CROSS-FLOW MEMBRANE FILTRATION OF CELL SUSPENSIONS

by

Norma Jean Ofsthun
B. S., Ch. E., California Institute
of Technology (1981)

Submitted in Partial Fulfillment
of the Requirements for the
Degree of Doctor of Philosophy
at the
Massachusetts Institute of Technology

February, 1989

Signature of Author: _____
Department of Chemical Engineering

Certified by: _____
C. K. Colton, Thesis Advisor

_____
C. Cooney, Thesis Committee Member

_____
W. M. Deen, Thesis Committee Member

_____
K. A. Smith, Thesis Committee Member

Accepted by: _____
R. Armstrong, Chairman
Dept. Comm. on Graduate Theses

This thesis is dedicated to my parents

Stanley O. Ofsthun

(1930-1987)

and

Mary S. Ofsthun

who have given me the courage, perseverance, and sense of humor needed to withstand life's many challenges,

and to my husband

Alexis Porras

whose love carries me through each day.

ACKNOWLEDGEMENTS

This project could not have been completed without the assistance of many people and corporations. Andrew Zydney assisted greatly by providing advice on a variety on subjects, particularly related to the mathematical modeling work. Visiting scientist Mitsuru Suzuki helped to improve the freeze-substitution technique and then carried out a large number of experiments during his stay at M. I. T. Eric Morrel kindly assisted with last-minute filtration experiments, while undergraduates Nhue Ho and Robin Zehr performed experiments with the rotating membrane system. I appreciate all of the help which these colleagues have given me.

Thanks are also due to those professors who served on my thesis committee: Clark Colton, my advisor, Charles Cooney, Bill Deen, Ken Smith, and Martin Yarmush. Contrary to what I had been led to expect, I found that some of the suggestions that I received at thesis committee meetings proved particularly useful. Clark lived up to his reputation, and provided detailed critical analysis of my thesis.

Many companies provided equipment used in my experiments. Hollow fibers were provided by Amicon/W. R. Grace, Enka A. G., Kinetek, and Sepracor. The Fenwal Automated Systems Division of Baxter Healthcare kindly loaned us the Hemascience Autopheresis-C rotating membrane system. Funding was provided by the N. S. F. Biotechnology Process Engineering Center at M. I. T., by Toyobo, Inc. (Japan), and by Baxter Healthcare. I would also like to thank Mike Lysaght at Baxter Healthcare for holding my future job in Renal Therapy open throughout the many delays of thesis writing.

Last, but not least, there are many lab-mates, teammates, lunch group members and other friends who made life enjoyable. I cherish the many friends I have made here at M. I. T. and hope we keep in touch despite the miles which will soon separate us.

CROSS-FLOW MEMBRANE FILTRATION OF CELL SUSPENSIONS

by

NORMA JEAN OFSTHUN

Submitted to the Department of Chemical Engineering
in partial fulfillment of the requirements for the
Degree of Doctor of Philosophy in Chemical Engineering

ABSTRACT

In order to better understand cross-flow membrane filtration of cell suspensions, experimental and theoretical work was carried out to meet the following goals: (1) to develop an experimental technique for observing cell concentration polarization boundary layers during cross-flow filtration, (2) to determine in what ways the cross-flow filtration behavior of rigid cell suspensions is different from that of deformable cells suspensions, and (3) to develop a mathematical model for rigid cell filtration.

We developed a freeze-substitution technique which permits visualization of cells which accumulate in the boundary layer near hollow fiber membrane surfaces. We have used this freezing technique to verify the occurrence of concentration polarization of red cells and to study the variation of concentration polarization with operating parameters which influence transport within the boundary layer and the hydraulic permeability of the dynamically-formed cell bed near the membrane surface.

Latex particles and bakers yeast were the two model rigid cell systems studied. Both are much less compressible than red cells; as a result, each has a much lower specific hydraulic resistance than the red cells. This lower resistance affects cross-flow filtration behavior because thick cakes of the rigid cells build up on the membrane during a long transient period before a steady-state balance between convection of cells toward the membrane and diffusion of cells away from the membrane is achieved. Significant differences in the cross-flow flux behavior with rigid and deformable cells were predicted theoretically and observed experimentally. Freezing experiments showed that cakes of rigid cells can significantly reduce the effective channel diameter and even clog fibers.

A theoretical model was developed for prediction of filtrate flux as a function of time for cross-flow filtration of rigid particle suspensions. The growth rate of the cake was calculated from the difference between the rate of particle convection toward the membrane and the rate of transport away from the membrane, using a stagnant film model to evaluate the particle mass transfer coefficient. Predicted fluxes were in good agreement with latex particle data. The filtration behavior suspensions of yeast in media or albumin solution (as required in the freezing experiments) was more complicated, requiring incorporation in the model of additional phenomena, including time-dependent membrane and cake resistances, and the effect of CO_2 generation by the yeast. The resulting yeast filtration model was able to qualitatively predict some important aspects of filtration behavior.

Thesis Advisor: Clark K. Colton, Professor of Chemical Engineering

TABLE OF CONTENTS

CHAPTER 1: INTRODUCTION

A. Historical Development of Membrane Filtration

Separation of cells from the fluid in which they are suspended has been important to the biotechnology and bio-engineering (medical) industries for many years. Reviews of the state of the art appeared as early as 1964 (Freeman), before the recent rapid growth in the membrane filtration industry. The first synthetic membranes developed provided the small molecular size cutoffs used in dialysis and reverse osmosis. With the development of higher-cutoff ultrafiltration and microfiltration membranes in the late 1960's, cross-flow membrane filtration emerged as a new unit operation in downstream processing (Michaels, 1968; Wang and Sinskey, 1970; Blatt, 1970). By 1980, biotechnology and membrane technology had each grown enough that an entire review was dedicated to the use of membranes in biotechnology (Michaels, 1980). Since then, such reviews have appeared in many journals (Short and Webster, 1982; Quinn, 1983; Short, 1983; Tutunjian, 1983; O'Sullivan et al., 1984; Bowden, 1985; Le and Billigheimer, 1985; Michaels and Matson, 1985; Strathmann, 1985; MacGregor, 1986; Mulder and Smolders, 1986; Biotechnology (anonymous) 1986; Belfort, 1987; and Olsen, 1987) and books (Gabler, 1985; Tutunjian, 1985; Drioli, 1986; and McGregor, 1986--a complete book on the subject), indicating the rapid progress in the field. None of these review articles provides a truly comprehensive picture of the current state of the art of membrane filtration in biotechnology. One reason why these reviews are incomplete is that pertinent articles are written in the journals of widely differing fields--microbiology, virology and bacteriology, biotechnology, chemistry and biochemistry, chemical and biochemical engineering, and waste water treatment. There is rarely overlap among such disparate bodies of literature, so it is easy to unwittingly omit relevant literature outside of one's specialty. Another reason is simply that many reviewers had no intention of surveying the entire literature: employees of membrane companies wrote reviews to introduce the concepts of cross-flow filtration to uninformed readers and to extol its virtues to potential users; extensive references were not necessary for achieving that goal. By utilizing a computerized literature search of several reference databases (available through the MIT Science Library) as a starting point, I have tried to put together a comprehensive review of membrane filtration in this chapter.

The main impetus for much of the development of membrane filtration systems has been medical applications--dialysis, hemofiltration (ultrafiltration of blood), and plasmapheresis (microfiltration of blood). The history and state of the art of membrane filtration in medicine has been discussed in detail elsewhere (Piskin and Chang, 1983; Zydney, 1985) and will be omitted here.

B. Membrane Filtration in Biotechnology

The two types of membrane filtration which are used for cell separations in biotechnology are microfiltration (MF) and ultrafiltration (UF). MF refers to the separation of particulates such as cells or cell fragments from water, small solutes, and macromolecules. UF refers to separations with membranes of smaller pore size which retain proteins and other macromolecules as well as cells. Whereas the pore size of UF membranes is usually reported as the nominal molecular weight cutoff (NMWCO), the nominal pore size (NPS) for MF membranes is usually given in microns or tenths of a micron. (For comparison, a NMWCO of 300,000 (or 300K) daltons is approximately equivalent to a NPS of 0.01 μm. The border between MF and UF is blurred when very small particles such as viruses must be filtered out; the membranes used for that separation are UF membranes, but the process is a solid/liquid separation like MF.)

Membrane filtration of cell suspensions is used in various stages of downstream processing of bioreactor effluents. The first step in purification of an extracellular product is to remove the cells from the broth. Depending on the size of the product, either MF or UF is used. MF results in a simple solid/ liquid separation of cells from broth. UF generally results in purification as well as solid/liquid separation: the extracellular product is separated from larger molecules in the broth. The smaller a product is, the more it can be purified in the initial filtration step. UF also allows retention of expensive serum proteins in the growth medium during recovery of products from animal cell culture.

For purification of an intracellular product, the first step is to remove water, residual nutrients, and waste products prior to cell disruption. Typically, microfiltration is used, often in combination with a cell-washing procedure. Next, filtration may be used to remove cell debris from the product stream after cell disruption. Membrane filtration may also be used to

recycle cells while removing a growth-inhibiting product from the broth. This allows higher cell concentrations (and product yields) to be achieved than is possible with traditional batch fermentations.

Most membrane filtration is carried out in cross-flow (CF) configurations, in which the bulk flow is parallel to the membrane surface while the filtrate flow is perpendicular to the membrane. The sweeping action of the bulk flow moving along the membrane minimizes the accumulation of retained species at the membrane surface. Cross-flow filtration (CFF) has numerous advantages over batch or "dead-end" filtration. CFF allows continuous, relatively steady operation, results in substantially higher fluxes, requires no filter aid, and is easily scaled up. The two common geometries for cross-flow systems are thin channels and hollow fibers. (Note: before CFF was developed, stirred cells were used. Stirring was the first method used to limit the buildup of retained species on the membrane.) Recently, rotating annular CF systems, in which the bulk flow moves between two cylindrical surfaces which are in relative motion, have been developed. The advantage of these systems is that the wall shear rate (and therefore the sweeping action) can be increased without affecting the axial pressure drop.

CFF also has advantages over other separation techniques. Unlike centrifugation, CFF is not dependent on the small density differences between cells and broth, and it is a gentle process with respect to both cell damage and protein (product) denaturation. Unlike flocculation and foam fractionation, CFF requires no chemical additives. Unlike freeze drying and spray drying, CFF is athermal and involves no phase change. Furthermore, energy and capital investment costs for CFF are small compared to those for continuous centrifugation. Consequently, CFF holds great promise for a variety of large-scale separations in the biotechnology industry.

Much of the recent progress in the use of membrane filtration in biotechnology has occurred in parallel developments which make a purely chronological review of the literature impossible. Therefore this review will be organized into three topics which are more manageable in size: filtration of intact organisms for product recovery; filtration of cell debris; and filtration for cell recycle. Reports of filtration of cell debris are grouped in a separate section because filtration of disrupted cells is distinctly more difficult than whole cell

filtration; increased viscosity, variation in particle sizes, and small average particle size make separation by either filtration or centrifugation difficult. Articles on cell recycle are discussed in a separate section because, in general, the emphasis of the work was not the filtration used but rather the effect of the recycling procedure on cell concentration achieved.

C. Review: Filtration of Intact Organisms for Product Recovery

The many examples of filtration of intact organisms for product recovery may be classified by the type of organism being filtered. To date, most membrane filtration in biotechnology involves yeast, bacterial cells, and viruses. Fewer reports discuss filtration of mycelial organisms and mammalian cells.

1. Yeast

Because of its industrial importance, availability, and low cost, Saccharomyces cerevisiae (baker's yeast) is the most common species of yeast used in filtration experiments. Use of other species will be specifically noted. In the 1970's, a number of membrane types and configurations were used for filtering yeast, but all reported experiments involved cell recycle and therefore will be discussed in Section 1.E.1. Although yeast cells are relatively large (diameter > 5 μm) compared to bacterial cells, UF membranes were used in early cell separation experiments. Lee et al. (1981) used 20K NMWCO polysulfone and "sulfonic acid" flat-sheet UF membranes (produced in their lab, on polyester support) in various configurations to filter beer stillage, and noted that the fouling properties of the membrane strongly influenced the flux. The homemade sulfonic acid membranes fouled less than the commercial polysulfone membranes. Cabral et al. (1985) studied the effect of antifoam agents (WPD 352 and WPD 700, "active oil-based defoamers from Westvaco," and X81-10, "a fatty-alcohol ester type product from Reilly-Whiteman") and cleaning procedures on hollow fiber UF with polysulfone 30K and 100K NMWCO membranes. They found that the cumulative fouling effect of the antifoam could be counteracted by washing with sodium hydroxide or ethanol, but not with water alone.

More recent studies often test MF membranes as well as UF membranes. Kroner and Nissinen (1986) measured filtrate flux vs. average transmembrane pressure, rotation rate, and

time with a rotating filter equipped with 1000K NMWCO polysulfone, 0.2 μm NPS Teflon, and 0.2 μm NPS polycarbonate membranes. Flux increased with increasing pressure, but began to level off at higher pressures. Increasing the rotation rate also increased the flux, but its effect became more, not less, pronounced at high rotation rates. The rotating device produced fairly constant filtration rates over a period of 24 hours. Bell and Davies (1987) filtered Apiotrichum curvatum, an oleaginous yeast whose low density causes centrifugation problems, with two 50K NMWCO (material not specified) hollow fiber UF membranes and with a pleated-sheet acrylic copolymer (0.2 μm NPS) MF membrane. They reported that flux increased with increasing shear rate, and decreased with increasing bulk cell concentration. This behavior is typical of cross-flow systems.

It has been observed that the flux obtained during cross-flow microfiltration of yeast declines very rapidly from pure-water permeability values. Kavanagh and Brown (1987) reported an order-of-magnitude decrease in flux within 40 sec of filtration with 2 μm NPS and 3 μm NPS microporous stainless steel tubes. Matsumoto et al. (1987) saw a 20 to 50-fold decrease in flux within one hour of filtration in a thin-channel system with 0.22 μm NPS cellulose triacetate MF membranes. In both studies, backflushing procedures were employed to enhance microfilter performance. As in all backwashing procedures in which product filtrate is the backwashing fluid, there was a trade-off between the resulting increase in the filtrate flux after backflushing and the negative filtrate flux during backflushing. Since membrane performance depends on operating procedures as well as device design and membrane properties, optimization of the entire process is necessary.

2. Bacteria

Over the past 15 years, a number of species of bacteria have been filtered in a wide variety of membrane systems. Although recently several engineering studies have appeared, most studies were largely anecdotal, employing a single set of operating conditions. Furthermore, details such as membrane material, pore size, and device configuration were not always reported. Nevertheless, let us begin with a brief review of the early "success stories" which provided the motivation for the development of cross-flow microfiltration.

Henry and Allred (1972) used a variety of MF and UF membranes to concentrate Micrococcus broth from batch fermentations in thin-channel (flat-sheet and spiral-wound) CFF systems. The filtrate flux decreased to its steady-state value over a period of 18 hours, and was "maintained for a week" at the steady-state value. The flux increased less than linearly with pressure as it was increased to 40 psi, but the flux never leveled off to a pressure-independent value. The flux in the thin-channel system was proportional to the shear rate to the one-half power, while that in the spiral wound system was proportional to shear rate to about the 0.8 power. (Note, the maximum shear rate studied, 12,000 sec^{-1}, was well within the laminar region, with a Reynolds number of 400.) The flux decreased with increasing bulk concentration, but the functional form of the concentration dependence varied from experiment to experiment. The observed increase in flux with increasing temperature was attributed to a drop in viscosity. Lastly, higher fluxes with asymmetric UF membranes than with homogeneous MF membranes were attributed to their lower susceptibility to plugging.

Reid and Adlam (1974) reported large-scale harvesting and concentration of Corynebacterium parvum using a Sartorius Membranfilter CF system. Cox (1975) used cellulose-acetate UF membranes in a CF system to purify toxin from Corynebacterium diphtheriae. Landwall and Holme (1977) used cellophane dialysis membranes to replenish media for Escherichia (E.) coli cultures without loss of cells. The universal conclusion was that cross-flow filtration is a useful technique for solid/liquid separation of bacterial suspensions.

By the end of the seventies, observations regarding the effects of varying operating parameters were being recorded in the literature, though systematic studies had not yet begun. Goto et al. (1979) harvested Methylomonas bacteria using stirred cell and thin-channel UF units, noting that the flux increased significantly with increasing Reynolds number, but only slightly with increasing pressure. Valeri et al. (1979) used both 0.22 μm NPS cellulosic MF membranes and 100K NMWCO polysulfone UF membranes in a thin-channel device to separate Bordetella pertussis from culture media and found that the UF flux decreased more gradually with time than did the MF flux. Tanny et al. (1980, 1982) concentrated and harvested both E. coli and Salmonella typhimurium using pleated cross-flow modules with 0.2

and 1.2 μm NPS acrylic-copolymer MF membranes. They found that raising the shear rate with or without raising the applied pressure resulted in increased fluxes. The flux decreased linearly with the log of the bulk cell concentration. Used membranes had a resistance of four times the original membrane resistance even after backflushing with water. However, an ethanol wash did effectively clean the membranes. Ackerman et al. (1982) used a CF microfilter to recover pseudomonad organisms continuously in a 600 L / 200 hr production run. Gallantree and Docksey (1983) used a relatively high pressure (200 psi) "ultrafilter" with 0.45 μm NPS polyvinylidene difluoride (PVDF) MF membranes and 100K NWMCO polysulfone UF membranes to separate E. coli, Lactobacillus, Streptococcus sanguius, Streptococcus faesciens, and Bacellus thuringensis. Eriksson (1985) conducted large-scale separation of Streptococcus pyogenes and E. coli cells from fermentation broths using CF MF and UF systems.

Recent studies in Germany sought not only to characterize the CF filtration behavior of bacteria, but also to determine the physical mechanisms involved. Schutte et al. (1983) studied the filtration of Bacillus cereus in 0.3 μm NPS polypropylene hollow fiber MF modules and found that the flux decreased with increasing cell concentration and increased with increasing temperature. Both effects were attributed to changes in the suspension viscosity. The authors recommended use of CFF in cases in which the required bacteria concentration is moderate, e.g. prior to cell disruption. Kroner et al. (1984) studied CFF of Bacillus sp., Bacillus cereus, Brevibacterium, Candida boidinii, E. coli, Klebsiella pneumonie, and Lactobacillus casei in polypropylene MF (0.3 μm NPS) hollow fibers, in a thin-channel microfilter with PVDF (0.45 μm NPS) membranes, in polysulfone (100K NMWCO) and polycarbonate (2000K NMWCO) UF hollow fibers, and in a polyacrylic (0.2 μm NPS) pleated membrane CF microfilter. In all cases, they found that plots of flux versus the log of the bulk cell concentration were sigmoidal in shape, with two regions of steep drop-off separated by a "constant operation" region. They attributed the low-concentration decrease to buildup of a bacterial cake on the membrane surface. While initial data indicated that the high-concentration drop-off could be caused by the large concomitant rise in the suspension viscosity, failure to recover higher fluxes by dilution of the bacterial suspension indicated that another mechanism--possibly cake compaction--was at least partially responsible. They also

observed that larger fluxes are obtained when larger cells are filtered. Backwashing was found to be of limited use in maintaining high fluxes. Furthermore, enzyme recovery was found to depend on operating parameters other than flux. They concluded "More research and development work is needed with regard to membrane properties, hydrodynamic aspects, cleaning procedures, and other improvements to establish cross-flow filtration in enzyme recovery processes." Riesmeier et al. (1986) studied MF of E. coli in polypropylene tubular membranes and in a relatively thick-channeled (2-6 mm) CF device with polypropylene and nylon membranes. Fluxes were "nearly steady" within 15 minutes, but continued their slight decline throughout 250 min experiments. Flux increased with increasing applied pressure up to a pressure of 1.5 bar, decreased with increasing bulk concentration, and decreased with increasing filter length. Use of antifoam lowered fluxes, presumably by membrane fouling. The thickness of the bacterial cake as a function of position was determined by measuring the total protein content of each of several axial segments of the filter after filtration. The thickest cakes were found in the region of high flux at the filter entrance, where the local pressure was highest. The cake height increased with increasing applied pressure and decreased with increasing length. The specific resistance of the cake was 3 orders of magnitude greater than that predicted by the Kozeny-Carman equation, and increased slightly with time, reportedly as a result of compaction. Changing the inlet reservoir from cell suspension to water sometimes increased the flux, probably by washing off portions of the cake. Other times, the flux remained constant, indicating that the cake was well-stuck to the membrane. Kroner and Nissinen (1986) filtered E. coli suspensions in the rotating membrane system with which they had also filtered yeast. Fluxes with E. coli were about half of those with yeast, but showed the same general behavior. Flux initially increased with transmembrane pressure, but began to level off at higher pressures. Increasing the rotation rate increased the flux, while increasing the bulk concentration decreased the flux. Fluxes were fairly constant with time. Enzyme transmission was much less pressure-dependent than it had been in hollow fiber experiments. They concluded that the rotating device, by virtue of its decoupling of shear rate and pressure, could be particularly useful for product recovery.

Other groups have also begun to characterize CF behavior of bacteria. Gabler and Ryan (1985) filtered E. coli suspensions with 0.45 μm PVDF membranes in a thin-channel

device and found that the CF filtrate flux increased more than linearly with the trans-membrane pressure, and asymptotically with recirculation rate. Le and Atkinson (1985) compared the performance of MF membranes of varying pore size for harvesting Erwinia carotovora and found 0.45 μm NPS membranes superior to both 0.2 μm and 0.6 μm NPS membranes. They also found that the flux decreased linearly with the log of the cell concentration in two regimes, with the slope in the low-concentration regime greater than the slope in the high-concentration regime. Zahka and Leahy (1985) studied CFF of E. coli, B. thuringiensis, and mycoplasma (a bacteria, the smallest known free-living organism) in a thin-channel system with both MF and UF membranes of unspecified materials. The flux obtained with E. coli increased with increasing pressure and with increasing shear rate, and decreased linearly with the log of the bulk cell concentration. The found significant differences in fouling among the membranes tested. Although MF fluxes decreased with time, they were significantly greater than UF fluxes. They reported that "chemical cleaning" of the membranes after filtration of E. coli restored original fluxes.

While these studies have characterized the performance of particular filtration systems with particular bacterial organisms, none has attempted to model the behavior so that the performance of a system could be predicted a priori. It is clear that development of a complete model must include the effects of the applied pressure, shear rate, cell concentration, axial pressure drop, particle size, membrane resistance, and cake resistance.

3. Viruses

Membrane filtration has been used to concentrate and purify viruses for over 50 years (Levaditi et al., 1926, with collodion membranes; Galloway and Elford, 1936, with gradocol membranes). Table I lists numerous reports of the use of modern membranes for virus concentration and purification. Except as otherwise noted, all of the studies below used UF membranes. (Because viruses are between 0.01 and 0.09 μm in diameter, MF membranes are not suitable.)

Belfort et al. (1974) reported that the flux remained constant throughout one hour experiments in which the poliovirus concentration was increased over 50-fold. They found that increasing the feed flow rate (and hence the shear rate) increased the filtrate flux. After

Table I. Membrane Filtration of Viruses

Author	Configuration	NMWCO	Virus
Strohmaier (1967)	thin channel	100K	foot & mouth disease
Morrow (1972)	"	"	"
Wang et al. (1968,1969)	stirred cell	10K,70K	bacteriophage SPO-1
Vaheri et al. (1969)	dialysis	---	rubella
Sweet et al. (1971)	osmotic UF	---	polio, coliophage
Sorber et al. (1972)	"	---	"
Rhim et al. (1969)	stirred cell	10K	leukemia, sarcoma
Klein et al. (1971)	"	100K	Rift Valley fever
Guskey & Wolff (1972)	"	50K	poliovirus
Kostenbader & Cliver (1973)	"	30K	enterovirus
Belfort et al. (1974,1976)	"	30K,10K	poliovirus
Colonno et al. (1977)	thin channel	---	vesicular stomatitus
Gangemi et al. (1977)	"	1000K	arenaviruses
Valeri et al. (1977)	"	1000K	influenza
Tamura & Takano (1978)	"	30K	C-type
Bellini et al. (1979)	"	1000K	Edmonston measles
Sekla et al. (1979)	"	100K	enteric
Berman et al. (1980)	thin channel	10K,30K	poliovirus
Leuthard & Schuerch (1980)	hollow fibers	100K	inducing
Shibley et al. (1980)	thin channel	1000K	Epstein-Barr
Trudel & Payment (1980)	hollow fibers	100K	rubella
Weiss (1980)	"	10K,50K	baboon endogenous
Ricketts et al. (1985)	thin channel	100K	lymphoma

initial experiments in which up to 60% of the virus stuck to the cellulose acetate membrane, backflushing was employed to maximize the recovery. The average rejection was 76% and the average recovery was 84%. In a subsequent study (Belfort et al., 1976), use of polysulfone hollow fibers resulted in complete rejection, higher filtration rates, and improved recovery. Most of the other studies reported filtration results only qualitatively. Usually neither the membrane material nor the filtrate flux was reported. However, the conclu ›n in all 23 studies was that ultrafiltration is a practical method for concentration and purification of viruses. Recently, the use of UF has extended beyornd the laboratory to large-scale production of biologicals (Shibley et al., 1980; Weiss, 1980; and Ricketts et al., 1985).

4. Mycelia

Molds, which are used industrially to produce antibiotics, organic acids, and enzymes, present interesting processing problems because of their mycelial structure. Their highly branched hyphae result in non-Newtonian (Bingham plastic) viscosity behavior which can make flow processes including filtration difficult. Nevertheless, within the past 10 years a few studies of filtration of mycelial organisms have been carried out. In 1979, Al-Obaidi and Berry incorporated a stirred cell microfilter (NPS not reported) in an external loop to periodically exchange the media and recover citric acid from an Aspergillus niger culture. Gallantree and Docksey (1983) used a CFF system with flat-sheet 0.45 μm NPS PVDF membranes for cell harvesting of Actinomycetes (a mycelial bacteria) and Streptomyces. Brown and Salam (1984) filtered the fungal organism Trichoderma reesei in a sterilizable CF filter constructed from sintered stainless steel tubes with a 75 μm NPS. They observed a steady decline in filtration rate which they attributed to "formation of a deposit in the surface of the filter tube." Backflushing resulted in a step increase of about one third of the flux decrease.

Ricketts et al. (1985) used polysulfone and cellulose flat-sheet and hollow fiber ultrafilters (10K and 20K NMWCO) to concentrate and purify largomycin from Streptomyces pluricolorescens prior to gel permeation chromatography. Zahka and Leahy (1985) used CFF to concentrate Streptomyces as well as the non-mycelial organisms mentioned previously. During the 6-fold concentration, the flux dropped to half its initial value four times; each

time the flux was almost completely restored by closing the filtrate port and thereby washing away the mycelial cake from the membrane surface.

As yet there are no reports comparing the performance of UF and MF membranes for filtration of a particular mycelial organism. The industrial importance of molds will probably lead to significant future work in this area.

5. Mammalian Cells

Because mammalian cells are much more fragile (shear-sensitive) than microbial cells, the gentleness of CFF is particularly advantageous when separation or concentration of mammalian cells is required. Consequently, the focus of many of the references which follow was cell viability rather than flux performance. Himmelfarb et al. (1969) equipped a culture vessel with a spin filter device based on a 3 μm NPS acrylic copolymer MF membrane and were able to produce mouse leukemia cells at a concentration fifty times greater than is possible in standard suspension cultures. Radlett (1972) used a cellulose-nitrate thin-channel filter to concentrate BHK 21 cells and found that 0.6 μm NPS MF membranes performed better than either 0.2 μm NPS membranes, whose filtrate fluxes were low, or 3.0 μm NPS membranes, which clogged after one hour.

Howlett et al. (1979) used a thin-channel MF (1.2 μm NPS) system to concentrate lymphoma cells prior to recovery of the plasma membranes for biochemical analyses. Maizel et al. (1981) used a CF UF system for recovery of Interleukin 1 from leukemia cells. Tanny et al. (1982) used an acrylic copolymer (0.2 μm) pleated CF MF module to filter the naturally stable dispersion of tissue homogenate from calf organs and consequently decided to build a pilot filtration system at a substantial cost savings over separation by a continuous centrifuge. Klein et al. (1984) used a 0.45 μm NPS nylon pleated CF filter for removing cells in the first step of the recovery of Interleukin-3 from mammalian cell suspensions. Ricketts et al. (1985) used thin-channel modules with polysulfone (10K, 30K, and 100K NMWCO) membranes to purify monoclonal antibodies from hybridoma cell suspensions and Interleukin-3 from murine cell suspensions.

DeLoach et al. (1986) used CF UF through 0.1 μm NPS hollow fibers to recover lipid-free hemoglobin from mammalian red blood cells. Shiloach et al. (1986) tested 0.2 μm NPS

polysulfone hollow fibers and 0.45 μm NPS PVDF thin-channel microfilters for the large-scale recovery of basophilic leukemia cells from tissue culture media and found that no loss in cells, nor decrease in cell viability, nor visible cell damage had occurred during the 80 min filtration procedures. A relatively linear decrease in flux with time (with a factor of two drop-off in 15 minutes) was attributed to membrane fouling and increased viscosity during the 30-fold concentration. As the authors themselves noted, their data "does not represent a systematic evaluation of hollow fiber tangential flow filters." It does, however, lay ground for future work.

Although no results have been reported as yet, it has been suggested that CFF of microcarrier cell cultures, using membranes with relatively large pore sizes (only somewhat smaller than the microcarrier beads) could be used for continuously removing products and wastes from the growth media. As the use of mammalian cell culture increases, perhaps report of this and other types of CFF of mammalian cells will appear regularly.

D. Review: Filtration of Cell Debris

In the last five years there have been many reports of using CFF for removing yeast and bacterial cell debris from the process stream. Most of these studies focused on enzyme (product) transmission through the membrane, which is not always proportional to the flux. Quirk and Woodrow (1983) used CFF to recover enzymes from disrupted Pseudomonas sp. and Pseudomonas fluorescens suspensions and found that 100K NMWCO polysulfone and 1000K NMWCO membranes (material not specified) gave very low enzyme yields in the filtrate while 0.45 μm NPS cellulosic and 0.5 μm PVDF MF membranes gave clear filtrates containing high enzyme yields. Datar (1985) filtered disrupted E. coli with flat-sheet MF (0.2 and 0.45 μm NPS) membranes made of a copolymer of polyvinyl chloride and acrylonitrile and found that use of turbulent flow resulted in greater recovery of enzyme in the filtrate than use of laminar flow. Eriksson (1985) obtained low flux and low enzyme yield when filtering disrupted E. coli in UF hollow fibers and found that MF with 0.45 NPS membranes in a thin-channel system (membrane materials not reported) resulted in better fluxes and yields, but filtrate quality no better than that obtained from centrifugal separators. Gabler and Ryan (1985) filtered E. coli lysate with 0.45 μm NPS flat-sheet PVDF MF membranes and found that the

flux increased with both transmembrane pressure and recirculation rate, and decreased with time. Thompson and Humphries (1985) found that recovery of cell walls from disrupted Micrococcus luteus by filtration with 0.2 μm NPS flat-sheet MF membranes produced better yields than recovery by centrifugation.

Le and co-workers (Le et al., 1984a; Le and Atkinson, 1985) filtered disrupted Pseudomonas fluorescens and Erwinia carotovora with various flat-sheet MF membranes and found enzyme transmission was influenced by both filtrate flux and other factors. The flux initially increased with pressure and then approached a pressure-independent maximum value. Increasing the shear rate increased the flux; the flux increased with the square root of the recirculation rate. The flux decreased a factor of two in the first 30 min and then gradually declined for the next 2.5 hr. Enzyme transmission decreased with time and increased with both increasing feed velocity and increasing applied pressure. Transmission through an asymmetric membrane dropped off most rapidly when the membrane was used in the "tight-side-up" configuration. In a subsequent study (1984b), they found CFF to be economically favorable compared to high speed centrifugation for the removal of Erwinia carotovora cell debris.

Kroner et al. (1984) filtered disrupted Candida boidinii cells with 2000 NMWCO polycarbonate UF hollow fibers and filtered disrupted yeast cells with a 0.2 μm NPS polypropylene flat-sheet MF membranes. Later, Kroner and Nissinen (1986, 1987) found that a rotating Teflon membrane filter with a NPS of 0.2 μm performed well in filtering disrupted B. ammoniagenes, B. cereus, B. licheniformis, C. boidinii, E. coli, and L. confusus. They found that the rotating filter resulted in 3-fold higher fluxes and enzyme transmission than was obtained with polysulfone 0.1 μm NPS hollow fibers and 0.2 μm NPS ceramic tube filters.

These studies have shown that the recovery of an intracellular product by membrane filtration after cell disruption depends on not only the filtrate flux but also factors such as adsorption onto the membrane and onto cell debris. Such factors will differ for each product/cell/membrane combination. Consequently, evaluation of CFF for cell debris removal will probably continue on a case-by-case basis.

E. Review: Filtration for Cell Recycle

The multitude of articles on membrane filtration for cell recycle will be separated into two sections: filtration for yeast recycle, and filtration for bacteria recycle. Because of the nature of cell recycle, CFF was used in all cases except those in which the filter was actually incorporated as part of the fermentor.

1. Yeast

According to a recent review article on "Recycle in Fermentation Processes" (Hamer, 1982), Pirt and Kurowski (1970) were the first to employ CFF to recycle yeast. Table II summarizes the subsequent reports of the use of membrane filtration for recycle of both Saccharomyces cerevisiae and Kluyveromyces yeast, listing details of device configuration, membrane material, and the size cut-off of the filter. All of the reports of use of CFF in yeast recycle were favorable.

Only a few authors discussed filter performance. Dostaltek and Haggstrom (1982) found porous stainless steel filter tubes superior to other MF membranes because of their mechanical strength after autoclaving and lack of cell adherence to the membrane. Nishizawa et al. (1983) reported that the filtrate flux during yeast recycle decreased rather steeply during the first hour, and continued to decline gradually for the next four hours. Plots of flux versus the log of the bulk concentration were linear, but data for different pressures fell on different lines. Increasing the pressure increased the flux.

In a comparison of a variety of MF and UF devices, Hoffmann et al. (1987) found that commercially available hollow fiber modules out-performed flat-plate devices. They noted that the flux obtained with MF membranes continued to fall over 25 hour experiments, though the rate of decrease became smaller and smaller. Failure of the flux to increase upon redilution of the yeast indicated that membrane fouling had occurred. (They concluded that relatively constant flux UF membranes are preferable to quickly-fouling MF membranes for yeast cell recycle.) Flux increased with increasing shear rate and decreased with increasing bulk concentration. The flux with washed and resuspended cells at a given concentration was always higher than that with original fermentation broth.

Table II. Use of Membrane Filtration for Yeast Recycle

SACCHAROMYCES CEREVISIAE:

Author	Channel Configuration	Dimension	Material	Cut-Off
Pirt & Kurowski (1970)	filter tubes	1.2 cm	glass fibers	2 μm
Margaritis & Wilke (1978)	rotating cylinder	10 cm	porous steel	5 μm
Haraldson & Rosen (1982)	"	"	"	"
Watson & Berry (1979)	stirred cell	N/A	cellulosic	1.2,0.2 μm
Rogers et al. (1980)	"	"	"	"
Hoffmann et al. (1985)	"	"	"	"
Dostaltek & Haggstrom (1982)	stirred cell	N/A	cellulosic	0.45 μm
	"	"	acrylic	"
	"	"	polycarbonate	0.4,0.8 μm
	"	"	polyester	1 μm
	"	"	porous steel	5 μm
Nishisawa et al. (1983)	hollow fibers	not reported	not reported	0.1 μm
Cheryan & Mehaia (1984)	hollow fibers	"	"	50 K
Kroner & Nissinen (1988)	rotating cylinder	0.4 cm	Teflon	0.2 μm
	"	"	polycarbonate	"
	"	"	polysulfone	1000 K
Hoffmann et al. (1987)	filter tubes	"	variety	variety
	thin channel	"	"	"
Lafforgue et al. (1987)	hollow fiber	0.6 cm	zirconium/carbon	0.14 μm

---

KLUYVEROMYCES:

Cheryan & Mehaia (1983)	hollow fiber	not reported	not reported	50 K
Jannssens et al. (1983)	thin channel	"	polysulfone	100 K

2. Bacteria

Reports of the use of membrane filtration for bacterial cell recycle are summarized in Table III. As with yeast recycle, most reports were concerned more with cell growth than with filter performance, and all reports of use of CFF for bacterial cell recycle were favorable.

Lee et al. (1980) reported flux decay in both cellulose acetate and polyamide filters. Charley et al. (1983) recommended use of a hollow fiber ultrafilter rather than either a thin-channel or hollow fiber microfilter for recycling bacteria because the filtrate flux could be maintained for a long period of time. Ohleyer et al. (1985) backflushed their PVDF MF membranes after 40, 100, 145, and 400 hours and found that the permeability remained constant after 40 hours at about two-thirds of its initial value. Taniguchi et al. (1987) noted the advantage of heat-sterilizability of the ceramic filters which they used for cell recycle.

Table III. Use of Membrane Filtration for Recycle of Bacteria

Author	Configuration	Channel Dimension	Material	Cut-off	Species
Fensom et al. (1974)	stirred cell	N/A	cellulosic	0.22 μm	Agrobacterium tumefaciens
Lee et al. (1980)	thin channel	*	cellulosic	0.2 μm	Zymomonas mobilis
	hollow fiber	*	polyamide	0.02 μm	"
Bull (1981)	filter tubes (w/inserts)	0.2 mm	ceramic	0.18 μm	Gluconobacter oxydans
					Serratia marcescens
Dostalek & Haagstrom (1982)	**	**	**	**	Pediococcus pentosaceus
					Propionibacterium
					Zymomonas mobilis
Charley et al. (1983)	hollow fiber	*	*	100 K	"
	thin channel	*	*	0.45 μm	"
	hollow fiber	*	*	0.45 μm	Escherichia coli
Anderson et al. (1984)	pleated sheet	*	acrylic	0.2 μm	Streptococcus dismutase
Holst et al. (1985)	hollow fiber	0.22 mm	polyamide	*	Lactobacillus delbrueckii
Ohleyer et al. (1985)	thin channel	*	PVDF	0.5 μm	Clostridium thermoaceticum
Reed & Bogdan (1985)	"	*	"	"	Clostridium acetobutylicum
Pierrot et al. (1985)	hollow fiber	0.5 mm	*	100 K	Streptococcus cremoris
Taniguchi et al. (1987)	filter tubes	4 mm	ceramic	0.2 μm	Lactobacillus casei

* not reported

** same as in Table 1

F. The Place of Membrane Filtration in Biotechnology

Review of the literature through 1987 indicates that membrane filtration can and will be an important separation process in the biotechnology industry. As in the development of any new technology, early experiments were exploratory in nature, searching for ways to use the process. It was shown that membrane filtration was a realistic alternative to centrifugation for separation of cells or cell debris from broth, and could be used for cell recycle as well as for downstream processing. Next came experiments with a variety of membrane and cell systems which demonstrated the breadth of possibilities. Engineers have recently begun to scale up membrane filtration systems for industrial use. Research is now necessary so that designs can be based on an understanding of the physical phenomena involved in filtration.

G. Brief Introduction to Concentration Polarization

The filtrate fluxes obtained when filtering cell suspensions are generally far below fluxes of cell-free media through the same membranes. It has been proposed that the flux is controlled by a concentrated layer of cells at the membrane surface, the so-called "concentration polarization boundary layer." While concentration polarization models have existed for about twenty years, no previous experiments proved that such boundary layers existed.

The essence of all concentration polarization models is that at steady state there is a balance between convection of the retained species toward the membrane and diffusion of that species away from the membrane (as a result of its concentration gradient). Blatt et al. (1970) found that a concentration polarization model for the filtrate flux in cross-flow ultrafiltration of macromolecules predicted fluxes very well, while an equivalent model for cross-flow microfiltration significantly underpredicted both the magnitude of the flux and its dependence on shear rate. Zydney and Colton (1982) proposed that the reason for the discrepancy between theory and experimental data was the inappropriate use of the Brownian-motion diffusivity of the cells in the model. They argued that the cell diffusivity was being significantly augmented by the fluid shear, which caused mutually-induced velocity fields due to both cell migrations and rotations. Zydney and Colton (1986) subsequently demonstrated that the fluxes measured in a variety of cross-flow microfiltration systems could be predicted by incorporation of an appropriate expression for the shear-induced diffusivity into the concentration polarization model.

The concentration polarization model hypothesizes that the pressure-independent flux observed arises because, at sufficiently high pressure, boundary layer phenomena (not the membrane resistance and applied pressure) limit the flux. With incorporation of the shear-enhanced diffusivity, the predicted filtrate flux increases linearly with the shear rate and decreases with the log of the bulk cell concentration.

Zydney (1985) also developed a detailed model of cross-flow microfiltration of blood which was in excellent agreement with experimental data. He found that the highly deformable blood cells pack to such high cell densities that only a few layers of cells on the membrane surface could provide sufficient hydraulic resistance to account for the entire

"transmembrane" pressure drop. As a result, the model predicted a pressure boundary layer much smaller than the concentration boundary layer over which the cell concentration decreased from its high concentration at the wall to its bulk value. This effectively decoupled the pressure gradient from the concentration gradient. The model predicted that the large concentration boundary layer, and the constitutive relations important in it--the concentration-dependent viscosity and the shear- and concentration-dependent diffusivity--were responsible for setting the flux.

While it appears that cross-flow microfiltration of deformable blood cells is well understood, the state of the art in CF MF of microbial cells lags far behind. The one modeling attempt in the literature to date (Matsumoto et al., 1987) is really only an exercise in curve-fitting, since the physical picture assumed in the original derivation of the model (Hermia, 1982)--small particles adsorbing onto the walls of large pores--directly contradicts the true physical picture--large yeast cells which cannot enter into small membrane pores. Some of the observed flux behavior of microbial cells is similar to that observed with deformable cells. Flux does not increase linearly with pressure as pure-water fluxes do; at normal operating pressures the flux is much smaller than the pure-water flux. The flux increases with increasing shear rate and decreases with increasing bulk concentration. These similarities suggest that concentration polarization phenomena are involved.

However, filtrate flux behavior with rigid cells is not identical to deformable cell behavior. With rigid cells, the approach to "steady state" (if such a state exists) is often very slow (hours; Henry and Allred, 1972; Nishizawa et al., 1983; Hoffmann et al., 1987) compared to the short time (<1 min; Zydney, 1985) required with blood cells. The flux may level off somewhat as the pressure is increased (Henry and Allred, 1972; Goto et al., 1979; Tanny et al., 1980; Le et al., 1984a; and Reismeier et al., 1986), but does not always approach a maximum value like that seen with deformable cells. The dependence of flux on shear rate (Henry and Allred, 1972; Tanny et al., 1982; Le et al., 1984a; Gabler and Ryan, 1985) and on the log of the bulk cell concentration (Schutte et al., 1983; Kroner et al., 1984; Gabler and Ryan, 1985) is not always linear. As data in Chapter 4 of this thesis will demonstrate, axial pressure drops are also greater than those observed with deformable cells.

As will be shown subsequently in this thesis, the reason for the observed differences in behavior may be directly related to the differences in deformability. Because of the lower hydraulic resistance, of the rigid cells, the pressure boundary layer may be made up of a thick cake of cells which would take a long time to build up. Such a cake could be thick enough to decrease the channel cross-section for flow, thereby leading to an increase in both the shear rate and the axial pressure drop. Increases in the effective shear rate would increase the apparent dependence of flux on shear rate, while increases in axial pressure drop could leave portions of the membrane exposed to the pressure-dependent regime (where the flux is lower) and therefore decrease the apparent dependence of flux on shear rate. Since the thickness of a rigid cell cake would have to change significantly as the pressure is raised, the shear rate, and therefore the flux, could continue to increase with pressure. Understanding the differences in the concentration polarization phenomena of rigid and deformable cells might allow prediction of filtrate fluxes with microbial cells.

Over the years there have been occasional references to the "unfilterability" of yeast cell suspensions (Tobler, 1981). Cross-flow channels can become completely blocked by cells. Because of its relatively large size (diameter > 5 μm) compared to other microbial cells such as E. coli (1 μm), the thickness of the pressure boundary layer (i.e. the yeast cake), may be as big as the channel itself. Also, the channel may plug because too great a fraction of the liquid is filtered out, "drying out" the bulk suspension so that its viscosity is so large that the bulk flow stops.

H. Thesis Program

The first goal of this thesis was to develop a freezing procedure which would allow observation of concentration polarization boundary layers. Since Zydney's detailed model for membrane plasmapheresis predicted concentration profiles which could be compared with freezing results, the first freezing experiments were carried out with blood. Variation of the observed boundary layer with wall shear rate, length, and applied pressure were compared with predictions. Experimental details and results are given in Chapter 2. Additional long-term experiments with blood were conducted by Mitsuru Suzuki, a visiting scientist. These experiments are discussed in Chapter 3.

The second goal of this thesis was to conduct experiments to determine the properties of yeast which affect filtration in order to provide the physical property relationships required for modeling. Batch filtration experiments were conducted to determine the hydraulic resistance of yeast cakes. Centrifugation experiments were used to measure the compressibility of yeast cakes. These experiments are discussed in Chapter 4.

The third goal of this thesis was to characterize the flux behavior of yeast in hollow fiber membrane systems. Yeast concentration, bulk flow rate, applied pressure and membrane material were varied. The flux data was taken in single hollow fibers as well as in hollow fiber cartridges. Membrane materials included polypropylene, polyamide, modified polysulfone, and polysulfone/Biopol. Internal diameters ranged from 300 to 2330 μm. Conditions under which the various hollow fibers clogged were studied. The fourth goal was to conduct freezing experiments to measure yeast cake layer thickness in hollow fibers. As with the blood-freezing experiments, variation with shear rate, applied pressure, and axial position were observed. The filtration experiments in which fluxes and cake thicknesses were measured comprise Chapter 5. The results of additional filtration experiments conducted with a novel annular rotating-membrane device are discussed in the Appendix to Chapter 5.

The fifth goal of this thesis was to develop a model to predict filtrate flux, cake thickness, and channel clogging during cross-flow filtration of yeast. To allow direct comparison with freezing data, a cylindrical geometry was chosen. Since experimental results had shown a relatively slow approach to steady-state fluxes, the model was designed to predict cake growth and flux decline as a function of time. The convective flux was calculated by

dividing the local applied pressure by the sum of the membrane and cake resistances. The effect of axial pressure drop, which can become particularly important as the channel narrows and as the axial increase in bulk concentration raises the suspension viscosity, was included. The shear-enhanced diffusion term was determined from a modified Leveque solution which incorporated the local variation of concentration, viscosity, and diffusivity in the boundary layer as well as the variation in shear rate with cake thickness. Chapter 6 contains modeling details and results. Source code and sample output are included in the Appendix to Chapter 6.

In summary, the goals outlined above were achieved, and our overall understanding of cross-flow filtration of cell suspensions has improved.

Chapter 1: Introduction

I. References

Ackerman, R. A., S. A. Meyers, J. F. Tobey, Jr., S. K. Birdsell, and S. G. Frasier (1982): Cross-flow Filtration to Recover Pseudomonad Organisms Abs. Pap. ACS 184: 56

Al-Obaidi, Z. S., and D. R. Berry (1979): Extended Production of Citric Acid Using an Exchange Filtration Technique Biotech. Letters 1(5): 221-224

Anderson, K. W., E. Grulke, and P. Gerhardt (1984): Microfiltration Culture Process for Enhanced Production of rDNA Receptor Cells of Escherichia coli Bio-Technology 2(10): 891-896

Anonymous (1986): High Expectations on the Downstream Side Biotechnology 4: 871-878

Belfort, G. (1987): Membrane Separation Technology: an Overview, in Advanced Biochemical Engineering Bungay, H.R., and G. Belfort, eds., John Wiley & Sons Inc., New York

Belfort, G., Y. Rotem, and E. Katzenelson (1974): Virus Concentration Using Hollow Fiber Membranes Water Res. 9: 79-85

Belfort, G., Y. Rotem, and E. Katzenelson (1976): Virus Concentration Using Hollow Fiber Membranes-II Water Res. 10: 279-284

Bell, D. J., and R. J. Davies (1987): Cell Harvesting of Oleaginous Yeast by Cross-Flow Filtration Biotech. Bioeng. 29(9): 1176-1178

Bellini, W. J., A. Trudgett, and D. E. McFarlin (1979): Purification of Measles Virus with Preservation of Infectivity and Antigenicity J. Gen. Virol. 43: 633-639

Berman, D., M.-E. Rohr, and R. S. Safferman (1980): Concentration of Poliovirus in Water by Molecular Filtration Appl. & Environ. Microbiol. 40(2): 426-428

Bertera, R., H. Steven, and M. Metcalfe (1984): Development Studies of Crossflow Microfiltration The Chemical Engineer Jun: 10-14

Blatt, W. F., A. Dravid, A. S. Michaels, and L. Nelson (1970): Solute Polarization and Cake Formation in Membrane Ultrafiltration: Causes, Consequences, and Control Techniques, in Membrane Science and Technology J. E. Flinn, ed., Plenum Press, New York, pp. 47-97

Bowden, C. (1985): Recovery of Micro-organisms from Fermented Broth The Chemical Engineer 415: 50-54

Brown, D. E., and F. R. Abdul Salam (1984): A New Filter for Cell Separation Biotech. Letters 6(6): 401-406

Bull, D. N., and M. D. Young (1981): Enhanced Product Formation in Continuous Fermentations with Microbial Cell Recycle Biotech. Bioeng. 23: 373-389

Cabral, J. M. S., B. Casale, and C. L. Cooney (1985): Effect of Antifoam Agents and Efficiency of Cleaning Procedures on the Cross-flow Filtration of Microbial Suspensions Biotech. Letters 7(10): 749-752

Charles, M., and M. Leh (1983): Biotechnological Applications of Cross Flow Microporous Filtration: Concentration and Cell Recycle Abs. Pap. ACS 186: 78

Charley, R. C., J. E. Fein, B. H. Lavers, H. G. Lawford, and G. R. Lawford (1983): Optimization of Process Design for Continuous Ethanol Production by Zymomonas mobilis ATCC 29191 Biotech. Letters 5(3): 169-174

Cheryan, M., and M. A. Mehaia (1983): A High-Performance Membrane Bioreactor for Continuous Fermentation of Lactose to Ethanol Biotech. Letters 5(8): 519-524

Cheryan, M., and M. A. Mehaia (1984): Ethanol Production in a Membrane Recycle Reactor: Conversion of Glucose Using Saccharomyces cerevisiae Process Biochem. Dec: 204-208

Cox, J. C. (1975): New Method for the Large-Scale Preparation of Diphtheria Toxoid: Purification of Toxin Appl. Microbiol. 29(4): 464-468

Datar, R. (1985): Studies on the Separation of Intracellular Soluble Enzymes from Bacterial Cell Debris by Tangential Flow Membrane Filtration Biotech. Letters 7(7): 471-476

DeLoach, J. R., C. L. Sheffield, and G. E. Spates (1986): A Continuous-Flow High-Yield Process for Preparation of Lipid-Free Hemoglobin Anal. Biochem. 157: 191-198

Dlouhy, P. E., and D. A. Dahlstrom (1968): Continuous Filtration in Pharmaceutical Production Chem. Eng. Prog. 64(4): 116-121

Dostalek, M., and M. Haggstrom (1982): A Filter Fermenter-Apparatus and Control Equipment Biotech. Bioeng. 24: 2077-2086

Drioli, E. (1986): Membrane Processes in the Separation, Purification, and Concentration of Bioactive Compounds from Fermentation Broths ACS Symposium Series 314: 52-66

Eriksson, A. (1985): Some Examples of the Use of Crossflow Filtration in the Downstream Processing in a Biochemical Industry Desalination 53: 259-263

Fensom, A. H., W. M. Kurowski, and S. J. Pirt (1974): The Use of Ferricyanide for the Production of 3-Keto Sugars by Non-growing Suspensions of Agrobacterium tumefaciens J. Appl. Chem. Biotechnol. 24: 457-467

Freeman, R. R. (1964): Biotechnology Report: Separation of Cells from Fluids Biotech. Bioeng. 6: 87-125

Gabler, F. R. (1985): Cell Processing Using Tangential Flow Filtration, in Comprehensive Biotechnology Vol 2, C. L. Cooney and A. E. Humphrey, eds., Pergamon Press, New York

Gabler, R., and M. Ryan (1985): Processing Cell Lysate with Tangential Flow Filtration ACS Symposium Series 217: 1-20

Gallantree, I., and S. Docksey (1983): Fermentation Cell Separations with High Performance Ultrafiltration Process Biochem. 18(3): R15-R19

Gangemi, J. D., E. V. Connell, B. G. Mahlandt, and G. A. Eddy (1977): Arenavirus Concentration by Molecular Filtration Appl. & Environ. Microbiol. 34(3): 330-332

Goto, S., T. Kuwajima, R. Okamoto, and T. Inui (1979): Separation of Biomass by Membrane Filtration and Continuous Culture with Filtrate Recycling J. Ferment. Technol. 57(1): 47-52

Gravatt, D. P., and T. E. Molnar (1986): Recovery of an Extracellular Antibiotic by Ultrafiltration, in Membrane Separations in Biotechnology, W. C. McGregor, ed., Marcel Dekker, Inc. New York, pp. 89-100

Guskey, L. E., and D. A. Wolff (1972): Concentration and Purification of Poliovirus by Ultrafiltration and Isopycnic Centrifugation Appl. Microbiol. Jul: 13-17

Hamer, G. (1982): Recycle in Fermentation Processes Biotech. Bioeng. 24: 511-531

Haraldson, A., and C.-G. Rosen (1982): Studies on Continuous Ethanol Fermentation of Sugar Cane Molasses II. Continuous Alcohol Fermentation and Product Removeal in a Laboratory Scale Plant Eur. J. Appl. Microbiol. Biotech. 14: 220-224

Henry, J. D. Jr., and R. C. Allred (1972): Concentration of Bacterial Cells by Cross Flow Filtration Dev. Indust. Microbiol. 13: 177-190

Himmelfarb, P., P. S. Thayer, and H. E. Martin (1969): Spin Filter Culture: The Propagation of Mammalian Cells in Suspension Science 164(May): 555-557

Hoffmann, H., T. Scheper, and K. Schugerl (1987): Use of Membranes to Improve Bioreactor Performance The Chem. Eng. J. 34(1): B13-B19

Hoffmann, H., W. Kuhlmann, H.-D. Meyer, and K. Schugerl (1985): High Productivity Ethanol Fermentations with Cross-flow Membrane Separation Techniques for Continuous Cell Recycling J. Memb. Sci. 22: 235-243

Holst, O., L. Hansson, A. C. Berg, and B. Mattiasson (1985): Continuous Culture with Complete Cell Recycle to Obtain High Cell Densities in Product Inhibited Culturess; Cultivation of Streptococcus lactis for Production of Superoxide Dismutase Appl. Microbiol. Biotech. 23: 10-14

Howlett, A. C., P. C. Sternweis, B. A. Macik, P. M. Van Arsdale, and A. G. Gilman (1979): Reconstitution of Catecholamine- sensitive Adenylate Cyclase J. Biol. Chem. 254(7): 2287-2295

Janssens, J. H., A. Bernard, and R. B. Bailey (1984): Ethanol from Whey: Continuous Fermentation with Cell Recycle Biotech. Bioeng. 26: 1-5

Kavanagh, P. R., and D. E. Brown (1987): Cross-flow Separation of Yeast Cell Suspensions Using Sintered Stainless Steel Filter Tubes J. Chem. Tech. Biotech. 38(3): 187-200

Klein, F., B. G. Mahlandt, H. B. Bonner, and R. E. Lincoln (1971): Ultrafiltration as a Method for Concentrating Rift Valley Fever Virus Grown in Tissue Culture Appl. Microbiol. Apr: 758-760

Klein, F., R. T. Ricketts, T. R. Rohrer, W. I. Jones, Jr., P. M. Clark, and M. C. Flickinger (1984): Membrane Ultrafiltration: Concentration of Interleukin-3 Appl. & Environ. Microbiol. 47(5): 1023-1026

Klein, W. (1982): Crossflow Microfiltration: a Membrane Process for Concentration of Suspensions Filtr. and Sep. Mar/Apr: 130-134

Kostenbader, K. D. Jr., and D. O. Cliver (1973): Filtration Methods for Recovering Enteroviruses from Foods Appl. Microbiol. Aug: 149-154

Kroner, K. H., H. Schutte, H. Hustedt, and M. R. Kula (1984): Cross-flow Filtration in the Downstream Processing of Enzymes Process Biochem. 19: 67-74

Kroner, K. H., and V. Nissinen (1986): Recent Studies with Dynamic Filtration of Microbial Suspensions using an Axial Rotating Filter, in 5th Int. Symp. Synth. Membr. in Science and Industry Tubingen, F. R. G.

Kroner, K. H., and V. Nissinen (1987): Dynamic Filtration Sudies with Cell Homogenates, in Proc. 4th Eur. Congr. Biotechnol. Vol. 2, Neijssel, O. M., R. R. van der Meer, and K. Ch. A. M. Luyben, eds., Elsevier Science Publishers, Amsterdam

Lafforgue, C., J. Malinowski, and G. Goma (1987): High Yeast Concentration in Continuous Fermentation with Cell Recycle Obtained by Tangential Microfiltration Biotech. Letters 9(5): 347-352

Landwall, P., and T. Holme (1977): Removal of Inhibitors of Bacterial Growth by Dialysis Culture J. Gen. Microbiol. 103: 345-352

Le, M. S., L. B. Spark, P. S. Ward, and N. Ladwa (1984): Microbial Asparaginase Recovery by Membrane Processes J. Membr. Sci. 21: 307-319

Le, M. S., L. B. Spark, and P. S. Ward (1984): The Separation of Aryl Acylamidase by Cross Flow Microfiltration and the Significance of Enzyme/Cell Debris Interaction J. Membr. Sci. 21: 219-232

Le, M. S., and P. J. Billigheimer (1985): Membranes in Downstream Processing The Chemical Engineer 416: 48-53 Le, M. S., and T. Atkinson (1985): Crossflow Microfiltration for Recovery of Intracellular Products Process Biochem. Feb: 26-31

Lee, K. J., M. Lefebvre, D. E. Tribe, and P. L. Rogers (1980): High Productivity Ethanol Fermentations with Zymomonas mobilis using Continuous Cell Recycle Biotech. Letters 2(11): 487-492

Lee, T. S., D. Omstead, N.-H. Lu, and H. P. Gregor (1981): Membrane Separations in Alcohol Production Ann. N. Y. Acad. Sci. 100: 367-381

Leuthard, P., and A. R. Schuerch (1980): A Simple and Rapid Method for Concentration of Interferon and Removal of Concentrated Inducing Virus Experientia 36: 1447

Maizel, A. L., S. R. Mehta, S. Hauft, D. Franzini, L. B. Lachman, and R. J. Ford (1981): Human T Lymphocyte/Monocyte Interaction in Response to Lectin: Kinetics of Entry into the S-Phase J. Immun. 127(3): 1058-1064

Margaritis, A., and C. R. Wilke (1972): Engineering Analysis of the Rotofermentor Dev. Ind. Microbiol. 13: 159-176

Margaritis, A., and C. R. Wilke (1978): The Rotofermentor. I. Description of the Apparatus, Power Requirements, and Mass Transfer Characteristics Biotech. Bioeng. 20: 709-726

Matsumoto, K., S. Katsuyama, and H. Ohya (1987): Separation of Yeast by Cross-flow Filtration with Backwashing J. Ferment. Technol. 65(1): 77-83

McGregor, W. C., ed. (1986): Membrane Separations in Biotechnology, Marcel Dekker, Inc., New York

Michaels, A. S. (1968): New Separation Technique for the CPI Chem. Eng. Prog. 64(12): 31-43

Michaels, A. S. (1980): Membrane Technology and Biotechnology Desalination 35: 329-351

Michaels, A. S. and S. L. Matson (1985): Membranes in Biotechnology: State of the Art Desalination 53: 231-258

Morrow, A. W. (1972): Concentration of the Virus of Foot-and-Mouth Disease in a Tangential Flow Ultrafiltration Unit J. Appl. Chem. Biotech. 22:501-505

Mulder, M. H. V., and C. A. Smolders (1986): Continuous Ethanol Production Controlled by Membrane Processes Process Biochem. 21(2): 35-39

Nishizawa, Y., Y. Mitani, K. Fukunishi, and S. Nagai (1984): Ethanol Production by Repeated Batch Culture with Hollow Fibers J. Ferment. Technol. 62(1): 41-47

Nishizawa, Y., Y. Mitani, M. Tamai, and S. Nagai (1983): Ethanol Production by Cell Recycling with Hollow Fibers J. Ferment. Technol. 61(6): 599-605

O'Sullivan, T. J., A. C. Epstein, S. R. Korchin, and N. C. Beaton (1984): Applications of Ultrafiltration in Biotechnology Chem. Eng. Prog. Jan: 68-75

Ohleyer, E., H. W. Blanch, and C. R. Wilke (1985): Continuous Production of Lactic Acid in a Cell Recycle Reactor Appl. Biochem. Biotech. 11: 317-332

Olsen, O. J. (1987): Membrane Filtration as a Tool in Biotechnical Down-stream Processing Desalination 62: 329-339

Pierrot, P., M. Fick, and J. M. Engasser (1986): Continuou cetone-Butanol Fermentation with High Productivity by Cell Ultrafiltration and k ycling Biotech. Letters 8(4): 253-256

Pirt, S. J., and W. M. Kurowski (1970): An Extension of the Theory of the Chemostat with Feedback of Organisms. Its Experimental Realization with a Yeast Culture J. Gen. Microbiol. 63: 357-366

Quinn, R. M. (1983): Ultrafiltration Membrane Processes - The Sleeping Giant Desalination 46: 113-123

Quirk, A. V., and J. R. Woodrow (1983): Tangential Flow Filtration - A New Method for the Separation of Bacterial Enzymes from Cell Debris Biotech. Letters 5(4): 277-282

Radlett, P. J. (1972): The Concentration of Mammalian Cells in a Tangential Flow Filtration Unit J. Appl. Chem. Biotech. 22: 494-499

Reed, W. M., and M. E. Bogdan (1986): Application of Cell Recycle to Continuous Fermentative Acetic Acid Production Biotech. Bioeng. Symp. 15: 641-647

Reid, D. E., and C. Adlam (1974): Large-scale Harvesting and Concentration of Bacteria by Tangential Flow Filtration J. Appl. Bacteriol. 41: 321-324

Rhim, J. S., L. B. Williams, Jr., R. J. Huebner, and H. C. Turner (1969): Concentration by Diaflo Ultrafiltration of Murine Leukemia and Sarcoma Viruses Grown in Tissue Culture Cancer Res. 29: 154-156

Ricketts, R. T., W. W. Lebherz III, F. Klein, M. E. Gustafson, and M. C. Flickinger (1985): Application, Sterilization, and Decontamination of Ultrafiltration Systems for Large-Scale Production of Biologicals ACS Symposium Series 217: 21-49

Riesmeier, B., K. H. Kroner, and M.-R. Kula (1986): Studies on Secondary Layer Formation and its Characterization during Cross-flow Filtration of Microbial Cells; Poster presented at 5th Intern. Symposium on Synth. Membr. in Sci. and Industry Sept. 1986, Tubingen, F. R. G.

Schneider, K., and W. Klein (1982): The Concentration of Suspensions by Means of Cross-flow Microfiltration Desalination 41:263-275

Schutte, H., K. H. Kroner, W. Hummel, and M.-R. Kula (1983): Recent Developments in Separation and Purification of Biomolecules Annals New York Acad. Sci. 413: 270-282

Sekla, L., W. Stackiw, C. Kay, and L. VanBuckenhout (1980): Enteric Viruses in Renovated Water in Manitoba Can. J. Microbiol. 26: 518-523

Shibley, G. P., M. Manousos, K. Munch, I. Zelljadt, L. Fisher, S. Mayyasi, K. Harewood, et al. (1980): New Method for Large-Scale Growth and Concentration of the Epstein-Barr Viruses Appl. & Environ. Microbiol. 4(6): 1044-1048

Shiloach, J., J. B. Kaufman, and R. M. Kelly (1986): Hollow Fiber Microfiltration Methods for Recovery of Rat Basophilic Leukemia Cells (RBL-2H3) from Tissue Culture Media Biotech. Prog. 2(4): 230-233

Short, J. L. (1983): Industrial Applications of Hollow Fibre Ultrafiltration The Chemical Engineer Aug/Sept: 47-51

Short, J. L., and D. W. Webster (1982): Ultrafiltration, a Valuable Processing Technique for the Pharmaceutical Industry Process Biochem. Mar/Apr: 29-32

Strathmann, H. (1985): Membranes and Membrane Processes in Biotechnology Trends in Biotechnology 3(5): 112-118

Tamura, T.-A., and T. Takano (1978): A New, Rapid Procedure for the Concentration of C-type Viruses from Large Quantities of Culture Media: Ultrafiltration by Diaflo Membrane and Purification by Ficoll Gradient Centrifugation J. Gen. Virol. 41: 135-141

Taniguchi, M., N. Kotani, and T. Kobayashi (1987): High- Concentration Cultivation of Lactic Acid Bacteria in Fermentor with Cross-Flow Filtration J. Ferment. Technol. 65(2): 179-184

Tanny, G. B., D. Hauk, and U. Merin (1982): Biotechnical Applications of a Pleated Crossflow Microfiltration Module Desalination 41: 299-312

Tanny, G. B., D. Mirelman, and T. Pistole (1980): Improved Filtration Technique for Concentrating and Harvesting Bacteria Appl. Envir. Microbiol. 40(2): 269-273

Thompson, J. S., and M. Humphries (1986): Bacterial Cell Wall Isolation by Filtration Enzyme Microb. Technol. 8: 93-96

Trudel, M., and P. Payment (1980): Concentration and Purification of Rubella Virus Hemagglutinin by Hollow Fiber Ultrafiltration and Sucrose Density Centrifugation Can. J. Microbiol. 26: 1334-1339

Tutunjian, R. S. (1983): Ultrafiltration Processes in Biotechnology Annals New York Acad. Sci. 413: 238-253

Tutunjian, R. S. (1985): Cell Separations with Hollow Fiber Membranes, in Comprehensive Biotechnology Vol 2, C. L. Cooney and A. E. Humphrey, eds., Pergamon Press, New York

Vaheri, A., C.-H. von Bonsdorff, T. Vesikari, T. Hovi, and P Vaananen (1969): Purification of Rubella Virus Particles J. Gen. Virol. 5: 39-46

Valeri, A., G. Gazzei and G. Genna (1979): Tangential Flow Filtration of Bordetella Pertussis Submerse Cultures Experientia 35: 1535-1536

Valeri, A., G. Gazzei, M. Morandi, B. Pende, and P. Neri (1977): Large-Scale Purification of Inactivated Influenza Vaccine Using Membrane Molecular Filtration Experientia 33: 1402-1403

Wang, D. I. C., T. Sonoyama, and R. I. Mateles (1968): Enzyme and Bacteriophage Concentration by Membrane Filtration Anal. Biochem. 26: 277-287

Wang, D. I. C., and A. J. Sinskey (1970): Collection of Microbial Cells ***Missing title of book*** 121-152

Watson, D. C., and D. R. Berry (1979): Use of an Exchange Filtration Technique to Obtain Synchronous Sporulation in an Extended Batch Fermentation Biotech. Bioeng. 21: 213-220

Weiss, S. A. (1980): Concentration of Baboon Endogenous Virus in Large-Scale Production by Use of Hollow-Fiber Ultrafiltration Technology Biotech. Bioeng. 22: 19-31

Zahka, J., and T. J. Leahy (1985): Practical Aspects of Tangential Flow Filtration in Cell Separations ACS Symposium Series 217: 51-69

Zydney, A. L., Cross-Flow Membrane Plasmapheresis: An Analysis of Flux and Hemolysis, Ph. D. Thesis, Massachusetts Institute of Technology (1985)

This page intentionally left blank.

CHAPTER 2

Short-term Filtration and Freeze-Substitution of Red Cell Suspensions

Introduction

The paper which follows discusses the first set of freeze-substitution experiments which were performed with suspensions of red blood cells in albumin. These were all short-term experiments, in which the fibers were frozen two to five minutes after filtration was initiated. The filtration devices used in these experiments were hand-potted five-fiber assemblies. Subsequent to the publication of this paper, single-fiber devices were developed and used in blood- and yeast-freezing experiments. In these experiments, the blood was pumped with a peristaltic pump. In subsequent single-fiber experiments, a syringe pump was employed.

Chapter 3 contains the results of later long-term experiments with blood. Chapter 5 contains the results of yeast filtration/freezing experiments.

Reprinted from ASAIO, July-September 1987
Vol. 10, No. 3

Visual Evidence of Concentration Polarization in Cross-flow Membrane Plasmapheresis

NORMA J. OFSTHUN AND CLARK K. COLTON

Membrane plasmapheresis is an alternative to centrifugation for the separation of plasma from the cellular components of blood. Commercially available clinical microporous membrane filters provide good cell retention and allow nearly complete passage of all plasma proteins.[1] The cross-flow configuration, in which blood flows parallel to the membrane, minimizes accumulation of cells at the membrane surface and results in larger filtration rates than can be obtained in a batch system.[2] Cross-flow also reduces hemolysis. The goal in design of such filters is to maximize flux while minimizing hemolysis.

The initial feasibility studies of membrane plasmapheresis[2] investigated filtrate flux in cross-flow microfiltration devices. Flux increased with transmembrane pressure drop (ΔP_{TM}), reaching a maximum, pressure independent value which increased with increasing wall shear rate (γ_w) and decreasing bulk cell concentration (C_b). The flux was much lower than that for filtering pure plasma under identical conditions.

The various models proposed to explain this kind of behavior and to provide a means for filtrate flux prediction have been reviewed elsewhere.[3] One approach is based on the notion that lift forces, which drive cells away from the surface, play a role in determining the flux.[4-13] A second assumes that layers of densely packed cells form at the membrane surface and are convected through the device with the flowing blood.[14,15] A third is based on the concept of concentration polarization of cells, in which it is assumed that the flux is governed by the balance between convection of cells toward the membrane surface and diffusion of cells away from the surface throughout the cell concentration boundary layer. When the red cell Brownian motion diffusivity is used in this model, the predicted maximum filtrate flux and its wall shear rate dependence are substantially less than are observed experimentally.[4,5,16] In 1982, Zydney and Colton[17] showed that if an experimentally determined shear-enhanced particle diffusion coefficient[18] is incorporated into a simple one-dimensional concentration polarization model, predictions of the model agree with plasmapheresis filtrate flux data within a factor of two over a wide range of operating conditions. The shear-enhanced diffusivity of the cells arises from mutually induced velocity fields in the shear flow of a concentrated suspension.[19] Others[20-24] have also proposed that shear-enhanced diffusion plays a role in the context of cell polarization.

Recently, numerical solutions have been developed using a detailed model for filtrate flux by directly solving the coupled partial differential equations describing conservation of mass and conservation of momentum in flowing blood undergoing filtration.[25,26] The resulting filtrate flux predictions were in excellent agreement with experimental data for a wide range of operating conditions in both the pressure-dependent and pressure-independent regimens. The results of this analysis indicate the formation of two boundary layers which each grow in thickness with increasing distance from the inlet. The concentration polarization boundary layer, in which the concentration drops from its maximum value at the wall to its bulk value, is tens of microns thick within a few centimeters of the inlet. Within this concentration boundary layer, the balance between diffusive and convective transport determines the filtrate flux. Buried within the concentration boundary layer is a very thin pressure boundary layer (a few microns thick) comprised of the very high concentration of cells near the membrane surface, across which the hydrostatic pressure decreases from its bulk value to the value at the membrane surface.[14,27] These results[25,26] further suggest that the transport of erythrocytes away from the membrane surface ultimately determines the filtration rate in cross-flow microfiltration, and that the details of the hydrostatic pressure reduction mechanism are not rate-determining because the properties of the pressure boundary layer adjust to provide the requisite hydraulic resistance to accommodate the imposed filtrate flux.

Despite good agreement between theoretical prediction and experimental data, the question of whether cell concentration polarization actually occurs is unresolved[28] and provides motivation for this study. The goal of the research reported here is to develop an experimental technique which would permit visualization of erythrocytes in the boundary layer near plasmapheresis membranes, to use that technique to determine whether concentration polarization occurs, and to determine any variation of concentration polarization with operating parameters. The technique we chose, freeze-substitution microscopy, was based upon experiments[29] in which this technique was used to measure

From the Department of Chemical Engineering, Massachusetts Institute of Technology, Cambridge, Massachusetts.
Supported in part by NSF grant CDR-850003.
Reprint requests: Clark K. Colton, Department of Chemical Engineering, Room 66-452, Massachusetts Institute of Technology, Cambridge MA 02139.

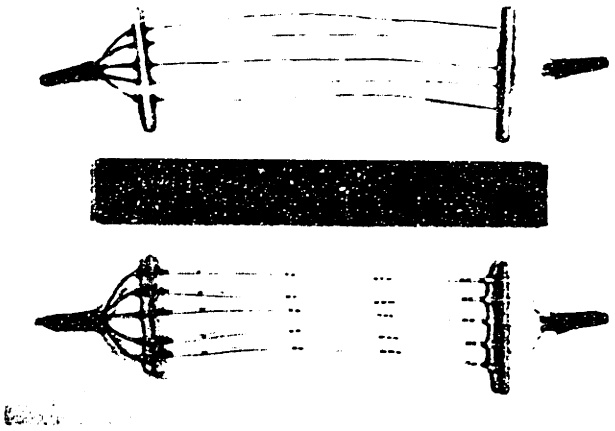

Figure 1. Free-fiber filtration device.

the distribution of leukocytes in blood flowing through 1 mm diameter rabbit arteries. The geometry of hollow fiber membranes, with diameters smaller than the rabbit arteries, renders them ideal for the fast-freezing technique necessary for preservation of cell concentration profiles during cross-flow filtration.

Materials and Methods

Filtrate flux measurements were first carried out with hollow fiber cartridges to define the relationship between flux and mean transmembrane pressure difference. The cartridges were graciously provided by Enka AG. Each cartridge contained 38 polyamide (nylon-6) fibers with an active length of 13 cm and a total area of 50 cm^2. According to the specifications of the manufacturer, the fibers had an internal diameter of 320 μm, a wall thickness of 100 μm, a maximum pore diameter of 0.35 μm, and a hydraulic resistance to water at 20°C of 1.2×10^{-9} cm^{-1}. The fibers were encased in an acrylic housing with two ports for filtrate collection.

Suspensions of 5 and 42% (by volume) of erythrocytes were obtained by diluting freshly drawn citrate phosphate dextrose anticoagulated blood with 6% (wtt vol) bovine serum albumin solution. Diluted blood was pumped in single pass from an inlet reservoir, through the cartridge, and into an outlet reservoir. Blood in the inlet reservoir was maintained at room temperature and kept in suspension by continuous stirring. The erythrocyte suspension was pumped through the cartridge using a peristaltic pump at flow rates corresponding to equivalent Poiseuille wall shear rates of 500 and 1000 s^{-1}. Inlet blood flow rates were measured before filtration by weighing timed collections of the outlet blood with the filtrate ports closed. Filtrate flow rates were determined by timed collection of fluid from a single open filtrate port. During filtration, the bulk inlet flow rate was verified by summing the filtrate and outlet flow rates. The outlet transmembrane pressure was varied from 0 to 275 mmHg by raising the height of the outlet reservoir. The pressure at the cartridge inlet and outlet was measured using a pressure transducer.

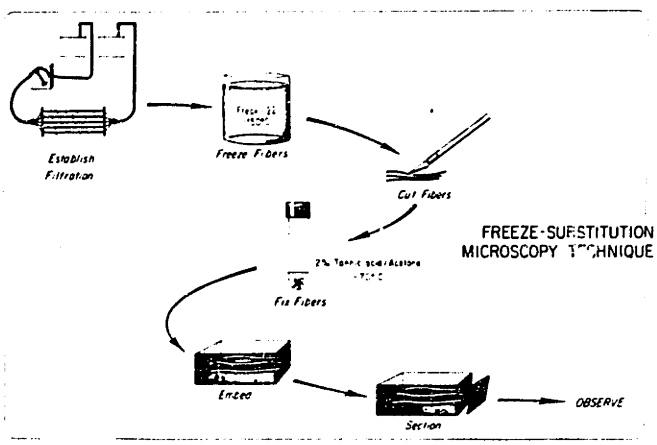

Figure 2. Freeze substitution technique.

The same Enka polyamide fibers were used in the freeze-substitution experiments. The fibers were arranged in a specially constructed free-fiber device. Five fibers were potted at each end and attached to wooden support bars near the ends to hold them apart and parallel so as to obtain the maximum heat transfer rate during subsequent freezing (**Figure 1**). The active length of the assembled device was approximately 10 cm. The inactive portions were coated with sealing compound to make them impermeable. The fibers were marked to keep track of axial position and fiber identity. The free-fiber devices were tested with doubly filtered distilled water to ensure that fibers were not blocked or broken during the assembly procedure.

The freeze-substitution procedure is summarized in **Figure 2**. Before freezing, steady-state filtration was established by the procedure described above. For the freezing experiments, the wall shear rate was varied from 50 to 500 s^{-1}, and the inlet transmembrane pressure was varied from 0 to 300 mmHg. Without interrupting filtration, the fibers were rapidly submerged into a trough of Freon-22 which had been cooled to its freezing point of −150°C with liquid nitrogen. The fibers, their potted ends, and a portion of the attached inlet and oulet tubing froze instantaneously. The pump was turned off after the fibers were frozen and the fibers were cut into 1 cm pieces while still in the Freon bath. The frozen fiber pieces were quickly transferred to vials containing a freeze-substitution solution of 2% tannic acid in acetone, which had been precooled to −95°C, the freezing point of acetone, and the vials were stored at −70°C for 1 week. During that time, acetone replaced the ice in the samples, and the tannic acid fixed both the cells and the protein solution surrounding them. The freeze-substitution vials were gradually brought to room temperature (overnight at −15°C, 2 hours at 5°C, then 1 hour at 20°C). The fibers were then rinsed in acetone and infiltrated overnight by a mixture of 50:50 Epon-812 epoxy resin (Ladd Industries, Burlington, VT) and acetone. The following day, the fibers were embedded in Epon and then cured at 60°C for 36 hours. Using a microtome, the hardened blocks were cut into sections of 1 or 5 μm thickness perpendicular to the fiber axis (flow direction). Sections were cut at different distances along the fiber length (x), usually near the inlet (x = 1 cm) or the outlet (x = 10 cm). One fiber was sectioned

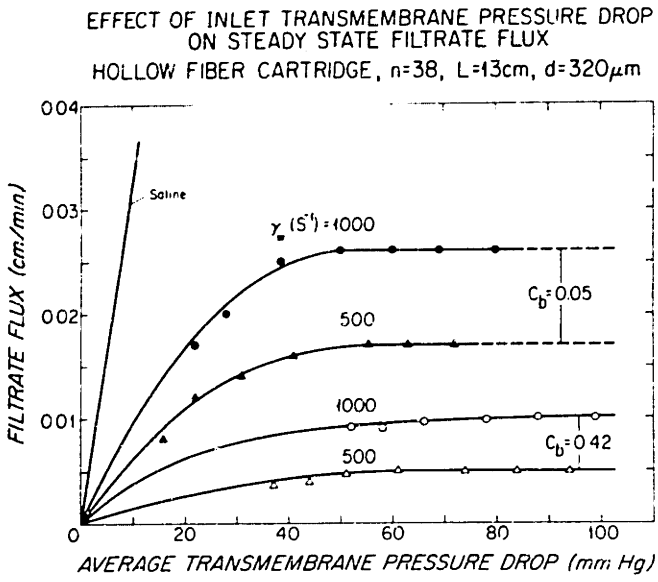

Figure 3. Effect of average transmembrane pressure drop on steady state filtrate flux.

parallel to the fiber axis. One micron sections were stained with methylene blue before coverslips were mounted. Specimens were viewed under phase contrast microscopy (Model ICM 405; Carl Zeiss, Inc., Thornwood, NY) for photography and under brightfield for image analysis.

In two experiments, the hollow fibers were rinsed after blood filtration. After filtration for 10 minutes at a shear rate of 50 s^{-1}, the inlet blood reservoir was replaced with a reservoir containing 6% albumin solution. The protein solution was pumped through the fibers at shear rates of either 50 or 500 s^{-1} for 5 minutes before freezing as usual. Protein solution was used rather than saline so that any cells in the lumen of the fibers would be fixed in place as in the blood experiments.

An Image Technology Corporation (Deer Park, NY) Model 3000 digital image analysis system was used to quantify erythrocyte concentration profiles. A 512 × 512 binary image was created from the incoming video image by adjustment of a grey-scale threshold level. The area fraction occupied by cells as a function of distance from the membrane was measured by counting pixels in the binary image.

Results

Filtrate Flux Measurement

Filtrate flux measured as a function of mean transmembrane pressure difference with the hollow fiber cartridge is plotted in **Figure 3**. In each experiment, the smallest average transmembrane pressure at which data are reported corresponds to the case in which the outlet pressure was zero (ambient) and the inlet pressure was that which arose from the axial pressure drop in the fibers. The pressure independent flux in each experiment was achieved with average transmembrane pressures of about 50 mmHg. This maximum, pressure independent flux occurs only when the local transmembrane pressure difference along the entire lengtn

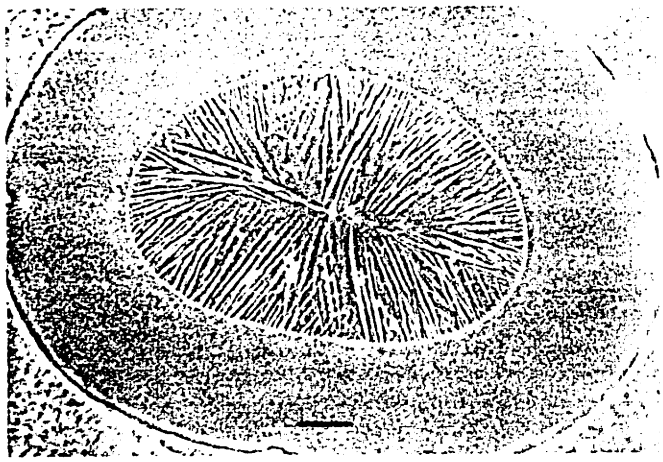

Figure 4. Fiber in which 6% albumin solution was freeze substituted (bar = 50 μm).

of each fiber was above the minimum threshold value required to reach the maximum flux. The trends reported previously[2] were also observed in our experiments, (*i.e.*, the asymptotic flux increased with increasing shear rate and with decreasing cell concentration).

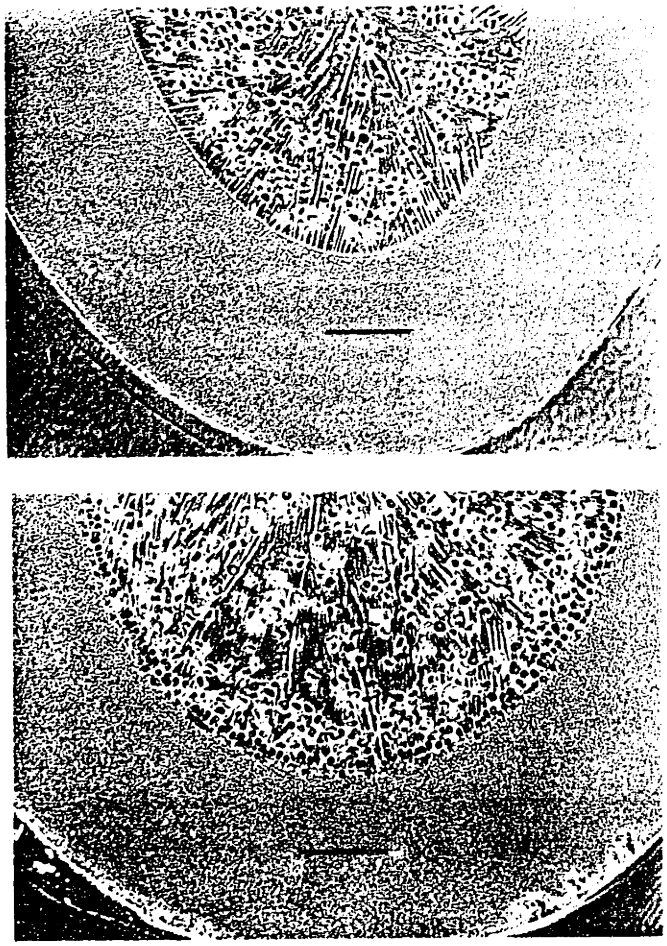

Figure 5. Sections (5 μm) from the same fiber in which diluted blood was flowing (γ_w = 500 s^{-1}, bar = 50 μm). Top, outlet, x = 10 cm, outlet ΔP_{TM} = 0. Bottom, inlet, x = 1 cm, inlet ΔP_{TM} = 25 mmHg.

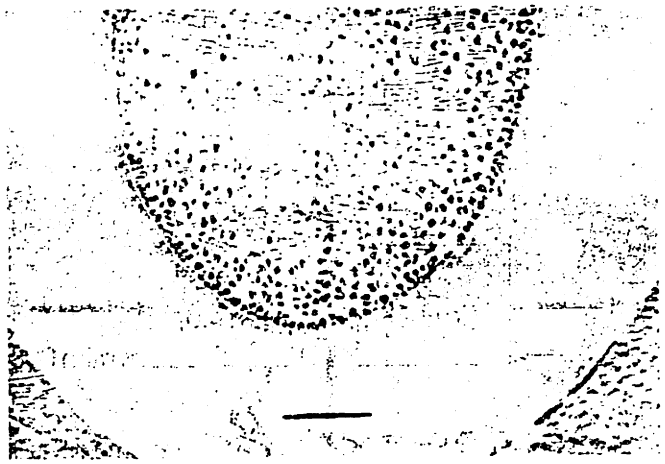

Figure 6. Section (5 μm) from the outlet of a fiber: x = 10, γ_w = 500 s^{-1}, inlet ΔP_{TM} = 100 mmHg, outlet ΔP_{TM} = 75 mmHg (bar = 50 μm).

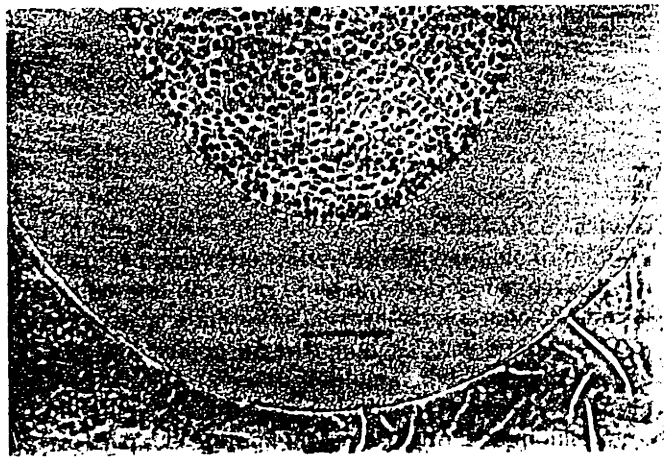

Figure 8. Section (5 μm) from the same fiber as in **Figure 7** taken at the inlet (x = 1 cm, bar = 50 μm).

Freeze Substitution Microscopy

The photomicrograph in **Figure 4** shows a cross section of a fiber in which protein solution alone was freeze substituted. As in many instances, the fiber cross-section was not circular. Freezing proceeded inward, generating nonuniformities in protein concentration which produced the radial streak patterns. When fluorescein isothiocyanate labeled albumin was used, the dark streaks fluoresced most strongly, indicating local protein accumulation.

Figure 5 shows diluted blood flowing in a fiber where the local transmembrane pressure difference was 0 at the outlet and 25 mmHg near the inlet. At the outlet the filtration flux is zero, and no concentration polarization is visible (**Figure 5 top**). This is not surprising because there is no filtrate flux to bring about such polarization. Instead, a cell-free zone occurs around the periphery of the lumen, as had been reported previously for flow of blood in impermeable tubes.[30,31] This cell-free zone arises as a result of lift forces acting on the cells near the membrane.[32] Near the inlet of the same fiber (**Figure 5 bottom**), where the local applied pressure is 25 mmHg (and filtration possibly occurred in the pressure-dependent regimen), the cell concentration is greater near the membrane than in the bulk, and a densely packed layer exists adjacent to the membrane surface. This phenomenon of concentration polarization became more pronounced in later experiments in which higher transmembrane pressure differences led to higher filtration rates.

Figure 6 is a section from the outlet of a fiber in which the outlet transmembrane pressure difference was raised to 75 mmHg, whereas the shear rate was again 500 s^{-1}. The distribution of cells is very different from that shown in **Figure 5A** because the filtrate flux is substantially greater than zero. Instead of a cell-free region at the wall, there is a concentrated region of cells, consisting of one or two tightly packed layers against the wall. Beyond this region, the concentration drops off to its bulk value within roughly 30 to 50 μm of the wall.

Reducing the shear rate to 50 s^{-1}, with the outlet transmembrane pressure drop again at 75 mmHg, results in the more pronounced concentration polarization shown in **Fig-**

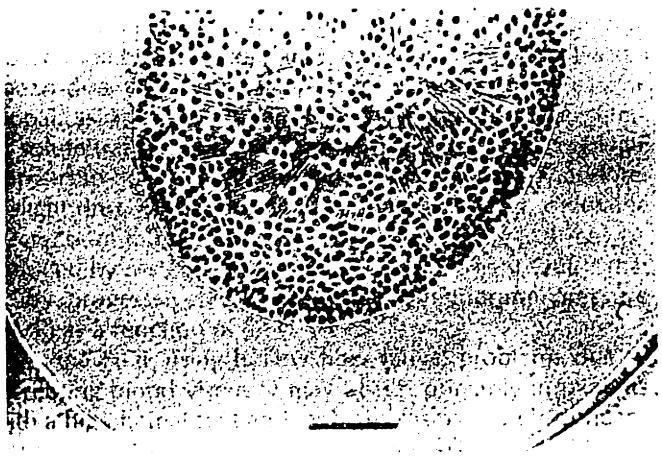

Figure 7. Same conditions as **Figure 6**, except γ_w = 50 s^{-1}, inlet ΔP_{TM} = 77.5 mmHg (bar = 50 μm).

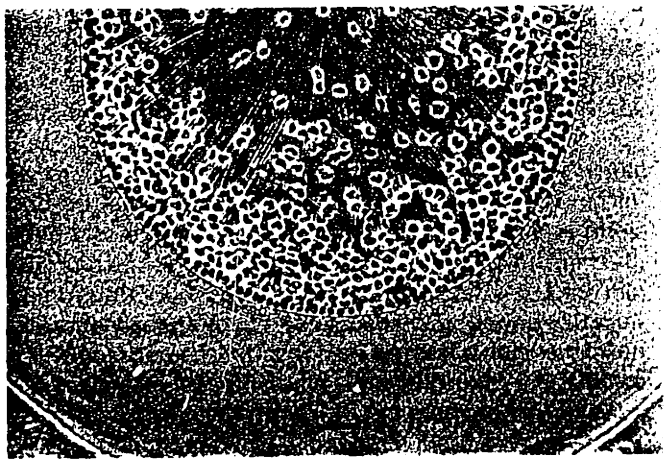

Figure 9. Section (5 μm) from the fiber outlet with same operating conditions as in **Figure 6**, except inlet ΔP_{TM} = 300 mmHg, outlet ΔP_{TM} = 275 (bar = 50 μm).

ure 7. In this section taken from the fiber outlet, there are more layers of cells tightly packed against the membrane at a higher concentration than in **Figure 6**. However, the boundary layer thickness is about the same, with the concentrated region extending roughly 30 to 50 μm into the bulk.

A section from the inlet of the same fiber is shown in **Figure 8**. There is less polarization at the inlet than at the outlet, as indicated by the smaller number of layers of tightly packed cells and the smaller polarization boundary layer. These and intermediate sections between the inlet and outlet (not shown) demonstrate that the thickness of the boundary layer increases with axial distance from the inlet.

Figure 9 shows the effect of increasing the outlet transmembrane pressure difference to 275 mmHg, with all other parameters kept the same as in **Figure 6**. No discernible change in the boundary layer is observed.

Digital image analysis was used to quantitate the average cell concentration as a function of distance from the membrane in the section shown in **Figure 6**. The results of this analysis (**Figure 10**) showed a cell concentration profile that decreased with distance from the membrane surface over a boundary layer nearly 40 μm thick.

Figure 11 shows the section in **Figure 7** under progressively higher magnification. These photomicrographs indicate that the erythrocytes are packed very tightly in the first few cell layers near most of the membrane surface. Using the digital image analysis system, area fractions of up to 97% were measured in some of the small, tightly packed regions. Randomly interspersed between these tightly packed regions were gaps or open spaces in the cell layer next to the wall. Serial 5 μm sections disclosed that these open spaces do not appear in the same position at the membrane in adjacent sections. Small, faint images were often observable within these spaces which may represent a small portion of an erythrocyte or a platelet at the membrane surface.

Figure 12 gives a high magnification view of sections from the inlet region of a fiber in an experiment run under low polarization conditions. **Figure 12, top**, is a standard cross-sectional view, whereas **Figure 12, bottom**, shows a section cut parallel to the fiber axis. In both cases, the cells at the membrane appear round, indicating that the cells have a spheroidal shape rather than their normal biconcave disc shape.

Most of the cells shown near the membrane surface in **Figure 11** are also spheroidal or have a similar, expanded shape. Some of these cells are deformed into the membrane surface pores. Other cells have migrated intact through these pores into the membrane wall. These observations suggest that most, if not all of the cells at the membrane surface have deformed into the membrane pores and that this deformation causes the lumenal portion of the cells to become spheroidal. Similar shape changes have been observed in micropipette experiments.[33]

The rinsing experiments were carried out to determine if the cells at the membrane surface were permanently lodged in the pores. The results are shown in **Figure 13**. When rinsed for 5 minutes at the same shear rate at which filtration was run, the cells at the membrane surface remained in

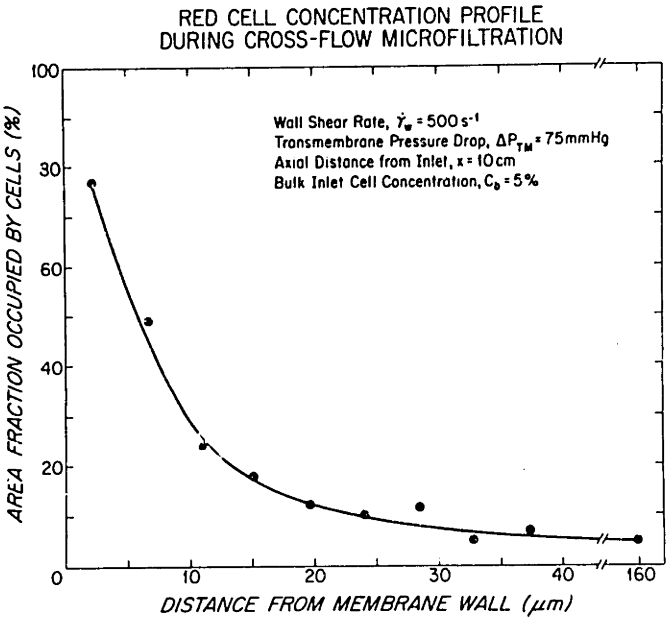

Figure 10. Erythrocyte concentration profile during cross-flow microfiltration. Area fraction occupied by cells was determined by digital image analysis of the section shown in **Figure 6** using a measurement field which was 4 μm wide in the radial direction.

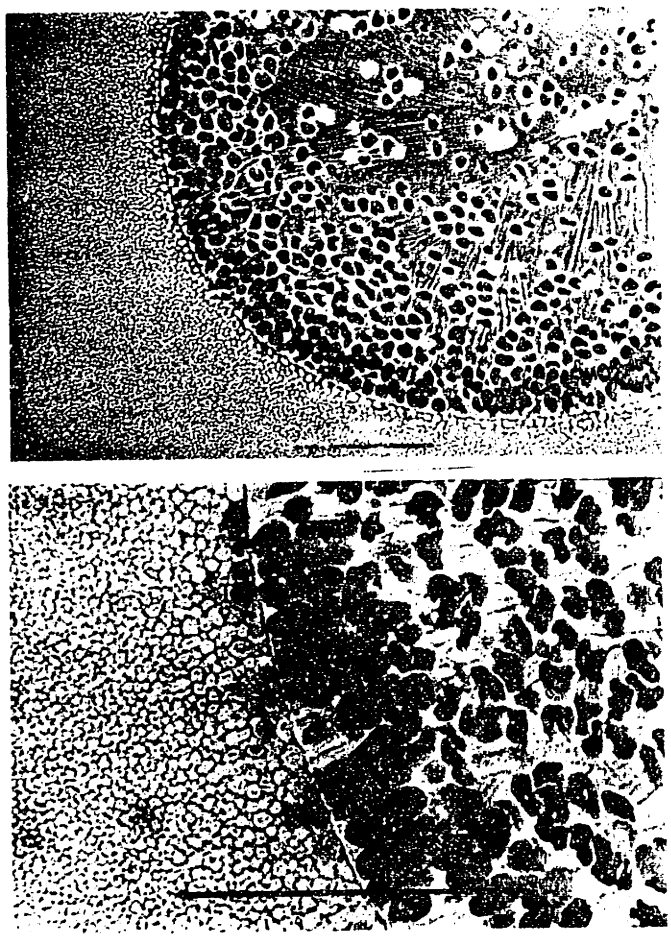

Figure 11. Higher magnification views of section shown in **Figure 7** (bar = 50μm).

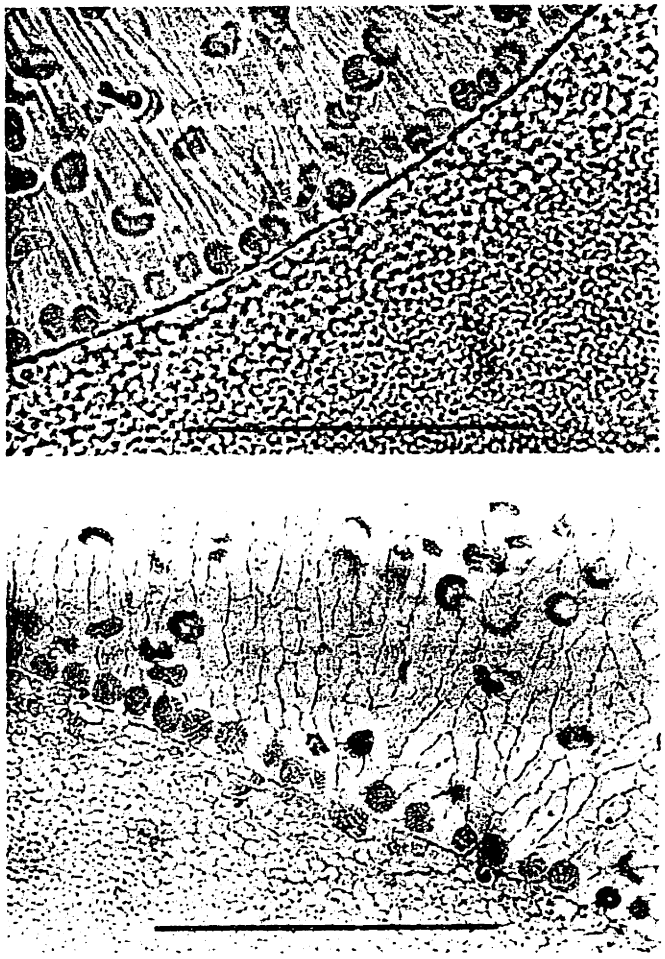

Figure 12. Sections (5 μm) from the inlet of a fiber in a low polarization experiment (x = 1 cm, γ_w = 500 s^{-1}, inlet ΔP_{TM} = 100 mmHg, outlet ΔP_{TM} = 75 mmHg, bar = 50 μm). Top, cut perpendicular to fiber axis (cross-sectional view). Bottom, cut parallel to fiber axis.

place. However, when rinsed at a shear rate ten times higher, the cells were washed away from the membrane surface.

Discussion

To visualize erythrocytes near the membrane surface in cross-flow microfiltration, we freeze substituted hollow fiber membranes in which diluted blood was filtered under a variety of operating conditions. We examined the freeze substituted fibers using light microscopy, and we used a digital image analysis system to quantify the concentration profiles. Our goal was to determine whether concentration polarization occurred and to examine variations in the extent of polarization with operating conditions.

The filtrate flux measurements with hollow fiber cartridges confirmed that the membranes used in this study displayed the asymptotic behavior which had been reported previously for cross-flow filtration devices. The freeze substititution experiments demonstrated that erythrocyte concentration polarization occurs in cross-flow membrane plasmapheresis, provided that sufficient filtration is occurring. Without filtration, a cell-free zone forms near the membrane surface. Freeze substitution experiments also showed that cells deform into membrane pores, causing the lumenal portion of the cells to become spheroidal, and that those cells resist mild rinsing but are washed away by rinsing at a higher wall shear rate.

Zydney and Colton proposed that hemolysis occurs by rupture of the erythrocyte membrane after deformation of cells into membrane pores.[17,34] The occurrence of such deformation has been verified in batch filtration experiments with flat plate membranes[33] but not previously in cross-flow filters. The observed deformation of cells into the hollow fiber membrane pores in this study lends support to the deformation mechanism of hemolysis. Furthermore, the demonstration that the effectiveness of cross-flow rinsing at removing the cells which have deformed into membrane pores depends on the wall shear rate supports the hypothesis that this deformation process is reversible and that the residence time in a pore, and hence the probability of lysis, decreases as the shear rate is increased.

Our results differ from previous attempts to determine whether concentration polarization occurs. Lewandowski *et*

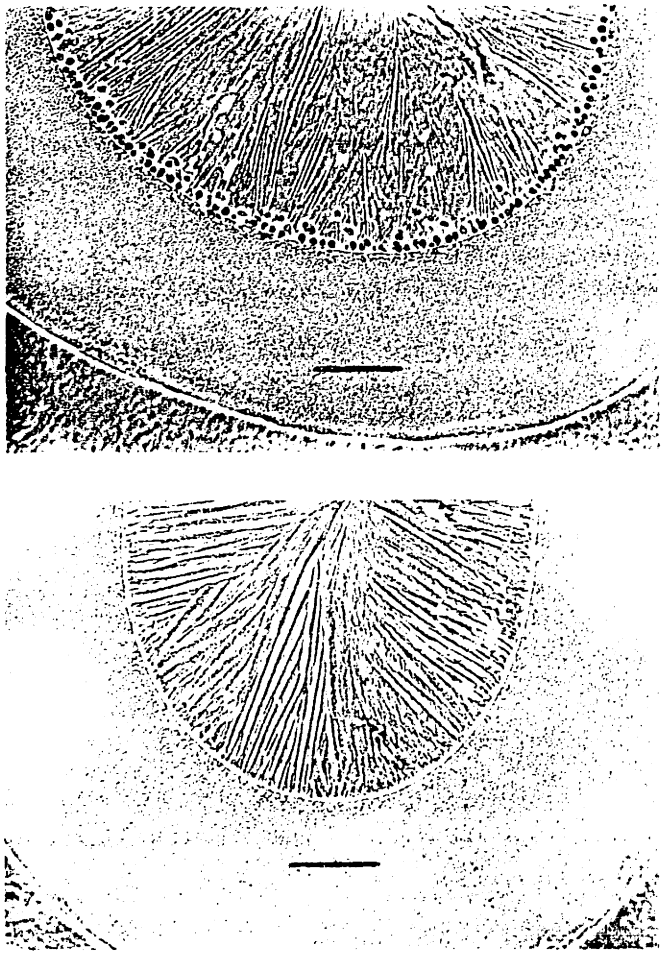

Figure 13. Sections (5 μm) from two different fibers after 10 minutes filtration at γ_w = 50 s^{-1}, outlet ΔP_{TM} = 75 mmHg, and 5 minute rinsing at: top, γ_w = 50 s^{-1}, outlet ΔP_{TM} = 75 mmHg. Bottom, γ_w = 500 s^{-1}, outlet ΔP_{TM} = 75 mmHg (bar = 50 μm).

al.[28] were unable to visualize cell polarization with any of three techniques. Their first technique, freezing hollow fibers with spray-on Freon, failed to provide any conclusive results because of hemolysis. Cell lysis may have occurred because the freezing rate was too slow or because thawing occurred during the sectioning procedure. Their second technique, glutaraldehyde fixation, showed only a monolayer of cells adherent to the membrane surface. The remainder of the polarization layer was probably rinsed away before fixation. The third method, microscopic flow observation of dialysis hollow fiber membranes, also failed to demonstrate cell polarization. This may have resulted because the very small filtrate flux achievable with dialysis membranes was not large enough to cause cell polarization. They observed cell-free layers similar to those seen previously during flow in impermeable tubes. This agrees with our observation that a cell-free layer occurs even in microfiltration fibers when the flux is zero because of the absence of a transmembrane pressure difference.

References

1. Gurland HJ, Lysaght MJ, Samtleben W, Schmidt B: Comparative evaluation of filters used in membrane plasmapheresis. *Nephron* 36: 173-182, 1984.
2. Solomon BA, Castino P, Lysaght MJ, Colton CK, Friedman LI: Continuous flow membrane filtration of plasma from whole blood. *TASAIO* 24: 21-26, 1978.
3. Zydney AZ, Colton CK: A concentration polarization model for the filtrate flux in cross-flow microfiltration of particulate suspensions. *Chem Eng Commun* 47: 1-21, 1986.
4. Henry JD Jr: Cross flow filtration, in Li NN (ed), *Recent Developments in Separation Science*, Vol II. Ohio, Chemical Rubber Company, 1972, pp. 220-225.
5. Porter MC: Concentration polarization with membrane ultrafiltration. *Ind Eng Chem Prod Res Develop* 11: 234-248, 1972.
6. Forstrom RJ, Bartlet K, Blackshear PL, Wood T: Formed elements deposition onto filtering walls. *TASAIO* 21: 602-607, 1975.
7. Madsen RF: *Hyperfiltration and Ultrafiltration in Plate and Frame Systems*, New York, Elsevier Scientific Publishing Co., 1977.
8. Asanuma Y, Smith JW, Suwa S, et al: Membrane plasmapheresis: platelet effects on filtration. *Proc Eur Soc Artif Organs* 6: 305-312, 1979.
9. Green G, Belfort G: Fouling of ultrafiltration membranes: lateral migration and the particle trajectory model. *Desalination* 35: 129-147, 1980.
10. Werynski A, Malchesky PS, Sueoka A, et al: Membrane plasma separation: toward improved clinical operation. *TASAIO* 27: 539-543, 1981.
11. Zawicki I, Malchesky PS, Smith JW, Harasaki H, Asanuma Y, Nose Y: Axial changes of blood and plasma flow, pressure, and cellular deposition in capillary plasma filters. *Artif Organs* 5: 241-247, 1981.
12. Altena FW, Belfort G: Lateral migration of spherical particles in porous flow channels: application to membrane filtration. *Chem Eng Sci* 39: 343-355, 1984.
13. Malchesky PS, Wokcicki J, Moorman M, Pentermann EJ, Lewandowski J, Nose Y: Blood cell effects in membrane plasma separation. *TASAIO* 30: 313-319, 1984.
14. Stepner TA, Vassilief CS, Leonard EF: Cell plasma interactions during membrane plasmapheresis. *Clin Hemorheol* 5: 15, 1985.
15. Vassilief CS, Leonard EF, Stepner TA: The mechanisms of cell rejection in membrane plasmapheresis. *Clin Hemorheol* 5: 7, 1985.
16. Blatt WF, Dravid A, Michaels AS, Nelson L: Solute polarization and cake formation in membrane ultrafiltration: causes, consequences, and control techniques, in Flinn JE, (ed), *Membrane Science and Technology*, New York, Plenum Press, 1970, pp. 47-97.
17. Zydney AL, Colton CK: Continuous flow membrane plasmapheresis: theoretical models for flux and hemolysis prediction. *TASAIO* 28: 408-411, 1982.
18. Eckstein EC, Bailey DG, Shapiro AH: Self-diffusion of particles in shear flow of a suspension. *J Fluid Mech* 79: 191-208, 1977.
19. Zydney AL, Colton CK: Augmented solute transport in the shear flow of a concentrated suspension. *J Col Interface Sci*, submitted, 1986.
20. Lysaght MJ, Schmidt M: Factors governing mass transport in filters for membrane plasmapheresis, in Nosé Y (ed), *Proc ISAO Symposium on Clinical Plasmapheresis*, New York, Raven Press, 1982, pp. 113-127.
21. Malbranq JM, Jaffrin MY, Bouveret E, Angleraud R, Vantgard G: Factors governing plasma filtration rate in membrane plasmapheresis by plane microporous membranes, *Proc 9th ESAO*, Brussels, Life Support Systems, 1982, p. 46.
22. Martin T, Jaffrin MY, Faure A: Interactions between platelets and red blood cells in plasma filtration. *TASAIO* 29: 735-738, 1983.
23. Malbranq JM, Jaffrin MY, Bouveret E, Angleraud R, Vantgard G: Plasmafiltration through a plane microporous membrane. *Am Soc Artif Intern Organs J* 7: 16-24, 1984.
24. Davis RH, Leighton DT: Shear-induced transport of a particle layer along a porous wall. *Chem Eng Sci* 42: 275-281, 1987.
25. Zydney AL: *Cross-flow Membrane Plasmapheresis: An Analysis of Flux and Hemolysis*. Ph.D. Thesis, Massachusetts Institute of Technology, Cambridge, MA, 1985.
26. Zydney AL, Colton CK: Fundamental studies and design analyses for cross-flow membrane plasmapheresis, in Andrade JD, (ed), *Artificial organs: the W. J. Kolff festschrift*, New York, BCH Publishers, 1987, in press.
27. Zydney AL, Saltzman WM, Colton CK: Hydraulic resistance of red cell beds in an unstirred filtration cell. *Chem Eng Sci* (in press).
28. Lewandowski JJ, Malchesky PS, Pentermann EJ, Breuer AC, Lynn M, Nose Y: Flow visualization of blood at the wall of a porous fiber. *TASAIO* 31: 419-423, 1985.
29. Phibbs RH: Distribution of leukocytes in blood flowing through arteries. *Am J Physiol* 210: 919-925, 1966.
30. Whitmore RL: Hemorheology and hemodynamics. *Biorheol* 1: 210-220, 1963.
31. Goldsmith HL, Marlow JC: Flow behavior of erythrocytes: II. Particle motions in concentrated suspensions of ghost cells. *J Coll Int Sci* 71: 383-407, 1979.
32. Ho BP, Leal LG: Inertial migration of rigid spheres in two dimensional unidirectional flow. *J Fluid Mech* 65: 365-400, 1974.
33. Dreher KL: *Induced Rigidity of Erythrocyte Membranes: A Mechanical and Chemical Assessment*. Ph.D. Thesis, University of Minnesota, Minneapolis, 1980.
34. Zydney AL, Colton CK: A red cell deformation model for hemolysis in cross flow membrane plasmapheresis. *Chem Eng Commun* 30: 191-207, 1984.

Discussion

DR. TURITTO: Was this done with whole blood or is this a suspension?

MS. OFSTHUN: We used diluted whole blood to which albumin had been added to bring up the albumin concentration to 6%; the albumin was added so that there would be enough protein around the cells to fix them in place.

DR. TURITTO: So you have platelets in this system?

MS. OFSTHUN: Yes.

DR. TURITTO: Do you also see the platelets?

MS. OFSTHUN: I haven't looked for the platelets, but they must be there.

DR. TURITTO: There are a lot of recent studies about exchanges between red cells and platelets and concentration profiles near the wall in nonfiltration type systems. I am just wondering if you saw any effects of this in yours where platelets might actually be plugging up holes, too?

MS. OFSTHUN: Yes, they might. We have seen spaces in the concentrated red cell layer at the membrane surface in which there are no red cells, only a small faint image which might be platelets. We haven't examined our sections specifically for platelets, but in the future we can stain sections to see them better.

DR. LYSAGHT: That's a good study. I have two questions.

Did you see any evidence of hemolysis at all when you were looking at the cells? Also, are your findings consistent with the picture that red cells are kind of rolling down the surface of the membrane and have a finite residence time over each pore which is the Colton-Zydney model for the onset of hemolysis?

MS. OFSTHUN: In answer to the first question, under the conditions I was using, there was not enough hemolysis to produce pink-colored filtrate. However, in high pressure experiments, the region of the fiber wall right near the lumenal surface was darker than the rest of the wall, possibly due to cells that had hemolyzed. No intact cells were visible in this region, but it was definitely darker than in any of the lower pressure experiments, so I think that some hemolysis may have been occurring. Future quantitation of hemolysis, by measuring the filtrate hemoglobin concentration, will help us answer your question better.

Could you please repeat the second question?

DR. LYSAGHT: The second part is, are your overall findings consistent with the concept from Zydney and Colton that red cells are kind of rolling down along the surface of a membrane and have a finite fixed residence time over each pore?

MS. OFSTHUN: We can't really tell whether those cells that were stuck at the membrane surface were rolling along or were stuck there permanently. The higher shear rate did wash them away, so it is possible that during filtration, if they were knocked out of pores by other cells, they could be moving along the surface.

DR. FISCHEL: You studied the rate at which the freezing occurred from the outside of the fiber toward the center and the relationship of that rate to the exchange in the flow dynamics. Could we be observing an artifact here?

MS. OFSTHUN: To test for possible artifacts, I conducted experiments in which the fibers were intentionally frozen more slowly, to magnify the effects of bad (i.e., too-slow) freezing.

When the freezing was done at a slower rate the freezing front produced a layer tens of microns thick next to the fiber wall in which there is no protein solution or cells. In addition, protein in the center of the fiber became granular. Since freezing is always from the outside in, any artifact would be a cell-free region near the wall, not a concentrated cell layer near the wall. Therefore, I don't believe that the cell concentration polarization which we have seen is an artifact of freezing. Rather, it is proof that the freezing was sufficiently fast to not produce a gross artifact.

DR. MALCHESKY: We haven't been able to get any decent results with freezing studies. We have carried out aldehyde fixation and then flow visualization studies, and we have never seen cells at the wall when the pressure gradient was less than 50 mmHg for devices which clinically operate in stable filtration at less than 50.

You showed results at 100 and 300 mmHg transmembrane pressure with cells on the wall. Such results have been reported before, and in the early days of clinical investigations on membrane systems people have reported such findings. Those pressures are not being used in the clinical area, and usually pressures less than 50, typically closer to less than 25 mmHg, are being applied. Could you restate what your results were at the lower transmembrane pressures?

MS. OFSTHUN: At the inlet of the fibers in which the only transmembrane pressure was due to the axial pressure drop in the fibers, the pressure was just 25 mmHg, yet there was a higher concentration near the wall than in the bulk, while at the wall there was a monolayer of tightly packed cells.

I agree that we should conduct more experiments at low pressure. However, an important distinction must be made when comparing the operating conditions in our experiments with those in clinical devices which are operated under demand mode, in which the filtrate flux is set by a pump. If the flux in a demand-mode device is too high, the pressure keeps going up, and the filtration is said to be unstable. Your group has shown that raising the flux only until the pressure is 25 mmHg ensures that demand-mode filtration remains stable. In our device, we set the pressure and allow the flux to adjust to that pressure. Even at 300 mmHg, the filtration is stable, reaching steady state in less than a minute.

DR. MALCHESKY: Okay. At the outlet of the filter did you have any deposition?

MS. OFSTHUN: No. At the outlet, where there was no applied pressure, there was a cell-free zone near the wall.

The participants of the discussion are identified as follows: Vincent Turitto, MD, Mt. Sinai Medical Center, New York, New York; Michael Lysaght, PhD, Travenol, Round Lake, Illinois; Halbert Fischel, PhD, Haemonetics Corporation, Los Angeles, California; and Paul S. Malchesky, DEng, Cleveland Clinic Foundation, Cleveland, Ohio.

This page intentionally left blank.

CHAPTER 3

Long-Term Filtration and Freeze-Substitution of Blood Cell Suspensions

ABSTRACT

This chapter describes the results of blood filtration experiments performed after the publication of Chapter 2. The purpose of the additional experiments was to study the time-dependence of both filtrate flux and cell concentration profiles. These experiments were performed by Mitsuru Suzuki, a visiting scientist from Toyobo Co., Ltd., working with the author.

Freeze-substitution experiments were conducted with polyamide (PA, 320 μm ID, 0.35 μm pore diameter), polypropylene (PP, 330 μm ID, 0.40 μm pore diameter), and modified polysulfone (PS, 950 μm ID, 0.75 μm pore diameter) hollow fibers. The PP and PA fibers were kindly supplied by Enka AG (Wuppertal, F.R.G.), while the modified polysulfone fibers were supplied by Sepracor, Inc. (Marlborough, MA). Unlike the experiments described in Chapter 2, the freeze-substitution experiments described here were performed with single hollow fibers fed by a syringe pump. Because acquisition of time-dependent flux data taken prior to freeze-substitution of the small PA and PP hollow fibers was limited by the slow rate of filtrate production, flux was also measured in manufacturer-supplied PA modules (38 fibers, with filtrate-side casing) and in homemade PP mini-modules (four fibers, no casing).

A gradual decline in filtrate flux occurred over the course of two-hour experiments. The flux decreased by a factor of two to three in all single-fiber experiments with red blood cells suspended in either saline or albumin solution. The same flux decline was observed in the PP mini-modules with no filtrate-side casing. However, with the PA modules with a filtrate-side casing, only a 10% decline in flux was observed during two-hour filtration of red cells suspended in either albumin solution or saline. This difference in behavior may be related to the presence of the filtrate-side casing which kept the outside of the fibers wet and reduced evaporation of filtrate.

Freeze-substitution experiments demonstrated that noticeable changes in the cell concentration profile near the membrane wall had occurred over a time scale of tens of minutes. After several minutes of filtration, the concentration polarization boundary layer in the FP fibers had disappeared except for the layer or two of cells closest to the wall. Based on the results of previous rinsing experiments (Chapter 2), those cells appear to be stuck in membrane pores. In many experiments a wide cell-free zone appeared next to the stuck cells, especially at the inlet end of the fibers. Similar results for the PA fibers were less dramatic and less conclusive because of problems with uneven distribution of cells in the bulk. No trends were evident in the results from the PS fibers because significant artifacts arose during the freeze-substitution of the large fibers.

Mr. Suzuki proposed that the cause of flux decline in the single-fiber experiments was rearrangement of the cells at the membrane surface into a more tightly packed configuration. He further proposed that since this rearrangement lowered the rate of convection toward the membrane below the rate of back-diffusion away from the membrane, mobile cells diffused out of the concentration boundary layer, leaving behind the cells stuck in membrane pores. He reasoned that the flux had become membrane-limited, with the membrane and those cells stuck to it acting as a composite membrane.

Additional experiments supported this hypothesis. In one experiment, the inlet reservoir was switched from a reservoir of red cells in albumin to a solution of albumin alone. Since the flux did not increase in the absence of cells, it appeared that the flux was membrane-limited. In other experiments, backflushing was shown to restore both initial fluxes and initial concentration polarization boundary layers. Furthermore, membrane-pretreatment experiments refuted the alternative explanation that the change in the boundary layer with time had been caused by a decrease in the permeability of the membrane itself.

Chapter 3: Long-Term Filtration and Freeze-Substitution of Blood Cell Suspensions

INTRODUCTION

Figure 3-1, reproduced from Zydney (1985), shows that the filtrate flux obtained when filtering a suspension of red cells in Eagles solution in a flat-plate microfilter appears to reach steady state in seconds. In that experiment the "steady-state" flux was about two orders of magnitude lower that the flux obtained when filtering pure Eagles solution under the same conditions. In other experiments, Zydney showed that this "steady-state" flux reached a pressure-independent maximum value at pressures lower than the conditions of the experiment shown here, and that the pressure-independent maximum depended on the parameters which influenced the rate of back-transport--wall shear rate and bulk concentration--but not on the parameters which influenced only the rate of convection--the applied pressure and the membrane resistance. These results suggested that the "steady-state" flux during microfiltration of red cells in saline was limited predominantly by the rate of back-transport of cells away from the membrane.

Other workers (Zawicki et al., 1981) have reported that the filtrate flux obtained during filtration of whole blood drops a factor of two or more during 90 min clinical plasmapheresis procedures. Generally this loss of performance has been attributed to membrane fouling. If blood cell filtration is a solely transport-limited process, changes in membrane permeability during filtration should have no effect on the filtrate flux obtained. The first goal of the experiments described below was to measure any long-term change in filtrate flux in controlled laboratory experiments without the inherent uncertainties and variability of clinical data.

As was reported in Chapter 2, freeze-substitution carried out after short-term (two to five min) filtration of red cells in albumin solution verified that concentration polarization boundary layers do form at the membrane surface and do vary with shear rate and axial position, supporting the transport-limited concentration polarization theory. Since at the time it appeared that the "steady-state" flux had been achieved, no long-term experiments were performed as part of that initial study.

Subsequent experiments demonstrated that during filtration of suspensions of yeast in albumin solution, thick cakes of yeast formed at the membrane surface quickly and then washed away as the membrane permeabiltiy increased with exposure to albumin

solution. The second goal of these experiments was to determine whether changes also occurred in red cell concentration polarization boundary layers during long-term filtration.

MATERIALS AND METHODS

The experimental procedure was essentially the same as that described in Chapter 4; therefore only the differences will be discussed here. In order to minimize variation among blood samples, Mr. Suzuki donated his own blood for use in these experiments, using the blood-drawing services of the M. I. T. Medical Department Laboratory. Standard 15 ml vacuum tubes were charged with approximately 1.0 ml of citrate phospate dextrose solution (recipe in Table I) as anticoagulant before they were filled with the donor's blood. The Medical Department determined the hematocrit H of the anticoagulated blood using standard medical protocol. The blood was then centrifuged for 15-20 min at 1800 RPM (744 × g) in an International Equipment Corporation Model PR-6 Centrifuge and the plasma and buffy coat were removed by aspiration. The red cells were then washed three times by resuspension in Eagles Solution (prepared according to the recipe in Table II) and centrifugation at the above conditions. Finally the cells were re-suspended in a solution of 6 g/100 ml bovine serum albumin (Fraction V Powder, Sigma Chemical Company, St. Louis, MO) in Eagle's solution which had been filtered through 8.0 μm nitrocellulose filters (Schleicher & Schuell, Keene, NH) to remove any particulate matter. (Note: once the cells have been thoroughly washed, no anticoagulant was needed.) The resulting concentration of red cells was checked by centrifugation for 20 min at the above conditions, and adjusted to the desired concentration by addition of albumin solution. The blood cell suspensions were stored at 4°C and used within three days of collection.

The apparatus for these experiments was identical to the single-fiber setup described in Chapter 4. The target inlet wall shear rate in all experiments was 85 s^{-1}. (This is in contrast to yeast experiments in the polypropylene and polyamide hollow fibers, which had to be performed at a ten-fold higher inlet wall shear rate to avoid clogging.)

Table I. Recipe for Citrate Phospate Dextrose Anticoagulant.

Component	Weight (g)
sodium citrate	25.80
dextrose	25.00
citric acid	3.20
$NaH_2PO_4 \cdot H_2O$	2.18

Add distilled H_2O to make 1000 ml. Use 14 ml CPD per 100 ml blood.

Three variations on the filtration procedure described in Chapter 4 were performed. The first variation was a flux experiment designed to determine whether the long-time flux was membrane-limited (by a composite membrane including the membrane itself and the attached layer of red cells) rather than boundary-layer limited. Suspensions of red cells in albumin were filtered for 60 min according to the usual procedure and then the bulk inlet tubing was switched to an inlet reservoir containing only albumin solution . In order to minimize disruption of flow, the two inlet reservoirs were syringes attached to the same pump, and a four-way connection shown in Figure 3-2 was constructed. Clamps initially blocked the two A positions, and the blood was pumped to the fiber while the albumin solution was discarded. Then the clamps were quickly moved from the A positions to the B positions, allowing the albumin solution to flow to the fiber. The flux was measured as a function of time before and after the switching procedure.

Table II. Recipe for Eagles Solution.

Component	Weight (g)
NaCl	6.20
KCl	0.36
$NaH_2PO_4 \cdot H_2O$	0.13
$NaHCO_3$	2.00
$CaCl_2$	0.18
$MgCl_2$	0.15
dextrose	0.90

Add distilled H_2O to make 1000 ml. Adjust pH to 7.4 by addition of NaOH or HCl. Adjust osmolarity to 295 mosmol/l by addition of NaCl or H_2O. Store at 4°C.

The second variation from the procedures in Chapter 4 involved interruption of filtration to perform back-flushing in order to determine whether the time-dependent changes were reversible. In single-fiber back-flushing experiments, after 60 min filtration of RBC in albumin at the desired applied pressure, the hollow fiber assembly was submerged in a graduated cylinder filled with either albumin solution or Eagles solution and the bulk outlet was lowered 113 cm below the hollow fiber, providing 83 mmHg of back-pressure at the outlet for two min. Then the back-flushing reservoir was removed, the outlet was restored to its initial height, and the standard filtration procedure was resumed. Back-flushing was also performed in PA modules by connecting the filtrate port to a reservoir of either albumin or saline, and lowering the bulk outlet 113 cm for two min.

The third variation of the filtration procedure was to pre-treat the PA hollow fiber with albumin solution in order to determine whether a reduction in the membrane permeability in the presence of albumin was responsible for differences in flux and in short and long-term concentration profiles. The pre-treatment was carried out by filtering albumin solution under the same conditions (shear rate and applied pressure) which would be used in the subsequent filtration of red cells in albumin. In one set of these experiments, pretreatment times of 20, 40, and 60 min were followed by one min filtration of RBC in albumin, and then freeze-substitution. In another set of pretreatment experiments, the hollow fibers were pretreated with albumin solution for about 150 min, until the flux of albumin had dropped to about 0.03 cm/min (one tenth of the initial flux), and then a suspension of RBC in albumin was filtered for various times (1, 15, and 30 min) prior to freezing.

RESULTS

Figure 3-3 shows the flux obtained when filtering 6% albumin solution alone through the PA, PP, and PS hollow fibers studied. The initial permeabilities of the membranes are within a factor of two, with the PS permeability the highest and the PA permeability the lowest. The permeability of the PS fibers remained fairly constant for the first 20 min and then gradually decreased a factor of two in the next 100 min. The

permeability of the PA hollow fibers declined steadily, dropping a factor of six in two hours. The permeability of the PP hollow fibers dropped off quickly at first--a factor of ten in 30 min--but then remained relatively constant for the next 90 min.

In each of the next three graphs, the albumin fluxes are re-plotted on a semi-log scale along with the fluxes measured with red cell suspensions. In each case, albumin data is plotted with as diamond symbols. Circles are used to represent red cell data from single-fiber experiments, while triangles are used to represent data from mini-module experiments. Open symbols indicate that the cells were suspended in Eagles' solution, while filled symbols indicate that the cells were suspended in 6% albumin solution.

Figure 3-4 shows results of the PA experiments. In the single-fiber experiments, each data point represents a single drop of filtrate collected. The number of data point is limited by the amount of filtrate obtained from the small fibers. Scatter results from uncontrollable secondary factors such as whether a drop falls all the way from the top of the fiber, or just partway. Figure 3-5 is a photograph of a PP fiber during filtration of Eagles solution alone. Although droplets consistently form in the same positions along the hollow fiber, the pattern of falling drops varies with time. Because of its surface-wetting properties, albumin solution runs more smoothly down fibers, yielding data which is a bit less scattered than the saline data. In the single PA fibers, the flux with red cells and albumin was slightly lower than the flux with red cells in saline, and both fluxes dropped off by a factor of about two in 90 min. In PA module experiments, fluxes obtained with red cells suspended in either albumin or saline dropped only about 10% in two hours. The smaller degree of scatter in the data from the module experiments results from the large surface area of the modules compared to surface area of the single fibers. Since the flux decline was significantly less in the only experiments in which a filtrate-side casing was present, it is possible that the greater dropoff in the other experiments is somehow related to the absence of a casing which served to keep the outside of the fibers wet and reduce evaporation of filtrate. As the outside of a fiber dried out, salt or protein crystals could form and block pore outlets. As the experiments went on, more and more pores could have become blocked, resulting in a gradual flux decline.

Figure 3-6 shows similar results for PP fibers. In general, the flux in the PP fibers was a factor of two to three less than the flux in the PA fibers. Again, in data obtained in single-fiber experiments, the flux with red cells in albumin was a bit lower than the fluxes with red cells in saline. Both fell about a factor of three in two hours. However, in the case of the PP mini-modules, the flux was not steady like the flux measured in the PA module; rather, it dropped off at the same rate as the single fiber data.

Figure 3-7 shows that the flux obtained with single PS fibers is about a factor of two higher than the flux obtained in the single PA fiber. The flux dropped off by about a factor of two during a one-hour experiment. Figure 3-8 shows the data from Figure 3-7 re-plotted along with data for four other runs with PS fibers. The data was fairly reproducible, though somewhat scattered.

Figure 3-9 through Figure 3-11 show the results of the freezing experiments. In Figure 3-9, inlet (~0.5 cm from the inlet), middle (~2.5 cm from the inlet), and outlet (~4.5 cm from the inlet) sections taken from PA hollow fibers after 1, 5, 10, 20, 40, and 60 min filtration. Similarly, Figure 3-10 shows sections taken from PP fibers after 1, 5, 10, 20, 40, and 60 min filtration. Figure 3-11 shows sections taken from modified PS fibers after 1, 5, 10, 20, 40, and 60 min filtration. Missing photos correspond to hollow fiber sections that were damaged at some point in the freeze-substitution procedure. Note that the magnification in Figure 3-11 is different than that of the previous two figures because the PS hollow fibers are much larger than the PP or PA hollow fibers.

The early-time photos display the same characteristics as were seen in Chapter 2: a tightly-packed region next to the wall contained within a thicker concentration boundary layer over which the concentration drops off to its bulk value. The bulk concentration appears uniform, with no cell-free zone during filtration at 75 mmHg.

In the PP fibers, after only five minutes the concentration polarization boundary layer has disappeared and a large cell-free zone has formed near the wall at the inlet of the fiber. Two distinct layers of cells remain next to the wall. Previous rinsing experiments performed with PA fibers (Chapter 2) have demonstrated that the cells at the membrane wall are stuck in membrane pores. Similar changes in the concentration

polarization boundary layer occur at later times in the PA hollow fibers. The reason for the uneven bulk concentration in the PA fibers is unknown.

The results of freezing the PS fibers (Figure 3-11) are inconclusive. Because more numerous artifacts (separation of the fiber wall from the lumen region, wrinkled and torn sections, etc.) occurred with the larger fibers, it is difficult to see any distinct changes in the red cell concentration profiles with time. However, it appears that even at 40 and 60 min a concentration polarization boundary layer remained, suggesting that the flux had not yet become membrane-limited in those fibers.

Mr. Suzuki hypothesized that after a certain period of filtration, the cells at the membrane wall had rearranged in such a way that the effective membrane resistance was high enough that the filtration rate had become membrane-limited, and that as a result the concentration polarization boundary layer was no longer needed to maintain the steady-state flux, and had "washed away" much like the disappearing yeast cakes described in Chapter 4. The rearrangement of cells could be a compaction phenomenon, in which the porosity of the cell bed was lowered, and/or a pore-blockage phenomenon, in which the effective membrane resistance increased as cells deformed into membrane pores. Since such a rearrangement should be reversible, removal of the trapped cells by back-flushing should result in restoration of the initial flux and the initial concentration polarization boundary layer. Figure 3-12 shows the filtrate flux as a function of time, before and after backflushing. The flux measured after backflushing was virtually identical to that measured initially, demonstrating that the long-term change in the steady-state flux is reversible. In Figure 3-13, the sections taken from fibers frozen one min after backflushing with either saline or albumin solution demonstrate that the changes in the concentration polarization boundary layer with time are also reversible.

If Mr. Suzuki's hypothesis is correct, and the flux at long time is membrane-limited, then the filtrate flux should not increase after switching from the inlet reservoir containing blood to the second reservoir containing albumin. Figure 3-14 shows the filtrate flux in the PA module as a function of time before and after switching. The flux did not increase, as it should if it were diffusion-limited. Mr. Suzuki attributed the loss of flux upon switching to plugging of some of the fibers in the PA module due to

inadvertent overpressurization during switching. This plugging could have obscured any increase in flux which might otherwise have occurred.

An alternative explanation for the disappearance with time of the concentration polarization boundary layers is that the membrane permeabilities had decreased sufficiently to lead to membrane-limited behavior (without any change in the cells at the wall). If this were the case, then membranes which were pretreated long enough should have no concentration polarization boundary layer even after short filtration times. Figure 3-15 shows that even after an hour pretreatment with albumin, the concentration boundary layer was observed after one minute filtration of red blood cells in albumin. Such boundary layers were not observed after one hour filtration of blood. Furthermore, Figure 3-16 shows that the time-dependent changes in the concentration boundary layer occur even in membranes pretreated to lower the membrane permeability by a factor of ten.

CONCLUSIONS

The above results support Mr. Suzuki's hypothesis that long-term changes in filtrate flux and concentration profiles during filtration of red cells in single hollow fibers are related to rearrangement of the cells at the membrane surface. However, since the flux measured in the polyamide module remained fairly constant, it appears that such long-term changes may not occur in an enclosed multi-fiber module, such as those used clinically. Unfortunately, the freezing technique employed here cannot be used on entire modules, so another approach is necessary in order to determine the reason for the differences seen here. It should also be mentioned that the peristaltic pumps used in clinical devices might also lead to different time-dependent behavior.

REFERENCES

Zawicki, I., P. S. Malchesky, J. W. Smith, H. Harasake, Y Asanuma, and Y. Nose (1981): Axial changes of blood and plasma flow, pressure, and cellular deposition in capillary plasma filters. Artif. Organs 5: 241-247 (1981)

Zydney, A. L., Cross-Flow Membrane Plasmapheresis: An Analysis of Flux and Hemolysis, Ph. D. Thesis, Massachusetts Institute of Technology (1985)

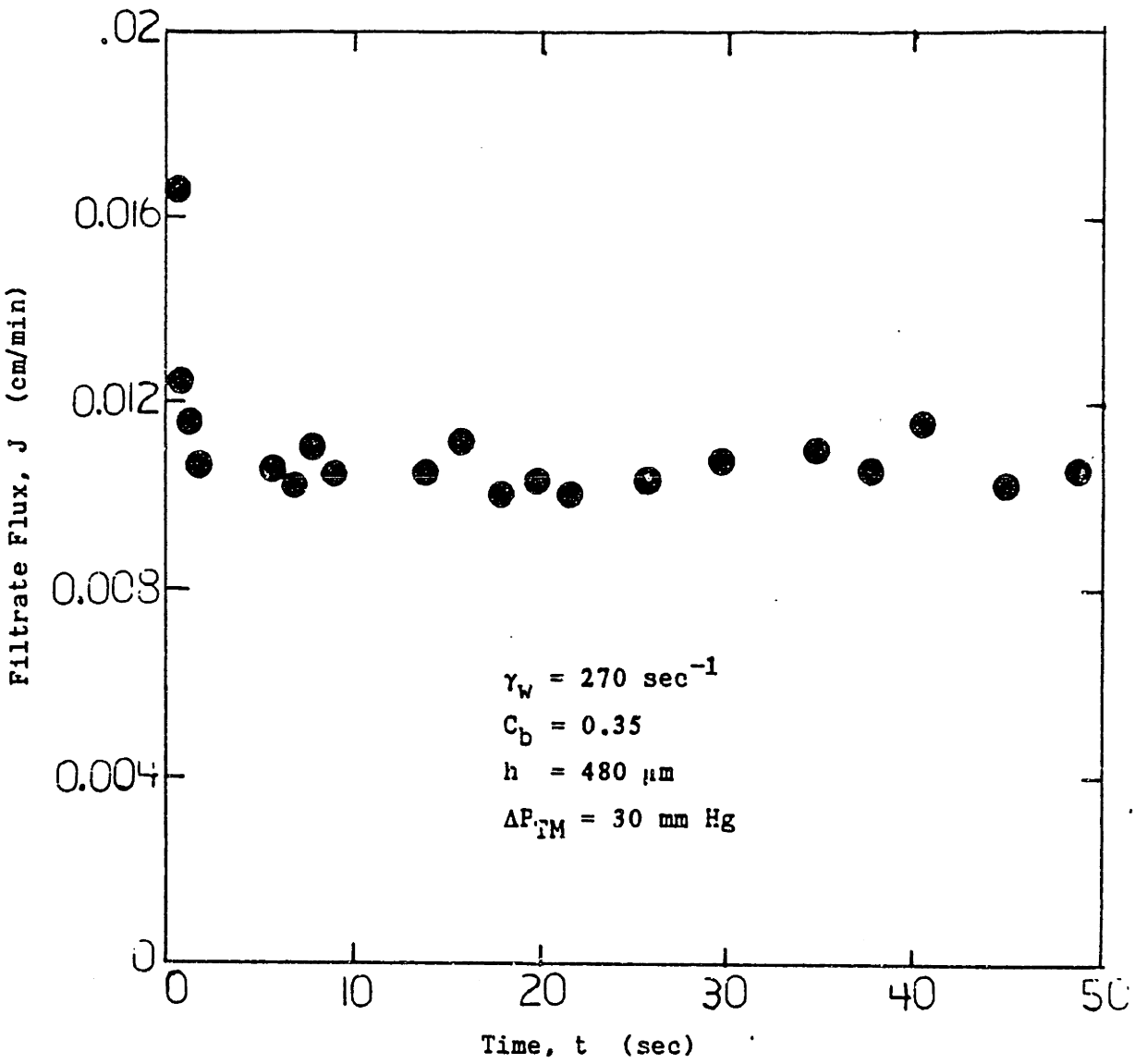

Figure 3-1. Flux as a function of time during filtration of red cells in Eagles solution in a flat-plate cross-flow filter (Zydney, 1985).

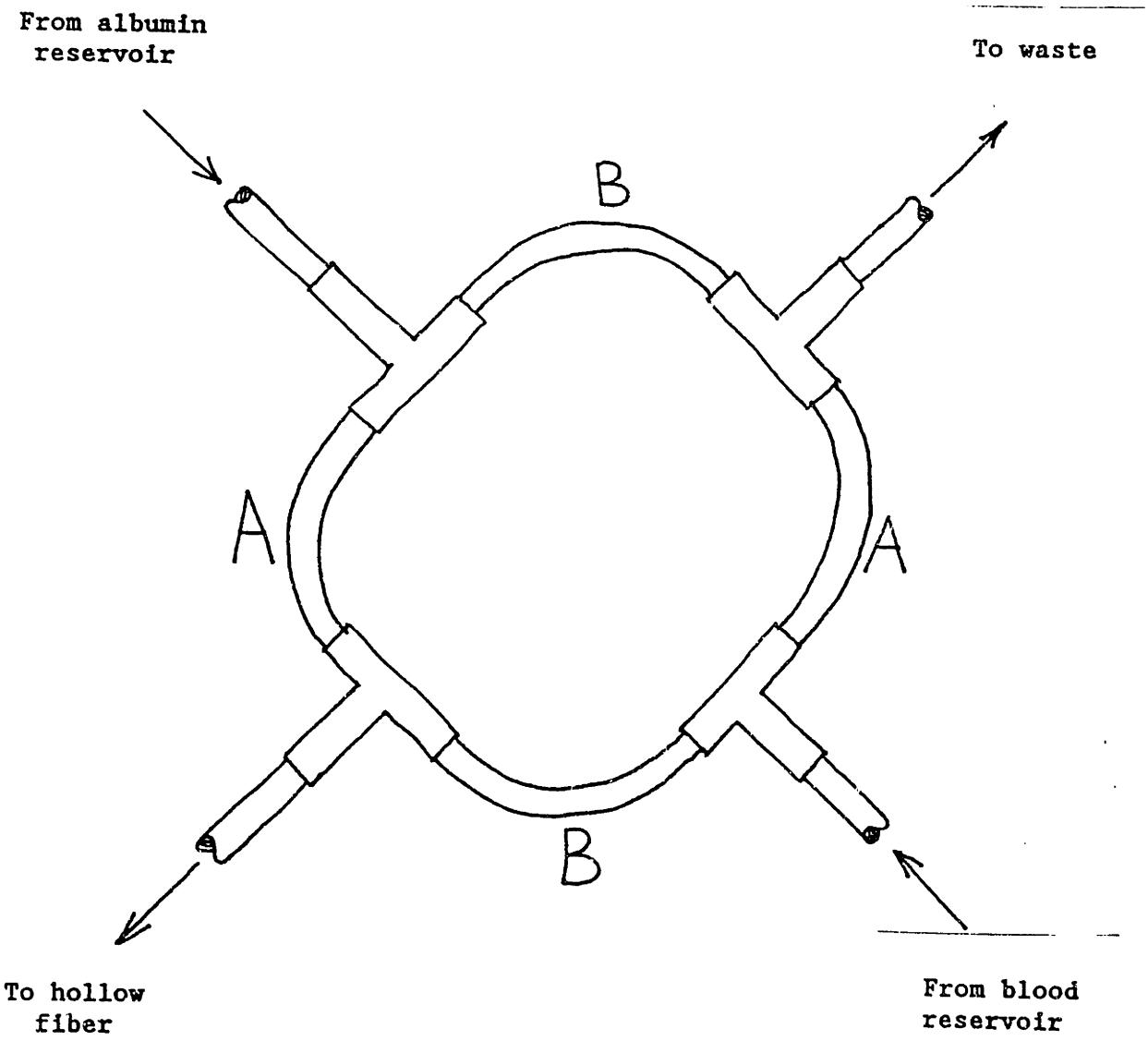

Figure 3-2. Four-way connector used in switching experiments.

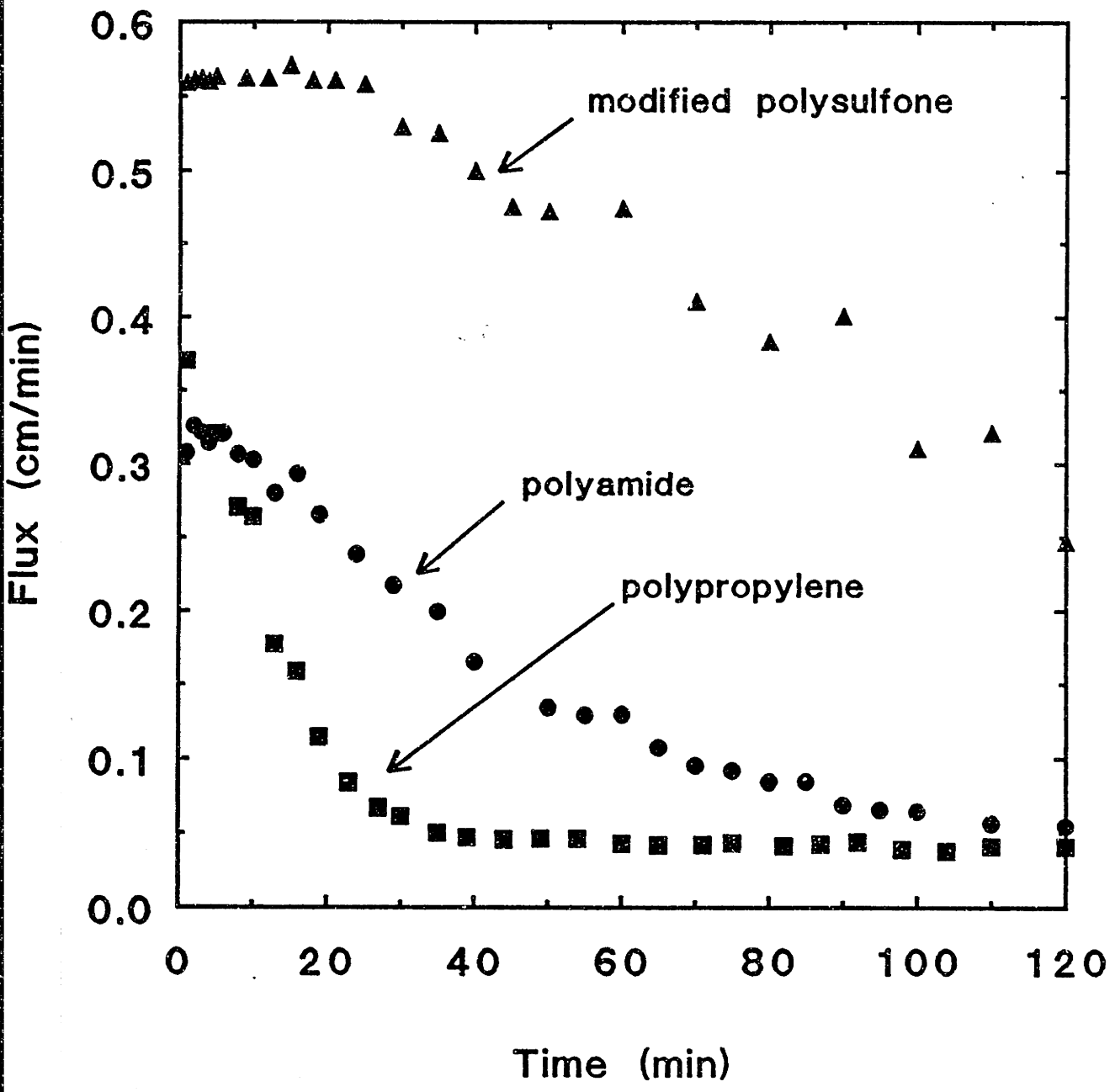

Figure 3-3. Flux as a function of time during filtration of 6% albumin solution in three types of hollow fibers at a pressure of 71 mmHg and an inlet wall shear rate of 800 s^{-1}.

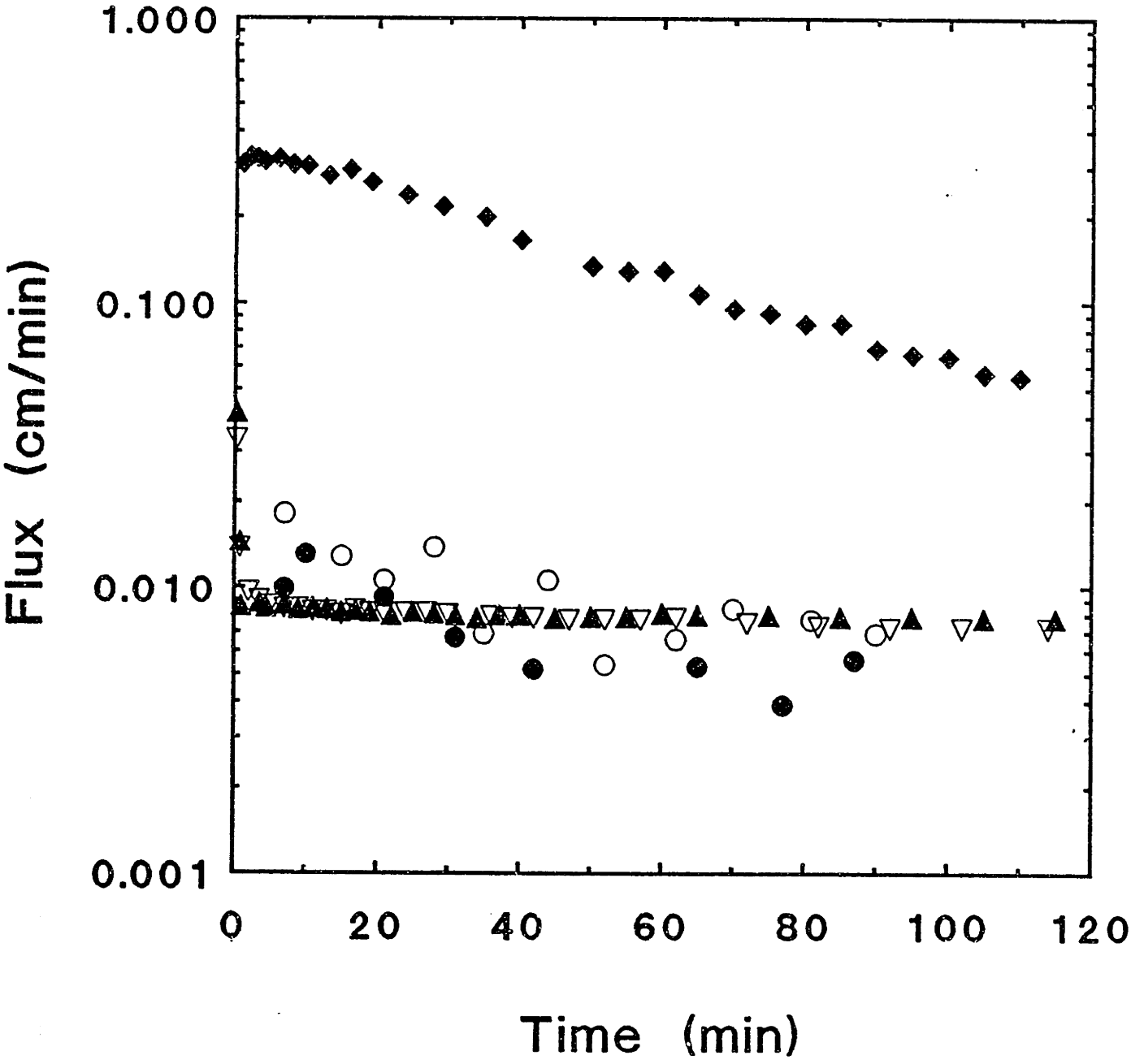

Figure 3-4. Filtrate flux as a function of time with 6% BSA (diamonds) and 5% red cells in 6% BSA (solid symbols) or saline (open symbols) in PA single fibers (circles) and modules (triangles) at P_{appl}=71 mmHg and $\gamma_{w,in}$=85 s^{-1}.

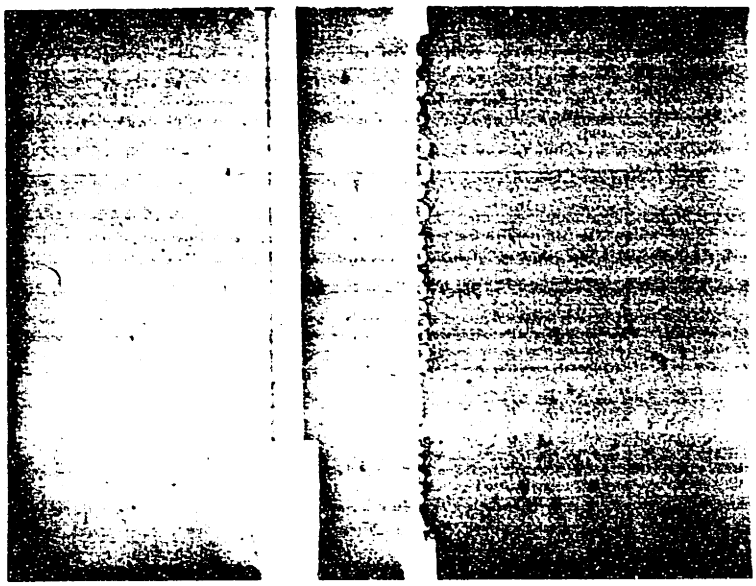

Figure 3-5. Photograph of polypropylene hollow fiber with saline filtrate droplets.

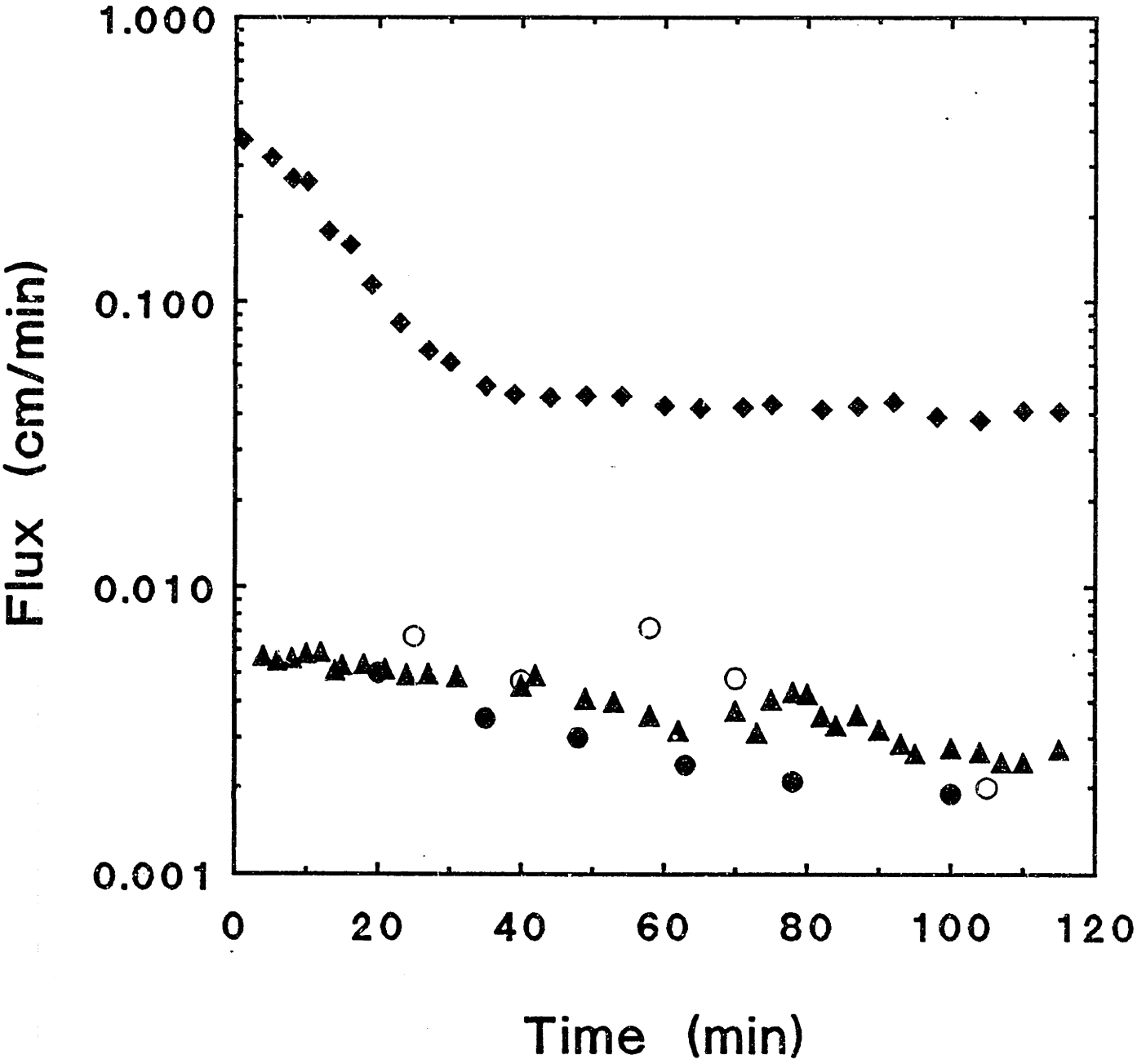

Figure 3-6. Filtrate flux as a function of time with 6% BSA (diamonds) and 5% red cells in 6% BSA (solid symbols) or saline (open symbols) in PP single fibers (circles) and mini-modules (triangles) at P_{appl}=71 mmHg and $\gamma_{w,in}$=85 s^{-1}.

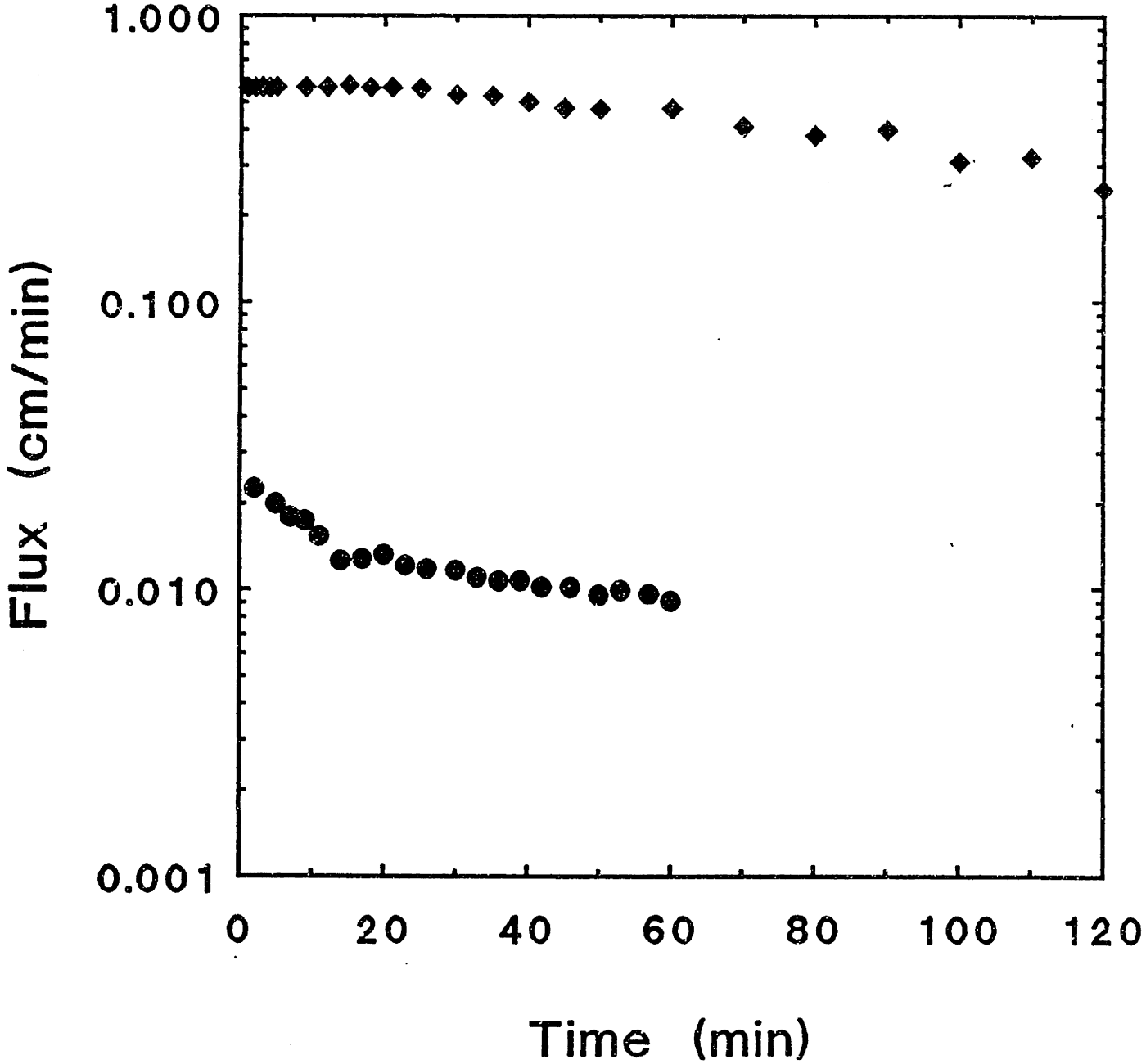

Figure 3-7. Flux as a function of time during filtration of 5% red cell suspensions in in PS fibers at a pressure of 71 mmHg and an inlet shear rate of 85 s^{-1}, and flux of 6% BSA in PS fibers, re-plotted from Figure 3.

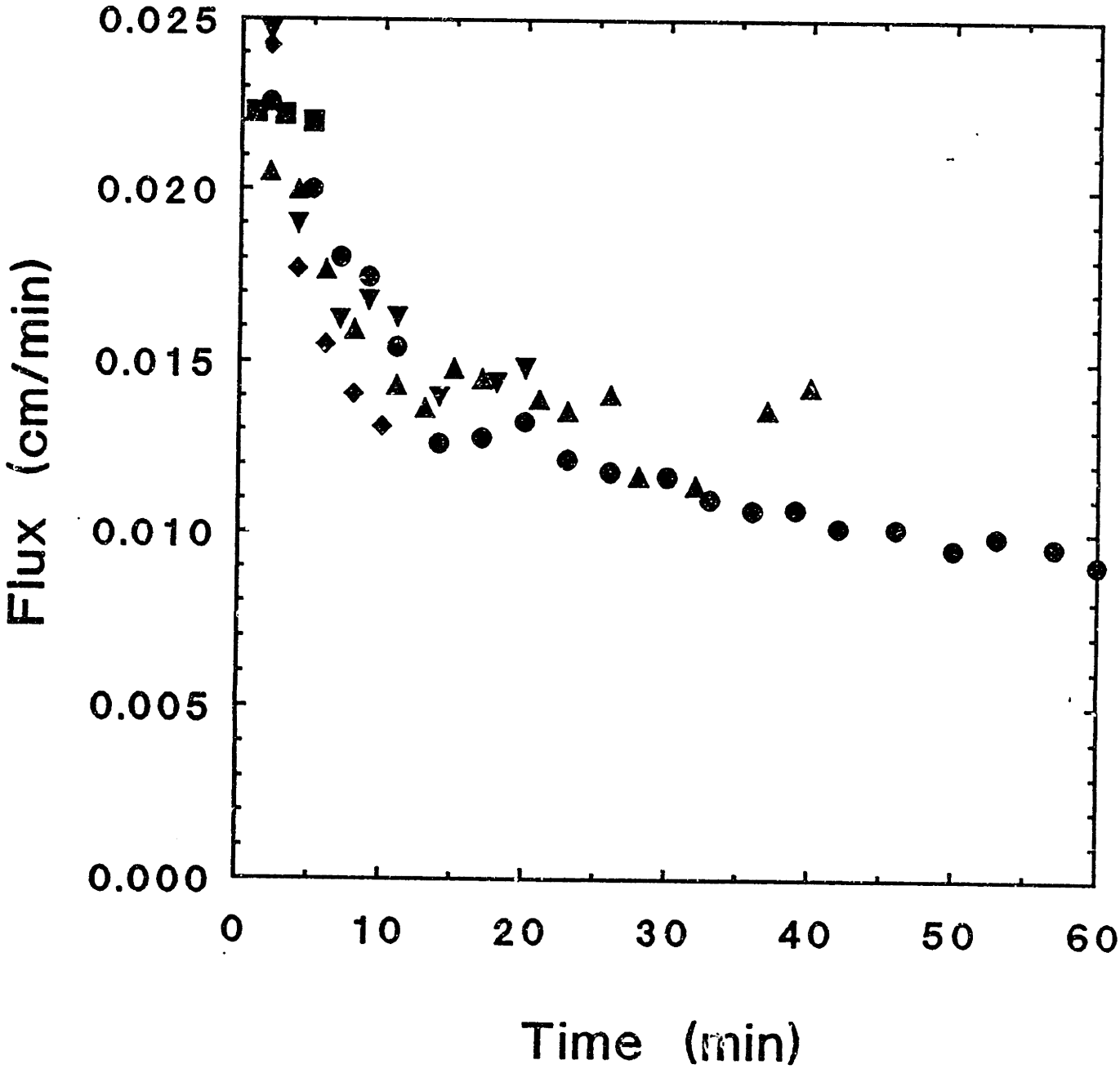

Figure 3-8. Flux as a function of time during filtration of 5% red cell suspensions in in PS fibers at a pressure of 71 mmHg and an inlet shear rate of 85 s^{-1}. (Five runs shown, one re-plotted from Figure 1-7.)

(Page intentionally left blank so that following captions and figures would appear side-by-side in double-sided copies)

(Photograph on following page.)

Figure 3-9. Polyamide (320 μm ID, 0.35 μm pore ID) fibers frozen after filtration of 5% red blood cells in 6% BSA for a)1, b)5, c)10, d)20, e)40 and f)60 min at P_{out}=71 mmHg, $\gamma_{w,in}$=80 s^{-1}, and 1)x=0, 2)x=2 and 3)x=5 cm.

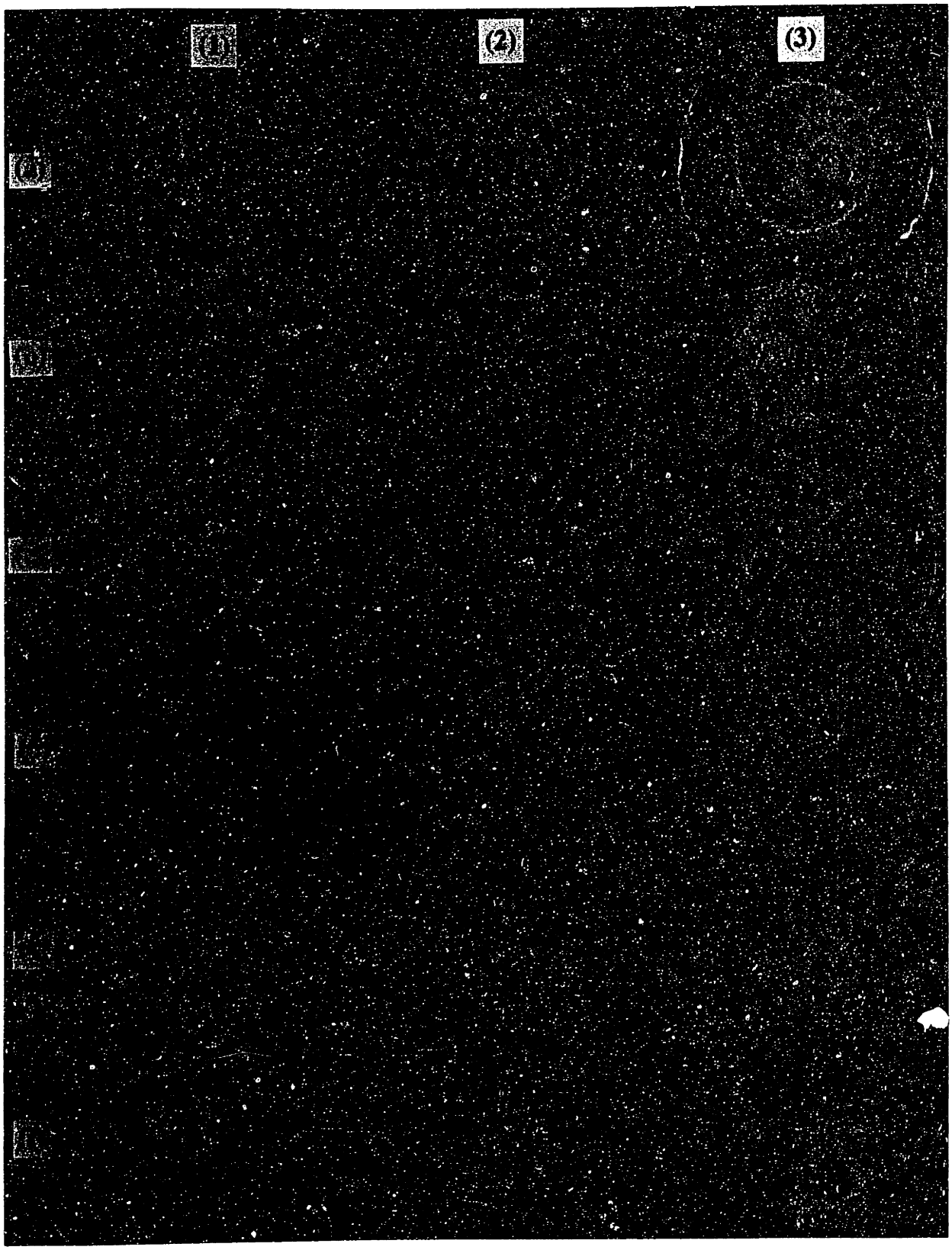

Fig 3-9

(Photograph on following page.)

Figure 3-10. Polypropylene (320 μm ID, 0.35 μm pore ID) fibers frozen after filtration of 5% red blood cells in 6% BSA for a)1, b)5, c)10, d)20, e)40 and f)60 min at P_{out}=71 mmHg, $\gamma_{w,in}$=80 s^{-1}, and 1)x=0, 2)x=2 and 3)x=5 cm.

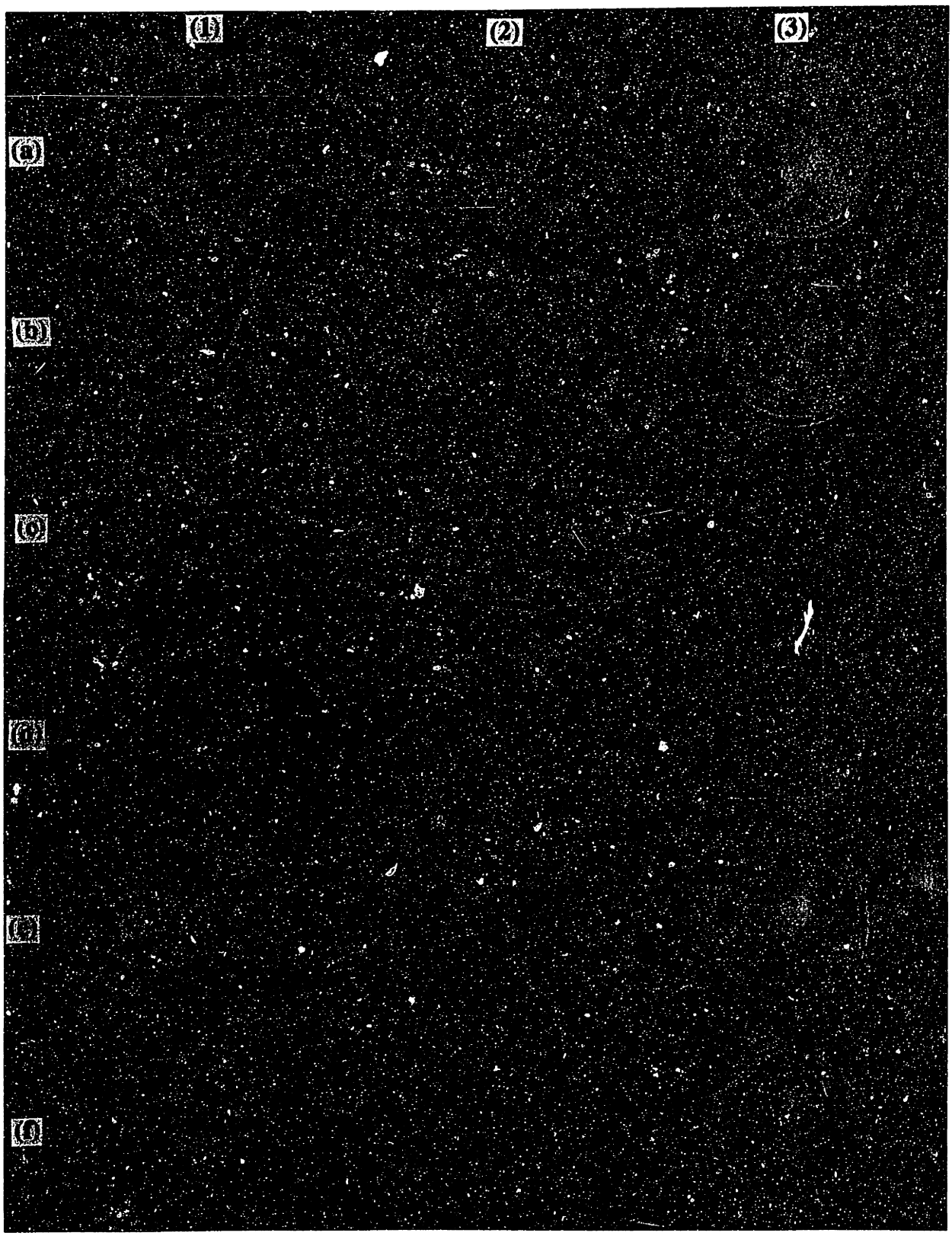

FIG 3-10

(Photograph on following page.)

Figure 3-11. Polysulfone (320 μm ID, 0.35 μm pore ID) fibers frozen after filtration of 5% red blood cells in 6% BSA for a)1, b)5, c)10, d)20, e)40 and f)60 min at P_{out}=71 mmHg, $\gamma_{w,in}$=80 s^{-1}, and 1)x=0, 2)x=2 and 3)x=5 cm.

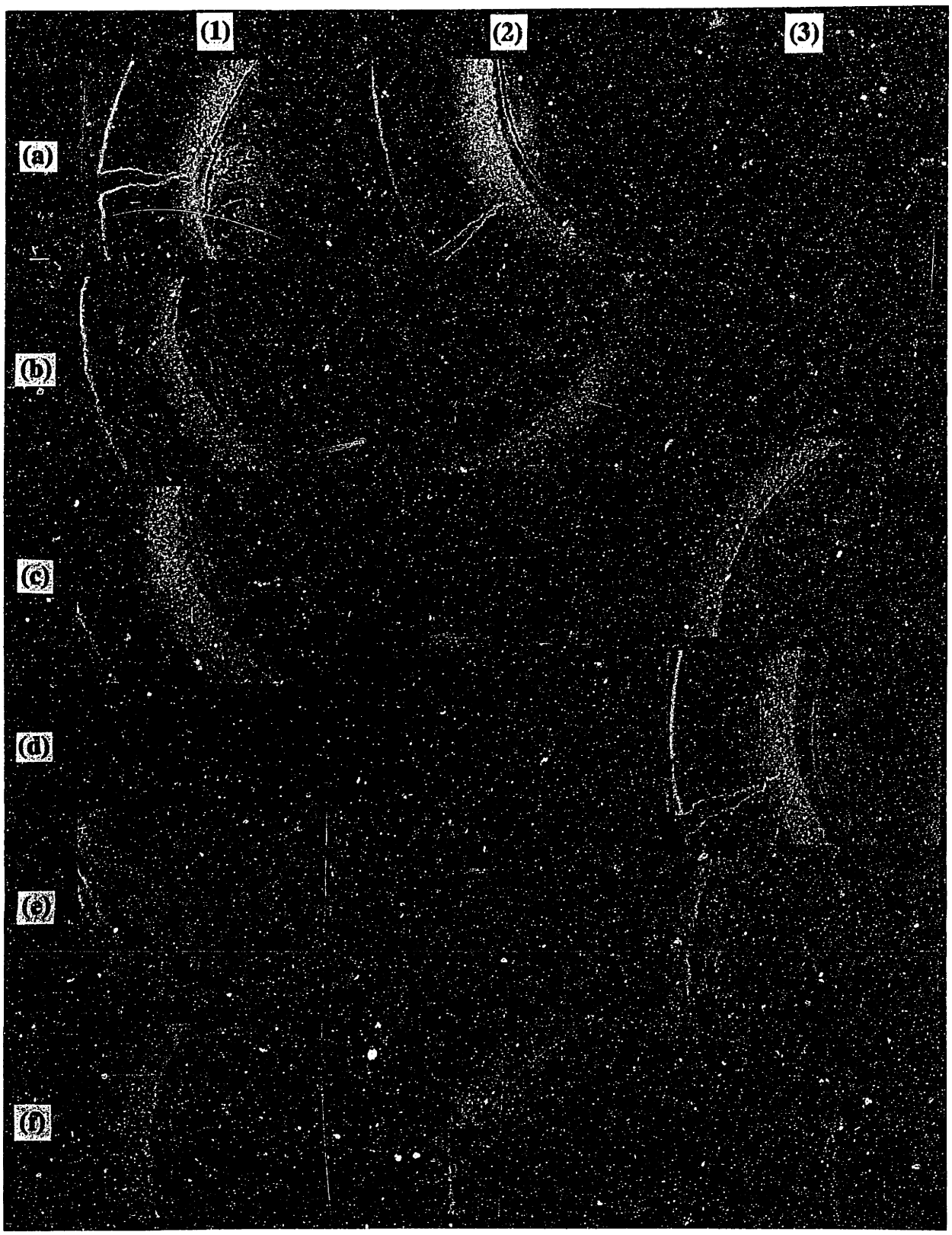

Fig 3-11

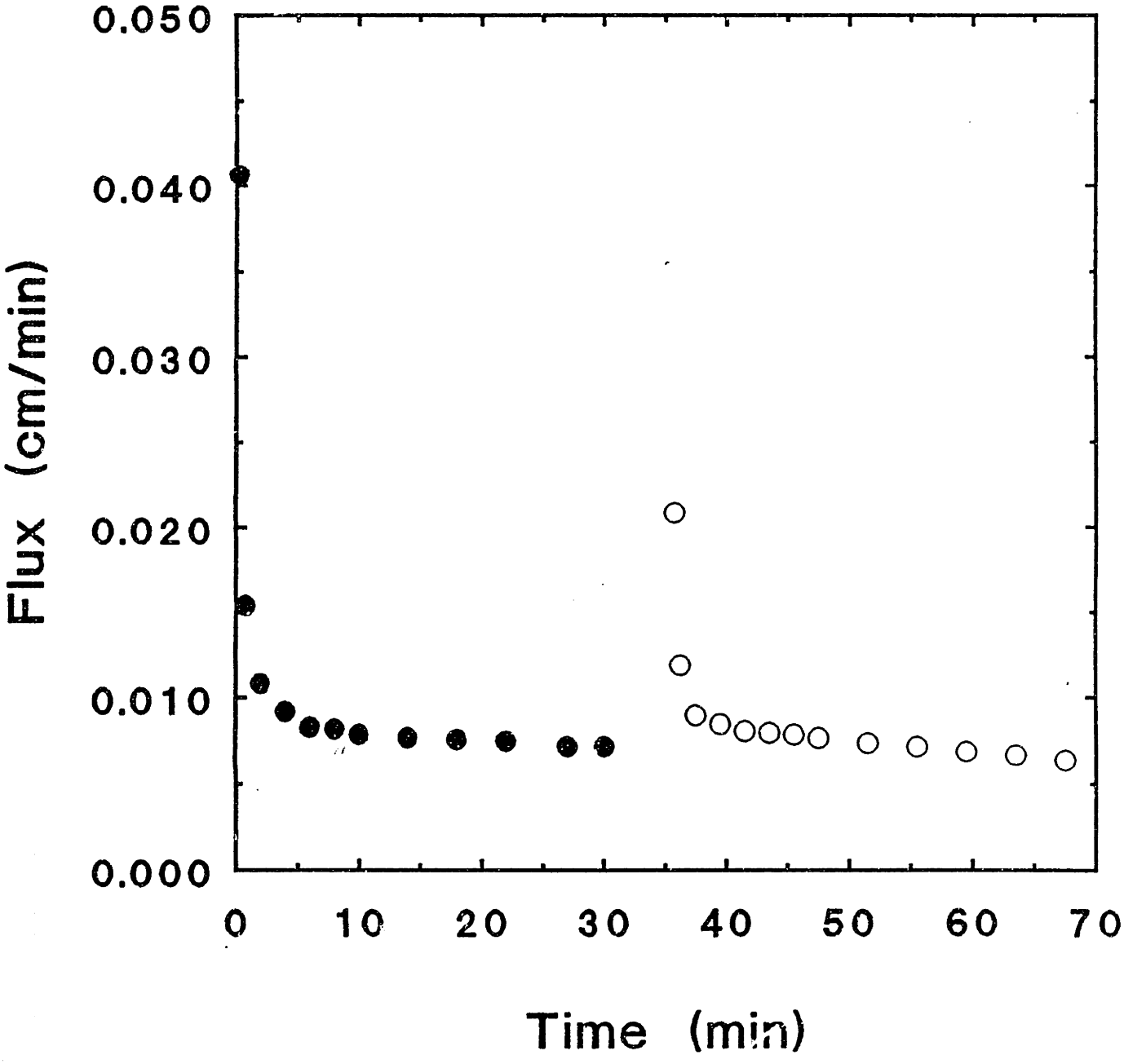

Figure 3-12. Filtrate flux as a function of time during filtration of 5% RBC in 6% BSA at P_{out}=71 mmHg and $\gamma_{w,in}$=85 s^{-1}, before and after 5 min backflushing with 6% BSA at P_{out}=-83mmHg.

(Photograph on following page.)

Figure 3-13. Polyamide fibers frozen after 60 min filtration of 5% RBC in 6% BSA at P_{out}=71 mmHg and $\gamma_{w,in}$=85 s^{-1}, 2 min backflushing with a) saline and b)6% BSA at P_{cut}=-83mmHg, and 1 min resumed filtration of RBC.

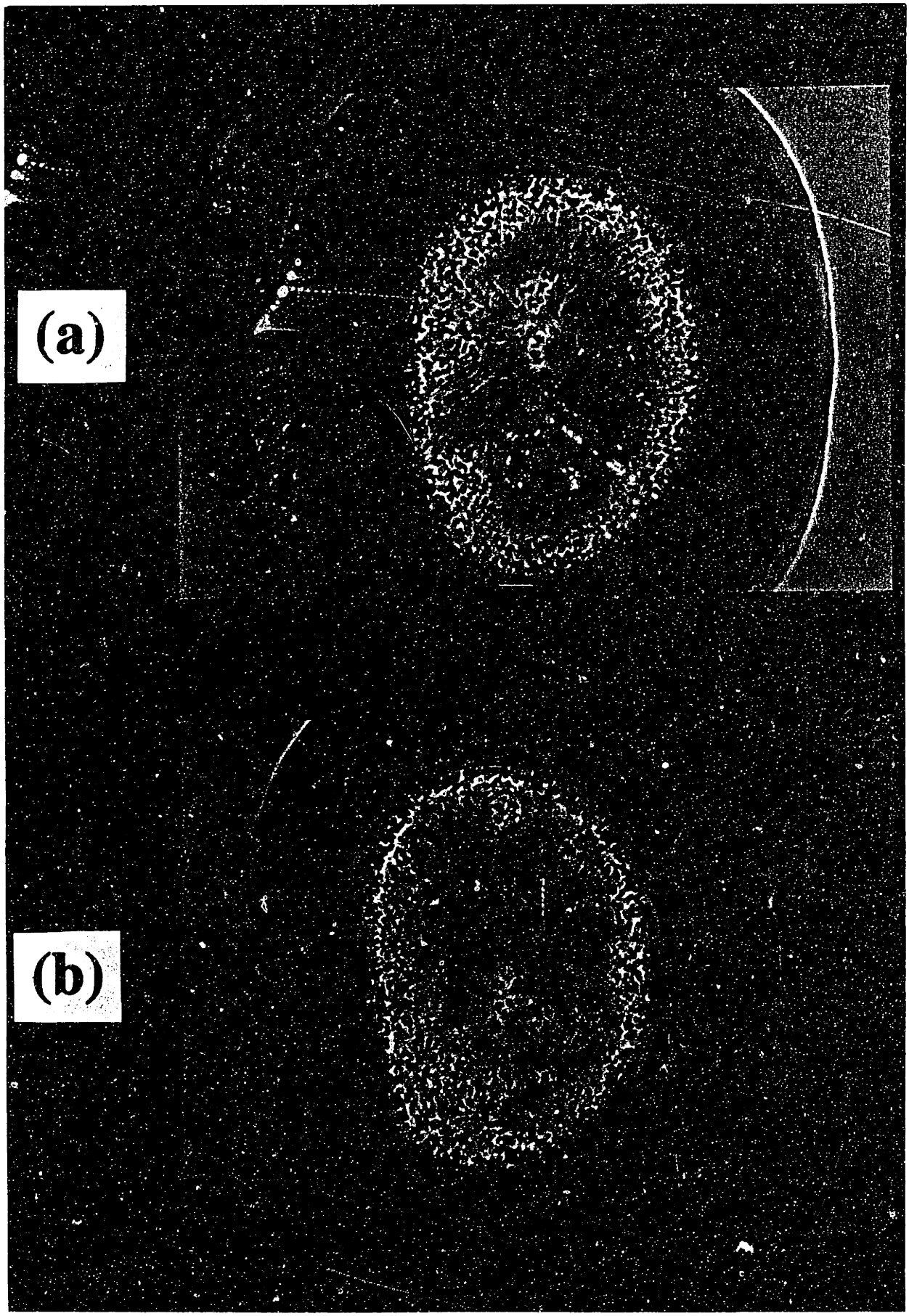

FIG 3-13

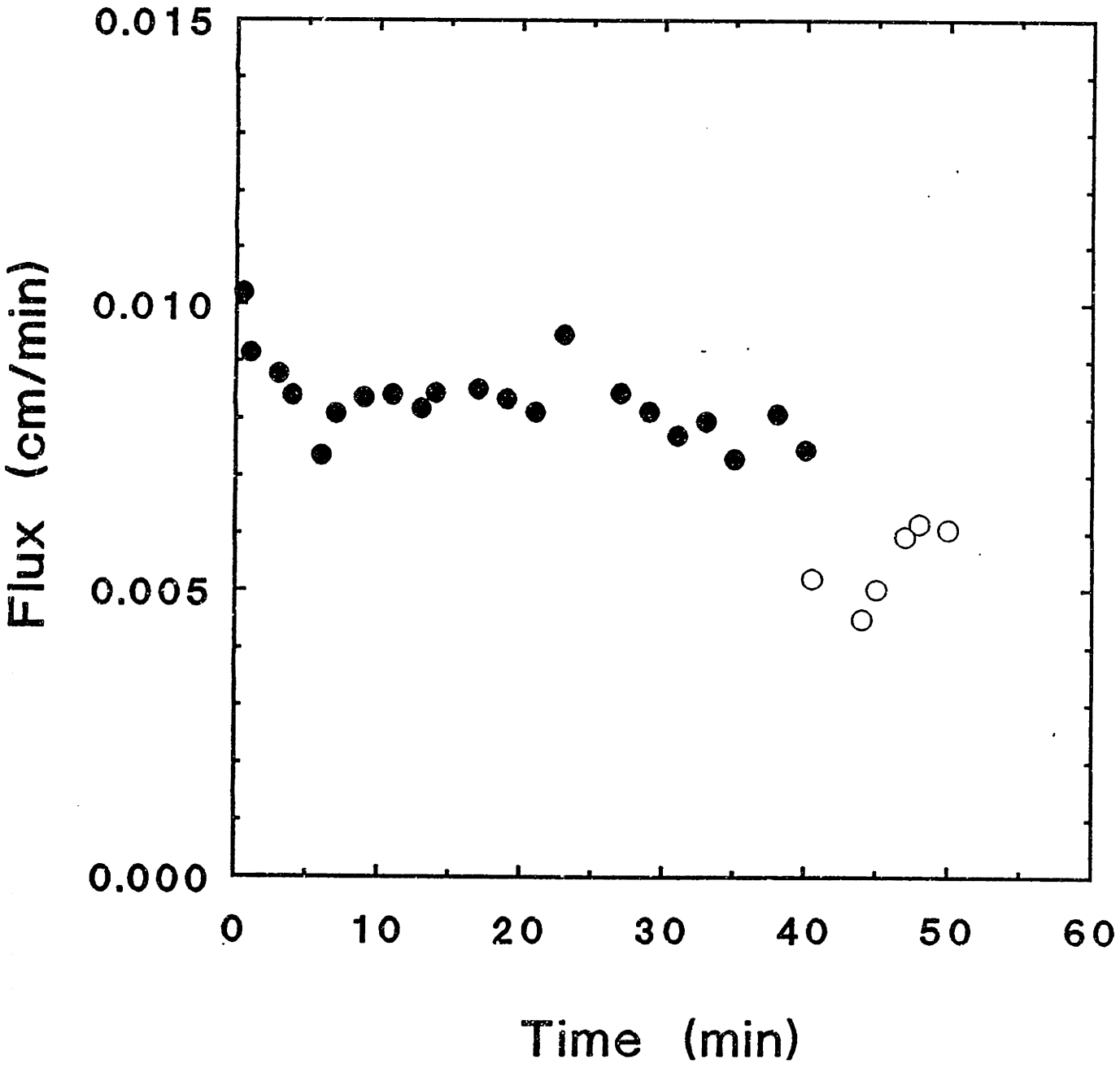

Figure 3-14. Filtrate flux as a function of time during filtration of 5% RBC in 6% BSA at P_{out}=71 mmHg and $\gamma_{w,in}$=85 s^{-1}, and during filtration of 6% albumin after switching inlet reservoirs.

(Photograph on following page.)

Figure 3-15. Polyamide fibers frozen after 1 min filtration of 5% RBC in 6% BSA at P_{out}=71 mmHg and $\gamma_{w,in}$=80 s^{-1}, after a)20, b)40, and c)60 min pretreatment with 6% BSA.

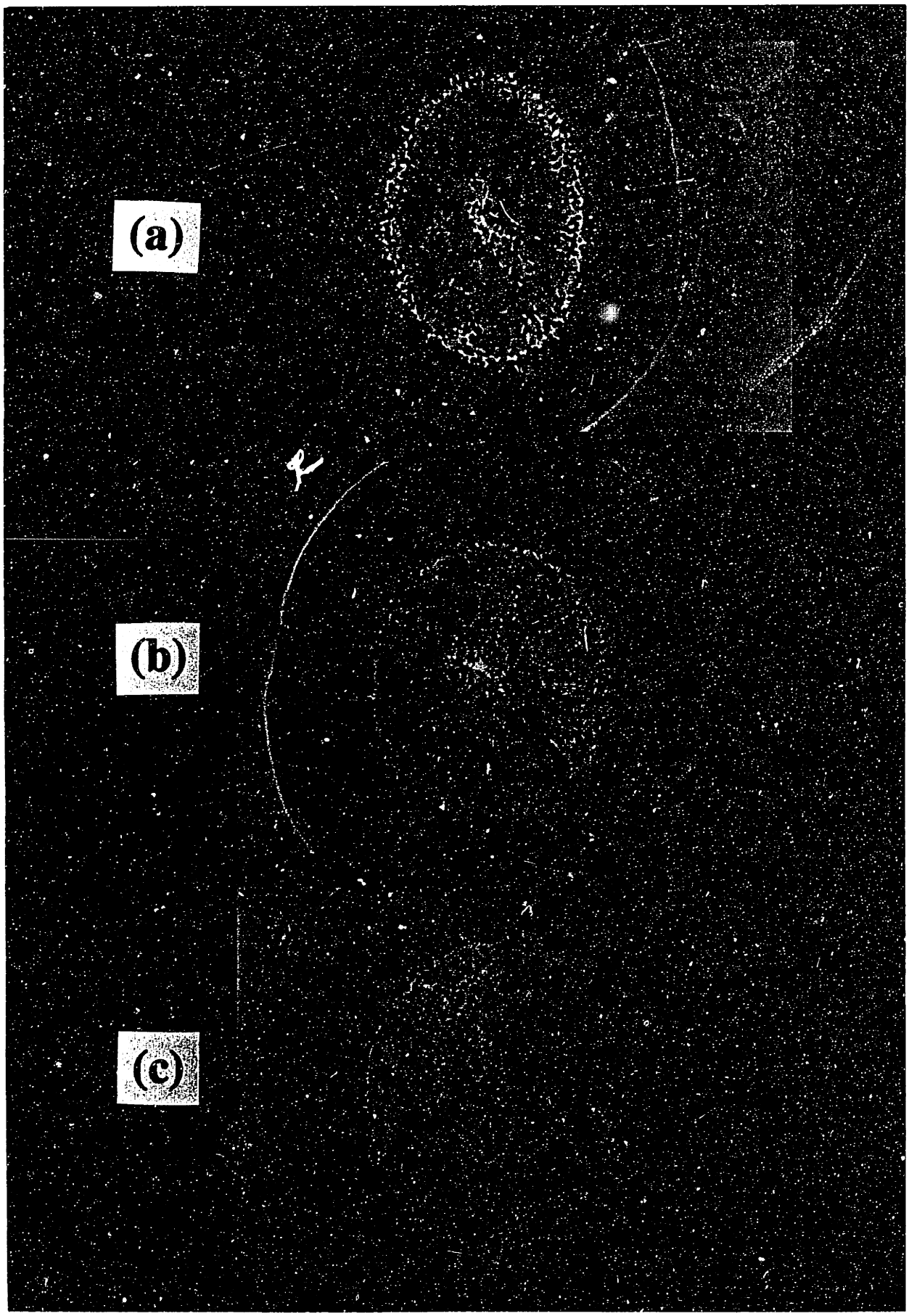

Fig 3-15

(Photograph on following page.)

Figure 3-16. Polyamide fibers frozen after a)1, b)15, and c)30 min filtration of 5% RBC in 6% BSA at P_{out}=71 mmHg and $\gamma_{w,in}$=85 s^{-1}, after 150 min pretreatment with 6% BSA.

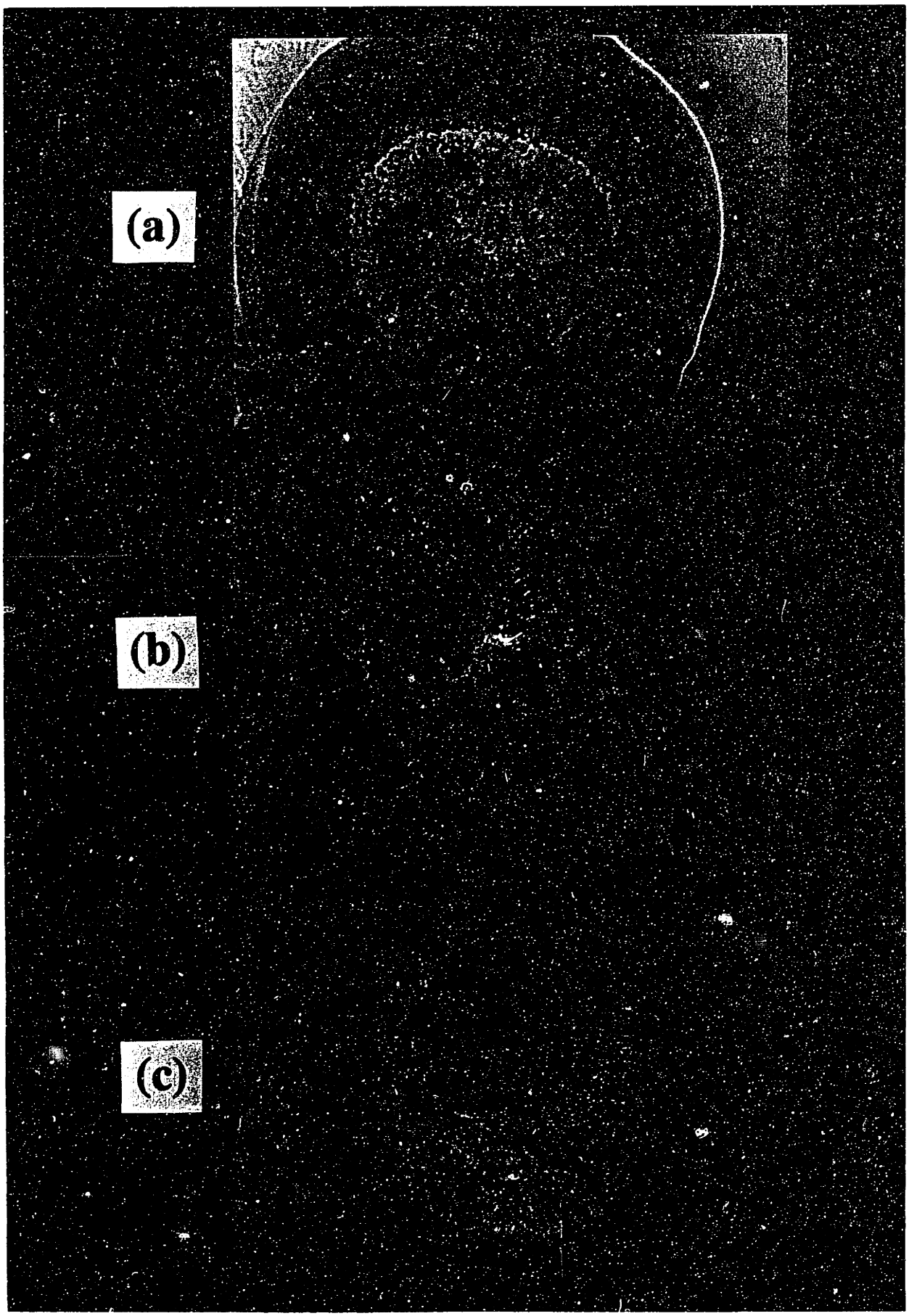

FIG 3-16

This page intentionally left blank.

A. ABSTRACT

Development of models to predict filtrate flux in cross-flow filtration of microbial cells requires information on the hydraulic resistance of cakes of cells which form at the membrane surface. In order to determine whether existing correlations for predicting the hydraulic resistance of a bed of particles are applicable to microbial cell systems, we have measured the size, packing characteristics, and hydraulic resistance of a model cell system, bakers yeast. We have compared the measured resistance with that predicted from particle size and packing information by the Kozeny-Carman correlation. Furthermore, we have sought to explain previously-observed variation in measured resistances by measuring the resistance under a variety of experimental conditions.

We found that yeast packs to higher concentrations than do rigid latex particles, but much lower concentrations than do highly deformable red blood cells. We found that while the resistance of glutaraldehyde-hardened yeast was within reasonable agreement with that predicted by the Kozeny-Carman equation, the resistance of freshly-rehydrated active dry yeast at room temperature was a factor of 20 or more greater than predictions. We found that the measured cell resistance varied significantly with experimental conditions; the resistance was an order-of-magnitude higher under conditions which allowed the yeast to produce large volumes of carbon dioxide than under conditions which precluded CO_2 production. This explained why a previous measurement of the resistance of well-rinsed yeast, with no available carbon source, had yielded a much lower resistance than a study with unrinsed yeast. In addition, by comparison of data with normal and hardened yeast cells, we found that cell deformability is responsible for only a factor of two in the resistance of normal yeast.

Under all conditions, the resistance of yeast was orders of magnitude lower than the resistance of highly deformable red blood cells, and significantly lower than the resistance of other microbial cells. As a result, yeast cakes which form at the membrane surface during cross-flow filtration should be thicker than those of other cells under similar conditions, and understanding cake formation will be crucial to predicting cross-flow fluxes. The functional

relationships between permeability, porosity, and compressive pressure developed here can be incorporated into future models for predicting the flux in cross-flow systems.

B. INTRODUCTION

Filtration is increasingly used as a first step in downstream processing of bioreactor effluents to separate microbial cells such as yeast from the media in which they are grown. The cross-flow configuration, in which the bulk flow is parallel to the filtering membrane, minimizes the accumulation of retained cells near the membrane surface, resulting in significantly larger filtration rates than can be obtained in a dead-ended system. Even so, the flux obtained in cross-flow microfiltration of cell suspensions may be orders of magnitude smaller than that obtained when filtering cell-free media under identical conditions (Blatt et al., 1970; and Porter, 1972). It has been proposed that a concentrated layer of cells at the membrane surface reduces the flux by (1) blocking membrane pores and (2) forming a cake which provides additional hydraulic resistance. Previous studies (Saltzman, 1984; Zydney, 1985; Zydney, et al., 1988) confirmed the importance of both mechanisms in reducing the flux obtained during filtration of highly deformable red blood cells. The objective of this work was to study the pore blockage and hydraulic resistance phenomena with relatively rigid yeast cells in a simple unstirred and unsheared system.

To do this, stagnant beds of yeast cells were formed by allowing a known mass of cells to settle in a batch filter. Then the filtrate flux of prefiltered media through the cell bed was recorded as a function of the applied pressure. Experiments were performed at room temperature (RT, 22±2°C) with freshly-rehydrated active dry yeast, with rehydrated yeast which had been washed three times with excess media, and with glutaraldehyde-hardened yeast. Experiments were also performed at 4°C with freshly-rehydrated yeast. At least two cell bed heights were studied under each set of conditions. In order to determine whether the presence of carbon dioxide bubbles in the cell bed could explain large variations in the measured resistances, we measured the volume of CO_2 produced under each set of conditions. Stagnant filtration experiments were also performed with rigid polystyrene spheres in distilled water.

Since the resistance of a bed of particles is known to depend on the void fraction or porosity of the bed, the dependence of yeast bed porosity on compressive pressure was studied by measuring cell bed heights in centrifugation experiments. Similar experiments were performed with the rigid polystyrene spheres.

Combining the stagnant filtration and centrifugation results allowed comparison of data with the Kozeny-Carman equation, a general correlation for the hydraulic resistance of a porous medium as function of packing fraction and specific surface area of the particles comprising the porous medium. The possible effects of non-sphericity, non-uniform size distribution, and surface roughness were analyzed using size information obtained with a light microscope and an image analysis system.

Two previous studies have measured the hydraulic resistance of yeast. Rushton and Khoo (1977) determined the resistance of Saccharomyces carlsbergensis (brewers yeast), a strain related to bakers yeast, from compression cell and unsteady-state stagnant filtration experiments with unrinsed yeast. They reported values of cell bed porosity ranging from 52.8% to 70.9%. Unless the yeast was highly flocculated, these porosities are probably erroneously high by a factor of two. This error arose from determining the solids content after drying and not taking into account the water lost by the yeast during drying. Had they compared their resistances with the Kozeny-Carman correlation, they would have found that the measured resistances were an order of magnitude higher than would be expected for yeast-sized particles, even assuming a porosity of 25-35%. (Note: the focus of the Rushton and Khoo study was (1) to determine the feasibility of using pressure for deliquoring yeast and (2) to predict the output of a rotary vacuum filter for processing yeast. They made no attempt to compare their measured resistances with porous media theory.)

In a more recent stagnant filtration study, Nakanishi et al. (1987) measured and modeled the effect of filter aid on the specific resistance of well-rinsed bakers yeast and other microorganisms. Their measured resistances were significantly lower than Rushton and Khoo's values; the authors were apparently unaware of the previous study and therefore did not discuss possible reasons for the discrepancy. Nakanishi et al. assumed that the Kozeny-Carman correlation held true, and calculated a yeast cake porosity of 40%, but did not attempt to determine the porosity independently. We have studied the resistance of both rinsed and

unrinsed yeast to determine why the results of Nakanishi et al. differed so significantly from the results of Rushton and Khoo. Our use of centrifugation experiments to determine porosity as a function of compressive pressure allows direct comparison with the Kozeny-Carman correlation. Our empirically-determined hydraulic resistance will be incorporated in a subsesquent cross-flow filtration model. (See Chapter 6.)

C. TERMINOLOGY

As was mentioned in the introduction, the hydraulic resistance offered by a porous medium such as a bed of particles depends on its porosity. Unfortunately, the terminology used to differentiate among distinct types of porosity changes in porous media is not uniform throughout the literature. The follow definitions were set down in the chemical engineering literature by Heertjes in 1964. Compression of a porous medium is a reversible process in which the porosity (and therefore the permeability) is reduced without relative displacement of particles in the medium. A compressed medium will swell when the flow through it stops. Compression is particularly important in porous media comprised of highly deformable particles. Consolidation, or compaction, is an irreversible process in which particles are rearranged to a more compact and less permeable configuration. Porous media made up of rigid particles are often significantly affected by consolidation, especially under high pressure.

Other uses of the terms compression and consolidation should be noted. Geologists use the term "consolidation" to describe a cementing together of grains in sedimentary rock. Such a process will not be discussed here. Some authors have used the term "compressible" to describe any porous medium which undergoes changes in porosity, for example, to describe a loose cake composed of flocculated rigid particles. Such a cake undergoes dramatic compaction, but no compression as defined above. Adoption of the adjective form "compactable" would avoid corruption of the above definitions. Occasionally the term "compressible" has been used to describe particles which change shape under pressure: to avoid confusion here we will employ the adjective "deformable" to describe an individual particle which is not rigid.

D. MATERIALS AND METHODS

1. Preparation of Yeast and Latex Particle Suspensions

All Saccharomyces cerevisiae suspensions were prepared from commercially available active dry yeast (ADY, Red Star Yeast Co., Randolph, MA). The 8% (wt/wt) moisture content of ADY previously reported by Thorn and Reed (1959) was verified by weighing before and after drying for 24 hours in a 100°C oven. Yeast "medium" (Wickerham, 1951) without a carbon source or vitamins was prepared according to the recipe in Table I. The osmotic pressure P_{osm} of the medium can be calculated from the total normality N_{tot} using the Van't Hoff equation (Sandler, 1979):

$$P_{osm} = N_{tot} R T \quad (1)$$

where R is the gas constant (0.08205 atm/mol°K) and T is the absolute temperature (295°K at RT). Using the value for N_{tot} given in Table I, we find P_{osm} = 13.8 atm.

A measured weight of ADY was placed in a flask containing approximately two-thirds of the desired final volume and stirred for about half an hour. Then the suspension was transferred to a volumetric flask or a graduated cylinder, filled to the desired volume with additional media, and stirred for the remainder of an hour. Sodium azide (0.1%) was added to yeast media and suspensions to prevent the bacterial growth which was seen in initial experiments without the preservative. Both the yeast media and the deionized water used in hydraulic resistance experiments were filtered sequentially through 8.0 μm and 0.45 μm membranes prior to use.

Samples used immediately after the one-hour stirring period will be referred to as "unrinsed freshly-rehydrated." Some samples were rinsed one or more times by spinning in a centrifuge (International Equipment Corporation Model PR-6) for one min at 2000 RPM (918 x g), decanting the supernatant liquid, and reconstituting with fresh media. These samples will be referred to as "nx-rinsed," where n is the number of rinsings.

Suspensions of glutaraldehyde-hardened yeast were prepared according to the procedure of Ju and Ho (1987). After the one-hour rehydration period, 100 ml of freshly-prepared yeast suspension was added to one liter of 3% (wt/vol) glutaraldehyde in distilled water and stirred for one hour at room temperature. The hardened yeast was then rinsed

Table I. Composition of Yeast Medium.

Species*	Concentration (g/L)	Molarity (M)	# of Ions**	Normality (N)
$(NH_4)_2SO_4$	17.8	0.135	3	0.405
KH_2PO_4	5.7	0.042	2.5	0.105
$MgSO_4$	1.2	0.010	2	0.020
$Na_3C_6H_5O_7$	0.5	0.002	4	0.008
$CaCl_2$	0.15	0.001	3	0.003
NaN_3	1.0	0.016	2	0.031
			total	0.572

* The first five species are the principal salts in the Wickerham yeast medium, as defined in USDA Technical Bulletin #1029 (1951). The complete medium contained trace amounts (<1 mg/L) of several other salts and varying amounts of several vitamins. The original recommended glucose concentration was 10 g/L (0.056 M); more recently glucose concentrations as high as 60 g/L (0.33 M) have been recommended. To avoid cell growth, no carbon source was used in our experiments. We added NaN_3 to avoid bacterial growth in long-term experiments.

** At pH 7; determined from pK_a's given in Butler (1964).

three times and resuspended in glucose-free yeast media. Ju and Ho found that the effect of the glutaraldehyde on the density and volume of yeast cells was insignificant. The presence of a cell wall is probably the reason why the yeast cells do not suffer from the glutaraldehyde-induced shrinkage which is common to animal cells.

Throughout this paper, the yeast concentration will be expressed as a volume fraction rather than as a dry weight per unit volume. The conversion of dry weights to volume fraction has reportedly been a source of error in literature on the concentration dependence of yeast viscosity (Reuss, 1979). Figure 4-1, an electron micrograph of a dried wine yeast cell (Bekers et al., 1979), graphically demonstrates one complicating factor--the volume shrinkage which occurs during drying. Reuss et al. (1979) developed a dye dilution technique with which they determined volume fraction vs. dry weight at several osmotic pressures. However, the dye which they used, Naphthol Green-B, has a molecular weight of 978, which is small enough to pass through the cell wall (but not the cell membrane) into the periplasmic space of the yeast cells (Gerhardt and Judge, 1964). The periplasmic space reportedly comprises

between 11% (Conway and Downey, 1949) and 15% (Arnold and Lacy, 1977) of the total volume of the yeast cell. Assuming that Reuss' dye was entering into 13% of the total cell volume, only 87% of the true volume occupied by the cells was being measured, and the reported volume fractions must be divided by 0.87 to give the true volume fraction. Taking this into account, the appropriate conversion factor for the glucose-free media used here was 2.3% (vol cells/vol suspension) yeast per 1 g ADY/100 ml suspension. (Ju and Ho, 1988, recently used 500,000 molecular weight dextran as a marker and found that the conversion factor for yeast cells suspended in distilled water was 2.572 cm^3/g dry, which is not consistent with Reuss' value of 3.0 cm^3/g dry at zero osmotic pressure, or 3.45 cm^3/g dry after the correction to account for the periplasmic space. However, because Ju and Ho rehydrated the yeast in 1% glucose solution (of unreported salt concentration) for one hour, and then hardened the cells in glutaraldehyde solution before suspending them in distilled water for the volume fraction measurements, it is unclear what osmotic state the cells were in at the time of the volume fraction measurement.)

Reuss' results indicated that steady-state volume fractions of yeast were achieved three to four hours after switching from a medium of one osmotic pressure to a medium of another osmotic pressure. Unfortunately, this data was not available to us prior to completion of the experiments described here. The decision to use a one-hour rehydration period was based on an earlier reference on active dry yeast (Thorn and Reed, 1959) which called for only a two- to three-minute contact period for rehydration. Since some experiments may have been conducted while the yeast was still in the process of rehydration, this may be a source of error in our experiments.

Suspensions of 3.98 μm diameter polystyrene latex particles in distilled water with no additives (Batch # 2-83-8, concentration = 8.4% (vol/vol), surface charge = 1.7 sulfate groups per 2000 $Å^2$, density ρ_p = 1.05 g/cm^2) were purchased from Interfacial Dynamics Corporation (Portland, OR). The concentration of the initial suspension of latex particles (C_I) was verified by measuring the mass of an aliquot of the suspension before (m_{wet}) and after (m_{dry}) drying using a Mettler H64 Balance (Mettler Instrument Co., Hightstown, NJ):

$$C_I = \frac{m_{dry}/\rho_p}{m_{wet}/\rho_{susp}} \tag{2}$$

where the suspension density ρ_{susp} is given by:

$$\rho_{susp} = C_I \rho_p + (1-C_I) \rho_f \tag{3}$$

The initial suspension was diluted with filtered distilled water to achieve lower particle concentrations. The initial (before-dilution) total mass of the suspension, M_I, and the final (after-dilution) total mass M_F were used to calculate the final particle concentration C_F as precisely as possible. High particle concentrations were achieved by decanting liquid off after the particles had settled overnight. The initial and final volumes were determined by weighing the total mass of the suspension before and after decanting step. The final concentration of particles was calculated as follows:

$$V_I = \frac{M_I}{\rho_p C_I + \rho_f (1-C_I)} \tag{4}$$

$$V_F = V_I + \frac{(M_F - M_I)}{\rho_f} \tag{5}$$

$$C_F = \frac{M_F/V_F - \rho_f}{\rho_p - \rho_f} \tag{6}$$

2. Cell Size and Shape Measurements

A dilute suspension of yeast in medium which had been prepared the previous day was placed on a glass slide, covered with a coverslip, and observed with a Zeiss ICM-405 Microscope equipped with a 100X oil objective. An Image Technology Systems Model 2000 image analysis system was connected to the video camera port of the microscope. The system was calibrated with a stage micrometer; the resolution was 0.14 μm, which is the width corresponding to a single pixel on the video camera. Since only 5-10 measurable cells appeared in the field of view, the microscope slide was moved randomly between

measurements to allow analysis of a larger sample size. Out-of-focus, overlapping, and partially-in-view cells were manually excluded from the sample. Once a total of at least 100 cells were measured, statistics on the cell population were determined. The system calculated the mean and standard deviation of the length and breadth of the cells. The length, or major axis, was defined as the longest distance between two parallel tangents to the cell surface; the breadth was defined as the longest distance between two tangents drawn parallel to the major axis.

3. Carbon Dioxide Evolution Measurements

Stock yeast suspensions of approximately 10% volume fraction were prepared from active dry yeast and pre-filtered glucose-free media as described above. Aliquots of 5 ml yeast suspension were drawn into sterile disposable 20-ml syringes, and the needle ports were tightly capped. The syringes were held vertically in racks which allowed free motion of the upwardly-facing plungers. At periodic intervals the total volume of suspension plus CO_2 produced was measured by recording the position of the plunger in the calibrated syringe. The volume of CO_2 was taken as the total volume minus the initial fluid volume.

4. Centrifugal Cell Packing Measurements

Suspensions of various concentrations of unrinsed freshly-rehydrated yeast were prepared as described above. Wintrobe hematocrit tubes were filled with yeast suspensions and spun at rotation rates of 1000 and 2000 RPM (230-918 × g) at 4°C in an International Equipment Corporation Model PR-6 centrifuge. The maximum initial concentration of cells used was 45% by volume because more concentrated suspensions produced carbon dioxide bubbles which interfered with height measurements. The centrifugation time was one hour except in time-dependent experiments during which samples were inspected at various times. The heights of the packed cells and total liquid column were recorded. Average packing densities in the cell columns were determined by dividing the true volume fraction (calculated from the dry weight) by the ratio of packed cell height to liquid height. These experiments were repeated with glutaraldehyde-hardened yeast.

Similar experiments were performed with suspensions of the 3.98 μm diameter latex particles. Because the latex particles are less dense than yeast, it was necessary to run a set of experiments at 3000 RPM (2070 × g) in order to achieve compressive pressures comparable to those with yeast at 2000 RPM.

5. Stagnant Filtration Experiments

The filtration assembly used to measure the yeast hydraulic resistance is shown in Figure 4-2. Polycarbonate track-etched membranes (Nuclepore Corp., Pleasanton, CA) were cut to fit the 47 mm diameter filter support (Nuclepore Corp.), which had an effective filtration area of 13.2 cm^2. The membranes used for the latex particle experiments had a rated pore diameter of 2.0 μm and a rated pore density of 2 x 10^6 pores/cm^2, while those used in the yeast experiments had a rated pore diameter of 1.0 μm and a rated pore density of 2 x 10^7 pores/cm^2. The cylindrical reservoir which screwed onto the filter support was filled with liquid and then closed with a one-holed number-10 rubber stopper with a glass tubing insert. A separation funnel on a ringstand served as a movable inlet reservoir. Tygon tubing was used to connect the inlet reservoir to the top of the filter assembly.

Prior to the yeast experiments, the membrane resistance was determined by measuring the flow of prefiltered (0.45 μm) media through the membrane as a function of applied pressure. The pressure was varied by adjusting the height of the inlet reservoir (1 cm water = 0.7355 mmHg). The filtration rate was measured by timed collection in graduated cylinders. For latex particle experiments, the membrane resistance was measured with prefiltered (0.45 μm) deionized water rather than with media.

To measure the yeast resistance, the inlet reservoir was temporarily disconnected while a small amount (< 1 ml) of a 3.2% (v/v) stock yeast suspension was added. The amount required was estimated based on the results of the yeast centrifugation experiments. After brief stirring, the yeast was allowed to settle overnight with the filtrate outlet closed. (The long settling time made use of the preservative essential.) The inlet reservoir was carefully reconnected to avoid disturbing the yeast cake. The sum of the membrane and yeast cake resistances was measured as before, by varying the applied pressure and measuring the flow rate. Then another volume of yeast was added, the contents of the reservoir was stirred, and

the entire process repeated. After the last resistance measurement, most of the water was decanted out of the funnel reservoir, and the remainder was removed by applying a slight vacuum to the filtrate side. Finally, the still-wet yeast cake was measured with a micrometer to verify the cake height which had been estimated from the initial yeast concentration. (The micrometer spindle was tightened in increments of 0.00025 in, 6 μm, and the smallest height at which no impression of the spindle was left on the yeast cake was recorded.) The measured cake heights were 102±6.0 μm, 198±6.0 μm, and 401±6.0 μm, respectively, for the experiments with 100, 200, and 400 μm estimated yeast cake heights.

E. DATA ANALYSIS

1. Defining Permeability and Hydraulic Resistance: Darcy's Law

The layer of cells which forms at a membrane surface is an example of a porous medium. A porous medium offers resistance to flow of a continuous fluid phase through the dispersed solid phase. Flow through porous media is generally described in terms of a permeability k which is defined by

Darcy's law:

$$V = -\frac{k}{\mu}\frac{dP}{dy} \tag{7}$$

where V is the superficial filtration velocity, or filtrate flux, μ is the fluid viscosity, and dP/dy is the pressure gradient. (Darcy's law is simply a differential representation of D'Arcy's observations of flow through beds of sand which were published over a hundred years ago; Darcy, 1856.) The permeability is a function of the microscopic details of a particular porous medium, and may vary with pressure and with time.

Several attempts have been made to derive Darcy's law from first principles (Slattery, 1969; Whitaker, 1973; and Willis and Tosun, 1980). These approaches lead to an expression for the permeability in terms of parameters which are difficult to measure experimentally. Another approach to flow in porous media is geometric modeling, in which one postulates a geometry thought to bear some resemblance to the actual porous media yet sufficiently simple to allow the governing equations of motion to be solved analytically (e.g. parallel capillaries--

Kozeny, 1927; skewed capillaries--Scheidegger, 1974; serial-parallel-type capillaries--Dullien, 1975; spatially periodic array--Happel and Brenner, 1973). The Kozeny-Carman equation, a geometric model slightly modified by experimental observations (Carman, 1937), is the most commonly used model for the permeability. The Kozeny-Carman (K-C) equation for the permeability of a bed of particles is:

$$k = \frac{1}{c_k S_0^2} \frac{\epsilon^3}{(1-\epsilon)^2} \qquad (8)$$

where S_0 is the surface-to-volume ratio of the particles and ϵ is the void fraction of the bed. S_0 is calculated using the gross particle dimensions and does not depend on the roughness of the surface. The constant c_k has been shown to range between four and five for a wide variety of experimental systems (Bird et al., 1960, p. 199), and here will be taken to be 5.0, the value suggested by Kozeny. According to Scheidegger (1960), "Kozeny himself (1927b), in an attempt to substantiate his formula experimentally, found discrepancies between calculated and measured surface areas of -69 to +86 percent." Therefore the value of c_k determined in any particular experiment might actually lie somewhere between two and ten. The surface roughness does not affect the K-C equation because it contains no inertial term. (The Modified Ergun equation, a generalized form of the K-C equation, contains both a viscous and an inertial term, and depends on surface roughness under "turbulent" conditions.) The K-C equation provides a relatively good correlation for a wide variety of porous media (Macdonald et al., 1979), but has not been evaluated for yeast or other microbial cell beds.

2. Measuring Hydraulic Resistance vs. Compressive Pressure

The permeability of a particle bed of known thickness can be determined by measuring the filtrate flux of pure solvent through a stagnant bed as a function of applied pressure. Because the particle bed acts in series with the membrane on which it is laid down, the total resistance to flow is the sum of the particle bed resistance and the membrane resistance. The particle bed resistance is inversely related to its permeability: $R_c = k^{-1}$. Note that R_c is a depth-specific resistance which must be multiplied by the bed height to

have the same units as a membrane resistance R_m. The hydraulic permeability L_p of a porous medium is defined as the flux divided by the pressure drop across the medium:

$$L_p = \frac{J}{\Delta P} = \frac{J}{P_{appl} - P_{atm}} \tag{9}$$

where P_{appl} is the applied pressure at the upstream side of the porous medium and P_{atm} is the atmospheric pressure at the downstream side of the porous medium. In all of the experiments described below, $P_{atm} = 0$ and $\Delta P = P_{appl}$. The hydraulic permeability L_p of the cell + membrane system is given by:

$$L_p = \frac{1}{\mu_f \, (R_m + R_c \delta)} \tag{10}$$

where δ is the thickness of the particle bed.

If a fraction ϕ of the membrane pores are blocked, the effective membrane resistance $R_{m,eff}$ must be used in place of the intrinsic membrane resistance R_m. $R_{m,eff}$ is given by:

$$R_{m,eff} = R_m / (1-\phi) \tag{11}$$

An upper bound estimate for ϕ is the concentration of cells at the membrane surface. We will calculate the cell resistance R_c for the limiting cases $\phi=0$ and $\phi=C_w$.

The flux through stagnant cell beds will be measured as a function of the applied pressure P. The data will be fit by an equation of the form:

$$J = c_1 P + c_2 \left(1 - \frac{1}{1 + c_3 P} \right) \tag{12}$$

The hydraulic resistance is calculated by rearranging Equation (9), (10) as follows:

$$R_c = \frac{\frac{1}{\mu_f L_p} - R_{m,eff}}{\delta} \tag{13}$$

The hydraulic permeability L_p may be calculated by differentiating the curve fit for the flux (Equation (12)) with respect to pressure:

$$L_p = \frac{dJ}{dP} = c_1 + \frac{c_2 c_3}{(1 + c_3 P)^2} \tag{14}$$

The hydraulic permeability calculated from this expression approaches the limit $L_p = c_1 + c_2c_3$ as P -> 0 and the limit $L_p = c_1$ as P -> ∞.

In order to convert the resistance versus applied pressure data to an expression for resistance as a function of porosity which can be compared with the Kozeny-Carman correlation, it is necessary to relate the average compressive pressure in the cell bed to the applied pressure. We will define the compressive pressure by constructing force balances on the fluid and solid phases. This analysis is patterned after Zydney et al. (1988).

Since the yeast is a non-homogeneous porous medium on the scale of a yeast cell, the force balance will be constructed on a differential element of the cell bed whose cross-sectional area is large compared to the size of a cell. At equilibrium, the sum of the pressure, gravitational, and interfacial forces on both cells and fluid within this differential element must be zero. The wall forces, which act via contact with cells and fluid near the walls, are negligible since the ratio of cell to bed diameter in our system is only 10^{-4} (Cohen and Metzner, 1981). The differential force balances in the y direction can be expressed as:

$$\text{fluid:} \quad \frac{d}{dz}(PA_f) + \frac{d}{dz}(F_{fs}) + \rho_f\, g\, A_f = 0 \tag{15}$$

$$\text{solid:} \quad \frac{d}{dz}(P_pA_p) + \frac{d}{dz}(F_{sf}) + \rho_p\, g\, A_p = 0 \tag{16}$$

where P and P_p are the fluid and particle pressures (force/area), respectively, A_f and A_p the cross-sectional areas, ρ_f and ρ_p the densities, and g the acceleration due to gravity. F_{sf} is the y component of the shear and pressure forces exerted on the solid by the flowing fluid along the fluid-solid interface. Since the interface is in equilibrium, the interfacial force exerted on the fluid by the solids (F_{fs}) must be balanced by F_{sf}, i.e.

$$F_{fs} = F_{sf} \tag{17}$$

Combination of Equations (15), (16), and (17) gives, upon rearrangement:

$$\frac{d}{dz}(P_pA_p) = -\frac{d}{dz}(PA_f) + \rho_p\, g\, A_p + \rho_f\, g\, A_f \tag{18}$$

The hydrostatic pressure difference between the cell interior and surrounding fluid causes surface stresses which can lead to conformational changes (deformation) in the cells if they are deformable. We will use the nomenclature of Zydney et al. (1988), who defined the compressive pressure π in terms of this pressure difference as:

$$A\,\pi = A_p\,(P_p - P) \tag{19}$$

The total cross-sectional area (A) appears in the left hand side of the definition for π because the compressive pressure is a characteristic of the solid-fluid matrix, i.e. it is a property of the particular porous medium and not a property of the solids alone. Other definitions for π are possible (Willis and Tosun, 1980), and there is no inherent advantage to any of these as long as one is consistent throughout the subsequent analysis.

Substitution of Equation (19) into (18) yields:

$$\frac{d\pi}{dz} = \frac{dP}{dz} + \rho_p\, g\, (1-\epsilon) + \rho_f\, g\, \epsilon \tag{20}$$

where the cross-sectional area occupied by cells, averaged over a region which is large compared to a single cell, is $A_p = A(1-\epsilon)$, while that occupied by the fluid is $A_f = A\epsilon$. In our filtration system the gravitational effects are negligible, thus the gradient in compressive pressure is simply the negative of the gradient in fluid pressure, a result derived previously using heuristic arguments (Tiller, 1953; McCabe and Smith, 1976). For a given porous medium, the permeability and porosity are unique functions of π (McCabe and Smith, 1976).

Equation (20) describes the solid mechanics in the cell bed. In order to complete the description of the filtration problem, a fluid momentum balance is required:

$$J = -\frac{k}{\mu}\frac{d}{dy}(P - \rho_f\, g\, y) \tag{21}$$

where J is the flux, or the superficial filtration velocity, in Zydney's nomenclature. This is Darcy's law, Equation (7), rewritten to include a gravitational term, which is negligible for the stagnant filtration system itself, but is important in the centrifugal system used to determine the porosity as a function of compressive pressure.

The compressive pressure is zero at the top of the cell bed, and increases with distance from the top of the bed. The compressive pressure at a distance z from the top of the bed is

equal to the cumulative pressure drop from the top of the bed to that point. If the porosity of the cell bed were perfectly uniform, then the resistance of the bed would be constant with z, and the compressive pressure would increase linearly with z. Then the average compressive pressure would equal one half the total pressure drop across the bed. If the membrane resistance were small compared to the resistance of the cell bed, the pressure drop across the bed would equal the applied pressure, and the average compressive pressure would be one half of the applied pressure. To compare the relative magnitude of R_c and R_m, one can assume that the yeast cells behave as rigid spheres with a diameter of 6 μm ($S_0 = 1 \times 10^4$ cm^{-1}), and that they are pack in a hexagonal close-packed arrangement with a void fraction $\epsilon = 0.27$. The resulting resistance calculated from the Kozeny-Carman equation is $R_c = 1.4 \times 10^{10}$ cm^{-2}. The total resistance of a 200 μm layer is then $R_c\,\delta = 2.8 \times 10^8$ cm^{-1}, which is an order of magnitude greater than the membrane resistance $R_m = 1.65 \times 10^7$ cm^{-1} specified by the manufacturer of the membranes used in the yeast resistance measurements. Since any deviation from rigid-sphere behavior will lead to an even higher yeast cake resistance, the assumption that the pressure drop across the bed is equal to the applied pressure is valid.

We will assume that the yeast and latex particles are rigid enough that we can approximate the average compressive pressure in the stagnant filtration experiments as one-half the applied pressure:

$$\pi_{avg} = P_{appl}/2 \qquad (22)$$

We will verify this assumption in the discussion section below.

3. Measuring Porosity vs. Compressive Pressure

In order to compare the measured resistance with the Kozeny-Carman correlation, the data must be expressed as a function of porosity. In this study, the dependence of porosity on compressive pressure was determined by studying the packing of particle beds in a centrifuge.

The compressive pressure in centrifuged cell beds arises from the effective centrifugal acceleration $\omega^2 R$, where ω is the rotational velocity of the centrifuge and R is the local radius. The hydrostatic fluid pressure drop in the centrifuge tube can be evaluated from Equation (21) with J=0:

$$\frac{dP}{dz} = \rho_f g \tag{23}$$

The compressive pressure can be evaluated from Equation (20) as:

$$\pi(z) = \int_0^z (\rho_p - \rho_f)\, \omega^2 R\, (1-\epsilon)\, dz \tag{24}$$

where the effective acceleration is $\omega^2 R$ rather than the gravitatioal acceleration g. R varies with the distance z from the top of the cell column:

$$R = R_0 - L + z \tag{25}$$

where R_0 is the total radial arm length of the centrifuge (20.7 cm in our system), and L is the total length of the cell column.

Since no porous medium is truly incompressible, the variation in compressive pressure along the length of the column results in local porosity variation. However, with rigid unflocculated particles, the extent of this porosity variation is expected to be much smaller than that seen with deformable particles. Centrifugation experiments yield the average porosity in the cell column, which is given by:

$$\epsilon_{avg} = \frac{1}{L} \int_0^L \epsilon\, dz \tag{26}$$

We will assume that the average porosity in the cell column can be characterized as a function of the average compressive pressure in the column. The average compressive pressure is calculated by integrating the centrifugal force on the entire cell column:

$$\pi_{avg} = \frac{1}{L} \int_0^L \pi\, dz \tag{27}$$

If the void fraction varies significantly with compressive pressure, it will be necessary to assume a functional form of ϵ vs π, carry out the integration above, and fit the centrifugal ϵ_{avg}-vs-π_{avg} data to determine the parameters in the ϵ vs π expression. (See Zydney et al., 1988, for the results of carrying out this procedure for highly deformable blood cells.) However, if the void fraction is relatively constant, as might be expected with rigid cells, one can carry out the integration of Equation (27) for constant ϵ_{avg} and calculate π_{avg} directly from measured ϵ_{avg} and L data:

$$\text{constant } \epsilon_{avg}: \quad \pi_{avg} = \Delta\rho\ \omega^2\ (1 - \epsilon_{avg}) \left\{ \frac{R_0 L}{2} - \frac{L^2}{3} \right\} \tag{28}$$

We will verify the assumption that Equation (28) is valid for determining the compressive pressure in the centrifugation experiments in the discussion section.

In order to obtain an expression for ϵ_{avg} vs. π_{avg}, we will assume a functional form similar to that suggested by Verhoff and Furjanic (1983):

$$\epsilon_{avg} = \epsilon_\infty + \frac{\epsilon_0}{1 + a\,\pi_{avg}} \tag{29}$$

and determine the parameters ϵ_∞, ϵ_0, and a using commercially-available software (RS/1, Bolt, Beranek, and Newman Software Product Co., Cambridge, MA) which performs a least-squares fit of the experimental data using a non-linear regression technique. We include the ϵ_∞ term (not present in Verhoff and Furjanic's equation) because the yeast and latex particles are fairly rigid and therefore will have a non-zero porosity even at high pressure.

4. Measuring Hydraulic Resistance vs. Compressive Pressure

The results of the stagnant filtration and centrifugation experiments can be combined to a single expression for the hydraulic resistance as a function of the average compressive pressure. Equation (29) can be rearranged to give the average compressive pressure π_{avg} in terms of the average porosity ϵ_{avg}:

$$\pi_{avg} = \frac{1}{a} \left\{ \frac{\epsilon_0}{\epsilon_{avg} - \epsilon_\infty} - 1 \right\} \tag{30}$$

Combining Equations (13), (14), (22), and (30), we get the following equation which may be solved for R_c as a function of ϵ_{avg}:

$$\mu\ (R_c \delta + R_{m,eff}) = \left\{ c_1 + \frac{c_2\ c_3}{\left\{ 1 + \frac{2c_3}{a} \left[\frac{\epsilon_o}{\epsilon_{avg} - \epsilon_\infty} - 1 \right] \right\}^2} \right\}^{-1} \qquad (31)$$

This complicated equation, with its six constants c_1, c_2, c_3, a, ϵ_{avg}, and ϵ_∞ yet to be determined from experimental data, cannot immediately be compared with other correlations. However, a graphical representation of our results along with the Kozeny-Carman equation (Equation (8)) will allow easy comparison of the two equations for resistance as a function of porosity.

Some data in the literature reports resistance data in terms of a compressibility index, n, defined as follows:

$$R_c \propto P^n \quad \text{or,} \quad \log R_c = n \log P + \text{constant} \qquad (32)$$

We will calculate the compressibility index from measured resistance-vs-pressure data and compare the results with previously reported values of n.

F. RESULTS

1. Cell Size and Shape Measurements

Minimum, maximum, and mean (± standard deviation) values for the length, breadth, and specific surface area of the yeast cells are given in Table II below. The resolution of the length measurements was 0.14 μm. The specific surface area S_o of each yeast cell was calculated from the following equation for the specific surface area of a prolate ellipsoid (Beyer, 1978):

$$S_o = 1.5 \left(\frac{1}{r_1} + \frac{\sin^{-1} e}{r_2\ e} \right) \qquad (33)$$

where the eccentricity e is given by:

$$e = \frac{\sqrt{r_1^2 - r_2^2}}{r_1} \qquad (34)$$

Table II. Yeast Cell Size Determined by Image Analysis

	Length (μm)	Breadth (μm)	Specific Surface Area (cm^{-1})
Minimum	5.1	3.3	7.48×10^3
Maximum	8.8	7.7	1.62×10^4
Mean	7.0	5.4	1.24×10^4
Standard Deviation	± 0.9	± 1.0	$\pm 1.63 \times 10^3$

where r_1 and r_2 are the major and minor radii, respectively. The equivalent diameter of a sphere with the same specific surface area of each yeast cell was calculated as follows:

$$D_{equiv} = 6/S_o \tag{35}$$

The calculated values of D_{equiv} are plotted as a histogram in Figure 4-3. The surface to volume ratio of a bed of yeast cells is given by the sum of the surface areas of each cell divided by the sum of the the volumes of the yeast cells. Again, assuming the yeast cells can be modeled as prolate ellipsoids (using surface area and volume formulas from Beyer, 1978), we have:

$$S_{o,bed} = \frac{\sum \left(n_i \, r_{2,i}^2 + \frac{r_{1,i} \, r_{2,i}}{e_i} \sin^{-1} e_i \right)}{\sum n_i \, r_{1,i} \, r_{2,i}^2} \tag{36}$$

The resulting specific surface area calculated for the above distribution of yeast cells was $S_{o,bed} = 9.61 \times 10^3$ cm^{-1}. This value will be used below in the calculation of yeast and particle cake resistances from the Kozeny-Carman equation.

2. Carbon Dioxide Evolution Measurements

The results of the carbon dioxide evolution measurements are summarized in Table III below. At 4°C, no measurable volume of CO_2 evolved. At RT, the volume of CO_2 which evolved in 16 hours from unrinsed freshly-rehydrated yeast was 24.0 times the volume

occupied by the cells. A single rinsing reduced the volume evolved to 7.0 times the cell volume, and two successive rinsings reduced the volume to 2.7 times the cell volume. After three rinsings, no measurable volume of CO_2 evolved.

Addition of 1% glucose to 3x-rinsed yeast resulted in an evolution volume of 23.6 times the cell volume, indicating that the rinsing had eliminated CO_2 production by removing a residual carbon source from the ADY. Addition of 0.1% glucose produced an evolution volume of 6.4 times the cell volume, which is approximately the same as was obtained from 1x-rinsed yeast. Addition of 1.0% glucose to unrinsed yeast resulted in a CO_2 evolution volume of 25.0 times the cell volume, which is only slightly greater than was obtained from the freshly-rehydrated unrinsed yeast.

Glutaraldehyde-hardened yeast produced no CO_2.

Table III. Carbon Dioxide Evolution from Yeast.

Exptl. Conditions	Temperature	Volume Gas/ml Cells
Freshly-rehydrated	20	24.0
(no added glucose)	4	0
Fresh + 1% glucose	20	25.0
Rinsed 1X	20	7.0
Rinsed 2X	20	2.7
Rinsed 3X	20	0
Rinsed 3X + 1% glucose	20	23.6
Rinsed 3X + 0.1% glucose	20	6.4
Glutaraldehyde-hardened	20	0

3. Centrifugal Cell Packing Measurements

The results of the centrifugation experiments are shown in Figures 4-4 through 4-10. The porosities for several reference packing arrangements of rigid spheres are shown for comparison: 48% for face-centered cubic, 33% for random close-packed, and 27% for rhombohedral, or hexagonal close-packed (Martin et al., 1951).

a. Latex Particles

Figure 4-4 shows the steady-state porosity of latex particles as a function of column height and rotation rate. No time-dependent data is shown because at times less than 10 min the particles had not settled enough to distinguish the top of the particle bed and at times greater than 10 minutes no change in porosity was seen. (Time-dependent data will be shown for the more dense yeast cells.)

Under gravity alone, the latex particles settled to an average porosity of about 39%. The average porosity of the latex particle columns was between 36% and 39% after centrifugation at 1000 RPM. The porosity decreased slightly as the cell column height was raised from 0.5 to 6.5 cm, which corresponds to an average compressive pressure of 3 to 35 mmHg. After centrifugation at 2000 RPM, with average compressive pressures of 13 to 143 mmHg, the porosities ranged from 39% down to 32%. Centrifugation at 3000 RPM, with average compressive pressures of 54 to 278 mmHg, resulted in porosities ranging from 36% down to 31%. (Average compressive pressures were determined using Equation (28).) The data for all three experiments is plotted versus compressive pressure in Figure 4-5. The constants for the curve fit (Equation (29)) shown along with the data are listed in Table IV below.

b. Yeast and Glutaraldehyde-Hardened Yeast

The time dependence of the packing of 4.8 cm yeast cell columns is shown in Figure 4-6. This data is representative of that seen at other cell column heights and centrifugation speeds. However, as the centrifugation speed (and hence the compressive pressure) increased, both the time required to reach steady state and the final porosity value decreased. In all experiments, the porosity after one hour was approximately constant.

The length-averaged porosity of columns of freshly-rehydrated bakers yeast after one hour centrifugation at 4°C is plotted as a function of bed height and rotation rate in Figure 4-7. Under gravity alone, the yeast settled to a porosity of 42%, which corresponds to a loose packing, roughly halfway between a face-centered cubic packing and a random close packing. The porosity decreased with both increasing column height and increasing centrifugation rate. At 1000 RPM, average compressive pressures of 11 to 67 mmHg resulted in porosities from 31% down to 24%. At 2000 RPM, average compressive pressures of 31 to 260 mmHg resulted in porosities from 28% down to 22%.

Porosity data from these two experiments is plotted as a function of compressive pressure in Figure 4-8. Note that given values of the centrifugation rate and the packed column height, the compressive pressure with yeast cells is twice as high as that with latex particles because of the difference in densities. (Specific gravities are 1.14 for yeast at 14 atm (Reuss, 1979) and 1.05 for polystyrene (manufacturer's literature). These experiments were repeated with glutaraldehyde-hardened yeast at RT: the resulting length-averaged porosity is plotted as a function of bed height and rotation rate in Figure 4-9 and as a function of compressive pressure in Figure 4-10. The data from Figures 5, 8, and 10 are replotted together in Figure 4-11. At 1000 RPM, average compressive pressures of 10 to 68 mmHg resulted in porosities from 33% down to 29%. At 2000 RPM, average compressive pressures of 41 to 269 mmHg resulted in porosities from 30% down to 27%. The curve fit (Equation (29)) constants for both the yeast and the glutaraldehyde-hardened yeast are given in Table IV below.

Table IV. Curve Fit Constants for Porosity-vs.-Compressive Pressure

Particle or Cell Suspension	ϵ_∞(%)	ϵ_o(%)	a ($mmHg^{-1}$)
3.98 μm latex particles at RT	26.7±1.1	12.9±0.9	0.0091±0.002
freshly-rehydrated yeast at 4°C	20.8±0.5	21.0±0.9	0.074±0.010
glutaraldehyde-hardened yeast at RT	26.3±0.3	14.5±0.6	0.075±0.009

4. Stagnant Filtration Experiments

a. Latex Particles

Data for the measurement of the hydraulic resistance of the latex particles is shown in Figure 4-12. The measured membrane resistance in this experiment was 9.9×10^7 cm^{-1}. In order to achieve steady-state compaction prior to measuring the resistance, this data was taken in order of decreasing pressure. The flux was linearly proportional to the applied pressure, as

is expected for an incompressible bed of rigid particles which is undergoing no further compaction. (Had these experiments been performed in order of increasing pressure, one would expect to see curvature in this data because the extent of compaction would increase with pressure as was seen in the centrifugation data.) The hydraulic resistance calculated from Equation (13), with L_p set equal to the slope of the data (and $\phi = 0$ since the particles are rigid spheres), was 1.5 x 10^{10} cm^{-2} for the 85 μm layer and 1.7 x 10^{10} cm^{-2} for the 180 μm layer. This is within a factor of two of the K-C prediction of 9.8 x 10^9 cm^{-2} for 3.98 μm rigid spheres packed to a volume fraction of 64% (porosity determined from centrifugation).

b. Yeast and Glutaraldehyde-Hardened Yeast

The resistance of the membranes used in the yeast experiments was 4.0 x 10^7 cm^{-1}. The flux of pre-filtered media through 100, 200, and 400 μm beds of freshly-rehydrated yeast at RT is plotted as a function of applied pressure in Figure 4-13. The 100 μm data is repeated in Figure 4-14, where similar data for an experiment with 1% added glucose in the yeast suspension and the media is shown. Flux through 200 and 400 μm layers of freshly-rehydrated yeast at 4°C is shown in Figure 4-15. Each set of experiments was conducted in order of decreasing pressure, after approximately one-hour filtration at the highest pressure. Approximately 5-10 min elapsed during the triplicate measurements at each pressure.

After the data from initial runs with freshly-rehydrated yeast displayed curvature with respect to applied pressure, the occurrence of hysteresis phenomena was tested by performing a series of flux experiments on a single bed. The flux was measured as the pressure was increased, then held steady at the high value, then decreased back to zero, and finally increased again. Figure 4-16 shows the up, down, and up-again phases observed with the 100 μm data from Figure 4-13. Hysteresis is seen in the first two series of data. Figure 4-17 shows that while the pressure was held at 75 mmHg, the flux decreased about 22% in 70 min; the rate of flux dropoff decreased with time. No hysteresis is seen in the third data series in Figure 4-16 (pressure up again). Figure 4-18 shows that the hysteresis seen in 200 μm data as the pressure was raised and then lowered was similar to that seen in the 100 μm data.

Flux through 200 and 400 μm layers of 3x-rinsed yeast at RT is shown in Figure 4-19, while similar data for 200 and 400 μm layers of glutaraldehyde-hardened yeast at RT is shown in Figure 4-20.

For each set of data, the constants c_1, c_2, and c_3 in Equation (12) were determined using commercially-available software (RS/1, Bolt, Beranek, and Newman Software Product Co., Cambridge, MA) which performs a least-squares fit of the experimental data using a non-linear regression technique. Resulting curve fits are shown on each graph, and the constants are listed in Table V below.

Table V. Curve Fit Constants for Flux-vs.-Pressure Data

Experimental Conditions	Cell Bed Height	c_1	c_2	c_3
freshly-rehydrated, RT, no glucose added	100	0.0014±0.0002	0.32±0.02	0.047±0.004
	200	0.00068±0.00006	0.148±0.008	0.048±0.004
	400	0.00039±0.00005	0.071±0.006	0.063±0.008
freshly-rehydrated, RT, 1% glucose added	100	0.0020±0.0002	0.17±0.02	0.13±0.02
freshly-rehydrated, cold (4°C)	200	0.0041±0.0009	0.44±0.14	0.034±0.012
	400	0.0019±0.0003	0.10±0.03	0.12±0.07
3X-rinsed, RT	200	0.0043±0.0014	0.51±0.24	0.025±0.011
	400	0.0032±0.0003	0.19±0.04	0.040±0.011
glutaraldehyde-hardened	200	0.0143±0.0005	0.25±0.05	0.073±0.027
	400	0.0075±0.0010	0.11±0.09	0.11±0.2
latex particles	85	0.0353±0.0007		
	400	0.020 ± 0.001		

The resistances calculated using Equation (31) with $\phi = 0$ ($R_{m,eff} = R_m$) are plotted as a function of applied pressure in Figure 4-21 through Figure 4-23 on a semi-logarithmic scale and in Figure 4-24 through Figure 4-26 on a log-log scale . (Results obtained assuming the maximum pore blockage, $\phi = C_w$, were at most 10% lower than the resistances calculated at $\phi = 0$, and are not shown.) The range of pressures plotted corresponds to the actual range of pressures over which the flux was measured; extrapolation of the curve fit data to the low and high pressure limits will be discussed below.

The resistance of unrinsed yeast at RT (10-40 x 10^{10} cm^{-2}) was about a factor of five greater than either the resistance of unrinsed yeast at 4°C or the resistance of 3x-rinsed yeast at RT, which were comparable (2-7 x 10^{10} cm^{-2}). The resistance of the glutaraldehyde-hardened yeast (2.0-2.5 x 10^{10} cm^{-2}) was roughly a factor of two smaller than the resistance of the rinsed or cold yeast.

In all experiments, the resistance increased with applied pressure. With glutaraldehyde-hardened yeast, the resistance increased only about 25% as the pressure was increased from 15 to 75 mmHg. With the rinsed yeast at RT and the unrinsed yeast at 4°, the resistance varied by a factor of about two as the pressure was increased from 7.5 mmHg to 75 mmHg. With the unrinsed yeast at RT, the resistance varied by a factor of about four over the same pressure range.

Values of the yeast resistance can be extrapolated to zero and infinite pressure using the limiting values of the hydraulic permeability given by Equation (14). These values can be compared to the predictions of the Kozeny-Carman equation calculated using the limiting values of the porosity given by (29). As can be seen in Table VI below, the resistances of cold and rinsed yeast calculated by extrapolation of the flux data to zero pressure are within a factor of two of the Kozeny-Carman extrapolation for normal yeast, while the extrapolation of the hardened yeast data to zero pressure shows even better agreement with the K-C extrapolation for hardened yeast. At the high pressure limit, there is excellent agreement between the resistances extrapolated from the cold and rinsed flux data and the K-C extrapolation for normal yeast and also between the resistance extrapolated from the hardened yeast data and the K-C extrapolation for hardened yeast.

The constants in Table IV provide a means for analytically differentiating the data with respect to pressure, but individual constants have no physical meaning. The sets of constants obtained with different bed thicknesses under equivalent conditions are equally valid. In subsequent modeling of yeast filtration in hollow fibers (Chapter 6), the constants obtained with 400 μm layers will be used. Depending on whether the yeast used in corresponding cross-flow experiments was rinsed or not, either the constants for 3x-rinsed yeast or the constants for freshly-rehydrated yeast at RT will be used.

Table VI. Limiting Resistances Calculated from Experimental Data

		Cell Bed Height (μm)	Extrapolated Resistances (cm^{-2}) Limit as P->0	Limit as P->∞
From flux data:				
Yeast:	freshly-rehydrated RT, no glucose added	100	4.5×10^{10}	5.7×10^{11}
		200	4.9×10^{10}	5.9×10^{11}
		400	4.0×10^{10}	5.1×10^{11}
	freshly-rehydrated, RT, 1% glucose added	100	1.9×10^{11}	3.9×10^{11}
	freshly-rehydrated, cold (4°C)	200	5.1×10^{9}	6.4×10^{10}
		400	9.0×10^{9}	7.0×10^{10}
	3X-rinsed, RT	200	2.2×10^{10}	9.0×10^{10}
		400	1.8×10^{10}	6.2×10^{10}
	glutaraldehyde-hardened	200	1.0×10^{10}	2.6×10^{10}
		400	9.3×10^{9}	2.6×10^{10}
Latex particles:		85	1.5×10^{10}	
		180	1.7×10^{10}	
From Kozeny-Carman and centrifugation data:				
Yeast:	normal		7.9×10^{9}	6.7×10^{10}
	hardened		7.4×10^{9}	2.7×10^{10}
Latex particles:			7.0×10^{9}	3.2×10^{10}

In order to calculate the compressibity index for comparison with data in the literature, our resistance data is replotted on log-log coordinates in Figure 4-24 through Figure 4-26. Values of n determined from the slope of the data are given in Table VII below. No value of n was reported for the one experiment conducted with added glucose because of the significant non-linearity of the log-log plot.

Table VII. Compressibility Index for Yeast and Latex Particles

Particle Type and Experimental Conditions	Compressibility Index, n
Unrinsed Yeast at RT	0.68
Unrinsed Yeast at 4°C	0.39-0.47
3×-Rinsed Yeast at RT	0.35-0.39
Glutaraldehyde-Hardened Yeast	0.158
4 μm Polystyrene Particles	0.0

The results from the centrifugation and stagnant filtration experiments are combined in Figure 4-27 through Figure 4-30, which are plots of the experimentally-measured hydraulic resistances as a function of porosity. Figure 4-27 shows the resistance of freshly rehydrated yeast at RT, with and without 1% added glucose. The measured resistances, 10-40 x 10^{10} cm^{-2}, are about 11-16 times greater than that predicted by the Kozeny-Carman equation. Figure 4-28 shows the resistance of freshly-rehydrated yeast at 4°C and the resistance of 3×-rinsed yeast at RT. These resistances, 2-7 x 10^{10} cm^{-2}, are about three times greater than that predicted by the Kozeny-Carman equation. Figure 4-29 shows the resistance of glutaraldehyde-hardened yeast, 2.0-2.5 x 10^{10} cm^{-2}, is about twice that predicted by the Kozeny-Carman equation.

To allow easier comparison of the data under various conditions, the data for 400 μm beds from Figures 4-27 through 4-29 is replotted in Figure 4-30. Figure 4-31 shows the same data with the x-axis expanded to show the porosities at which the Kozeny-Carman correlation yields resistances as large as the measured yeast resistances.

G. DISCUSSION

1. Validity of Assumptions

a. Compressive Pressure in Stagnant Filtration Experiments

The compressive pressure in the stagnant filtration experiments was assumed to be one-half the applied pressure. To test that assumption, we will assume that the expression for ϵ_{avg} as a function of π_{avg} (Equation (29)) holds locally, and calculate the compressive pressure profile across the bed. Using an Euler technique, Equation (7) may be expanded as:

$$\pi_{z+\Delta z} = \pi_z + \left(\frac{\mu}{k} V\right)\Big|_z \Delta z$$

with the boundary condition that $\pi = 0$ at $z = 0$, i.e. that the compressive pressure is zero at the top of the bed. The porosity and permeability at $z+\Delta z$ are evaluated directly from Equations (29) and (31). The value of V is determined iteratively. One assumes a value for the flux, and calculates the pressure profile in the cake using the Euler technique. The value of the pressure at the wall is used to calculate the flux through the membrane, which is then compared with the guessed value. The calculated compressive pressure profile in a 180 μm layer of latex particles is shown in Figure 4-33. For comparison, the assumed linear profile is also shown. The difference between the calculated compressive pressure at the membrane surface (89 mmHg) and the applied pressure at the top of the bed (100 mmHg) is the calculated pressure drop across the membrane (11 mmHg). The average compressive pressure in the calculated profile is 36.7 mmHg, which is 27% lower than the assumed value of 50 mmHg. Much of this difference is related to neglecting the membrane resistance, i.e. to assuming that the compressive pressure at the bottom of the cake is the same as the applied pressure at the top of the cake. This error was much smaller in the yeast experiments because the ratio of total yeast cake resistance to membrane resistance (of the more open membranes used in those experiments) was significantly greater.

b. Compressive Pressure in Centrifugation Experiments

Similarly, the error in using an average porosity in calculating the compressive pressure in centrifugation experiments is small. The extrapolated cell concentrations at zero

pressure ($1-\epsilon_\infty-\epsilon_0$) for latex particles, normal yeast, and glutaraldehyde-hardened yeast, respectively, are only 18%, 26%, and 20% smaller than the extrapolated cell concentrations at infinite pressure ($1-\epsilon_\infty$). This is the maximum error in the cell concentration at any position in the cell column. Thus, the error in the calculated average compressive pressure must also be less than 26% in all cases.

2. Compaction and Compression of Yeast Cell Beds

Measurement of the porosity of yeast cell beds as a function of time of centrifugation revealed that the porosity dropped steeply during the first 10 to 15 min. The time dependence of the porosity of a cell bed on a microfiltration membrane, particularly one used in a cross-flow configuration, might be significantly different because the cells laid down during filtration would not necessarily be arranged the same as those which settle under centrifugation.

The porosity achieved with normal yeast cells at a given compressive pressure was lower than that of either rigid latex particles or glutaraldehyde-hardened yeast at the same compressive pressure. In general, the porosity of normal yeast was lower than the porosity of the latex particles by 10% volume fraction, while the porosity of the hardened yeast was midway between that of normal yeast and that of latex particles. The difference between the porosity of the hardened yeast and the latex particles is due to the non-sphericity and non-uniform size distribution of the yeast, while the difference between the normal and hardened yeast cells is due to a difference in cell deformability.

A previous study (Zydney et al., 1988) measured the porosity of highly deformable red blood cells as a function of compressive pressure. The porosity of red cell beds was much lower than the porosities measured here. The porosities ranged from 8.9% at a compressive pressure of 15 mmHg to 3.3% at a compressive pressure of 80 mmHg. Even the extrapolated red cell concentration at zero compressive pressure, 80%, was greater than the maximum yeast concentration observed in our experiments. Thus, compared to blood cells, yeast is quite rigid.

The hysteresis seen in the first two series of data in Figures 4-16 and 4-18 indicates that an irreversible compaction of the yeast cake occurred. Such compaction could be the result of rearraangement of yeast cells and carbon dioxide bubbles within the cake. The lack of hysteresis in the third data series in Figure 4-16 demonstrates that after steady-state

compaction is achieved, no further hysteresis is seen. The remaining curvature must be due to a reversible compression of the cake with pressure. The greater curvature seen in experiments with freshly-rehydrated yeast at RT than in the other experiments which follow indicates that the presence of CO_2 in the cake affects cake compression, presumably by deformation of the gas bubbles in the cake.

3. Hydraulic Resistance of Yeast

a. Non-Sphericity and Non-Uniform Size Distribution Effects

Glutaraldehyde-hardened yeast serves as a model system with the same shape and size distribution as normal yeast (Ju and Ho, 1987) but without the complicating factors of cell compressibility or carbon dioxide bubble formation. Figure 4-23 revealed that the resistance of the hardened yeast was relatively constant with pressure, while the resistance of normal (unhardened) yeast under a variety of conditions showed varying increases with pressure (Figures 4-21 and 4-22). The variation in index of compressibility will be discussed below. When plotted versus porosity, the resistance of the glutaraldehyde-hardened yeast was only a factor of two larger than that predicted by the the Kozeny-Carman correlation. Puttock et al. (1986) recently reported that the K-C prediction for the hydraulic resistance of alumina trihydrate particle beds was over a factor of two less than experimentally measured values.

In comparing our measured resistances with the predictions of the Kozeny-Carman correlation, we were careful to account for the non-sphericity and non-uniform size distribution of the yeast by calculating the specific surface area from the image analysis data. Our value of 9.61×10^3 cm^2 is similar to the value of 1.26×10^4 cm^2 which was recently reported by Nakanishi et al., 1987. Since a recent study of microbial cells (Nakanishi et al., 1987) had highlighted the effect of cell shape on hydraulic resistance, and since an earlier (Sohn and Moreland, 1968) study of Ottawa Silica sand had demonstrated the influence of size distribution on packed bed characteristics, we will calculate the magnitude of these two effects on the yeast resistance.

The effect of the non-uniform size distribution can be estimated by comparing the specific surface area calculated from individual cell dimensions with that calculated for a prolate spheroid with radii equal to the mean values measured. Using Equation (33), a

5.4 μm x 7.0 μm prolate spheroid has an S_0 of 1.03 x 10^4 cm^2. The S_0 calculated from individual cell data was 9.61 x 10^3 cm^2, which is only 7% lower, and would be expected to give a slightly lower resistance than a bed of uniform ellipsoids.

To determine the importance of non-sphericity, consider a sphere with the same volume as the prolate ellipsoid above. Its radius would be 5.9 μm, and its specific surface area 1.02 x 10^4 cm^2, only 1% less than the the prolate spheroid of the same volume. Therefore the only significant effect of the non-sphericity of bakers yeast on its resistance is its effect on the porosity of the cell bed, which was independently measured in the centrifugation experiments.

b. Effect of the Yeast Cell Deformability

By comparing the resistance of normal and hardened yeast cells under conditions in which no carbon dioxide is produced, we can isolate the effect of yeast cell deformability on the hydraulic resistance of yeast cell beds. The centrifugation experiments revealed that at a given compressive pressure, hardened yeast packs to lower concentrations than normal yeast. These experiments detect only irreversible compaction of the bed, in which the porosity of the bed is permanently reduced by particle rearrangement, because the packed cell height is measured after centrifugation is terminated, when the compressive pressure is zero. The experiments may not be able to measure any reversible compression of the bed in which the kinetics of reversibility are fast, and the porosity is reduced as a result of cell deformation while the bed is under compressive pressure, but rebounds as soon as that pressure is released. (These experiments could detect reversible compression of the bed in which the kinetics of reversibility are slow, and the bed remains compressed for some time after the compressive pressure is released.) Therefore it is conceivable that normal yeast cells under pressure have somewhat lower porosities than were measured in the centrifugation experiments. This would reveal itself in a higher resistance in normal cells at a given porosity than in hardened cells at the same porosity. As can be seen in Figure 4-30, this phenomenon was observed. The extent of the cell compression can be estimated by determining what decrease in porosity would shift the cold and rinsed yeast resistance data to the left far enough to reach a continuation of the hardened yeast data, equidistant from the Kozeny-Carman curve of Figure 4-31. A 5%

decrease in the porosity of normal yeast under pressure would account for the observed difference between the resistance of normal yeast and that of glutaraldehyde-hardened yeast.

Cell deformability also affects the extent of pore blockage. We assumed an upper bound pore blockage of $\phi = C_w$ and found that the effect on the calculated cell resistance was less than 10%. This is because the membrane resistance is less than ten percent of the total cake resistance, as we calculated above. Since Zydney (1985) found that highly deformable blood cells block only about 60% of the membrane pores, the actual error resulting from the $\phi = C_w$ assumption must be even lower.

c. Effect of Carbon Dioxide Evolution

One possible explanation why the resistance of freshly-rehydrated bakers yeast is so much higher than would be expected for a bed of particles of that size and packing density is that small carbon dioxide bubbles formed by the yeast remain trapped in the cake, effectively blocking channels and reducing the void fraction available for flow of liquid through the cell bed. Almost 40 years ago, Pillsbury (1950) reported that the hydraulic resistance of silica sand which had been "thoroughly acid-cleaned and washed" decreased until all entrapped air had been dissolved. Since the volume of CO_2 produced varies with experimental conditions, we were able to test this hypothesis.

Carbon dioxide evolution experiments showed that large volumes of CO_2 are produced by freshly-rehydrated active dry yeast, with or without added glucose. Rinsing the yeast reduces the volume of CO_2 produced. The effect of repeated rinsing is cumulative; after three rinsings no CO_2 is produced. However, when 1% glucose was added to 3x-rinsed yeast immediately after rinsing, CO_2 production resumed, indicating that the rinsing cut down CO_2 production by removing any residual carbon sources from the yeast. Under refrigeration at 4°C, unrinsed yeast produced no CO_2, presumably by slowing metabolic processes.

Stagnant filtration experiments revealed that both 3x-rinsed at RT and unrinsed yeast at 4°C have significantly lower hydraulic resistances ($2\text{-}7 \times 10^{10}$ cm^{-2} at pressures of 10-75 mmHg) than unrinsed yeast at RT ($10\text{-}40 \times 10^{10}$ cm^{-2} at pressures of 10-75 mmHg), lending credence to the above hypothesis. The observed difference in hydraulic resistance of rinsed and unrinsed yeast can also explain differences in previously reported yeast resistance. In

experiments with unrinsed yeast, Rushton and Khoo (1977) found that the resistance of the strain Saccharomyces carlsbergensis (whose size and shape are very similar to Saccharomyces cerevisiae) was 4-20 x 10^{10} cm^{-2} at pressures of 10 to 40 mmHg. In more recent experiments with well-rinsed yeast, Nakanishi et al. (1987) found that the resistance of Saccharomyces cerevisiae was only 1-6 x 10^{10} cm^{-2} at pressures of 30-1000 mmHg. Thus, variations in the measured resistances of yeast, both in the literature and reported here, can be explained by differences in experimental conditions which affect the production of carbon dioxide by the yeast.

Variation in the observed pressure-dependence of the yeast resistance data was also similar to that previously reported. For the cold and rinsed experiments, in which no CO_2 was produced, the compressibility index n ranged from 0.35 to 0.47. Nakanishi et al. (1987) reported n = 0.45 for well-rinsed bakers yeast. (Both that report and this study also found that n = 0.0 for latex particles.) Rushton and Khoo (1977) reported that there was no clear relationship between hydraulic resistance and pressure for unrinsed brewers yeast in complete media at room temperature. When we plotted log(resistance)-vs.-log(applied pressure) for our only experiment conducted in the presence of added glucose, we were unable to calculate n because the data was very non-linear. Given the presence of a carbon source, and the reported variation in yeast culture age from one experiment to the next in the Rushton and Khoo study, the presence of varying amounts of CO_2 could have resulted in inconsistent pressure-dependence results.

To estimate how much CO_2 is necessary to result in the observed order-of-magnitude variation in yeast resistances, a model for the resistance as a function of gas volume is needed. Rapoport and Leas (1951) studied the resistance of porous media containing a discontinuous gas phase (as shown in Figure 4-32) to flow of a continuous liquid phase through it. They demonstrated that existing correlations for simple two-phase porous media systems (one solid, one fluid) could be adapted to account for the presence of the immobile fluid by appropriate corrections to the porosity and specific surface area terms. The porosity was taken to be the volume fraction not occupied by either the solid or the discontinuous fluid, and the specific surface are was taken to be the interfacial area between the mobile fluid and the composite

porous medium of solids + immobile fluid, divided by the volume occupied by the two immobile phases.

If we assume (for lack of a better approximation) that the CO_2 bubbles are uniformly distibuted within the yeast bed and that the specific surface area of the composite system is equal to that the simple yeast + media system, we can estimate the volume fraction occupied by gas bubbles by measuring the horizontal distance between the measured resistance and the Kozeny-Carman resistance on Figure 4-31. The resulting 16% of the total volume of the cake which is estimated to be occupied by gas bubbles represents an upper bound to the volume of CO_2 bubbles required to account for the high unrinsed yeast resistance since a 5% change in volume fraction may be accounted for by yeast cell compression as discussed above. Nevertheless, even a volume fraction of 16% would be only 20-25% of the volume occupied by the cells (whose volume fraction is 65-75%). Since the CO_2 evolution experiments indicated that unrinsed yeast at room temperature produces that much CO_2 in 10 min, it is certainly plausible that sufficient CO_2 remained trapped in the cake to account for the factor-of-five variation in observed resistances.

d. Comparison with Other Cell Types

The resistance of a bed of cells depends on the specific surface area of the cells and the porosity of the cell bed, which depend on cell characteristics such as cell size, shape, deformability, and tendency to flocculate. In comparing the hydraulic resistance of yeast to that of other cell types, the importance of each of these characteristics becomes apparent.

One significant difference between yeast cells and animal cells is the presence of the cell wall, which is much more rigid than a cell membrane. The resistances measured here, even under conditions in which carbon dioxide is produced, are more than two orders of magnitude lower than the resistance of red blood cells measured using similar experiments (Zydney et al., 1988). This is not surprising given that red cell deformation allows packing to concentrations above 95%.

While most microbial cells are considered to be fairly rigid, yeast is known for having the most rigid and unbreakable cell wall. Since yeast is also one of the most spherical cell

types, one would expect that yeast beds would have higher porosities than beds of other microbial cells. Yeast is also larger than most bacteria or other microbial cells. Consequently, one would expect that the resistance of yeast would be lower than that of other microbial cells. Nakanishi et al. (1987) found that the resistance of well-rinsed yeast was one to two orders of magnitude lower than that of 4 other cell types. Not surprisingly, E. coli, the smallest cell studied, had the highest resistance.

Two types of cells which one would expect would yield fairly low resistances at low pressure, but higher resistances as the pressure is increased, are cells with mycelial structures and cells which flocculate. Highly-branched mycelial structures lead to high bed porosities and low resistances, but their loosely-packed structures break down if sufficient compressive pressure is applied. Flocculated cells have large effective particle sizes (low specific surface areas) and low resistances, but flocs also break apart under high compressive pressures. Both of these processes may lead to time- and pressure-dependent resistances which are difficult to compare with the resistances of other cells. At the present time, no hydraulic resistance data is available for these systems.

Thus, whereas blood cells represent the high end of the spectrum of cell bed resistances observed to date, yeast represents the low end of the spectrum.

e. Implications for Cross-flow Filtration under Process Conditions

As we have shown, the resistance of yeast cell beds depends not only on the packing characteristics of the yeast, but also on metabolic state of the yeast, which depends on factors such as temperature, metabolite and catabolite concentrations in the media, and yeast age. One might expect that different flow patterns and higher fluxes present in cross-flow configurations could affect the yeast resistance by changing the tendency of carbon dioxide bubbles to remain trapped in the cell cake. Furthermore, use of cross-flow configurations might affect the packing density of the yeast. (Based on our stagnant filtration results, effects related to carbon dioxide bubbles would probably be greater than effe^Ts related to yeast packing.) Nevertheless, the value of the yeast resistance under process conditions in a cross-flow filter probably lies between the limits seen in our stagnant filtration results.

Regardless of the exact value of the yeast resistance, its relatively low value would lead to the buildup of thick cakes of cells on the membrane. The influence of low hydraulic resistance on cross-flow flux behavior of rigid cells will be studied experimentally in Chapter 4. Its importance will also be analyzed theoretically in Chapter 5.

4. Summary

The purpose of this work was to determine the filtration properties of yeast under a variety of experimental conditions and to explain previously-observed variation in measured resistances. Centrifugal cell packing experiments revealed that yeast packs to higher volume fractions than do rigid latex particles or hardened yeast, but significantly lower volume fractions than do highly deformable red blood cells. We found that the resistance of glutaraldehyde-hardened yeast was within reasonable agreement with that predicted by the Kozeny-Carman equation. The resistance of 3x-rinsed yeast at RT and unrinsed yeast at 4°C was about twice the resistance of glutaraldehyde-hardened yeast. This difference can be accounted for by a 5% change in the porosity due to reversible compression of the slightly deformable yeast cells. THe resistance of unrinsed yeast at RT was approximately 5 times greater than the resistance of the cold or rinsed yeast (10 times greater than that of the glutaraldehyde-hardened yeast). We propose that the presence of CO_2 bubbles within the cake of unrinsed yeast at RT leads to the higher resistances. CO_2 evolution experiments confirmed that more-than-sufficient quantities of CO_2 are produced by unrinsed yeast at RT but not by either cold or well-rinsed yeast. In all experiment the measured resistance observed was orders of magnitude lower than the resistance of highly deformable red blood cells, and significantly lower than the resistance of other microbial cells. Yeast represents the low-resistance limit of known cell resistances, and consequently the expected thickness of cakes formed at the membrane surface during cross-flow filtration should be greatest with yeast.

H. REFERENCES

Arnold, W. N., and J. S. Lacy, "Permeability of the Cell Envelope and Osmotic Behavior in Saccharomyces cerevisiae," J. Bacteriology 131(2):564-571 (1977)

Bekers, M. J., Damberga, B. E., Krauze, I. J., Ventina, E. J., and J. G. Kontakevich, "Factors of Wine Yeast Resistance at their Dehydration," J. Bacteriology 131(2):564-571 (1977)

Beyer, W. H., ed., CRC Standard Mathematical Tables, CRC Press, Inc., Boca Raton, FL, pp. 129 and 287 (1978)

Bird, R. B., Stewart, W. E., and E. N. Lightfoot, Transport Phenomena, John Wiley & Sons, Inc., New York (1960)

Blatt, W. F., Dravid, A., Michaels, A. S., and L. Nelson, "Solute Polarization and Cake Formation in Membrane Ultrafiltration: Causes, Consequences, and Control Techniques," in Membrane Science and Technology, J. E. Flinn, ed., Plenum Press, New York, pp. 47-97 (1970)

Butler, J. N., Ionic Equilibrium: A Mathematical Approach, Addison-Wesley Publishing Co., Reading, MA (1964)

Carman, P. C., "Fluid Flow through Granular Beds," Trans. Instn. Chem. Eng. 15:150-166 (1937)

Cohen, Y., and A. B. Metzner, "Wall Effects in Laminar Flow of Fluids through Packed Beds," AIChe J 27:705 (1981)

Conway, E. J., and M. Downey, "An Outer Metabolic Region of the Yeast Cell," Biochem. J. 47:347-355 (1950)

Darcy, H. P. G., Les Fontaines Publiques de la Ville de Dijon, Dalmont, Paris (1856)

Dullien, F. A. L., "Single Phase Flow through Porous Media and Pore Structure" Chem. Eng. J. 10:1 (1975)

Gerhardt, P. and J. A Judge, "Porosity of Isolated Cell Walls of Saccharomyces cerevisiae and Bacillus megaterium," J. Bacteriology 87(4):945-951 (1964)

Happel, J., and H. Brenner, Low Reynolds Number Hydrodynamics with Special Applications to Particulate Media, Noordhoff International Publishing (1973)

Heertjes, P. M., "Filtration," Trans. Instn. Chem. Engrs. 42:T266-T274 (1964)

Ju, L.-K., and C. S. Ho, "Correlation of Cell Volume Fractions with Cell Concentrations in Fermentation Media," Biotech. Bioeng. 32:95-99 (1987)

Kozeny, J., Hydralik, Springer-Verlag, Wein (1927)

Kozeny, J., Wasserkraft und Wasserwirtschaft 22:67,86 (1927)

Macdonald, I. F., El Sayed, M. S., Mow, K., and F. A. L. Dullien, "Flow Through Porous Media--The Ergun Equation Revisited," Ind. Eng. Chem. Fund. 18:199-208 (1979)

Martin, J. J., McCabe, W. L., and C. C. Monrad, "Pressure Drop Through Stacked Spheres," Chem. Eng. Prog. 47(2):91-94 (1951)

McCabe, W. L., and J. C. Smith, Unit Operations in Chemical Engineering, McGraw-Hill Publishing Co., New York (1976)

Nakanishi, K., Tadokoro, T., and R. Matsuno, "On the Specific Resistance of Cakes of Microorganisms," Chem. Eng. Comm. 62:187-201 (1987)

Pillsbury, A. F., "Effects of Particle Size and Temperature on the Permeability of Sand to Water," Soil Sci. 70:299-300 (1950)

Porter, M. C., "Concentration Polarization with Membrane Ultrafiltration," Ind. Eng. Chem. Prod. Res. Develop. 11:234-248 (1972)

Puttock, S. J., Fane, A. G., Fell, C. J. D., Robins, R. G.., and M. S. Wainwright, "Vacuum Filtration and Dewatering of Alumina Trihydrate--The Role of Cake Porosity and Interfacial Phenomena," Intl. J. Mineral Processing 17:205-224 (1986)

Rapoport, L. A., and W. J. Leas, "Relative Permeability to Liquid in Liquid-Gas Systems Petroleum," Trans. AIME 192:83-98 (1951)

Reuss, M., Josic, D., Popovic, M., and W. K. Bronn, "Viscosity of Yeast Suspensions," European J. Appl. Microbiol. 8:167-175 (1979)

Rushton, A., and H. E. Khoo, "The Filtration Characteristics of Yeast," J. Appl. Chem. Biotechnol. 27:99-109 (1977)

Saltzman, W. M., An Investigation of the Hydrodynamic Resistance of Concentrated Layers of Erythrocytes, M. S. Thesis, Massachusetts Institute of Technology (1984)

Sandler, S. I., Chemical and Engineering Thermodynamics, John Wiley & Sons, Inc., New York (1979)

Scheidegger, A. E., The Physics of Flow through Porous Media, The MacMillan Co., New York (1960)

Scheidegger, A. E., The Physics of Flow through Porous Media, University of Toronto Press, Toronto (1974)

Slattery, J. C., "Single-Phase Flow through Porous Media," AIChE J. 15:866 (1969)

Thorn, J. A., and G. Reed, "Active Dry Yeast," Cereal Sci. Today 4(7):197-213 (1959)

Tiller, F. M., "The Role of Porosity in Filtration," Chem. Eng. Prog. 49(9):467-479 (1953)
Verhoff, F. H., and J. J. Furjanic, Jr., "Compressible Packed Bed Fluid Dynamics with Application to a Glucose Isomerase Reactor," Ind. Eng. Chem. Proc. Des. Dev. 22:192-198 (1983)

Whitaker, S., "The Transport Equations for Multi-Phase Systems," Chem. Eng. Sci. 28:139 (1973)

Wickerham, L. J., Technical Bulletin 1029, United States Department of Agriculture, Washington, D.C. (1951)

Willis, M. S., and I. Tosun, "A Rigorous Cake Filtration Theory," Chem. Eng. Sci. 35:2427-2438 (1980)

Zydney, A. L., Cross-Flow Membrane Plasmapheresis: An Analysis of Flux and Hemolysis, Ph. D. Thesis, Massachusetts Institute of Technology (1985)

Zydney, A. L., Saltzman, W. M., and C. K. Colton, "Hydraulic Resistance of Red Cell Beds in an Unstirred Filtration Cell," Chem. Eng. Sci. (in press, 1988)

I. FIGURES

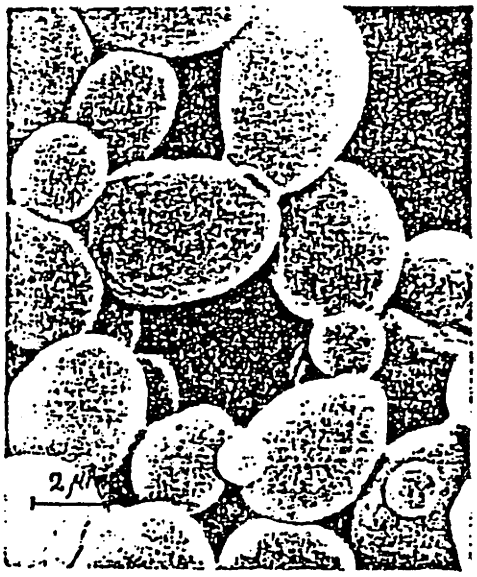

a. Wine yeast cells before dehydration

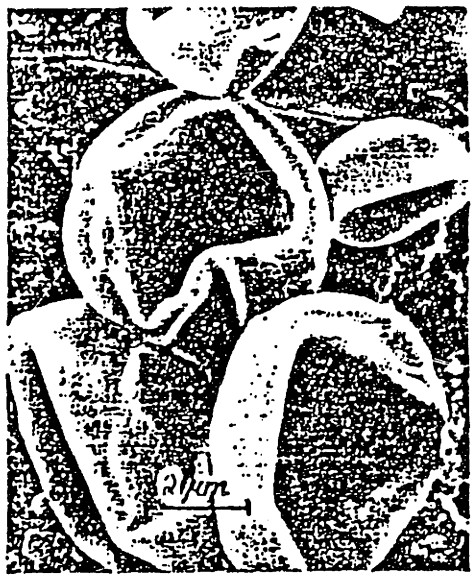

b. Dried wine yeast cells (preparation was obtained without preliminary fixation).

Figure 4-1. Dehydrated wine yeast cell (Bekers et al., 1979).

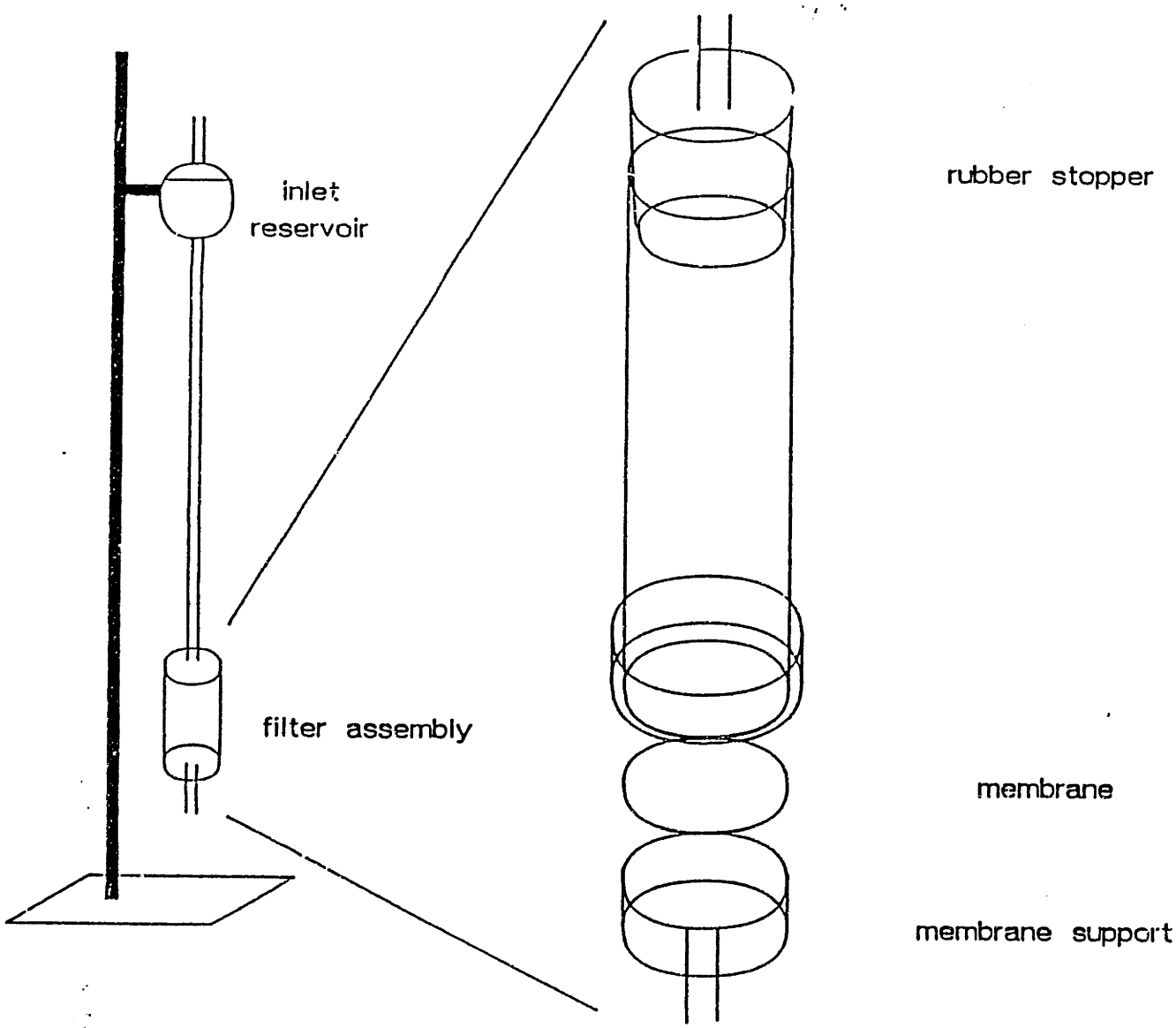

Figure 4-2. Stagnant filtration funnel assembly.

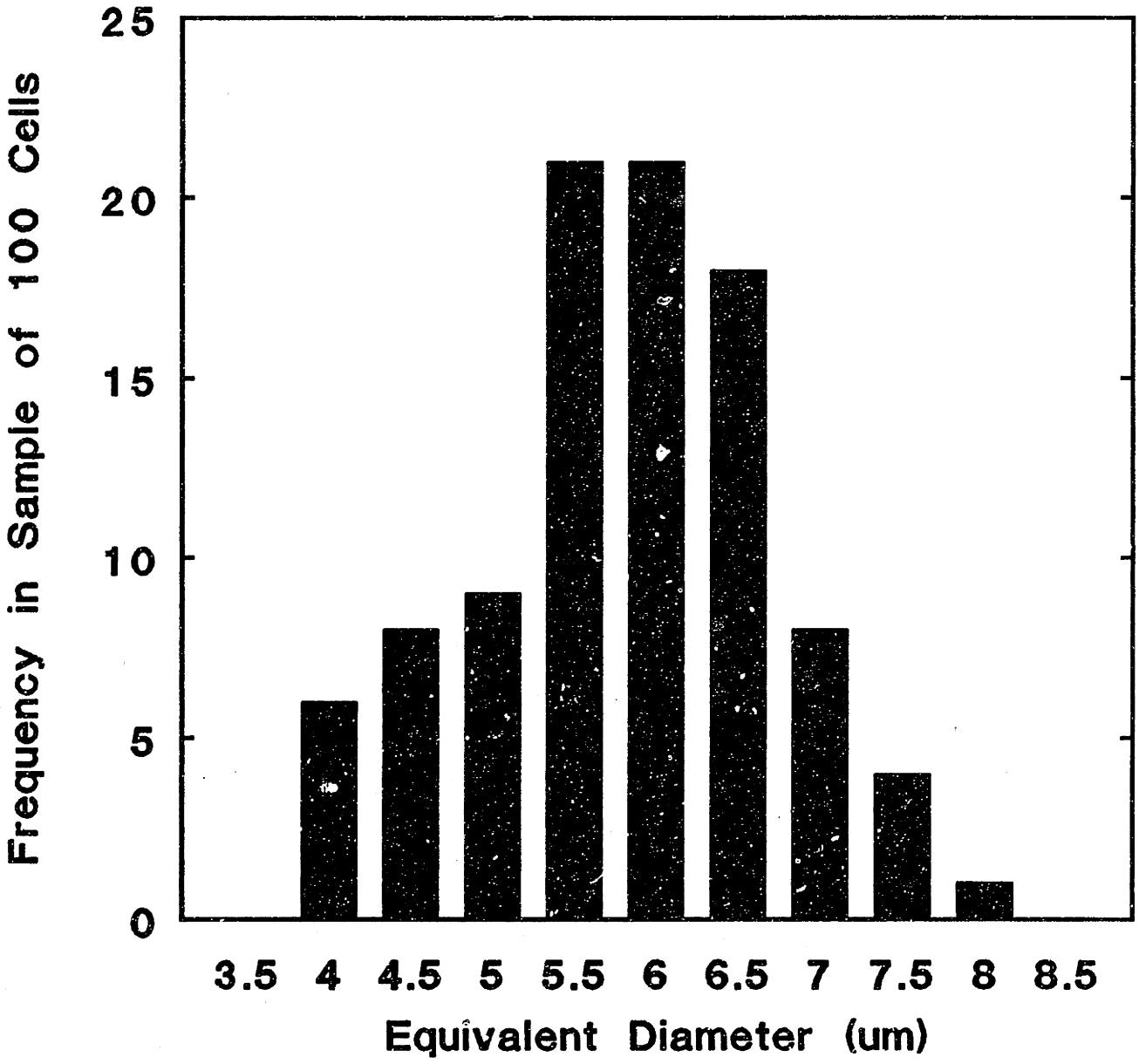

Figure 4-3. Histogram showing the distribution of equivalent sphere diameters (d_{eq}) of yeast cells measured by image analysis. Bar at x=n μm indicates the number of cells in a sample of 100 cells with (n-0.25) < d_{eq} < (n+0.25).

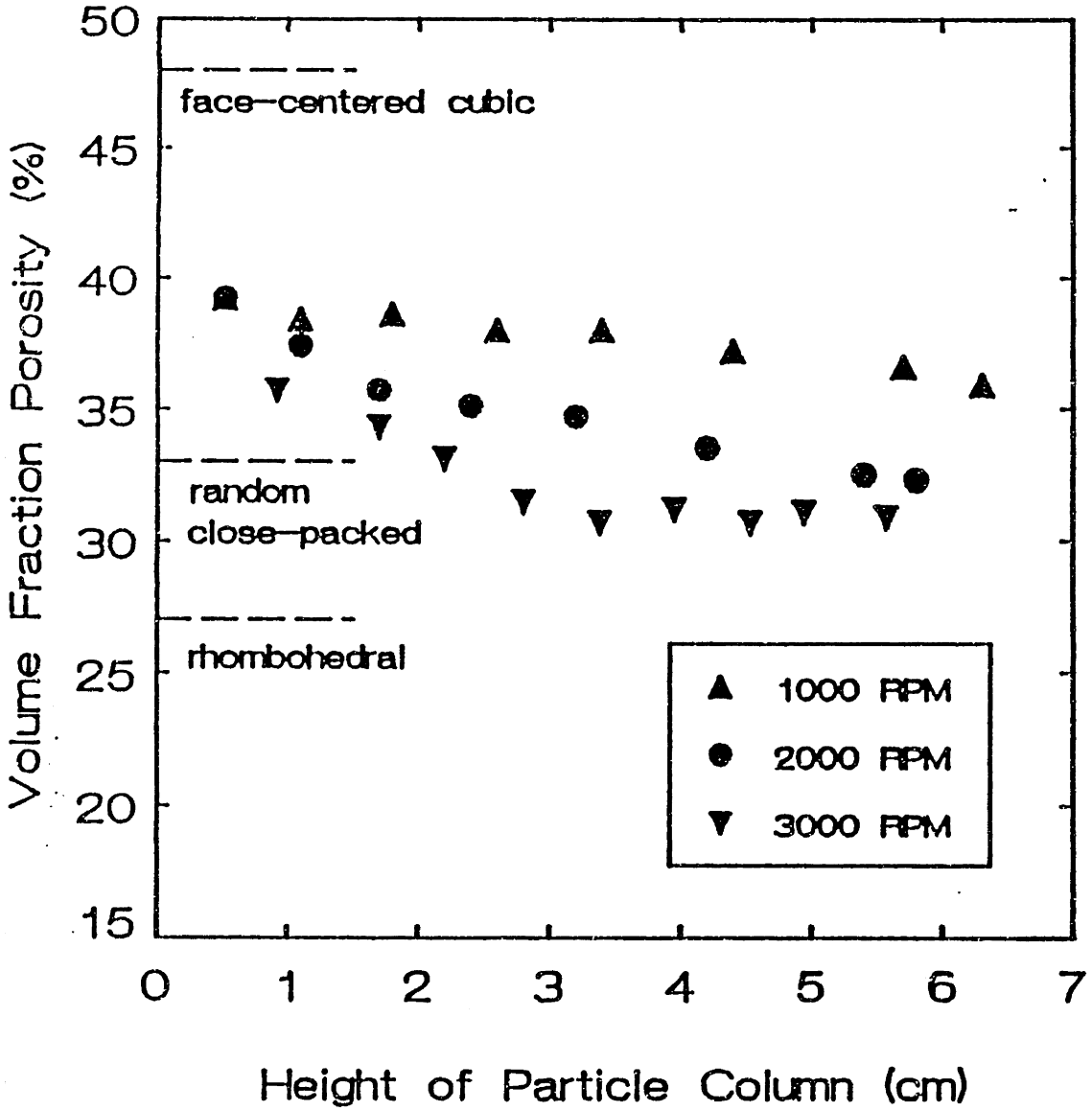

Figure 4-4. Length-averaged porosity of columns of 4 μm polystyrene particles after 1 hr centrifugation, as a function of bed height and rotation rate.

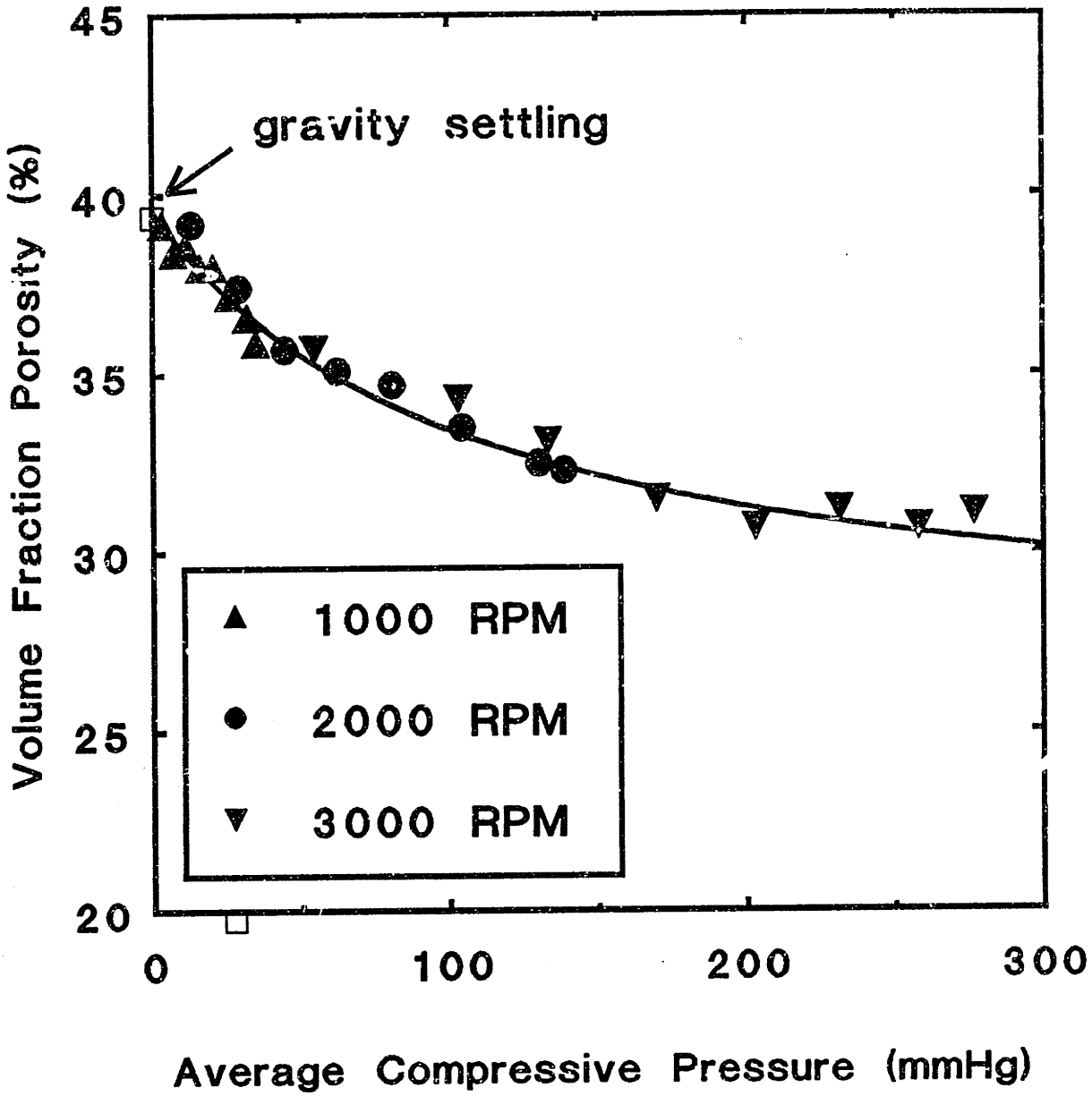

Figure 4-5. Length-averaged porosity of columns of 4 μm polystyrene particles after 1 hr centrifugation, as a function of compressive pressure.

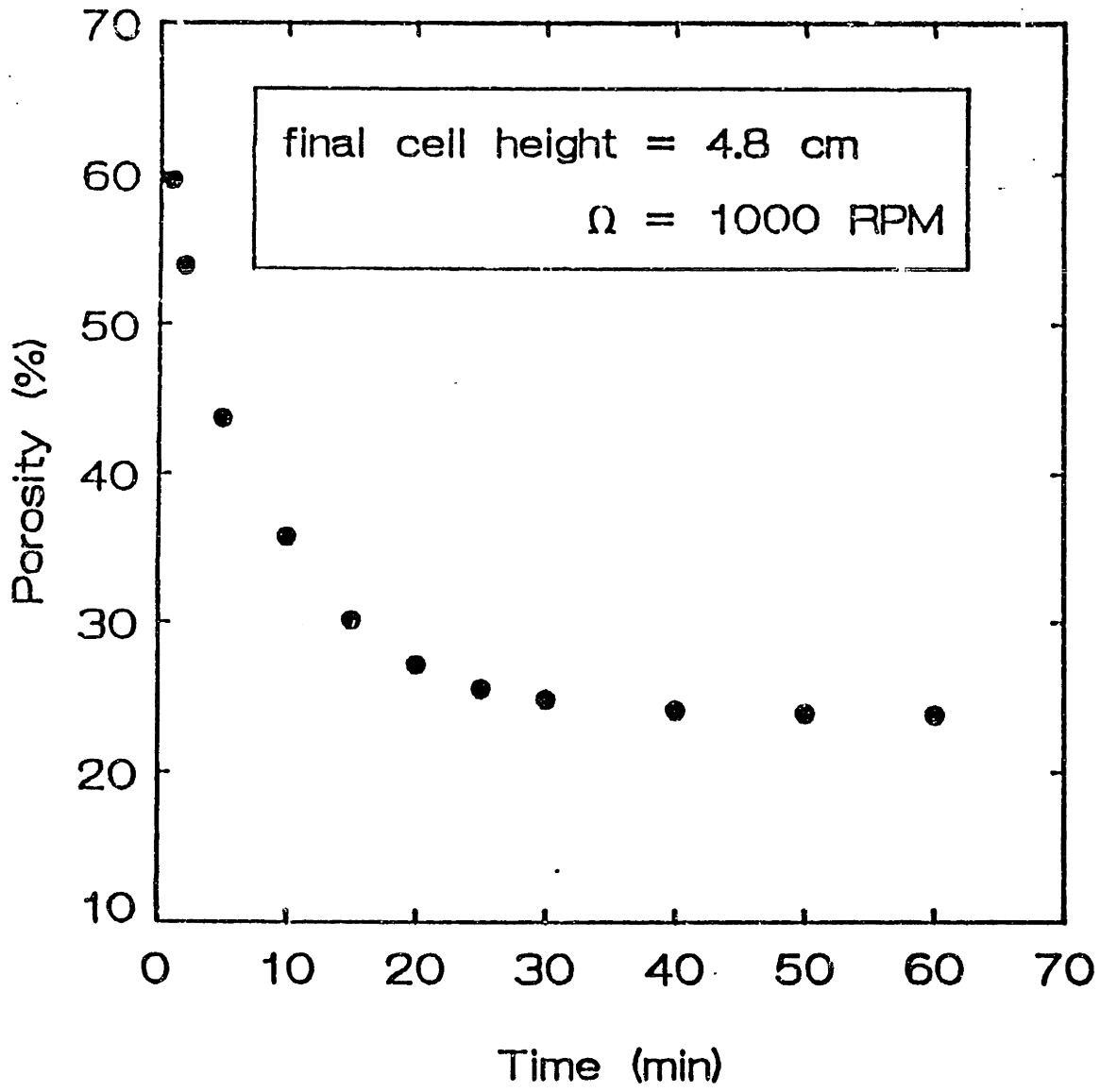

Figure 4-6. Length-averaged porosity of columns of freshly-rehydrated bakers yeast as a function of time of centrifugation at 4°C.

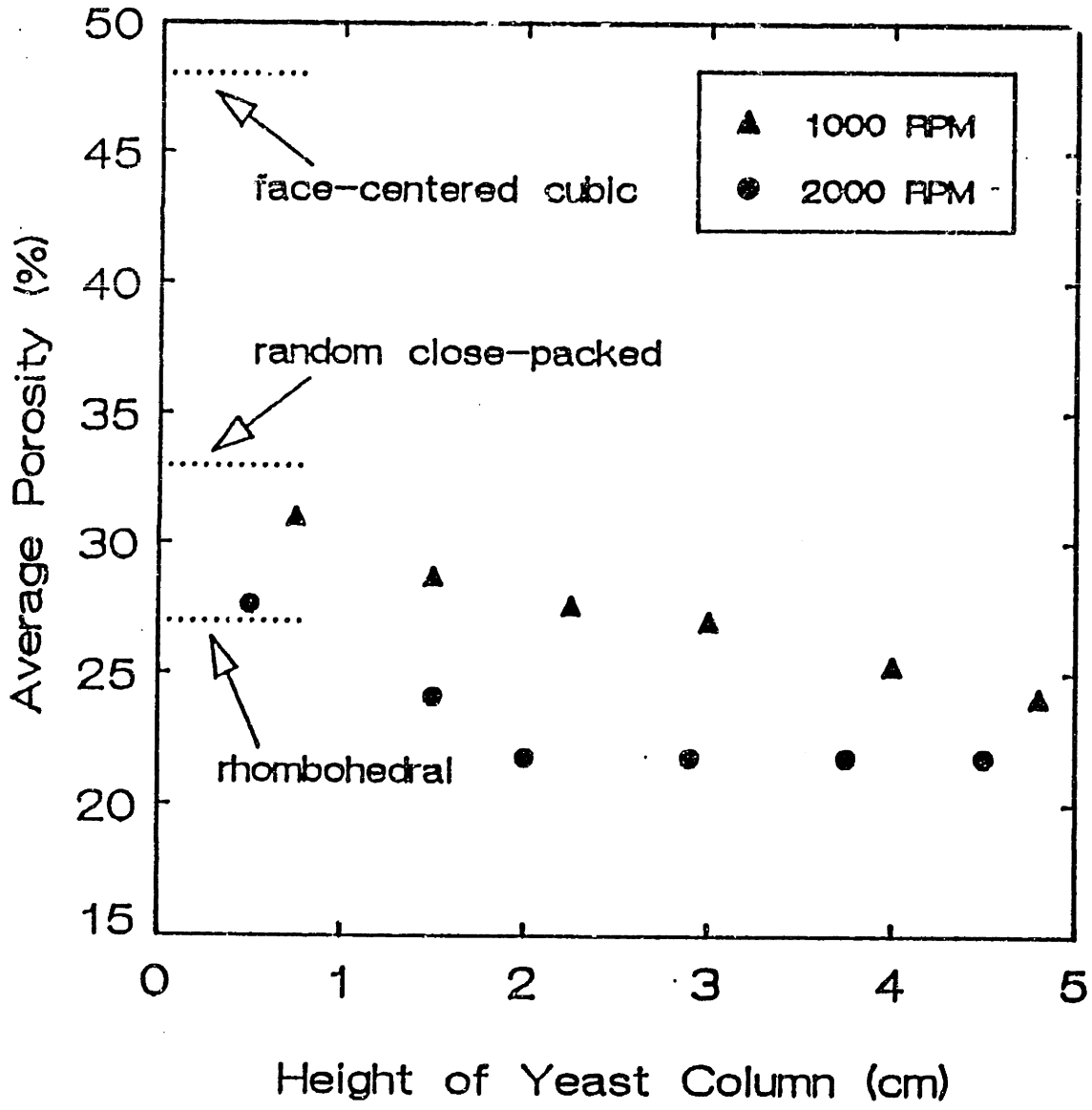

Figure 4-7. Length-averaged porosity of columns of freshly-rehydrated bakers yeast after 1 hr centrifugation at 4°C, as a function of bed height and rotation rate.

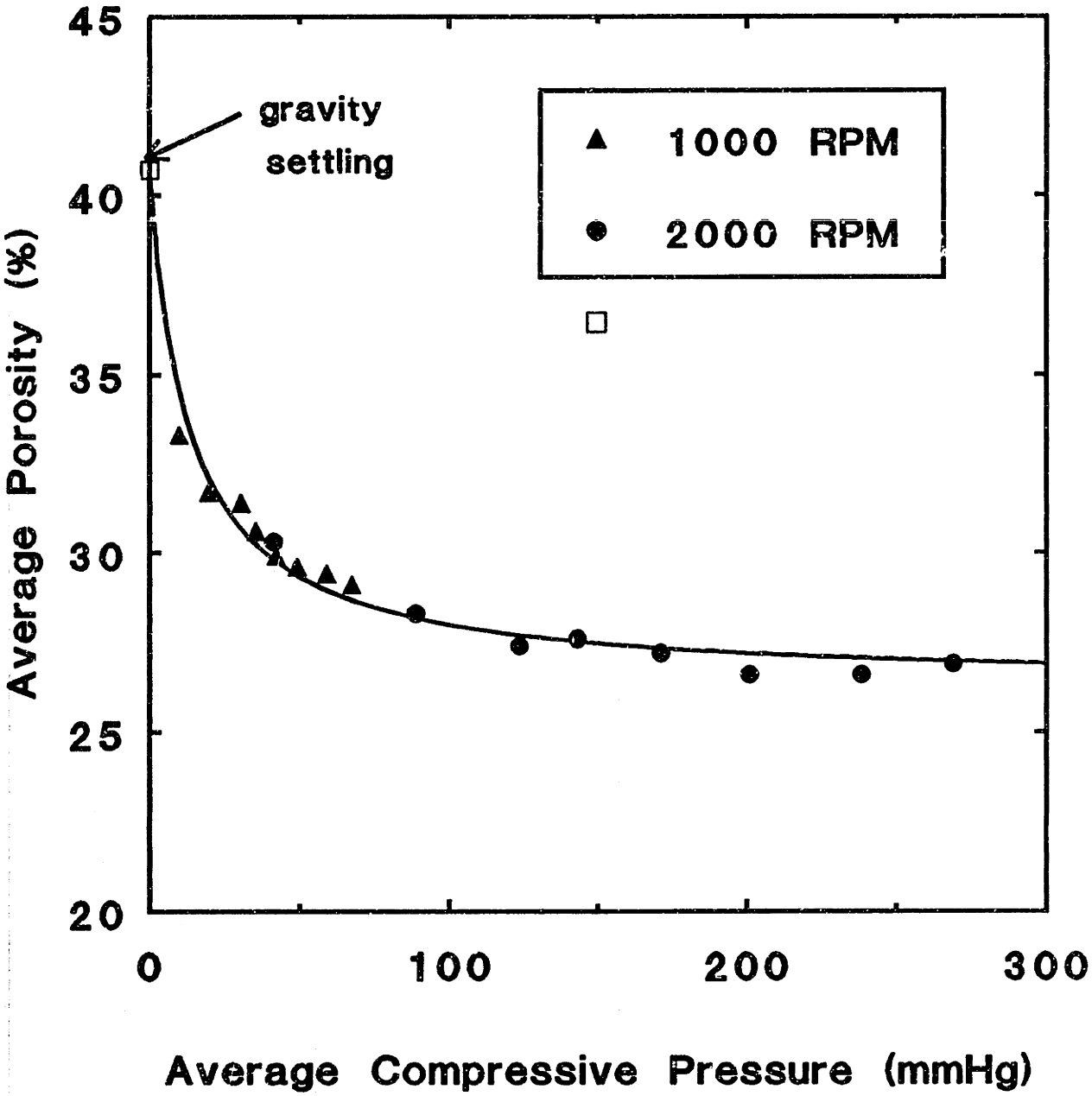

Figure 4-8. Length-averaged porosity of columns of freshly-rehydrated bakers yeast after 1 hr centrifugation at 4°C, as a function of compressive pressure.

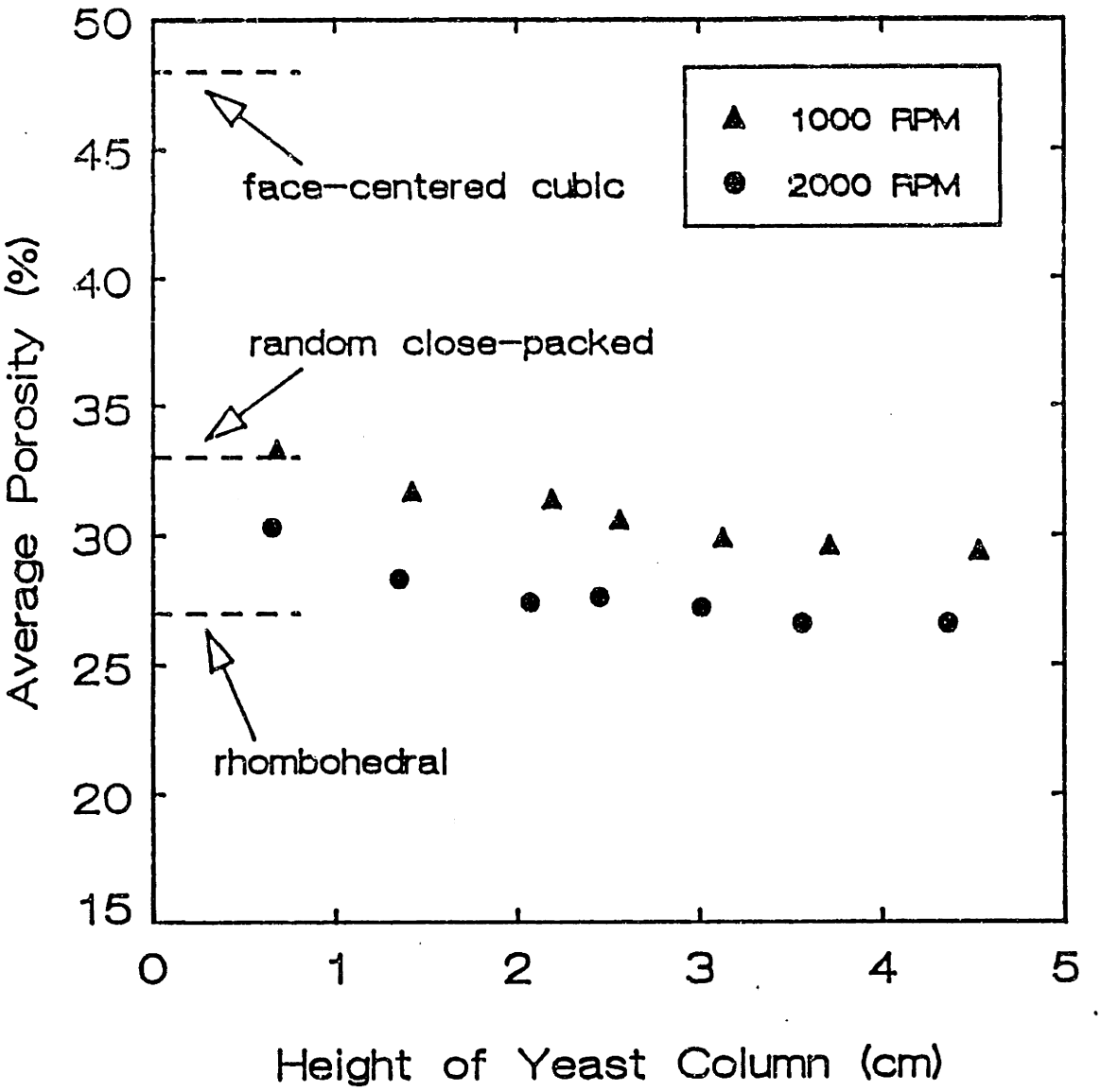

Figure 4-9. Length-averaged porosity of columns of glutaraldehyde-hardened bakers yeast after 1 hr centrifugation at RT, as a function of bed height and rotation rate.

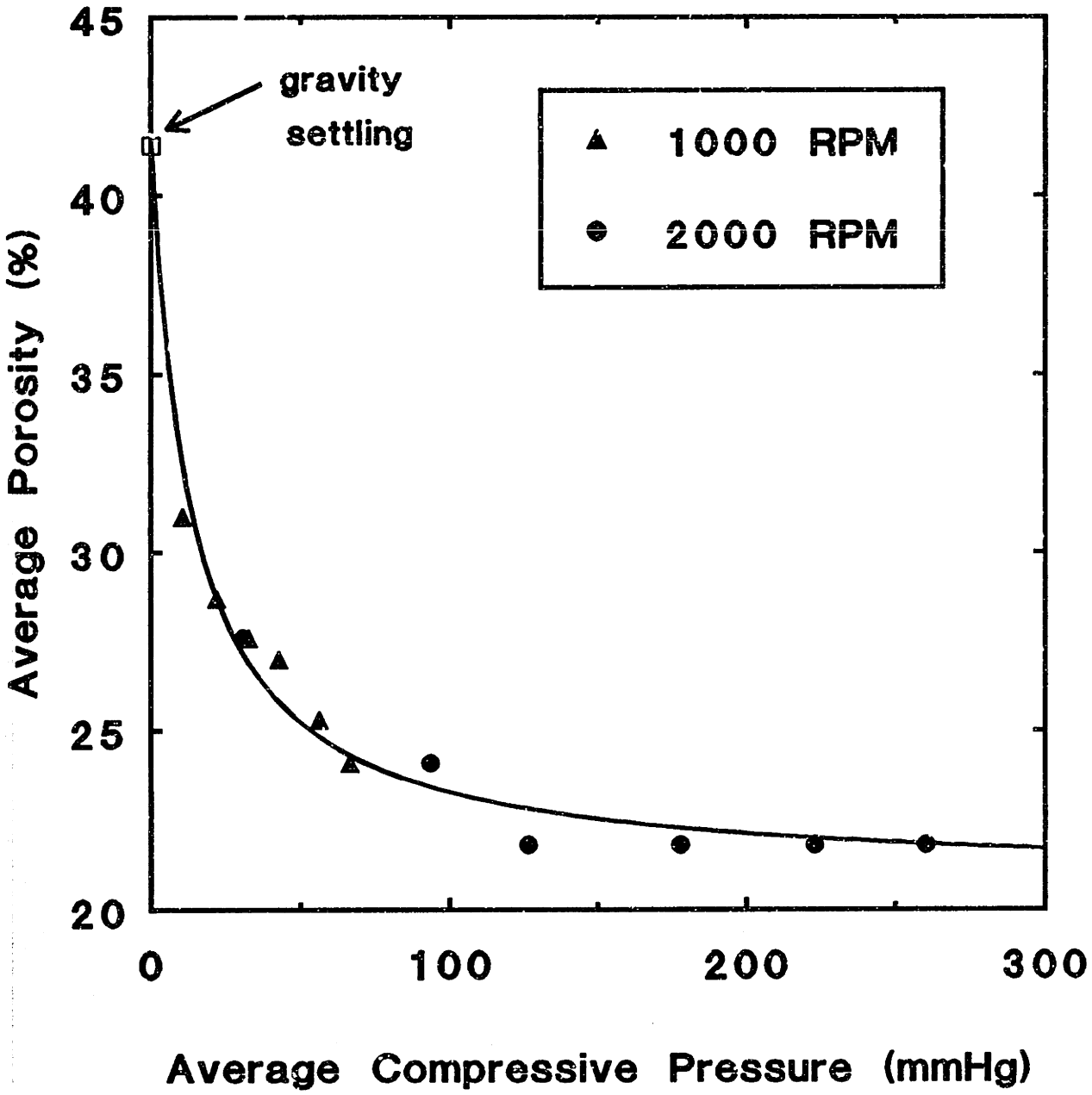

Figure 4-10. Length-averaged porosity of columns of glutaraldehyde-hardened bakers yeast after 1 hr centrifugation at RT, as a function of average compressive pressure.

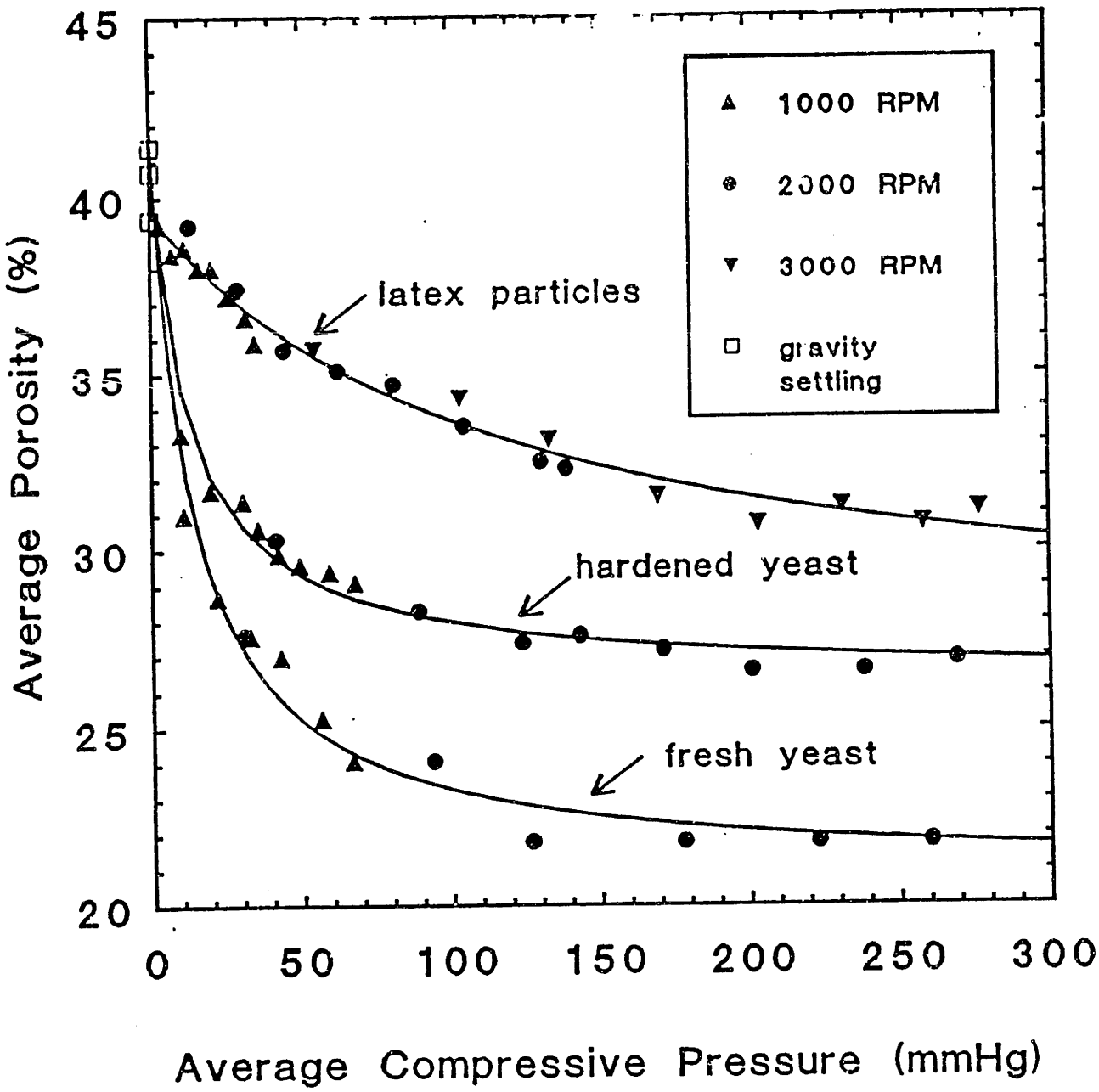

Figure 4-11. Length-averaged porosity as a function of average compressive pressure for latex particles, freshly-rehydrated bakers yeast, and glutaraldehyde-hardened bakers yeast (data re-plotted from Figures 5, 8, and 10).

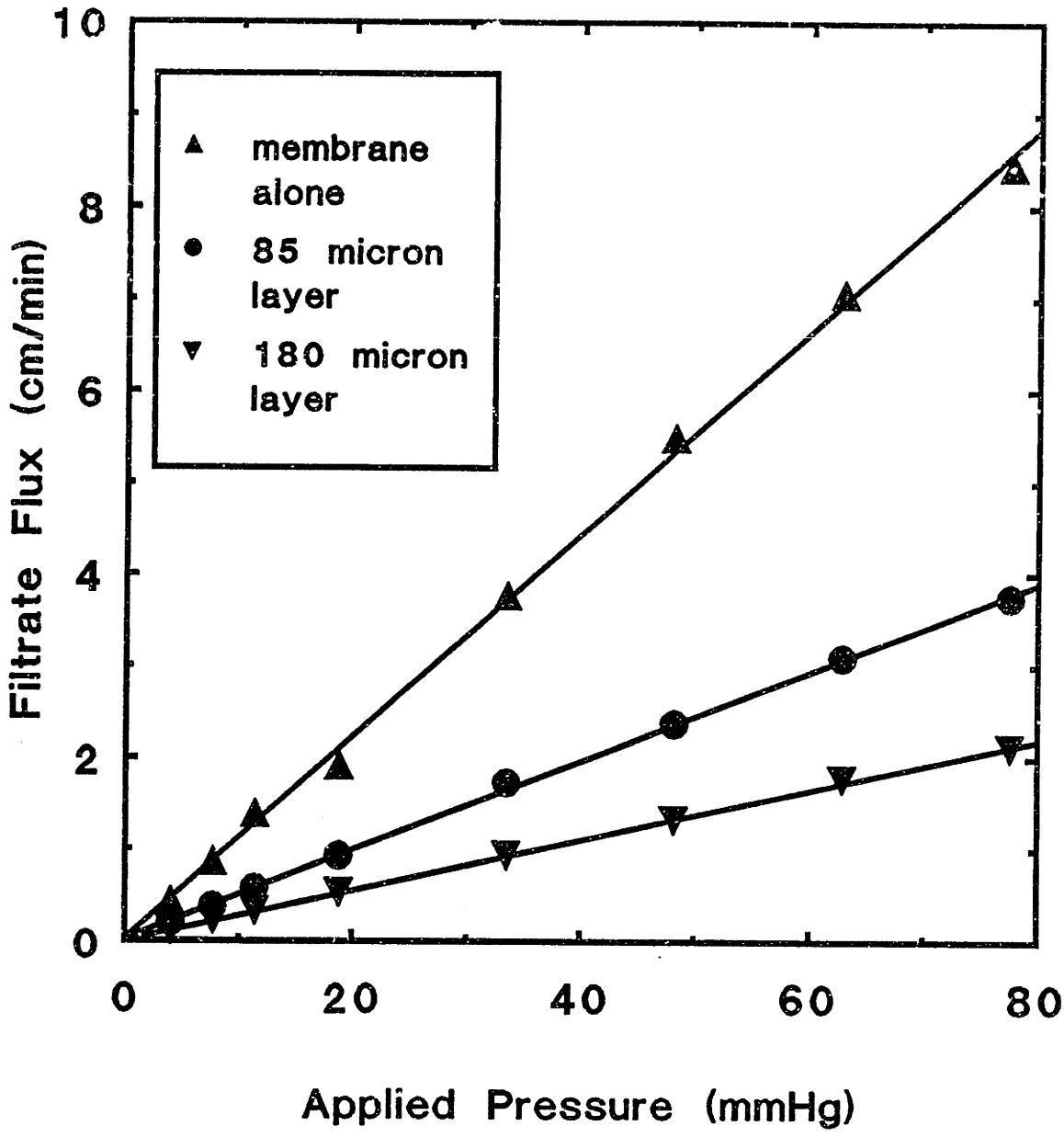

Figure 4-12. Filtrate flux through stagnant beds of latex particles.

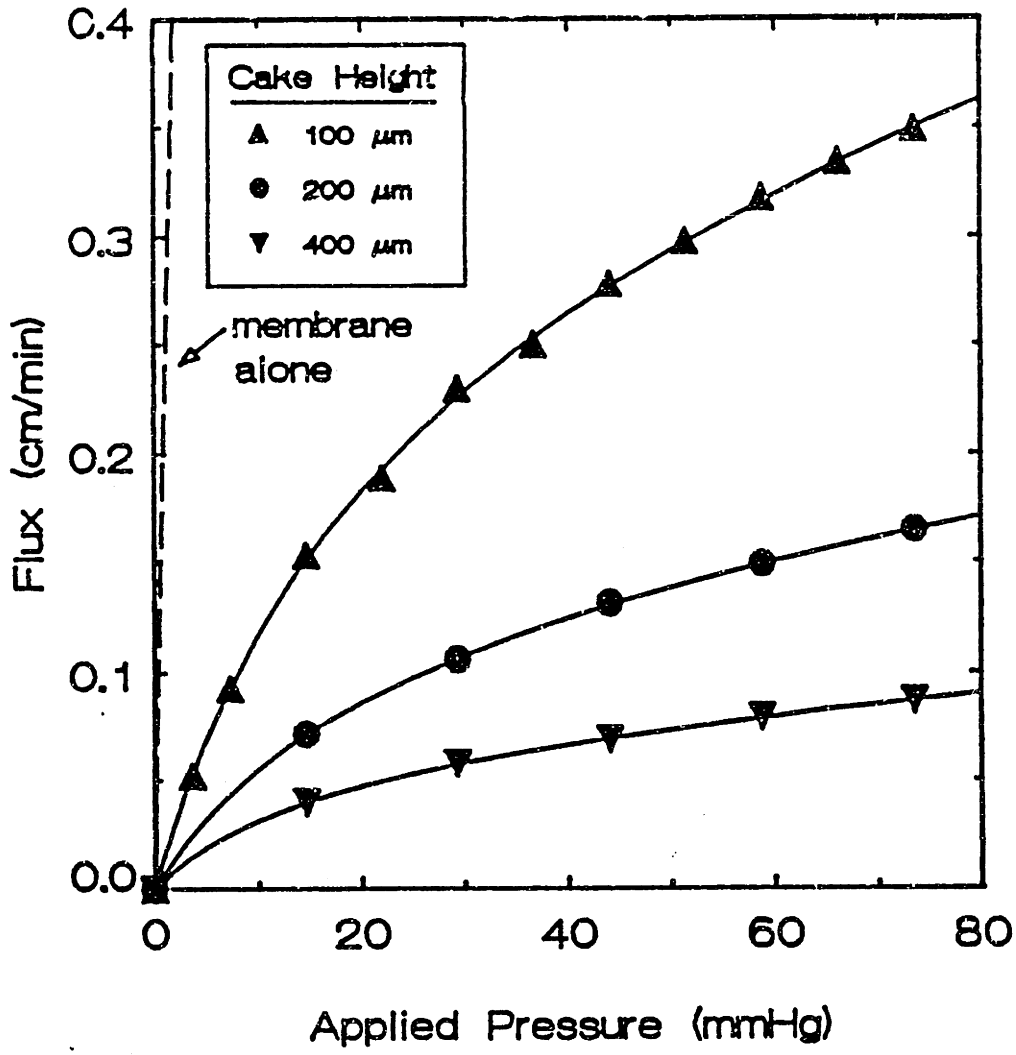

Figure 4-13. Filtrate flux through stagnant beds of unrinsed freshly-rehydrated bakers yeast at RT (with no added glucose).

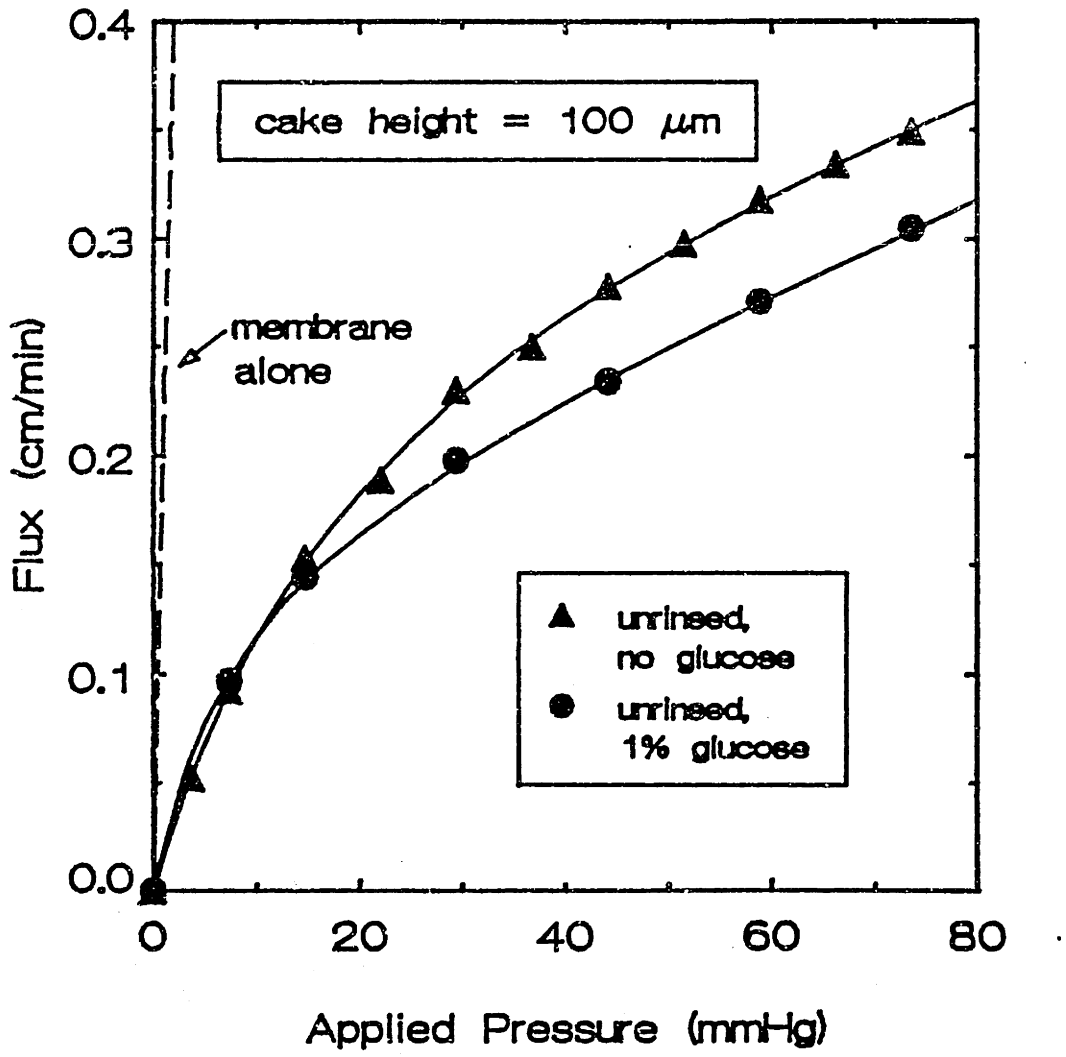

Figure 4-14. Filtrate flux through 100 μm thick stagnant beds of unrinsed freshly-rehydrated bakers yeast at RT, with and without 1% added glucose.

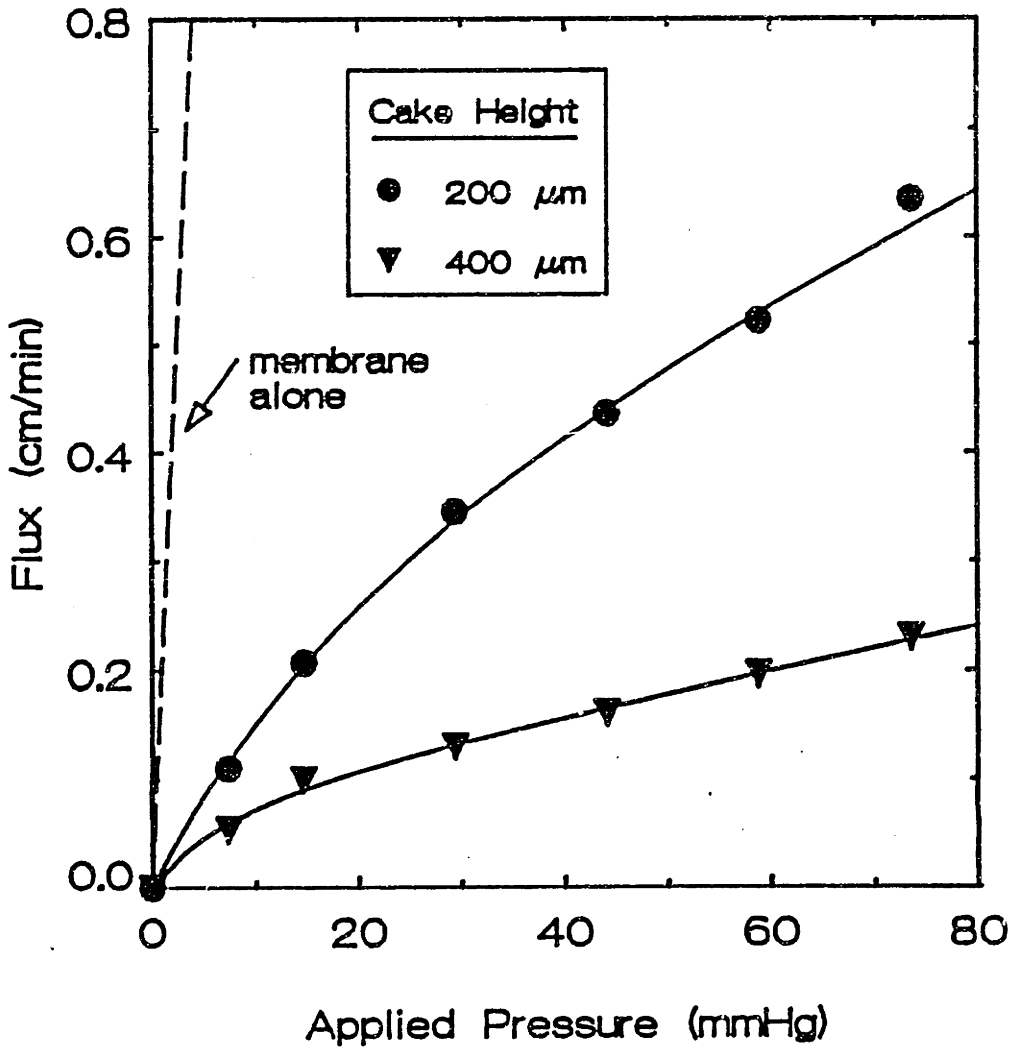

Figure 4-15. Filtrate flux through stagnant beds of unrinsed freshly-rehydrated bakers yeast at 4°C.

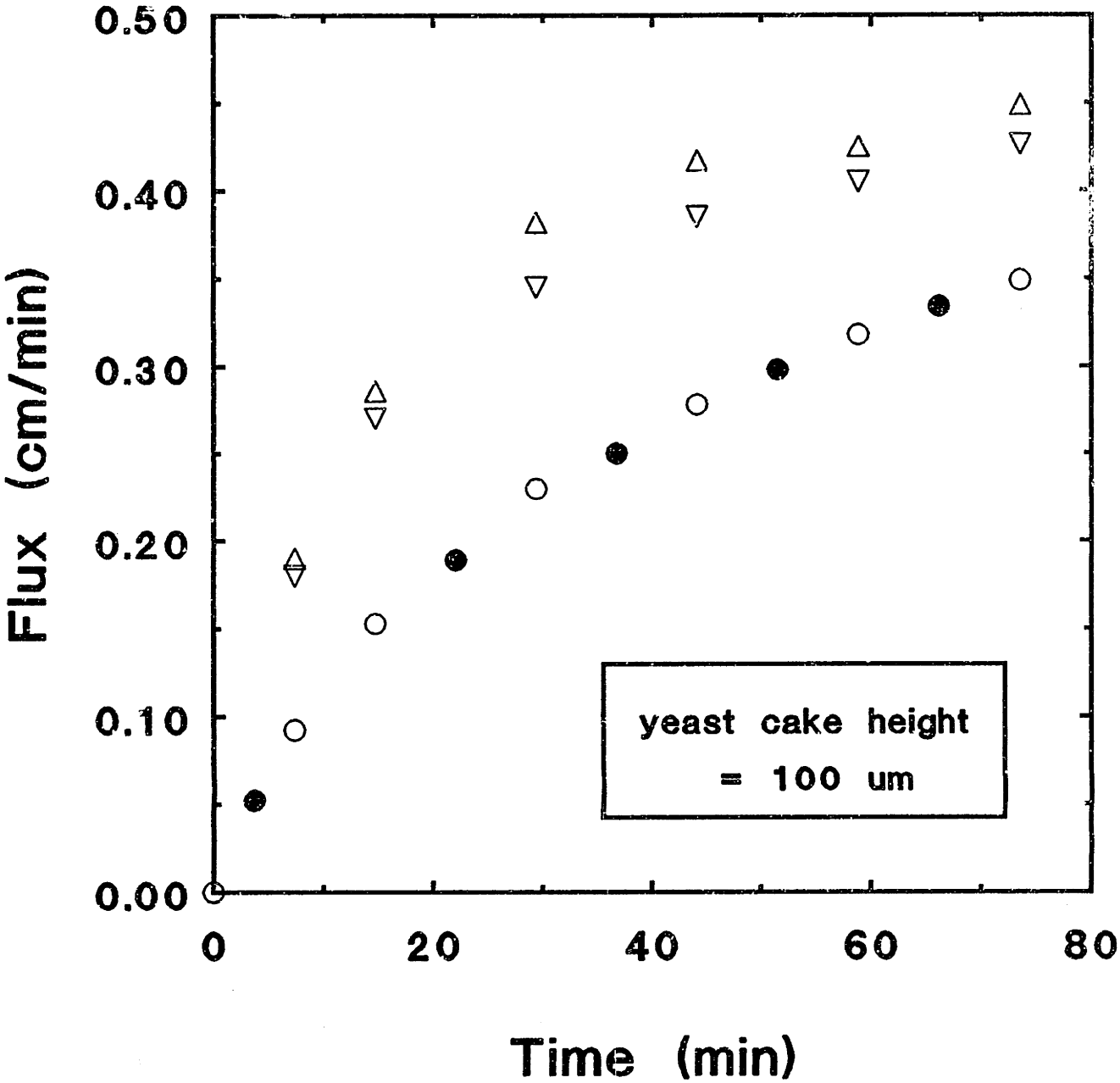

Figure 4-16. Hysteresis in 100 μm stagnant filtration data. Data represented by triangles are initial measurements taken in order of increasing pressure. The Δ data was taken two min after raising the pressure. The ∇ data was taken three min later, and then the pressure was raised to the next value. After one hour at the maximum pressure, the ● data was taken in order of decreasing pressure, at intervals of approximately two min. Then the ○ data was taken in order of increasing pressure, at intervals of approximately two minutes.

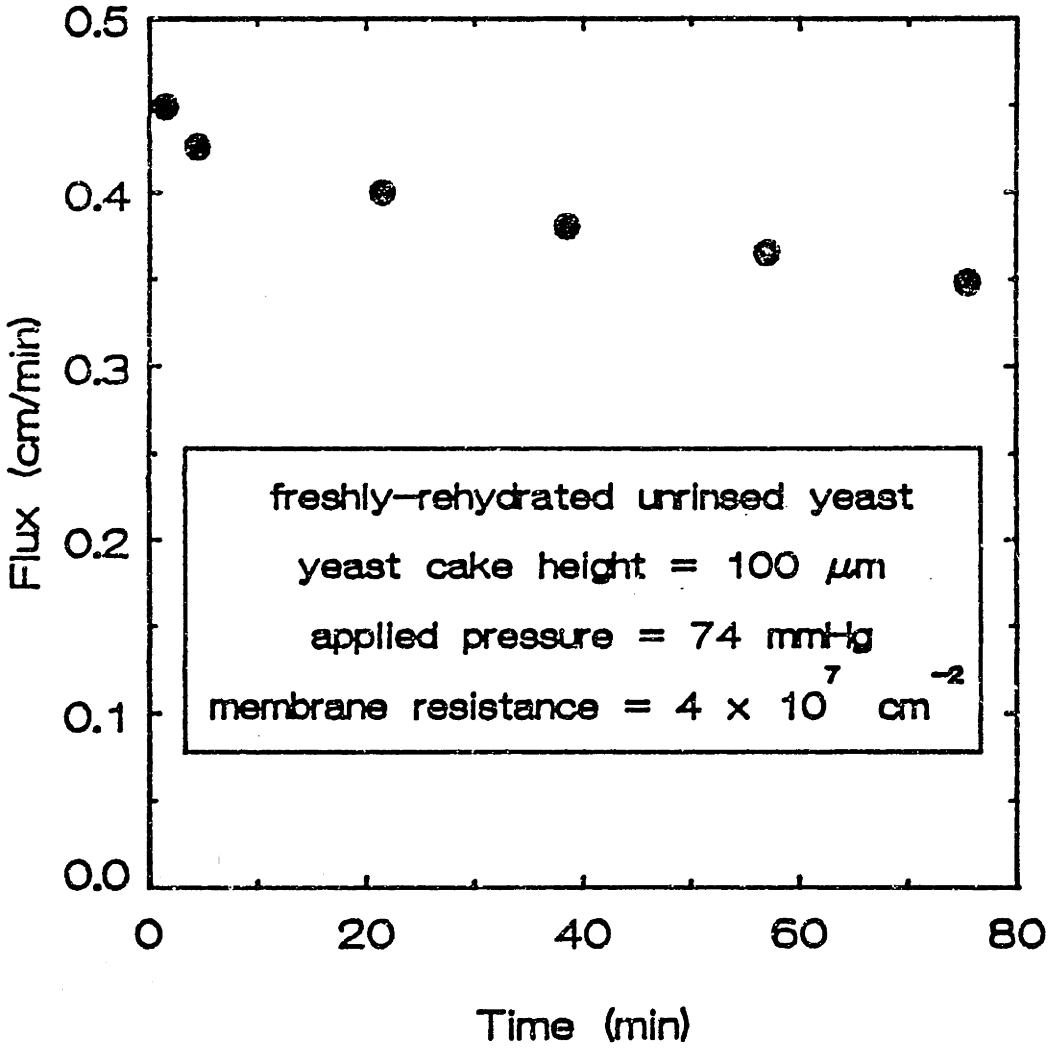

Figure 4-17. Time dependence of filtrate flux through a stagnant bed of bakers yeast.

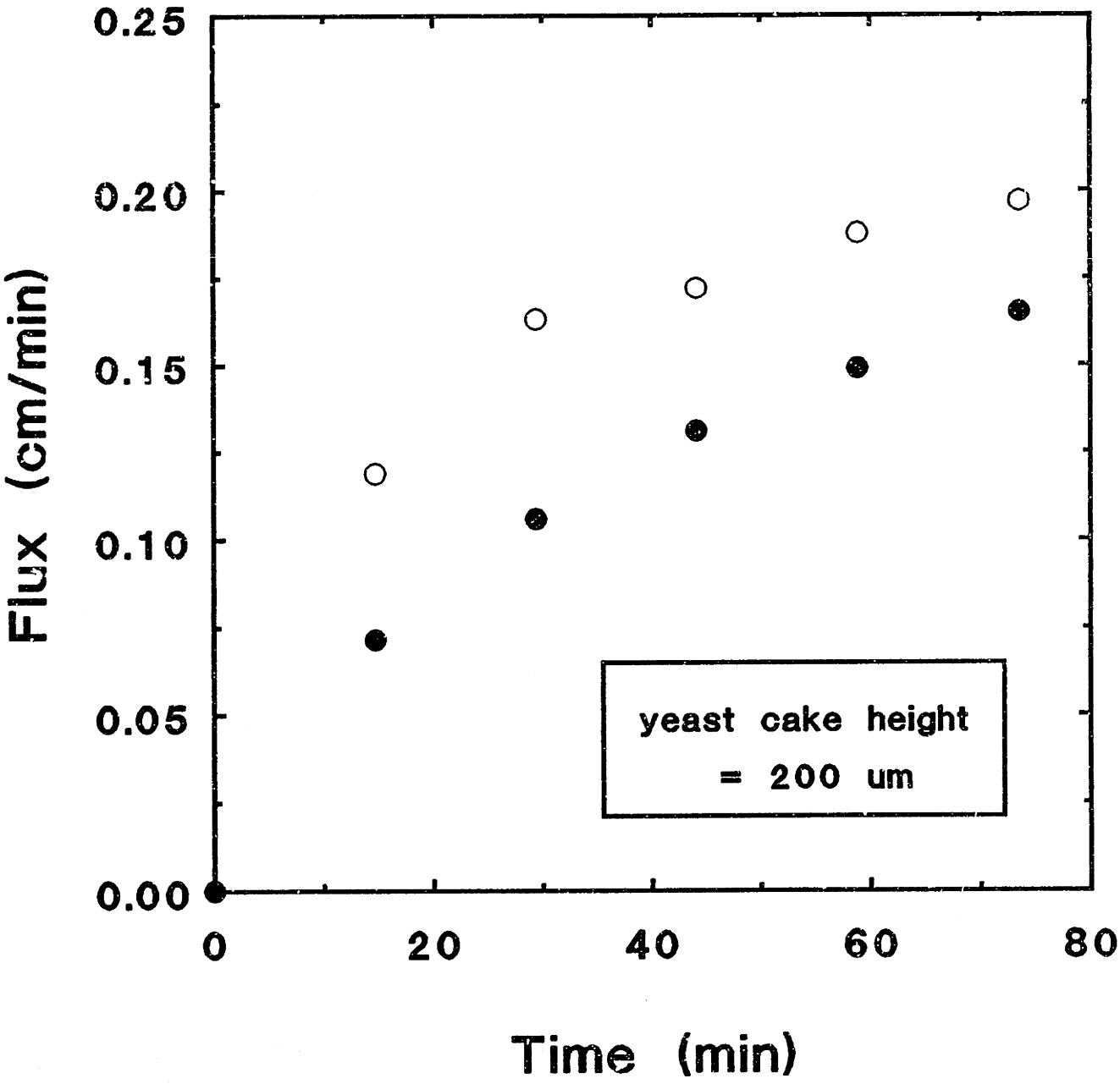

Figure 4-18. Hysteresis in 200 μm stagnant filtration data. The ○ data was taken in order of increasing pressure, with approximately 5 min between data points. Then, after 30 min at the highest pressure, the ● data was taken in order of decreasing pressure, again with approximately 5 min between data points.

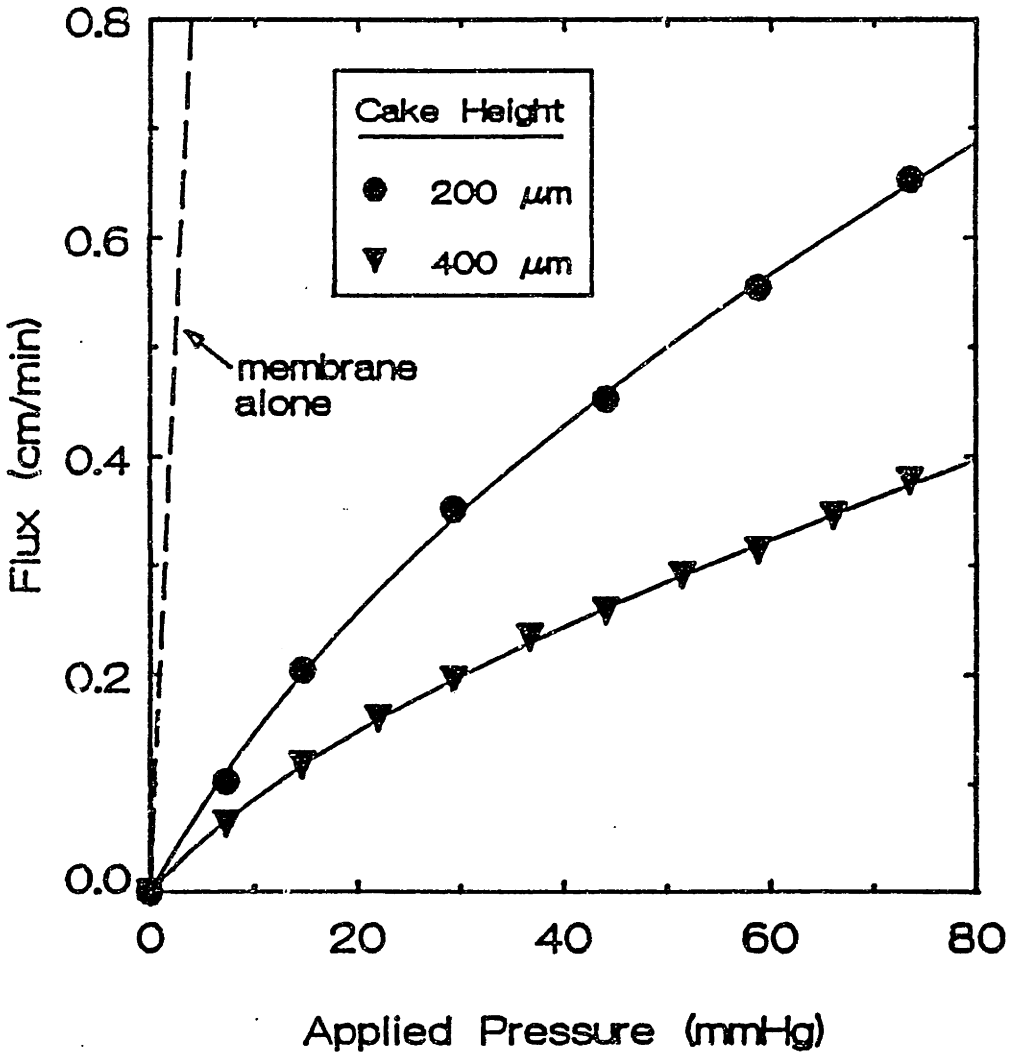

Figure 4-19. Filtrate flux through stagnant beds of 3x-rinsed freshly-rehydrated bakers yeast at RT.

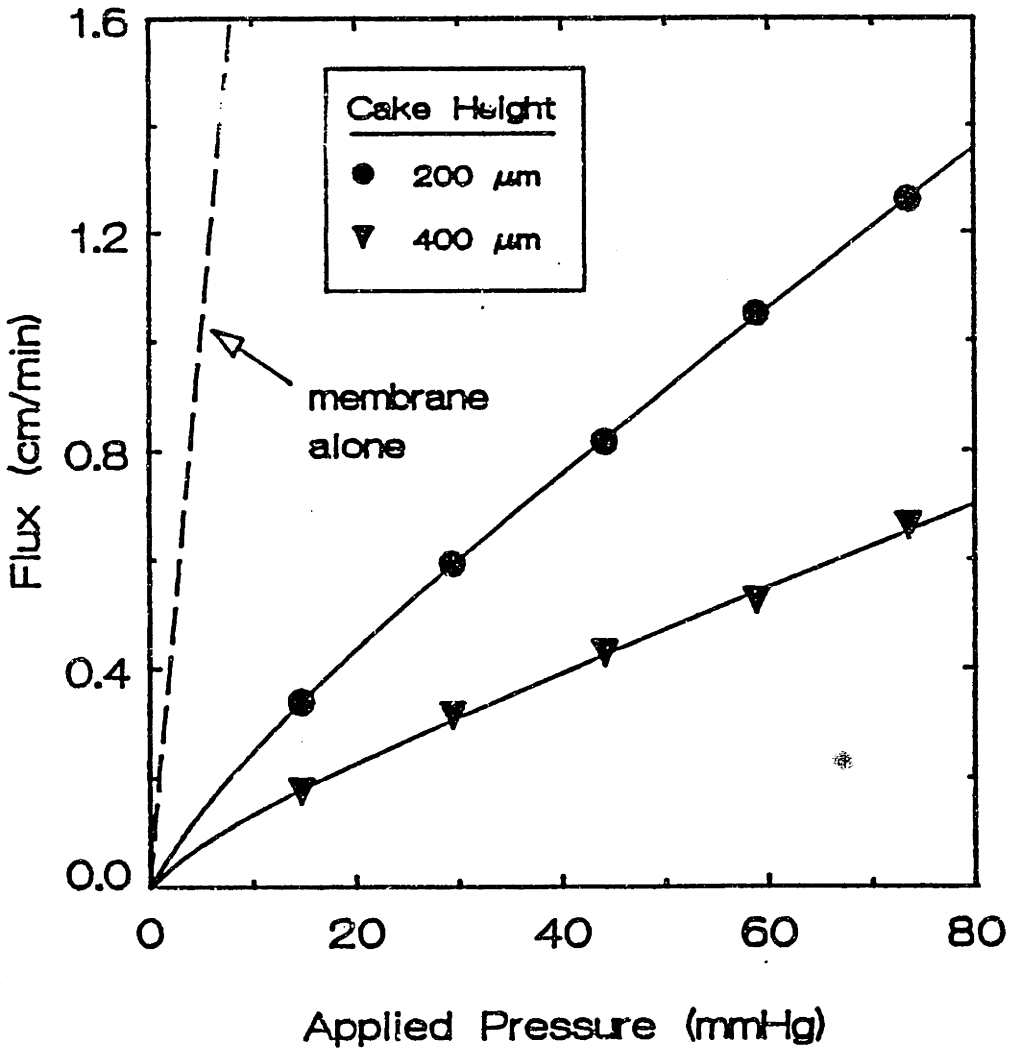

Figure 4-20. Filtrate flux through stagnant beds of glutaraldehyde-hardened bakers yeast at RT.

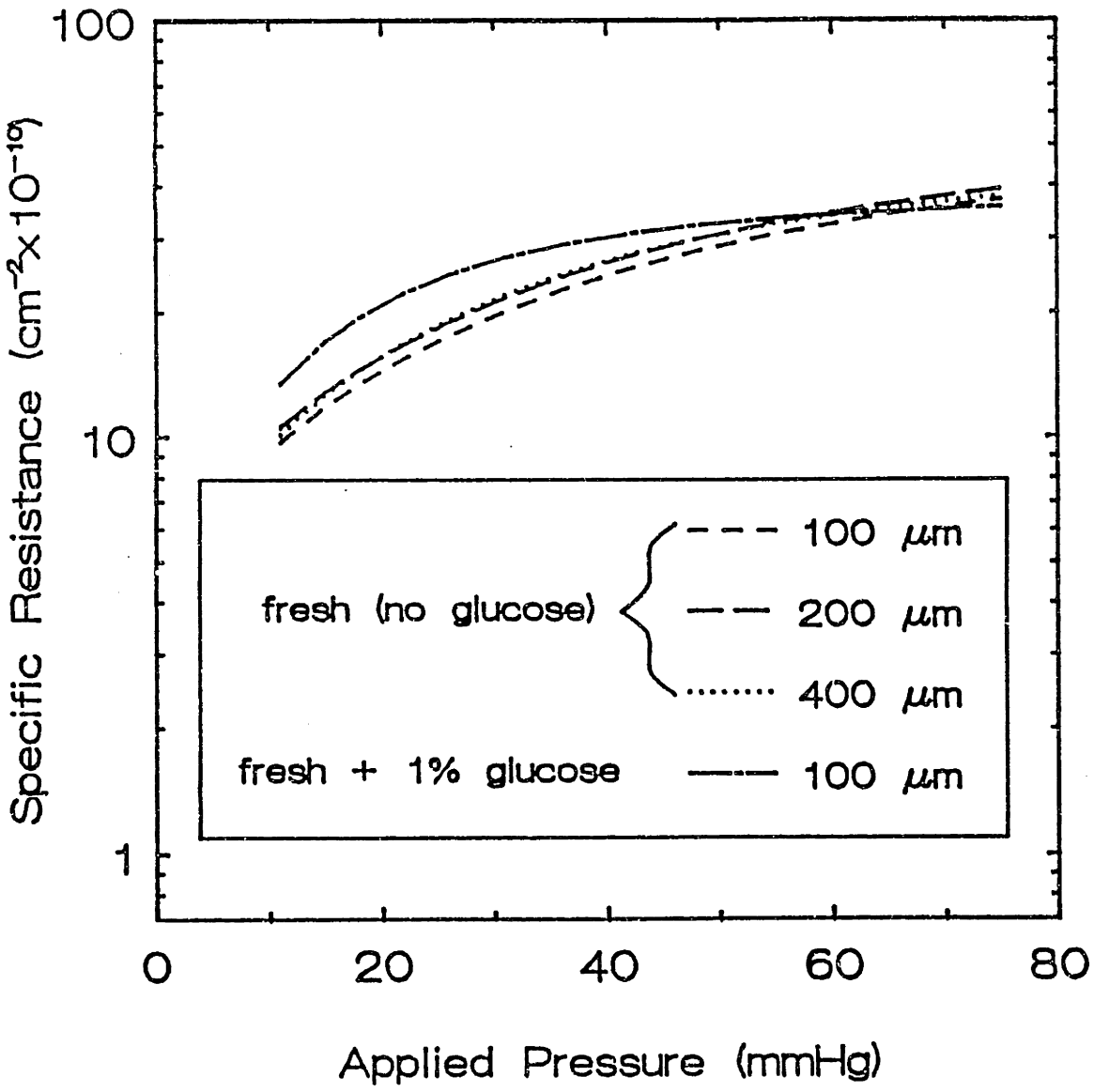

Figure 4-21. Hydraulic resistance of unrinsed freshly-rehydrated bakers yeast at RT, with and without 1% added glucose, as a function of applied pressure.

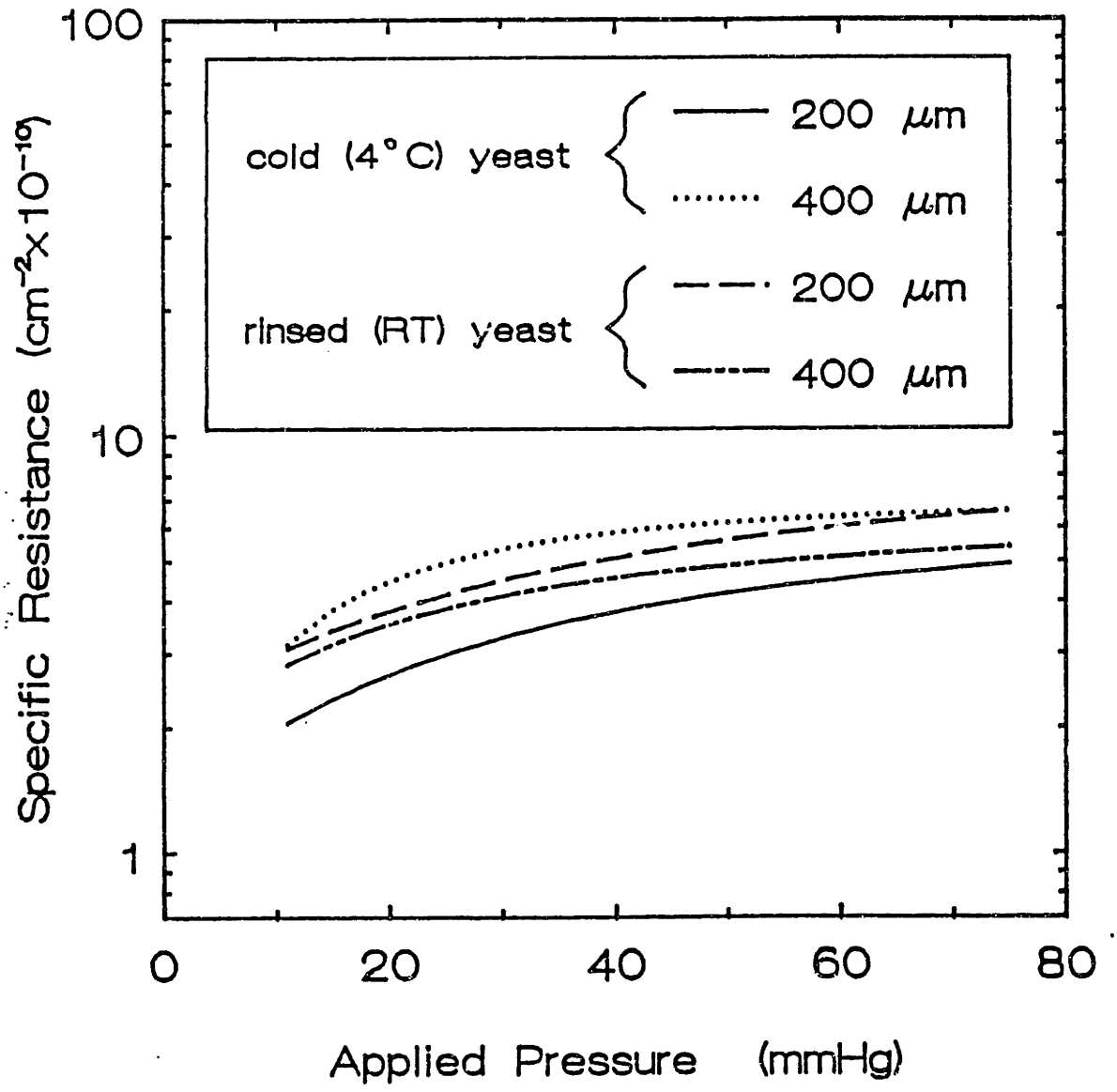

Figure 4-22. Hydraulic resistance of unrinsed freshly-rehydrated bakers yeast at 4°C and of 3x-rinsed freshly-rehydrated bakers yeast at RT.

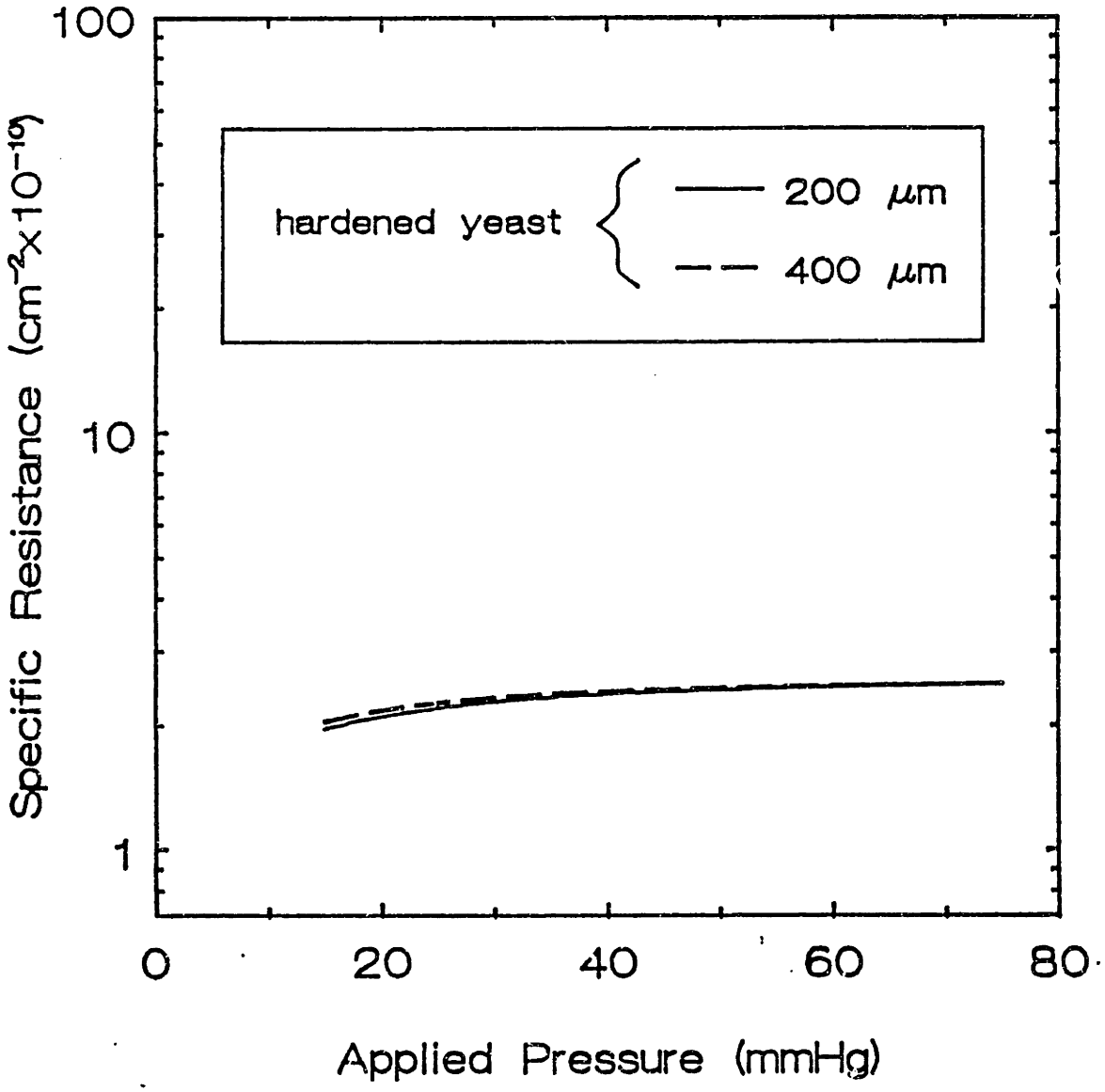

Figure 4-23. Hydraulic resistance of glutaraldehyde-hardened bakers yeast at RT.

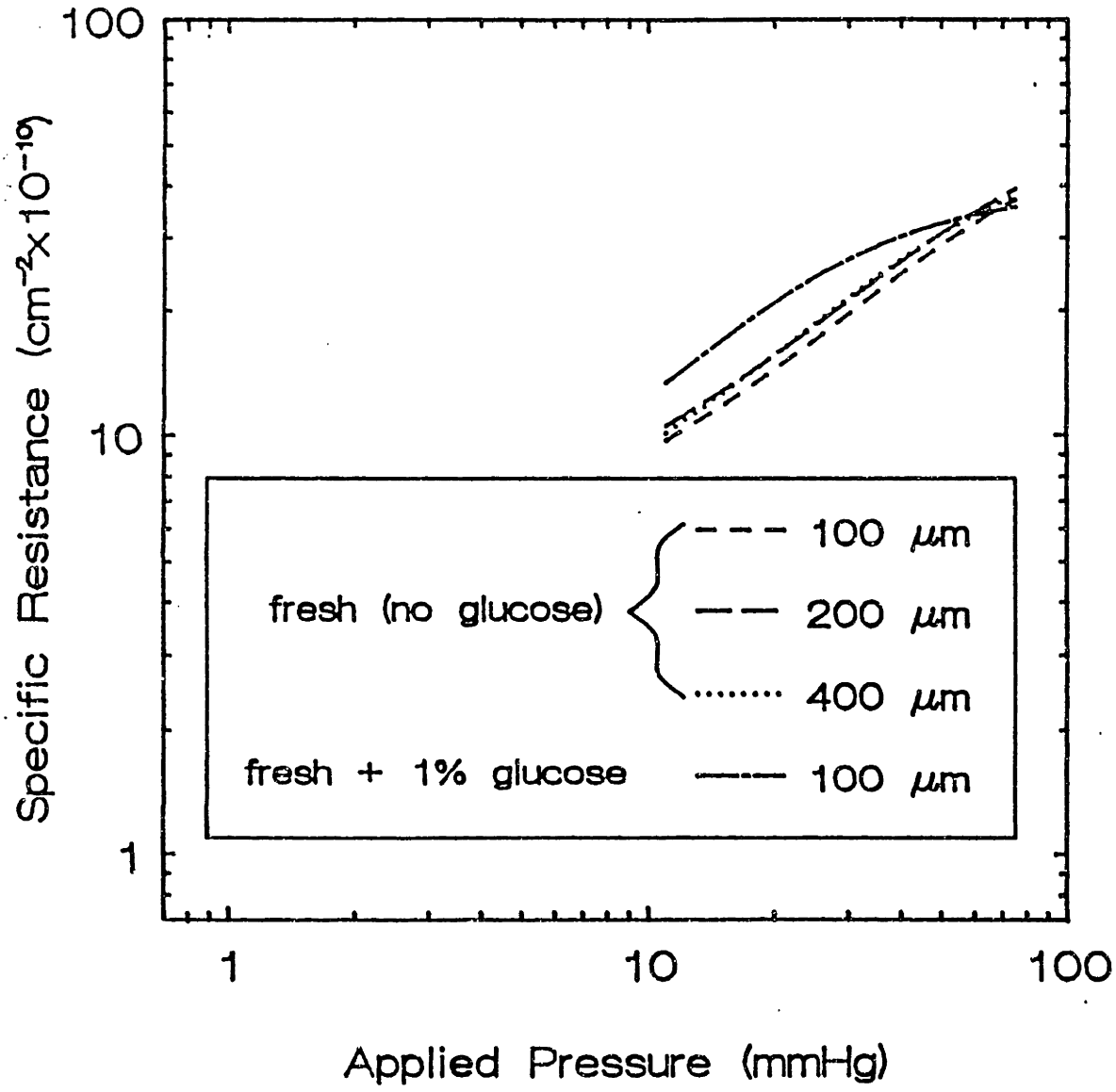

Figure 4-24. Hydraulic resistance of unrinsed freshly-rehydrated bakers yeast at RT, with and without 1% added glucose, as a function of applied pressure. (Same data as Figure 4-21, replotted on log-log scale.)

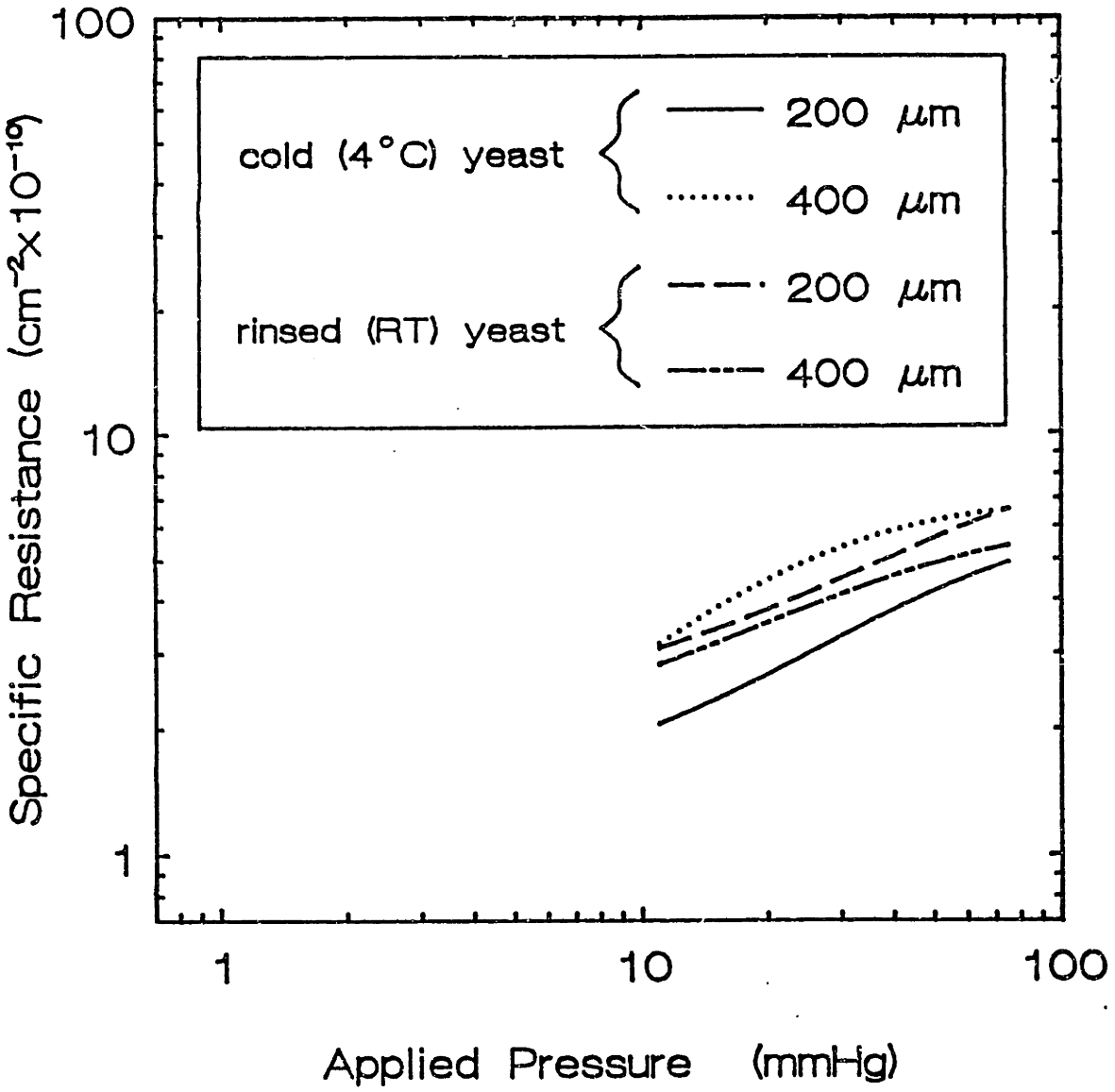

Figure 4-25. Hydraulic resistance of unrinsed freshly-rehydrated bakers yeast at 4°C and of 3x-rinsed freshly-rehydrated bakers yeast at RT. (Same data as Figure 4-22, replotted on log-log scale.)

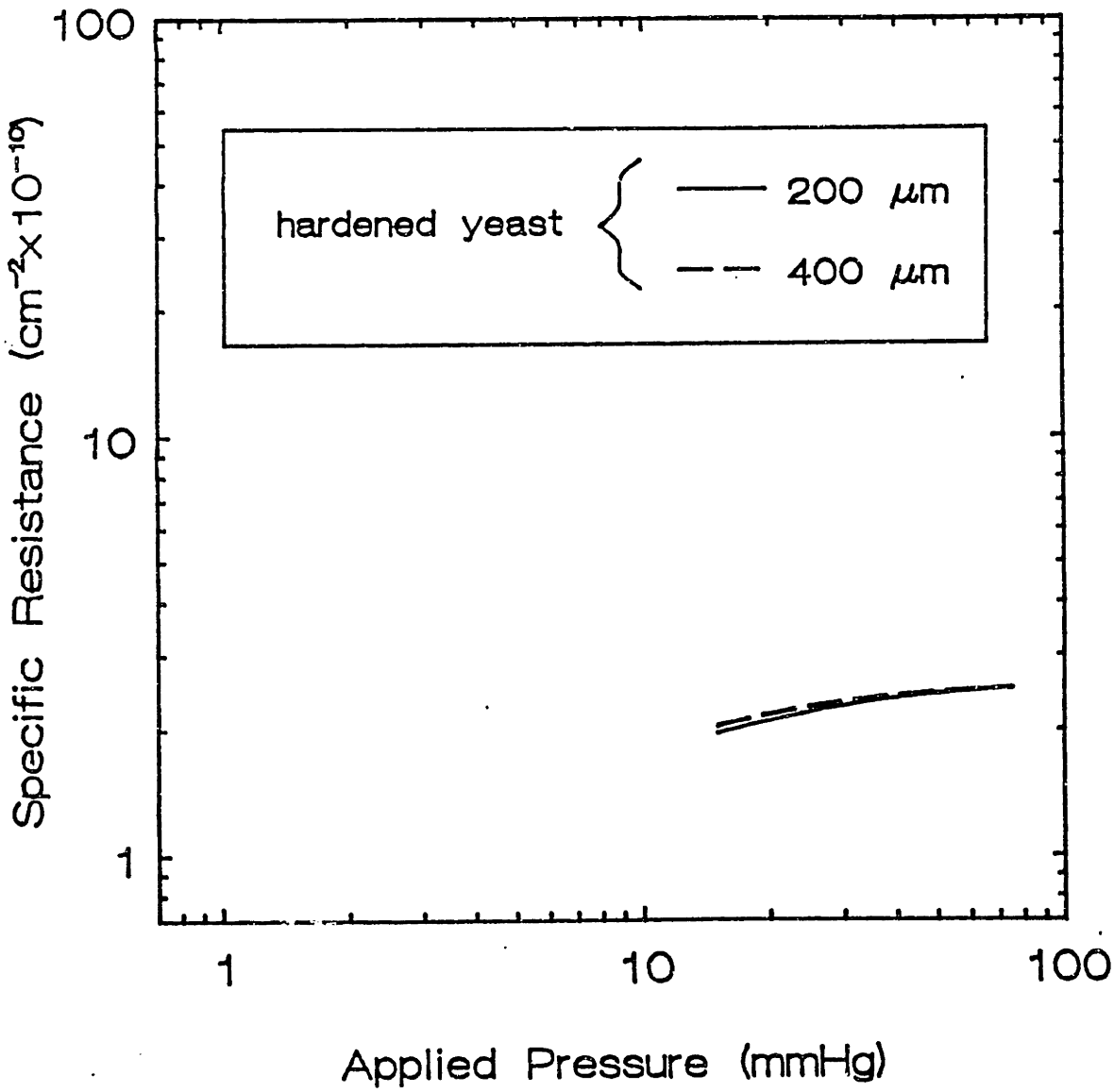

Figure 4-26. Hydraulic resistance of glutaraldehyde-hardened bakers yeast at RT. (Same data as Figure 4-23, re-plotted on log-log scale.)

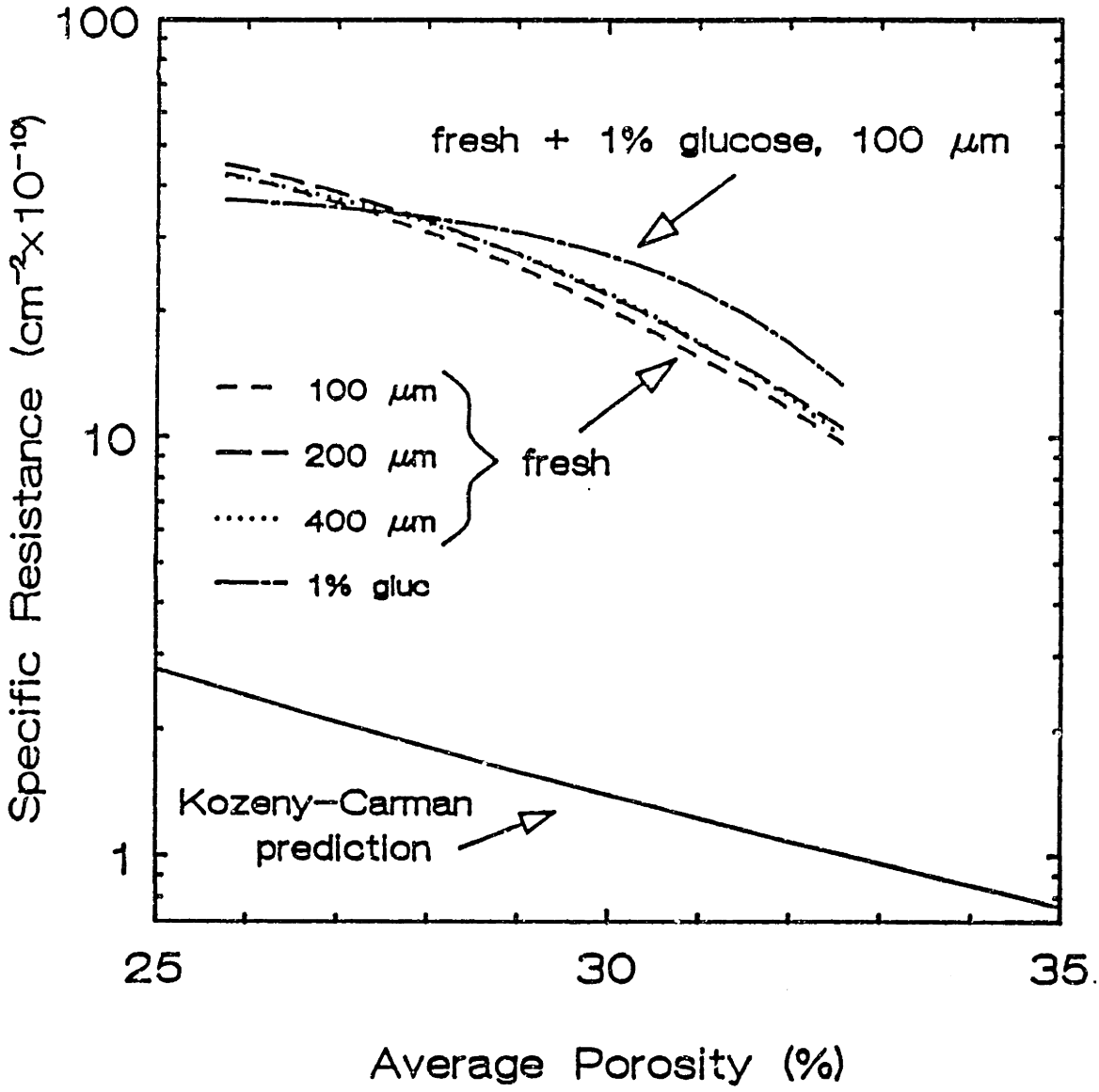

Figure 4-27. Hydraulic resistance of unrinsed freshly-rehydrated bakers yeast at RT (with and without 1% added glucose) as a function of the porosity of the cell bed, and the resistance predicted by the Kozeny-Carman equation.

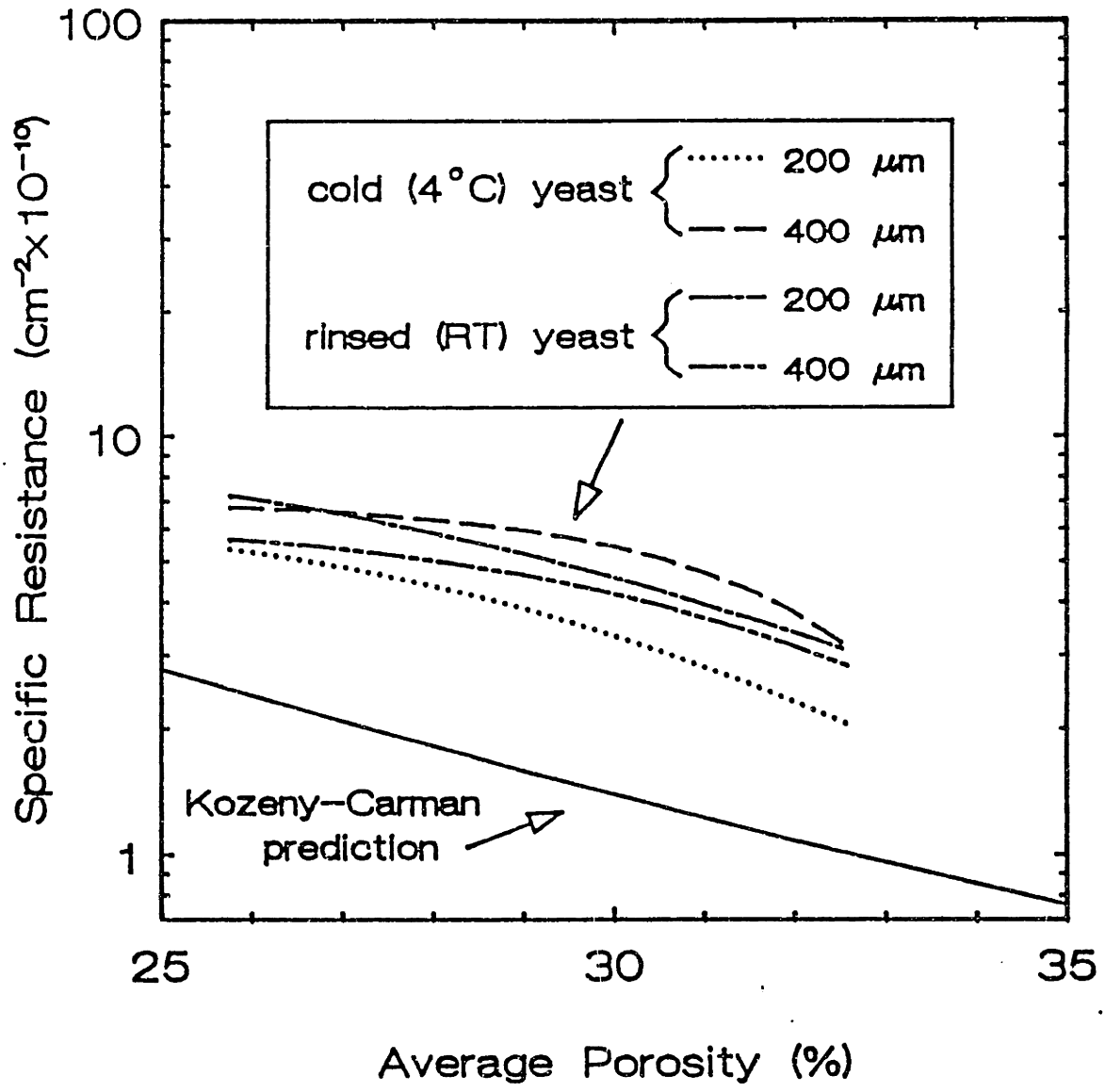

Figure 4-28. Hydraulic resistance of unrinsed freshly-rehydrated bakers yeast at 4°C and 3×-rinsed freshly-rehydrated bakers yeast at RT as a function of the porosity of the cell bed, and the resistance predicted by the Kozeny-Carman equation.

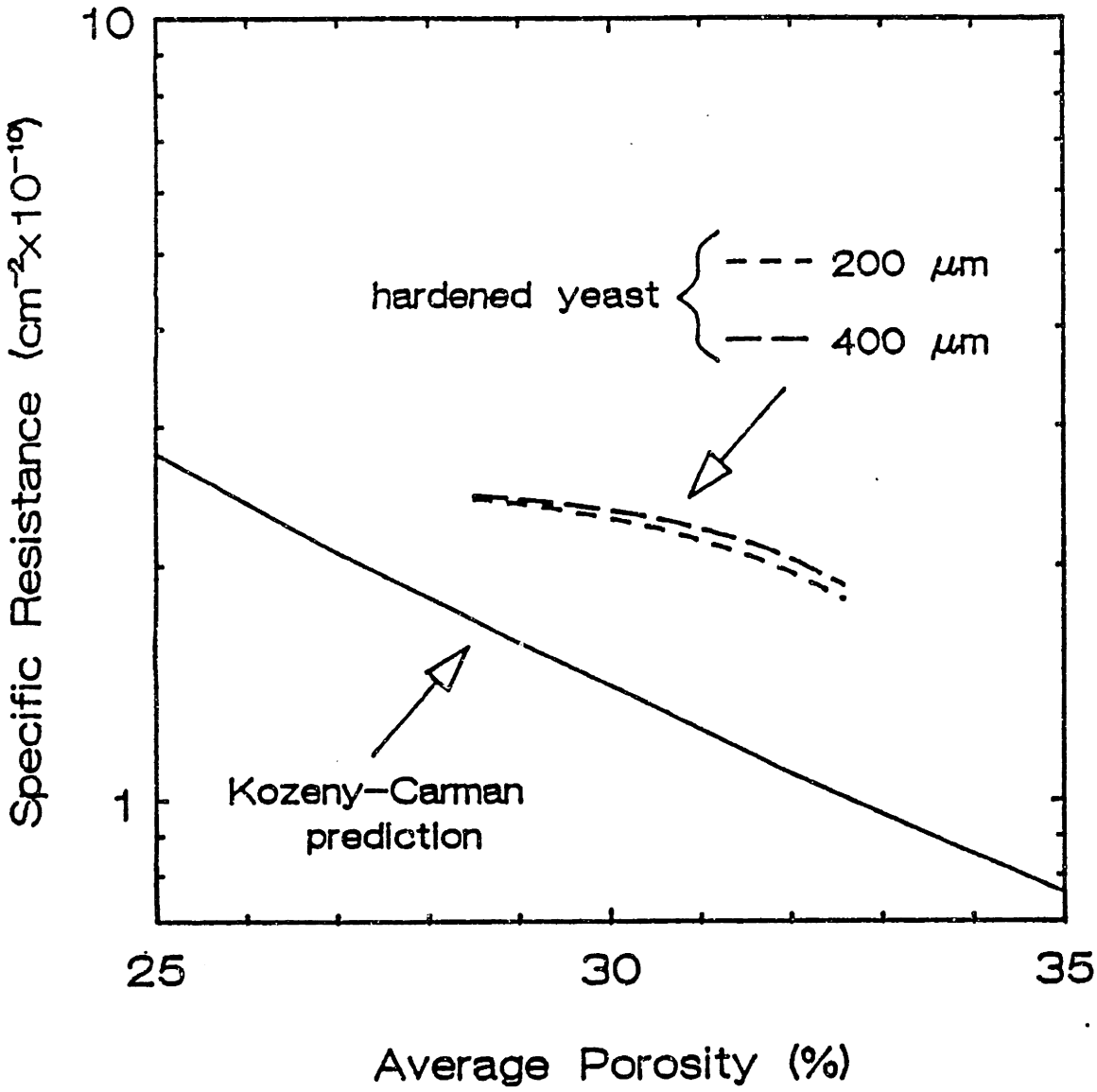

Figure 4-29. Hydraulic resistance of glutaraldehyde-hardened bakers yeast at RT as a function of the porosity of the cell bed, and the resistance predicted by the Kozeny-Carman equation.

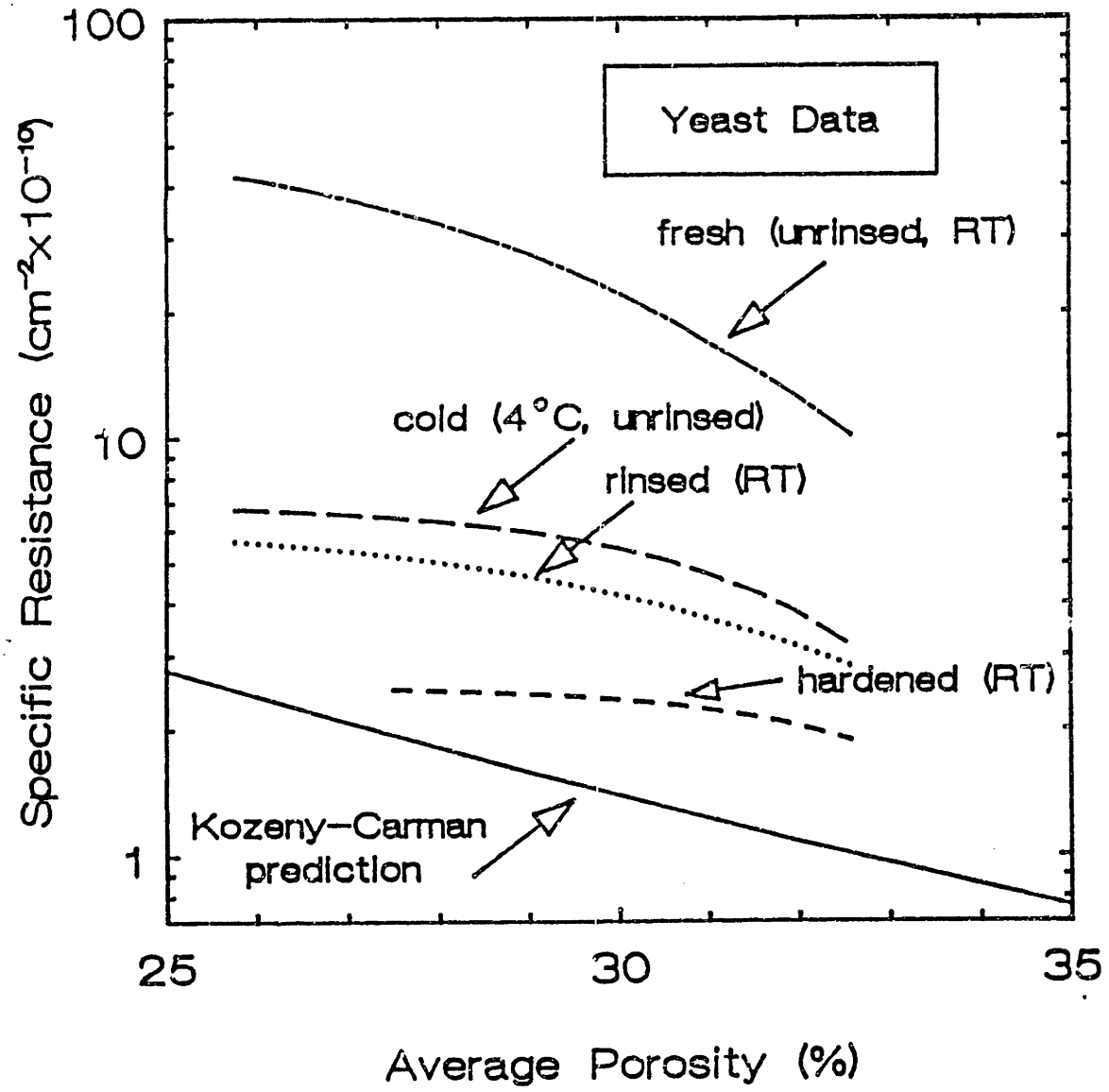

Figure 4-30. Hydraulic resistance of 400 μm stagnant beds of unrinsed, 3x-rinsed, and glutaraldehyde-hardened yeast at RT, and unrinsed yeast at 4°C, and the resistance predicted by the Kozeny-Carman equation.

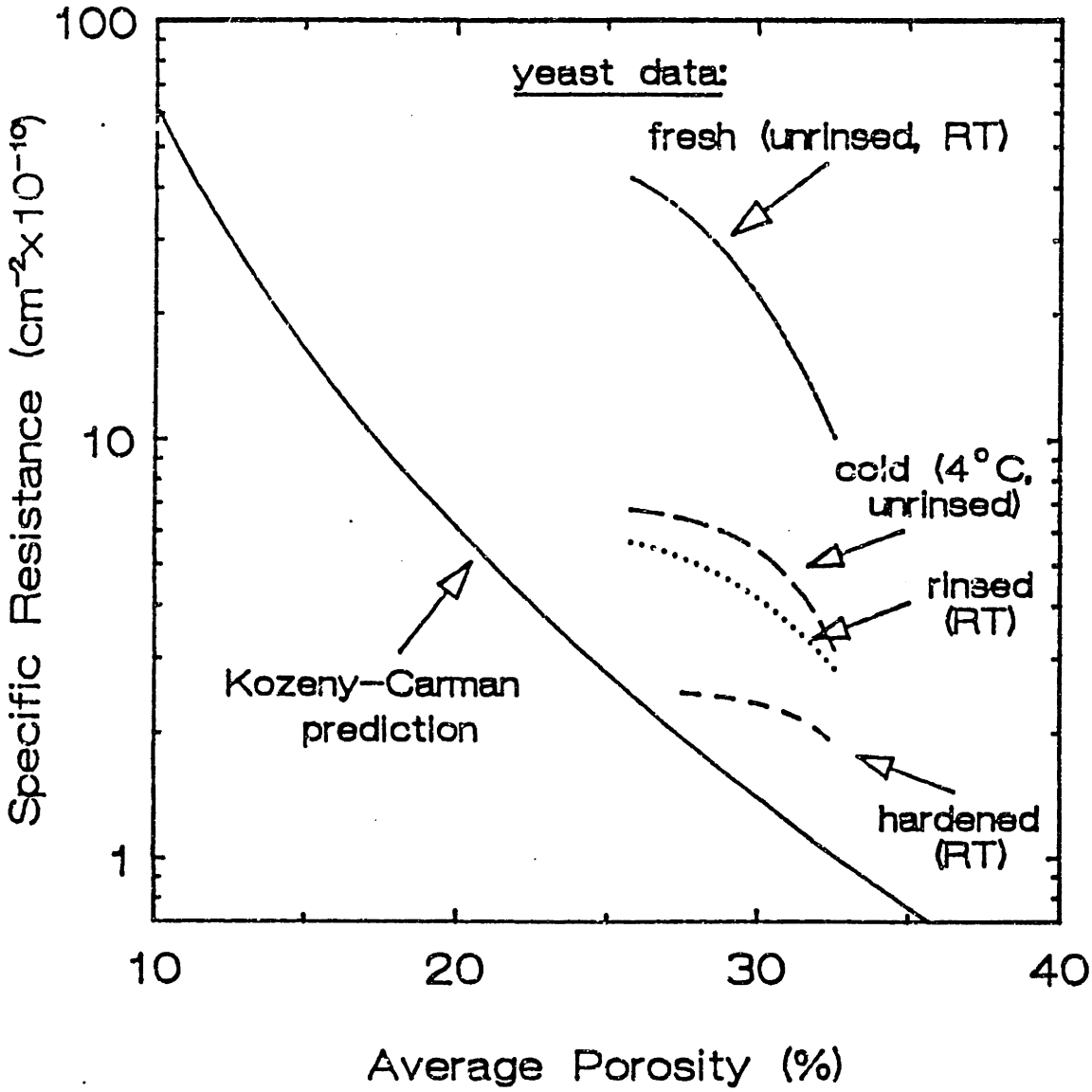

Figure 4-31. Hydraulic resistance of 400 μm stagnant beds of yeast. (Same data as Figure 4-30, re-plotted to show Kozeny-Carman predictions at low porosity.)

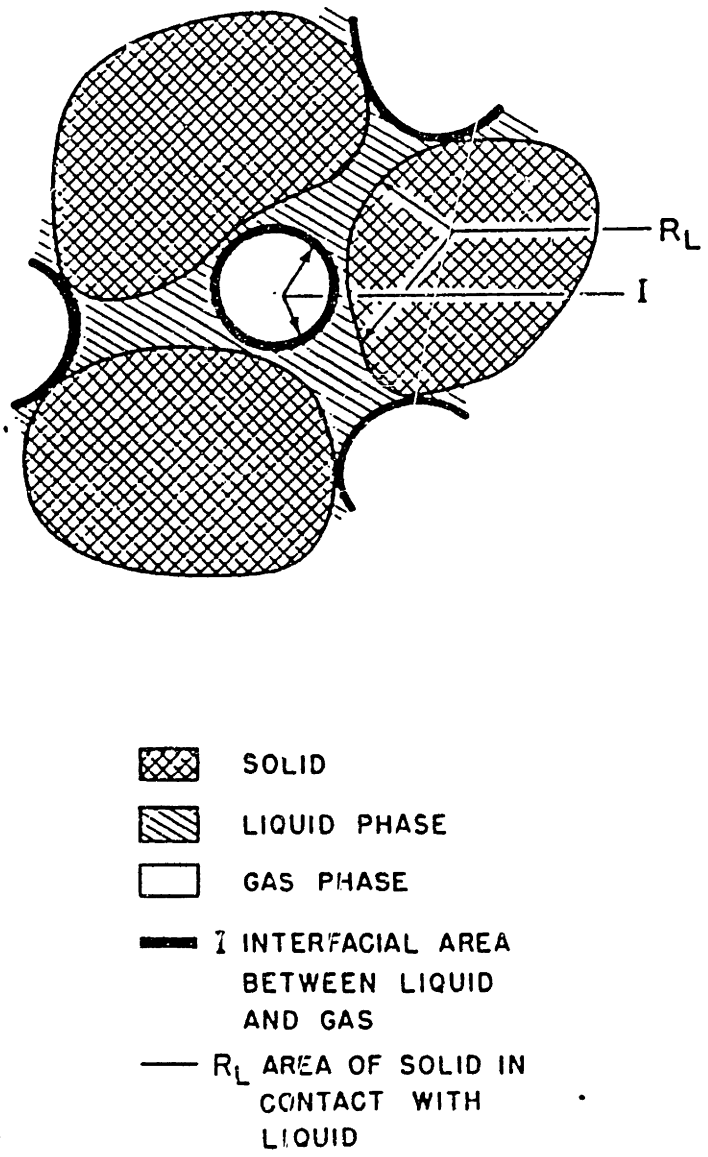

Figure 4-32. Porous medium in which bubbles of a stationary gas phase reduce the void fraction open for flow of a liquid phase, increasing the measured hydraulic resistance (Rapoport and Leas, 1951).

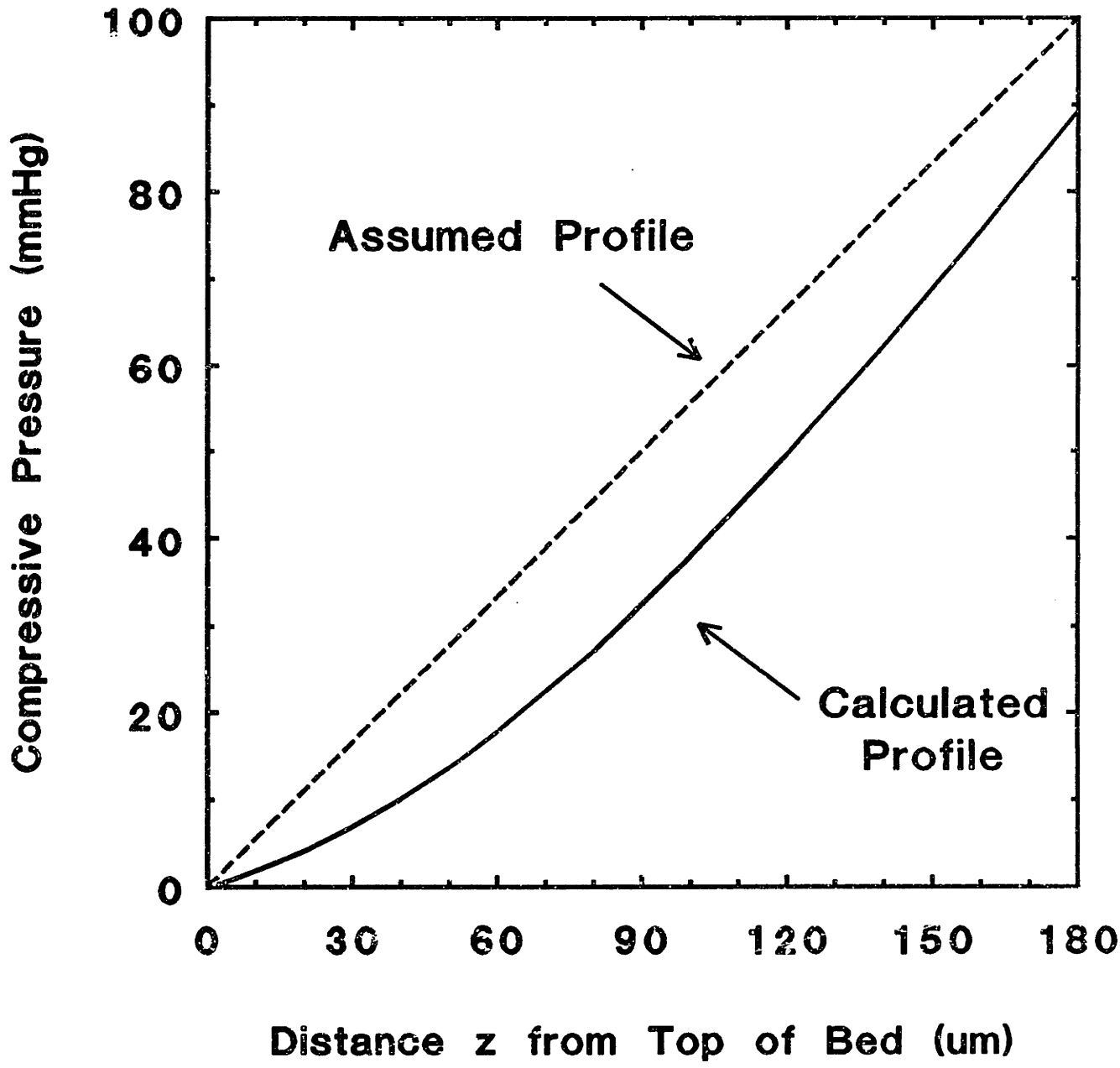

Figure 4-33. Calculated and assumed compressive pressure profiles as a function of the distance from the top of the latex particle bed.

CHAPTER 5

Filtrate Flux and Cake Thickness during Cross-Flow Filtration of Yeast and Latex Particle Suspensions

A. ABSTRACT

With the advent of genetic engineering and the growth of biochemical engineering, microbial cells are increasingly used to produce complex biological molecules which cannot be economically produced by traditional chemical processes. The first step in recovery of such products is to separate the cells from the fermentation broth. Cross-flow filtration with microporous hollow fiber membranes is an effective means of carrying out that separation.

In order to design a membrane filtration system, one must know how the filtration rate depends on design and operating parameters. Previous studies have demonstrated the general feasibility of separation of microbial cells with membranes, but have fallen short of providing adequate data for evaluating theoretical models which predict filtrate flux. Therefore, the first goal of this study was to characterize the filtrate flux behavior of a model microbial cell system in hollow fiber microfiltration membranes. We chose Saccharomyces cerevisiae, bakers yeast, as the model system and measured the filtrate flux as a function of applied pressure, bulk flow rate, concentration and time. By studying several types of hollow fibers, we also analyzed the effects of hollow fiber geometry and membrane resistance.

Because the filtration rate is believed to be limited by the buildup of cakes of cells on the membrane surface, our second goal was to measure yeast cakes formed during cross-flow filtration in hollow fibers. Using an experimental technique which we had previously developed for observing red blood cell polarization layers, we measured the yeast cake thickness as a function of time, axial position, and filtration conditions. Our third goal was to compare flux and cake thickness data to previous results with more deformable red cells.

Flux experiments demonstrated significant differences between the filtration behavior of yeast and red cells. While the flux with red cells dropped to a steady-state value in less than a minute, the flux with yeast dropped rapidly for the first 20 minutes, and continued to decrease slowly throughout 2 hr experiments. Increasing the wall shear rate increased the flux, but the dependence was weaker than the previous linear dependence reported for blood.

Attempts to determine whether a pressure-independent maximum flux was attained with yeast as well as blood revealed a serious problem: hollow fiber clogging by the yeast. We found that hollow fibers with internal diameters optimized for blood (~300 μm) were terribly susceptible to clogging. Larger (1 mm) fibers worked better, but still clogged if the applied pressure was raised to its final value (75 mmHg) too quickly. Because large fractions of the inlet flow rate of the yeast suspensions were removed, fiber lengths had to be shorter than those normally used for blood. Whereas avoiding cell lysis has been an imporatant constraint in designing blood filtration systems, avoiding fiber clogging will be the primary constraint in designing yeast filtration systems.

Freezing experiments revealed significant buildup of yeast cakes on the membranes, and confirmed the occurrence of fiber clogging under certain conditions. Thick yeast cakes formed rapidly, more rapidly than fluxes dropped off. The cakes grew with distance from the inlet, particularly as the local bulk flow rate decreased. In fibers whose membrane resistance increased significantly with time, the cakes washed away in long-term experiments. The observed yeast cakes were thick enough to affect the local shear rate and the axial pressure drop as well as the total resistance to flow through the membrane. In combination with flux measurements, this cake thickness data can be used to assess mathematical models for cross-flow filtration of yeast.

B. INTRODUCTION

Filtration with microporous membranes is increasingly used as a first step in downstream processing of bioreactor effluents, to separate microbial cells such as yeast from the media in which they are grown. Cross-flow configurations, in which the bulk flow is parallel to the filtering membrane as shown in Figure 5-1, minimize the accumulation of retained cells near the membrane surface, resulting in significantly larger filtration rates than can be obtained in dead-ended systems. Even so, the flux obtained in cross-flow microfiltration of cell suspensions is orders of magnitude smaller than that obtained when filtering cell-free media under identical conditions (Blatt et al., 1970; and Porter, 1972). It has been proposed that a concentrated layer of cells at the membrane surface reduces the flux

by (1) blocking membrane pores and (2) forming a cake which provides additional hydraulic resistance.

Red blood cells are the only cell system whose cross-flow filtration properties have been studied in detail. The filtrate flux obtained when filtering red cells drops down to a steady-state value within about 1 min (Zydney, 1985; see Chapter 2 of this thesis). This steady-state flux has been shown to reach a pressure-independent, maximum value which increases with increasing wall shear rate and decreases with increasing cell concentration (Zydney and Colton, 1982). Recent studies (Saltzman, 1984; Zydney, 1985; Zydney, et al., 1988) have demonstrated that pore blockage and cell layer hydraulic resistance are the mechanisms responsible for flux reduction in cross-flow filtration of red cells. Those studies have also shown that the value of the maximum flux is determined by a balance between convection toward the membrane and shear-augmented diffusion away from the membrane; during the transient approach to steady state, cells continue to accumulate in the boundary layer until the rate at which they are carried toward the membrane by the convective flow has decreaed to the rate at which they are transported away from the membrane. Because only a very thin layer of red cells is required to reduce the flux to its steady-state value, this layer does not significantly affect the shear-augmented diffusion which is taking place throughout a much larger concentration boundary layer. As a result, the maximum flux is a function of factors which influence shear-augmented diffusion--shear rate and bulk concentration--but is not a function of factors which influence convection--membrane resistance, applied pressure, cell bed hydraulic resistance, or pore blockage.

One might expect that microbial cells such as yeast, which are about the same size as red cells, would undergo comparable rates of shear-augmented diffusion, and hence display filtration behavior similar to that seen with red cells. However, there is reason to believe that the conclusions regarding red cell filtration might not be applicable to filtration of microbial cells. In particular, the decoupling of the flux-reduction mechanism from the flux-determining balance between convection and diffusion results from the very high specific resistance of red cells, which is related to their extreme deformability. Previous work (Chapter 3) has shown that yeast cells are much less compressible than red cells, and, as a result, have a much lower specific hydraulic resistance. Therefore the yeast cell layers formed

on membrane surfaces are expected to be significantly thicker than red cell layers under corresponding conditions. Since such thick layers could cause significant differences in flux behavior, it is important to characterize the filtration behavior of such microbial cell systems in order to provide a sound basis for the design of effective systems.

The objectives of this work were to characterize the filtrate flux behavior of a model microbial cell system, bakers yeast, to measure the thickness of yeast cakes which build up on membranes during cross-flow filtration, and to compare flux and cake thickness data to previous data with red cells. While the experimental techniques used in measuring fluxes were standard engineering-laboratory procedures, the freeze-substitution technique used in measuring yeast and red cell cake heights was developed specifically for those experiments. The results of flux and cake thickness measurements can be used to test theoretical models for the filtrate flux in cross-flow microfiltration of yeast.

Hollow fiber membranes were used in these experiments because their geometry is uniquely suitable for the freeze-substitution technique used to measure yeast cake heights. Better design of hollow fiber systems is a relevant industrial goal since the use of membrane systems, in general, and hollow fiber membranes, in particular, is growing. Cross-flow membrane filtration offers several advantages over other separation techniques such as centrifugation: low capital and energy costs, continuous processing, gentle process conditions, no aerosol formation, and easy scale-up. Hollow fiber modules offer the additional advantages of large surface areas and small holdup volumes.

C. MATERIALS AND METHODS

Many of the experiments described here were carried out by Mitsuru Suzuki, a visiting scientist from Toyobo Ltd. (Japan), and Eric Morrel, a postdoctoral associate. Mr. Suzuki was primarily responsible for the freeze-substitution experiments with yeast, while Dr. Morrel was primarily responsible for flux experiments with latex particles. Both contributed substantially to the completion of this project, and I am grateful for their help.

All yeast filtration experiments consisted of the following steps: (1) preparation of the yeast suspension, (2) set-up of the experimental apparatus, (3) measurement of the membrane resistance, (4) measurement of the flux during yeast filtration, and, in some experiments,

(5) freeze-substitution of the hollow fiber. A detailed description of each of these steps will follow a brief explanation of differences among three types of experiments performed.

In the results and discussion sections which follow, the yeast filtration experiments described in this section will be grouped into four categories based on the composition of the suspending fluid and the configuration of hollow fiber system used. It is important to discuss the results of the four types of experiments separately because the nature of the suspending fluid and the geometry of the system can affect the observed filtration behavior. However, the experimental techniques are best discussed together since all consist of variations of the steps outlined above.

One category is comprised of freeze-substitution experiments only, since those experiments were the only ones in which suspensions of yeast in albumin solution were filtered through single hollow fibers. In these experiments, the choice of suspending fluid and system configuration were dictated by the freezing procedure. Albumin solution was used to suspend the yeast cells because the fixation procedure required protein (albumin) in solution in order to fix the cells in place. Use of single hollow fibers allowed rapid freezing and avoided the potential problem of uneven flow distribution among fibers potted together.

Unfortunately, the presence of protein influences filtration behavior as well as the subsequent fixation procedure. Previous reports on membrane fouling have shown that exposure to protein solution reduces membrane permeability (Fane et al., 1983; Randerson and Taylor, 1983; Roberts et al., 1983). Since the membrane resistance could not be measured after freeze-substitution (because the fibers were fixed and embedded), changes in membrane permeability had to be estimated from separate experiments. Therefore albumin filtration experiments (without yeast) were conducted to measure membrane resistances in the presence of albumin. Other (non-freezing) filtration experiments were carried out with yeast suspended in protein-free medium to minimize changes in membrane resistance.

The three types of non-freezing filtration experiments differ in the hollow fiber configuration used. In single-fiber experiments with the 300 μm and 1000 μm ID hollow fibers, the experimental setup was exactly the same as that used in the freeze-substitution experiments. Experimental procedures were identical, except that instead of ultimately freezing the fiber, the membrane resistance was re-measured after yeast filtration. In

experiments with 28-fiber cartridges (1000 μm ID, W. R. Grace), suspensions of yeast in medium (without albumin) and suspensions of latex particles in distilled water were filtered. The specific equipment and procedures used in the cartridge experiments were different from those used in the single-fiber experiments because of the substantial difference in bulk flow rates required. The membrane resistance was again measured both before and after yeast filtration. The single-fiber experiments with the 4.66 mm cartridges used equipment and procedures taken from both the single-fiber experiments with the smaller fibers and the cartridge experiments.

1. Preparation of Yeast Suspensions and Latex Particle Suspensions

All Saccharomyces cerevisiae suspensions were prepared from commercially available active dry yeast (ADY, Red Star Yeast Co., Randolph, MA). The low moisture content (8% wt/wt) of the ADY was verified by weighing before and after drying for 24 hours in a 100°C oven. Yeast "medium" (Wickerham, 1951) without a carbon source or vitamins was prepared according to the recipe in Chapter 4, and then filtered sequentially through 8.0 μm (type SCWP-047-00, Millipore Corp., Bedford, MA) and 0.45 μm (type ME25, Schleicher & Schuell, Keene, NH) nitrocellulose membranes prior to use. A measured weight of ADY was placed in a flask containing approximately two-thirds of the desired final volume and stirred for about half an hour. Then the suspension was transferred to a volumetric flask or a graduated cylinder, filled to the desired volume with additional medium, and stirred for the remainder of an hour. Sodium azide (0.2%) was added to yeast medium and suspensions to prevent the bacterial growth.

Throughout this paper, the yeast concentration will be expressed as a volume fraction rather than as a dry weight per unit volume. As was discussed in Chapter 4, the appropriate conversion factor for the glucose-free medium used here is 2.3% (vol cells/vol suspension) yeast per 1 g ADY/100 ml suspension. (This value was determined by correcting the results of Reuss et al. (1979) to account for an error in their dye dilution technique; see Chapter 4 for details.)

Albumin solution (6 g/100 ml solution) was prepared by adding bovine serum albumin (Fraction V Powder, Sigma Chemical Co., St. Louis, MO) to pre-filtered medium, sirring for

one hour, and filtering through an 8.0 μm nitrocellulose membrane. Suspensions of yeast in albumin were prepared by rehydrating the yeast as described above, decanting off the medium after allowing the yeast to settle, and resuspending the yeast in albumin solution.

Suspensions of polystyrene latex particles (density ρ_p = 1.055 g/cm^2) in distilled water with no additives were purchased from Interfacial Dynamics Corporation (Portland, OR). The particle diameters, surface charge densities, initial particle concentrations, and batch numbers are listed in Table I. In some experiments the particle suspensions were diluted with filtered distilled water prior to use. The initial concentrations of the suspensions were verified and the concentrations after dilutions were determined as described in Chapter 4.

Table I. Latex Particle Suspensions used in Flux Experiments.

Particle Diameter (μm)	Initial Concentration (vol/vol)	Surface Charge Density (μC/cm^2)	Lot. No.
0.264±1.7%	7.7±0.1	1.28	10-59-28
0.711±1.1%	8.9±0.1	7.01	10-4-7
2.17±3.0%	10.9±0.1	5.32	10-50-83
3.98±11.3%	8.4±0.1	7.27	2-83-8

2. Hollow Fibers Used

Nominal manufacturer's specifications for the several types of hollow fibers employed are listed in Table II. All of the hollow fibers studied here were graciously supplied by the manufacturers.

3. Experimental Setup

a. Single fiber experiments with 300 μm and 1000 μm fibers

The filtration assembly used in all single-fiber experiments is shown in Figure 5-2. The fiber length in all of the experiments reported here was 5 cm. (Serious clogging problems had been encountered in initial experiments with 10 cm lengths.) For freezing experiments,

Table II. Manufacturer's Specifications for Hollow Fibers

Material of Construction	Manufacturer and Location	Fiber Diameter ID (μm)	Wall Thickness (μm)	Pore Diameter (μm)	Hydraulic Resistance (cm^{-1})
polyamide	Enka AG (Wuppertal, F. R. G)	320	100	0.35	1.2×10^9
polypropylene	Enka AG	330	110	0.40	5.8×10^8
modified polysulfone	Sepracor (Marlborough, MA)	1000	300	0.7-0.8	1.2×10^9
polysulfone -Biopol	W. R. Grace (Lexington, MA)	950	300	0.20	5.0×10^8
XM formulation	W. R. Grace	4660	20	< 0.01	1.2×10^9
polysulfone-dextran	Kinetek (St. Louis, MO)	1000	300	< 0.1	1.2×10^9

the fibers were marked with a permanent ink magic marker at 1 cm intervals to prevent loss of axial position information.The specifics of the auxiliary apparatus (pump, tubing, connectors) used in experiments with the 4.66 mm fibers will be discussed separately below. In all of the other single fiber experiments, the inlet and outlet lines made of polyethylene tubing (Intramedic, Clay Adams, Parsipanny, NJ) with internal diameters of 580 μm or less were attached to the hollow fiber by inserting the ends of the tubing and fiber into a short piece of narrow Tygon tubing. The outer diameters of the polyethylene tubing and the hollow fiber were closely matched to the inner diameter of the Tygon tubing so that no potting material or glue was required. The fiber was then suspended from a ringstand in a special apparatus which held the fiber taut and vertical without damaging the fiber. The inlet line, which always led to the bottom of the hollow fiber, was attached to a syringe pump (Sage Instruments Model 355, Orion Research, Inc., Cambridge, MA) by inserting a syringe needle into the other end of the tubing. The needle was then attached to a disposable plastic syringe which served as an inlet reservoir. The twist-on connection between the needle and syringe allowed easy switching from one reservoir to another. A small magnetic stirring bar was placed inside the syringe and a small stirring plate (Submersible Magnetic Stirrer Model 700, Troemner, Inc., Philadelphia, PA) was held directly above the syringe.

Both the syringe pump and an Erlenmeyer flask which served as the outlet reservoir were placed on a laboratory jack so that they could be raised simultaneously. In order to raise the applied pressure for flux measurements, it was only necessary to raise the outlet reservoir. However, because the inlet line would be cut near the pump during the freezing procedure, the pump was raised so that cutting the line would not cause a drop in the applied pressure.

b. Cartridge experiments

The setup for cross-flow experiments with hollow fiber cartridges is shown in Figure 5-3. The manufacturer of the polysulfone/Biopol hollow fibers supplied cartridges containing 28 fibers, approximate 8.5 cm long (effective area 55 cm^2, reported by the manufacturer, takes into account losses due to wicking of potting material onto fibers). Tygon tubing (ID = 2 to 4 mm, depending on shear rate) was used as inlet and outlet tubing. Smaller tubing was used in low-shear-rate experiments, in which avoidance of yeast settling in the lines was the primary concern. Larger tubing was used in high-shear-rate experiments, in which minimizing pressure drop in the lines was more of a problem than avoiding settling. The inlet line ran from the inlet reservoir (an Erlenmeyer flask on a magnetic stirring plate) to a Masterflex peristaltic pump (Model 7520-35, Standard Console Drive with Quick-Load Pump Head, Cole-Parmer Instrument Co., Chicago, IL) and from the pump to the bulk inlet port at one end of the cartridge. The outlet line ran from the bulk outlet port immediately to a tee-shaped joint which allowed connection of a pressure transducer, and then on to an Erlenmeyer flask on a laboratory jack, which served as an outlet reservoir. The outlet applied pressure was adjusted by raising the outlet reservoir.

c. Single fiber experiments with 4.66 mm fibers

For single-fiber flux measurements with the 4.66 mm fibers, a 5-cm active length fiber was mounted vertically as shown in Figure 5-2. However, in order to attain desired shear rates, it was necessary to use the relatively large-capacity peristaltic pump used in the cartidge experiments rather than the syringe pump used in the other single-fiber experiments. To avoid large axial pressure drop in the inlet and outlet tubing, the large-diameter tubing

used in the cartridge experiments was used here also. The fibers were potted singly in polyethylene connectors using an epoxy resin provided by the manufacturer of the fibers.

4. Membrane Resistance Measurements

a. Fiber Wetting Procedures

The first step in all experiments was to wet the membrane using a procedure appropriate to the membrane material. The polyamide, polysulfone/Biopol, and modified polysulfone fibers were initially primed with prefiltered (0.45 μm) deionized water by attaching water-filled syringes to the inlet and outlet lines and depressing the plungers with gentle thumb pressure. The filtered water was then replaced with pre-filtered (0.45 μm) media in the same manner. The polysulfone/Biopol cartridges were primed by pumping filtered deionized water into the cartridge using the peristaltic pump, with the filtrate ports open, the bulk outlet raised slightly to provide transmembrane pressure, and the bulk outlet open and pointed upwards so that the entire shell side would fill with filtrate. The filtrate side was then drained and the process was repeated with filtered media.

Because of their hydrophobicity, the polypropylene fibers could not be wetted by the same procedure. The first step in preparing a polypropylene fiber was to fill the fiber lumen with water via a single syringe attached to the inlet line. Next the syringe was replaced with a syringe filled with 95% ethanol, and the water in the fiber lumen, inlet tubing, and outlet tubing was flushed out with ethanol. (Note: if the fiber was not initially filled with water, it was difficult to fill the entire lumen with alcohol because the alcohol would all flow out of the upstream portion of the fiber wall.) A second syringe of ethanol was attached to the fiber outlet and the two plungers were pressed simultaneously in order to wet the fiber as evenly as possible. Next the 95% ethanol was replaced with prefiltered deionized water by first flushing out the line using a single syringe and then forcing the water into the pores using two syringes as before. After several ml of water had passed through the membrane, the water was replaced with media by repeating the one syringe/two syringe procedure.

b. Permeability to Media Before and after Yeast Filtration

Prior to the yeast experiments, the membrane resistance was determined by measuring the flow of prefiltered (0.45 μm) media through the membrane as a function of applied pressure. For experiments with individual fibers, the fiber was wetted and primed as described above, and both ends of the fiber were placed in a single reservoir. Then the pressure was varied by adjusting the height of the reservoir (1 cm water = 0.7355 mmHg), and the resulting filtration rate was measured by timed collection and weighing of filtrate droplets. For experiments with hollow fiber cartridges, the bulk outlet port was closed, and the bulk inlet port was attached to the peristaltic pump via an inlet line which included a tee connection to the pressure transducer. Then the flow rate of media through the membrane was varied by adjusting the pump flow setting and the resulting inlet pressure was measured with the pressure transducer. The flow rate was measured by timed collection in graduated cylinders.

The same experimental procedures were used to measure the membrane resistance after completion of yeast filtration experiments in which no freezing was performed. At the end of each experiment with a polysulfone/Biopol cartridge, the hollow fibers were thoroughly rinsed by flowing fresh filtered media through the cartridge (with the outlet lowered to bench level and the filtrate port closed) until no further turbidity in the outlet stream was seen. In most experiments, the membrane resistance was re-measured at this point. In one experiment, the fibers were backflushed by lowering the bulk outlet about 40 cm below bench level and connecting the filtrate port to a reservoir of filtered media. This allowed backflow of media across the membrane from the filtrate side to the retentate side, which removed additional yeast from the membrane. Backflushing was continued until the outlet stream again became clear, usually for 10-15 min. In one case, the back-flushing period was extended to an hour. In the single-fiber experiments without freezing, the fibers were rinsed using a syringe of fresh media attached to either the inlet or outlet tubing. The membrane resistance was re-measured after the outlet stream became clear. (Since individual fibers were not saved for re-use, and since the single-fiber setup ensured that the entire membrane surface was in contact with the rinsing stream, no backflushing was employed.)

c. Permeability to 6% Albumin Solution and to Yeast Filtrate

The freeze-substitution procedure requires albumin in solution in order to fix the cells in place. While the initial permeability to albumin solution could be calculated from the measured permeability to media and the relative viscosities of the two solutions, exposure to protein solution generally lowers a membrane's permeability (increases its resistance) over time. Because it has been suggested (Baker and Strathman, 1970) that the shear rate to which the protein molecules in solution are exposed may influence the rate at which protein adsorbs on membrane surfaces (and thereby increases the membrane's resistance), we measured the hollow fiber resistances in the same cross-flow system used in the yeast filtration experiments. Inlet wall shear rates were maintained at the values to be used in the yeast filtration experiments: 800 s^{-1} for the polypropylene and polyamide fibers, and 80 s^{-1} for the modified polysulfone fibers. The outlet applied pressure was set at 70 mmHg by raising the outlet reservoir 95 cm above the fiber outlet. The filtration rate was measured by timed collection of filtrate drops into pre-weighed glass vials. The vials were capped to avoid evaporation, and were later weighed to the nearest 10^{-5} g with a Mettler H64 balance (Mettler Instrrument Co., Hightstown, NJ).

To test whether increases in membrane permeability observed in initial experiments with yeast in media could be caused by some substance given off by the yeast, filtrate from a previous experiment with 5% yeast was filtered through a new cartridge at 75 mmHg. The membrane resistance was then calculated as a function of time of exposure to the yeast filtrate.

d. Conversion of Permeability Data to Membrane Resistance

The flux of pure solvent through a membrane is a linear function of applied pressure. The hydraulic permeability (L_p) of a membrane to a particular solvent is defined as the slope of the flux-versus-pressure data for that solvent:

$$L_p = \frac{dJ}{dP} \tag{1}$$

The slope of the permeability data was determined by least squares regression of a straight line passing through the origin. The hydraulic resistance (R_m) of the membrane is calculated from the hydraulic permeability and the viscosity of the solvent (fluid) μ_f:

$$R_m = \frac{1}{\mu_f L_p} \tag{2}$$

In these calculations, the fluid viscosity was 1.0 cP for media permeability experiments and 1.5 cP (Kozinsky and Lightfoot, 1972) for albumin permeability experiments. The units conversion factor used (to leave R_m in units of cm^{-1}) was 1.25×10^{-7} mmHg min/cP.

5. Flux Measurements

a. Single fiber experiments

After measurement of the permeability to media, the hollow fiber was primed with the suspending fluid to be used in the yeast filtration (media or media plus albumin), using syringes as described above. Then the inlet line was connected to an inlet reservoir (syringe) containing the yeast suspension, and the outlet line was placed in an outlet reservoir (flask) at bench level. The syringe pump was turned on before the outlet pressure was raised, and the bulk flow rate was measured by collecting a timed sample in a pre-weighed vial and weighing the vial plus sample with a Mettler H64 balance. Stirring prevented settling of the yeast in the inlet reservoir, while use of the narrow gauge tubing prevented settling in the inlet line. After the yeast suspension had reached the outlet reservoir, the outlet transmembrane pressure was raised to the desired value by gradually elevating the jack supporting the pump and the outlet reservoir. (When the pressure was raised, too quickly, the fiber irreversibly clogged. Typically, the pressure was raised in a series of equal steps to its final value over a period of two min. As will be discussed in Chapter 6, the occurrence of early-time clogging with the yeast may be related to the time-dependent resistance of quickly-formed yeast cell beds.) Flux was measured by timed collection and weighing of the filtrate droplets as described in the above procedures for measuring the membrane resistance.

Immediately prior to freezing, the outlet bulk flow rate was measured by timed collection and weighing of the outlet stream. The fraction of the inlet flow rate being

removed as filtrate was calculated by dividing the difference between the inlet and outlet flow rates by the inlet flow rate.

b. Cartridge experiments

After measurement of the membrane resistance, the inlet line was placed in an Erlenmeyer flask which served as the inlet reservoir, and the outlet line was placed in a flask containing filtered media. (The outlet reservoir was partially filled so that the outlet transmembrane pressure could be maintained even at early times in the low-shear-rate experiments, when backflow at the outlet would otherwise have lowered the height of the liquid in the outlet line. Such backflow occurred because the relatively high initial filtration rate was larger than the small bulk flow rate.) The inlet reservoir was placed on a magnetic stirring plate at bench level, while the outlet reservoir was placed at the height corresponding to the desired outlet applied pressure (1 cm water = 0.7355 mmHg). Clamps on the bulk inlet, bulk outlet, and filtrate outlet lines were removed just as the pump was turned on. Timed collection of filtrate into graduated cylinders was initiated as soon as the yeast suspension reached the cartridge. As the filtration rate dropped off, the filtrate was collected into pre-weighed 10 ml flasks and weighed to allow accurate measurement of the filtration rate. Whereas in the single-fiber experiments it was necessary to gradually raise the outlet pressure to avoid clogging, with the cartridges containing the 1 mm ID polysulfone/Biopol hollow fibers it was possible to immediately raise the pressure because even when initial backflow at the outlet occurred, the outlet flow recovered and filtration continued. Since the hollow fibers are opaque and the cartridges are too large to freeze, it was impossible to see whether any of the fibers had clogged during filtration. Large cylindrical chunks of yeast which appeared when the cartridges were back-flushed suggested that some fibers had clogged.

6. Freeze-Substitution Procedure

The freeze-substitution procedure is summarized in Figure 5-4. After filtration for the desired time period, the hollow fiber membrane was frozen in situ. An insulated vessel (Dewar flask) containing Freon-22 which had been cooled to its freezing point of -150°C with liquid nitrogen was rapidly raised up from below the suspended fiber, instantaneously

freezing the fiber and a portion of the attached inlet and outlet tubing. Results of an early experiment with the syringe pump suggested that just after freezing the fiber, the pump had overpressurized the inlet line and had forced the fiber contents partway out of the fiber (into the outlet tubing). In all subsequent experiments, the inlet tubing was cut with scissors just as the fiber was frozen. To avoid inadvertently changing the applied pressure, the pump was kept at the same height as the outlet reservoir, and the line was cut near its attachment to the pump.

The fiber was cut into 1 cm pieces while still in the Freon bath. The frozen fiber pieces were quickly transferred to vials containing a freeze-substitution solution of 2% tannic acid in acetone, which had been pre-cooled to -95°C, the freezing point of acetone, and the vials were stored at -70°C for one week. During that time, acetone replaced the ice in the samples, and the tannic acid fixed both the cells and the protein solution surrounding them (Usukura et al., 1982). To avoid the formation of ice crystals during warmup (Porter and Anderson, 1982), the freeze-substitution vials were gradually brought to room temperature (overnight at -15°C, 4 hours at 5°C, then 1 hour at 20°C). The fibers were then rinsed in acetone and infiltrated overnight by a mixture of 50:50 Epon-812 epoxy resin (Ladd Industries, Burlington, VT) and acetone. The following day, the fibers were embedded in Epon and then cured at 60°C for 36 hours. Using a microtome, the hardened blocks were cut into 5 μm sections perpendicular to the fiber axis (flow direction). Sections were cut at different distances along the fiber length (x).

D. RESULTS

1. Membrane Resistance Measurements

Membrane resistances measured before and after yeast-in-media filtration in the polysulfone/Biopol hollow fibers and hollow fiber cartridges are listed in Table III. Corresponding media fluxes at 75 mmHg are reported in the legends of Figure 5-9 through Figure 5-12. In general, the resistance of new membranes increased by a factor of two to four in 35-120 min experiments. Had extensive backflushing been performed in all experiments, smaller changes in membrane resistance may have been measured after filtration. However, the data shown here may give a more accurate picture of what happens to the

Table III. Polysulfone/Biopol Membrane Resistances

Membrane Configuration	Inlet Yeast Conc. (%)	Inlet Wall Shear Rate (s^{-1})	Filtration Time (min)	Membrane Resistance (cm^{-1}) Before*	After
Cartridge	1	100	180	1.38×10^{9}**	1.87×10^{9}
Cartridge	1	600	90	3.30×10^{8}	1.13×10^{9}
Cartridge	5	100	60	1.57×10^{8}	2.00×10^{8}***
Cartridge	5	600	60	2.77×10^{8}	1.41×10^{9}
Single Fiber	1	600	180	3.48×10^{8}	1.29×10^{9}
Single Fiber	1(75mmHg)	1900	90	3.57×10^{8}	8.64×10^{8}
Single Fiber	1(37.5mmHg)	1900	90	3.49×10^{8}	2.62×10^{9}
Single Fiber	5	600	60	5.47×10^{8}	6.52×10^{8}
Single Fiber	5	1900	60	1.54×10^{8}	(not measured)

* Manufacturer's specification: 4.98×10^{8}

** Used membrane, not backflushed

*** After extensive (1 hr) backflushing

membrane resistance during yeast filtration.

Figure 5-5 shows the results of the experiment in which filtrate from a previous experiment was filtered through a new cartridge. Figure 5-6 shows the time-dependent membrane resistance calculated from that data. The resistance rose a factor of 20 in one hour, which is much more than the changes in resistance which occurred during yeast filtration experiments. This difference in membrane resistance behavior could be atributed to two factors. First, the smaller change measured before and after the yeast filtration experiments could be caused by the rinsing procedure which was used to remove the yeast cake from the fiber. Fresh media might wash the unknown yeast substance out the pores. The observed change in resistance might also be smaller in the yeast filtration experiments because a smaller volume of filtrate had passed through the membrane.

The filtration rates of albumin through the various hollow fibers are plotted together in Figure 5-7. (The albumin filtration data for each type of fiber is also shown as the open circles in later plots of yeast filtration data, Figure 5-17 through Figure 5-18.) The membrane resistances calculated from this data are plotted as a function of time in Figure 5-8. The presence of albumin causes the membrane resistance to increase with time, presumably because adsorbed protein narrows the membrane pores. The polypropylene membrane resistance increased rapidly within the first half hour, while the polyamide membrane resistance increased gradually over two hours. The resistance of the modified polysulfone fibers remained approximately constant for the first 30 min and then increased slowly over the following 90 min. After two hours, the resistance of the modified polysulfone fibers was approximately the same as the initial membrane resistance of the other fibers. The flux with the Kinetek fiber remained constant with time but was too low for further study. (No attempt was made to determine why the resistances of the various membranes changed at different rates. This phenomenon is currently being studied in detail with other membranes by another student in the M. I. T. Chemical Engineering Department, Arun Chandarvarkar.)

2. Filtrate Flux in Cross-flow Filtration Experiments

a. Yeast in Media (without Albumin)

The filtrate flux measured during filtration of 1% and 5% yeast in media (without added albumin) at shear rates of 1900 and 600 s^{-1} in single polysulfone/Biopol hollow fibers is shown in Figure 5-9. Similar data for filtration of 1% and 5% yeast at shear rates of 600 and 100 s^{-1} in cartridges containing 28 fibers of approximately the same length is shown in Figure 5-10. The flux obtained when filtering 1% yeast in either device decreased rapidly during the first 15-20 min, and then gradually decreased throughout the remainder of the experiment. With 5% yeast, the flux decreased rapidly in the first 5-10 min, and thereafter continued to decrease slowly. After the first minute of filtration, the flux obtained from 5% yeast was at least a factor of 2 smaller than that obtained from 1% yeast. As can be seen in both Figure 5-9 and Figure 5-10, the time-dependent flux shows a weak dependence on inlet wall shear rate.

Figure 5-11 shows the above data for 1% yeast filtered at a shear rate of 1900 s^{-1} and an outlet applied pressure of 75 mmHg replotted along with data from another experiment at

identical conditions except that the pressure was reduced by a factor of two. For the first 10 min, the flux obtained at the lower pressure was approximately half that obtained at the higher pressure. Between 10 and 30 min, the gap between the fluxes disappeared as the flux at 75 mmHg dropped faster than the flux at 37.5 mmHg. At longer times, the flux measured at 75 mmHg fell somewhat below that measured at 37.5 mmHg. Additional experiments at 150 mmHg all resulted in fiber clogging.

Figure 5-12 shows a comparison of cartridge and single fiber data with inlet wall shear rates of 600 s^{-1}. The two sets of 1% data roughly coincide at times greater than 20 min, while the two sets of 5% data coincide at times greater than 10 min. At early times, the flux obtained in the cartridges is smaller than that obtained in the single fibers. If this difference in early-time fluxes is interpreted as a difference in time scales, then the time constant for the flux dropoff is shorter in the cartridge experiments than in the single fibers.

Figure 5-13 shows flux data for filtration of suspensions of 1% bakers yeast in single 4.66 mm ID hollow fibers at an inlet wall shear rate of 80 s^{-1} and an outlet applied pressure of 75 mmHg. The triangles are data obtained with freshly-rehydrated unrinsed yeast, and the circles are data obtained with 3x-rinsed yeast. The early-time data is re-plotted on an expanded scale in Figure 5-14. Figure 5-15 shows similar data obtained in the 1000 μm ID modified polysulfone hollow fibers at an inlet wall shear rate of 80 s^{-1} and an outlet applied pressure of 75 mmHg. In both types of fibers, the flux decreased more slowly with rinsed yeast than with unrinsed yeast. Stagnant filtration experiments in Chapter 4 demonstrated that the resistance of unrinsed yeast is higher than that of rinsed yeast. As was discussed in Chapter 4, this difference in resistances can be explained by the presence of CO_2 bubbles in cakes of unrinsed yeast.

b. Yeast in Albumin Solution

The filtrate fluxes measured during filtration of suspensions of 1% yeast in 6% albumin through polypropylene, polyamide, and modified polysulfone fibers are plotted in Figure 5-16, Figure 5-17, and Figure 5-18, respectively. On each graph, multiple runs are indicated by different symbols. In all experiments, the outlet applied pressure was 70 mmHg. The inlet wall shear rate was 800 s^{-1} for experiments in the small (~300 μm ID) polypropylene

and polyamide hollow fibers, and 80 s^{-1} for the larger (~1 mm ID) modified polysulfone hollow fibers. The flux was measured during the filtration phase of the two longest freeze-substitution experiments in the polypropylene and polyamide hollow fibers and during the filtration phase of all five freeze-substitution experiments in the modified polysulfone hollow fibers. In each series of data, the last data point indicates the time at which the fiber was frozen.

In all cases, the fluxes decreased rapidly over the first 15-30 min and then continued to decrease slowly during the remainder of one-hour experiments. The polypropylene membrane experiments plotted in Figure 5-16 show good reproducibility, as do the modified-polysulfone membrane experiments plotted in Figure 5-18. Data from the two polyamide experiments (Figure 5-17) agreed only at times greater than 20 min.

Because the polypropylene and polyamide hollow fibers have similar dimensions and initial permeability, the experiments shown in Figure 5-16 and Figure 5-17 are directly comparable. The fluxes measured in the polyamide and polypropylene experiments coincide at times greater than 20 min. At earlier times, the two polyamide curves straddle the polypropylene data. While the yeast-in-albumin fluxes in the polypropylene and polyamide fibers show similar time-dependent behavior, the albumin fluxes in the two membranes diverge considerably during one-hour experiments. After 20 min exposure to albumin, the polypropylene membrane permeability has decreased so much that the albumin flux is only slightly greater than the yeast-in-albumin flux. The permeability of the polyamide fibers decreases more slowly, and the albumin flux is significantly greater than the yeast-in-albumin flux throughout one-hour experiments.

Figure 5-19 shows the data from Figure 5-18 plotted together with the polypropylene and polyamide data (Figure 5-16 and Figure 5-17) on a log-log scale. Despite differences in fiber diameter and inlet wall shear rate, the flux measured in experiments with the modified polysulfone fibers is similar to the fluxes observed with the polypropylene and polyamide fibers. The data is also comparable to that measured during filtration of 1% yeast in media in cartridges containing similarly-sized polysulfone/Biopol fibers (Figure 5-10).

The fraction of the inlet bulk fluid removed as filtrate (calculated from inlet and outlet bulk flow rates just prior to freezing) in each of these experiments is tabulated in Table IV. In

all cases, initially the fraction removed is very high. In the case of the modified polysulfone hollow fibers, initially there was backflow at the outlet because the filtration rate was greater than the bulk flow rate. In all of the fibers, after an hour, the fraction removed has decreased to about 10% of the inlet bulk flow.

In initial single-fiber experiments in which the pressure was raised rapidly from 0 to 70 mmHg, the fibers clogged in less than two minutes. The small hollow fibers, with internal diameters optimized for blood filtration (300 μm) were particularly susceptible to clogging. About half of those fibers clogged even when the pressure was raised slowly. Individual fibers with above-average initial permeabilities most often clogged. Therefore the "best" hollow fibers for yeast filtration are not necessarily those with the highest permeabilities. It is clear that devices and procedures which have been proven to work well for filtering blood will not necessarily be good for filtering yeast or other microbial cell suspensions.

Table IV. Fraction of Inlet Flow Removed as Filtrate

Filtration Time (min)	Fraction Removed (%) Polypropylene	Polyamide	Modified Polysulfone
1			>100
3	74	93	
5			78
10	31	58	41
20	18	60	24
35		11	
38	9.8		
40			9.3
60			8.5
63	7.5	5.1	

c. Latex Particles in Distilled Water

Figure 5-20 shows experimental data for filtration of an 8.9% suspension of 0.711 μm diameter latex particles in the 4.66 mm ID XM hollow fibers at three different bulk flow rates, corresponding to equivalent Poiseuille wall shear rates of 72, 153, and 302 s^{-1}. All three experiments were carried out at 75 mmHg. The membrane resistances in these experiments

were 2.68 x 10^9, 1.99 x 10^9, and 1.90 x 10^9, respectively. In all cases the time required to reach steady state was over 15 min, much longer than the time required to reach steady-state during filtration of red blood cells. Figure 5-21 shows the data at a shear rate of 153 s^{-1} re-plotted along with data at the same shear rate but a pressure of 37.5 mmHg. Figure 5-22 shows the same data plotted again along with data for a 0.89% suspension at the same wall shear rate and pressure.

Figure 5-23 shows experimental data for filtration of a 7.7% suspension of 0.264 μm diameter latex particles at a shear rate of 55 s^{-1} in the same type of hollow fiber. The steady-state flux obtained with these smaller particles is significantly lower than that measured with the 0.711 μm particles. Also, a longer time (more than four hours) was required to reach the lower steady-state flux. Figure 5-24 shows experimental data for filtration of a 0.2% suspension of 0.264 μm diameter latex particles at shear rates of 12 and 500 s^{-1} in the same type of hollow fiber. The lower bulk concentration dramatically increased the time required to reach steady state to over 10 hrs at 500 s^{-1}. The data for 12 s^{-1} had not yet reached steady state after 2 days.

3. Cake Thickness in Cross-flow Filtration Experiments

a. Experimental Artifacts

The photomicrographs below demonstrate the formation of thick cakes of cells on the membrane surface during cross-flow microfiltration of yeast. Accurate interpretation of the photographs requires an understanding of what features are attributable to experimental artifact. The existence of the cakes cannot be explained as an artifact of the freezing procedure; rather, the cakes serve as evidence that an adequate freezing rate was used. During the initial development of the freeze-substitution procedure (Chapter 2), experiments in which the freezing rate was intentionally reduced showed that slow ("bad") freezing pushed cells away from the wall, as would be expected since the freezing front moves from the outside of the fiber in. Unfortunately, not all artifacts could be avoided by simply freezing more quickly. In the photomicrographs which follow two types of artifacts are present: cracks in yeast cakes and separation of the membrane from the yeast cake. Fortunately,

although these artifacts can be distracting, they do not prevent measurement of the yeast cake thickness.

Panel a2 of Figure 5-25 shows a fiber containing a thick yeast cake with a noticeable freezing artifact. In the middle of the fiber, a bit off-center, there is an open region with only a few cells. This region contained flowing yeast suspension when it was frozen. The radial lines seen in this open area are concentrated regions of protein which formed during freezing. Because such lines form perpendicular to the freezing front, they converge at the point in this cross-section that was frozen last. Inside the cake itself, there is a large crack in which there are neither yeast cells nor protein lines. The lack of protein indicated that this crack was not present prior to freezing. The two sides of the crack, with their corresponding jagged edges, are further evidence that an abrupt fissure occurred. Such cracks rarely occurred in previous freezing of hollow fibers containing red blood cells in albumin (Chapter 2); apparently the thicker and more rigid yeast cakes are less able to withstand the stresses which build up during freezing.

An example of the second type of artifact can be seen in Figure -34. The separation of the fiber wall from the yeast cake occurred in the modified polysulfone fibers but not in the either the polyamide or polypropylene fibers. During the fixation procedure, the acetone caused the modified polysulfone membranes to expand and, in many cases, to pull away from the yeast cake inside them. A few cells stuck to the membrane and were separated from the rest of the cake. Some of the hardened lumen regions slid out of the hollow fiber as it was being transferred to the embedding solution. The fibers shrunk back to their normal size during the embedding process, but return to the original alignment was virtually impossible.

b. Results with Narrow (Polypropylene and Polyamide) Hollow Fibers

Figure 5-25 shows the results of five experiments in which polypropylene fibers were frozen after filtration times of 3, 10, 20, 38, and 63 min, respectively, from top (a) to bottom (e). In each case, three axial positions are shown: x=0, 2, and 5 cm, respectively, from left (1) to right (3). Similarly, Figure 5-26 shows sections cut 0, 2, and 5 cm from the inlet of polyamide fibers frozen after filtration times of 3, 10, 20, 38, and 63 min. The sections denoted x=0 were cut as close to the inlet of the fiber as possible. However, because

in some cases the fibers broke during freezing, the actual distance may be as far as 0.5 cm from the inlet.

In each case, the cake thickness grows from inlet to outlet. At t=3 min, the outlets of both polypropylene and polyamide fibers appear to be blocked, but highly concentrated yeast was still flowing in the outlet line. After varying periods of time, the cake thickness begins to decrease. Preliminary experiments in which suspensions of yeast in albumin were filtered in polypropylene and polyamide fibers for 3 hr showed no yeast cakes.

The next several figures are the results from freezing experiments for which no flux data is shown. Figure 5-27 shows a polypropylene fiber frozen after filtration of 0.65% yeast in 6% albumin at $\gamma_{w,in}$ = 2000 s^{-1} and $P_{appl,out}$ = 70 mmHg. A thick yeast cake has formed in only 2 min even though the shear rate was relatively high.

Figure 5-28 a polyamide fiber frozen after filtration of 6.5% yeast in 6% BSA for 60 min at $\gamma_{w,in}$ = 140 s^{-1} and $P_{appl,out}$ = 122 mmHg. The cake grows with axial position. The unevenness of the cake can be seen more clearly in part (a) of Figure 5-29. Part (b) is an example of an uneven cake forming even in a very round polypropylene hollow fiber. The conditions for part (b) were x = 5 cm, C_b = 6.5%, $\gamma_{w,in}$ = 612 s^{-1}, $P_{appl,out}$ = 22 mmHg, and t=10 min.

Figure 5-30 shows a polypropylene fiber frozen after filtration of 0.65% yeast in 6% albumin at $\gamma_{w,in}$ = 359 s^{-1} and $P_{appl,out}$ = 70 mmHg for 3 min. The cake is occupies a large fraction of the channel and grows with distance from the fiber inlet.

Part (a) of Figure 5-31 shows sections from a polypropylene fiber frozen after filtration of 6.5% yeast in 6% albumin at $\gamma_{w,in}$ = 88 s^{-1} and $P_{appl,out}$ = 4 mmHg for t=2 min. The cake height first grows and then decreases with axial position. Part (b) shows sections from three fibers after filtration times of 2, 10, and 15 min. These photos show the cake washing away with time.

Figure 5-32 shows a fiber which clogged within the first two minutes of filtration. Such clogging occurred in many experiments, particularly those in which the pressure was quickly raised to its final value. Figure 5-33 shows partial channel clogging of a flat plate channel during filtration of 4 μm white latex particles in a solution of fluorescein in distilled

water. Frame (a) shows the dark-colored suspension flowing from left to right in the channel prior to opening the filtrate port. In frames (b) and (c), which were taken 30 sec and 2 min after filtration was begun, parts of the membrane appear slightly lighter in color as the white particles start to form a cake on the membrane surface. Frames (d) through (f), taken 3 min, 5 min, and 30 min after the onset of filtration, show the subsequent development of a light-colored cake which grows in from the side walls, filling portions of the channel. Frames (g) through (i) show the same cake 2 min, 4 min, and 6 min after the filtrate port is closed, allowing the bulk flow to "rinse" the channel. The immobile cake is washed away chunk by chunk, in a shear-dependent erosion process. (In experiments not shown here, raising the shear rate increased the rate of erosion.) In other experiments, partial channel clogging was observed at shear rates of up to 20,000 s^{-1}.

c. Results with Wide (Modified Polysulfone) Hollow Fibers

Figure 5-34 shows the results of freeze-substitution of modified polysulfone fibers during filtration of 0.65% yeast in 6% albumin solution. Because of the large size of these fibers (1 mm ID), only a portion of the fiber cross-section appears in each photo. Filtration times of 1, 5, 10, 20, 40, and 60 min are shown in rows (a) through (f), respectively. Where possible, sections taken at axial positions of 0, 2, and 5 cm are shown in columns (1) through (3), respectively. Blank panels correspond to fiber segments whose yeast cakes had slid out of the swelled fiber prior to embedding. Although we attempted to embed the separated lumen regions, the unprotected cakes did not survive the subsequent handling. These experiments could not be repeated because only a small number of pre-production sample fibers were available.

This set of experiments was conducted at an inlet shear rate of 80 s^{-1}, a factor of 10 lower than the shear rate used in experiments with the smaller fibers. A low shear rate was chosen for several reasons. First of all, higher shear rates could not be maintained throughout one-hour experiments with the syringe pump because of the limited capacity of the syringes. Switching to a peristaltic pump would have resulted in large fluctuations in bulk flow rate and pressure in the single fiber experiments, which clearly is undesirable in experiments used to

evaluate a theoretical model. Use of a low shear rate also ensured operation in a regime in which cake buildup would be significant.

With the large modified polysulfone fibers, cakes heights as large as 350 μm are observed. The cake height generally increased with distance from the inlet. After reaching 250 μm in 5 min, the inlet cake height varied randomly from about 100 to 250 μm in longer experiments. The outlet cake height grew steadily from 50 μm at 1 min to 350 μm at 20 min, and then diminished slightly over the next 40 min.

E. DISCUSSION

1. Filtrate Flux Behavior

a. Time Dependence

In both single fiber and cartridge experiments, the flux decreased more rapidly with 5% yeast than with 1% yeast. This is because, for a given filtrate flux, the rate of buildup of cells on the membrane is greater if the bulk suspension which is carried toward the membrane contains a higher concentration of cells.

In all of the yeast filtration experiments, with and without albumin present in solution, the rate of flux drop-off with yeast was much slower than was previously reported for red blood cells in either flat plate (Zydney and Colton, 1982) or hollow fibers (Ofsthun and Colton, 1987). The flux obtained with red cells reached steady state flux within 30 to 60 sec, while the flux with yeast dropped rapidly over two to ten minutes and continued to decrease for an hour or more. There are two possible explanations for this difference in time scales. First, because the yeast cell resistance is much smaller than the red cell resistance, much thicker cakes of yeast must build up in order to reduce the flux the same amount. Second, the thick yeast cakes may undergo a relatively slow period of consolidation, in which cells are rearranged to more dense (and more resistive) packing arrangement, while the highly deformable red cells may reach their final packing arrangement very quickly.

The faster drop in flux observed in the cartridge experiments may be related to the use of a peristaltic pump in the cartridge experiments and a syringe pump in the single-fiber experiments. The pulsatile nature of the peristaltic pump might cause the yeast cake to achieve its pseudo-steady-state configuration more quickly in the cartridge experiments.

Non-uniformities in bulk flow distribution and fiber permeabilities among the hollow fibers in the cartridges might also influence the time-dependent behavior.

b. Pressure Dependence

Previous data with red cell suspensions demonstrated that a maximum, pressure-independent flux is achieved at pressures of 20 mmHg (in a flat-plate system: Zydney and Colton, 1982; Zydney, 1985) to 50 mmHg (in hollow fiber cartridges: Chapter 2; Ofsthun and Colton, 1987). Yeast fluxes measured here at an inlet wall shear rate of 1900 s^{-1} and outlet applied pressures of 37.5 and 75 mmHg are about the same for times greater than 20 min, suggesting attainment of a similar pressure-independent flux. However, because of the long transients and the clogging problem, it was impossible to determine whether the flux had truly reached a maximum value.

While the pressure dependence of cartridge fluxes was not studied, it is conceivable that the observed pressure dependence would be influenced by the initial start-up procedure, since some of the fibers might clog as the pressure is initially raised.

c. Shear Rate Dependence

Previous data with red cell suspensions in a flat-plate system (Zydney and Colton, 1982; Zydney, 1985) showed a linear dependence of steady-state, pressure-independent fluxes on wall shear rate, while the hollow fiber data of Chapter 2 of this thesis (Ofsthun and Colton, 1987) showed a slightly weaker dependence. As can be seen in Figure 5-9 and Figure 5-10, the dependence of flux on inlet shear rate was much weaker with yeast. Several factors may cause this difference in shear rate dependence with yeast and red cells. Since a large fraction of fluid is removed, particularly at early times (Table IV), a significant portion of the fiber may be exposed to a value substantially smaller than the inlet value of the wall shear rate. Conversely, buildup of a thick yeast cake would decreases the effective membrane area and increase the effective shear rate. The results of analysis with a theoretical model in Chapter 6 gives further insight on the causes of the shear rate dependence observed with rigid particle suspensions.

d. Concentration Dependence

As was discussed in Chapter 1, previous workers have shown that the filtrate flux obtained when filtering yeast and other microbial cell suspensions decreases as the bulk cell concentration increases. In some cases, the fluxes were inversely proportional to the log of the bulk concentration. The same logarithmic dependence has been observed in the filtration of red cells, and is predicted by a simple concentration polarization model (Zydney, 1985; Zydney and Colton, 1982). As will be discussed in Chapter 6, such a relationship is expected if (1) the flux is determined by the rate of back-diffusion of cells from the membrane surface, as it would be if steady state were established, (2) the cross-flow channel is not significantly narrowed by development of a particle cake on the membrane surface, and (3) the membrane resistance is constant. In Chapter 6, we will see examples (taken from the data reported here) in which each of these conditions is not met.

If the observed time-dependence of fluxes obtained during yeast filtration reflects the time required to build up a cell cake, then one would expect that the rate of flux dropoff would increase as the bulk cell concentration increased. The data clearly shows that the rate of flux dropoff is greater with 5% cells than with 1% cells, as is expected.

e. Influence of Membrane Resistance

The influence of membrane resistance on flux can be analyzed by comparing results obtained from similarly-sized membranes of different materials. Although the resistances of the 330 μm polypropylene membranes and 320 μm polyamide membranes are approximately equal (within about ±20%) for the first 10 min of filtration with albumin present, after 10 min filtration the polypropylene resistance rises faster, and during the period from 30 to 60 min the polypropylene resistance is about three times the polyamide resistance. No observable difference in the filtrate flux obtained with 0.65% yeast in 6% albumin was noted in this range. To better analyze the influence of membrane resistance, hollow fibers of constant membrane resistance are needed. Since membrane resistances increased during filtration of yeast in media but recovered somewhat with rinsing and backflushing, this may involve not only non-fouling membrane materials, but also membrane surfaces which do not entrap cells.

2. Yeast Cake Thickness

a. Non-uniformities

In many cases the yeast cakes formed during filtration are not uniform in thickness around the circumference of the fiber. Gravitational settling cannot explain the non-uniformity because the fibers were held vertical throughout all experiments. An asymmetric axial flow pattern in the fiber might produce non-uniformity in cake thickness, but use of tubing similar in internal diameter to the hollow fibers along with the smooth method of connecting the tubing to the fiber makes this explanation unlikely. Another possibility is that the hollow fibers are not uniformly permeable around the circumference of the fibers. There is no data in the literature on circumferential variation in membrane permeability, though it is conceivable that such non-uniformities could be caused by irregularities in the nozzle used to make the hollow fiber. If so, a thicker cake would form on the more permeable side of the fiber. Even concentration polarization boundary layers were seen in similar blood-freezing experiments (Ofsthun and Colton, 1987; Chapter 2 of this thesis), but the high resistance of even a thin layer of blood cells could have hidden any variation in fiber permeability.

Many of the examples of uneven yeast cakes occurred during the period in which the yeast cake was being washed away as the membrane permeability decreased. If the yeast is removed by shear-dependent erosion similar to that seen with latex particles in the flat-plate system (Figure 5-33), then such unevenness may reflect non-uniform wall shear rates in the non-circular fibers.

b. Differences among Fiber Types

Since the polypropylene and polyamide fibers have approximately the same internal diameters, any differences in cake thickness are probably due to differences in membrane resistance. As was seen in Figure 5-8, the resistance of the polypropylene membrane starts out approximately equal to the polyamide fiber resistance, but rises much more rapidly in the presence of albumin. Comparison of the first rows of Figure 5-25 and Figure 5-26 reveals that the cakes observed after three min filtration are similar. However, in the later photos it is apparent that the yeast cakes wash away more quickly in the polypropylene fibers. Increases in membrane resistance decrease the rate of convection of cells to the membrane.

Assuming that the rate of diffusion has not changed, convection of cells toward the membrane is less than diffusion away from the membrane, and consequently yeast cells are taken out of the cake, back into the bulk suspension. This behavior is qualitatively shown in Figure 3-35. This process occurs sooner in polypropylene fibers than in polyamide fibers because the polypropylene resistance increases more rapidly. After 30 min, the flux with yeast-in-albumin in the polypropylene fibers is about 60% of the albumin flux, and falls roughly parallel to it. Since this difference could be accounted for by partial blinding of the membrane with yeast, the flux may be membrane-limited at this point. Since no yeast cakes were observed in either polypropylene or polyamide fibers after 3 hr filtration, the flux must be completely membrane-limited by that time.

Another noticeable difference between the two types of fibers is that even yeast cakes rarely formed in the polyamide fibers; in most cases, one side of the fiber was completely clear, while the other had a significant cake. As discussed above, this might indicate that none of the polyamide fibers are uniformly permeable around the circumference of the fibers. With the polypropylene fibers, even cakes often formed, indicating that at least some of the polypropylene fibers are uniformly permeable.

The dropoff in cake heights in the modified polysulfone fibers did not occur until the 40 and 60 min samples. Until that time, the flux with albumin alone was approximately constant, and therefore the membrane resistance had not caused any changes in cake thickness. If the flux with albumin alone were to continue its steady dropoff with time, one would expect that the flux with yeast in albumin would become membrane-limited after 3-4 hours of filtration with these fibers.

c. Comparison of Time Scales of Cake Growth and Flux Drop-off

At the outset of this study, when preliminary flux data revealed a much slower approach to "steady state" than had been previously observed with red cells, we hypothesized that time scale for flux dropoff was a measure of the time required to build up the cell cake responsible for the flux reduction. Since yeast and red cells are approximately the same size, we expected that the shear-augmented diffusion of the two types of cells would be similar, and that therefore the steady-state flux would be about the same. Because previous

experiments (Chapter 3) had demonstrated that the resistance of yeast cells was much lower, we knew that thick cakes of yeast would be required to reduce the flux to its steady-state value. We expected that such thick yeast cakes would build up slowly, gradually reducing the flux toward its steady-state value.

The freeze-substitution experiments proved that thick cell cakes do form during cross-flow filtration of yeast. However, the same experiments demonstrated that the time scale over which the observed cake thickness grew was shorter than the time scale over which the flux varied. In fact, cakes often grew thick enough to completely clog the hollow fibers in less than two minutes.

Another early observation was that if filtration with albumin present was carried out for three hours prior to freezing, no yeast cakes would be observed. This suggested that loss of membrane permeability might be responsible for the slow flux decay seen with yeast. This possibility was ruled out when fluxes obtained when filtering suspensions of yeast in albumin in polypropylene and polyamide membranes were the same, while the fluxes obtained with albumin solution alone were significantly different in the two membranes. Although changing membrane resistance is not the answer to the question at hand, it is clearly an important factor in understanding cross-flow filtration of yeast suspensions.

Another possibility is that although the yeast cakes build up quickly, the cakes undergo a relatively slow compaction process in which the void fraction of the cake is reduced by rearrangement of the cells. Such a gradual reduction in void fraction, and corresponding increase in the hydraulic resistance of the cake, might be responsible for the slow flux decay observed with yeast. Such changes were seen in batch filtration exp^Aiments in Chapter 3. In a subsequent study (Chapter 5), the effects of cake growth, increasing membrane resistance, and increasing cake resistance will be incorporated into a time-dependent model for predicting the flux during yeast filtration in hollow fiber membranes.

d. Effects on Effective Shear Rate and Axial Pressure Drop

The freeze-substitution experiments revealed that the yeast cakes which form on the membrane surface can significantly affect the area of the flow channel available for flow. Because the wall shear rate varies inversely with the cube of the channel radius, at constant

flowrate the effect on shear rate, and hence the shear-augmented diffusion coefficient, can be substantial. The effective membrane area is also reduced, which decreases the apparent flux (based on membrane area), partially counteracting the increase in the diffusion term. Since axial pressure drop increases with the fiber radius to the minus four power, growth of thick cakes can also influence the axial pressure drop in the fiber. If the inlet pressure is fixed, this may lead to backflow at the outlet, and channel clogging. If the outlet pressure is fixed, the pressure at the inlet of the fiber may grow large enough to exceed "optimal" pressures recommended by the hollow fiber manufacturers, which will also affect the flux achieved.

The effects of the thick yeast cake on channel height, effective wall shear rate, and axial pressure drop will all be incorporated into the time-dependent model in Chapter 5.

e. Implications for Device Design and Operation

Our experiments with yeast filtration in hollow fibers have shown that fibers whose dimensions have been established for use in blood filtration are not suitable for filtration of yeast. For yeast filtration, larger diameters and/or shorter lengths are needed. We have also seen that operating procedures as well as device designs influence clogging. In particular, we found that start-up procedures should include a gradual increase in the applied pressure to avoid initial "drying out" of the suspension.

Since the steady-state filtration rate achieved with blood is solely diffusion-limited, no improvement in filtrate flux is achieved by increasing the membrane permeability. Because of the relatively short single-use filtration time, an increasing membrane resistance does not affect operation of blood filters. However, if membrane filters are to be used in large-scale industrial separations, much longer lifetimes and reuse will be required. Since after 3 hr filtration of yeast-in-albumin solutions, fluxes are membrane limited, and since bioreactor suspensions may contain a variety of membrane-fouling materials, development of non-fouling and non-blinding membranes is crucial to designing membrane filters for industrial use in biotechnology. Since increasing the initial permeability will aggravate the problem of hollow fiber clogging, raising the entire flux-vs-time curve is less desirable than achieving fairly constant membrane permeability.

4. Summary

The goals of this study were to characterize the filtrate flux behavior of a model microbial cell system under cross-flow microfiltration, to study the formation of cakes of microbial cells on the membrane surface, and to compare the observed flux and cake formation behavior to the results of similar experiments performed with more deformable red blood cells. We chose bakers yeast as the model cell system, and conducted experiments in several types of hollow fibers. We found significant differences in the flux behavior of yeast and red cells, and confirmed expectations that thick yeast cakes would form on the membrane surface.

The flux obtained when filtering yeast dropped much more slowly than the flux obtained when filtering blood under similar conditions. The freeze-substitution experiments showed that the longer approach to steady state with yeast cells could not be explained simply as the time required for buildup of the thick cakes, since the cakes reached their maximum height much sooner than fluxes reached their minimum values. This longer time dependence might be related to the time required for the microbial cell cakes to compact to their final configuration. Furthermore, with yeast, no true steady state was ever reached: increasing membrane resistance in the presence of albumin resulted in slow flux decline at long times. (In contrast, the flux achieved in cross-flow filtration of red cells was virtually independent of membrane resistance.) While steady-state cross-flow filtration models have adequately predicted filtrate flux with red cells, time-dependent models are needed to predict fluxes with microbial cells. Microbial cell filtration models must take into account changes in both membrane resistance and cell resistance with time.

The occurrence of fiber clogging made comparison of yeast and red cell flux behavior difficult. With yeast, the applied pressure could not be raised very far into the pressure-independent regime for blood cells. Raising the applied pressure further resulted in fiber clogging before the existence of a pressure-independent asymptote could be verified or disproven. With yeast, increasing the wall shear rate increased the flux achieved at an outlet applied pressure of 75 mmHg, but the dependence was weaker than the previous linear relationship reported for blood at the same pressure (in the pressure-independent regime).

Fiber clogging presents a serious problem to the engineers who design filtration systems for separation of microbial cells. Whereas the primary design constraint with deformable cells has been to avoid cell lysis, the primary constraint with more rigid microbial cells will be to avoid clogging of the hollow fibers. Therefore any mathematical models developed to predict filtration performance must be able to predict channel clogging as well as filtration rate. Furthermore, it is clear that hollow fiber systems which have been designed for blood separation will not work well for filtering microbial cells. To avoid clogging, the hollow fibers used for microbial cell filtration must be larger in diameter than those used for blood filtration. The procedures for operating hollow fiber systems must also be designed to avoid clogging. In particular, start-up procedures should avoid raising the applied pressure too quickly, since doing so can clog even large-diameter fibers. If possible, models developed for predicting filtration behavior should allow testing of procedures for variation of the applied pressure with time.

Design of devices for long-term industrial use will also require further development of membrane materials, since the fluxes obtained with all of the membranes studied here became membrane-limited after only a few hours of filtration. Since increasing the initial membrane permeability will worsen clogging problems, membranes with fairly constant membrane resistances are needed.

Freezing experiments not only confirmed the occurrence of fiber clogging under certain conditions, but also revealed significant buildup of yeast cakes on the membranes under non-clogging conditions. Yeast cakes of 100-350 μm formed within minutes. The cakes grew with distance from the inlet, particularly as the local bulk flow rate decreased. In fibers whose membrane resistance increased significantly with time, the cakes washed away in long-term experiments. The observed yeast cakes were thick enough to affect the local shear rate and the axial pressure drop as well as the total resistance to flow through the membrane. All of these effects must be incorporated into models of cross-flow filtration of yeast or other microbial cells.

Filtrate flux experiments also revealed that large fractions of the inlet flow rate of the yeast suspensions were removed as filtrate at early times when the flux was highest. Since the fraction removed was significantly higher than the fraction removed from red cell suspensions

under comparable filtration conditions, fiber lengths had to be shorter than those normally used for blood. Clearly models which predict filtrate flux behavior must take into account changes in bulk concentration and flow rate along the device length.

In Chapter 6, a time-dependent model for predicting filtrate flux, cake thickness, and channel clogging for cross-flow filtration of yeast in hollow fiber membranes will be developed. The rate of accumulation of yeast of the membrane will be taken to be the rate at which the cells are convected to the membrane surface minus the rate at which they are carried away from the membrane by shear-augmented diffusion. The model will account for the effect of the cell cake on the effective channel height as well as its effect on the total resistance to convective flow through the membrane. Axial changes in bulk concentration, bulk flow rate, and local applied pressure will be incorporated. Time-dependent variation of membrane resistance, cell resistance, and outlet applied pressure will also be included. To allow comparison with data taken at fixed outlet applied pressure, the model will iterate to determine the appropriate value of the inlet applied pressure. In short, all of the effects shown to be important in these experiments will be incorporated into the model. The predicted fluxes and cake thicknesses will be compared to the data taken here.

F. REFERENCES

Baker, R. K., and H. Strathman (1970): "Ultrafiltration of Macromolecular Solutions with High-Flux Membranes: A Uniform Correlation?" J. Appl. Polym. Sci. 14: 1197

Fane, A. G., C. J. D. Fell and A. G. Waters (1983): "Ultrafiltration of Protein Solutions through Partially Permeable Membranes--The Effect of Adsorption and Solution Environment" J. Memb. Sci. 16: 211-224

Kozinsky, A. A., and E. N. Lightfoot (1972): "Protein Ultrafiltration: A General Example of Boundary Layer Filtration" A. I. Ch. E. J. 18(5): 1030-1040

Porter, K. R., and K. L. Anderson (1982): "The Structure of the Cytoplasmic Matrix Preserved by Freeze-Drying and Freeze-Substitution" Eur. J. Cell Biol. 29: 83-96

Randerson, D. H., and J. A. Taylor (1983): "Protein Adsorption and Flux Decay in Membrane Plasmapheresis," in Y. Nose, P. S. Malchesky and J. W. Smith, eds., Plasmapheresis: New Trends in Therapeutic Applications, ISAO Press, Cleveland

Roberts, C. G., K. Schindhelm, and P. C. Farrel (1983): "Protein-Membrane Interactions in Membrane Plasma Separation," in Y. Nose, P. S. Malchesky and J. W. Smith, eds., Plasmapheresis: New Trends in Therapeutic Applications, ISAO Press, Cleveland

Reuss, M., Josic, D., Popovic, M., and W. K. Bronn, "Viscosity of Yeast Suspensions," Europeın J. Appl. Microbiol. 8:167-175 (1979)

Saltzman, W. M., An Investigation of the Hydrodynamic Resistance of Concentrated Layers of Erythrocytes, M. S. Thesis, Massachusetts Institute of Technology (1984)

Usukura, J., Yorifuji, H., and E. Yamada (1982): "Freeze-Substitution Using Various Kinds of Fixative," J. Electron Microscopy 31(3): 301

Zydney, A. L. (1985): Cross-Flow Membrane Plasmapheresis: An Analysis of Flux and Hemolysis, Ph. D. Thesis, Massachusetts Institute of Technology (1985)

Zydney, A. L., and C. K. Colton (1982): Continuous Flow Membrane Plasmapheresis: Theoretical Models for Flux and Hemolysis Prediction Trans. Am. Soc. Artif. Intern. Organs 28: 408 (1982)

Zydney, A. L., and C. K. Colton (1986): A Concentration Polarization Model for the Filtrate Flux in Cross-Flow Microfiltration of Particulate Suspensions Chem. Eng. Commun. 47: 1-21

Zydney, A. L., Saltzman, W. M., and C. K. Colton, (1988): Hydraulic Resistance of Red Cell Beds in an Unstirred Filtration Cell Chem. Eng. Sci. (in press)

G. FIGURES

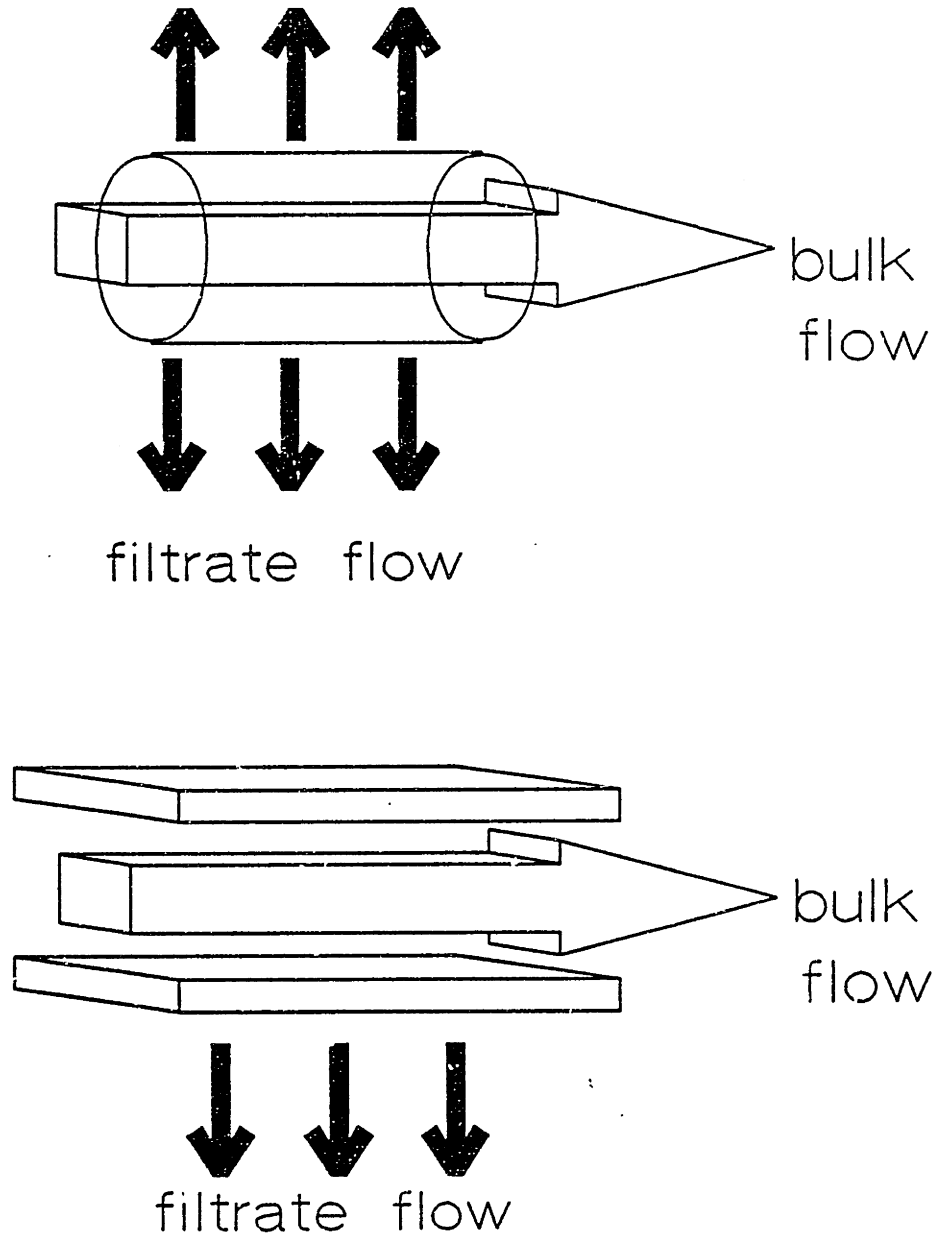

Figure 5-1. Cross-flow configurations.

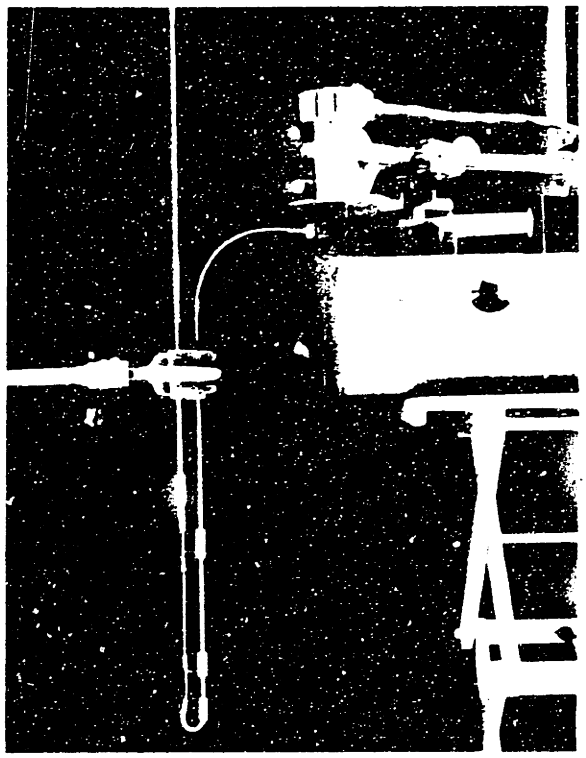

Figure 5-2. Apparatus for single-fiber experiments.

Figure 5-3. Apparatus for cartridge experiments.

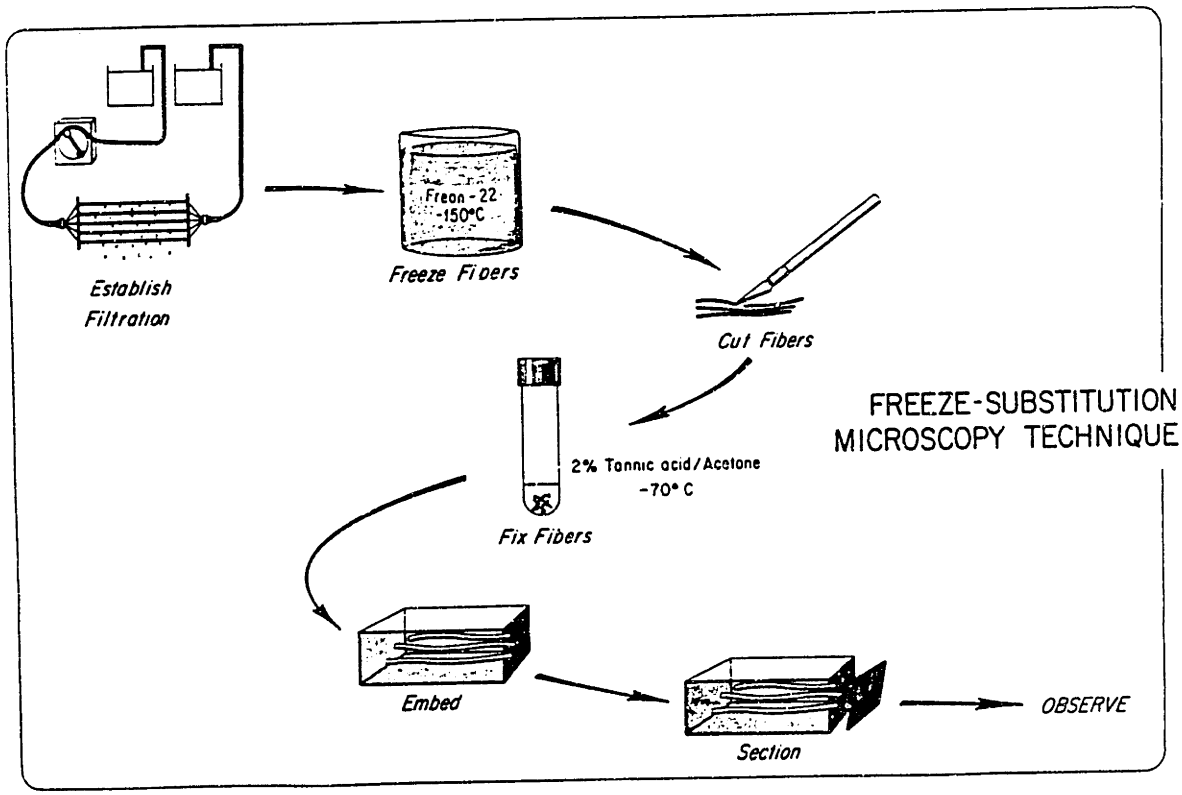

Figure 5-4. Freeze-substitution procedure.

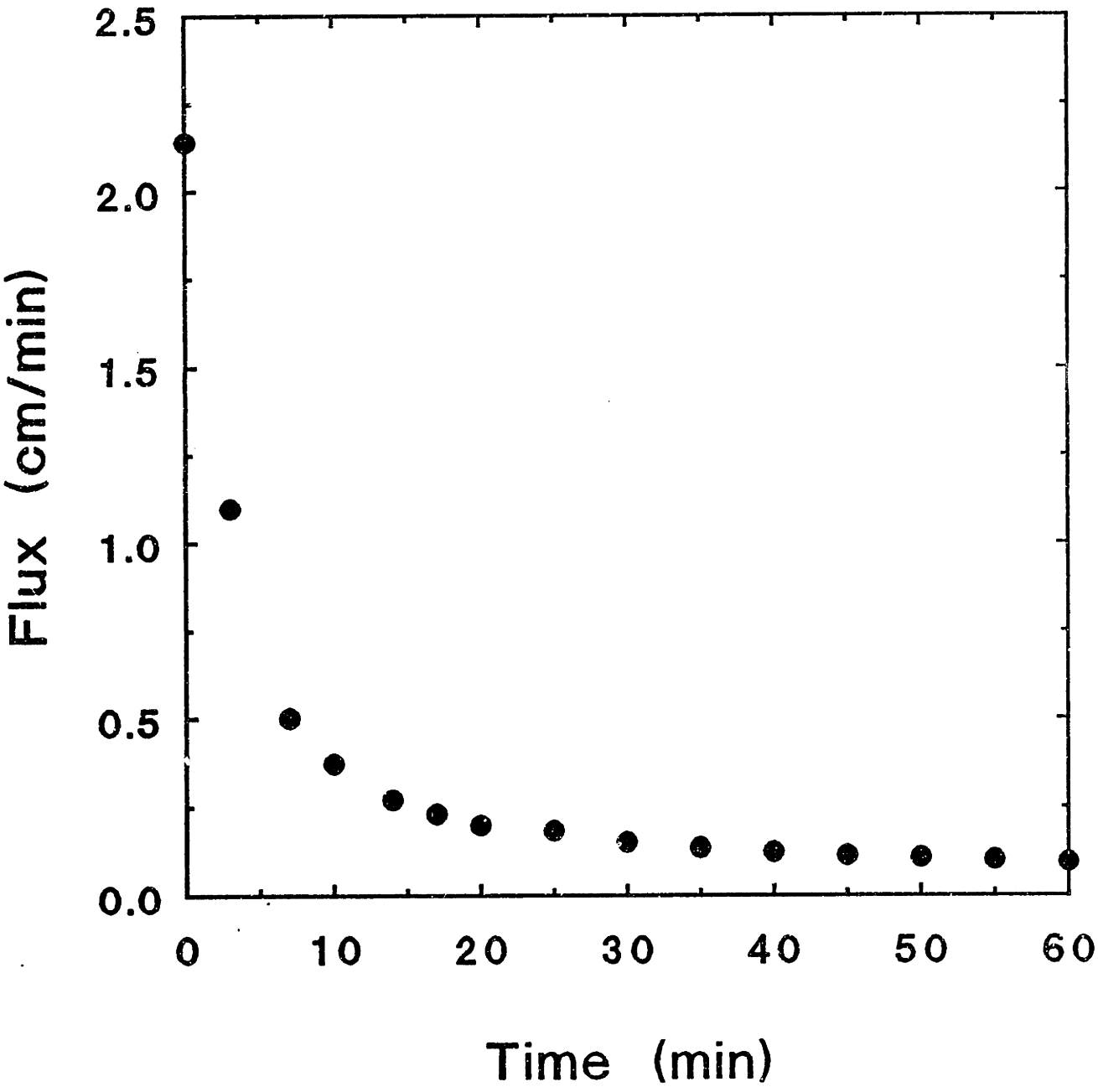

Figure 5-5. Flux as a function of time during filtration of filtrate from a previous 5% yeast experiment through a new polysulfone/Biopol hollow fiber cartridge (N=28, L=8.5 cm, ID=475 μm, pore ID=0.2 μm) at a pressure of 75 mmHg.

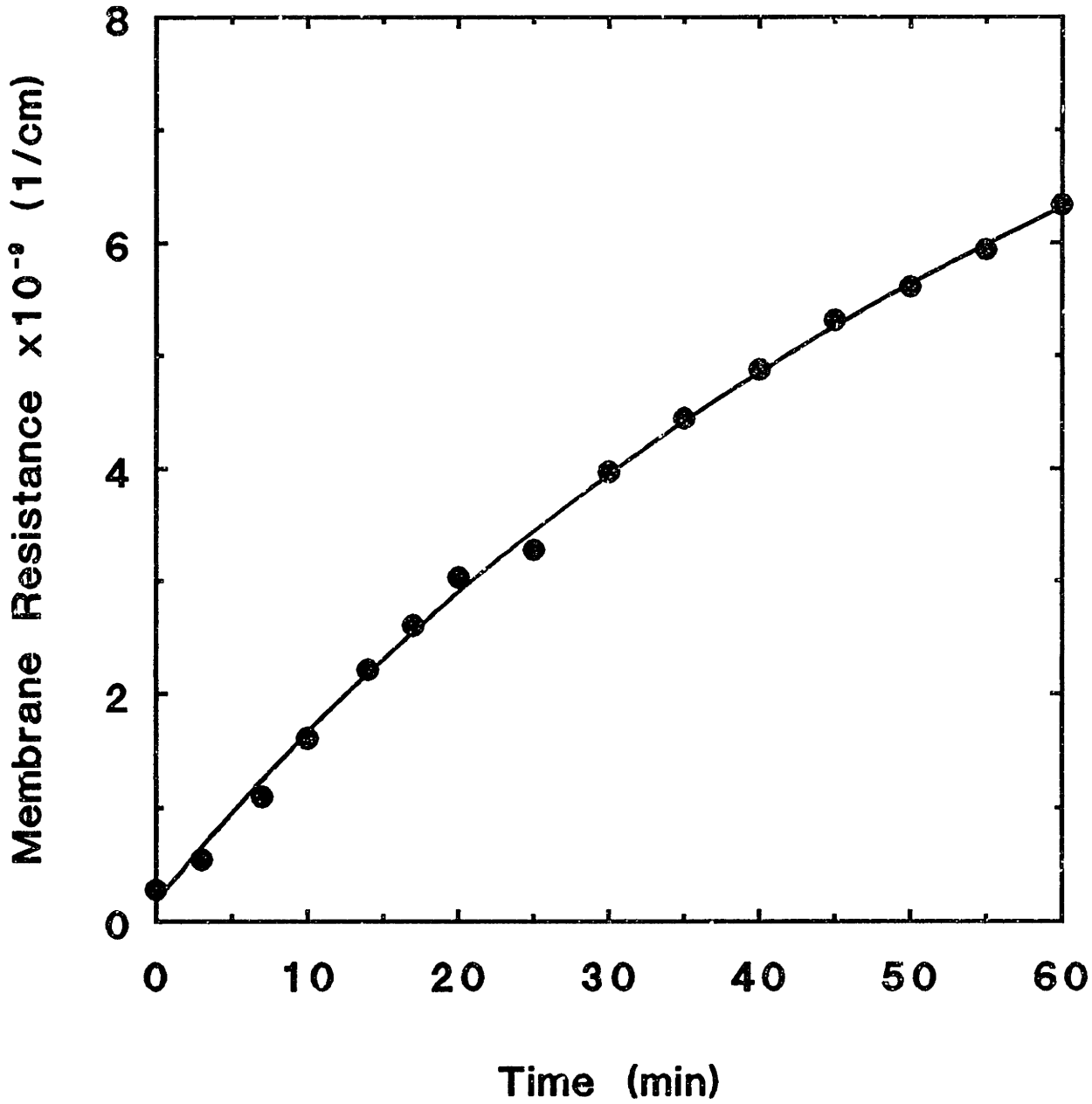

Figure 5-6. Membrane resistance of a new polysulfone/Biopol hollow fiber cartridge (N=28, L=8.5 cm, ID=475 μm, pore ID=0.2 μm) as a function of time of exposure to yeast filtrate calculated from the flux data in Figure 5-5.

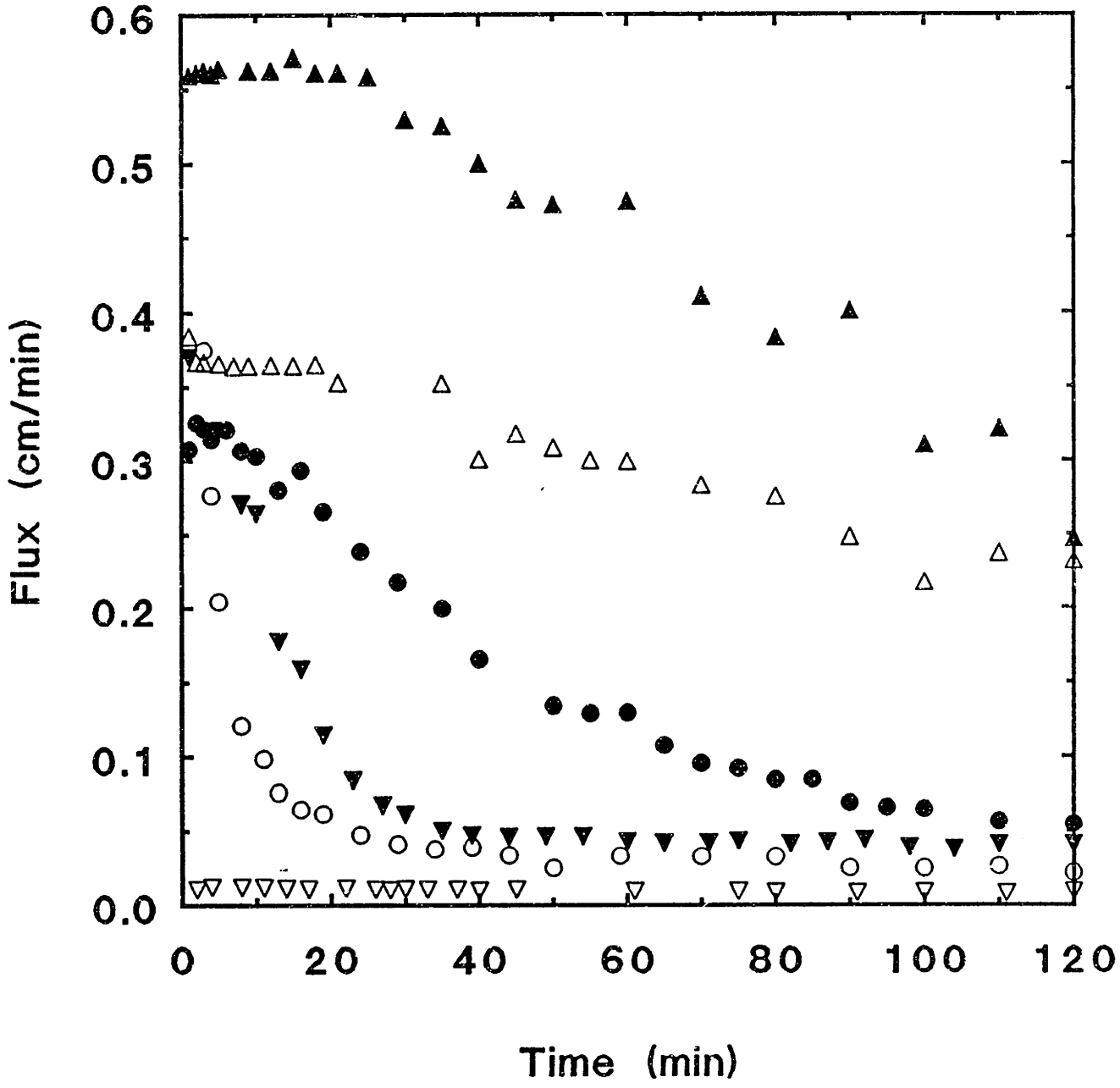

Figure 5-7. Flux of 6% albumin through Sepracor modified polysulfone (activated ▲ and unactivated △ forms), Enka polyamide (●) and polypropylene (▼), W. R. Grace polysulfone-Biopol (○), and Kinetek polysulfone-Dextran (▽) hollow fiber membranes.

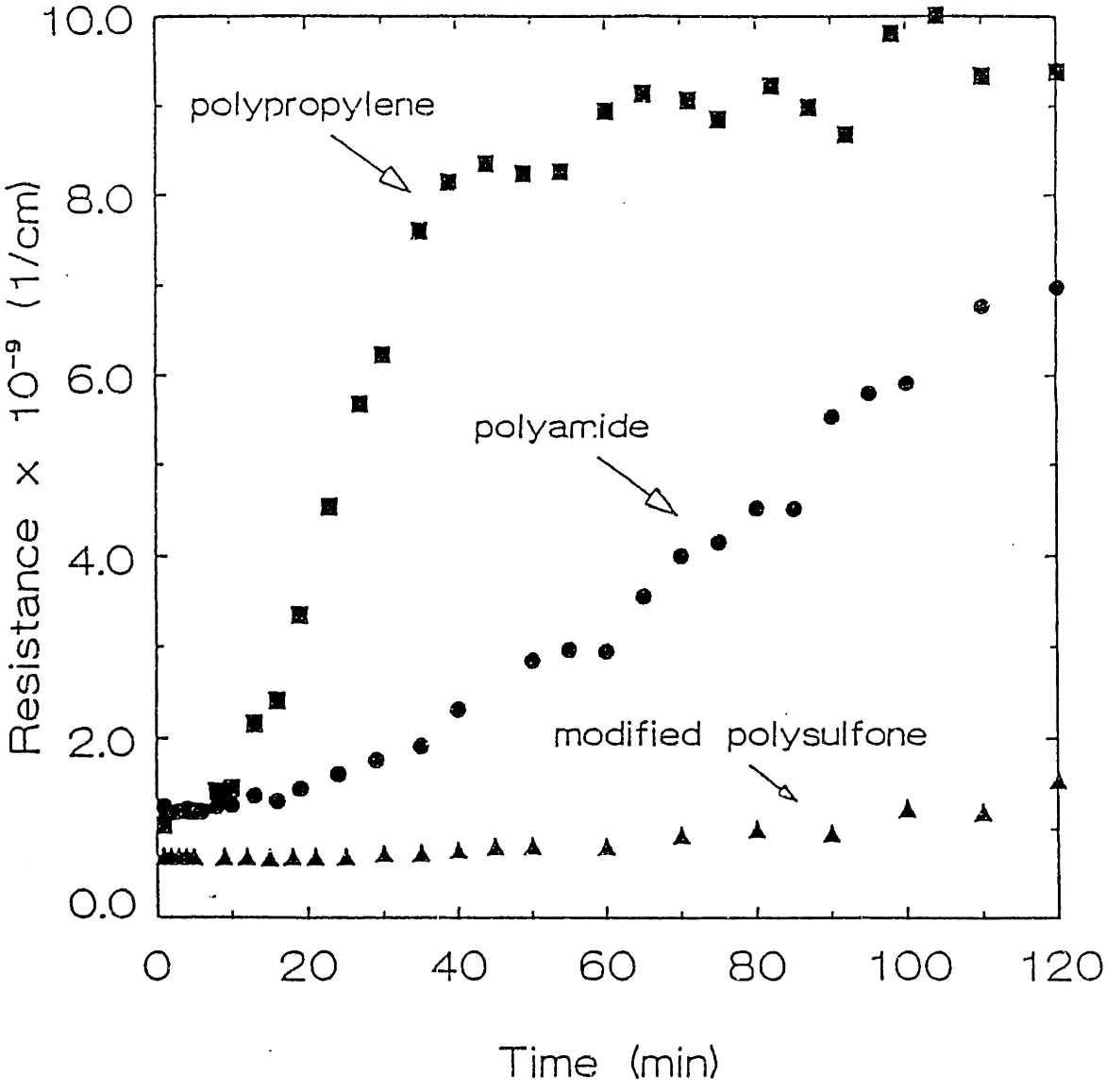

Figure 5-8. Membrane resistances as a function of time of albumin filtration.

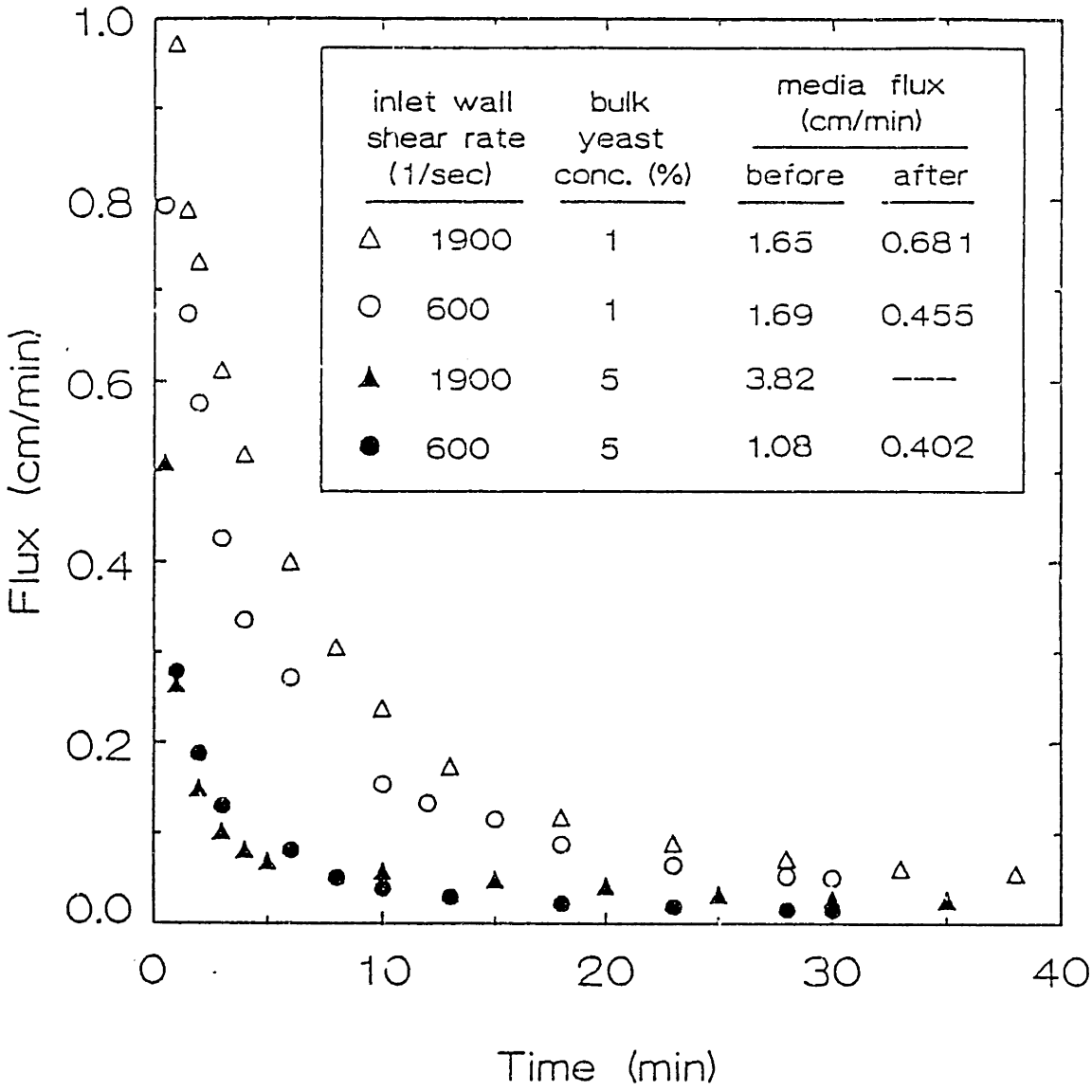

Figure 5-9. Time-dependent filtration rate of 1% and 5% yeast in media (w/o albumin) in single polysulfone/Biopol hollow fibers (L=10 cm, ID=475 μm, pore ID=0.2 μm) at an outlet applied pressure of 74 mmHg, at two inlet wall shear rates.

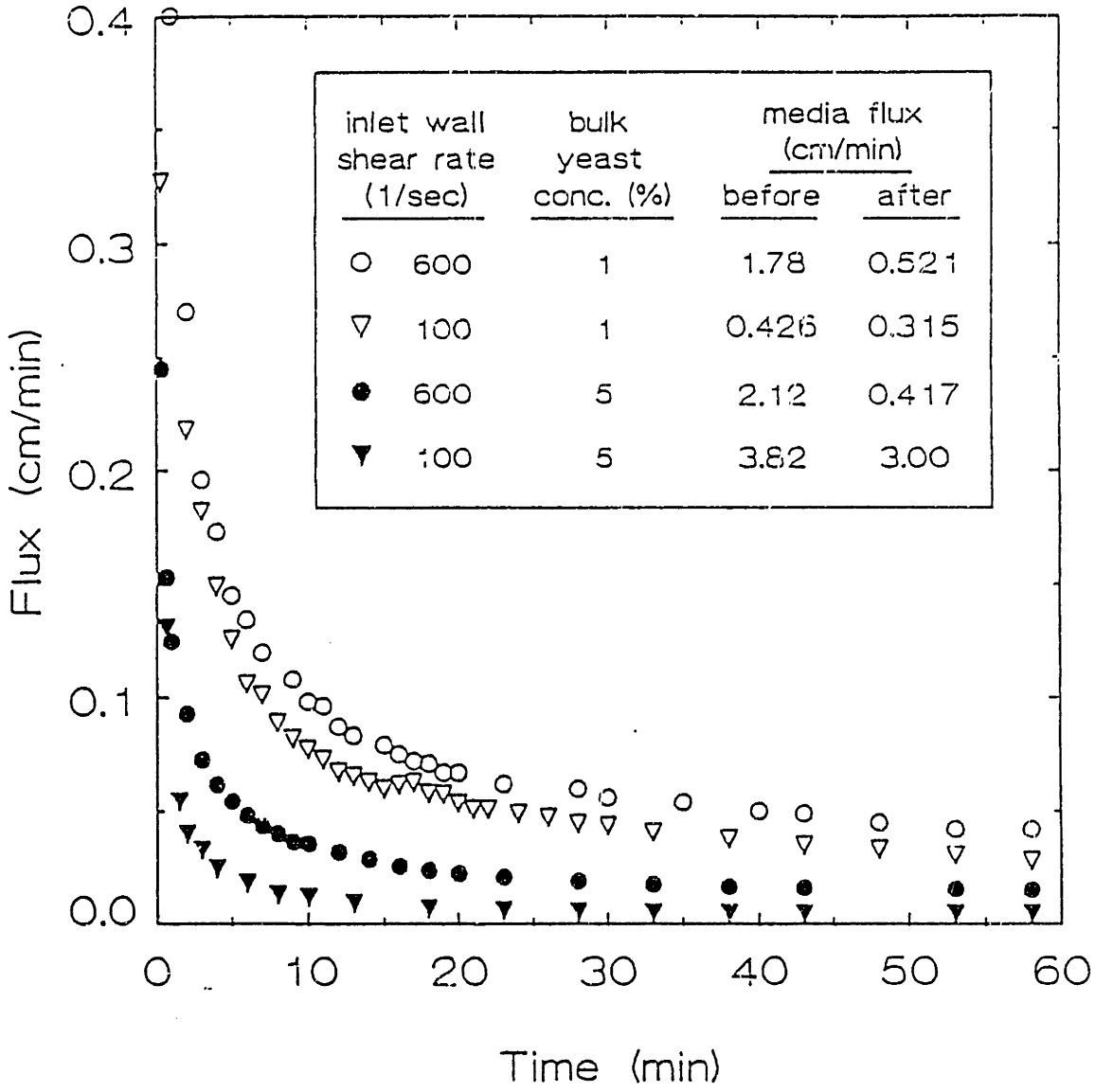

Figure 5-10. Time-dependent filtration rate of 1% and 5% yeast in media (w/o albumin) in polysulfone/Biopol hollow fiber cartridges (N=28, L=8.5 cm, ID=475 μm, pore ID=0.2 μm) with P_{out}=74 mmHg, at two inlet wall shear rates.

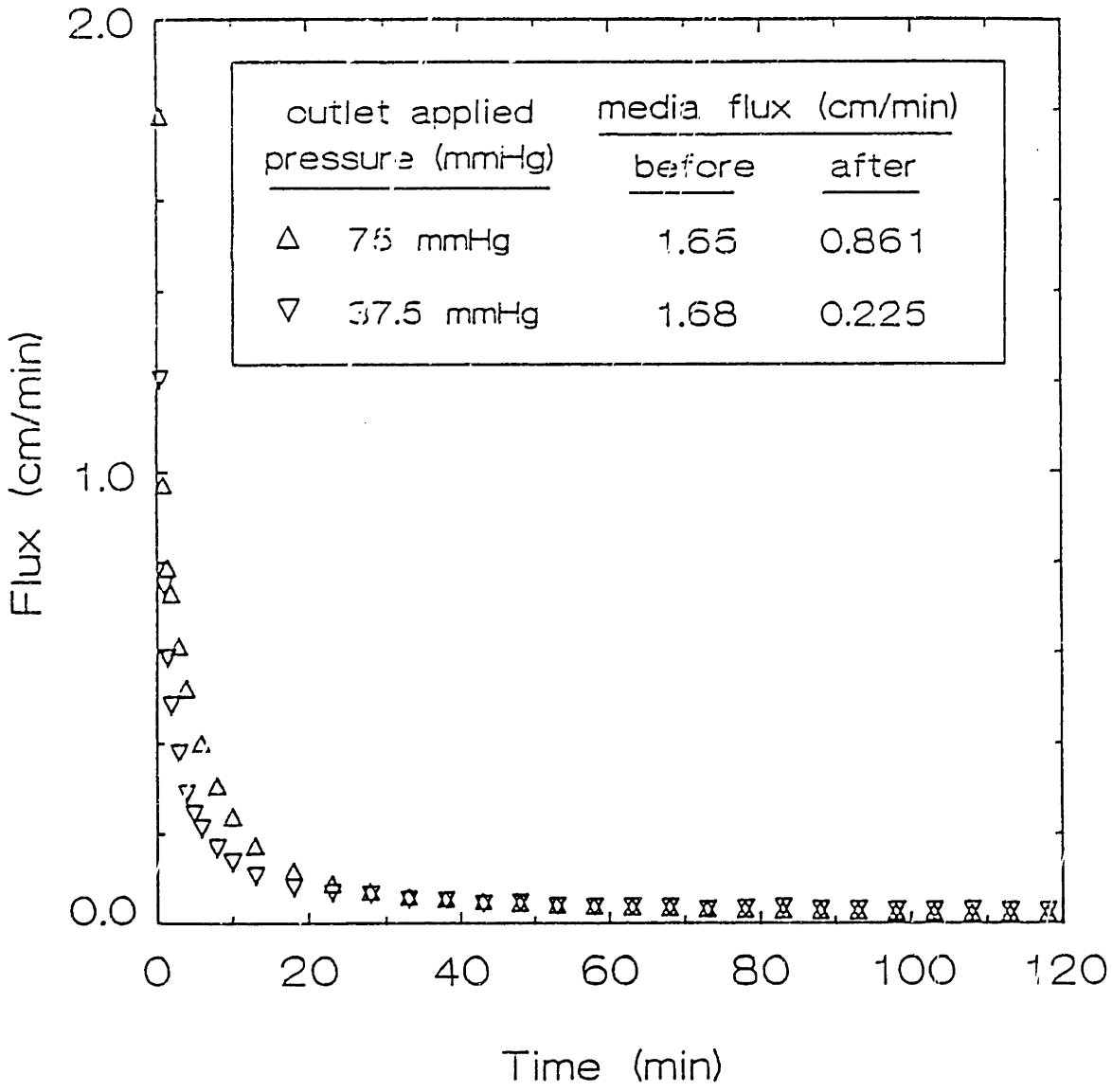

Figure 5-11. Time-dependent filtration rate of 1% yeast in media (w/o albumin) in single polysulfone/Biopol hollow fibers (L=10 cm, ID=475 μm, pore ID=0.2 μm) at an inlet wall shear rate of 1900 s^{-1}, at two outlet applied pressures.

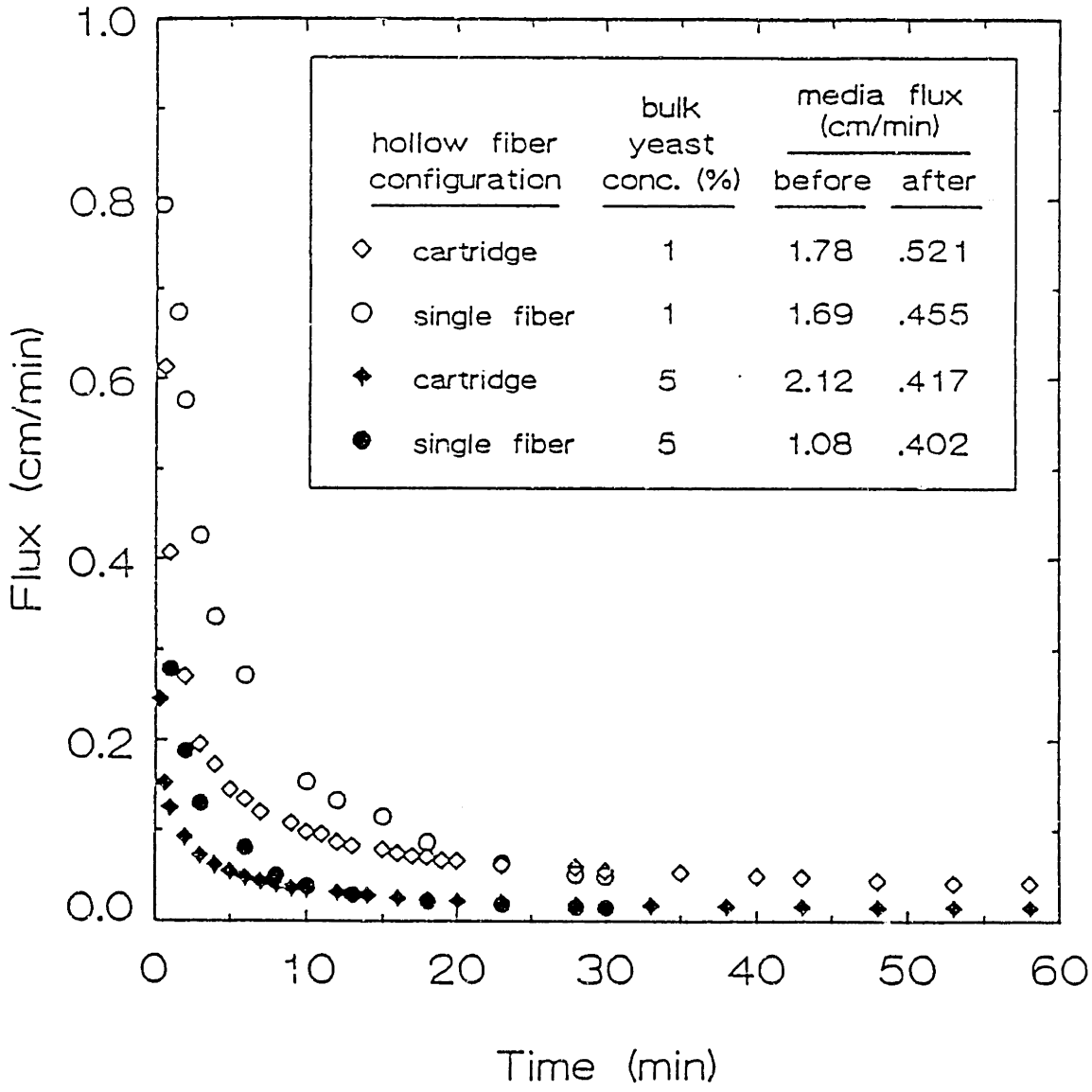

Figure 5-12. Time-dependent filtration rate of 1% and 5% yeast in media in single polysulfone/Biopol hollow fibers (L=10 cm, ID=475 μm, pore ID=0.2 μm) and in cartridges (N=28, L=8.5 cm) at P_{out}=74 mmHg and γ_{in} = 1900 s^{-1}.

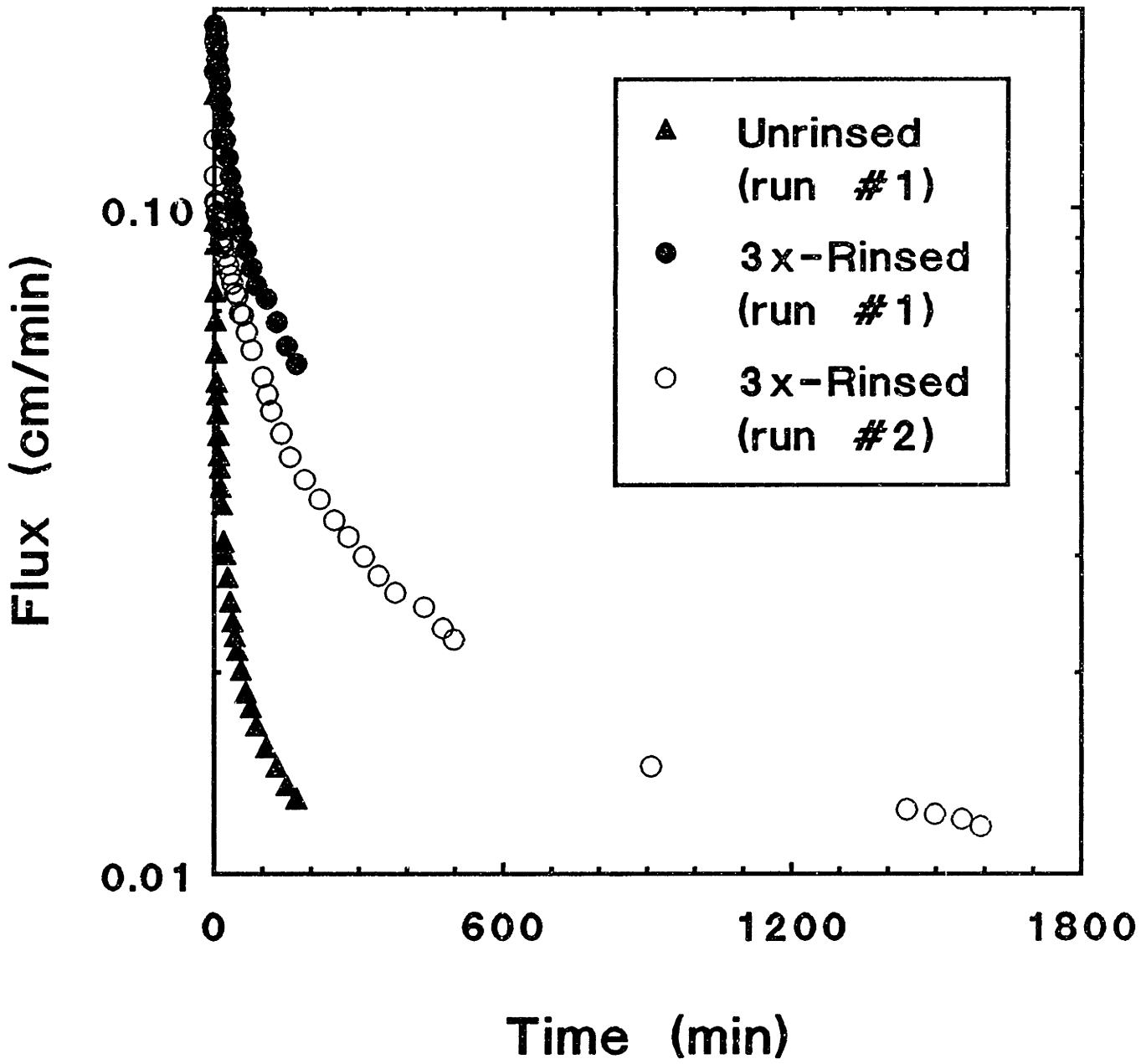

Figure 5-13. Filtrate flux as a function of time during filtration of suspensions of 1% bakers yeast in single 4.66 mm ID hollow fibers at an inlet wall shear rate of 80 s^{-1} and an outlet applied pressure of 75 mmHg.

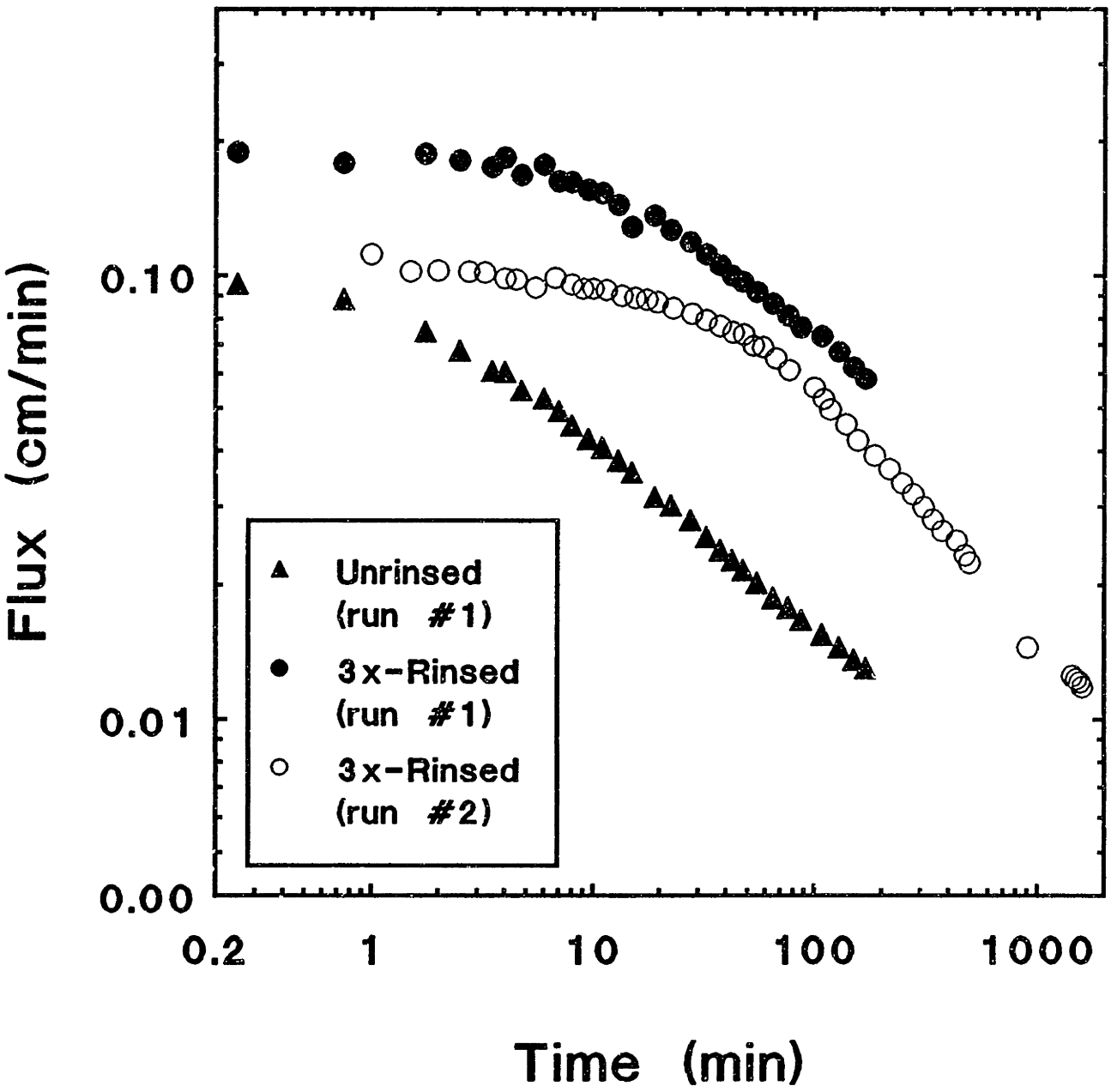

Figure 5-14. Filtrate flux as a function of time during filtration of suspensions of 1% bakers yeast in single 4.66 mm ID hollow fibers; data from Figure 5-13 replotted on an expanded scale.

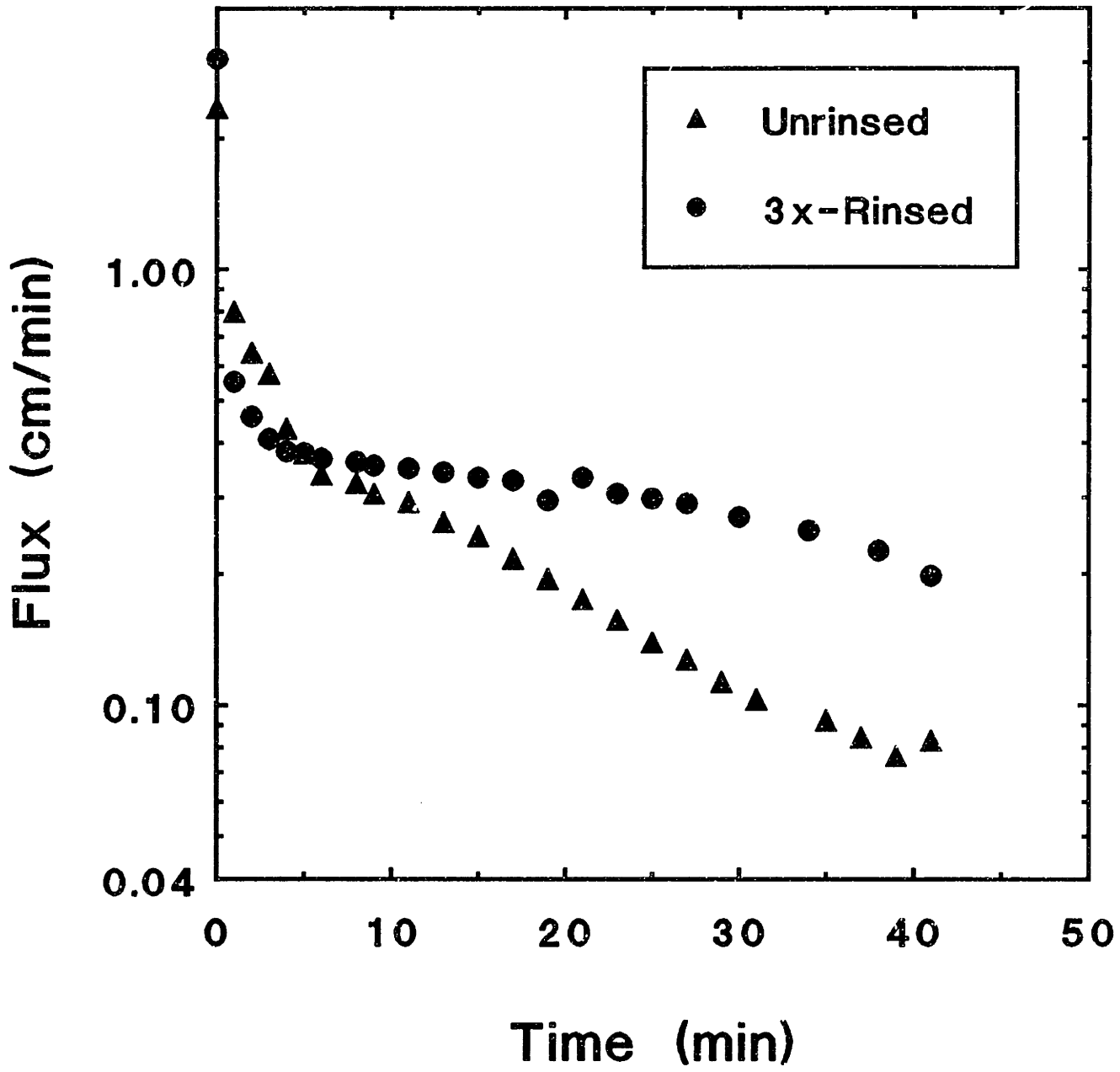

Figure 5-15. Filtrate flux as a function of time during filtration of suspensions of 1% bakers yeast in single 1000 μm ID modified polysulfone hollow fibers at an inlet wall shear rate of 80 s^{-1} and an outlet applied pressure of 75 mmHg.

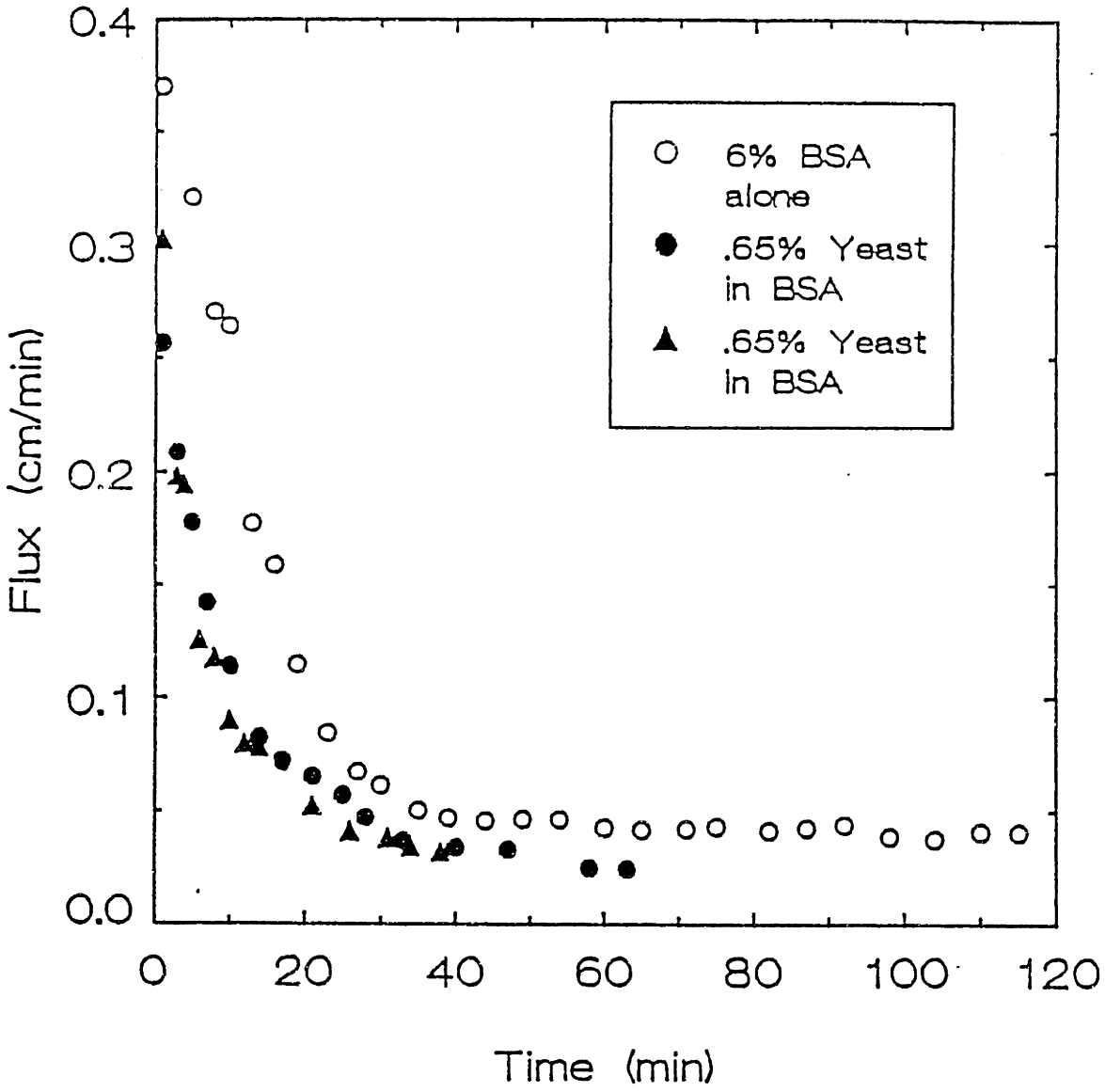

Figure 5-16. Flux of yeast and albumin suspensions through polypropylene hollow fibers, with an inlet wall shear rate of 800 s^{-1} and an outlet applied pressure of 70 mmHg.

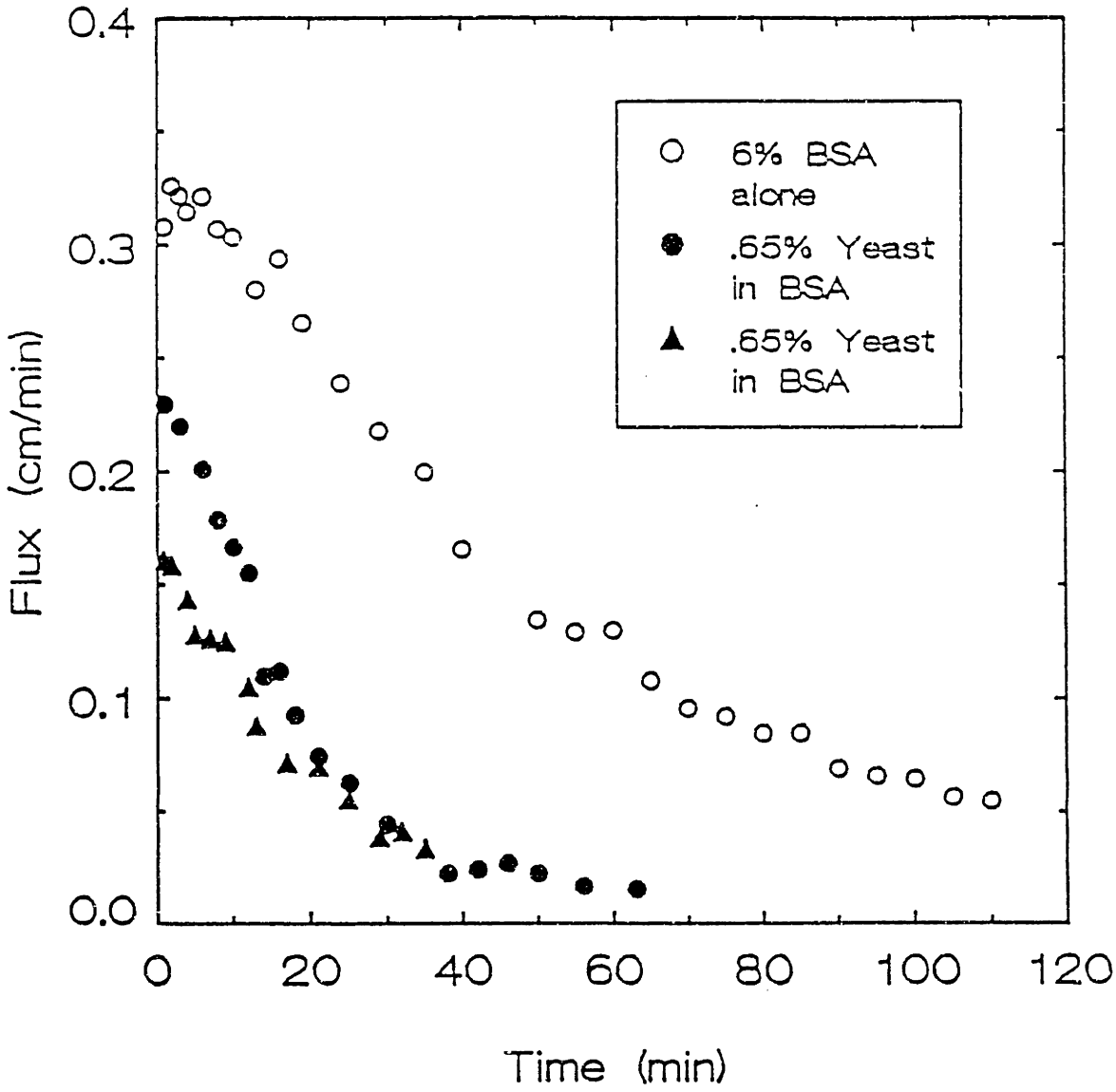

Figure 5-17. Flux of yeast and albumin suspensions through polyamide hollow fibers, with an inlet wall shear rate of 800 s^{-1} and an outlet applied pressure of 70 mmHg.

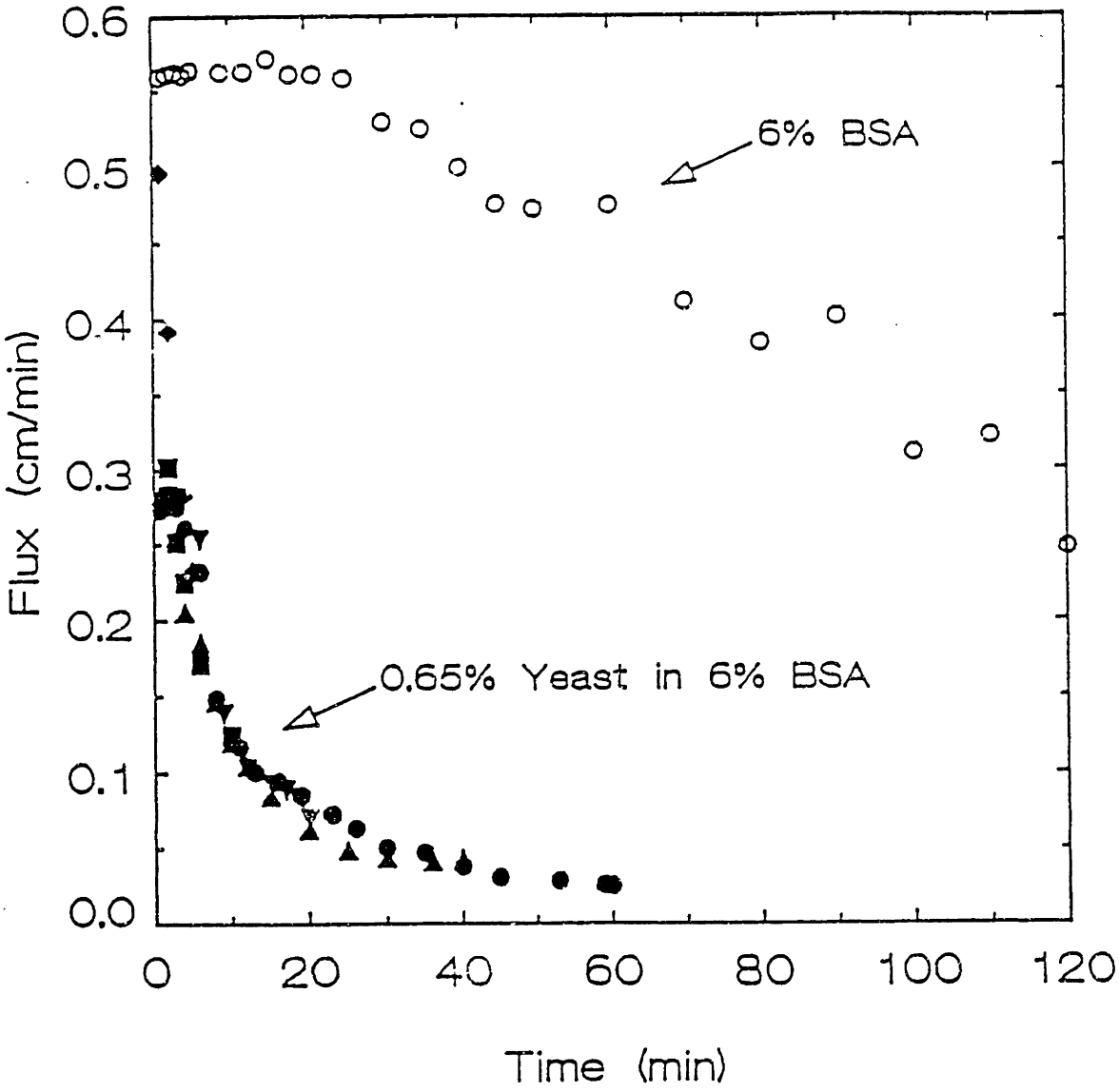

Figure 5-18. Flux of yeast and albumin suspensions through modified polysulfone hollow fibers, with an inlet wall shear rate of 80 s^{-1} and an outlet applied pressure of 70 mmHg.

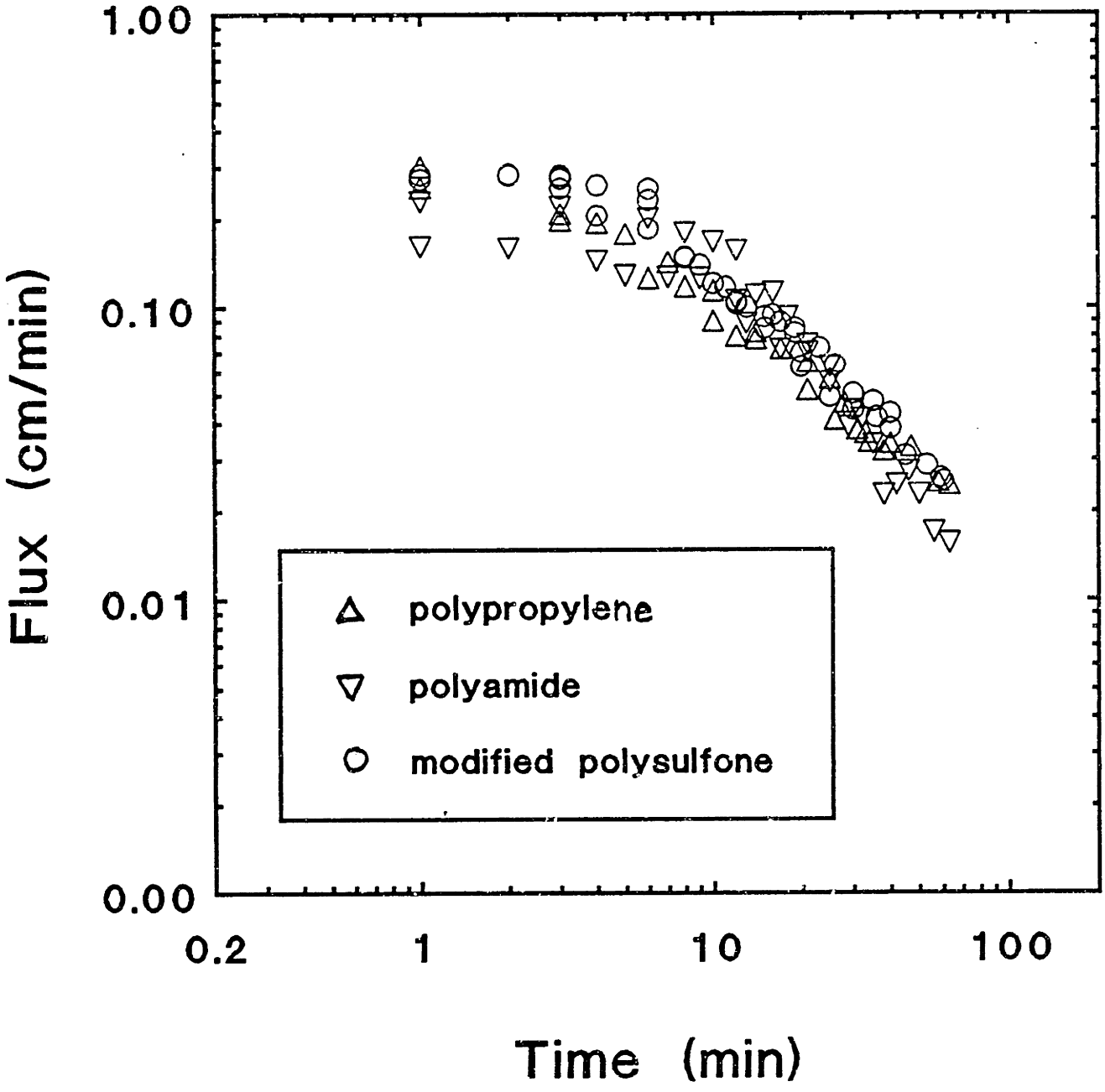

Figure 5-19. Flux of yeast and albumin suspensions through polypropylene, polyamide, and modified polysulfone hollow fibers (data from previous three figures re-plotted).

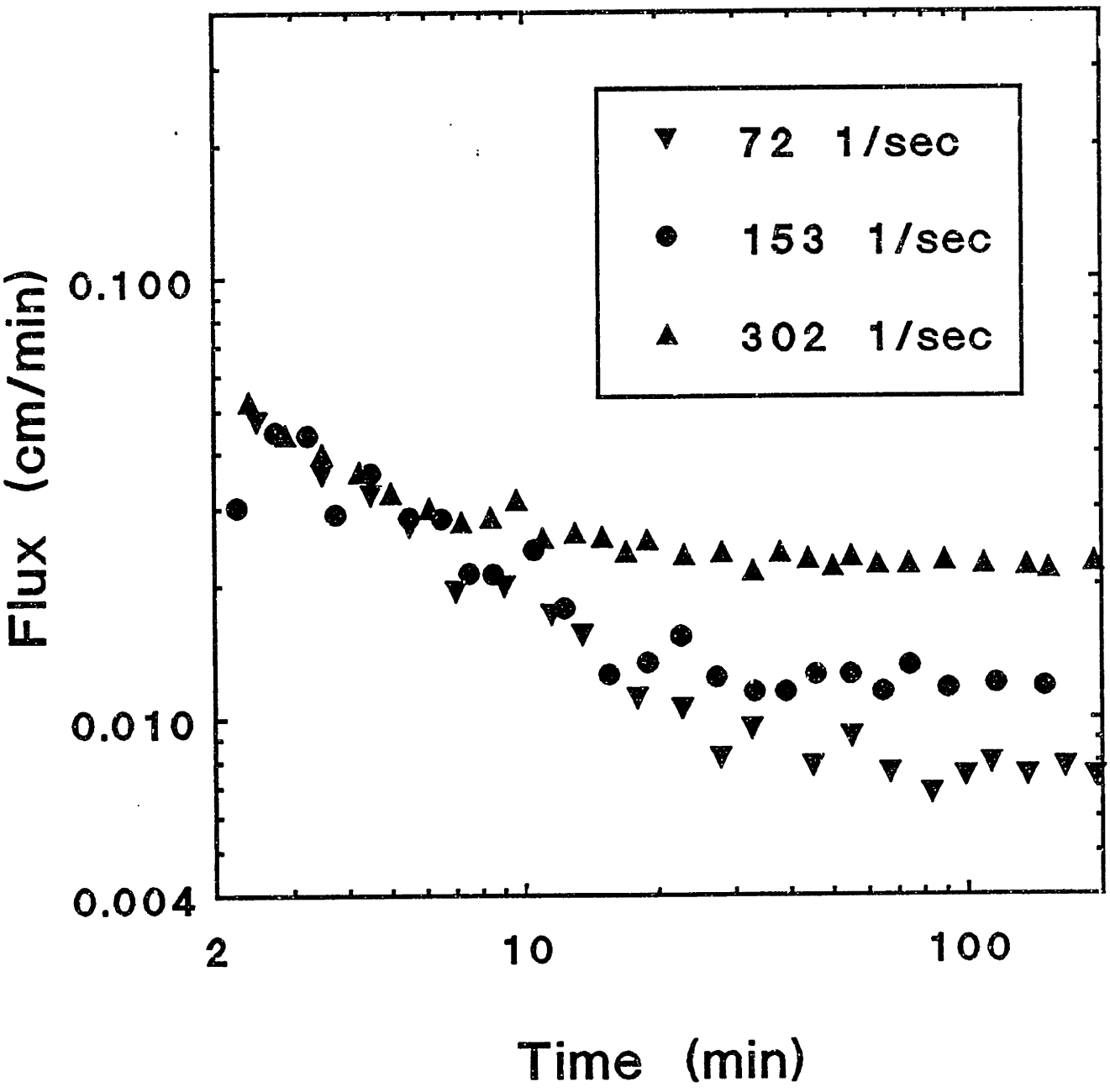

Figure 5-20. Filtrate flux as a function of time during filtration of an 8.9% suspension of 0.711 μm diameter latex particles in single 4.66 mm ID hollow fibers at $P_{out,appl}$ = 75 mmHg and three different shear rates.

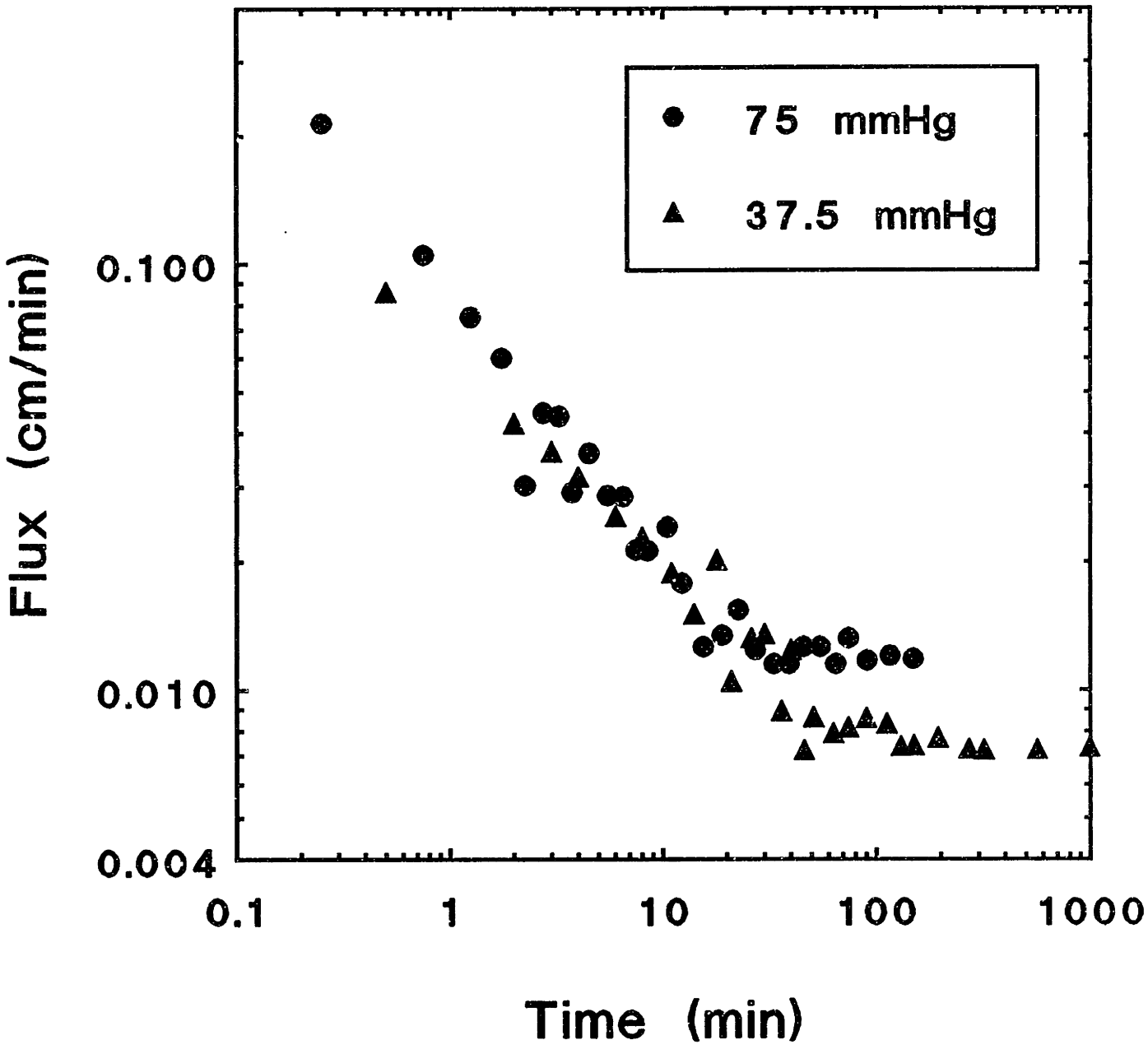

Figure 5-21. Filtrate flux as a function of time during filtration of an 8.9% suspension of 0.711 μm diameter latex particles in single 4.66 mm ID hollow fibers at an inlet wall shear rate of 250 s^{-1} and $P_{out,appl}$ = 75 mmHg and 37.5 mmHg.

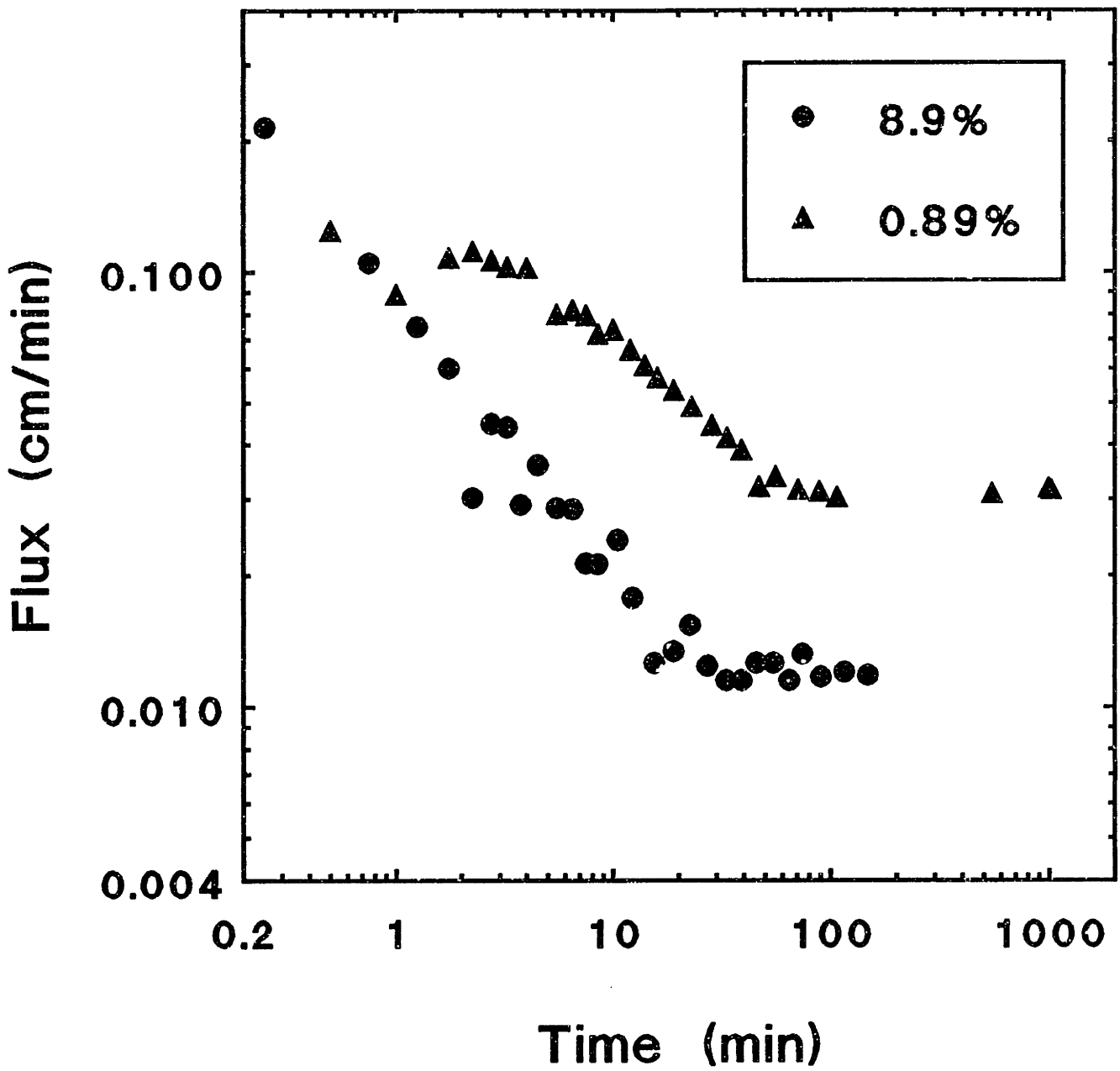

Figure 5-22. Filtrate flux as a function of time during filtration of 0.89% and 8.9% suspensions of 0.711 μm diameter latex particles in single 4.66 mm ID hollow fibers at an inlet wall shear rate of 250 s^{-1} and $P_{out,appl}$ = 75 mmHg.

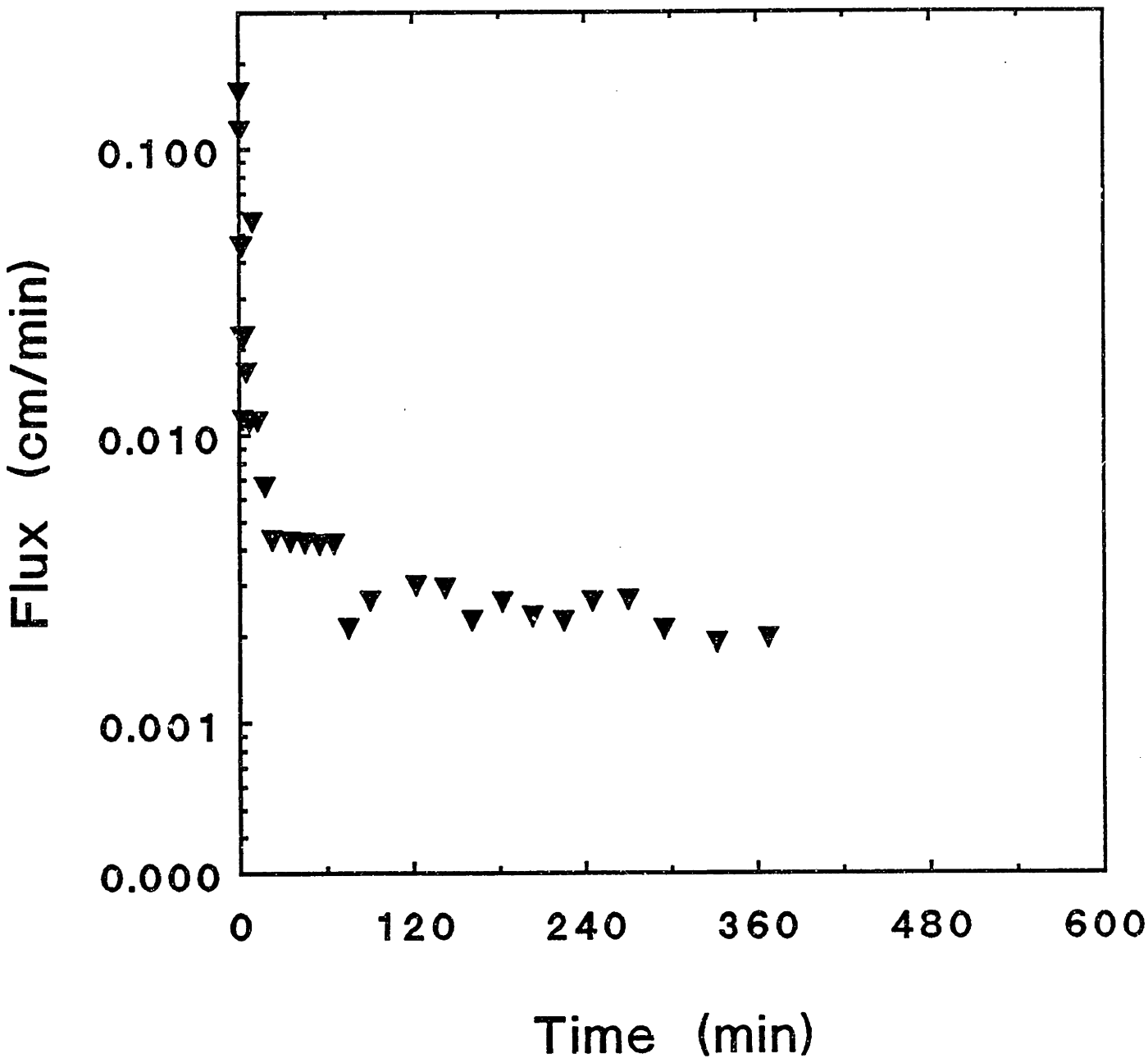

Figure 5-23. Filtrate flux as a function of time during filtration of a 7.7% suspension of 0.264 μm diameter latex particles.

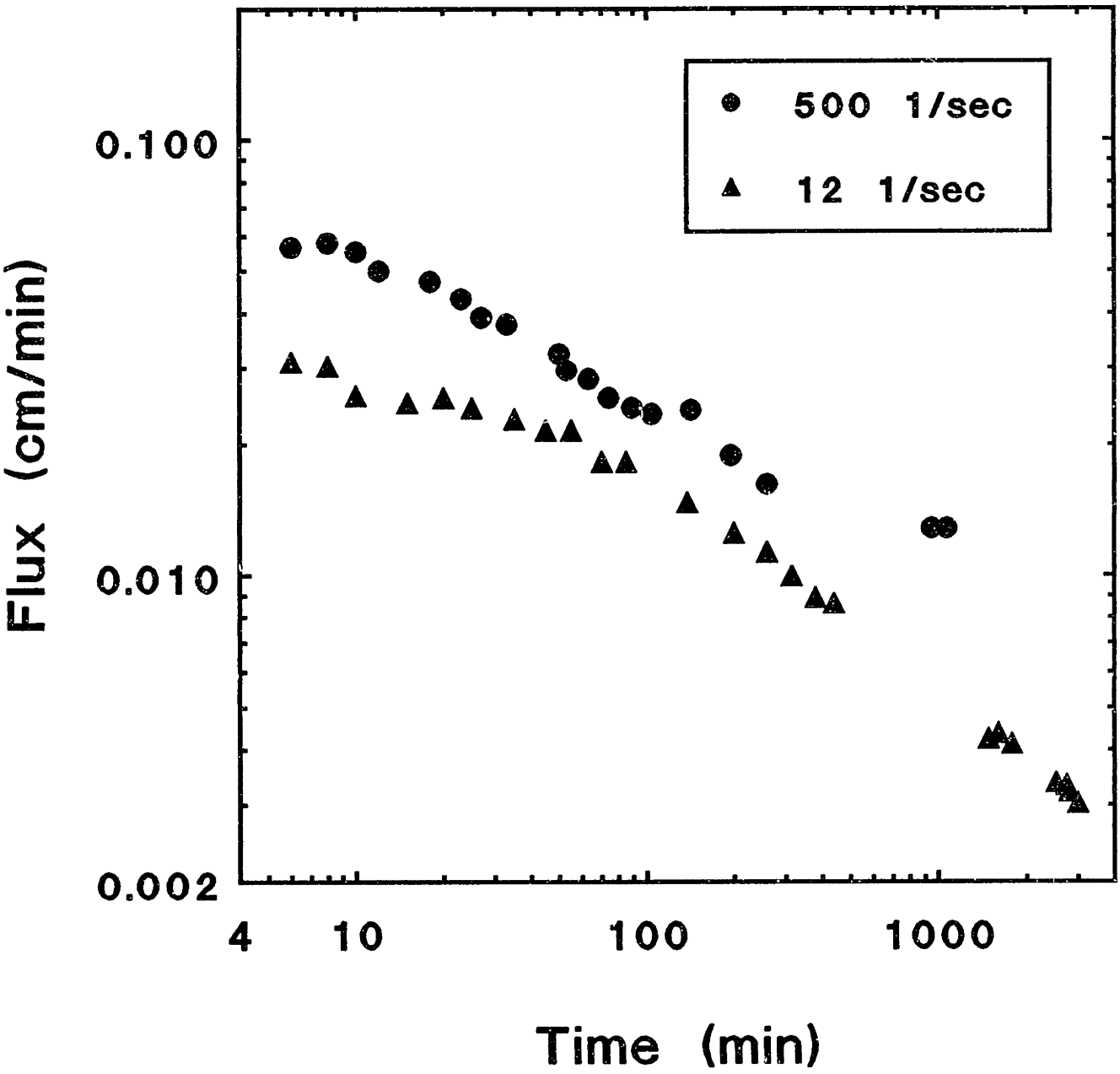

Figure 5-24. Filtrate flux as a function of time during filtration of a 0.2% suspension of 0.264 μm diameter latex particles.

(Photograph on following page.)

Figure 5-25. Polypropylene (330 μm ID, 0.4 μm pore ID) fibers frozen after filtration of 0.65% yeast in 6% albumin for a) 3, b) 10, c) 20, d) 38 and e) 63 min at an inlet shear rate of 800 s^{-1}. Axial positions shown: 1) 0, 2) 2 and 3) 5 cm.

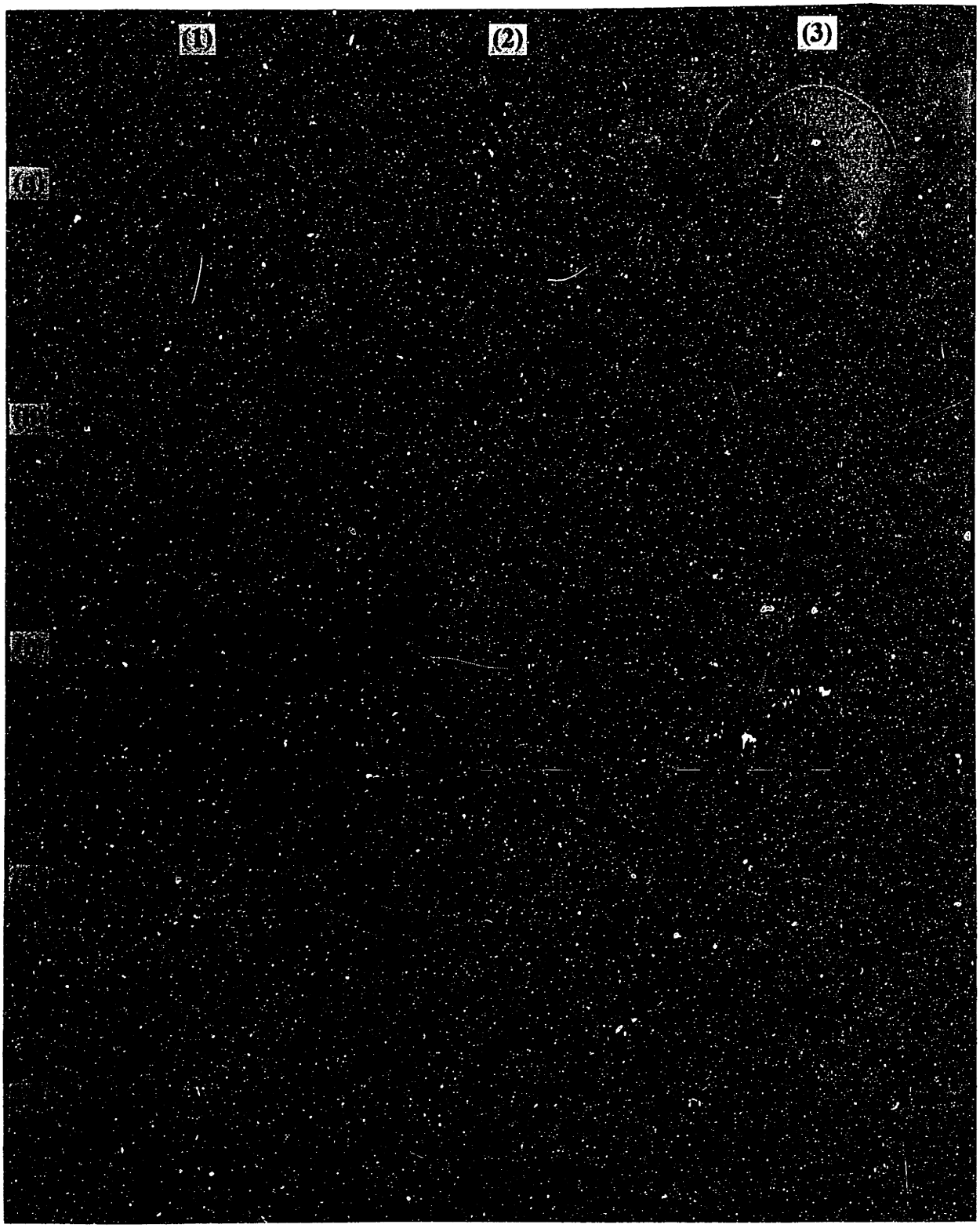

FIG 5-25

(Photograph on following page.)

Figure 5-26. Polyamide (320 μm ID, 0.35 μm pore ID) fibers frozen after filtration of 0.65% yeast in 6% albumin for a) 3, b) 10, c) 20, d) 35 and e) 63 min at an inlet shear rate of 800 s^{-1}. Axial positions shown: 1) 0, 2) 2 and 3) 5 cm.

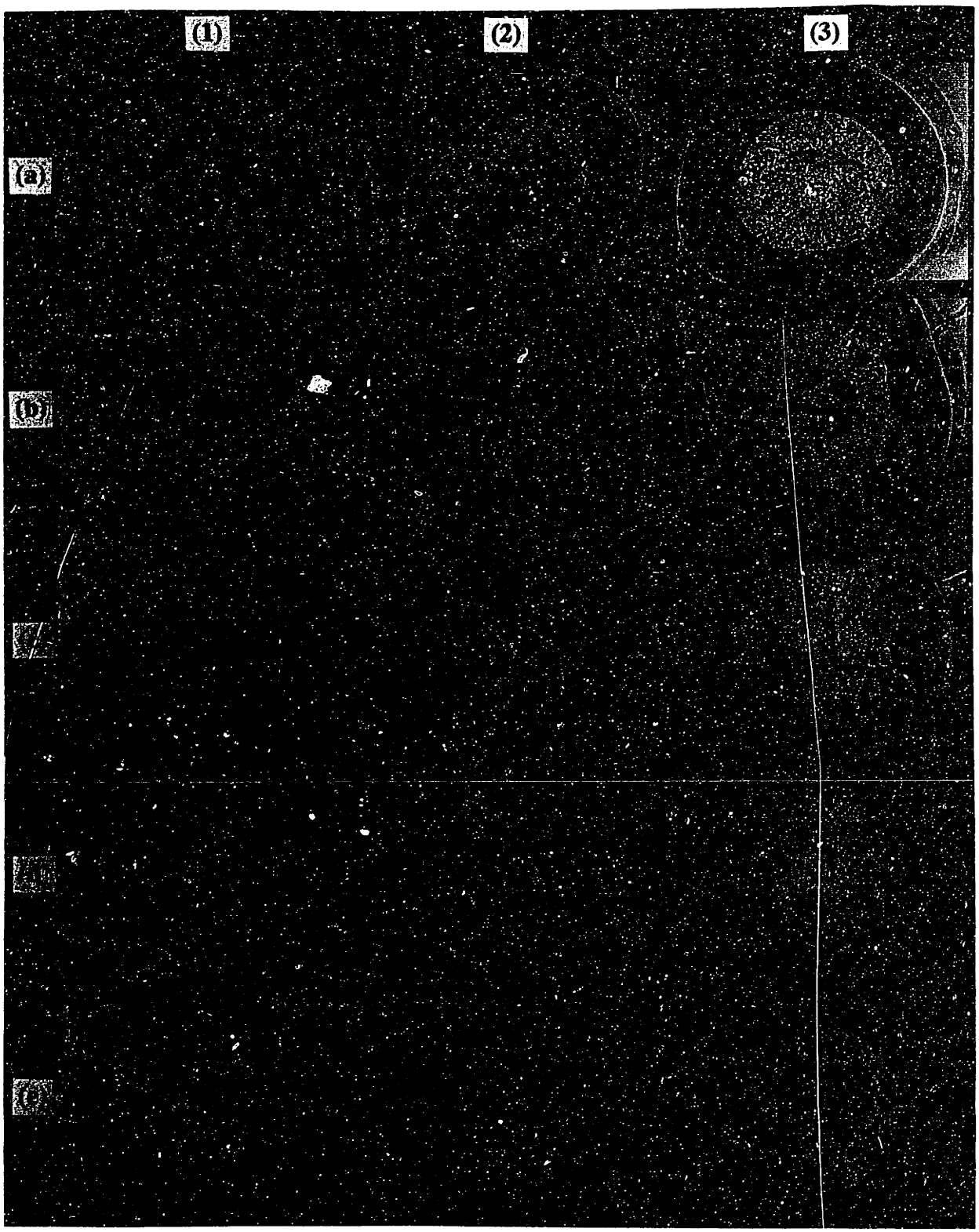

Fig 5-26

(Photograph on following page.)

Figure 5-27. Polypropylene fiber frozen after filtration of 0.65% yeast in 6% albumin at $\gamma_{w,in} = 2000\ s^{-1}$ and $P_{appl,out} = 70$ mmHg for t=2 min.

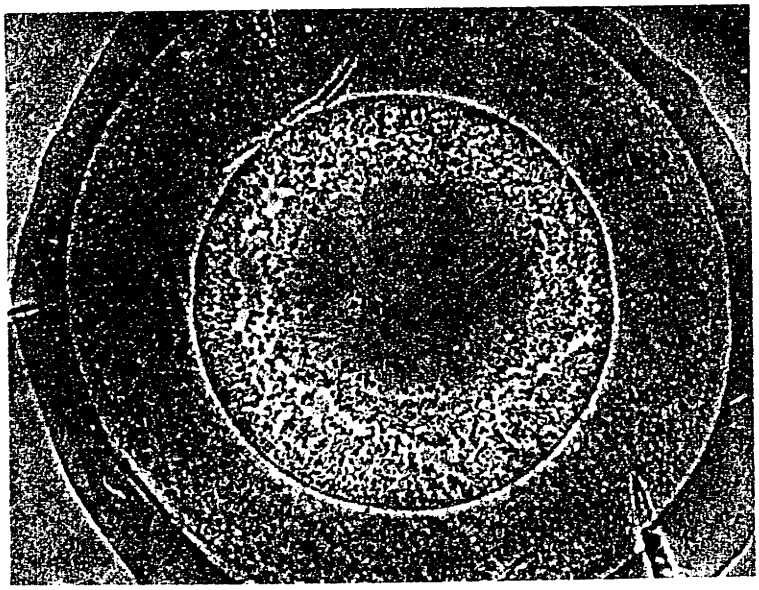

Fig 5-27

(Photograph on following page.)

Figure 5-28. Polyamide (320 μm ID, 0.35 μm pore ID) fiber frozen after filtration of 6.5% yeast in 6% BSA for 60 min at $\gamma_{w,in}$ = 140 s^{-1} and $P_{appl,out}$ = 122 mmHg. Axial positions shown: a) 0 b) 2, and c) 4 cm.

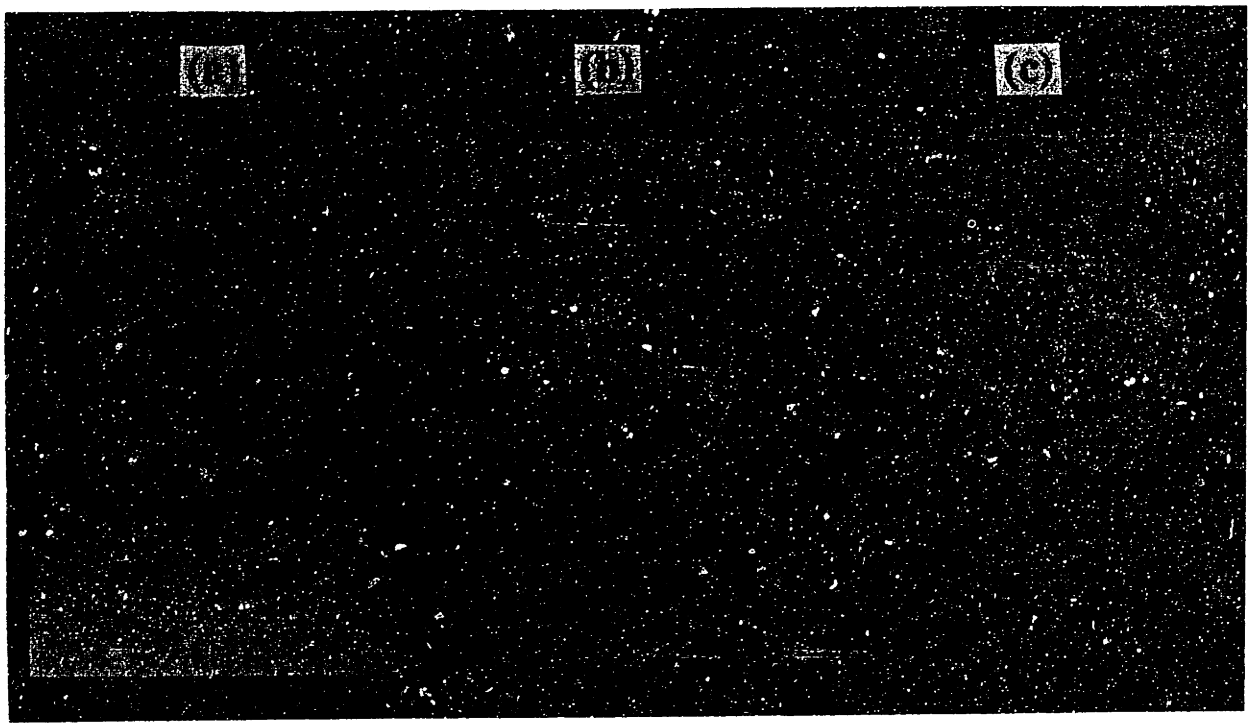

Fig 5-28
217

(Photograph on following page.)

Figure 5-29. Examples of uneven yeast cakes which formed in both (a) polyamide (320 μm ID, 0.35 μm pore ID) and (b) polypropylene (210 μm ID, 0.40 μm pore ID) hollow fibers. (For conditions of experiments, see text.)

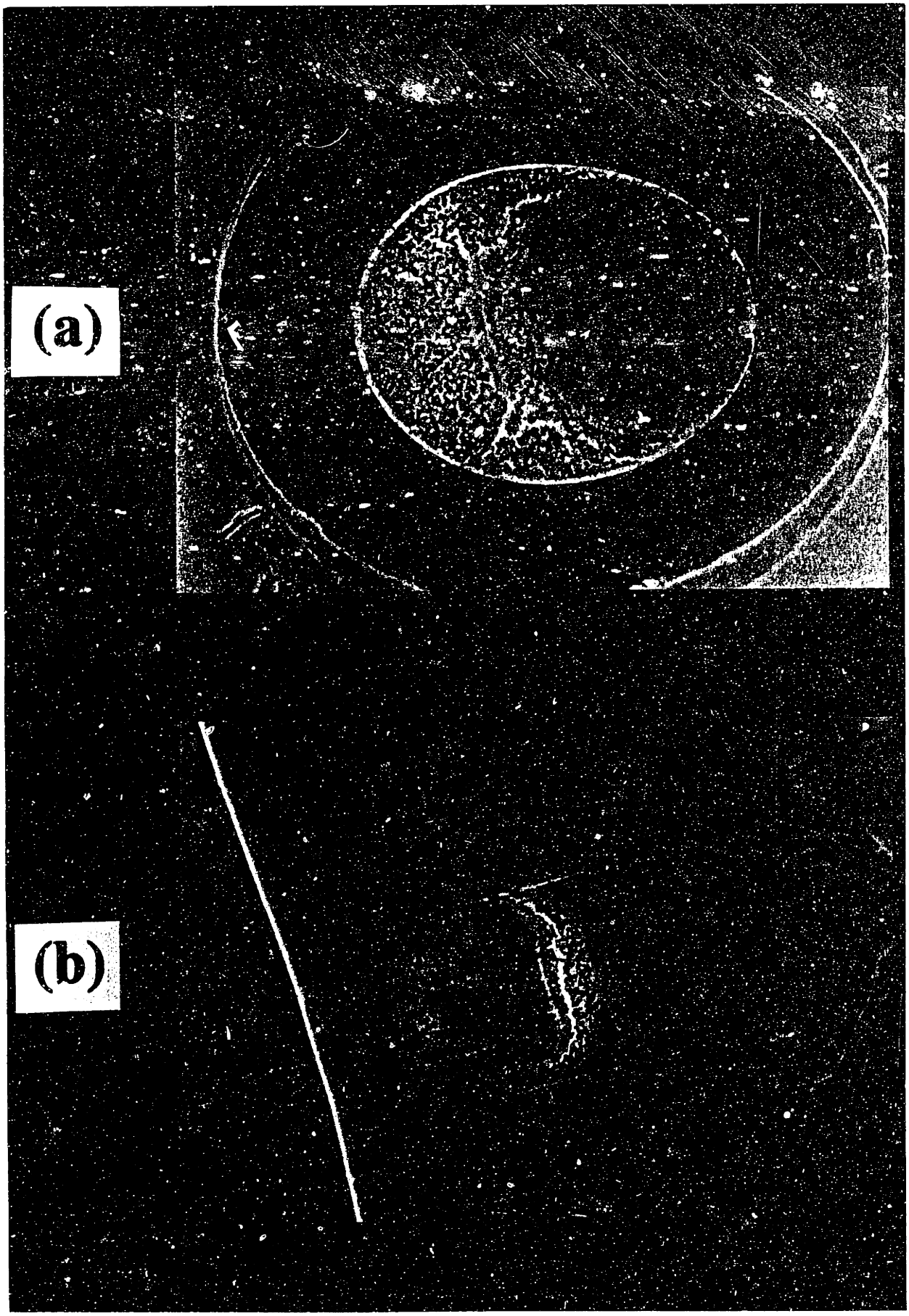

Fig 5-29

(Photograph on following page.)

Figure 5-30. Polypropylene fiber frozen after filtration of 0.65% yeast in 6% albumin at $\gamma_{w,in} = 359\ s^{-1}$ and $P_{appl,out} = 70$ mmHg for 3 min. Axial positions shown: a)x=0, b)x=1, c)x=2, d)x=3, e)x=4, and f) x=5 cm.

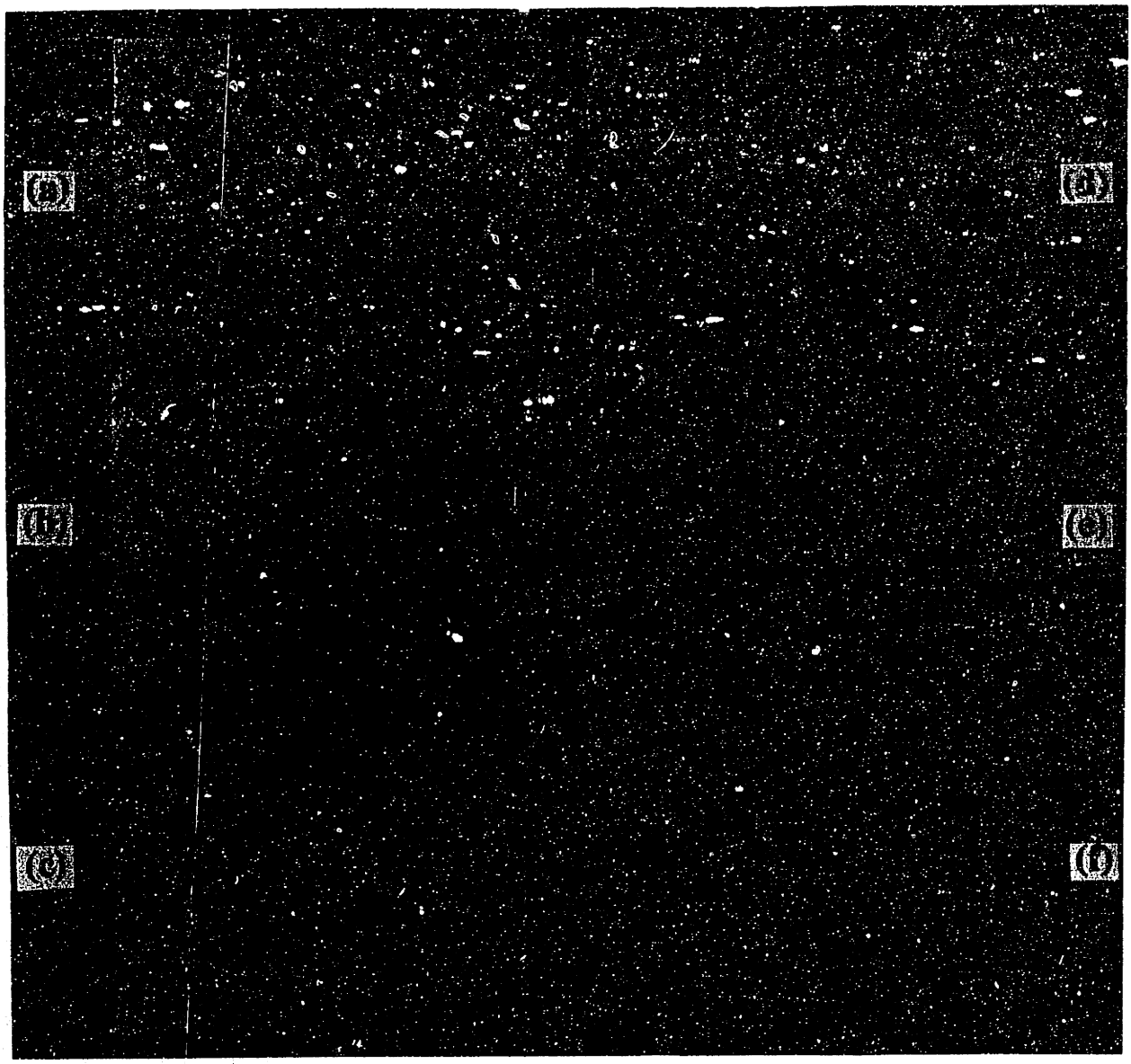

Fig 5-30

(Phctograph on following page.)

Figure 5-31. Polypropylene fiber frozen after filtration of 6.5% yeast in 6% albumin at $\gamma_{w,in}$ = 88 s^{-1} and $P_{appl,out}$ = 4 mmHg for a) t=2 min and 1)x=0, 2)x=2, 3)x=5 cm; b)x=2 cm and 1)t=2, 2) t=10 and 3) t=15 min.

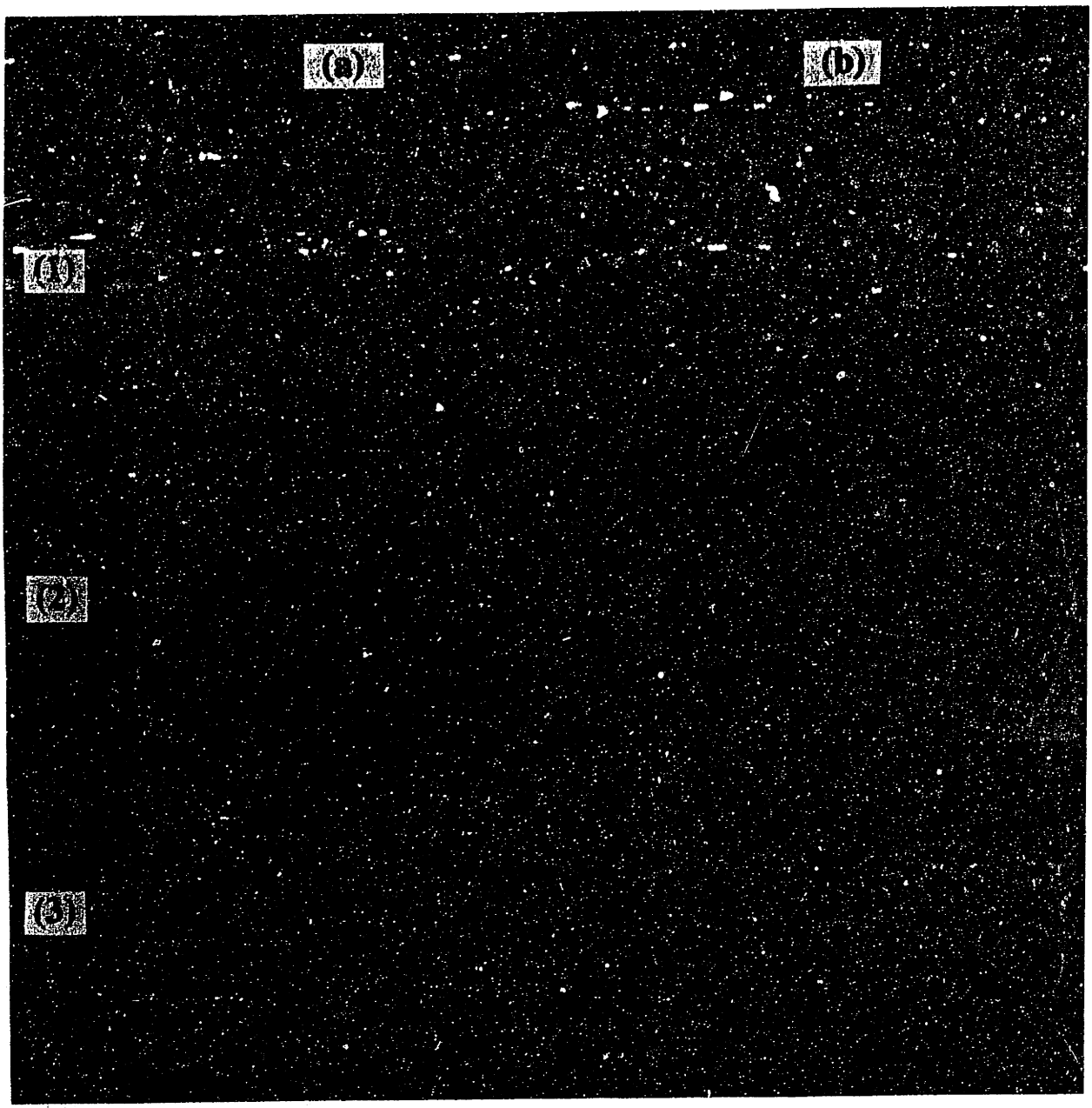

FIG 5-31
223

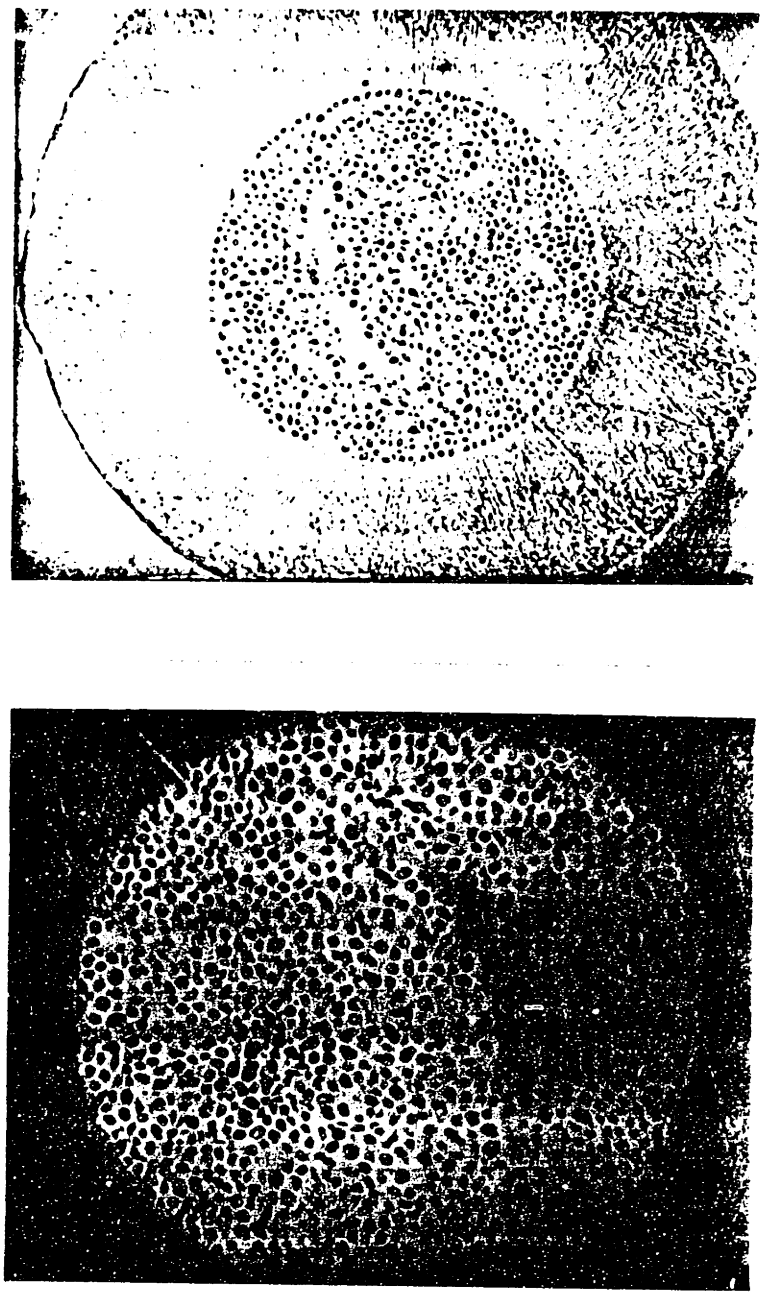

Figure 5-32. Section taken from a hollow fiber which clogged during startup of yeast filtration.

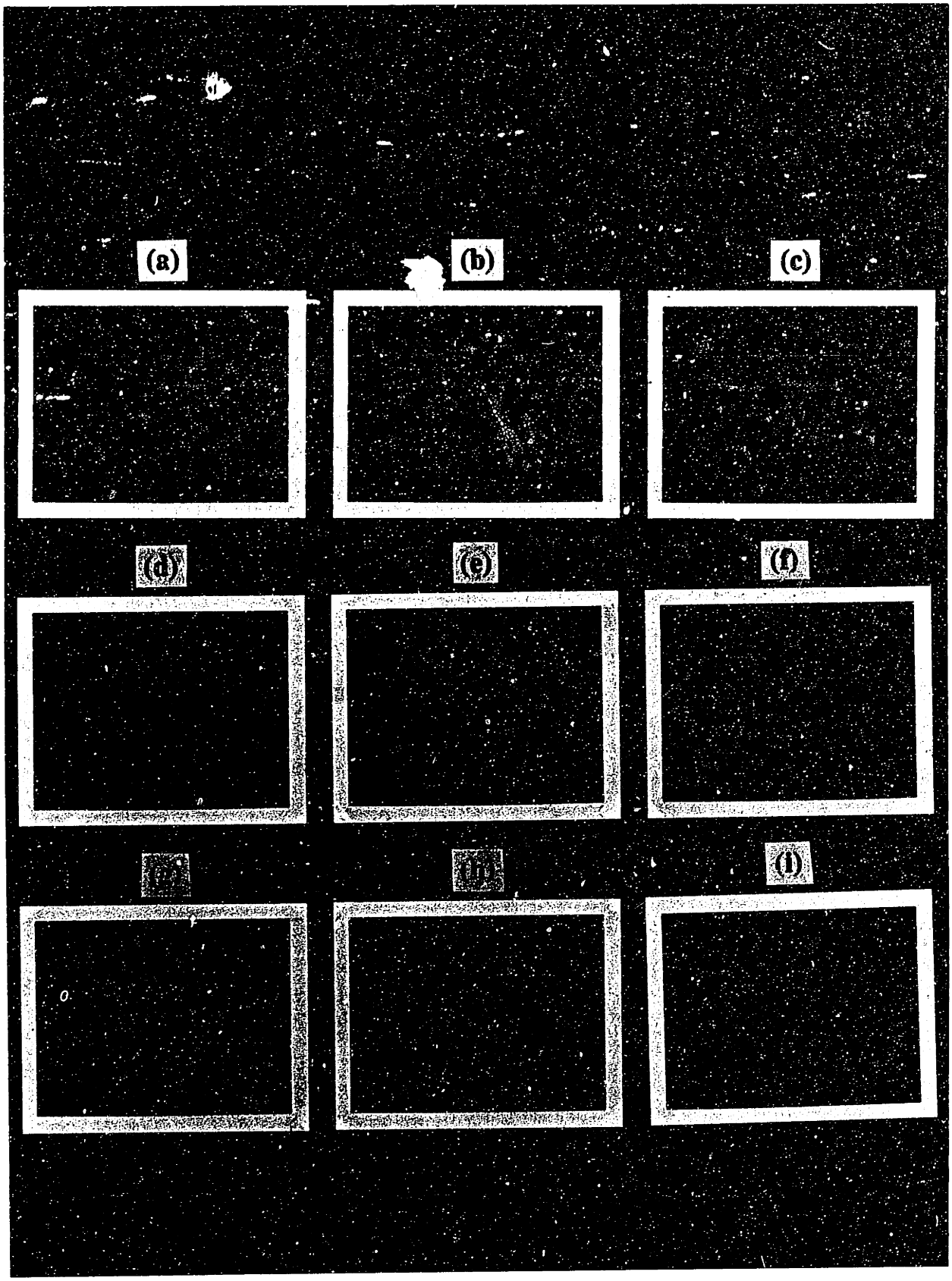

Figure 5-33. Partial clogging of a flat-plate channel (flow left to right) during filtration of 3.98 μm latex particles for (a) 0, (b) 0.5, (c) 2, (d) 3, (e) 5, and (f) 30 min, and re-opening of channel after rinsing for (g) 2, (h) 4, and (i) 6 min.

(Photograph on following page.)

Figure 5-34. Modified polysulfone (1 mm ID, 0.4 μm pore ID) fibers frozen after filtration of 0.65% yeast in 6% BSA for a) 3, b) 10, c) 20, d) 38 and e) 63 min at an inlet shear rate of 80 s^{-1}. Axial positions shown: 1) 0, 2) 2 and 3) 5 cm.

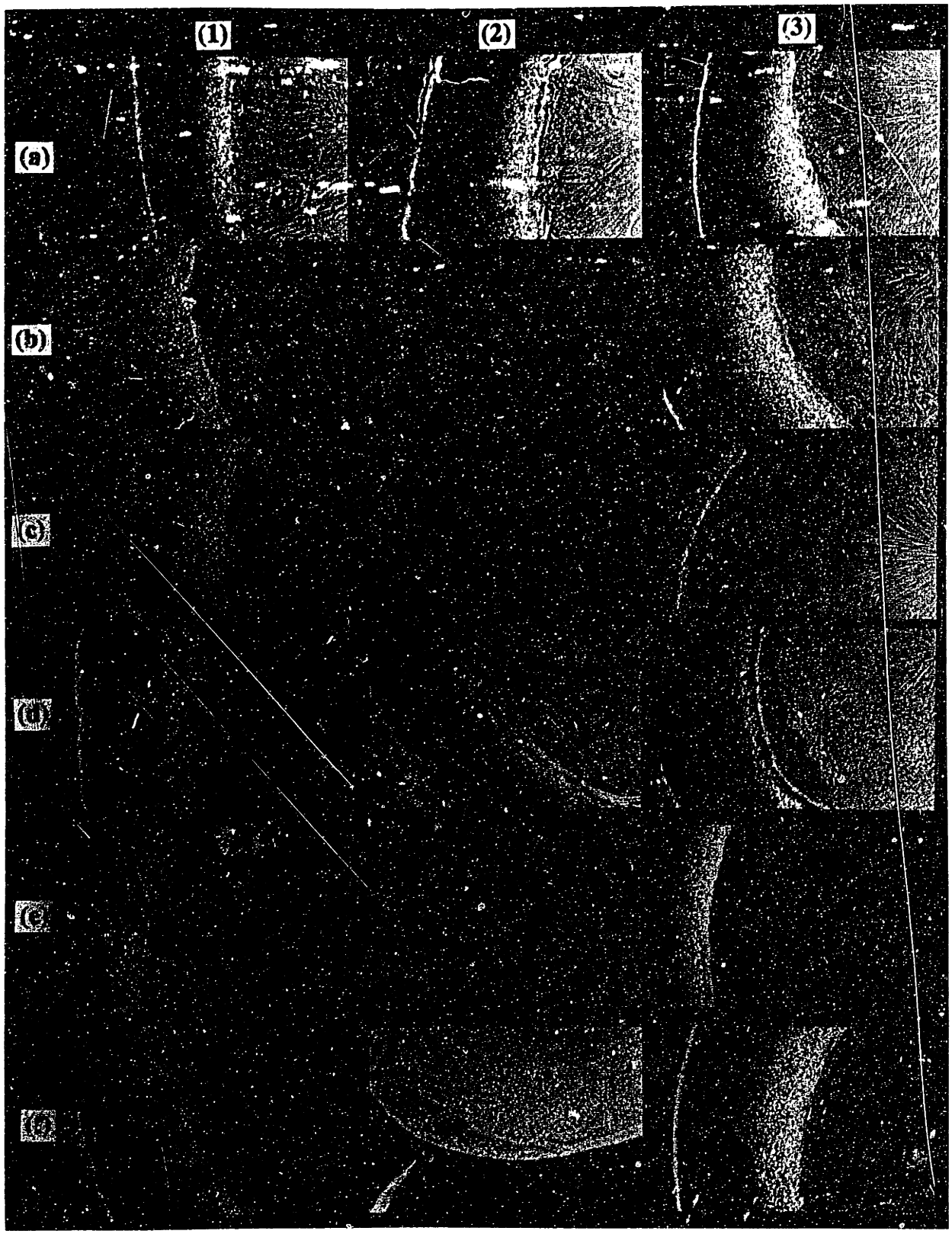

FIG 5-34

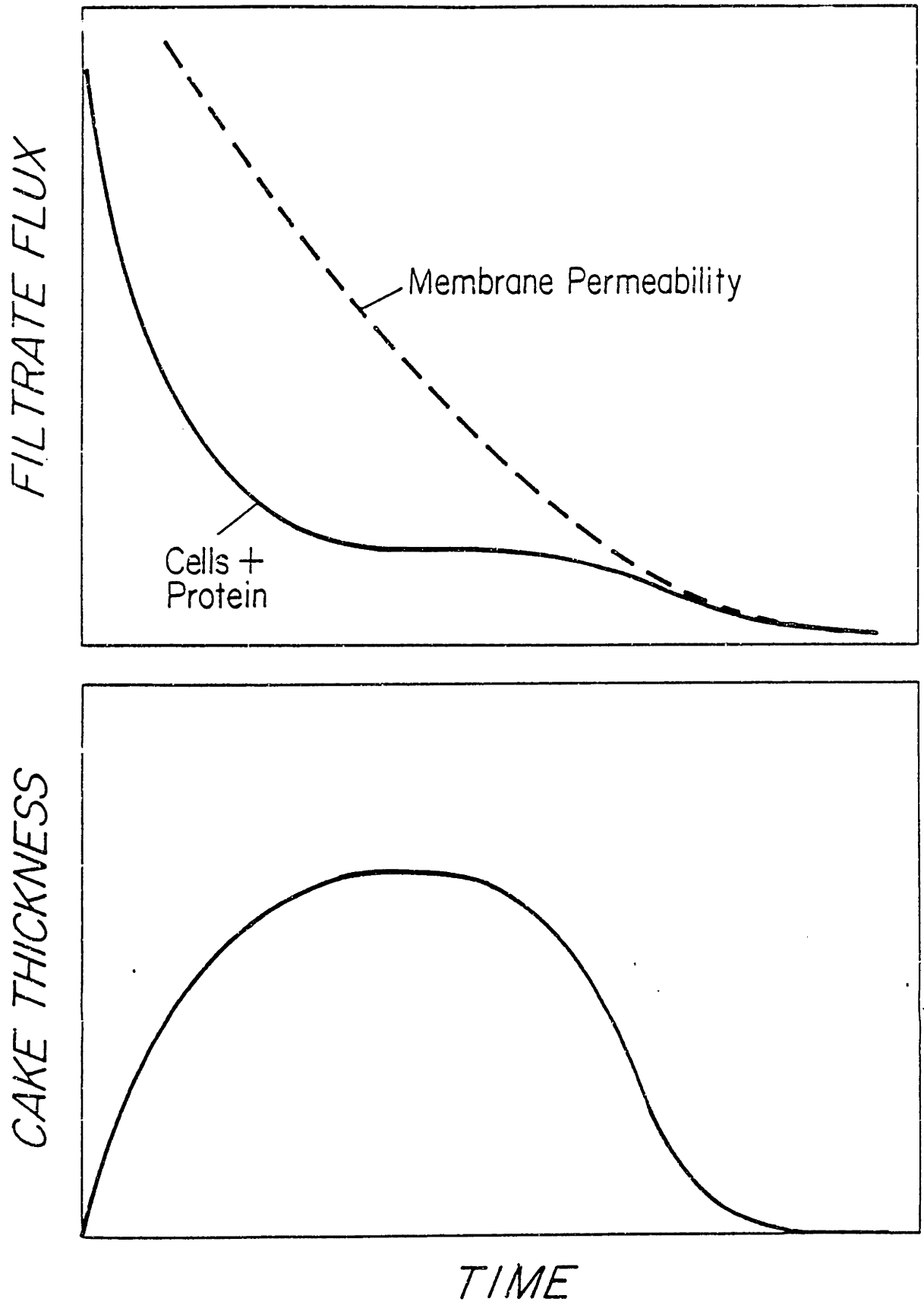

Figure 5-35. Postulated explanation for disappearance of yeast cakes with time.

CROSS-FLOW MEMBRANE FILTRATION

OF CELL SUSPENSIONS

by

Norma Jean Ofsthun
B. S., Ch. E., California Institute
of Technology (1981)

Submitted in Partial Fulfillment
of the Requirements for the
Degree of Doctor of Philosophy
at the
Massachusetts Institute of Technology

February, 1989

Signature of Author: Norma J. Ofsthun
Department of Chemical Engineering

Certified by: Clark K. Colton
C. K. Colton, Thesis Advisor

C. Cooney, Thesis Committee Member

W. M. Deen, Thesis Committee Member

K. A. Smith, Thesis Committee Member

Accepted by: Robert C Armstrong
R. Armstrong, Chairman
Dept. Comm. on Graduate Theses

APPENDIX TO CHAPTER 5

Filtration of Yeast in a Novel Rotating Membrane System

A. ABSTRACT

Rotating membrane systems have been shown to outperform traditional cross-flow devices in separation of plasma from whole blood. The purpose of this study was to evaluate the performance of a rotating membrane system in filtration of a model microbial cell system, bakers yeast. Results indicate that the rotating system allows high fluxes to be achieved without clogging problems. Furthermore, demand-mode operation allows independent control of throughput and yield without the development of prohibitive retentate-side pressures. The dependence of filtrate flux on applied pressure, rotation rate, bulk concentration, membrane material, and pore size were studied. It was noted that under some conditions (at sufficiently high rotation rate), the flux appeared to be membrane-limited, and decreased with time as the membrane permeability decreased. Thus, improvement of membrane permeability and resistance to fouling may play an even more important role in the development of rotating membrane systems than it does in development of traditional cross-flow systems such as hollow fibers.

B. INTRODUCTION

In annular rotating membrane devices such as that shown in Figure 5A-1, the bulk fluid to be filtered flows through a narrow annular channel in which the membrane is attached to a rotating inner cylinder. Such devices have been shown to achieve filtrate fluxes several times higher than can be achieved in conventional cross-flow devices (Beaudoin and Jaffrin, 1987). Higher fluxes are achieved by reducing the buildup of cells on the membrane surface. In traditional cross-flow devices, the ability to increase the wall shear rate is limited by the concurrent increase in axial pressure drop. However, in rotating membrane systems, the wall shear rate is varied independently from the axial pressure drop by adjusting the membrane rotation rate. Two other mechanisms present in the rotating membrane system also serve to reduce cell buildup on the membrane surface. Under certain conditions, the rotation of the inner cylinder also causes the development of Taylor vortices such as those pictured in Figure 5A-2. The torus-shaped flow patterns further increase the shear rate at the membrane

surface, and reduce cell buildup. The rotating membrane also causes the fluid near the membrane surface to rotate. Since the cells are more dense than the suspending medium, they are subjected to a centrifugal force which drives them away from the membrane. The combined effects of high rotational shear rate, increased shear due to Taylor vortices, and centrifugal forces reduce cell buildup on the membrane surface and result in high filtration rates compared to traditional cross-flow devices.

Figure 5A-2, reproduced from Ohashi et al. (1988), shows the dependence of wall shear rate on rotation rate for filtration of a 35% suspension of bovine red blood cells in 6.5% BSA in an Autopheresis-C filter. The straight dashed line indicates the wall shear rate due to rotation alone, assuming Couette flow. The solid line represents the wall shear rate in the presence of Taylor vortices. At rotation rates of less than 1000 the two curves coincide. However, at rotation rates of 3000 or more the wall shear rate with Taylor vortices is more than twice that present with simple Couette flow. While no theory is currently available for predicting the effect of Taylor vortices on flux obtained during microfiltration of rigid particles in rotating membrane systems, a non-linear increase in flux with rotation rate is expected to be seen in the rotation rate regime in which Taylor vortices develop.

The rate at which cells are driven away from the membrane by centrifugal force may be calculated using the no-slip condition at the wall, and assuming that the velocity of the cells immediately adjacent to the wall is approximately equal to the velocity of the membrane wall. The centrifugal velocity u in cm/s is related to Ω, the rotational velocity in RPM, as follows (Perry and Chilton, 1973):

$$u = \frac{(2\pi\Omega)^2 \, R \, (\rho_c - \rho_f) \, a^2}{18 \, \mu} \qquad (1)$$

Calculation of the centrifugation velocity in the boundary layer near the membrane surface requires knowledge of the viscosity μ in the boundary layer. Figure 5A-3 shows the centrifugation rate calculated by neglecting particle-particle interactions and setting μ equal to the bulk viscosity. Since the viscosity of particle suspensions are concentration-dependent, if significant concentration polarization occurs, and the concentration in the boundary layer is significantly greater than the bulk concentration, then the actual viscosity in the boundary

layer will be significantly larger than the bulk viscosity, and the true centrifugation rate will be much lower than that shown in Figure 5A-3.

As a first step in understanding the performance of rotating membrane systems for filtration of rigid particle suspensions, this study was designed to characterize the flux behavior of a model rigid cell system. We filtered suspensions of bakers yeast in a Hemascience Autopheresis-C filter and measured the dependence of filtrate flux on applied pressure, rotation rate, bulk concentration, membrane material, and pore size. We also examined simple models for predicting the effects of rotational shear rate, centrifugation, and Taylor-vortices on filtrate flux.

C. MATERIALS AND METHODS

The Autopheresis-C and associated disposables were kindly provided by Fenwal Automated Systems (Irvine, CA). Figure 5A-1 is a schematic of the Hemascience membrane module. The dimensions of the device are L = 7.7 cm, R = 1.325 cm, and d = 0.0635 cm. The bulk fluid flows in the annular channel between the membrane, which is attached to the rotating inner cylinder, and the stationary outer cylinder. The filtrate flows down thin channels under the membrane surface and is collected into a central exit port at the bottom of the module. The membrane is rotated by a magnetic coupling to the drive motor. To avoid overheating of the bearing seals, it is necessary to prime the module before initiating rotation.

Three types of membrane modules were studied. The first type contained polycarbonate track-etched membranes manufactured by Nuclepore Corp. (Pleasanton, CA). These membranes have straight-through cylindrical pores of diameter 0.8 μm. The second and third types contained nylon-66 membranes manufactured by Pall Trinity Micro Corp. (Cortland, NY). These membranes have a fibrous mesh structure. The reported maximum pore sizes (determined by bubble point measurement) for these membranes were 0.45 μm and 3.0 μm.

Figure 5A-4 is a diagram of the Autopheresis-C plasmapheresis system (Hemascience, Inc., Santa Ana, CA). When used for blood filtration, the operation of all pumps, valves, and monitors is microprocessor-controlled. As supplied to us, with LabSep software, the operator can set the membrane rotation rate and the flow rates of the inlet and

outlet pumps. The pumps can be operated at flow rates of up to 130 ml/min, in increments of 1 ml/min. In demand mode operation, the operator sets the inlet flow rate and filtration rate; the outlet flow rate is set implicitly as the difference between those values. The pressure is monitored via a pressure transducer which is connected to the inlet line by a T-connection. The pressure readout is given in units of mmHg, and the maximum pressure which can be read is 500 mmHg.

Although the system is designed to be used in demand mode, most of the experiments were performed using the configuration shown in Figure 5A-5. In this configuration, the outlet line bypassed the outlet pump and terminated in a flask on a laboratory jack, which served as a movable outlet reservoir. The retentate side pressure was varied by adjusting the height of the bulk outlet reservoir. The net transmembrane pressure was increased further by lowering the outlet reservoir for the filtrate line.

The net transmembrane pressure ΔP_{net} in a rotating membrane system is equal to the difference between the retentate-side pressure P_r and the filtrate-side pressure P_f. The retentate pressure in free-flowing filtrate mode is given by the hydrostatic head of the bulk outlet line. The filtrate pressure is made up of two terms, the hydrostatic head of the filtrate line and the filtrate back-pressure P_{cent} which results from centrifugation of the fluid on the filtrate side of the membrane, given by (Beaudoin and Jaffrin, 1987):

$$P_{cent} = \frac{\rho_f (2\pi\Omega R)^2}{2} \qquad (2)$$

where ρ_f is the fluid density. Note that although there is only a thin layer of fluid under the membrane, at the filtrate outlet there is a column height R of fluid being rotated. The data points in Figure 5A-6 are measured values of the back-pressure, while the curve shows the values calculated from Equation (2), using a conversion factor of 7.5×10^{-4} mmHg/(dynes/cm^2). Back-pressures were measured by filtering distilled water with the outlet and filtrate reservoirs at the same height as the membrane module.

The rotation rate can be set in increments of 1 RPM between 0 and 4000 RPM. However, rotation rates below 500 RPM are not reliable. The setting of the rotation rate was calibrated using a stroboscopic tachometer (Strobotac Type 1531, General Radio Co., Concord,

MA). Before connecting the inlet and outlet tubing to a new cartridge, a drop of dye was dropped onto the non-filtering edge of the membrane through each bulk port. Experiments were performed with two cartridges. In the first experiment, distilled water was pumped through the cartridge, with the filtrate outlet open, during the calibration. The second calibration was performed during filtration of 6% yeast. The strobe light was directed toward the membrane, the flash rate of the strobe was adjusted until the dot appeared to be stationary, and the flash rate was recorded. As can be seen in Figure 5A-7, the results of both experiments indicated that the actual rotation rate was approximately 5% less than the nominal setting.

The inlet and outlet pumps were calibrated by timed collection. As can be seen in Figure 5A-8, the flow rate of the inlet pump was about 6% greater than the inlet flow rate setting, and the flow rate of the outlet pump was about 8% below the outlet flow rate setting. These calibrations were used as a guide for obtaining the desired flow rate in each experiment; the actual flow rate was measured at the beginning of each yeast filtration experiment.

The membrane resistance was measured by closing the bulk outlet, adjusting the setting on the inlet pump, and recording the retentate-side pressure while simulataneously measuring the fitltration rate by timed collection. Figure 5A-9 shows data taken for measurement of the membrane resistance in a typical experiment. The flux increases linearly with the applied pressure.

The experimental procedure for yeast filtration conducted in the free-flowing filtrate mode was as follows. Suspensions of yeast in either media or distilled water were prepared as described in Chapter 4. After the measurement of the membrane permeability, the bulk outlet was opened, the filtrate outlet was clamped, and the cartridge was primed with yeast suspension. The inlet reservoir of yeast was continuously stirred using a magnetic stirrer. At this point the inlet pump flow rate was calibrated and adjusted to the desired value. Then the filtrate line was opened and the rotation rate was adjusted to the desired value. Finally, the transmembrane pressure was adjusted to the desired value by raising the height of the outlet reservoir and/or lowering the height of the filtrate reservoir, and the filtration rate as a function of time was measured by timed collection. In experiments in

which measurements were desired at several pressures, the pressure was raised to the next desired value once the flux had stabilized. Typically the pressure was increased in increments of 20-30 mmHg. After completion of a set of measurements at a particular rotation rate, the membrane module was rinsed with suspending fluid and the membrane resistance was re-measured. Membranes were re-used for additional experiments as long as the membrane resistance was within an order of magnitude of the initial membrane resistance. In one set of experiments the membrane resistance was measured after measurement of each pressure data point.

One demand-mode experiment was completed to test the performance of the rotating membrane system as designed. An initial 4L suspension of 3% yeast in distilled water was concentrated batchwise to determine the maximum concentration at which the filter could operate. In the first ten steps, a bulk flow rate of 100 ml/min and a filtration rate of 25 ml/min were employed. Then, since the processing volume was less than 250 ml, the bulk flow rate was reduced to 40 ml/min. At that time the filtration rate was simultaneously reduced to 5 ml/min in order to approach the maximum concentration more gradually. The experimented was terminated when the extremely high bulk concentration of yeast jammed the device (breaking the magnetic coupling).

D. RESULTS

Figure 5A-10 shows the steady-state flux as a function of pressure at spin rates of 0, 1000, and 2000 RPM. As noted in the figure caption, the initial water flux J_0 at 100 mmHg was 5.3 cm/min. The dashed lines are the pure-water fluxes at each rotation rate. The x-intercept is the back-pressure which must be overcome to obtain any filtrate; the back-pressure increased with rotation rate as expected. In the rotating experiments, steady-state values over a factor of 20 less than the membrane limit were achieved in 10-15 minutes. Longer times (1 hour) were required to reach steady state in the no-spin experiments. The data shown in all of the following figures is the flux measured at a net transmembrane pressure of 100 mmHg. For the zero-spin experiments, the flux at 100 mmHg is clearly within the pressure-independent regime.

Figure 5A-11 shows device-averaged fluxes measured at a spin rate of zero and a

pressure of 100 mmHg. Fluxes with 14% yeast were about one half those with 3% yeast, and in both cases the flux increased approximately linearly with bulk flow rate. Comparison of the fluxes measured at zero rotation rate with existing theoretical predictions for cross-flow microfiltration of particulate suspensions (Zydney and Colton, 1988) is not possible because large portions of the channel were completely clogged by a thick yeast cake, as can be seen in Figure 5A-12. (Similar partial channel clogging was previously seen in a flat-plate channel; see Chapter 5, Figure 5-33.) To increase the contrast between the caked yeast and the flowing yeast in the experiment shown in Figure 5A-12, brilliant blue-R dye was added to the inlet yeast reservoir about five minutes after initiating filtration. The dark region is the only portion of the annulus which remained open for flow of bulk suspension.

After the photograph in Figure 5A-12 was taken, rotation was begun. Although the rotation rate was set to 1000 RPM, at first the membrane moved very slowly. Figure 5A-13 shows that during that time, dark horizontal streaks appeared as portions of the channel began to clear. After the membrane reached 1000 RPM, all of the visible yeast cake had been washed away, as can be seen in Figure 5A-14. Removal of the yeast cake resulted in much higher fluxes. Figure 5A-15 shows the increase in flux with rotation rate for the two yeast concentrations. The filled symbols are data from experiments with yeast in distilled water, and the open symbols are data from experiments with yeast in media. The composition of the suspending fluid had no apparent effect on steady-state flux in the rotating system. The dotted lines are simply curve fits through the data. Measured fluxes are lower than the calculated centrifugation rates shown in Figure 5A-3, indicating that inter-particle effects including the concentration-dependent viscosity cannot be neglected.

In order to determine whether the steady-state flux was affected by membrane characteristics, similar experiments were performed with polycarbonate and nylon membrane modules. The results are shown in Figure 5A-16. Although the initial permeability of the polycarbonate membranes was about 50% higher than the initial permeability of the nylon membranes (as indicated in the figure captions), the steady-state yeast fluxes were consistently lower in the polycarbonate membranes. This could be related to differences in membrane fouling and/or differences in pore blockage properties. The nylon membranes consist of a network of interconnected pores with a relatively wide size distribution while the

polycarbonate membranes consist of straight-through pores of a relatively narrow size distribution.

In order to test whether some substance given off by the yeast was fouling the membranes, we took yeast filtrate from a previous experiment and filtered it through new membranes. (Protein analysis (Modified Lowry assay with BSA standard; Sigma Chemical Co.) of the light-yellow -colored filtrate indicated a protein concentration of 0.3 g/L.) The results are shown in Figure 5A-17. The polycarbonate membrane fouled dramatically over the course of one hour, while the permeability of the mylon membrane remained fairly constant. This explained why the polycarbonate membranes generally did not meet our above requirement for reuse (permeability > 1/10 initial permeability) after completion of a single series of flux measurements.

The dependence of flux on pore size was studied by conducting experiments with nylon membranes with pore diameters of 0.45 and 3.0 μm. In experiments with ΔP_{net} = 100 mmHg, the 3.0 μm membranes had an initial water flux of 8.3 cm/min, which is 57% higher than the initial water flux of the 0.45 μm membranes. As can be seen in Figure 5A-18, the flux with 3 μm pores was about 30% greater than the flux with 0.45 μm pores. Measurement of the membrane resistance between consecutive data points in one experiment with yeast also revealed the true reason for the apparent leveling off of flux with pressure seen in Figure 5A-10. (The author's initial incorrect assumption was that at low transmembrane pressure, the cross-flow flux was membrane-limited, while at higher pressures, concentration polarization of yeast dominated.) As can be seen in Figure 5A-19, the change in flux with pressure in the presence of yeast merely paralleled the change in permeability of the membrane. With the 3.0 μm membrane, the difference between the cell-free flux and the flux with cells present is small enough to be explained by pore blockage alone. One might expect high pore blockage in the rotating membrane system because the back-pressure can deform the membrane so that a large fraction of the membrane is in contact with the cells at the membrane surface. In the absence of cake formation, the fraction of unblocked pores is sgiven by the ratio of flux with cells present to flux without cells present at the same conditions. Figure 5A-20 shows the calculated fraction of unblocked pores (assuming no cake formation) at each rotation rate studied. Notice that the fraction of

open pores increases dramatically between 1000 and 2000 RPM and then again between 3500 and 4000 RPM, while it remains fairly constant at about 50% between 2000 and 3500 RPM. This suggests that two mechanisms may be involved in achieving the highest fluxes. Note that a rotation rate of 4000 RPM is apparently sufficient to keep the membrane clean.

The data in Figure 5A-19 could also be explained by formation of a relatively thin cake layer whose thickness decreases as the rotation rate increases. In the absence of pore blockage, the cake thickness h could be calculated by assuming a value R_c for the specific resistance of the cake and setting the ratio $(R_m+R_ch)/R_m$ equal to the ratio of the flux without cells present to the flux with cells present at the same conditions. Using a resistance of 4×10^{11} cm^{-2} (taken from data for unrinsed freshly-rehydrated yeast in Chapter 4), a cake height of 3.77 μm (less than one yeast cell diameter) would be equivalent to a pore blockage of 50%. (Using the resistance for rinsed yeast, the calculated cake height would be 25 μm.

The results of the demand-mode experiment are shown in Figure 5A-21. The device did not jam until I tried to raise the yeast concentration from 62% to 70%. This maximum concentration is close to the maximum achieved in the centrifugation experiments. This performance is remarkable compared to the hollow fiber experiments which were plagued by channel clogging even when the outlet concentration was far from the yeast cake concentration. Using demand mode, any desired concentration could be achieved in one pass because the method of shear rate generation is independent of the bulk flow rate.

E. CONCLUSIONS AND RECOMMENDATIONS

The advantages of the rotating system are summarized in Table I. The LabSep version of the Autopheresis-C performed well in laboratory-scale experiments. However, the membrane modules tested would be expected to have a limited lifetime if used to filter fermentation broths containing high concentrations of membrane-fouling materials. Also, the scale-up for pilot-plant or industrial operations requires considerations of other factors, such as energy consumption.

Table I. Advantages of the Rotating Membrane System.

- continuous one-pass operation
- high flux
- high concentration factor
- low axial pressure drop
- easy avoidance of channel clogging

G. REFERENCES

Beaudoin, G., and M. Y. Jaffrin (1987): "High Efficiency Plasmapheresis using Rotating Membrane Devices Life Support Systems 5:(in press)

Ohashi, K., K. Tashiro, F. Kushiya, T. Matsumoto, S. Yoshida, M. Endo, T. Horio, K. Ozawa and K. Sakai (1988): "Rotation-Induced Taylor Vortex Enhances Filtrate Flux in Plasma Separation" Trans. ASAIO (in press)

Perry, R. H., and C. H. Chilton, eds., (1973): Chemical Engineers' Handbook, Fifth Edition, McGraw-Hill Book Co., New York

H. FIGURES

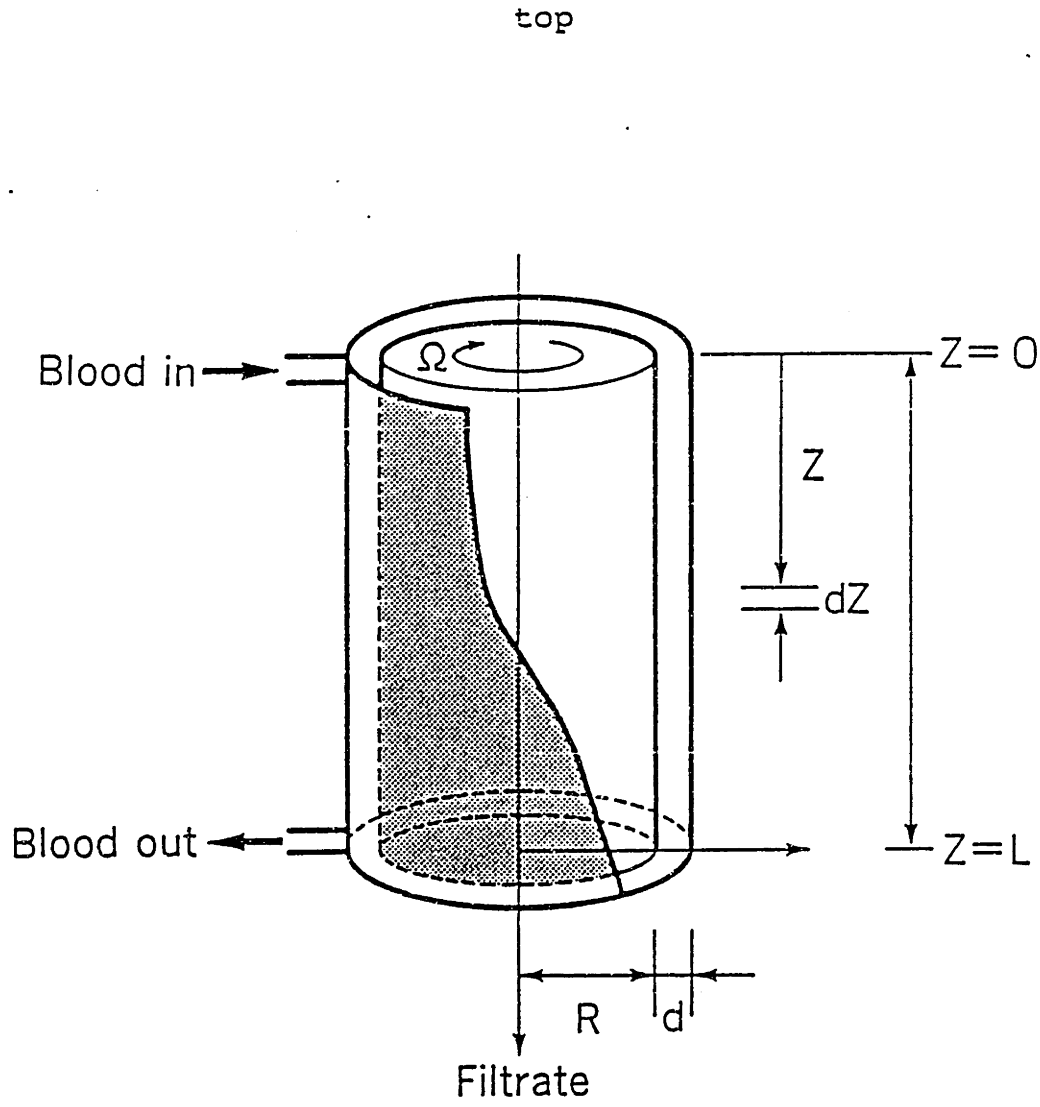

Figure 5A-1. Rotating membrane filter (reproduced from Ohashi et al., 1988).

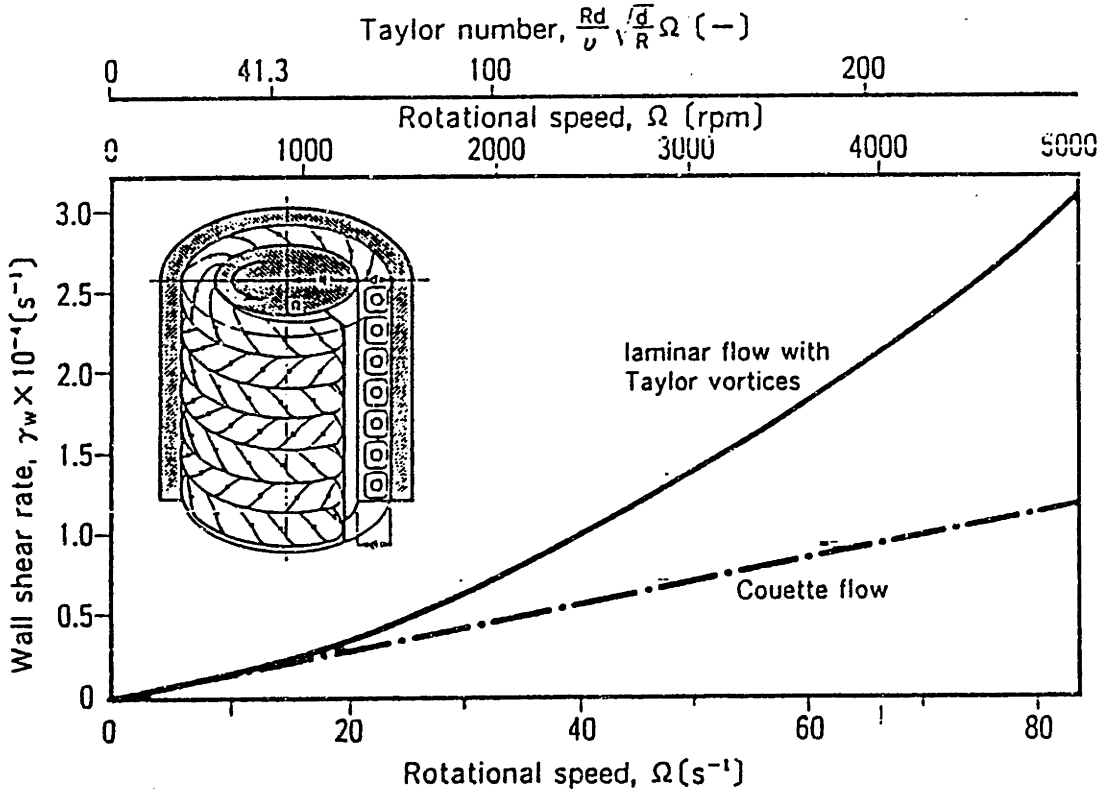

Figure 5A-2. Wall shear rate as a function of rotational speed (reproduced from Ohashi et al., 1988).

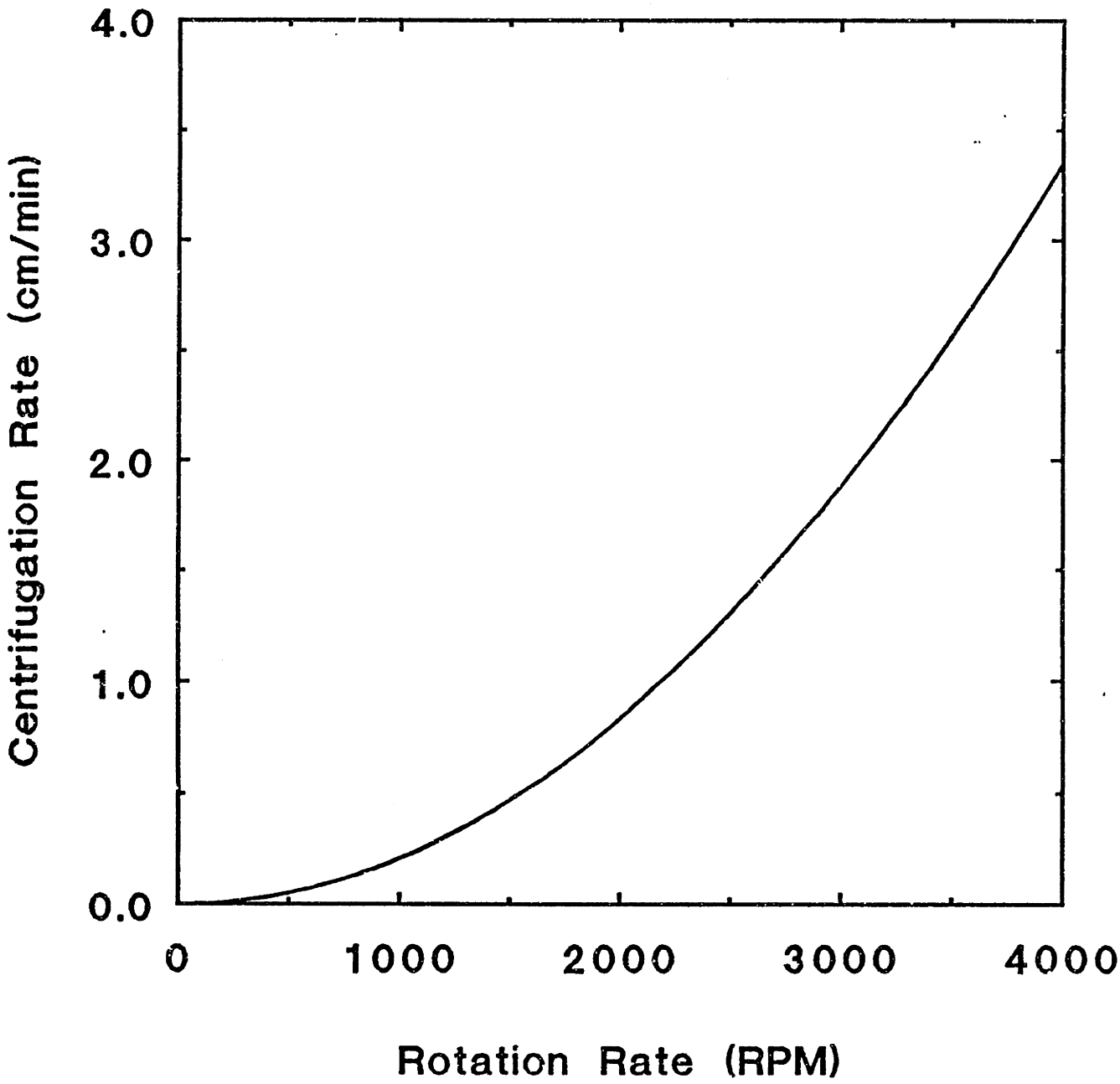

Figure 5A-3. Centrifugation velocity of yeast cells as a function of rotation rate.

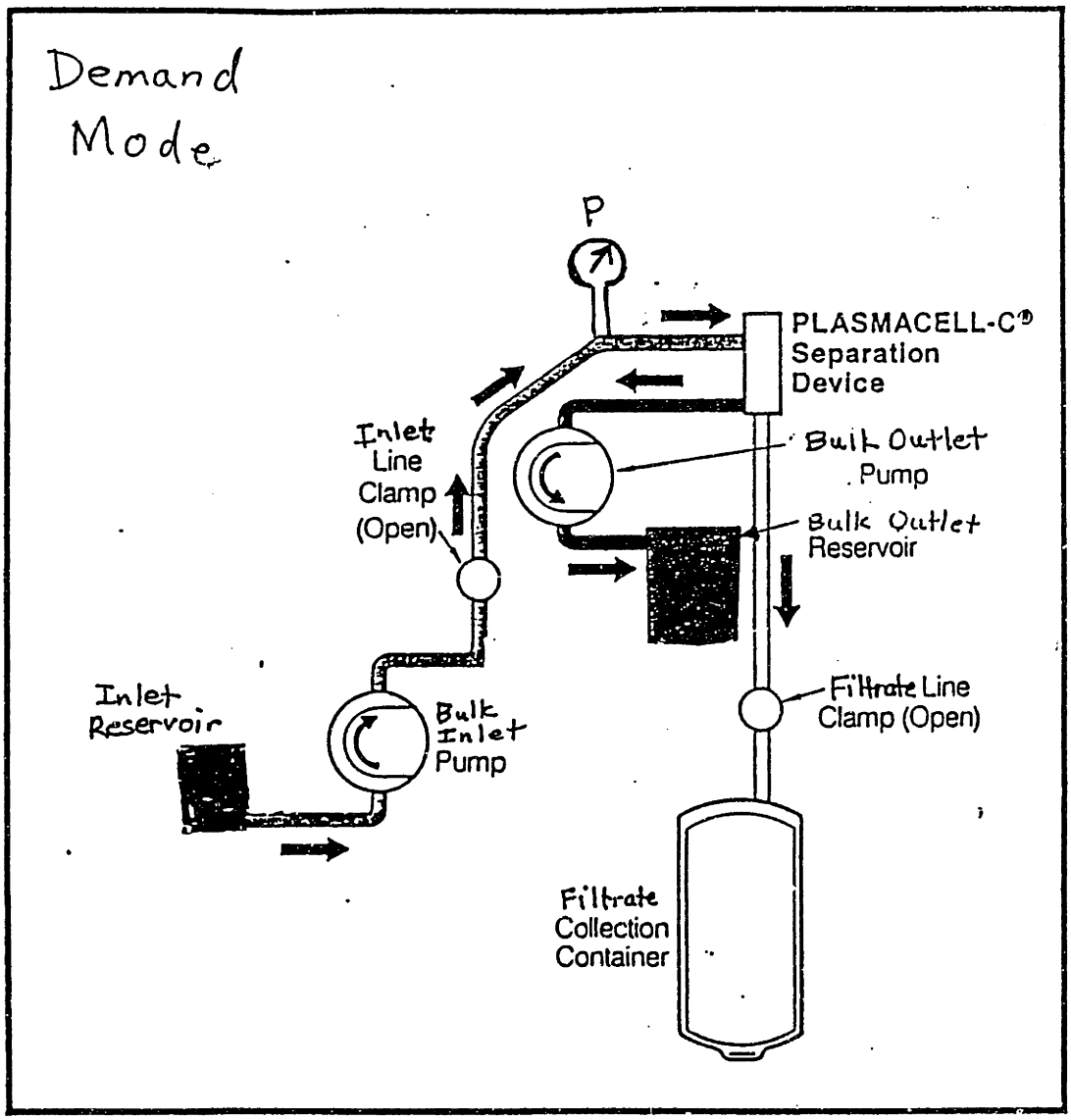

Figure 5A-4. Normal demand-mode configuration of the Autopheresis-C.

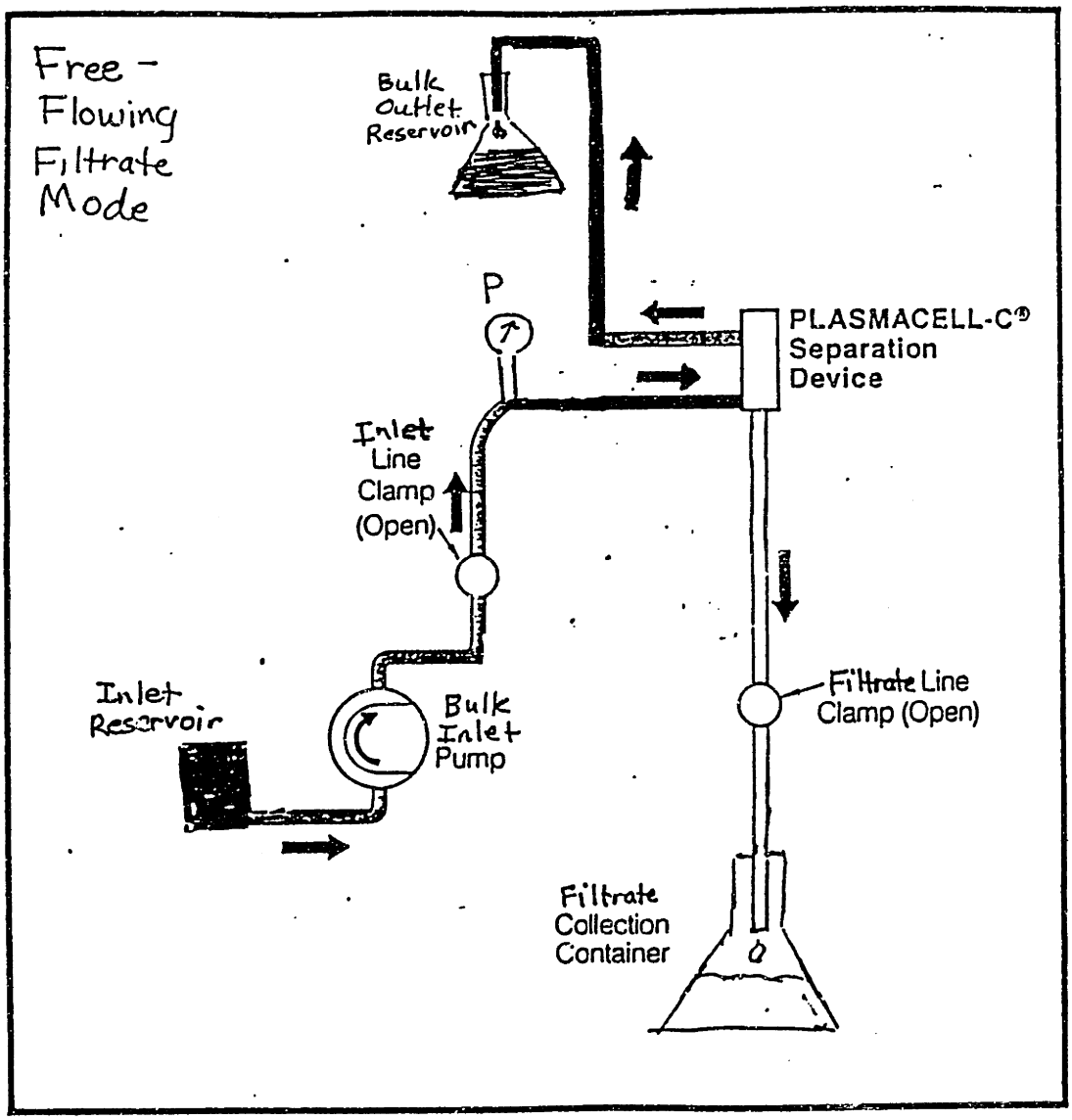

Figure 5A-5. Revised setup for free-flowing filtrate experiments.

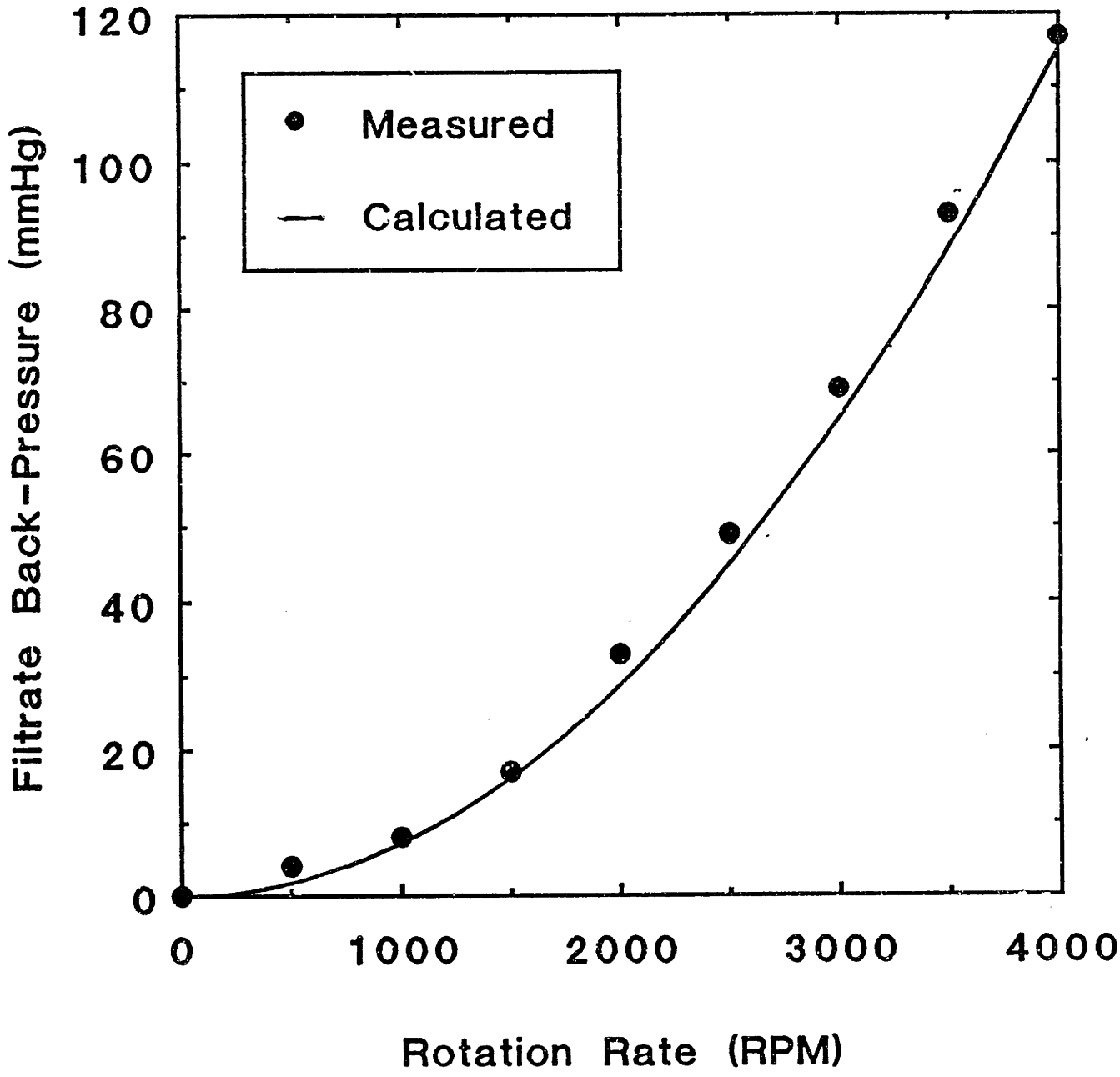

Figure 5A-6. Calculated and measured values of the filtrate back-pressure as a function of rotation rate.

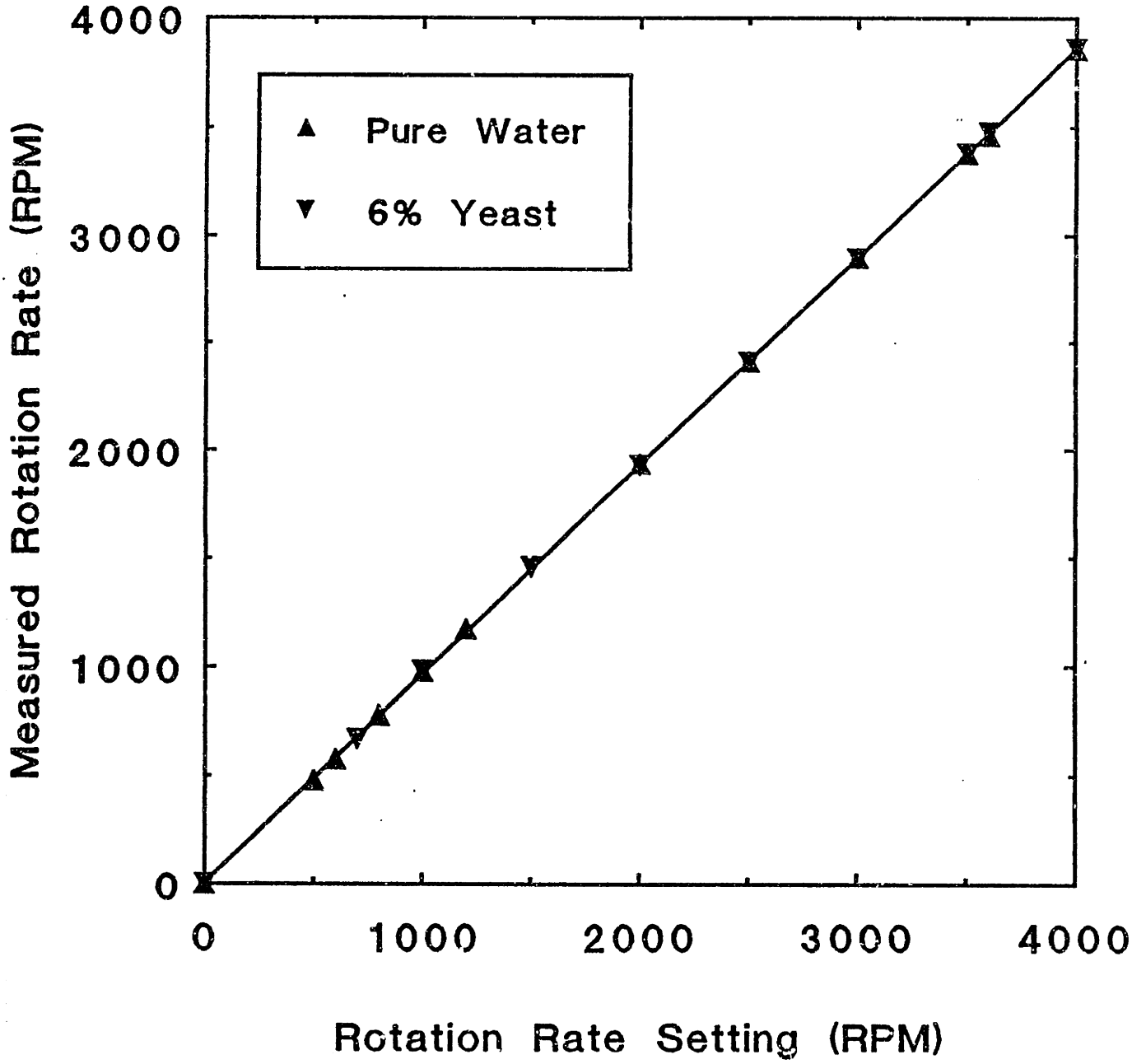

Figure 5A-7. Calibration curve for the rotation rate setting.

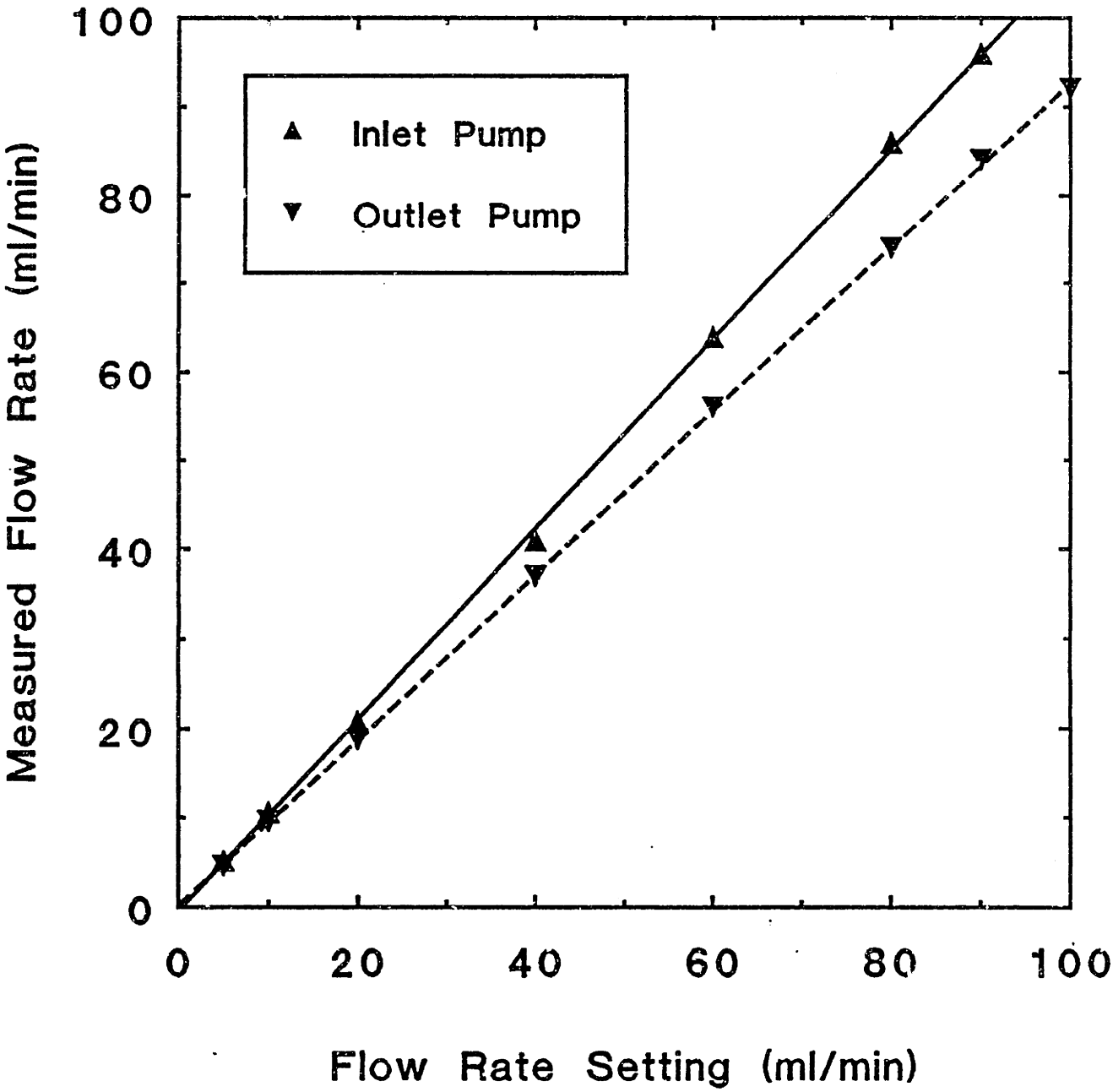

Figure 5A-8. Calibration curves for pump flowrates.

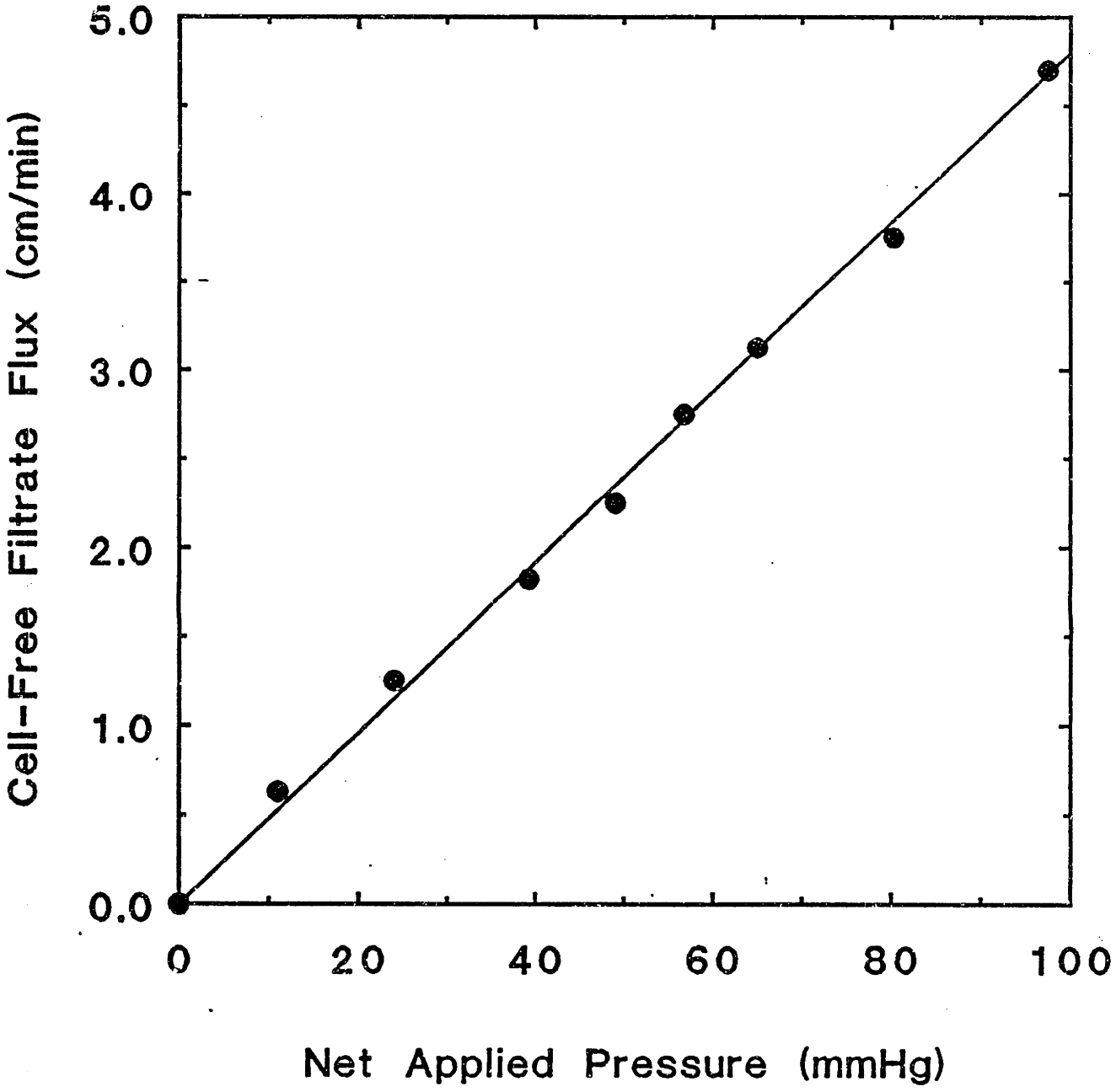

Figure 5A-9. Representative data for measurement of membrane resistance.

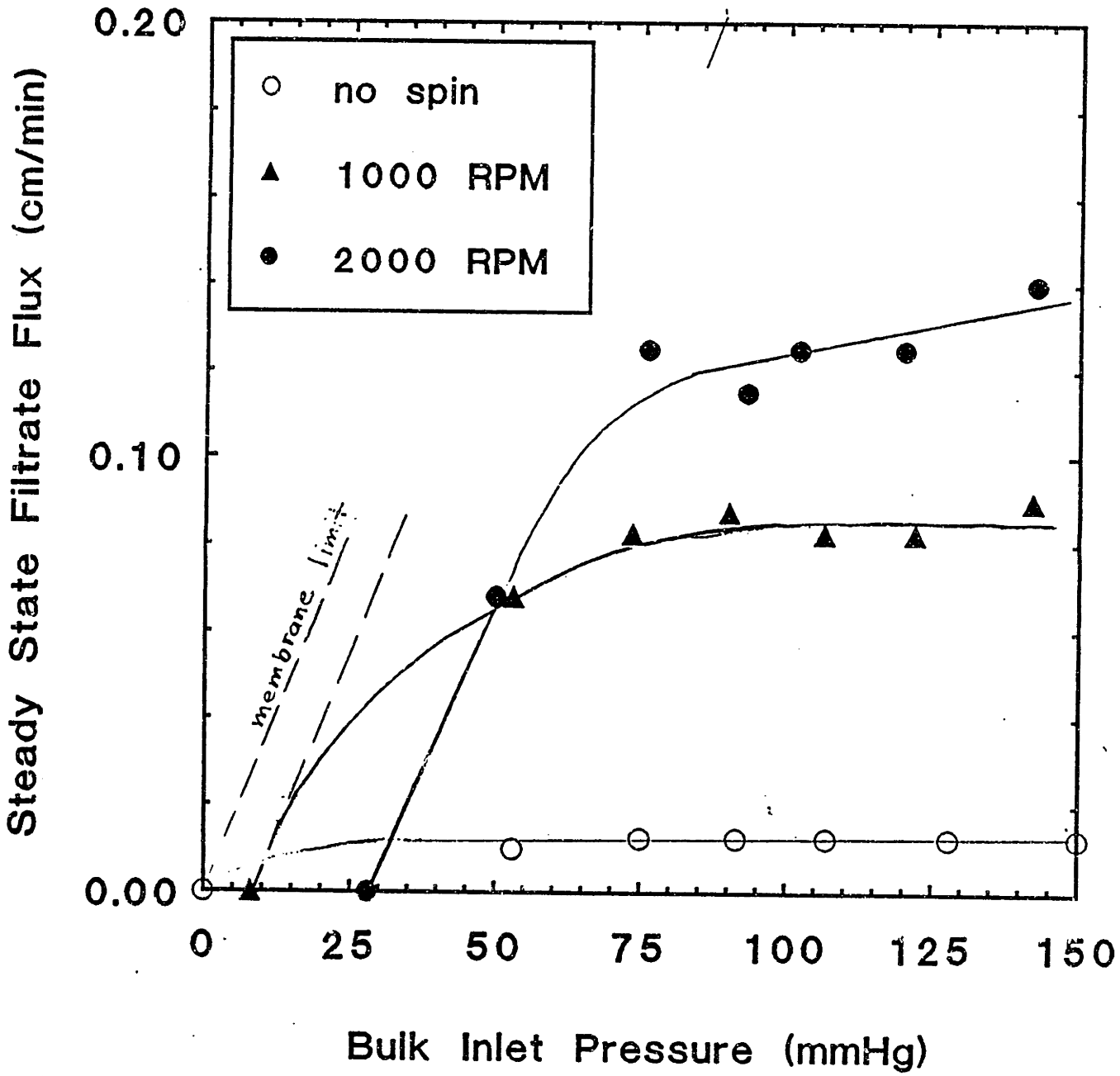

Figure 5A-10. Steady-state filtrate flux as a function of bulk inlet pressure in polycarbonate membrane module with pore ID=0.8 μm, C_b=14%, Q_b=50 ml/min, and J_0=7.2 cm/min.

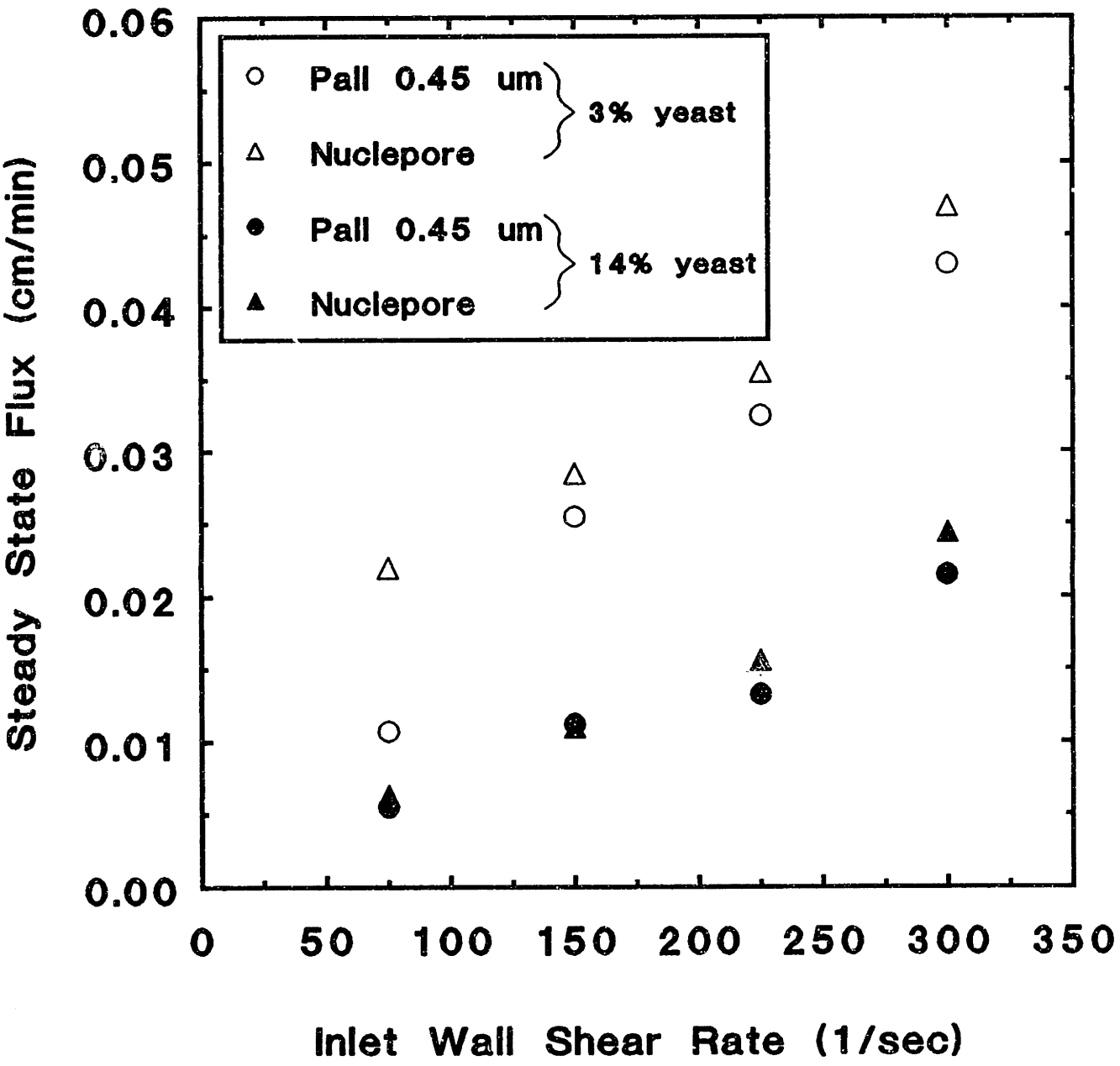

Figure 5A-11. Steady-state filtrate flux as a function of inlet wall shear rate for Ω=0 RPM and P_{net}=100 mmHg in polycarbonate (pore ID=0.8 μm, J_0=7.2 cm/min) and nylon (pore ID=0.45 μm, J_0=5.3 cm/min) membrane modules.

Figure 5A-12. Photograph of membrane module during filtration at 0 RPM. (Setup shown in Figure 5A-5, with bulk flow from bottom to top.) Yeast cake fills most of the channel, leaving only a narrow river through which the bulk fluid flows.

Figure 5A-13. Photograph of membrane module from Figure 5A-12 approximately 30 sec after initiation of rotation. Dark horizontal streaks indicate clearing of portions of the channel which had previously been clogged by yeast.

Figure 5A-14. Photograph of membrane module from previous two figures after achievement of a rotation rate of 1000 RPM. The thick yeast cake which had previously clogged most of the annular channel is gone.

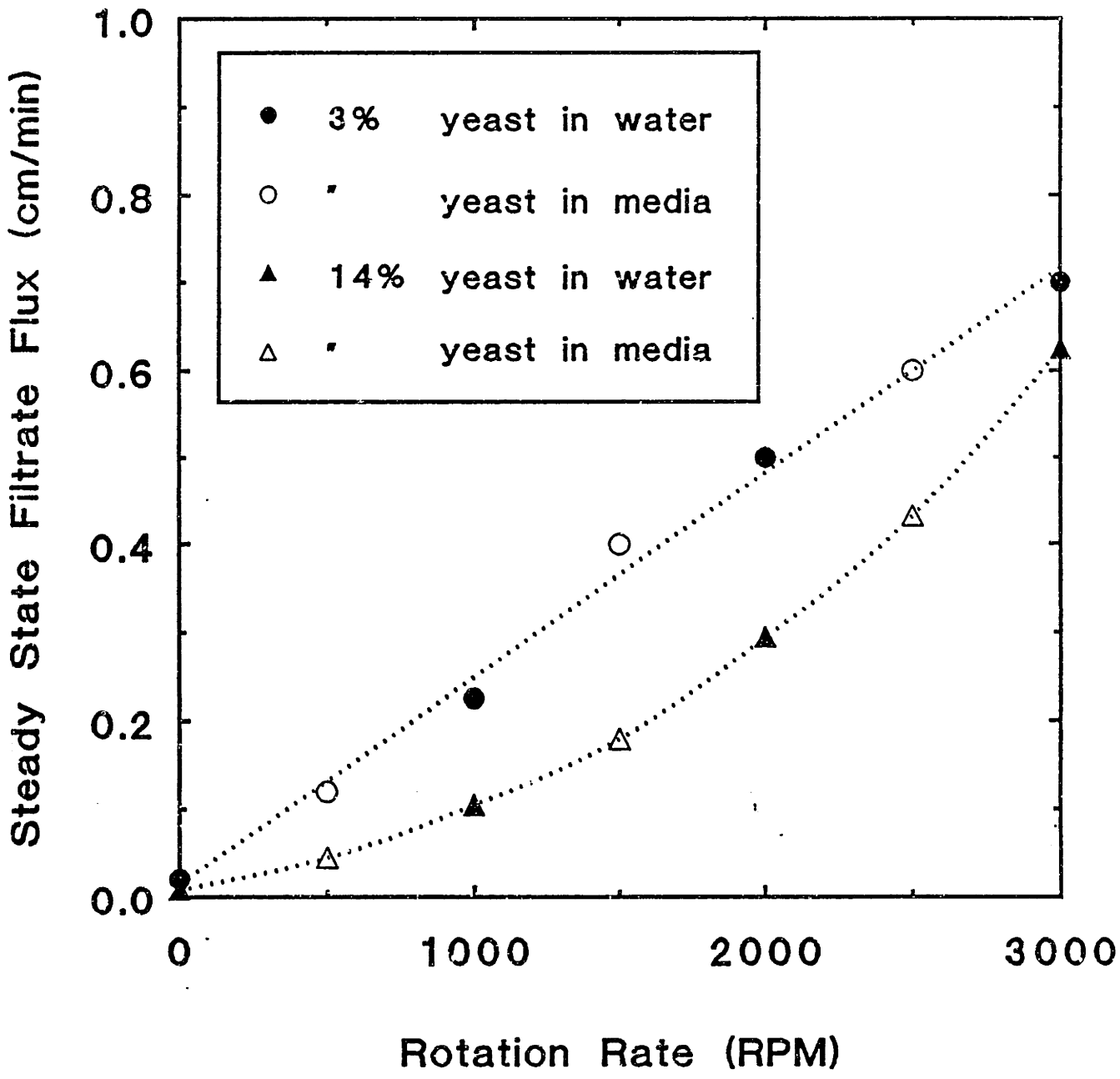

Figure 5A-15. Steady-state filtrate flux as a function of rotation rate in nylon membrane module (pore ID=0.45 μm, J_0=5.3 cm/min) with P_{net}=100 mmHg and Q_b=50 ml/min.

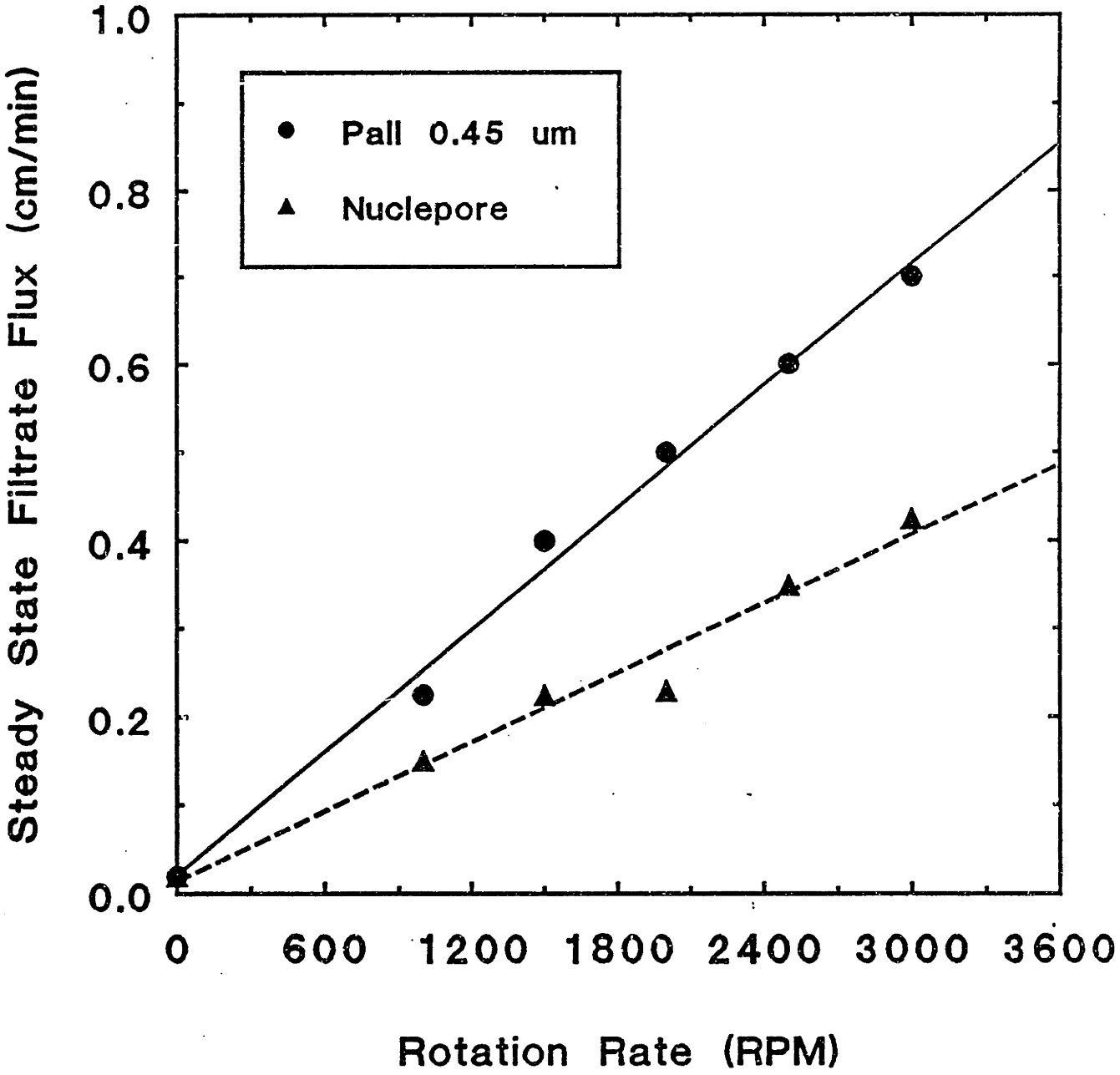

Figure 5A-16. Steady-state filtrate flux as a function of rotation rate for Q_b=50 ml/min and P_{net}=100 mmHg in polycarbonate (pore ID=0.8 μm, J_0=7.2 cm/min) and nylon (pore ID=0.45 μm, J_0=5.3 cm/min) membrane modules.

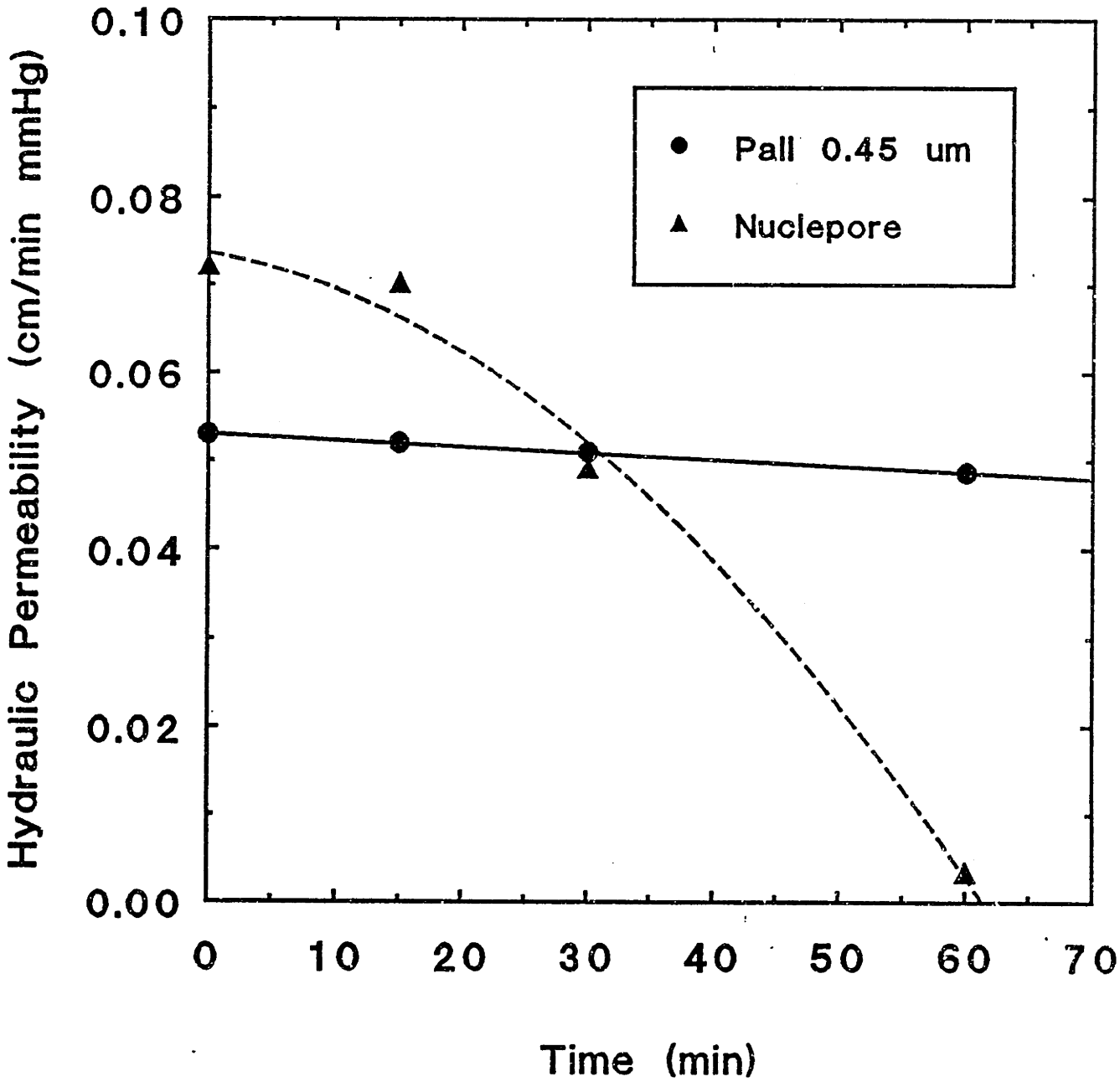

Figure 5A-17. Hydraulic resistance as a function of time during filtration of yeast filtrate in polycarbonate (pore ID=0.8 μm, J_0=7.2 cm/min) and nylon (pore ID=0.45 μm, J_0=5.3 cm/min) membrane modules, at P_{net}=100 mmHg.

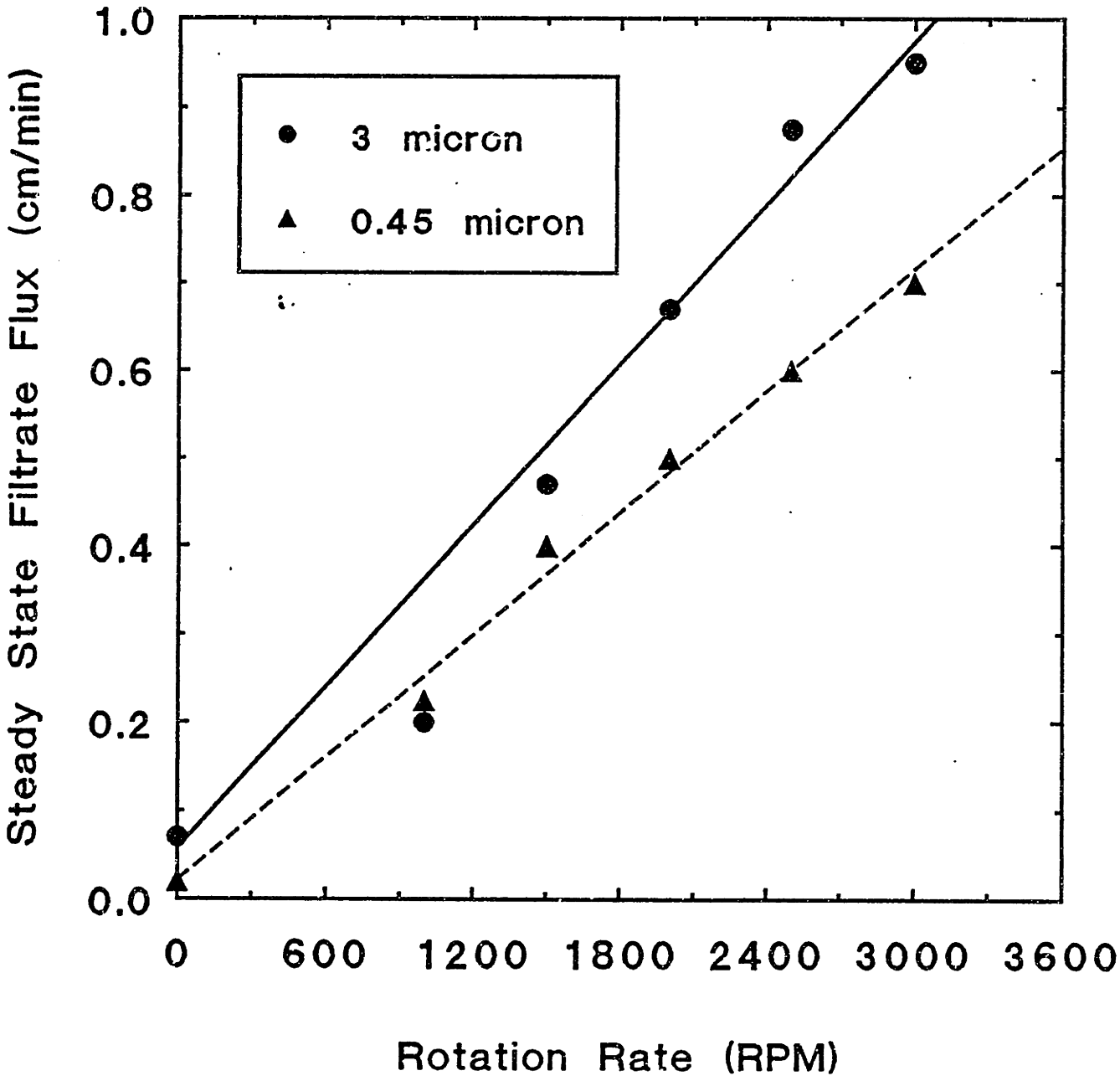

Figure 5A-18. Steady-state filtrate flux as a function of rotation rate for Q_b=50 ml/min and P_{net}=100 mmHg in nylon membrane modules with pore ID=0.45 μm (J_0=5.3 cm/min) and pore ID=3.0 μm (J_0=8.3 cm/min) membrane modules.

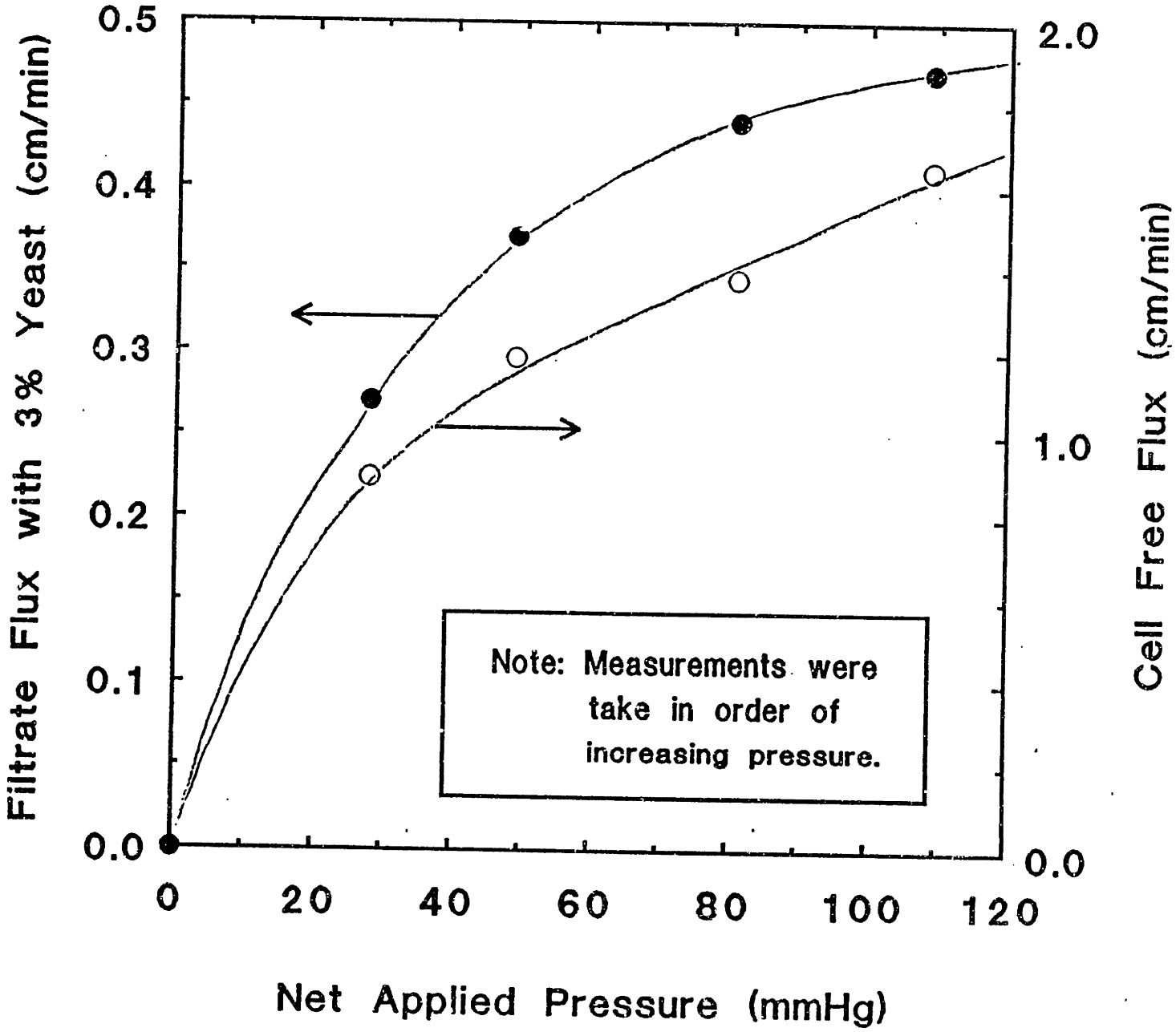

Figure 5A-19. Steady-state filtrate flux and cell free-filtrate flux as a function of net applied pressure in nylon membrane module (pore ID=3.0 μm, J_0=8.3 cm/min) at Q_b=50 ml/min and Ω=1500 RPM.

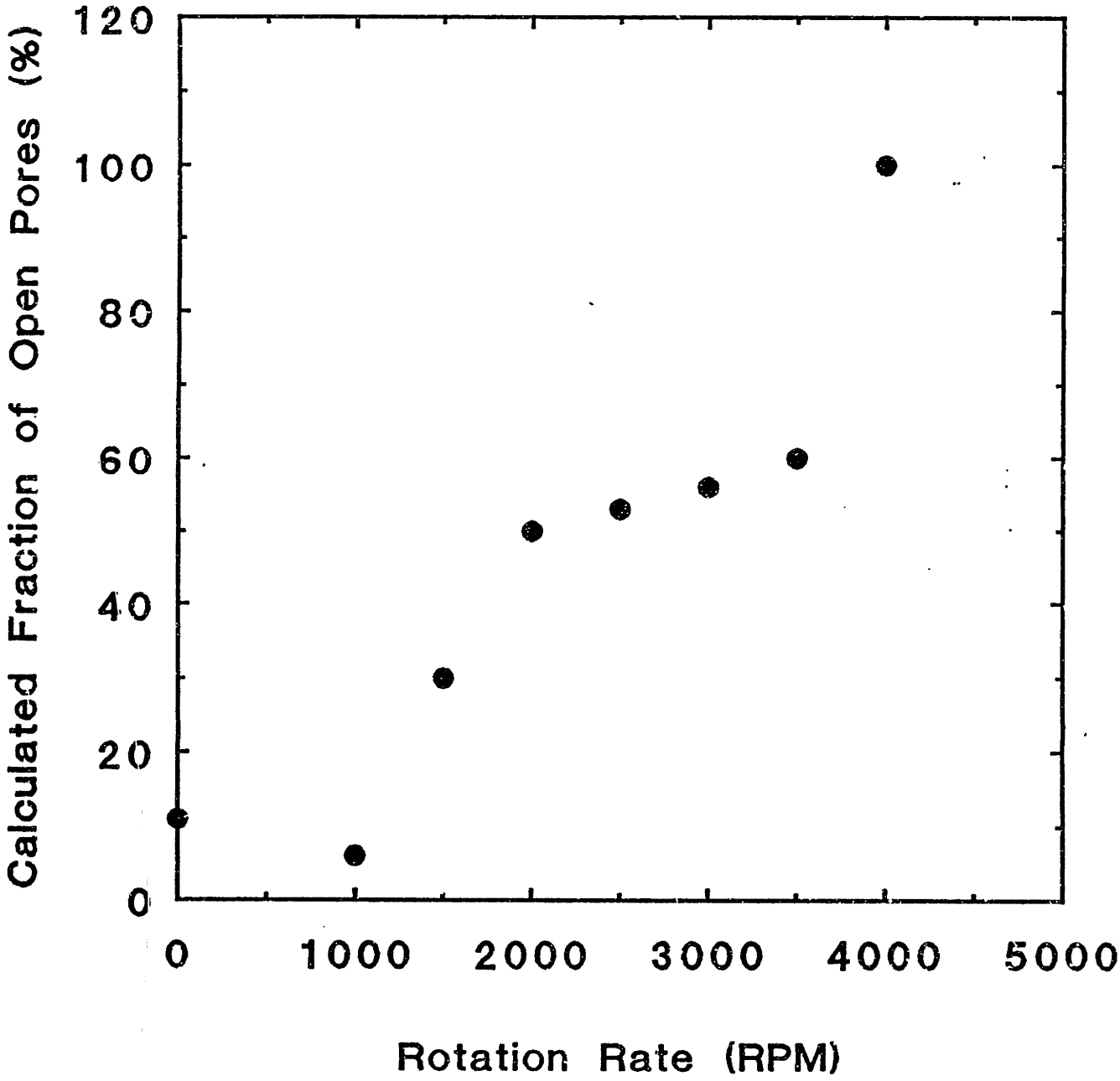

Figure 5A-20. Calculated fraction of open pores as a function of rotation rate in nylon membrane module (pore ID=3.0 μm, J_0=5.3 cm/min) at Q_b=50 ml/min ΔP_{net}=100mmHg.

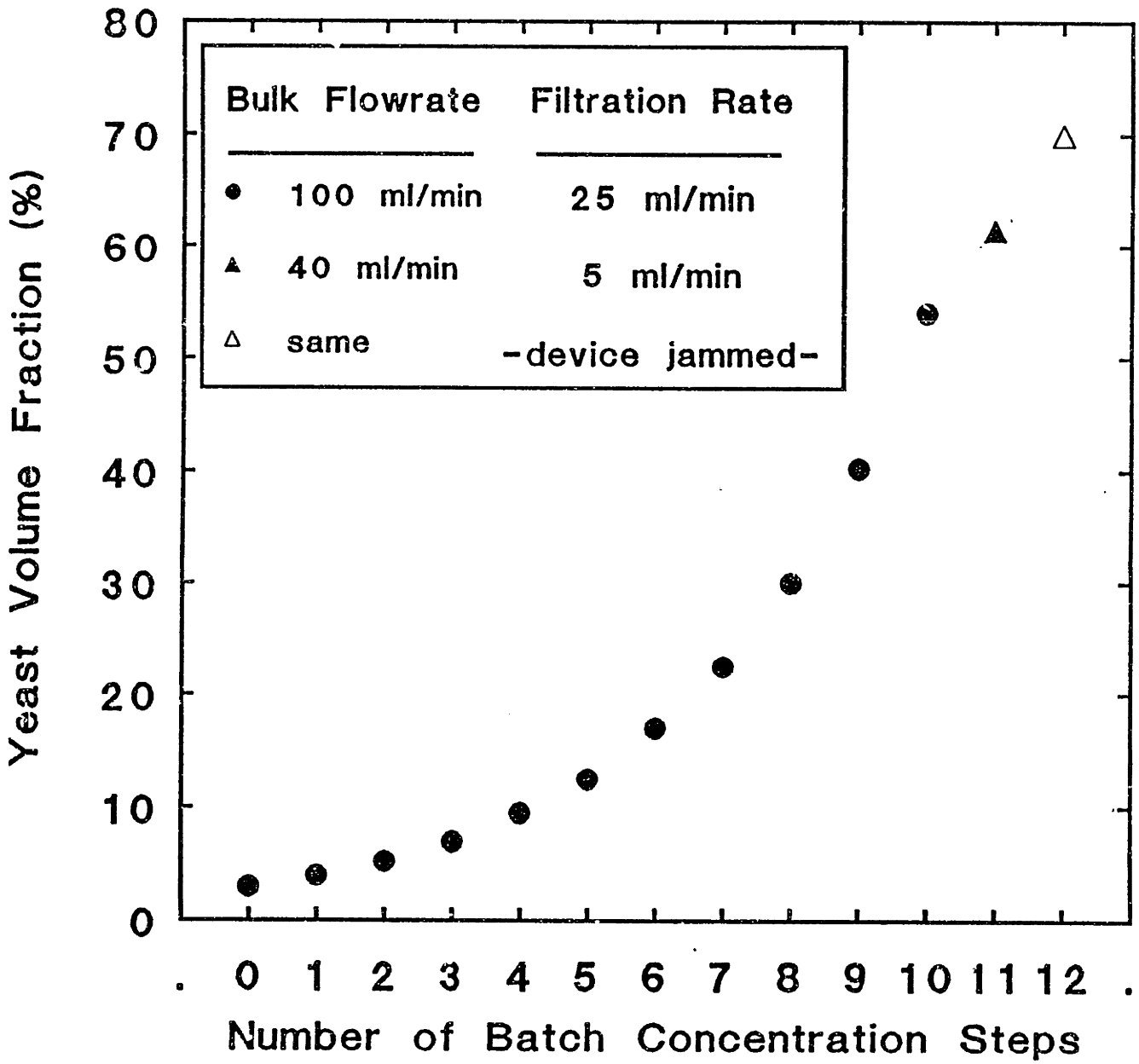

Figure 5A-21. Yeast volume fraction as a function of number of batch concentrations in demand mode experiment with nylon (pore ID=0.45 μm, J_o=5.3 cm/min) membrane module at ΔP_{net}=100mmHg, Ω=1500 RPM, and flow rates as shown.

Chapter 6:

Prediction of Filtrate Flux, Cake Thickness, and Channel Clogging during Cross-flow Filtration of Yeast and Latex Particle Suspensions in Hollow Fiber Membranes

A. ABSTRACT

The goal in designing hollow fiber devices for cross-flow filtration of rigid particle suspensions is to maximize filtrate flux (i.e. minimize membrane area) while avoiding fiber clogging. In order to achieve this goal, one must predict the extent of particle cake formation on the membrane wall, and understand its effects on filtration behavior. We have developed a mathematical model for predicting filtrate flux, cake thickness, and channel clogging during filtration of rigid particles in hollow fiber membranes. Model predictions for both latex particle and yeast suspensions are compared with experimental data which has been reported elsewhere. (See Chapter 5.)

B. INTRODUCTION

Consider the case of a suspension of rigid particles undergoing cross-flow filtration with a membrane which completely rejects the particles. Particles accumulate at the membrane wall if the rate at which they are convected toward the wall along with the filtrate is greater than the rate at which they are transported away from the wall via shear-enhanced diffusion and axial convection. This accumulation increases the concentration of particles at the wall until the maximum particle concentration, C_{max}, is reached. Continued accumulation leads to buildup of a cake, i.e. a layer of uniform concentration C_{max}, at the membrane wall. Growth of the cake increases the hydraulic resistance to filtrate flow, thereby reducing the rate of convection of particles toward the membrane. Because the cake layer reduces the effective fiber diameter, the axial pressure drop in the fiber increases; in cases where the axial pressure drop is significant, this effect decreases the pressure driving force for filtrate flow and further reduces the rate of convection. Conversely, the restriction of the channel by the cake also increases the effective shear rate, thereby increasing the rate of back-transport of particles from the wall. Steady state is achieved when the cake is thick enough that the rate of back-transport equals the rate of convection toward the wall. At steady state there is no further net accumulation of particles at the wall.

There are three ways in which rigid particles can clog fibers during filtration. First, the cake layer can grow so thick that it fills the channel. In this case there is no cake thickness smaller than the fiber radius at which steady state is achieved (i.e. at which the rate of convection toward the membrane is balanced by the rate of back-transport away from the membrane). Second, if too great a fraction of the suspending liquid is removed, the suspension may cease to flow because the bulk concentration has reached a critical value at which the concentration-dependent suspension viscosity is infinite. It is not clear a priori whether such a "drying out" of the suspension can occur before the channel has already clogged due to cake buildup. Third, the axial pressure drop can exceed the inlet applied pressure, causing backflow at the outlet which may lead to fiber clogging at the stagnation point where the axial velocity is zero. At the stagnation point the only mechanism of back-transport of the particles is Brownian diffusion, so the cake builds up at the same rate as in a batch filter. The cake continues to build up at the stagnation point until (1) the cake fills the channel, clogging the fiber, or (2) enough cake has built up on the membrane upstream of the stagnation point so that a positive axial velocity is restored. Stagnation point clogging will occur as the outlet pressure is initially raised even under conditions at which steady-state operation is possible, if the cake fills the channel at the stagnation point before the steady-state cake thickness can be achieved in the entire fiber.

Clearly the ability to predict both filtrate flux and channel clogging requires analysis of particle cake buildup as a function of operating parameters. The model developed below calculates the growth of the cake thickness with time, with the operating conditions (inlet applied pressure and bulk flow rate), suspension characteristics (particle size, bulk concentration, suspending fluid viscosity, suspension viscosity, and particle diffusivity), particle bed characteristics (cake concentration and resistance), and hollow fiber specifications (internal diameter, length and membrane resistance) specified for each particular system under study. Experimentally-observed time-dependent membrane and cake resistances (Chapter 4) which were specific to the type of membrane and particle suspension, were incorporated in the model as appropriate. The resulting model can predict both the filtrate flux and the occurrence of channel clogging under a wide variety of conditions.

C. PREVIOUS WORK

The early attempts to model filtrate flux in cross-flow filtration also assumed that at steady state the rate of convection toward the wall was balanced by the rate of back-transport from the wall. To determine the rate of back-transport, the classical solution of Leveque (for the case of a linear velocity gradient across the boundary layer) was used to evaluate the mass transfer coefficient, and, until recently, the cell diffusivity was evaluated from the Stokes-Einstein equation for Brownian motion. This mathematical representation for boundary layer transport had been successfully used in the ultrafiltration of macromolecules (Blatt et al., 1972; Colton et al., 1975), but quantitative agreement with experimental data for the cross-flow filtration of colloidal suspensions was poor. More recently, Zydney and Colton (1982) suggested that the appropriate diffusion coefficient for particulate suspensions was a shear-enhanced diffusion coefficient in which the particle diffusivity is proportional to the shear rate times the square of the particle radius. (The correlation they used is given in the model development section below.) They developed a simple model for predicting steady-state filtrate flux in cross-flow filtration by incorporating this shear-enhanced diffusivity into the Leveque solution. As Zydney (1985) indicated, the good agreement between the simple model predictions and cross-flow microfiltration data was surprising in view of many severe limitations of the model.

Zydney subsequently developed a more complete model for predicting the steady-state filtrate flux in cross-flow microfiltration of red blood cells by solving the governing conservation equations for cell and fluid motion based on a macroscopic-continuum two-phase flow model. This formulation led to a set of coupled differential conservation equations for cell and fluid motion which were expressed in terms of the following macroscopic properties: the effective red cell diffusivity, the blood viscosity, the compressibility and hydraulic permeability of the red cell layers, and the fractional blockage of membrane pores. In this model, Zydney again used the correlation for the shear-enhanced diffusivity. The other physical properties were determined in independent experiments. Zydney solved the resulting set of partial differential equations numerically using a finite difference technique. Predictions of this model gave excellent agreement with measured filtrate fluxes. The results revealed that the region over which the pressure dropped from its bulk value to that at the

membrane surface was only a few μm (one to two cell layers) thick. This pressure boundary layer comprised only a small part of the concentration polarization boundary layer over which the concentration rose from its bulk value to its wall value. The thinness of the pressure boundary layer was a direct result of the high compressibility and concomitant high hydraulic resistance of the red cells. Zydney also found that predicted steady-state flux in the pressure-independent region depended on the parameters which influence the rate of back diffusion--wall shear rate, bulk concentration, cell diffusivity, and suspension viscosity--but not on the parameters and properties which directly controlled the rate of convection--the applied pressure, the membrane resistance, or the specific form of the cell hydraulic resistance and pore blockage functions.

Zydney also developed a modified stagnant film model to incorporate the effect of the concentration-dependent suspension viscosity on the shear rate within the concentration polarization boundary layer by assuming constant shear stress (rather than constant shear rate) across the boundary layer. After incorporation of the concentration-dependent viscosity, no analytical solution was available, and the resulting integration across the boundary layer was carried out numerically. Predictions gave excellent agreement with experimentally-measured fluxes.

More recently, Romero and Davis (1988) developed a steady-state model for cross-flow filtration of rigid particles that was also based on the concept of shear-enhanced diffusion. Their model is based on an integral solution of the governing differential equations. Both models assume that the suspension acts as a Newtonian fluid with a concentration-dependent viscosity, that the shear stress is constant across the concentration boundary layer, that the shear-enhanced diffusion coefficient is proportional to the particle radius squared and linearly proportional to shear rate. The main difference between the Zydney's modified Leveque solution and Romero and Davis's integral solution is the method of including the contribution of axial convection to the overall particle mass balance in the concentration boundary layer .

The time-dependent model developed here is based on a film-theory approach in which we evaluate the rate of back-transport by assuming that the concentration boundary layer is quasi-steady (under the current conditions of pressure, concentration, effective

channel diameter, etc.) and using the Leveque solution for the mass transfer coefficient, and then calculate the rate of cake buildup as the difference between the rate of convection toward the membrane and the rate of back-transport. Cake accumulation occurs because, even though the concentration boundary layer is quasi-steady, the rate of convection toward the membrane is greater than back-transport. The assumption that the concentration boundary layer is quasi-steady is valid as long as the transverse Peclet number is small. This is true except at early time, when the rate of convection is much larger than the rate of diffusion and any error in determining the rate of back-transport is not important.
At steady state, the model developed here is more general than that of Romero and Davis because we do not assume that the pressure and bulk concentration remain constant down the length of the device. However, it does require selection of some appropriate average diffusivity in the boundary layer (in order to evaluate the mass transfer coefficient), for which we have made use of the results from the integral solution of Davis and Leighton (1987). In the yeast version of the model, we also have incorporated expressions for a time-dependent membrane resistance and a time-dependent yeast cake resistance.

D. MODEL DEVELOPMENT

Figure 6-1 is a diagram of a cross-section of a hollow fiber during filtration of a particle suspension. The membrane is represented by the solid-colored circle. The darkly-shaded region next to the membrane is the particle cake, a stagnant layer of retained particles of thickness h and particle concentration (volume fraction) C_c. Because curvature effects may be important, the model is developed in cylindrical coordinates. The effective channel radius r_{eff} is given by the fiber radius r_f minus the cake height h. The adjacent region of medium shading is the concentration boundary layer, the region of thickness δ over which the particle concentration C drops from C_c down to C_b, its value in the lightly-shaded bulk region. Particle concentration is defined as the volume fraction of the suspension occupied by particles. Radial position will be denoted in two ways, with r denoting the distance from the centerline of the fiber and y denoting the distance from the inner surface of the cake toward the bulk. The axial distance from the fiber inlet (not shown in this cross-sectional view) will be denoted z. Axial and radial velocities will be denoted u and v, respectively, while $\underline{V}$ will

denote the velocity in vector notation. The radial velocity at the membrane wall (the filtrate flux) will be denoted v_w. In some equations it will be more convenient to express the axial velocity in terms of the bulk flow rate Q, which is given by the average bulk velocity $\bar{u}$ times the cross-sectional area πr^2. The applied pressure will be denoted P. To predict filtrate flux and channel clogging, we must solve for $\bar{u}$, v, C_b, P, and h as a function of axial position and time.

1. Strategy

We assume that suspension flow in the axial direction is laminar, fully-developed, and quasi-steady, and that the boundary layer thickness is small compared to the local effective tube radius. We begin with an overall mass balance on the particles in a differential volume element within the boundary layer. We further assume that the boundary layer is quasi-steady and that axial diffusion is negligible compared to axial convection. Even with these simplifications, a complete solution to the steady-state problem alone would require a two-dimensional numerical solution of the particle mass balance equation together with the momentum conservation equations in a manner analagous to that carried out by Zydney (1985) for red cell suspensions. In this study, we develop an approximate solution of the time-dependent problem by making use of the equivalent stagnant film concept. To account for axial variations in cake height, axial velocity, and pressure, a one-dimensional numerical solution was employed which is simpler to implement than a full two-dimensional, time-dependent numerical solution.

2. Overall mass balance on particles

An overall mass balance on the particles is given by

$$\frac{\partial}{\partial t}(C) + \nabla\cdot(C\underline{V}) = \nabla\cdot D(\nabla\cdot C) \qquad (1)$$

Expanding this equation using cylindrical coordinates leads to

$$\frac{\partial C}{\partial t} + \frac{\partial}{\partial z}(uC) + \frac{1}{r}\frac{\partial}{\partial r}(rvC) = \frac{\partial}{\partial z}\left(D\frac{\partial C}{\partial z}\right) + \frac{1}{r}\frac{\partial}{\partial r}\left(D\,r\frac{\partial C}{\partial r}\right) \qquad (2)$$

where v is the suspension velocity (assumed to be the same as the fluid) in the radial direction. Using the quasi-steady state assumption, we will neglect the first term on the left hand side. The axial diffusion term (the first term on the right hand side) is negligible compared to the axial convection term (the second term on the left hand side). The resulting equation is

$$\frac{\partial}{\partial z}(uC) + \frac{1}{r}\frac{\partial}{\partial r}(rvC) = \frac{1}{r}\frac{\partial}{\partial r}\left(D\, r\, \frac{\partial C}{\partial r}\right) \tag{3}$$

At this point, solution of Equation 3 is, in effect, broken up into two separate problems. The first is to assume that locally (at any value of z) the boundary layer may be represented as an equivalent stagnant film which has the same transport properties as the (actual) boundary layer represented by Equation 3 but in which there is no axial convection. Dropping the axial convection term leads to

$$\frac{1}{r}\frac{\partial}{\partial r}(rvC) = \frac{1}{r}\frac{\partial}{\partial r}\left(D\, r\, \frac{\partial C}{\partial r}\right) \tag{4}$$

Later, axial convection and radial diffusion will be incorporated in a separate description of the boundary layer characteristics. Returning now to Equation 4, multiplying both sides by r and integrating once leads to the following form of the local mass balance on particles in the boundary layer:

$$rvC - D\, r\, \frac{\partial C}{\partial r} = k_{integ} \tag{5}$$

The constant of integration k_{integ} can be evaluated using the boundary condition at the edge of the cake, $r=r_{eff}$, which relates the net particle flux (the difference between radial convection and radial diffusion) to the rate of cake growth, to give:

$$rvC - r\, D\, \frac{\partial C}{\partial r} = r_{eff}\, C_c\, \frac{\partial h}{\partial t} \tag{6}$$

In order to evaluate Equation 6, we next derive an equivalent expression for $D\,\partial C/\partial r$. When the steady-state cake thickness is reached ($\partial h/\partial t=0$), the convection and diffusion terms in Equation 5 exactly balance, and the constant of integration equals zero. Let v_{ss} denote the steady-state filtrate flux (radial velocity) which would be attained at the conditions pertinent to any instant of time if the radial convection and diffusion were actually in equilibrium. Under these conditions, Equation 5 becomes

$$v_{ss}C = D\,\frac{\partial C}{\partial r} \tag{7}$$

Substituting Equation 7 into Equation 6 yields

$$rvC - r\,v_{ss}\,C = r_{eff}\,C_c\,\frac{\partial h}{\partial t} \tag{8}$$

Evaluating Equation 8 at the edge of the boundary layer, and neglecting the small effect of curvature (since $\delta << R_{eff}$) leads to

$$C_c\,\frac{\partial h}{\partial t} = (v_c - v_{c,ss})\,C_b \tag{9}$$

where v_c is the instantaneous radial velocity at the edge of the cake (at $r=r_{eff}$), and $v_{c,ss}$ is the value of v_c at which particle convection would be exactly balanced by radial diffusion within the boundary layer. Thus, the rate of cake growth can be evaluated if $v_{c,ss}$ is known. As will be seen subsequently, $v_{c,ss}$ itself is a function of both z and t, and it does not attain a true steady state until cake growth ceases.

To evaluate $v_{c,ss}$, we return to Equation 7. Using separation of variables and integrating across the boundary layer we obtain the following expression for the $v_{c,ss}$:

$$v_{c,ss} = \frac{1}{\delta(z)} \int_{C_b}^{C_c} \frac{D(C,\gamma)}{C}\,dC \tag{10}$$

In deriving Equation 10, we have assumed that the wall concentration C_w (at the membrane surface) is equal to C_c at all points along the membrane. In reality, there is a small distance

from the inlet of the channel over which C_w increases from C_b to C_c (Romero and Davis, 1988). For the experimental conditions in this study, this region is estimated to be very small.

For rigid particles (including yeast cells), the diffusion coefficient $D(C,\gamma)$ within the concentration polarization boundary layer is taken to be the shear-induced diffusion coefficient determined by Leighton and Acrivos (1987):

$$D = 0.33\ a^2\ \gamma\ D^*(C) \tag{11}$$

where $$D^*(C) = C^2\ (1 + 0.5\ e^{8.8C}) \tag{12}$$

As can be seen in Figure 6-2, a plot of $D^*(C)$ on log-log coordinates, D^* is very strongly dependent on concentration. Except for the difference in concentration dependence, the form of Equation 11 is similar to a previous correlation of Eckstein (1975):

$$D = 0.03\ a^2\ \gamma\ D'(C) \tag{13}$$

where $$D'(C) = \begin{cases} C/0.20 \text{ if } C \le 0.20 \\ 1 \text{ if } C \ge 0.20 \end{cases} \tag{14}$$

Zydney and Colton used Eckstein's correlation for the shear-enhanced diffusivity in previous steady-state models for filtrate flux (1982, 1985).

Since our purpose here is to predict the behavior of rigid particles or cells, we will use Equations 11 and 12 in the remainder of this discussion and in the subsequent numerical implementation. This correlation for the shear-enhanced diffusivity of rigid particles is plotted for various particle sizes at a shear rate of 1000 s^{-1} in Figure 6-3 and for various shear rates and a particle radius of 1.0 μm in Figure 6-4. Under certain conditions (small particle size, low concentration and/or low shear rate), the shear-induced diffusion coefficient can fall below the Brownian diffusivity. Under such conditions, the above equation for the shear-induced diffusivity is not a valid expression for the particle diffusivity. Since the model implementation below inadvertently used Equation 11 for all conditions, and did not properly account for the diffusivity due to Brownian motion, the model results for small particle size and low concentration could be in error.

In applying Equation 11, γ will be evaluated at the local shear rate in the boundary layer. We assume that $\delta << r_{eff}$, so that the shear stress τ_w may be assumed constant across the boundary layer and is given by the wall shear stress calculated assuming Poiseuille flow with a fluid of constant viscosity $\mu(C_b)$. With these assumptions, the local shear rate γ is related to γ_{eff}, the equivalent Poiseuille wall shear rate in a tube of radius r_{eff}, by

$$\tau_w = \gamma\ \mu(C(y)) = \gamma_{eff}\ \mu(C_b)$$

so that

$$\gamma = \gamma_{eff}\ \ \mu(C_b)\ /\ \mu(C(y)) \tag{15}$$

and where the equivalent Poiseuille wall shear rate γ_{eff} is defined by

$$\gamma_{eff} = \left.\frac{du}{dr}\right|_{r=r_{eff}} = \frac{4Q}{\pi\ r_{eff}^3} \tag{16}$$

where $\mu(C)$ is the concentration-dependent suspension viscosity, which will be discussed below. Combining Equations 10, 11, 12, and 15 leads to the following:

$$v_{c,ss} = \frac{0.33\ a^2\ \gamma_{eff}\ \mu(C_b)}{\delta(z)} \int_{C_b}^{C_c} \frac{D^*(C)}{C\ \mu(C)}\ dC \tag{17}$$

3. Leveque Solution

In order to evaluate $\delta(z)$, we return to Equation 3 which governs transport within the boundary layer. We assume that the radial velocity does not significantly affect the transport characteristics of the boundary layer. Dropping the radial convection term yields

$$\frac{\partial}{\partial z}\ (uC)\ \ = \ \ \frac{1}{r}\ \frac{\partial}{\partial r}\ (D\ r\ \frac{\partial C}{\partial r}) \tag{18}$$

By this means, the effect of axial convection is incorporated into the solution.

We have used the solution to Equation 18 of Leveque (1928) for the analogous heat transfer problem which applies to the case of constant physical properties, constant

concentration at the wall, and $\delta << r_{eff}$, with the shear rate taken to be constant across the boundary layer. By use of Equation 15, we have already accounted for the variation of shear rate across the boundary layer.

Trettin and Doshi (1980) examined the effect of the radial velocity on the flux predicted using the Leveque solution with the equivalent stagnant film model (and constant properties). In the limit of $C_w/C_b \rightarrow 1.0$, the film theory is exact. With $C_w/C_b = 4$, the error is about 2%. However, with large values of C_w/C_b, neglecting the radial velocity results in significant underestimatation of the flux because convection normal to the membrane tends to compress the boundary layer, thereby increasing the flux.

The Leveque solution gives

$$k(z) = 0.538 \left[\frac{D^2 \gamma_{eff}}{z} \right]^{1/3} \tag{19}$$

for the local mass transfer coefficient k(z). In the context of the equivalent stagnant film theory, we set

$$k(z) = \frac{D}{\delta(z)} \tag{20}$$

which leads to

$$\delta(z) = 1.86 \left[\frac{D^2 z}{\gamma_{eff}} \right]^{1/3} \tag{21}$$

Incorporating Equation 11 for D yields

$$\delta(z) = \frac{D}{k(z)} = 1.28 \left\{ a^2 z D^*_{avg} \right\}^{1/3} \tag{22}$$

where D^*_{avg} is an appropriate average of D^* across the boundary layer. Interestingly, the shear rate dependence of $\delta(z)$ vanishes in Equation 22 because of the shear rate dependence of D.

Substituting Equation 22 into Equation 17 gives

$$v_{c,ss} = 0.778 \left[\frac{a^4}{z\, D^*_{avg}} \right]^{1/3} \gamma_{eff}\, \mu(C_b) \int_{C_b}^{C_w} \frac{D^*(C)}{C\, \mu(C)}\, dC \tag{23}$$

In order to evaluate the boundary layer thickness from the Leveque solution, it is necessary to calculate the appropriate average value of $D^*(C)$ in the concentration boundary layer. There is no clear a priori definition of what averaging method should be used to determine D^*_{avg}. In the context of the equivalent stagnant film model, we have chosen to employ a value of D^*_{avg} which gives the same mass transfer resistance as a stagnant film having the concentration profile which occurs in the boundary layer.

The particle flux N is given by:

$$N = D(C(y)) \frac{dC}{dy} \tag{24}$$

Assuming that C(y) is known, so that D=D(y), we separate variables and integrate over the boundary layer:

$$N \frac{dy}{D(y)} = - dC \tag{25}$$

$$N \int_0^{\delta} \frac{dy}{D(y)} = - \int_{C_c}^{C_b} dC = \Delta C \tag{26}$$

We can then calculate the value of D^*_{avg} which provides the correct representation of diffusional mass transfer resistance R of an equivalent stagnant film with a concentration difference ΔC from the following expression for the flux N:

$$N = \frac{\Delta C}{R} \tag{27}$$

where

$$R = \frac{\delta}{D^*_{avg}} \tag{28}$$

Combining Equations (26), (27), and (28) gives

$$D^*_{avg} = \left\{ \frac{1}{\delta} \int_0^{\delta} \frac{dy}{D^*(y)} \right\}^{-1} \tag{29}$$

As an approximation of the actual concentration profile, we have used the steady-state non-dimensional concentration profile determined by Davis and Leighton (1987) from an integral solution of the steady-state differential equations. Their concentration profile is given in terms of a dimensionless distance y', which is valid for all z. This concentration profile is shown in Figure 6-5. Figure 6-6 shows the variation of $D^*(C(y'))$ with dimensionless distance calculated from that profile, and Figure 6-7 shows the variation of $1/D^*(C(y'))$ with dimensionless distance. The final form of the equation used to determine D^*_{avg} is:

$$D^*_{avg} = \left\{ \frac{1}{y'_{max}} \int_0^{y'_{max}} \frac{dy'}{D^*(y')} \right\}^{-1} \tag{30}$$

where y'_{max} is the value of y' at which $C=C_b$. The largest possible value of y'_{max} is 0.083 at which $C_b=0$. The integration was carried out numerically. Curve 1 of Figure 6-8 shows D^*_{avg} calculated as a function of bulk concentration. D^*_{avg} is a very sensitive function of C_b. Also shown for comparison are calculations of D^*_{avg} using five other averaging techniques. Curve 1 gives the lowest D^*_{avg} because the high concentration values of $D^*(C)$ are given the least weight. Curve 2 is the value of D^*_{avg} evaluated at the geometric mean of C_c and C_b, i.e. $D^*_{avg} = D^*[(C_cC_b)^{1/2}]$. Curve 3 is given by $D^*_{avg} = [\, D^*(C_c)\, D^*(C_b)\,]^{1/2}$. Curve 4 was determined by numerical integration of:

$$D^*_{avg} = \frac{1}{C_c - C_b} \int_{C_b}^{C_c} D^*(C)\, dC \tag{31}$$

Curve 5 is given by $D^*_{BL,avg} = [\, D^*(C_c) + D^*(C_b)\,]/2$, and Curve 6 is given by $D^*_{BL,avg} = D^*[(C_c + C_b)/2\,]$. These averaging methods give progressively more weight to the maximum value of $D^*(C)$ in the boundary layer. We chose to use the first averaging method, which gave most weight to the region with the highest mass transfer resistance, because it was consistent with modeling the boundary layer as an equivalent stagnant film.

Illustrative calculations of the boundary layer thickness $\delta(z)$ predicted with Equation 21 are shown in Figure 6-9 for latex particles of various sizes at a shear rate of 1000 s^{-1}, in Figure 6-10 for latex particles of radius 0.5 μm at various concentrations, and in Figure 6-11 for latex particles of radius 3.0 μm at various concentrations. In all cases, the boundary layer thicknesses are relatively small compared to the tube radii tested in this study, which justifies the assumption that $\delta << r_{eff}$.

The concentration-dependent viscosity which appears in the integral in Equation 23 depends on the particle suspension of interest. Leighton (1985) used a Couette viscometer to determine the following expression for the viscosity of rigid (polystyrene) spheres:

$$\mu(C) = \left[\, 1 + 1.5 \left(\frac{C}{1 - C/0.58} \right) \right]^2 \tag{32}$$

Reuss et al. (1979) measured the viscosity of yeast as a function of volume fraction, using a dye-dilution technique to determine the relationship between volume fraction and dry weight. In the following expression for the yeast viscosity, the constants employed are those which Reuss reported for an osmotic pressure of 14 atm (which is appropriate to the glucose-free media used here), corrected to account for the periplasmic space error previously discussed in Chapter 4 :

$$\mu(C) = \frac{1}{1 - (1.98\, C)^{0.5}} \tag{33}$$

The above viscosity expressions are shown graphically in Figure 6-12. In the simulations which follow, Equation (32) was used for latex particle calculations and Equation (33) was used for yeast calculations.

The integral in Equation 23, including the appropriate expressions for $D^*(C)$ and $\mu(C)$, was evaluated numerically as a function of the bulk concentration C_b. Figure 6-13 shows the integrand as a function of concentration for the case of latex particles. The value of the integrand first increases because the shear-enhanced diffusivity in the numerator is increasing with concentration and then decreases because the viscosity in the denominator increases with concentration. Because the viscosity becomes very large as C_b approaches the maximum concentration in the viscosity expression C_{max} (0.58), the value of the integral is only slightly dependent on the cake concentration C_c because as can be seen in Figure 6-14, where the results of the numerical integration for latex particles with wall concentrations of 0.50, 0.54, and 0.58 are plotted as a function of bulk concentration. The integral obtained using any cake concentration greater than 0.58 would be the same as that obtained with $C_c = 0.58$ because the correlation for the viscosity is infinite at such concentrations.

4. Darcy's Law (y-component momentum balance)

The integrated form of Darcy's Law which is commonly employed in the filtration literature is that which relates the convective flux of filtrate through a flat-sheet membrane and cake to the applied pressure as follows:

$$v_w = \frac{P_{applied}}{\mu \left(R_{M,eff} + h\, R_c \right)} \tag{34}$$

where $R_{M,eff}$ is the effective membrane resistance and R_c is the average specific cell resistance (per unit height of the cell bed). This form may be used to describe flow through a hollow fiber membrane only if the cake height is small enough that curvature can be neglected, i.e. $h << r_f$. The appropriate form for flow through a cylindrical cake can be derived from the y-component momentum equation in cylindrical coordinates:

$$\frac{\partial}{\partial r} \left[rv \right] = 0 \tag{35}$$

This momentum balance holds both in the membrane and the cake. The pressures at the inside surface of the cake, at the interface between the cake and the membrane, and at the outside wall of the membrane (exposed to the atmosphere) will be denoted P_{app}, P_{int}, and P_{atm}, respectively. Integrating across the membrane, we have:

$$r\,v = \text{constant} = r_f\,v_w \qquad r \geq r_f \tag{36}$$

where v_w, the flux relative to the inner membrane surface (wall), is the experimentally-measured value which is used to define the membrane resistance as follows:

$$v_w = \frac{P_{int} - P_{atm}}{\mu\,R_{M,eff}} \tag{37}$$

(Note: Although we will define all pressures relative to the atmospheric pressure, i.e. $P_{atm} = 0$, we will retain P_{atm} in the following derivation for completeness.) Next, applying the momentum balance in the cake:

$$r\,v = \text{constant} = r_{eff}\,v_c \qquad r_{eff} \leq r \leq r_f \tag{38}$$

where v_c is the flux at the edge of the cake (at the interface with the concentration polarization boundary layer). (The radial velocity v_c is the flux which acts in opposition to the diffusive flux in the concentration polarization boundary layer. For large cake heights, v_w will be significantly lower than v_c.) Next, using the definition of the cake resistance, we write:

$$v = -\frac{1}{\mu\,R_c}\,\frac{dP}{dr} \qquad r_{eff} \leq r \leq r_f \tag{39}$$

where R_c is thate appropriate average hydraulic resistance of the cake over its entire thickness. At the interface between the cake and membrane, both Equation 36 and Equation 38 are valid. Combining these two expressions leads to the following relationship between v_w and v_c:

$$r_f \, v_w = r_{eff} \, v_c \tag{40}$$

In order to obtain an expression for either v_w or v_c in terms of P_{app}, r_f, and r_{eff}, we must combine Equations 36 through 39 and solve the resulting first-order differential equation for the pressure in the cake as a function of r to determine the unknown pressure P_{int}. Using separation of variables, we find:

$$\frac{r_f \, (P_{int}-P_{atm}) \, R_c}{R_{M,eff}} \int_{r_{eff}}^{r_f} \frac{dr}{r} = -\int_{P_{app}-P_{atm}}^{P_{int}-P_{atm}} d(P-P_{atm}) \tag{41}$$

Carrying out the integration leads to the following result:

$$r_f \, (P_{int}-P_{atm}) \, \frac{R_c}{R_{M,eff}} \ln \frac{r_f}{r_{eff}} + P_{int}-P_{atm} = P_{app}-P_{atm} \tag{42}$$

which can be rearranged to give an expression for P_{int}:

$$P_{int}-P_{atm} = \frac{P_{app}-P_{atm}}{1 + r_f \, \frac{R_c}{R_{M,eff}} \ln \frac{r_f}{r_{eff}}} \tag{43}$$

Substituting this expression into Equation 37 results in the following equation for v_w:

$$v_w = \frac{P_{app}-P_{atm}}{\mu \left(R_{M,eff} + r_f \, R_c \ln \frac{r_f}{r_{eff}} \right)} \tag{44}$$

The effective membrane resistance is a function of the intrinsic membrane resistance R_{M0} and the fraction of blocked pores ϕ:

$$R_{M,eff} = R_{M0}/(1-\phi) \tag{45}$$

The larger the fraction of blocked pores, the higher the resistance.

For simulations of experiments with latex particles in distilled water, the intrinsic membrane resistance is assumed to be constant. For simulations of experiments with yeast in albumin solution, the albumin permeability data of Chapter 5 was used to determine the following equations for the time-dependent membrane resistance of each type of fiber. The resistance of the polypropylene fibers is given by:

$$R_{M0}\ (cm^{-1}) = \begin{cases} (9.99\times10^{-10} - 3.64\times10^{-9}\ t)^{-1} & \text{for } t < 16 \text{ min} \\ (2.93\times10^{-9} - 2.82\times10^{-9}\ [1-e^{-0.140t}])^{-1} & \text{for } t \geq 16 \text{ min} \end{cases} \quad (46)$$

The resistance of the polyamide fibers for times less than 120 min is given by:

$$R_{M0}\ (cm^{-1}) = (8.94\times10^{-10} - 1.27\times10^{-11}\ t + 5.40\times10^{-14}\ t^2)^{-1} \quad (47)$$

For $t > 120$ min, the polyamide resistance is taken to be constant at $R_{M0}(t) = R_{M0}(120)$. The resistance of the modified polysulfone fibers at times greater than 18 min is given by:

$$R_{M0}\ (cm^{-1}) = (1.66\times10^{-9} - 7.95\times10^{-12}\ t - 2.08\times10^{-10}\ e^{-0.817t})^{-1} \quad (48)$$

For $t < 18$ min, the polyamide resistance is taken to be constant at $R_{M0}(t) = R_{M0}(18)$. These resistances were previously plotted in Chapter 5. These time-dependent membrane resistances were used in all simulations of experiments with yeast in albumin.

In Chapter 4, the specific resistances of latex particles and yeast cells were determined by measuring the flux of pure solvent through stagnant particle beds as a function of applied pressure. The experimentally-determined specific resistance of polystyrene latex particles agreed well with the resistance predicted using the Kozeny-Carman equation, which we rewrite here:

$$R_c^{-1} = k = \frac{1}{5\ S_0^{\,2}}\ \frac{\epsilon^3}{(1-\epsilon)^2} \quad (49)$$

where S_0 is the specific surface area of the particles (3/a for spherical particles of radius a). This equation for the resistance of the particle cake was used in the latex particle version of

the model. To evaluate the porosity ϵ of the latex particle cake, we used the results of the centrifugation experiments in Chapter 4:

$$\epsilon_{avg} = \epsilon_{\infty} + \frac{\epsilon_o}{1 + a\,\pi_{avg}} \tag{50}$$

where $\epsilon_{\infty} = 0.267$, $\epsilon_o = 0.129$, and $a = 0.0091$ mmHg^{-1} for latex particles. The average compressive pressure was evaluated from

$$\pi_{avg} = \frac{P_{appl} - P_{atm}}{2} \tag{51}$$

The error associated with this approximation is thought to be small. In Chapter 4, an illustrative calculation was carried out to test this assumption for the case where the resistance of a 180 μm layer of 4.0 μm latex particles was measured in a stagnant filtration cell at an applied pressure of 100 mmHg. The compressive pressure profile within the cake was calculated using an Euler technique, and the true value of π_{avg} was calculated to be 36.7 mmHg, while Equation (51) gave $\pi_{avg} = 50$ mmHg. The corresponding values of ϵ_{avg} determined from Equation (50) were 0.364 using the true π_{avg} and 0.356 using the approximation of Equation (51). The resistance calculated from the Kozeny-Carman equation using $\epsilon_{avg} = 0.356$ is only 10% higher than the resistance calculated using $\epsilon_{avg} = 0.364$.

The experimentally-determined specific resistance of freshly-rehydrated yeast cells was over an order of magnitude greater that the resistance predicted by the Kozeny-Carman equation, while that of three-times rinsed yeast was about a factor 4 greater than Kozeny-Carman predictions. Therefore we used the following relationship relating the yeast resistance to the applied pressure which were determined by fitting resistance data in Chapter 4.

$$R_c = \frac{\dfrac{1}{\mu_f\, L_p} - R_{m,eff}}{h} \tag{52}$$

where the hydraulic permeability L_p is given by:

$$L_p = \frac{dJ}{dP} = c_1 + \frac{c_2\, c_3}{(\,1 + c_3\, P\,)^2} \tag{53}$$

For the simulations here, we used the data for experiments with a cake height h = 0.04 cm, a membrane resistance $R_{M,eff} = 4.0 \times 10^7$ cm^{-1}, and a fluid viscosity $\mu_f = 1.25 \times 10^{-7}$ mmHg min. For unrinsed yeast, we used the following constants from Table V of Chapter 4: $c_1 = 0.00039$, $c_2 = 0.071$, and $c_3 = 0.063$. For rinsed yeast, we used $c_1 = 0.0032$, $c_2 = 0.19$, and $c_3 = 0.040$.

To this point, we have developed equations that permit estimation of cake thickness h from which v_w can be evaluated for the case where all other variables (bulk flowrate Q, bulk concentration C_b, and applied pressure P_{appl}) are known. If there are no axial variations in these variables, the solution is complete throughout the tube. In what follows, we develop additional relationships to account for axial varation in these other variables.

5. Overall mass balance on suspension

As shown by Zydney (1985), an overall mass balance on the suspension reduce to the continuity equation for the mixture:

$$\frac{\partial}{\partial z}(u) + \frac{1}{r}\frac{\partial}{\partial r}(rv) = 0 \tag{54}$$

or

$$\frac{\partial}{\partial z}(ru) + \frac{\partial}{\partial r}(rv) = 0$$

Integrating from r=0 to $r=r_{eff}$:

$$\frac{\partial}{\partial z}\left\{ \int_0^{r_{eff}} ur\, dr \right\} + (rv)\Big|_0^{r_{eff}} = 0 \tag{55}$$

v_c is the radial velocity evaluated at $r=r_{eff}$, and $\bar{u}$, the average axial velocity, is defined by

$$\bar{u} = \frac{2}{r_{eff}^2} \int_0^{r_{eff}} ur\, dr \tag{56}$$

Using these definitions, Equation (55) may be rewritten as

$$\frac{r_{eff}^2}{2}\frac{\partial \bar{u}}{\partial z} = v_c\, r_{eff} \tag{57}$$

If we multiply each side by ($2\pi\Delta z$), we get

$$\pi\ r_{eff}^2\ d\bar{u} = (2\ \pi\ r_{eff}\ dz)\ v_c \tag{58}$$

where the quantity in the parentheses on the right hand side is the area dA_c of the inner surface of the cake in a differential segment of axial distance dz. Rewriting the left hand side in terms of the volumetric bulk flow rate Q, which is equal to the product of the average axial velocity times the cross-sectional area of the open portion of the fiber, we get:

$$dQ = v_c\ dA_c \tag{59}$$

6. Axial particle concentration variation

To account for axial changes in C_b which arise from removal of fluid by filtration, we have employed

$$-\frac{r_{eff}}{2}\frac{\partial(v_b\bar{u})}{\partial z} - C_c\frac{\partial h}{\partial t} = (v_c - v_{c,ss})\ C_b \tag{60}$$

Equation (60) is conveniently expressed in terms of flowrate Q through multiplication by $2\pi r_{eff}$ which yields

$$-\frac{\partial}{\partial z}(C_bQ) = 2\ \pi\ r_{eff}\ (v_c - v_{c,ss})\ C_b \tag{61}$$

These equations imply that the particles which are deposited in the cake represent all of the particles which are removed from the bulk. The axial growth of the mass in the boundary layer is not included. The term neglected in Equation (60) can be derived by employing the overall mass balance on particles, Equation 3.

Multiplying by r and integrating from r=0 to $r=r_{eff}$, the edge of the cake, we have:

$$\frac{\partial}{\partial z}\left\{\int_0^{r_{eff}}(uC)rdr\right\} + (rvC)\Big|_0^{r_{eff}} - (D\frac{\partial C}{\partial r})\Big|_0^{r_{eff}} \tag{62}$$

Expanding the axial convection term:

$$\frac{\partial}{\partial z}\left\{\int_0^{r_{eff}}(uC)rdr\right\} = \frac{\partial}{\partial z}\left\{\int_0^{r_{eff}}u(C-C_b)rdr\right\} + \frac{\partial}{\partial z}\left\{C_b\int_0^{r_{eff}}urdr\right\}$$

$$-\frac{\partial}{\partial z}\left\{\int_{r_{eff}-\delta}^{r_{eff}}u(C-C_b)rdr\right\} + \frac{r_{eff}^2}{2}\frac{\partial(C_b\bar{u})}{\partial z} \qquad (63)$$

using the definition of $\bar{u}$ (Equation (56)) and the fact that $C = C_b$ for $r < r_{eff}-\delta$.

Incorporating Equation (63) into Equation (62), and making use of Equation 6 evaluated at r=0 and $r=r_{eff}$, as well as Equation 9, we find:

$$\frac{\partial}{\partial z}\left\{\int_{r_{eff}-\delta}^{r_{eff}}u(C-C_b)rdr\right\} + \frac{r_{eff}^2}{2}\frac{\partial(C_b\bar{u})}{\partial z} = r_{eff}\,C_c\frac{\partial h}{\partial t} = r_{eff}\,(v_c - v_{c,ss}) \qquad (64)$$

The first term (which was neglected in the above analysis) represents the axial rate of change of the net excess flux of particles which are entrained in the concentration boundary layer. The second term represents the axial rate of change of the axial particle flux in the bulk. The terms on the right represent the local cake growth rate.

If $\delta << r_{eff}$, which has already been assumed, it seems reasonable to conclude that the first term may be neglected. However, some error must be incurred in the estimated axial change in C_b. The maximum error occurs at steady state, when the right hand side is zero. The two terms on the left must then be of equal magnitude, and the estimated rate of change in C_b will be high by a factor of two. Prior to steady state, the neglected term is the same magnitude as its value at steady state provided that δ is the same, while the axial bulk convection term v_c is larger. Therefore the relative magnitude of the error is smaller prior to steady state. In reality, the larger v_c present prior to steady state will compress the boundary layer (making δ smaller than at steady state), and the error will be even smaller.

7. z-component momentum balance

In order to estimate the pressure drop along a short segment of the fiber (over which the bulk flow rate and concentration are approximately constant), we will neglect the effect of

filtration on flow through the fiber, i.e. assume that the suspension is flowing through an impermeable tube of radius r_{eff}. In this case, the z-momentum balance simplifies to Poiseuille's equation for the axial pressure drop in a tube of radius r_{eff}:

$$\frac{\partial P}{\partial z} = -\frac{8\ \mu(C_b)\ \Delta z\ Q_b}{\pi\ r_{eff}^4} = -\frac{2\ \mu(C_b)\ \Delta z\ \gamma_{eff}}{r_{eff}} \tag{65}$$

Equation 65 provides a reasonable approximation for the case where $\delta << r_{eff}$, and the fluid has a constant viscosity $\mu(C_b)$ except in the very thin boundary layer.

8. Initial Conditions

The initial conditions used in all simulations were $C_b = C_{b0}$, $Q_b = Q_{b0}$, and h=0 at t=0. For simulations of experiments in the wide-bore (4.66 mm) tubes, the outlet applied pressure was instantaneously raised to $P_{appl,out}$ at t=0. For simulations of the experiments with yeast in albumin solution in the smaller fibers, the outlet applied pressure was raised linearly from 0 to its final value $P_{appl,out}$ over a period of two minutes. This approximates the procedure which was actually used in those experiments after it was found that instantaneously raising the pressure led to immediate fiber clogging by the yeast.

9. Summary

Table I summarizes the governing equations, the variables solved for, and the equation numbers for both differential and finite difference forms of the those equations. Table II contains the differential forms of governing equations written together for easy reference.

Table I. Summary of Governing Equations.

	variable solved for	differential form Eq. #	difference form Eq. #
equivalent stagnant film concept	h	9	71
Leveque solution	$v_{c,ss}=f(\delta)$	23	74
Darcy's law	v_w	44	75
overall mass balance on suspension	u,Q	57,59	76
axial particle concentration variation	C_b	60,61	78
z-component momentum balance	P	65	79

Table II. Summary of governing differential equations.

$$C_c \frac{\partial h}{\partial t} = C_b \, (v_c - v_{c,ss}) \tag{9}$$

$$v_{c,ss} = \frac{D}{\delta(z)} \frac{\mu(C_b)}{D^*_{avg}} \int_{C_b}^{C_w} \frac{D^*(C)}{C \, \mu(C)} \, dC$$

$$= 0.778 \left(\frac{a^4}{z \, D^*_{avg}} \right)^{1/3} \gamma_{eff} \, \mu(C_b) \int_{C_b}^{C_w} \frac{D^*(C)}{C \, \mu(C)} \, dC \tag{23}$$

where $D = 0.33 \, a^2 \, \gamma_{eff} \, D^*(C) = 0.33 \, a^2 \, \gamma_{eff} \, C^2 \, (1 + 0.5 \, e^{8.8C})$

and $\mu(C) = \left[1 + 1.5 \left(\frac{C}{1 - C/0.58} \right) \right]^2$

$$v_w = \frac{P_{app} - P_{atm}}{\mu \left[R_m + r_f \, R_c \, \ln \frac{r_f}{r_{eff}} \right]} \tag{44}$$

$$\frac{r_{eff}^2}{2} \frac{\partial \bar{u}}{\partial z} = v_c \, r_{eff} - v_w \, r_f \tag{57}$$

$$- \frac{r_{eff}}{2} \frac{\partial (C_b \bar{u})}{\partial z} = C_c \frac{\partial h}{\partial t} = C_b \, (v_c - v_{c,ss}) \tag{60}$$

$$\frac{\partial P}{\partial z} = \frac{8 \, \mu(C_b) \, \Delta z \, Q}{\pi \, r_{eff}^4} = \frac{2 \, \mu(C_b) \, \Delta z \, \gamma_{eff}}{r_{eff}} \tag{65}$$

Nomenclature: h = cake height
C = particle concentration (C_b=bulk concentration, C_c= cake concentration)
v = radial (filtration) velocity (v_w=velocity at wall; v_c=velocity at edge of cake; and ss denotes steady-state)
$\bar{u}$ = average axial velocity; Q = bulk flow rate; γ_{eff}=equivalent Poiseuille wall shear rate
r_f = fiber radius; r_{eff} = effective fiber radius = r_f - h
D = shear-enhanced particle diffusivity
μ = viscosity
R_m = membrane resistance; R_c = specific cake resistance
z = axial position; t = time; δ = boundary layer thickness

E. SIMPLIFIED SOLUTIONS FOR LIMITING CASES

1. Time-dependent solution for $v_w >> v_{c,ss}$

Under certain conditions, the rate of back-transport is much smaller than the rate of convection toward the membrane and the last term in Equation 9 is negligible, leaving

$$C_c \frac{\partial h}{\partial t} = v_c \, C_b \tag{66}$$

A simplified version of the above model was developed which uses Equation 66 rather than Equation 9. There is no restriction on the cake height since this model is developed in cylindrical coordinates, and axial changes in bulk concentration and applied pressure are included. Since the rate of cake buildup in this revised model is equal to the rate at which cake is deposited on the membrane by convection, this version of the model will be termed the "non-uniform cake deposition model." This solution is valid at early time, before the convective flux approaches its steady-state value.

2. Time-dependent solution for $v_w >> v_{c,ss}$, $h << r_f$, constant C_b and constant P_{appl}

If the rate of back-transport is negligible compared to the rate of convection and the cake height is small compared to the fiber radius, then $v_c = v_w$ and Equation 66 becomes

$$h(t) = \int \frac{C_b \, v_w(t)}{C_c} \, dt \tag{67}$$

where

$$v_w(t) = \frac{\Delta P}{\mu_0 \, [R_{M,eff} + R_c \, h(t)]} \tag{68}$$

If axial changes in bulk concentration and applied pressure are negligible, Equations 67 and 68 can be solved analytically (Chudacek and Fane, 1984) to give:

$$v_w = \left\{ \left[\frac{R_{M,eff}\ \mu_0}{\Delta P_{appl}} \right]^2 + \left[\frac{2\ C_b\ R_c\ \mu_0}{\Delta P_{appl}\ C_c} \right] t \right\}^{-1/2} \qquad 69$$

This solution will be termed the uniform cake deposition solution. This solution is valid at very early times, when convection is much greater than its steady-state value and the cake height is small enough that curvature effects are not important. This solution is only valid in wide-bore hollow fibers in which axial changes in C_b and P_{appl} are negligible.

3. Steady-state solution for constant C_b and constant P_{appl}

It should be noted that the steady-state flux for the case of constant C_b and P_{appl} may be calculated directly as follows. At steady state, $\partial h/\partial t = 0$ and $v_c = v_{c,ss}$ by Equation 9. v_c is given by Equation 44, Darcy's law, and Equation 40, which relates v_c and v_w. $v_{c,ss}$ is given by Equation 23. Combining these three equations, we have

$$v_{c,ss} = 0.778 \left[\frac{a^4}{z\ D^*_{avg}} \right]^{1/3} \gamma_{eff}\ \mu(C_b) \int_{C_b}^{C_w} \frac{D^*(C)}{C\ \mu(C)}\, dC$$

$$= v_c = \frac{r_f}{r_{eff}} v_w \qquad (70)$$

$$= \frac{P_{app} - P_{atm}}{\mu \left[R_{M,eff} + r_f\ R_c\ \ln \dfrac{r_f}{r_{eff}} \right]}$$

Since r_{eff} appears in γ_{eff} as well as in Darcy's law, this equation must be solved iteratively for r_{eff} (or h). If h is small relative to r_f ($r_{eff} \approx r_f$), then Equation 70 reduces to a simple cubic equation in r_{eff}.

F. FINITE DIFFERENCE IMPLEMENTATION

Consider the schematic diagram of a hollow fiber shown in Figure 6-15. The axial distance from the fiber inlet is z. The cylindrical fiber is divided into N equal segments of length $\Delta z = L/N$. The n^{th} such segment is the control volume over which overall mass balances will be carried out. Time will be divided into M timesteps of varying length; the length of the m^{th} timestep will be denoted Δt_m.

The bulk flow, concentration, and pressure at the inlet of the n^{th} segment at the m^{th} timestep will be denoted $Q_{n,m}$, $C_{b,n,m}$, and $P_{n,m}$, respectively. The corresponding outlet variables at the timestep are $Q_{n+1,m}$, $C_{b,n+1,m}$, and $P_{n+1,m}$.

1. Equivalent stagnant film concept

The finite difference form of Equation 9 is:

$$\frac{\Delta h_{n,m}}{\Delta t_m} = \frac{C_{b,n,m}}{C_c} \left(v_{c,n,m} - v_{c,ss,n,m} \right) \tag{71}$$

The cake height at timestep m+1 is related to the cake height at timestep m as follows:

$$h_{n,m+1} = h_{n,m} + \Delta h_{n,m} \tag{72}$$

The effective tube radius at timestep m+1 is given by:

$$r_{eff,n,m+1} = r_f - \Delta h_{n,m+1} \tag{73}$$

2. Leveque solution

The finite difference form of Equation 23 is

$$v_{c,ss} = 0.538 \left[\frac{a^4}{z_{n+\frac{1}{2},m} D^*_{avg,n,m}} \right]^{1/3} \gamma_{eff,n,m} \mu(C_{b,n,m}) \int_{C_{b,n,m}}^{C_w} \frac{D^*(C)}{C \mu(C)} dC \tag{74}$$

where $z_{n+\frac{1}{2},m} = z_{n,m} + \Delta z/2$. The integral in Equation 74 is carried out numerically.

3. Darcy's Law

The finite difference form of Equation 44 is:

$$v_{w,n,m} = \frac{P_{n+\frac{1}{2},m} - P_{atm}}{\mu \left(R_{M,eff} + r_f R_c \ln \frac{r_f}{r_{eff,n,m}} \right)} \tag{75}$$

4. Overall mass balance on suspension

The finite difference form of Equation 59 is:

$$Q_{out} - Q_{in} = A_c v_c$$

or

$$Q_{n+1,m} - Q_{n,m} = A_{c,n,m} v_{c,n,m} \tag{76}$$

5. Axial particle concentration variation

The finite difference form of Equation 61 is:

$$Q_{out} C_{b,out} - Q_{in} C_{b,in} = A_c (v_c - v_{c,ss})$$

or, upon rearrangement,

$$C_{b,out} = \frac{Q_{in} C_{b,in} - A_c (v_c - v_{c,ss})}{Q_{out}} \tag{77}$$

Finally, using the above notation for the n^{th} axial step and m^{th} timestep, the overall particle mass balance becomes:

$$C_{b,n+1,m} = \frac{Q_{n,m} C_{b,n,m} - A_{c,n,m} (v_{c,n,m} - v_{c,ss,n,m})}{Q_{n+1,m}} \tag{78}$$

6. z-component momentum balance

The finite difference form of Equation 65 is:

$$\Delta P_{n,m} = \frac{8\ \mu(C_{b,n,m})\ \Delta z\ Q_{b,n,m}}{\pi\ r_{eff,n,m}^4} = \frac{2\ \mu(C_{b,n,m})\ \Delta z\ \gamma_{eff,n,m}}{r_{eff,n,m}} \tag{79}$$

The average pressure in segment n is calculated from the average pressure in segment n and the pressure drops in the segments n-1 and n:

$$P_{n+\frac{1}{2},m} = P_{n-\frac{1}{2}} - \Delta P_{n-1}/2 - \Delta P_n/2 \tag{80}$$

7. Details of algorithm

The algorithm for calculating $h_{n,m}$ is shown in Figure 6-16. The size of the timesteps and axial steps were chosen by progressively reducing the step size by a factor of two until no further change in predicted flux was seen (< 0.1% difference in average predicted flux). The resulting timestep pattern consisted of 24 timesteps each of length 5, 10, 15, 30, and 60 sec, followed by 36 steps of length 2 min and 12 or more steps of length 5 min. This timestep pattern was used in all runs. For modeling fibers of length 5 cm, it was found that an axial step length of 0.5 cm was sufficient for most runs. Step sizes of 0.1 cm were used in runs in which fiber clogging was predicted and/or the axial pressure drop was large.

The length-averaged flux and cake height were determined as follows:

$$\bar{v}_{w,m} = \frac{1}{N} \sum_n v_{w,n,m} \tag{81}$$

$$\bar{h}_m = \frac{1}{N} \sum_n h_{n,m} \tag{82}$$

G. RESULTS AND DISCUSSION

Model predictions for latex particles and yeast will be discussed in separate sections. Since there is less uncertainty in the viscosity, shear-enhanced diffusivity, cake resistance, and membrane resistance for latex particles, those results will be discussed first. In each of the two sections we will begin with a comparison of predicted and measured fluxes. The latex particle section will then continue with a parametric analysis which examines the influence of various parameters on predicted fluxes and cake thicknesses. In the yeast section, a comparison of predicted and measured cake heights will be included. Each section will conclude with a section on prediction of clogging phenomena.

(1) Modeling Results for Latex Particles

(a) Comparison of flux predictions with experimental data

Figure 6-17 shows experimental data and model predictions for filtration of an 8.9% suspension of 0.711 μm diameter latex particles in single 4.66 mm ID ultrafiltration hollow fibers (XM formulation, W. R. Grace) at three different bulk flow rates, corresponding to inlet equivalent Poiseuille wall shear rates of 72, 153, and 302 s^{-1}. All three experiments were carried out at an outlet applied pressure of 75 mmHg. Since there was no appreciable axial pressure drop throughout the course of these experiments, a cake concentration of 0.635, which corresponds to π_{avg} = 37.5 mmHg, was assumed. In these and all the following model predictions of latex particle data, the corresponding cake resistance was determined from the Kozeny-Carman equation (Equation 49), and the bulk viscosity was calculated from Leighton's correlation, Equation 32. The membrane resistances in these experiments were 2.68 x 10^9, 1.99 x 10^9, and 1.90 x 10^9 cm^{-1}, respectively. For filtration of pure water at 75 mmHg, the corresponding values of filtrate flux would be 0.224, 0.302, and 0.316 cm/min, respectively. In all cases the time required to reach steady state was over 15 min, much longer than the time required to reach steady-state during filtration of red blood cells. (See Chapter 3 for red cell data.) The data and predictions from Figure 6-17 are re-plotted on a log-log scale in Figure 6-18. The flux predictions from Figure 6-17 are replotted in Figure 6-19 along with the corresponding length-averaged cake thickness predictions. The model predictions indicate that the time required for the flux to reach steady

state in these experiments corresponds to the time required for the cake to build up to its steady-state value.

Figure 6-20 shows the predicted growth of the cake height with time as a function of axial distance for the 153 s^{-1} case. Except close to the inlet, the cake height is relatively constant with z until steady state is approached. Figures 6-21 and 6-22 show the 153 s^{-1} data again along with predicted flux and length-averaged cake height on semi-log and log-log coordinates. The non-uniform cake deposition solution does well at predicting early-time data when convection is substantially greater than back-diffusion. At longer times, the flux predicted with the non-uniform cake deposition model drops rapidly as the entire channel is filled with a particle cake. The uniform cake deposition solution, which ignores the effect of curvature, predicts a slower rate of flux dropoff (because the effective membrane area is unchanged). This results in over-predicting the flux at filtration times of 5 to 45 min. At long times, when back-transport becomes important, the uniform cake deposition model underpredicts the flux. Overall, the uniform cake-deposition model predictions fit the data from this two-hour experiment better than do the non-uniform cake deposition predictions. This is surprising since the predicted cake heights occupied a large portion of the channel radius. The relative agreement of the uniform cake deposition model with experimental data results because the errors in neglecting back-transport and in neglecting curvature act in opposition, and partially cancel each other. Notice that the slope of the flux data on log-log coordinates in the cake-growth region (where the flux is decreasing) is approximately minus one-half, as is predicted by the uniform cake deposition model.

Figure 6-23 shows the γ=153 s^{-1}, $P_{app,out}$=75 mmHg flux data and predictions re-plotted along with data and predictions for the same shear rate and $P_{app,out}$=37.5 mmHg. For this lower pressure case, a cake concentration of 0.622, which corresponds to π_{avs} = 18.8 mmHg, was assumed. (Again, there was no appreciable change in pressure, so C_c was constant.) The model predictions for both the cake-growth region (in which the flux is decreasing) and the steady-state region (in which the flux is constant) agree well with the experimental data at both pressures. Again the slope of both data and predictions in the cake growth region is approximately minus one-half.

Figure 6-24 shows the γ=153 s^{-1}, C_b = 8.9% flux data and predictions re-plotted along with data and predictions for the same shear rate and a bulk concentration of 0.89%. Again, the model predicts the rate of flux decline in the cake-growth region quite well. However, the model underpredicts the steady-state flux of the low-concentration data by a factor of two.

Figure 6-25 shows experimental data and model predictions for filtration of a 7.7% suspension of 0.264 μm diameter latex particles at an inlet equivalent Poiseuille wall shear rate of 55 s^{-1} in the same type of hollow fiber. The steady-state flux obtained with these smaller particles is significantly lower than that measured with the 0.711 μm particles. Also, a longer time (more than four hours) was required to reach the lower steady-state flux.

Figures 6-26 and 6-27 shows experimental data and model predictions for filtration of a 0.2% suspension of 0.264 μm diameter latex particles at shear rates of 12 and 500 s^{-1} in the same type of hollow fiber on semi-log and log-log coordinates. The lower bulk concentration dramatically increased the time required to reach steady state to over 10 hrs at 500 s^{-1}. The data for 12 s^{-1} had not yet reached steady state after 2 days. In this case, the virtually-identical predictions of both the uniform and non-uniform cake deposition models were very similar to the predictions of the complete model. This indicates that even after two days, back-transport is not yet significantly affecting filtrate flux and that the cake height is small relative to the fiber radius. Figure 6-28 shows the predicted cake heights at t=3000 min as a function of axial position for the two cases shown in Figure 6-27. The predicted cake height for the higher shear rate data, which has already achieved steady state, varies more significantly with distance from the inlet than does the predicted cake height for the lower shear rate data, which is not yet as steady state. In both cases, the predicted cake height increases with distance from the inlet, and the maximum cake height predicted occupies less than 15% of the channel radius.

In all of the experiments reported in this section, the estimated values of Q ($\bar{u}$), C_b, and P_{appl} changed negligibly between the inlet and outlet. This reflects the use of a wide bore (d~0.5 cm), short (L=5 cm, L/d~10) tube in these experiments. For example, a membrane resistance of 2 x 10^9 cm^{-1} results in a pure-water filtration rate of 2.2 ml/min at 75 mmHg. The inlet bulk flow rate at a shear rate of 100 s^{-1} is 60 ml/min. Thus, the maximum fraction removed during filtration of a particle suspension at a shear rate of 100 s^{-1} and an applied pressure of 75 mmHg is 3.7%. Any decrease in flux due to buildup of a particle cake reduces the fraction

removed. Increasing the shear rate increases the bulk flow rate and therefore decreases the maximum fraction removed. These small fluid removal rates result in negligible changes in bulk concentration. The axial pressure drop is also negligible. The pressure drop calculated at a shear rate of 1000 s^{-1} is 0.3 mmHg, less than the resolution (1 mmHg) of the pressure transducer used to measure the pressure. Since pressure drop in a tube is linearly proportional to bulk flow rate, the axial pressure drop was negligible in all of the experiments reported above.

(b) Parametric analysis of predicted flux and cake thickness for latex particle filtration

In this section we will examine the influence of various parameters on model predictions for latex particles. In order to first examine the effects of cake formation in the absence of complications such as axially-dependent bulk flow rate and concentration, we will consider a base case in which the fiber is about the same size as the large ultrafiltration fibers described above. We will also use similar membrane resistance and pressure to those above. Table II lists the parameters used in the base case. Only variations from the standard parameters will be noted in figure captions. Except as noted, only one parameter was varied in each figure.

For these runs, the cake concentration was determined from Equation 50, and the resulting cake resistance was determined from the Kozeny-Carman equation (Equation 49). The

Table III. Parameters used in base case for parametric analysis.

Parameter	Value
outlet applied pressure	75 mmHg
inlet equivalent Poiseuille wall shear rate	1000 s^{-1}
particle diameter	1.0 μm
inlet bulk concentration	0.10 (vol. fract.)
membrane resistance	2 x 10^9 cm^{-1}
filtrate flux with water at 75 mmHg	0.30 cm/min
fiber length	5 cm
fiber radius	2500 μm

cake concentration and resistance were allowed to vary with both time and position, as the local applied pressure changed. In all of these runs, D^*_{avg} was determined by numerically integrating the data of Leighton and Acrivos (1987) as described in the model development section (Equation 30).

Figure 6-29 shows the predicted length-averaged flux and cake height as a function of time for the base case. Under these conditions, the axial changes in bulk flow rate and concentration were less than 0.3%, and axial pressure drop was less than 1% of the applied pressure. Even at the fairly large inlet equivalent Poiseuille wall shear rate of 1000 s^{-1}, a significant fraction of the fiber is blocked by the cake. The time dependence of the flux drop-off is directly related to the time required to build up such a thick cake. Even though the bulk concentration chosen for the base case is quite high, several minutes are required to reach steady state. As will be demonstrated below, this time scale will broaden considerably as the inlet bulk concentration is lowered.

Figure 6-30 shows the variation of the predicted steady-state cake height with axial position. The cake grows with distance from the inlet because the rate of back-diffusion decreases with z, thereby decreasing the local flux and requiring a thicker cake to provide the requisite hydraulic resistance. As can be seen in Figure 6-31, which expands the first 0.1 cm shown in Figure 6-31, the cake height grows rapidly with distance.

Figure 6-32 shows the influence of applied pressure on length-averaged steady-state flux and cake height. As was mentioned previously, the axial pressure drop is negligible under these conditions. At very low pressure (< 5mmHg), there is no cake on the membrane and consequently the flux increases linearly with pressure. At higher pressures, a cake forms. Increasing the applied pressure leads to a thicker cake, which narrows the radius available for flow, leading to a higher effective shear rate, which in turn leads to a higher flux. As a result, the flux does not reach a pressure-independent value. As will be discussed in the next section, this behavior is different from that observed with deformable blood cells. The time-dependent plots from which these data were taken are shown in Figure 6-33.

Figure 6-34 shows the variation of steady-state flux with shear rate. The solid line is the flux predicted for variations of the base case, with a fiber radius of 2500 μm and a length of 5 cm. The presence of thick cakes at low shear rates causes the shear rate dependence to deviate

greatly from the linear dependence predicted and observed with deformable red cells (Zydney, 1985). At very high shear rates, the cake eventually disappears, and the membrane-limited flux is achieved. The dotted line shows results in which the particle diameter was reduced to 0.125 μm and the length was reduced to 1 cm in order to minimize cake effects. For comparison, the dashed line drawn approximately through these data has a slope of 0.97, indicating an approximately linear relationship between steady-state flux and inlet wall shear rate under these conditions.

Figures 6-35 and 6-36 show the variation of cake height and effective equivalent wall shear rate with axial position for two extreme cases in which a thin cake ($h << r_f$) has little effect, and in which a thick cake has a very large effect, on the local effective shear rate. Figure 6-35 shows the effective shear rate for the example in Figure 6-34 with 0.125 μm diameter particles at a an inlet wall shear rate of 8000 s^{-1}. In this case, the effective wall shear rate rises less than 10% along the length of the fiber due to the presence of the cake. Figure 6-36 shows the effective shear rate for the example with 1 μm particles at an inlet wall shear rate of 100 s^{-1}. In this case, the effective shear rate is over 10 times higher than the inlet shear rate throughout about 90% of the fiber.

Figures 6-37 and 6-38 show the influence of particle diameter on the predicted length-averaged steady-state flux and cake height. Figure 6-37 shows predictions for variation of the base case, with a shear rate of 1000 s^{-1} and a fiber radius of 2500 μm, while Figure 6-38 shows predictions for a shear rate of 8000 s^{-1} and a fiber radius of 5000 μm (other parameters at base case values). In each graph, flux is indicated by the solid line and cake height is indicated by the dashed line. The dotted line is a reference line with a slope of 4/3, which is the dependence of predicted flux with deformable red cells (Zydney, 1985) and with rigid particles in the absence of cake effects.

In the base case predictions plotted in Figure 6-37, the dependence on shear rate is greater than 4/3 for particle sizes less than about 1.5 μm and less than 4/3 for particle sizes greater than 1.5 μm. Initially the predicted length-averaged cake thickness increases with particle diameter, as a result of the inverse dependence of specific cake resistance on particle size. This increase in cake thickness with particle diameter reduces the effective channel diameter, thereby increasing the effective shear rate, and increasing the flux. This causes a greater-than-4/3 dependence of

flux on particle diameter in this regime. However, beyond a certain point (particle diameter ~ 2 μm), the cake height decreases as the predicted steady-state flux approaches the membrane limit (0.3 cm/min). In this regime, the influence of membrane resistance on flux results in a less-than-4/3 dependence of flux on particle diameter.

For the case of high shear rate (8000 s^{-1}) and large fiber radius (5000 μm) plotted in Figure 6-38, at particle diameters less than 0.5 μm, the cake is thin enough that the 4/3 power dependence is seen. However, with larger particles, the shear-induced diffusion coefficient is large enough that the cake disappears and the membrane-limited flux is attained.

Figure 6-39 shows the dependence of steady-state flux on bulk inlet concentration. As was mentioned previously, under the conditions described here only a small fraction of the bulk flow is removed as filtrate, and no noticeable change in bulk concentration along the length of the fiber occurs. The steady state flux decreases with increasing bulk concentration. In the absence of a concentration-dependent diffusivity and concentration-dependent viscosity, one would expect the flux to be linearly proportional to the log of the ratio of wall to bulk concentration, which would lead to a straight line which would intercept the x-axis at the wall concentration, which for an applied pressure of 75 mmHg is 0.635. The curvature seen here reflects the importance of the concentration-dependence of the diffusivity and the viscosity. The time-dependent plots from which these data were taken are shown in Figure 6-40. Note that increasing the bulk concentration decreases the time required to reach steady state.

Figure 6-41 shows the influence of membrane resistance on model predictions. An order-of-magnitude change from the base case resistance of 2 x 10^9 cm^{-1} barely effects the steady-state flux. In this regime, the cake resistance is much greater than the membrane resistance, and the cake height only changes slightly as the membrane resistance is varied. At higher resistances (R_m > 4 x 10^{10} cm^{-1}), no cake is formed and the flux is inversely proportional to the membrane resistance. The time-dependent plots for several of these runs are shown in Figure 6-42.

Figure 6-43 shows the dependence of steady-state flux on hollow fiber length. The dotted line, with a slope of -1/3, shows the dependence observed with deformable blood cells (Zydney, 1985). The deviation from this line is a result of the variation of cake height with distance. Because the cake thickness increases with z, the effective shear rate also increases with z, as was

shown in Figures 6-35 and 6-36. This increase in effective shear rate partially counteracts the decrease in mass transfer coefficient with z.

Figure 6-44 shows the dependence of steady-state filtrate flux on fiber radius. (The time-dependent plots from which these data were taken are shown in Figure 6-45.) In the absence of cake effects, one would expect the flux at a given shear rate to be independent of fiber diameter. Here we see that, in the presence of a cake, the flux decreases with increasing fiber diameter. There is a trade-off between maximizing flux and minimizing fiber-clogging problems, however. Model predictions for $r_f < 250$ μm are not shown because the model predicted that under these conditions the cake would fill the channel, i.e. that channel clogging would occur.

Figure 6-46 shows the predicted axial pressure profile at several times for the $r_f = 500$ μm case shown in Figures 6-44 and 6-45. Steady-state was reached in three minutes, at which time the axial pressure drop had risen to about 38 mmHg, half the value of the outlet applied pressure. Even though the steady-state cake height occupies approximately one-half of the fiber radius, the fraction of fluid removed at steady-state is only 2.8%, and the outlet bulk concentration is only 3% higher than the inlet bulk concentration. (The maximum predicted fraction of fluid removed in this experiment was 8.1% at t=0.)

(c) Parametric analysis of clogging predictions for latex particle filtration

As was mentioned previously, the model for latex particle filtration predicted that under certain conditions the steady-state cake thickness would be greater than the fiber radius, i. e. that the fiber would clog. The results in the previous section also showed that increasing the shear rate reduces the steady-state cake thickness. Thus, at any given set of conditions, there is a minimum shear rate for operation without clogging. In this section we will study the variation of this minimum shear rate on other operating conditions, and in doing so define clogging and non-clogging regimes of operation. The point of incipient clogging is taken to be that combination of parameters which causes the steady-state thickness at any point in the fiber to equal the fiber radius. In the simulations which follow, clogging always occurred at the channel outlet.

Figure 6-47 shows clogging predictions in which only the shear rate and fiber radius were varied from the base case values. The line representing the model predictions of the minimum

shear rate for non-clogging operation will be denoted the critical shear rate line. Clogging occurs in the shaded region to the left and below the critical shear rate line.

Figures 6-48 and 6-49 show similar predictions in which the particle radius was varied from its base case value of 0.5 μm to 0.125 μm and 2.0 μm, respectively. These three plots are combined in Figure 6-50. For the shear rates and fiber radii shown here, the critical shear rate line for the 0.125 μm particles is always to the left and below the critical shear rate line for the 0.5 μm particles. However, increasing the particle radius by the same factor of four does not show the same trend. Changing the particles leads to two competing effects which influence the tendency to clog. Smaller particles have a higher resistance, and therefore a smaller cake thickness required to achieve a given steady-state flux. However, smaller particles have a lower shear-enhanced diffusion coefficient, so the steady state flux is lower and a greater total cake resistance is required to reach steady state. Apparently for the particular conditions shown here the first effect dominates as the particle size is reduced from 0.5 μm to 0.125 μm. This effect also dominates in the low shear rate regime when one increases the particle size from 0.5 to 2.0 μm. However, at higher shear the size-dependence of the shear-enhanced diffusion coefficient apparently dominates. In fact, for the conditions examined here, at shear rates of about 3000 s^{-1} the membrane limit is achieved, the critical shear rate line is flat, and clogging is not expected to occur in any size fiber.

Figures 6-51 and 6-52 show clogging predictions for cases in which the membrane resistance was changed from its base case value of 2×10^9 cm^{-1} to 2×10^8 cm^{-1} and 2×10^{10} cm^{-1}, respectively. Plots for all three membrane resistance are combined in Figure 6-53. Reducing the membrane resistance by a factor of 10 greatly expands the clogging regime, limiting the non-clogging region to high shear rates and large fiber diameters. Increasing the membrane resistance extends the non-clogging regime to lower shear rates and smaller fiber diameters. Raising the applied pressure would have the same effect on clogging as reducing the membrane resistance. More cake would be required to reduce the flux to its steady-state value. Thus, in designing membrane filters for rigid particles there is a trade-off between obtaining high fluxes and risking the occurrence of clogging.

In systems in which the bulk flow rate is fixed (i.e. the bulk fluid is being pumped), once particle cakes grow too thick the axial pressure drop in the system results in high inlet pressures

which further exacerbate the problem. Figure 6-54 shows the predicted inlet pressure as a function of time for a 500 μm fiber at a shear rate of 150 s^{-1} (and all other parameters at base case values). This increase in pressure could serve as a warning of impending clogging if the inlet pressure is monitored. Whether such a warning arrives early enough to prevent problems depends on the rate at which the cake can build up. For example, high bulk concentrations could pose a serious problem in this regard. The conditions modeled here generally resulted in clogging within a few minutes if clogging was to occur at all.

Futher insight into the mechanism of clogging is gained by expamination of model prediction for Q and C_b prior to clogging. For the conditions of Figure 6-54, the fraction of fluid removved as filtrate just prior to clogging was 0.357, while the outlet bulk concentration was just 6.4%. Clogging occurred because the cake filled the channel at the outlet, not because of any "drying out" of the suspension. Similar results were seen under other clogging conditions.

We have not yet tested these clogging predictions in a systematic way. However, we have found that latex particles with a radius of 1.1 μm will clog a 1 mm diameter hollow fiber with a membrane resistance of about 1×10^9 cm^{-1} at a shear rate of 100 s^{-1} but not at a shear rate of 500 s^{-1}. Characterization of clogging behavior is an aspect of this project which could definitely be carried further in future experiments.

Predicting clogging phenomena in multiple-fiber cartridges may be more difficult than predicting clogging of single fibers. We found that yeast and latex particles will not clog entire 28-fiber cartridges under identical conditions at which single fibers clog. Because of uneven flow distribution among hollow fibers, it is possible that the fibers in which the initial shear rate is lowest clog, which raises the shear rate in the remaining fibers and thereby prevents clogging in those fibers. We found that cylindrically-shaped chunks of yeast approximately the size of the hollow fibers were released from the hollow fiber cartridges during back-flushing after filtration at single-fiber clogging conditions. These chunks appeared to be large enough to clog entire fibers.

(2) Modeling Results for Yeast

As was previously mentioned in the modeling section, the yeast cake concentration was calculated from the centrifugation results of Chapter 4 (Equation 50 in this chapter) by assuming that the average compressive pressure in the cake was equal to one-half the applied pressure. The hydraulic resistance of the yeast cake was evaluated from stagnant filtration results of Chapter 4. Since it was anticipated that the local applied pressure could vary significantly during development of relatively thick yeast cakes in the small hollow fibers, the cake concentration and hydraulic resistance were calculated locally. Different values for the constants in the yeast cake resistance expression (Equation 52) were employed for predicting the flux with rinsed and unrinsed yeast.

For the simulations of filtration of yeast in medium, the membrane resistance was taken to be constant. For the simulations of filtration of yeast in albumin solution, the resistance expressions (Equations 45-47) previously listed in the model development section were employed. These membrane resistance expressions were previously plotted in Chapter 5. The albumin permeability data from which these expressions were derived were also previously plotted along with yeast filtration data in Chapter 5.

As was mentioned in the model development section, the time-dependence of the outlet applied pressure in model simulations was chosen to match experimental procedures. For all simulations of filtration in the large ultrafiltration fibers (including the parametric analysis section), the outlet applied pressure was instantaneously raised to its final value at $t = 0$. However, for simulations of the experiments with yeast in albumin solution in the other fibers, the outlet applied pressure was raised linearly with pressure over a period of two minutes. Flux was not measured in this period. Flux and cake height data was reported relative to the time at which the final pressure was attained. In graphs comparing predicted and measured fluxes, the predicted fluxes are plotted on a time scale which does not include the two-minute start-up period. However, graphs showing flux and cake height predictions alone include the start-up period, since predictions for this period may be important for the understanding of the occurrence of clogging during start-up.

After initial simulations using cake concentrations and resistances which depended solely on the local applied pressure failed to account for the observed time-dependence of fluxes and cake heights, the model was to revised to incorporate a time-dependent cake resistance due to either gradual compaction of the yeast cake or gradual buildup of CO_2 within the cake. Compaction was modeled by incorporating a cake concentration C_c which varied linearly from $C_{c,final} - \Delta C_c$ to $C_{c,final}$ over a time period τ_c. In this case the cake height $h_{n,m}$ from the m^{th} timestep was reduced by the ratio of $C_{c,n,m} / C_{c,n,m+1}$ before adding $\Delta h_{n,m}$ in Equation 72. The effect of gradual buildup of a CO_2 was incorporated by assuming that the volume fraction C_{CO2} of CO_2 would vary linearly from zero at t=0 to ΔC_{CO2} at time $\Delta\tau_{CO2}$. The time-dependent resistance of the cake was calculated by using the Kozeny-Carman equation to relate the resistance at a porosity $\epsilon(t) = 1-C_{c,final}-C_{CO2}(t)$ to the final resistance at a porosity of $\epsilon_{final} = 1-C_{c,final}-\Delta C_{CO2}$, which was taken to be the resistance measured in stagnant filtration experiments.

(a) Comparison of flux predictions with experimental data

Figures 6-55 through 6-57 show predicted and measured fluxes for filtration of 0.65% yeast in 6% albumin in 1mm ID polysulfone, 330 mm ID polypropylene, and 320 μm ID polyamide hollow fibers. (See Chapter 5 for experimental details.) In each case, four model prediction curves are shown. The solid line represents predictions obtained using the Leighton and Acrivos correlation, Equations 11 and 12, for the shear-enhanced diffusivity and the corrected version of Reuss' fit to data for yeast viscosity at an osmotic pressure of 14 bar, Equation 32. The dotted line is the result of using a diffusivity equal to one-tenth of the Leighton-Acrivos correlation value. The dashed line is the result of using the Leighton-Acrivos diffusivity and incorporating a time decay in the yeast resistance using a compaction term in which C_c varies linearly from $C_{c,final} - \Delta C_c$ to $C_{c,final}$ over a time period τ_c. In all cases, $C_{c,final}$ was determined from the applied pressure using Equation 50, with $\epsilon_0 = 0.208$, $\epsilon_\infty = 0.210$, and $a = 0.074$ mmHg^{-1}. For the small fibers, $\Delta C_c = 0.1$ and $\tau_c = 10$ min were used. For the 1 mm fibers, $\Delta C_c = 0.15$ and $\tau_c = 30$ min were used. Similar runs in which a time decay due to CO_2 production was incorporated (using $\Delta C_{CO2} = \Delta C_c$ and $\tau_{CO2} = \tau_c$) produced results which were virtually identical to the cake compaction results, and are not shown here. The dot-

dash line is the result of simultaneously reducing the Leighton-Acrivos diffusivity by a factor of ten and incorporating the time decay in the resistance by use of a compaction term.

Figure 6-55 shows the results for the modified polysulfone hollow fibers, which were shown in Chapter 5 to exhibit a fairly constant membrane resistance during one-hour exposure to 6% albumin. The results in Figure 6-55 show that using the Leighton-Acrivos diffusivity and no time decay (solid line) results in (1) underpredicting the flux at early time, and (2) overpredicting the flux at later times. Incorporating the time decay (dashed line) improves the early-time prediction, while reducing the diffusivity (dotted line) improves the later-time predictions. Incorporating both effects (dot-dash line) results in correctly predicting the shape of the data, although more precise knowledge of the correct functional form of $R_c(t)$ and the true value of D is needed. Longer-time experiments are also needed to determine whether steady state is actually reached, as is predicted by the model. As will be seen more clearly in a later graph of cake thickness predictions, the steady state predicted here is related to achievement of a steady-state thickness of yeast cake. The difference in early-time fluxes for the two cases with no decay in the resistance (solid and dotted), which differ only in the magnitude of the diffusivity, indicate that even at early time back-transport is playing a role in controlling the rates of cake buildup and flux decline.

Figure 6-56 shows the results for the polypropylene hollow fibers, which show the fastest decrease in membrane permeability with exposure to albumin. Both curves which use the Leighton-Acrivos diffusivity (solid and dashed) predict a significant influence of membrane permeability on flux. The shoulder in the those curves is the point at which the membrane resistance has become large enough to control the flux. The model predictions with a reduced diffusivity and a time decay in the resistance due to cake compaction (dot-dash) agree fairly well with the data except at long time. In this case, the "steady-state" flux predicted by all four methods indicates that the flux has sbecome membrane iimited. The predicted flux mirrors the leveling off of the albumin permeabiiity data after one hour. By this time the yeast cake has washed away. The flux data suggests that the membrane resistance increased even further than the permeability measurements with albumin solution had indicated. Use of the time-dependent resistance was essential to understanding why the yeast cakes disappeared with time during filtration of yeast in albumin solution. Since unrinsed yeast was used in these experiments, and

other experiments with unrinsed yeast in polysulfon/Biopol fibers showed that the membrane permeability decreased, it is conceivable that the further decay of the membrane permeability suggested by Figure 6-56 resulted from use of unrinsed yeast.

Figure 5-57 shows the results for the polyamide membranes, which have a membrane resistance which increases more slowly than the polypropylene membrane resistance, but more rapidly than the modified polysulfone membrane resistance, according to the results of permeability measurements with albumin solution. In this case, all of the model predictions severely overpredict the experimental data at times greater than 20 min. As in Figure 6-56, The data suggests that the membrane permeability in the presence of albumin and yeast drops more rapidly that the permeability in the presence of albumin alone.

Figure 5-58 shows predicted and measured fluxes for the filtration of 2% yeast in media in 4.66 mm ultrafiltration fibers. The solid symbols and solid line represent data and predictions for unrinsed yeast, using the resistance of freshly-rehydrated yeast measured in Chapter 4, a diffusivity equal to one-tenth the Leighton-Acrivos diffusivity, and no compaction term. The open symbols are data with rinsed yeast. According to the hypothesis of Chapter 5, the flux with rinsed yeast drops off more slowly than the flux with unrinsed yeast because the cake resistance of the unrinsed yeast is greater, due to the presence of CO_2 bubbles in the unrinsed yeast cake which arise from a carbon source on the surface of the yeast which is not rinsed away. The dashed line shows model predictions obtained using the resistance of rinsed yeast measured in Chapter 4, a diffusivity equal to one-tenth the Leighton-Acrivos diffusivity, and no compaction term. This suggests that the difference in final yeast cake resistances arising from CO_2 generation is not the sole reason for the difference in the time-dependence of the flux. Incorporation of a cake compaction term with $\Delta C_c = 0.15$ and $\tau_c = 30$ min as in the 1 mm fibers results in the predictions represented by the dotted line. Increasing τ_c to 120 min results in the predictions shown by the dot-dash line. The incorporation of the time decay in the resistance brings the theoretical predictions closer to the flux measured with the rinsed yeast. Why no compaction term was required to predict the unrinsed yeast flux is not clear. Further study into the effect of CO_2 on the resistance of yeast cakes formed during cross-flow filtration is required.

(b) Comparison of cake thickness predictions with experimental data

Figures 6-59 through 6-61 show predicted length-averaged flux and cake thickness for experiments in polypropylene, polyamide, and modified polysulfone fibers, the results of which were plotted in Figures 6-55 through 6-57. These results are those which incorporated both a reduced diffusivity and a time decay in the membrane resistances. In all cases, the flux increases during the start-up period, and then decreases due to both yeast cake buildup and loss of membrane permeability. The cake height firest increases and then decreases as a result of the decrease in membrane permeability. The cake washes away quickly in the polypropylene fibers, gradually in the polyamide fibers, and only slightly in the polysulfone fibers.

Figures 6-62 through 6-64 show predicted cake height as a function of axial position at several times for the experiments with polypropylene, polyamide, and modified polysulfone fibers. Comparing Figure 6-62 with the freeze-substitution results in Figure 5-25, we find that the experimentally observed cake heights are generally greater than the predicted cake heights, especially at the outlet at early time. Both predicted and observed cake heights increase with axial position. Except for the section shown in (2a) of Figure 5-25, the experimental data confirms the predicted trend that the yeast cake washes away with time as the membrane resistance increases. The reason why the cake height at the outlet is so large at early time may be related to the large fraction of fluid initially removed. Since cake buildup is proportional to C_b at early time, the cake should grow fastest at the outlet where C_b is highest.

Comparing the yeast cake thickness observed in the polyamide fibers shown in Figure 5-26 with the predicted cake height in Figure 6-63, we again find that experimentally-observed cake heights are greater than model predictions. Both predicted and measured cake heights increase with axial position. Both theory and data also show that the yeast cake thickness increases between t=1 min and t=5 min, then remains fairly steady between t=10 min and t=20 min, and then decreases at later times.

Comparing the yeast cake thickness observed in the modified polysulfone fibers shown in Figure 5-34 with the predicted cake height in Figure 6-64, we find that experimentally-observed cake heights are approximately equal to the predicted cake heights. This may reflect the lesser effect of membrane resistance on cake height in these fibers. Both predicted and measured cake heights increase with axial position, as in the other fibers. However, in this case the predicted cake thickness continues to grow for the first 20 min and then remains fairly constant between the 20 min and 40 min samples. The experiments show a greater decrease in cake thickness between the 40 min and 60 min samples than the theory predicts. This suggests that the

membrane resistance may be decreasing more rapidly in the presence of yeast plus albumin than it did in permeability experiments with albumin alone.

The difference in cake-washout behavior in these fibers reflects the difference in the rates of fouling of the three types of membranes. The polypropylene membranes foul most quickly, causing the yeast cake to wash away at relatively early time. The modified polysulfone membranes foul the most slowly, and consequently the yeast cake remains the longest in those fibers.

These experiments clearly demonstrate that the yeast cakes which develop on hollow fiber membrane surfaces are thick enough to effect both effective shear rate and axial pressure drop in the fibers. More accurate prediction of yeast cake thickness and filtrate flux will require a better understanding of the effects of compaction phenomena and CO_2 buildup on the resistance of yeast cakes which form in cross-flow systems, as well as accurate knowledge of the time-dependence of membrane resistance during the yeast filtration experiments.

d. Clogging predictions for yeast

As was previously mentioned in Chapter 5, clogging occurred during startup of yeast filtration experiments in which the initial pressure was raised too quickly. This clogging occurred at identical conditions of shear rate, pressure, and bulk concentration under which no clogging occurred when the pressure was raised more slowly. Although the occurrence of such clogging was not studied in detail either experimentally or theoretically, the clogging phenomenon involved here appears to be different from the clogging phenomenon discussed in the section on clogging by latex particles.

As was reported in Chapter 5, in experiments in which the pressure was raised gradually, very large fractions of the incoming fluid were removed as filtrate just after reaching the final applied pressure. Modeling results with τ_p = 2 min predicted similar high removal rates. Modeling runs in which the time constant for raising the pressure was reduced from two min to 0.5 min or less predicted clogging during start-up. Distinguishing between true drying out of the suspension and clogging due to rapid buildup of the cake in sections of the fiber where the bulk suspension has become highly concentrated is difficult. Nevertheless, the model was able to successfully predict the occurrence of this start-up (non-steady-state) clogging phenomenon.

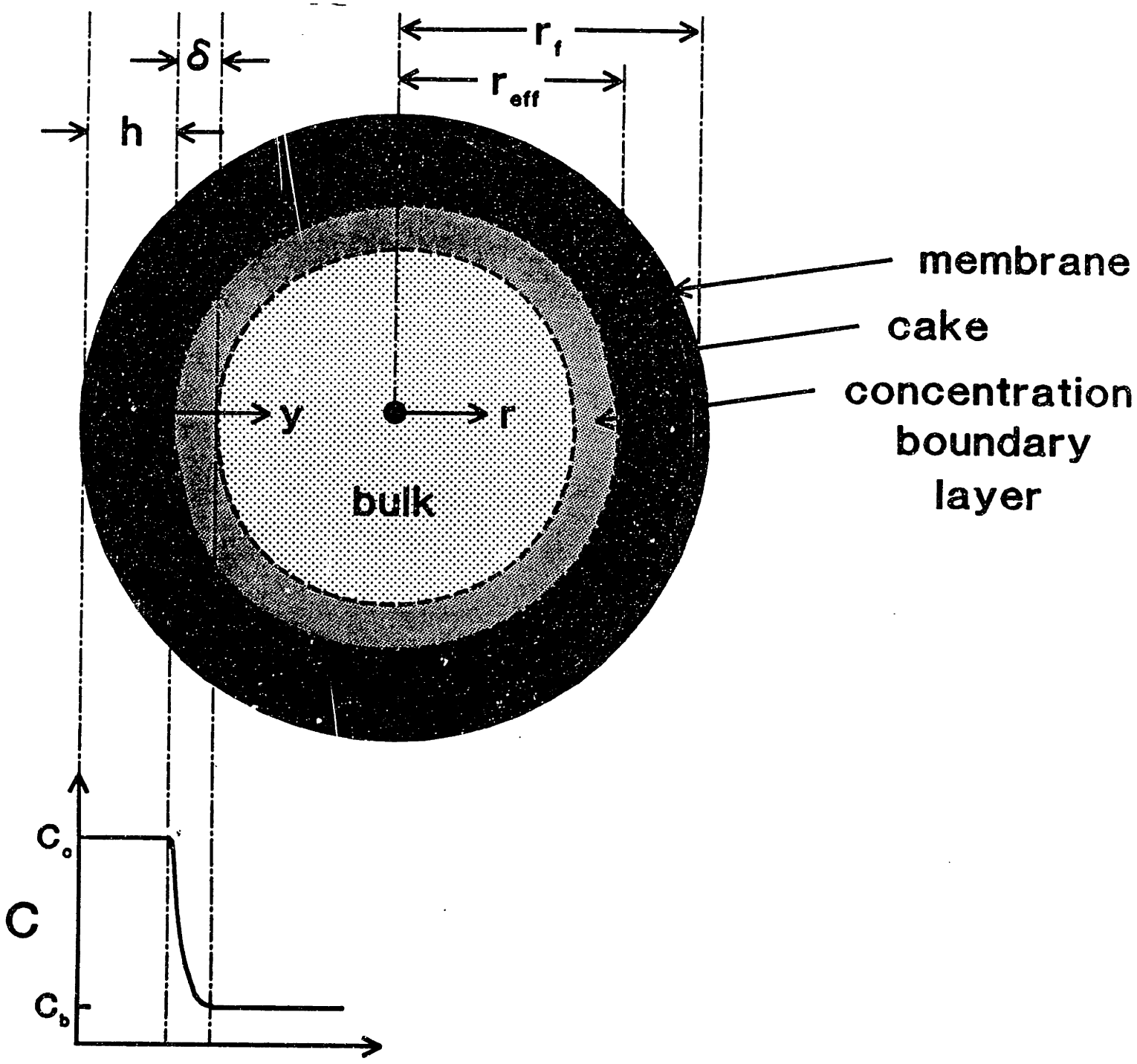

Figure 6-1. Cross-sectional view of hollow fiber.

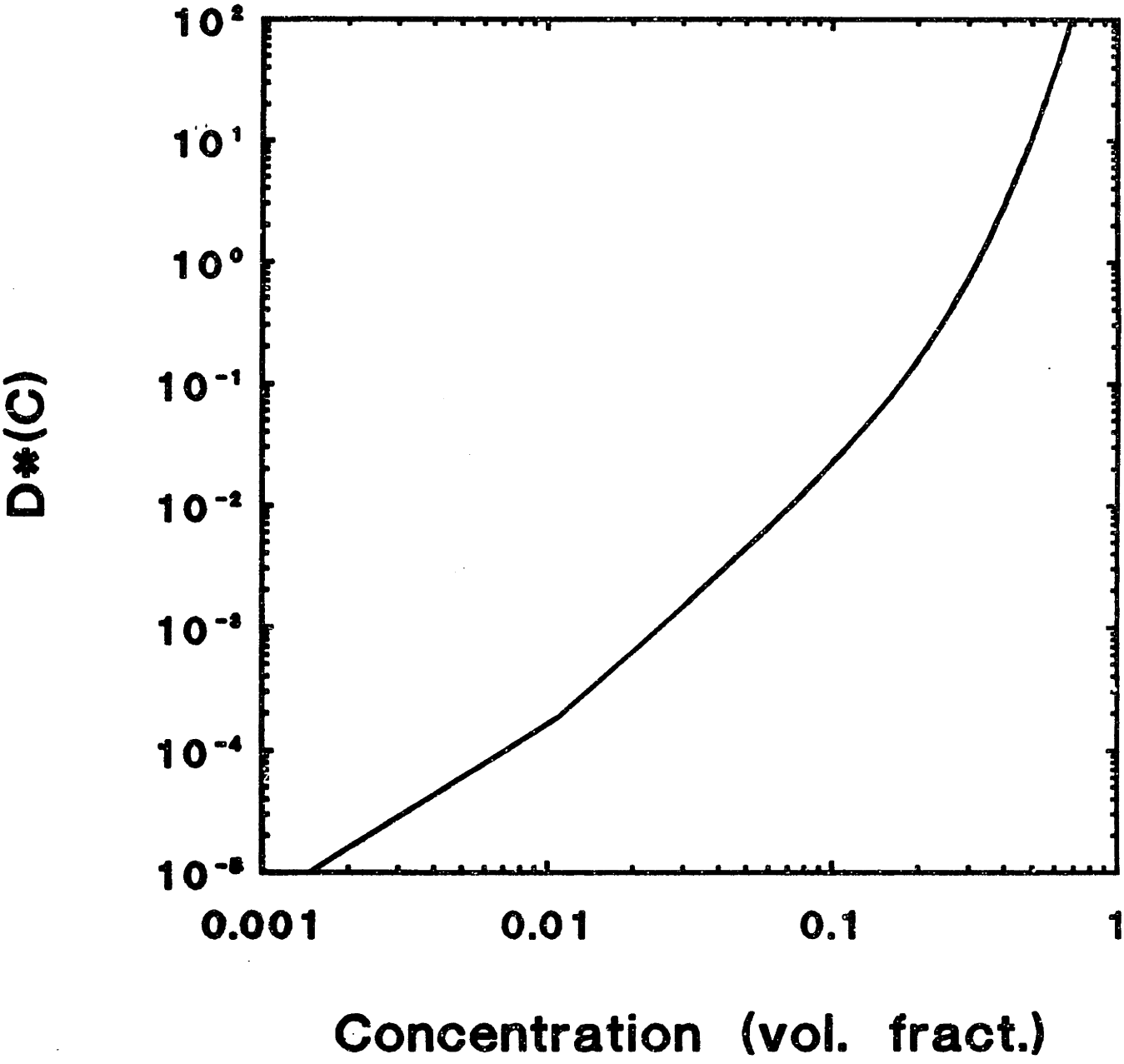

Figure 6-2. Concentration dependence $D^*(C)$ of the shear-induced diffusion coefficient of rigid particles (Leighton and Acrivos, 1987).

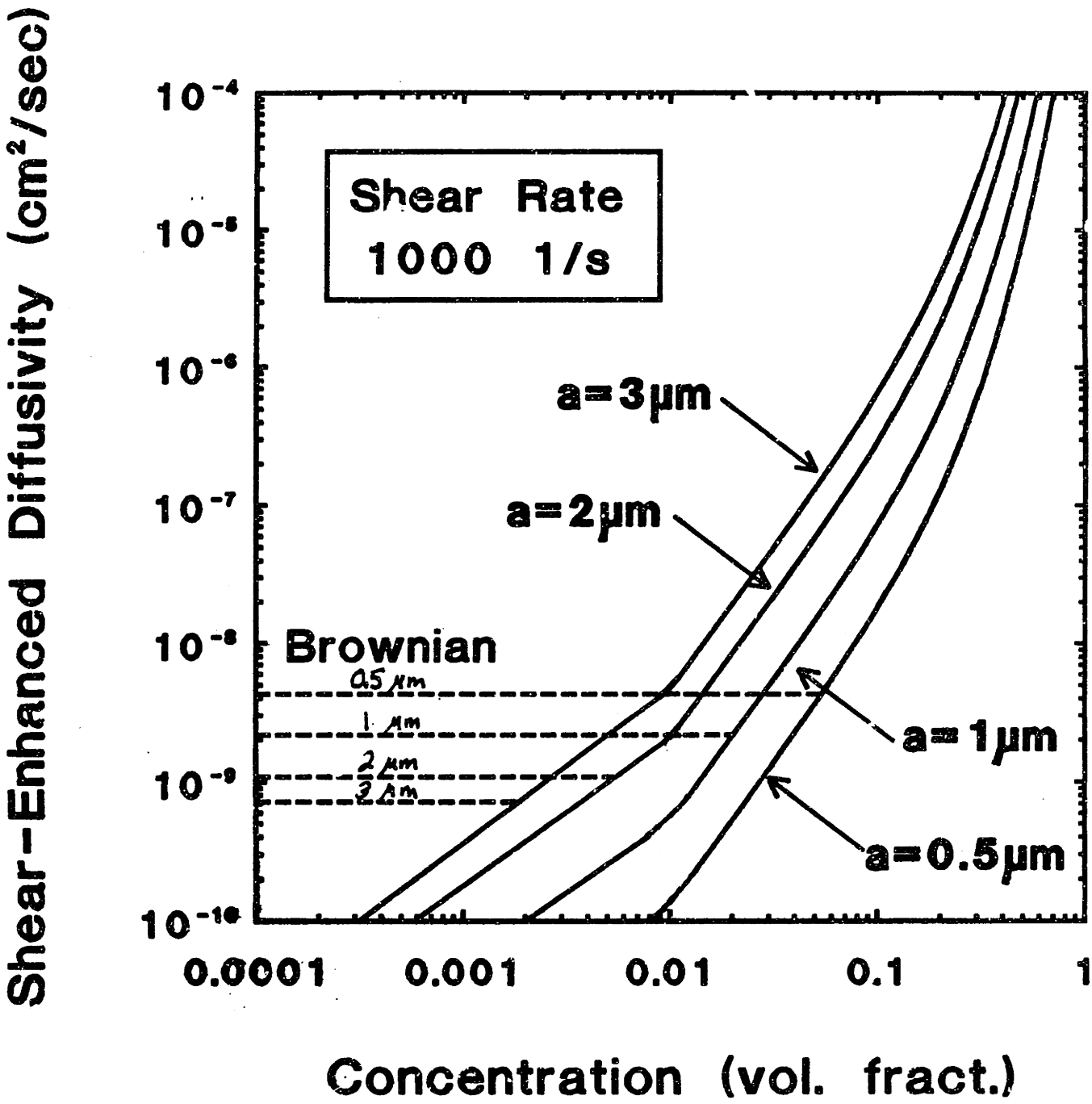

Figure 6-3. Shear-enhanced diffusivity of suspensions of latex particles of various sizes (radius a) at a shear rate of 1000 s^{-1}.

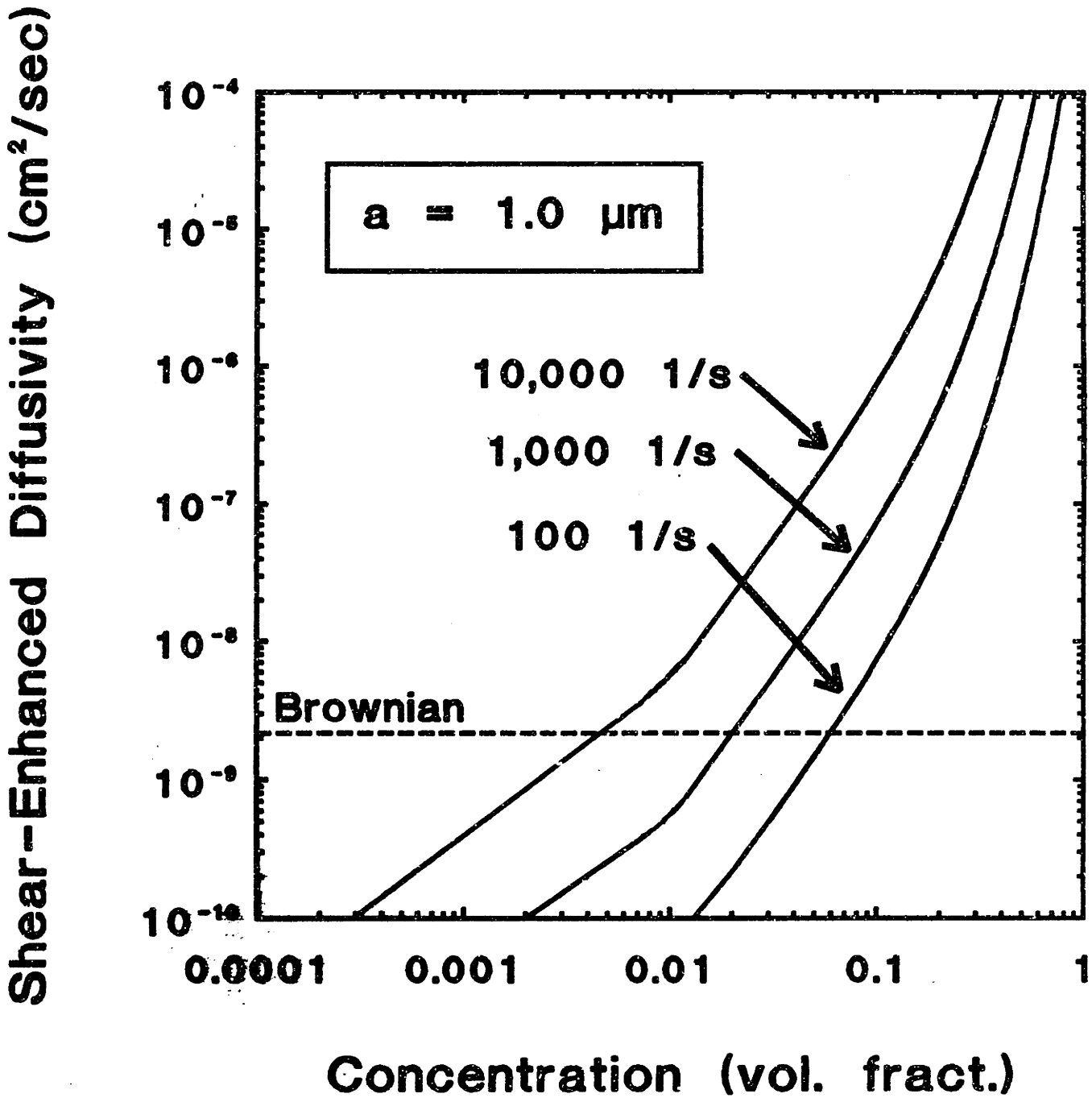

Figure 6-4. Shear-enhanced diffusivity of suspensions of latex particles of radius a=1 μm at various shear rates.

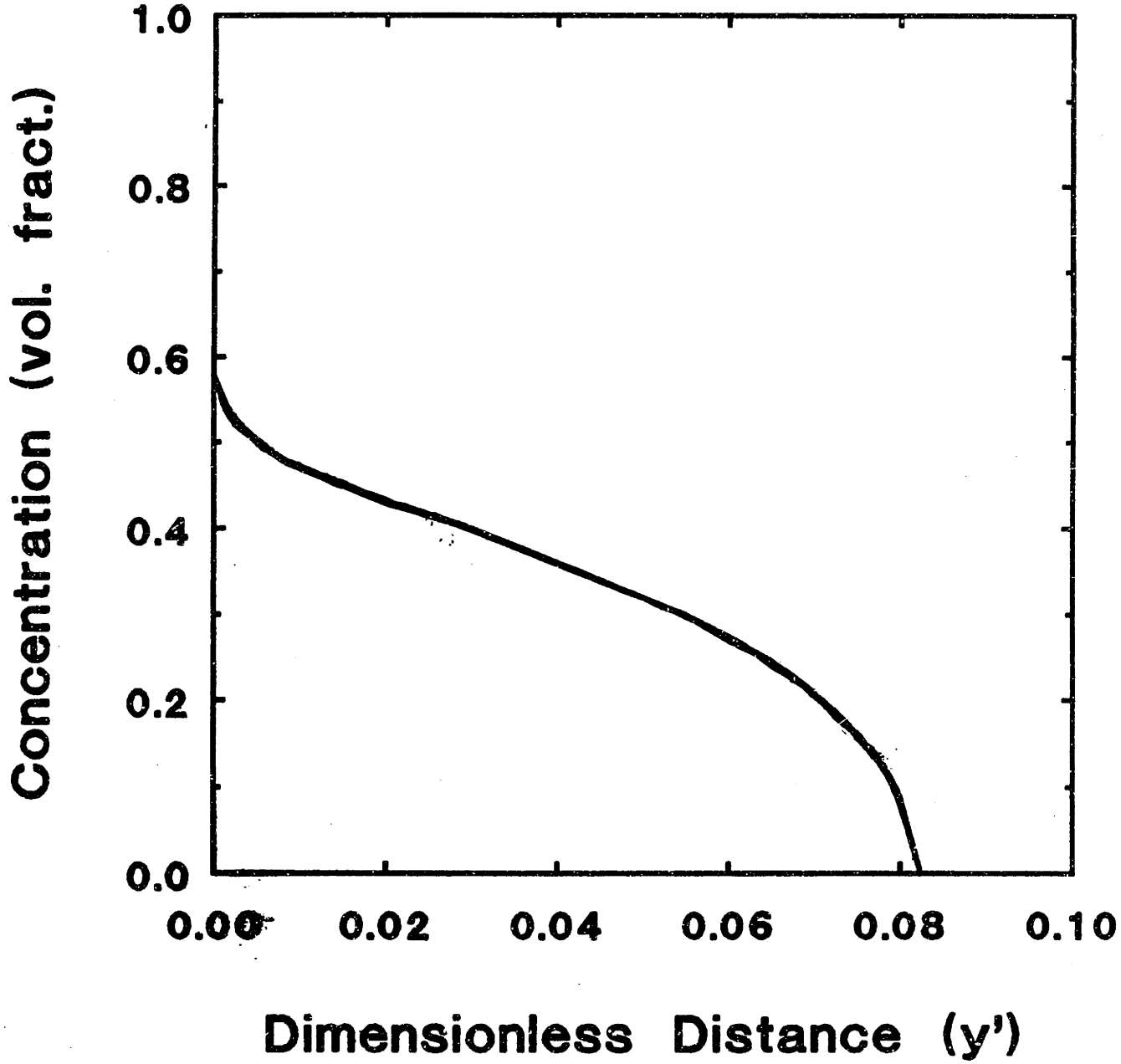

Figure 6-5. Concentration profile predicted by Davis and Leighton (1987).

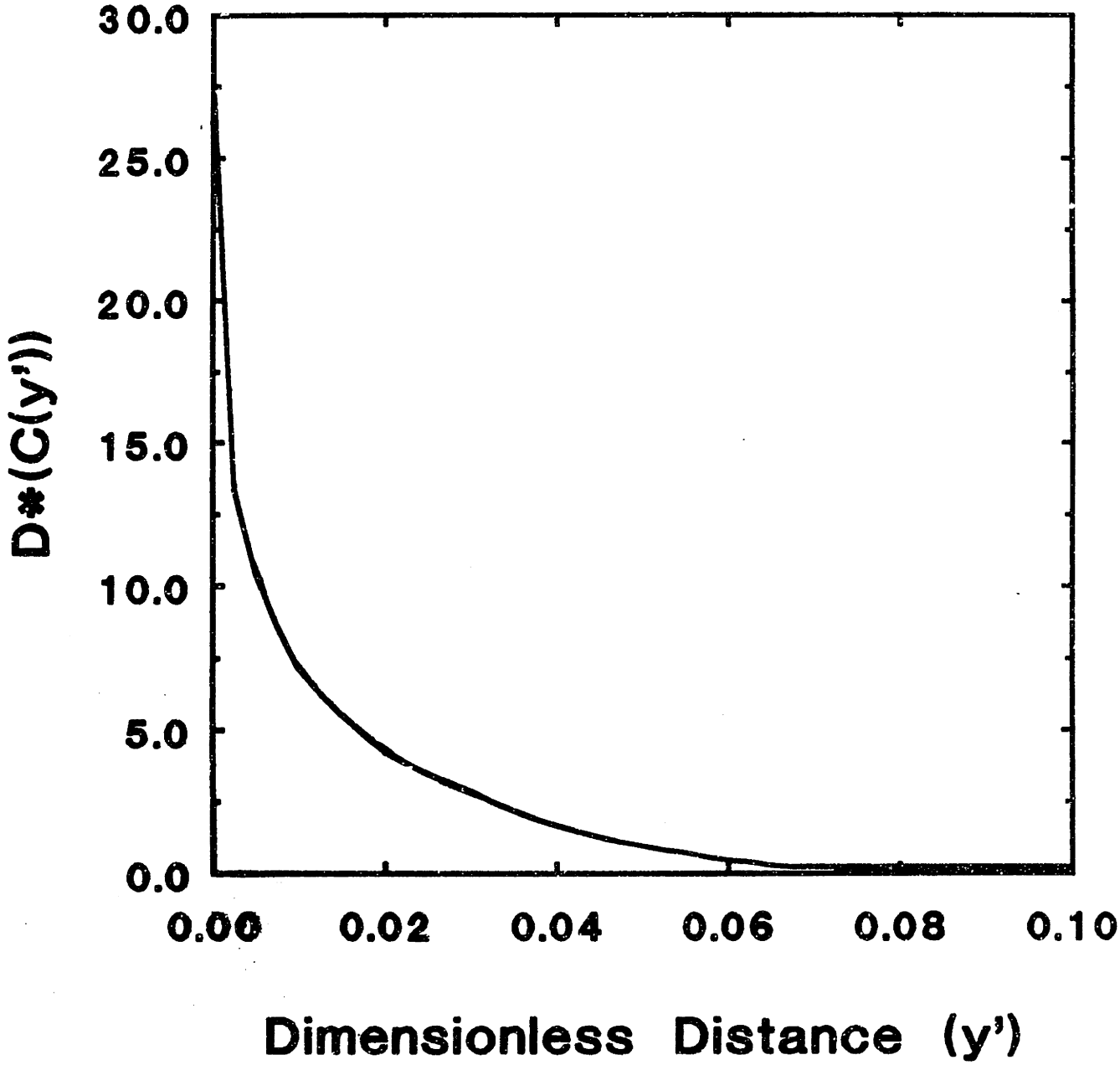

Figure 6-6. $D^*(C)$ as function of dimensionless distance, calculated from concentration profile of Davis and Leighton (1987).

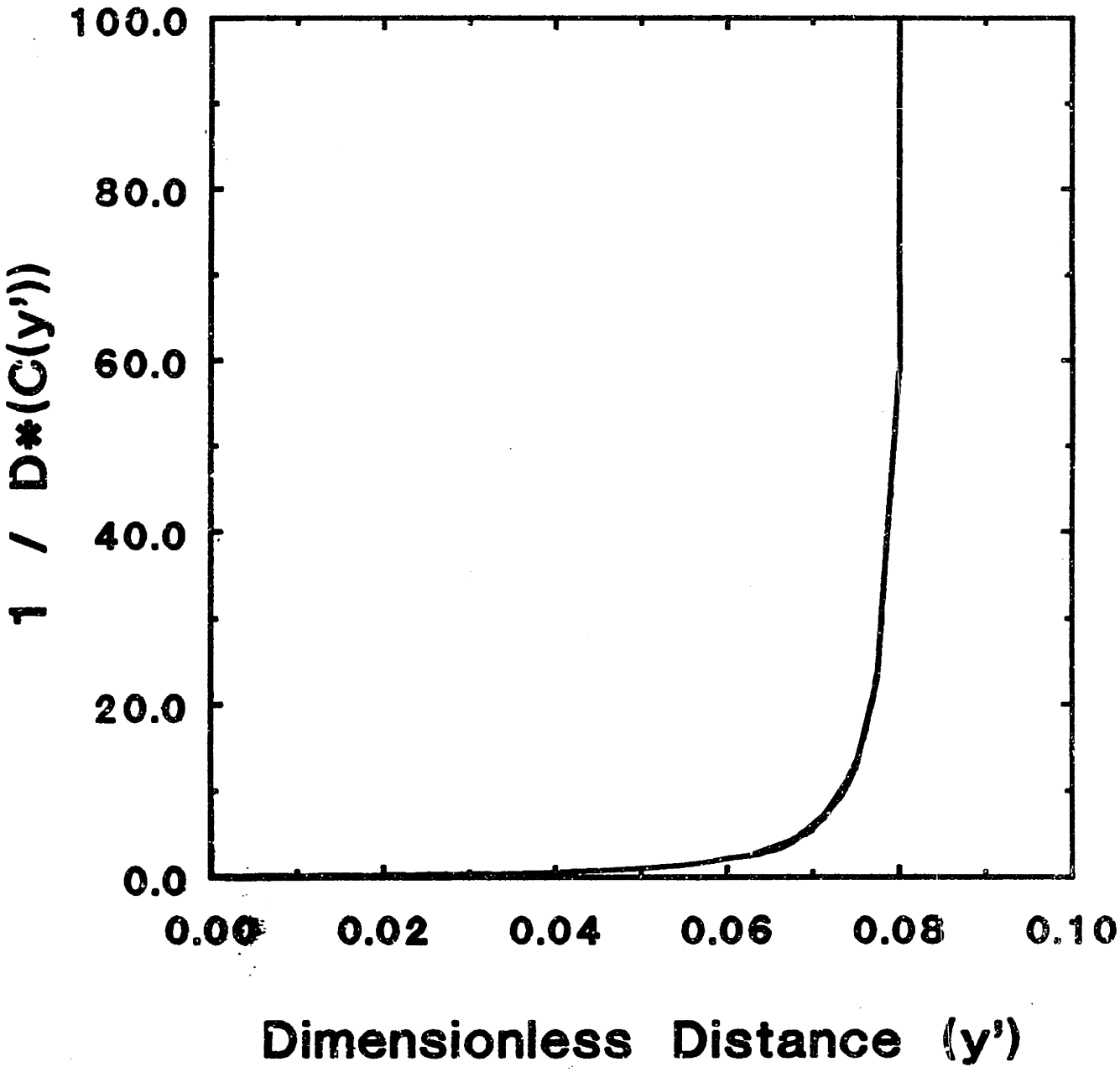

Figure 6-7. $1/D^*(C)$ as function of dimensionless distance, calculated from concentration profile of Davis and Leighton (1987).

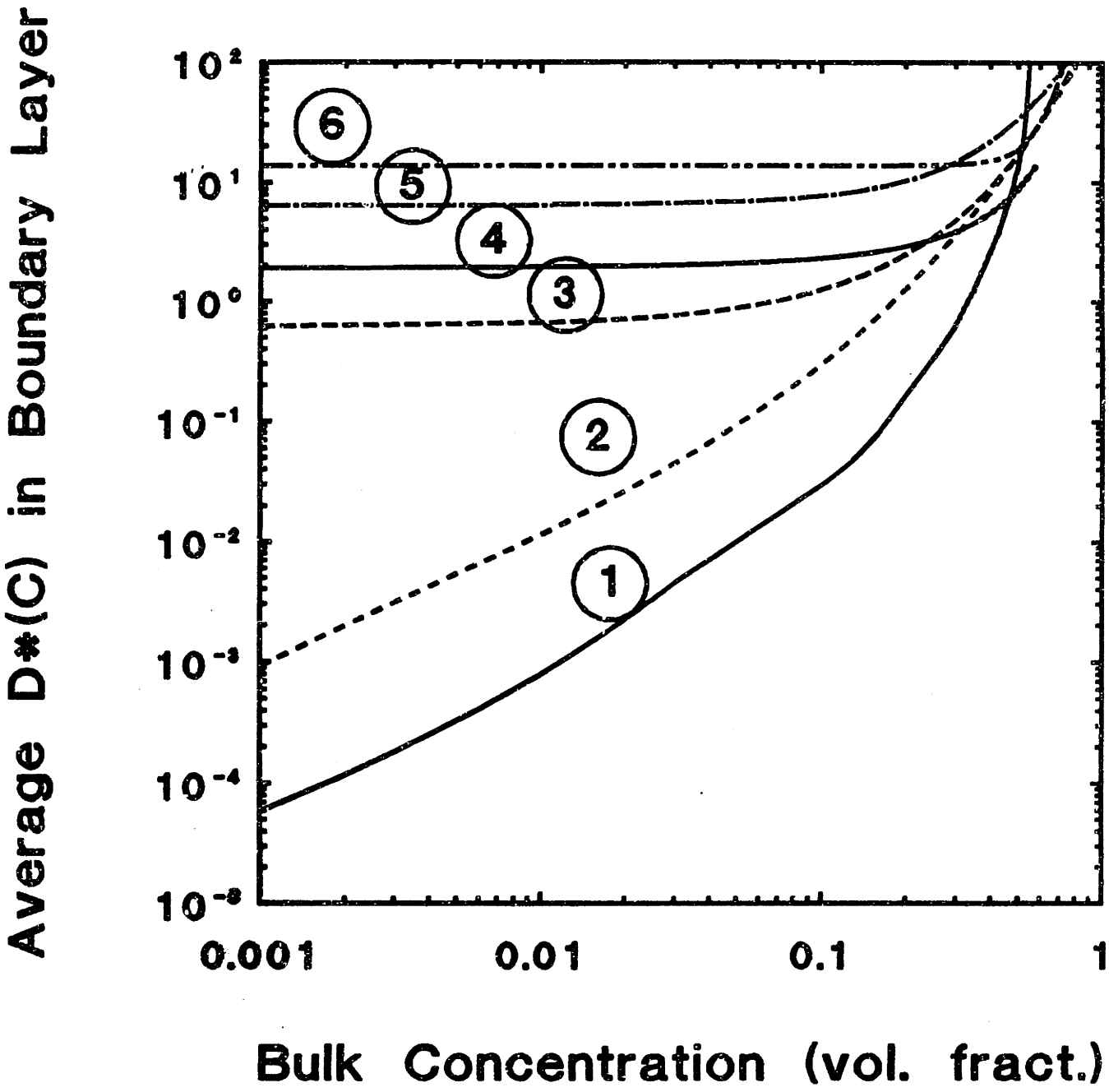

Figure 6-8. Average $D^*(C)$ in the concentration boundary layer, as function of bulk concentration, calculated using six averaging techniques. (See discussion in text.)

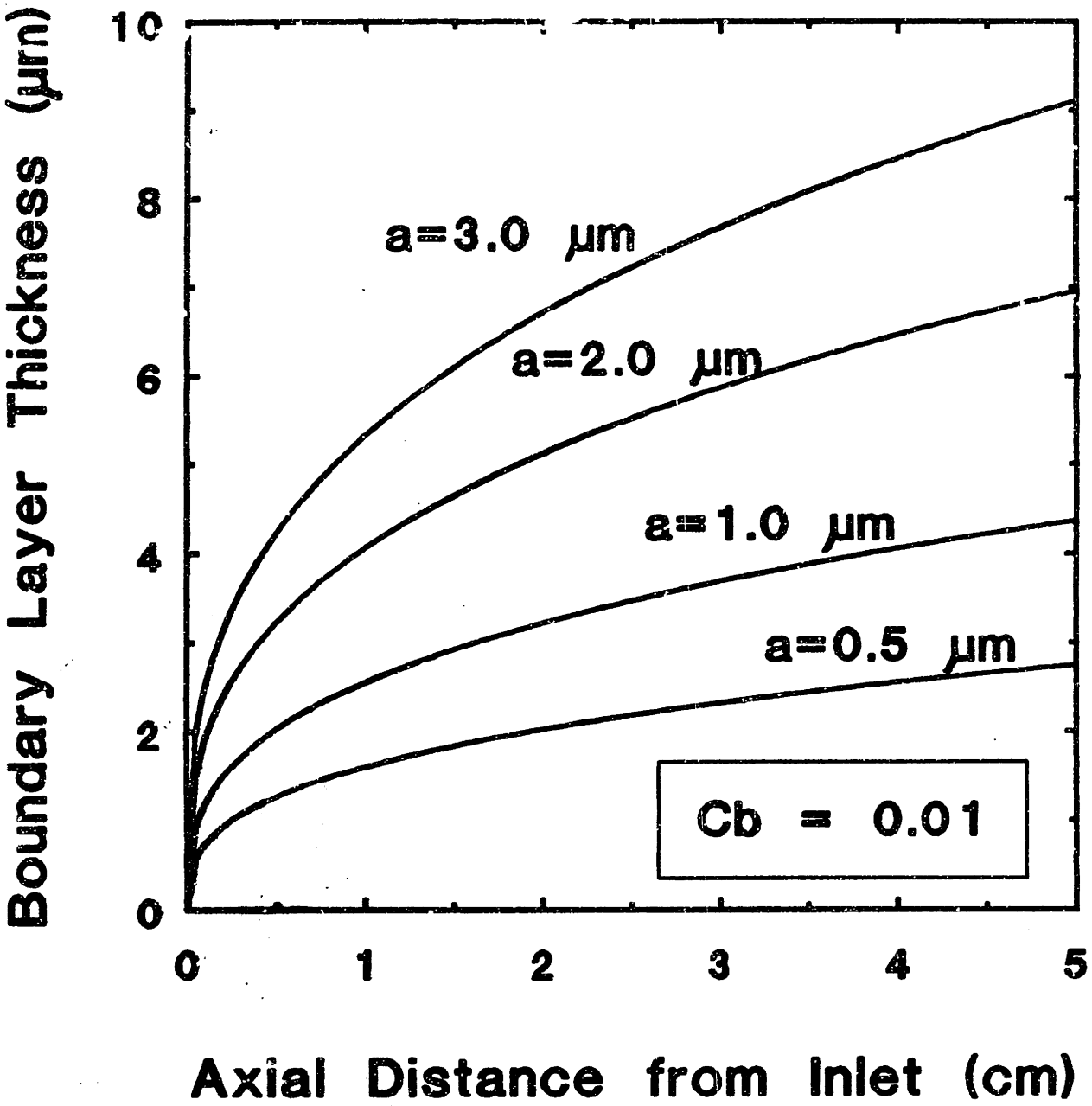

Figure 6-9. Calculated concentration boundary layer thickness as a function of axial distance from inlet for latex particles of various sizes (a=radius) at a bulk concentration of 0.01. (δ is independent of shear rate.)

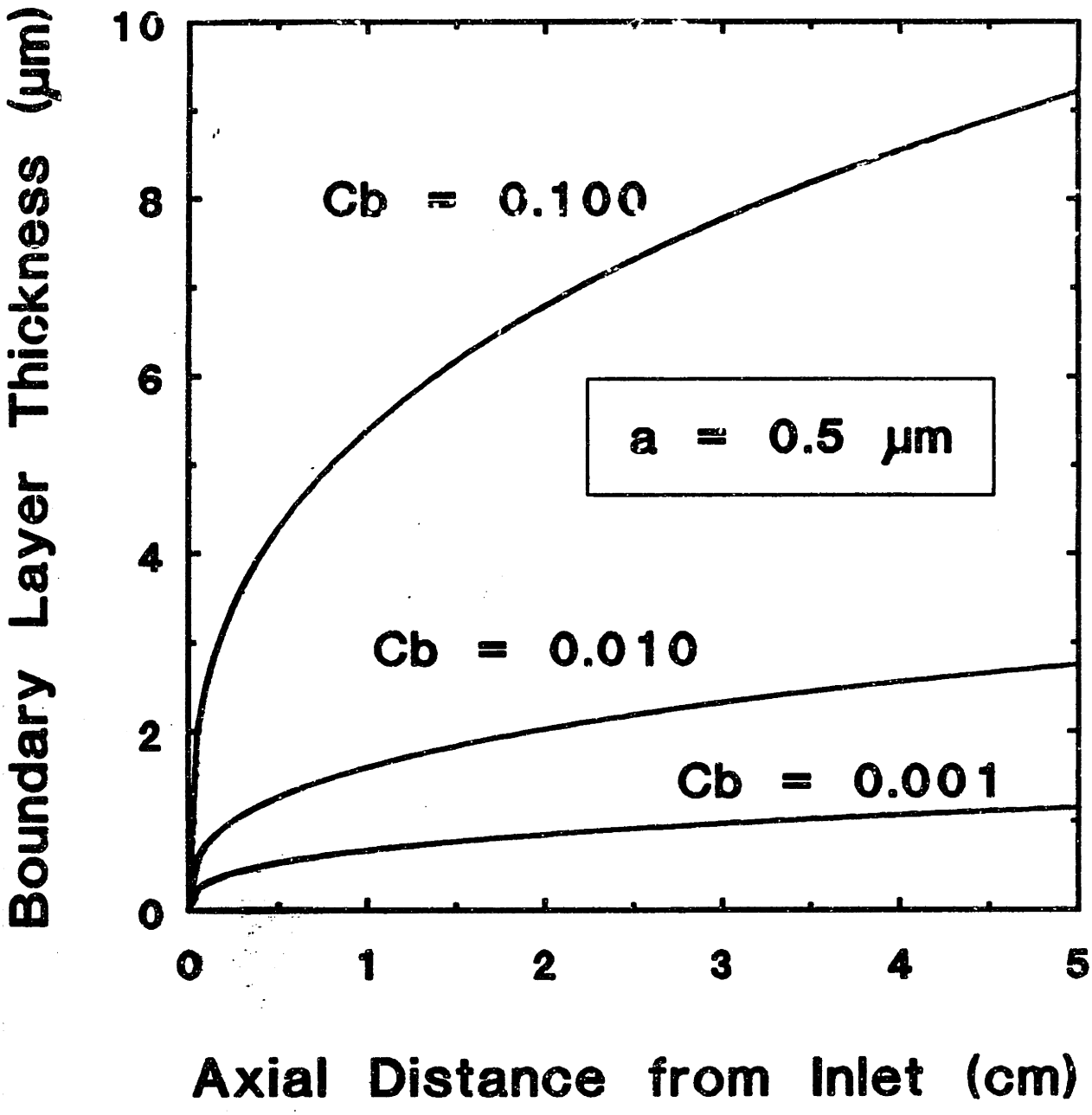

Figure 6-10. Calculated concentration boundary layer thickness as a function of axial distance from inlet for latex particles of radius a=0.5 μm at various bulk concentrations. (δ is independent of shear rate.)

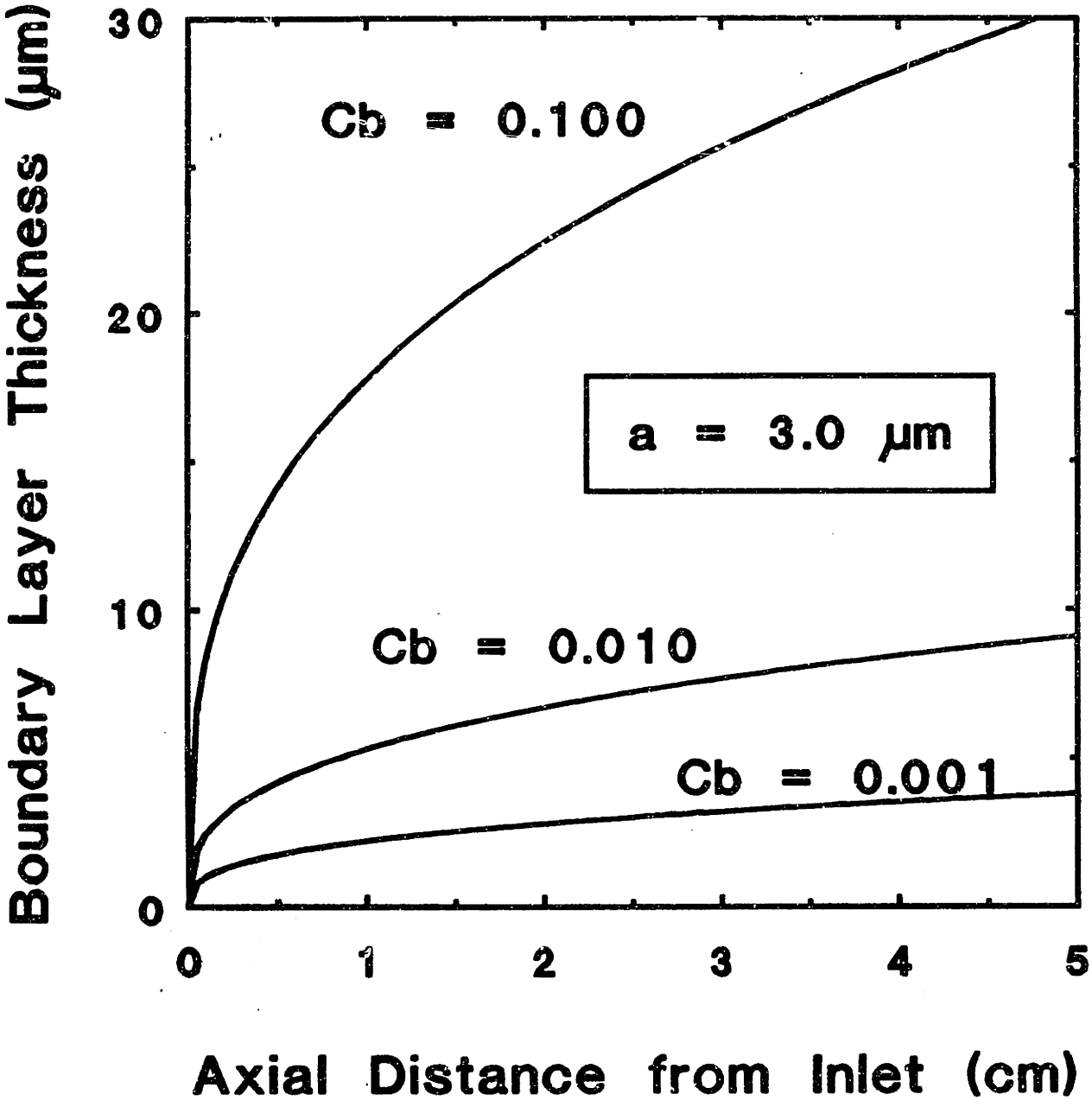

Figure 6-11. Calculated concentration boundary layer thickness as a function of axial distance from inlet for latex particles of radius a=3.0 μm at various bulk concentrations. (δ is independent of shear rate.)

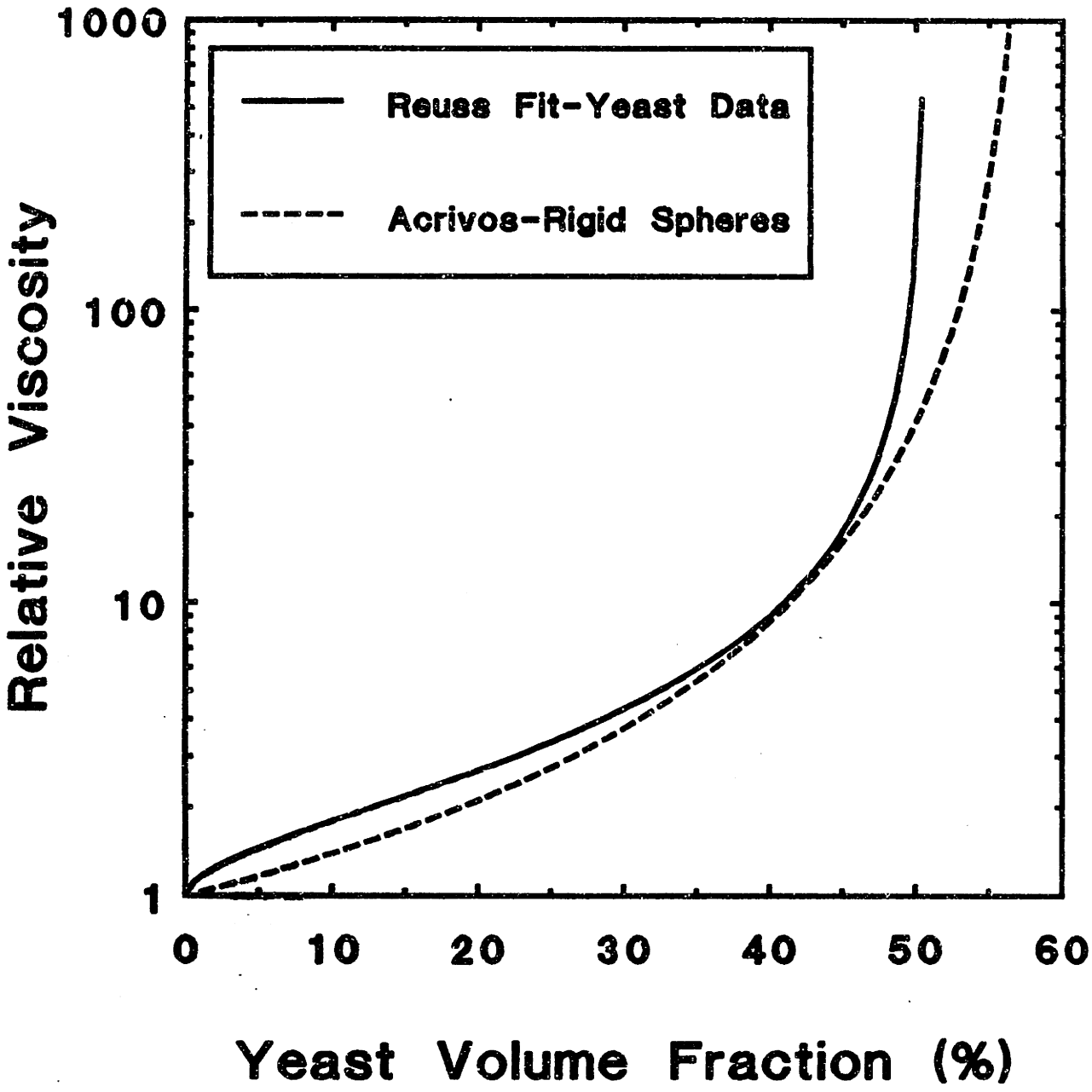

Figure 6-12. Viscosity of yeast and latex particle suspensions as a function of bulk concentration.

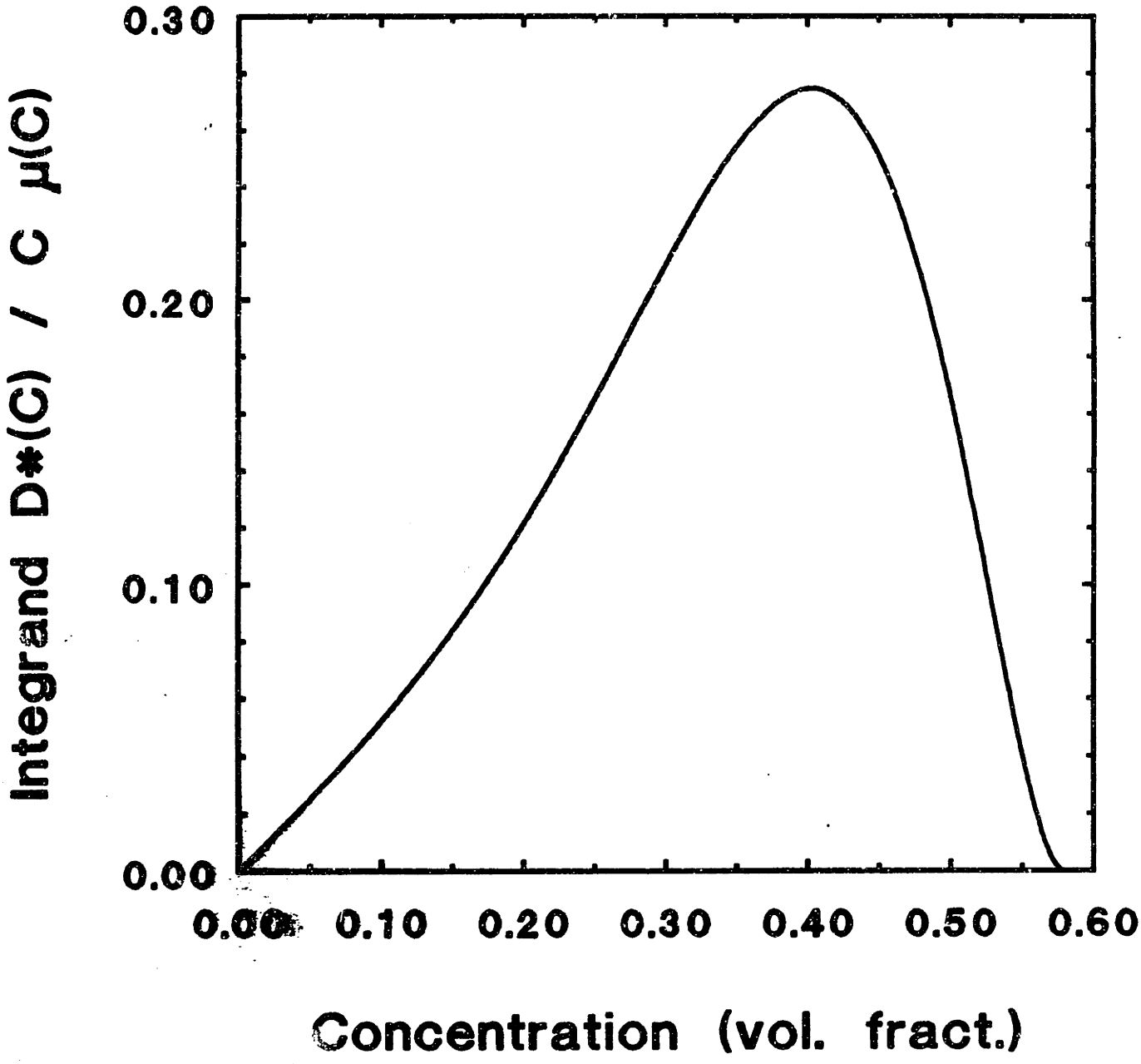

Figure 6-13. Integrand $D^*(C)/C\,\mu(C)$ as a function of C.

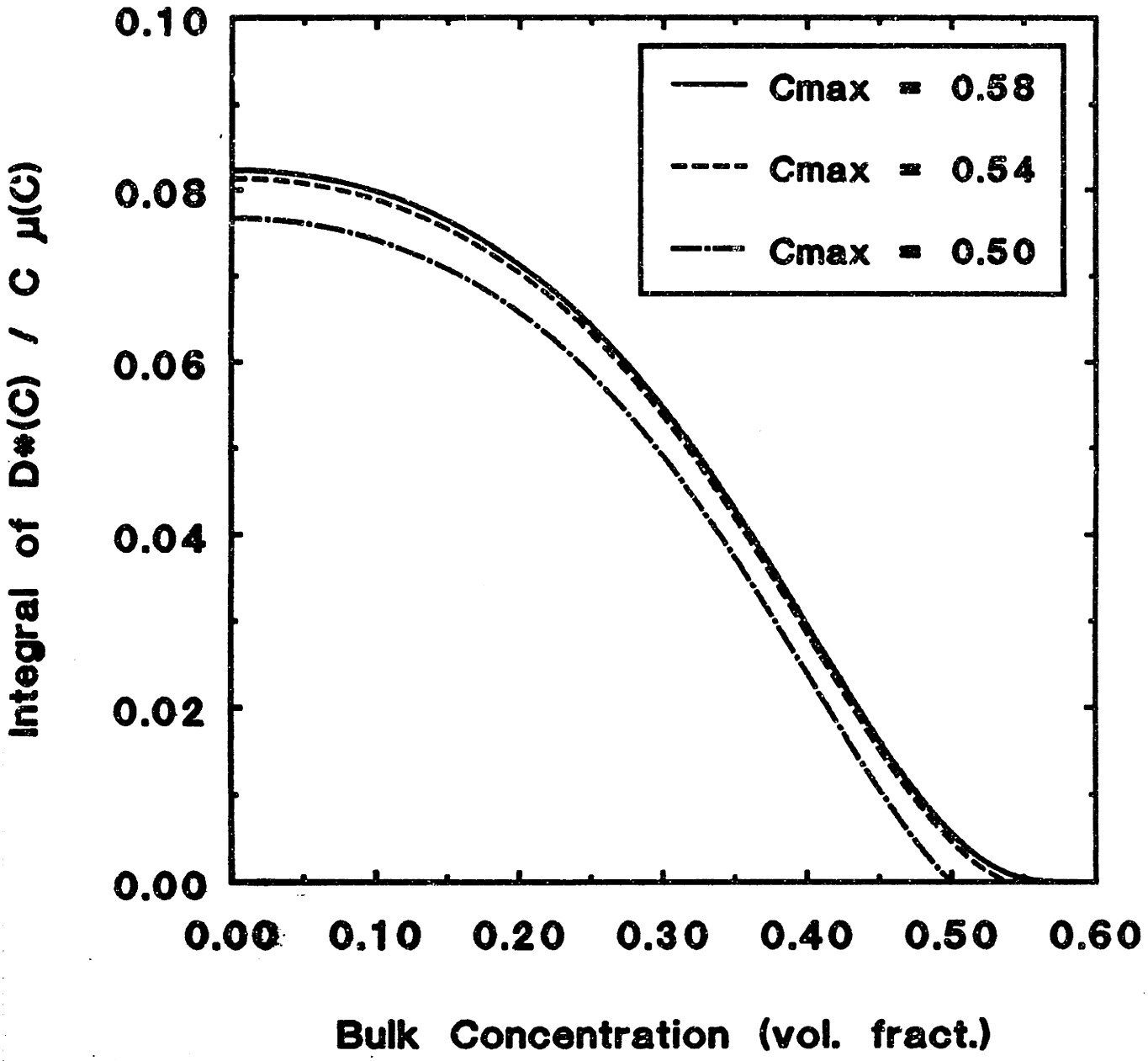

Figure 6-14. Integral of $D^*(C)/C\ \mu(C)$ across the boundary layer as a function of bulk concentration.

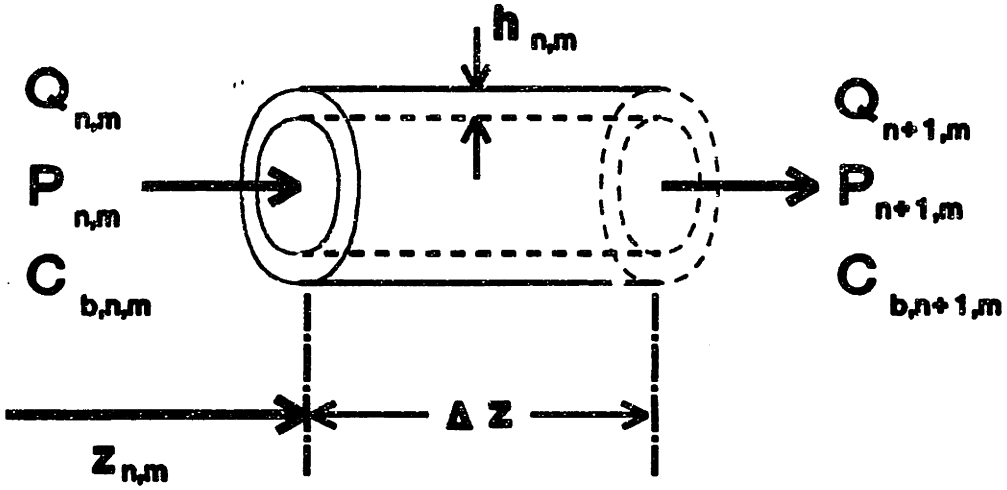

$$z_{n+\frac{1}{2},m} = z_{n,m} - \frac{\Delta z}{2}$$

$$P_{n+\frac{1}{2},m} = P - \frac{\Delta P_{n,m}}{2} \quad ; \quad P_{n+1,m} = P_{n+\frac{1}{2},m} - \frac{\Delta P_{n,m}}{2}$$

Figure 6-15. Schematic of axial segment of hollow fiber.

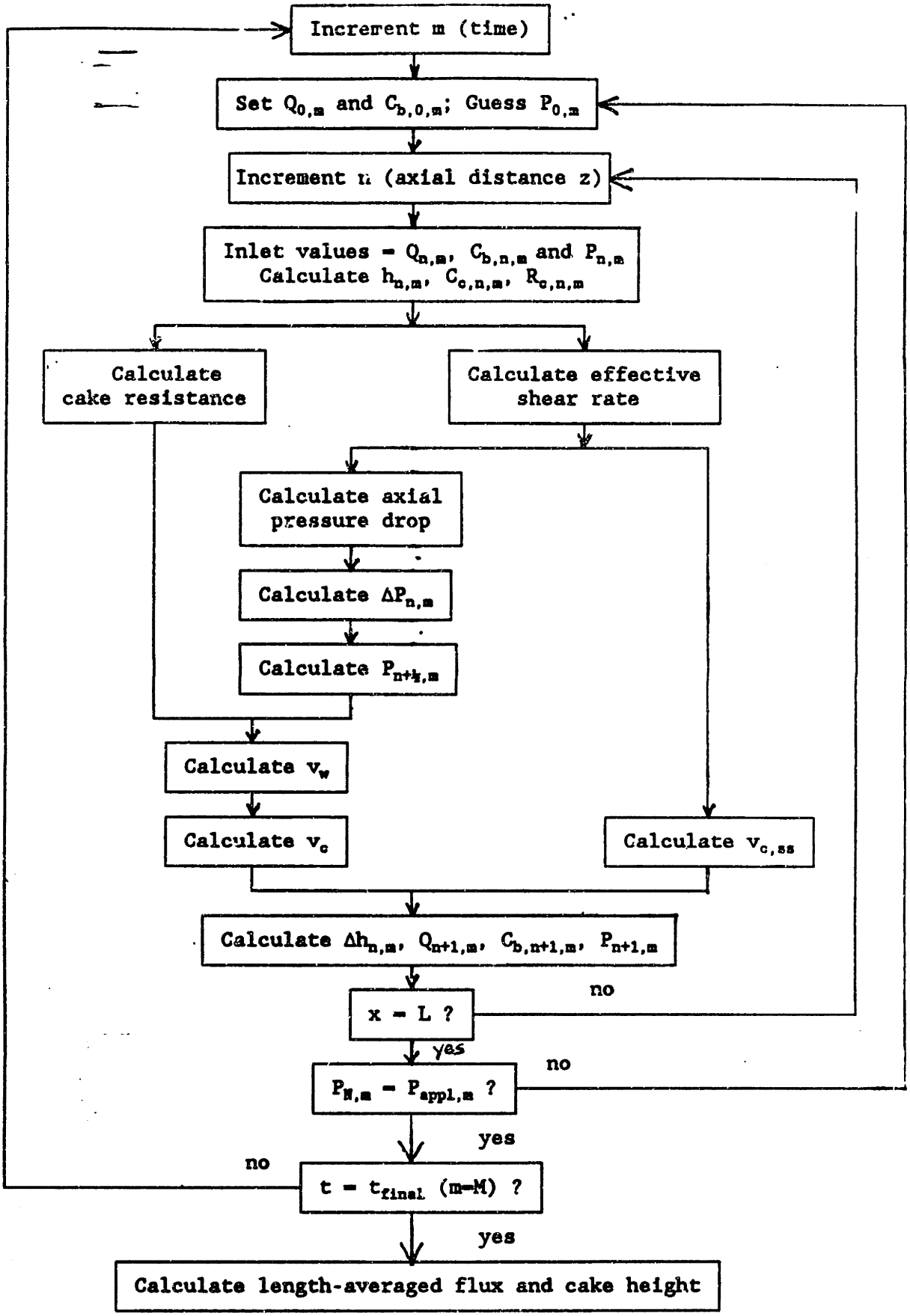

Figure 6-16. Algorithm for calculating $h_{n,m}$

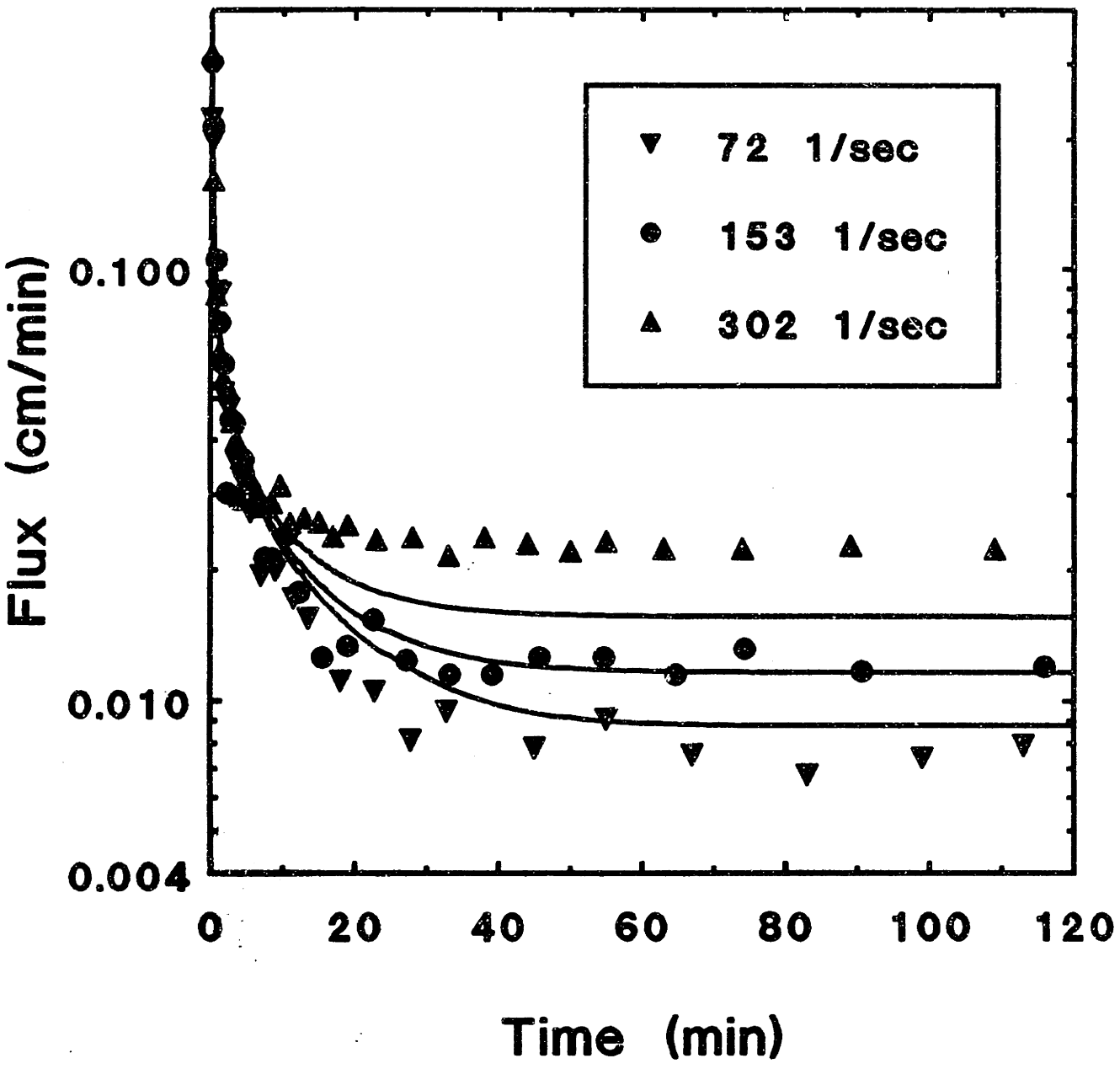

Figure 6-17. Experimental data and model predictions for filtration of an 8.9% suspension of 0.711 μm diameter latex particles in single 4.66 mm ID hollow fibers at $P_{app,out}$ = 75 mmHg and three different shear rates,.

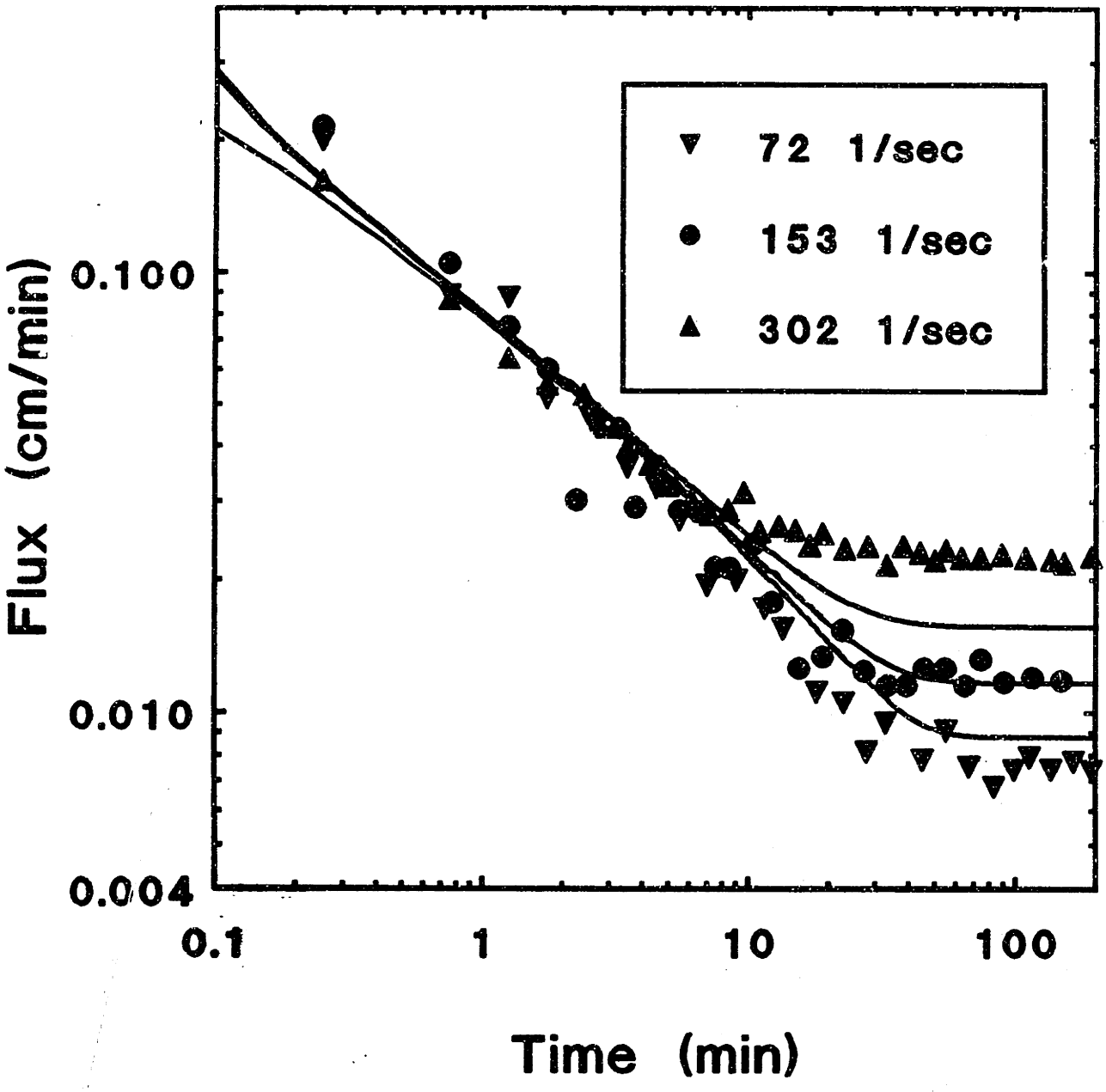

Figure 6-18. Experimental data and model predictions for filtration of an 8.9% suspension of 0.711 μm latex particles in single 4.66 mm ID hollow fibers at $P_{app,out}$ = 75 mmHg and three different shear rates, re-plotted on log-log coordinates.

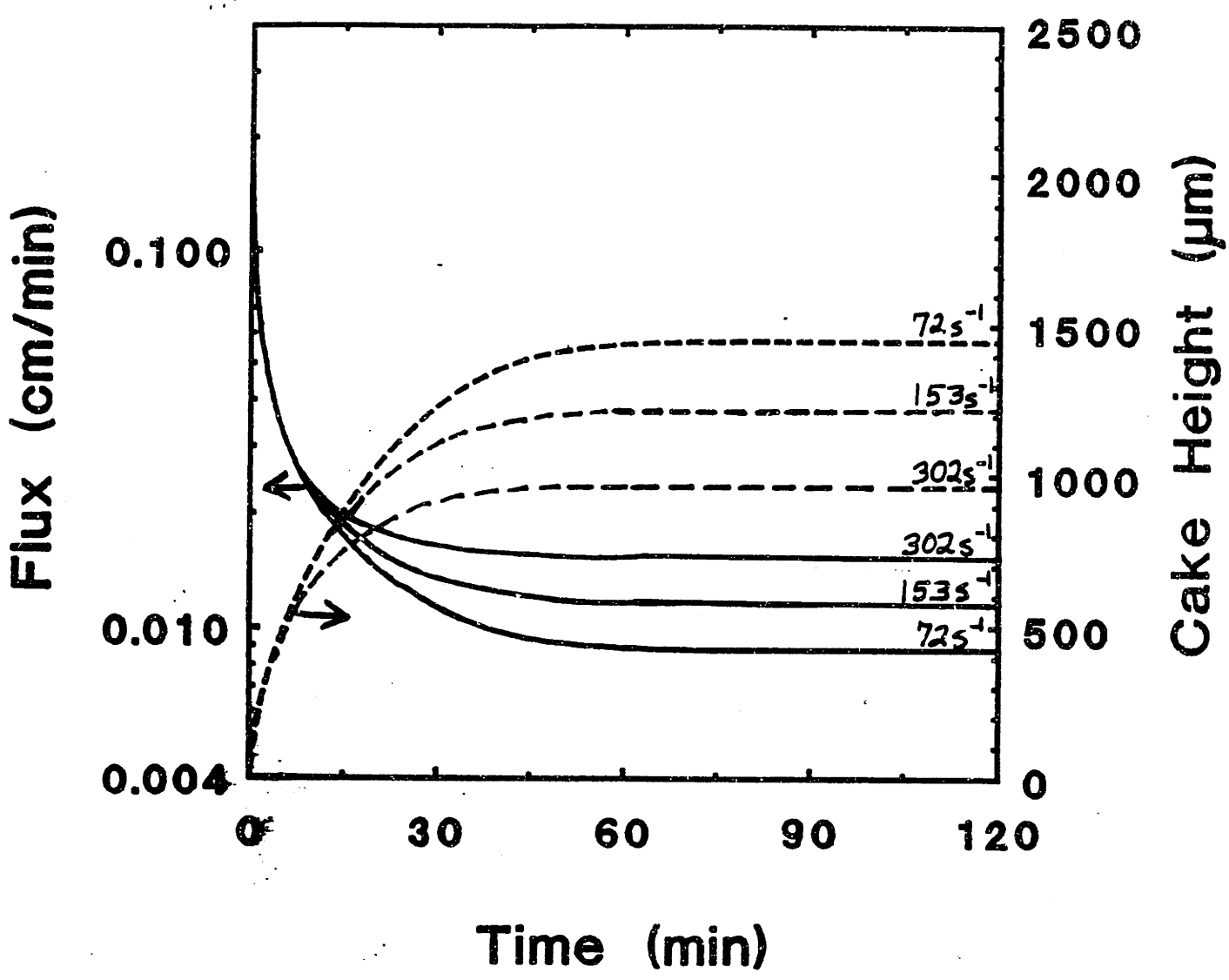

Figure 6-19. Predicted length-averaged flux and cake height as a function of time for filtration of an 8.9% suspension of 0.711 μm latex particles in single 4.66 mm ID hollow fibers at $P_{app,out}$ = 75 mmHg and three shear rates.

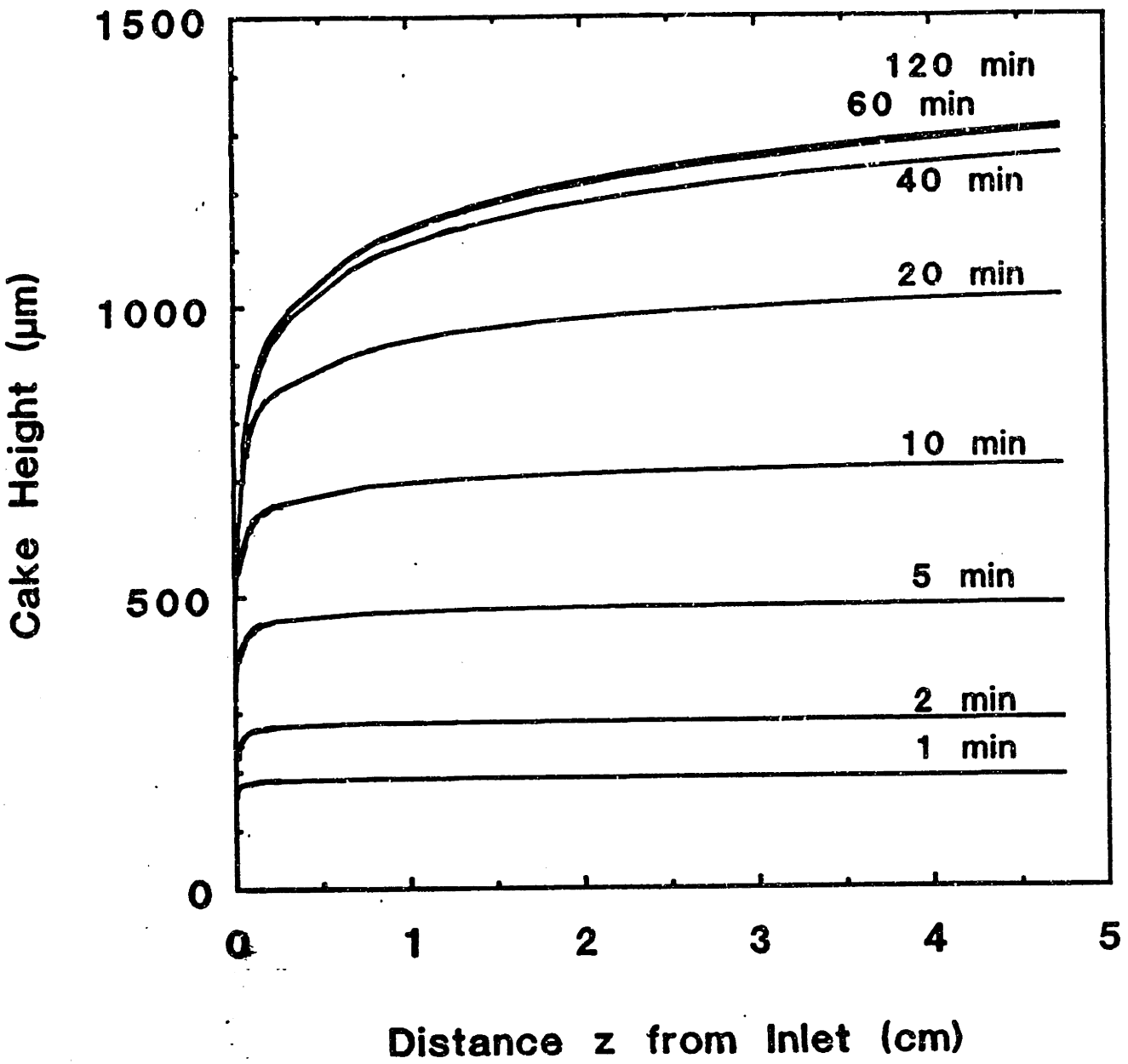

Figure 6-20. Predicted cake height vs. axial position at various times for filtration of an 8.9% suspension of 0.711 μm latex particles in single 4.66 mm ID hollow fibers at $P_{app,out}$ = 75 mmHg and $\gamma_{w,in}$ = 153 s^{-1}.

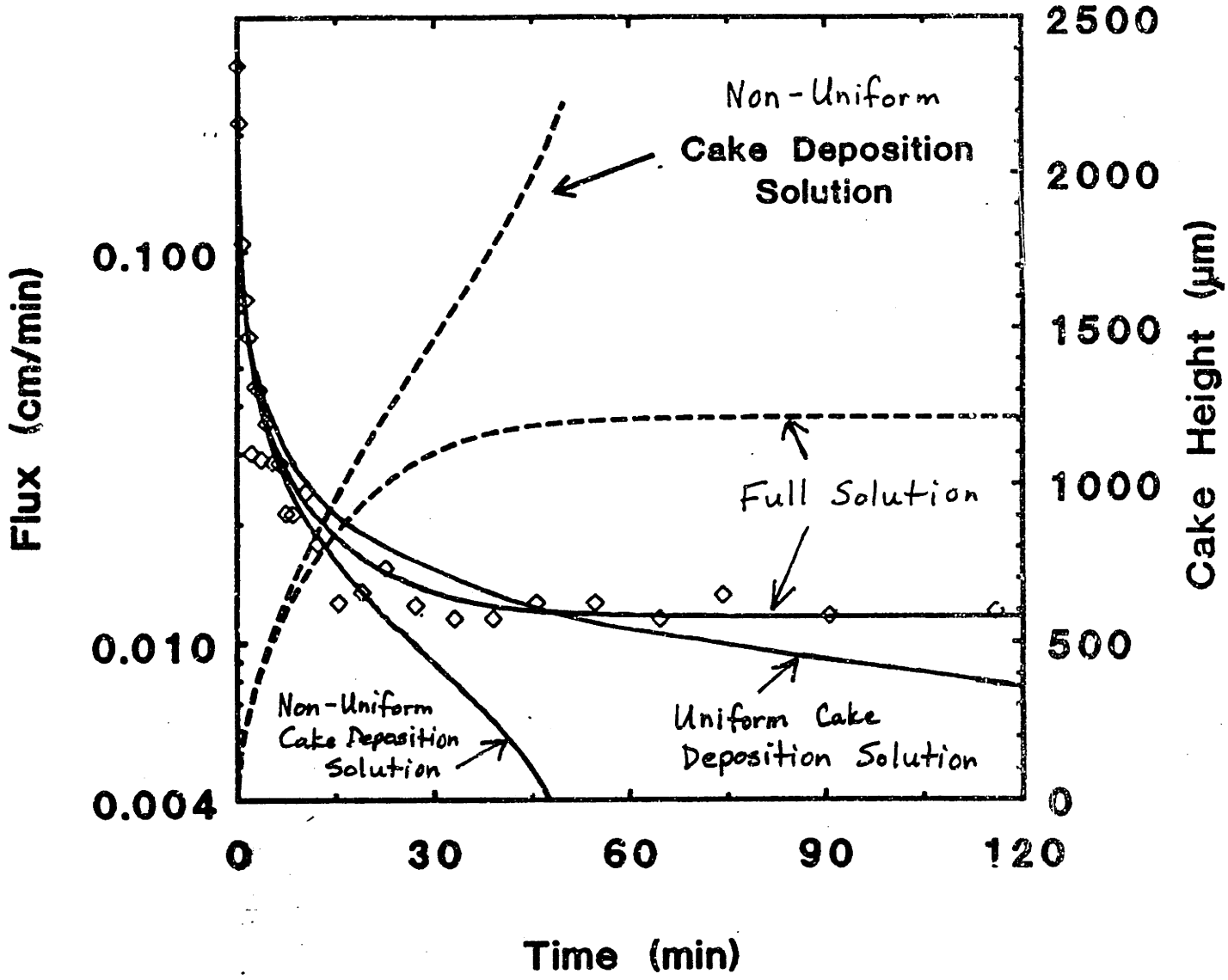

Figure 6-21. Predicted and measured length-averaged flux and predicted length-averaged cake height, re-plotted from Figure 6-18 along with the uniform and non-uniform cake deposition solutions.

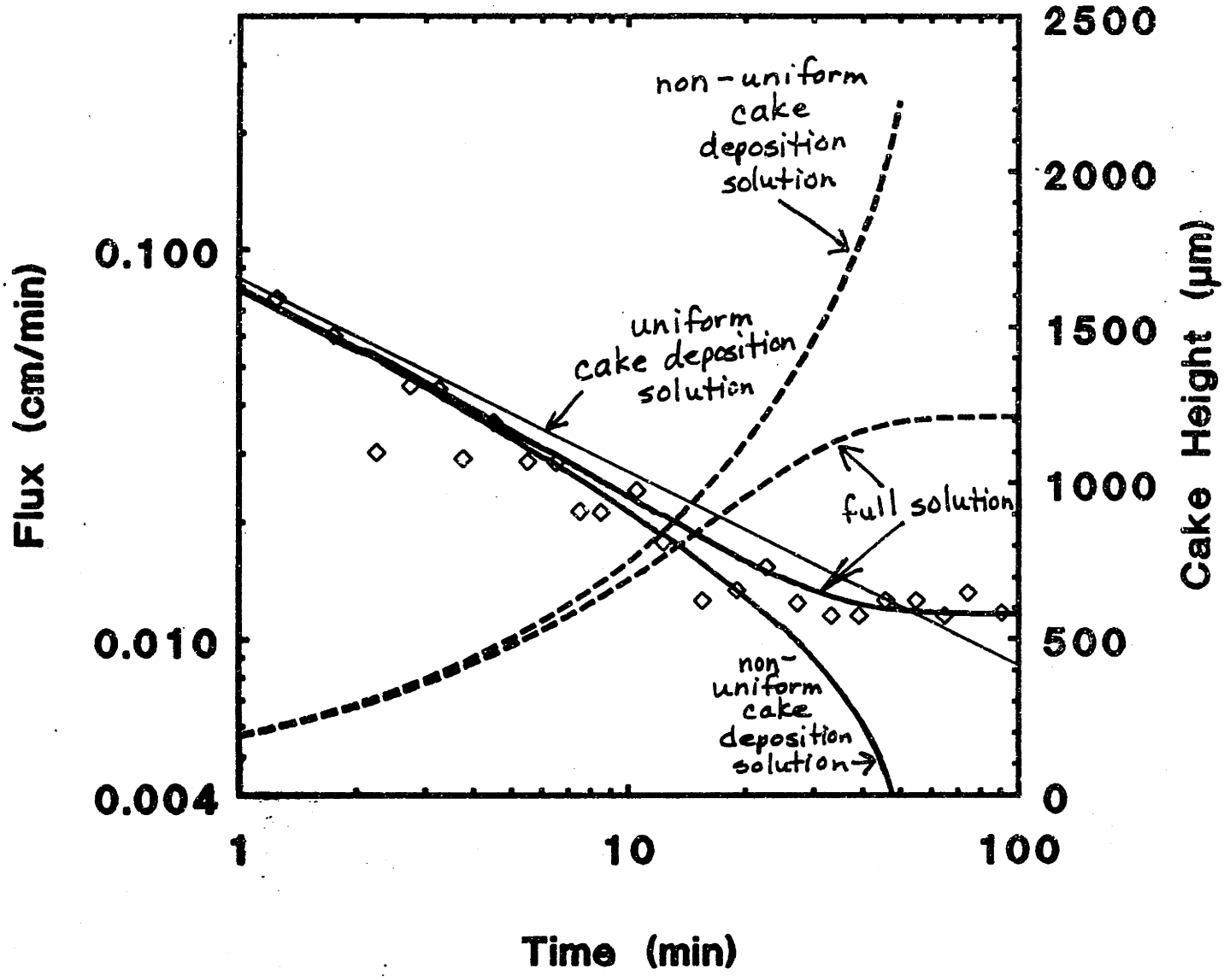

Figure 6-22. Predicted and measured length-averaged flux and predicted length-averaged cake height, re-plotted from Figure 6-21 on log-log coordinates.

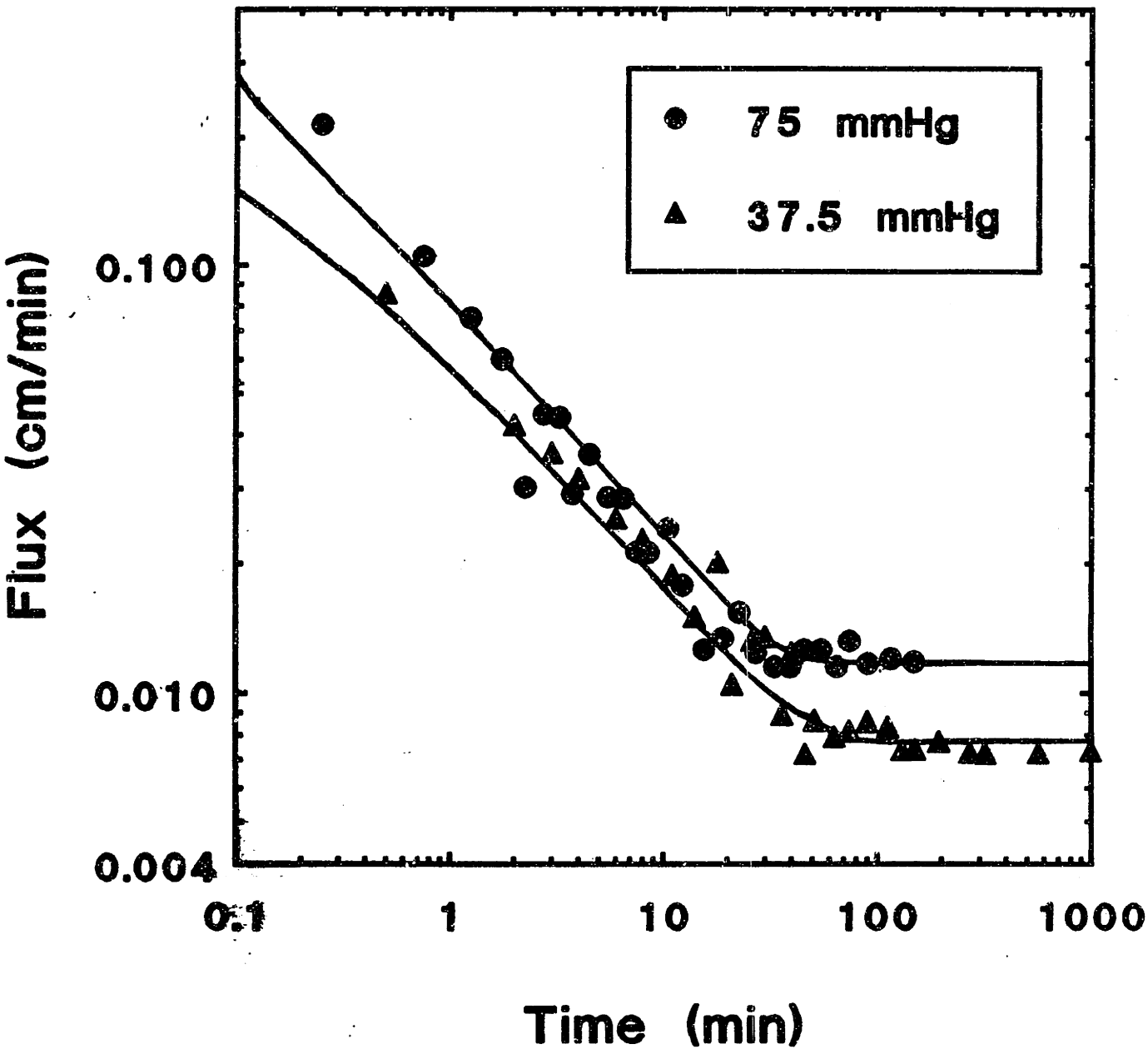

Figure 6-23. Predicted length-averaged flux and cake height as a function of time for filtration of an 8.9% suspension of 0.711 μm latex particles in single 4.66 mm ID hollow fibers at $\gamma_{w,in} = 153\ s^{-1}$ and two applied pressures.

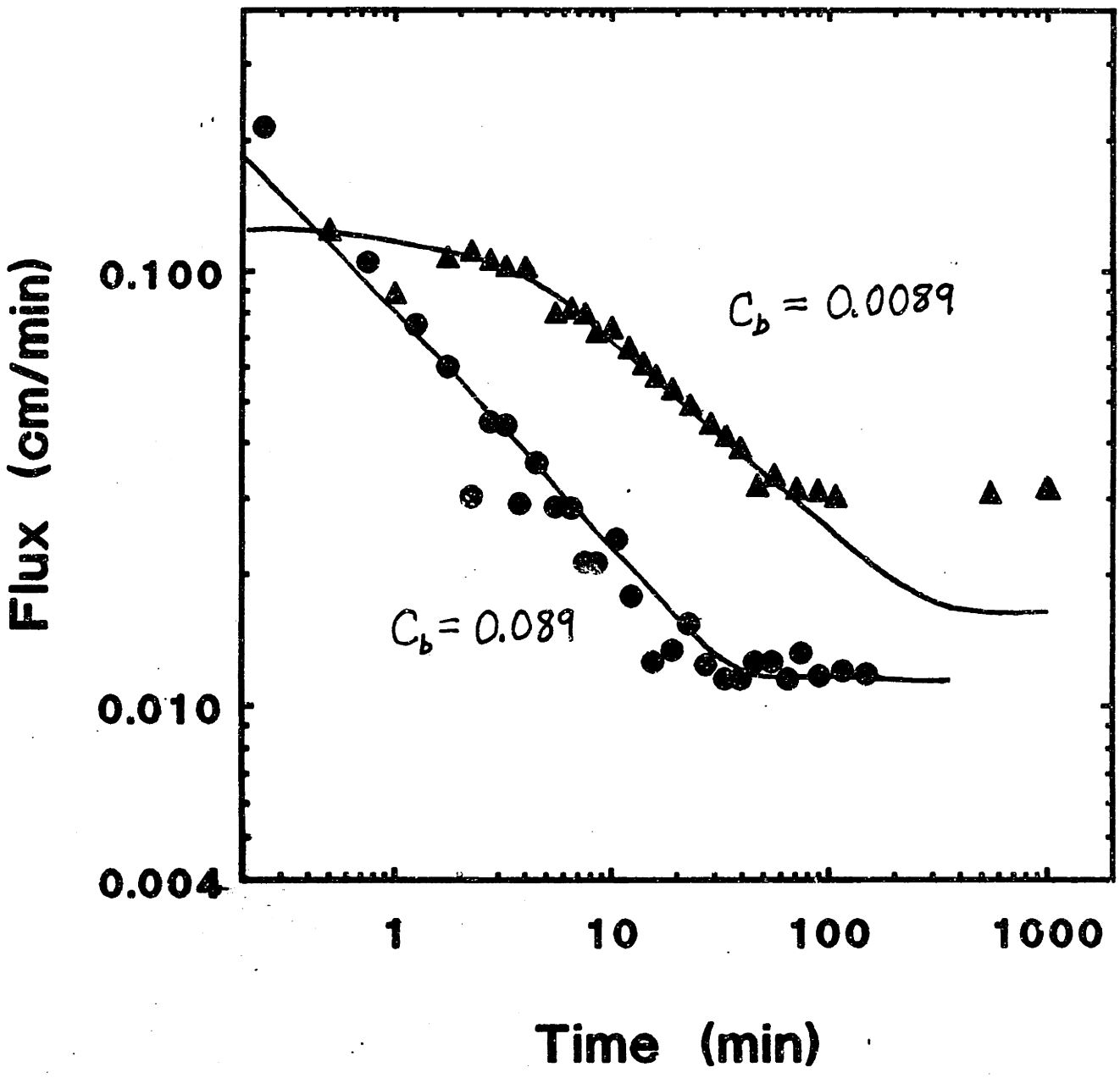

Figure 6-24. Predicted length-averaged flux and cake height as a function of time for filtration of 8.9% and 0.89% suspensions of 0.711 μm latex particles in 4.66 mm ID hollow fibers at $\gamma_{w,in}$=153 s^{-1} and $P_{app,out}$=75 mmHg.

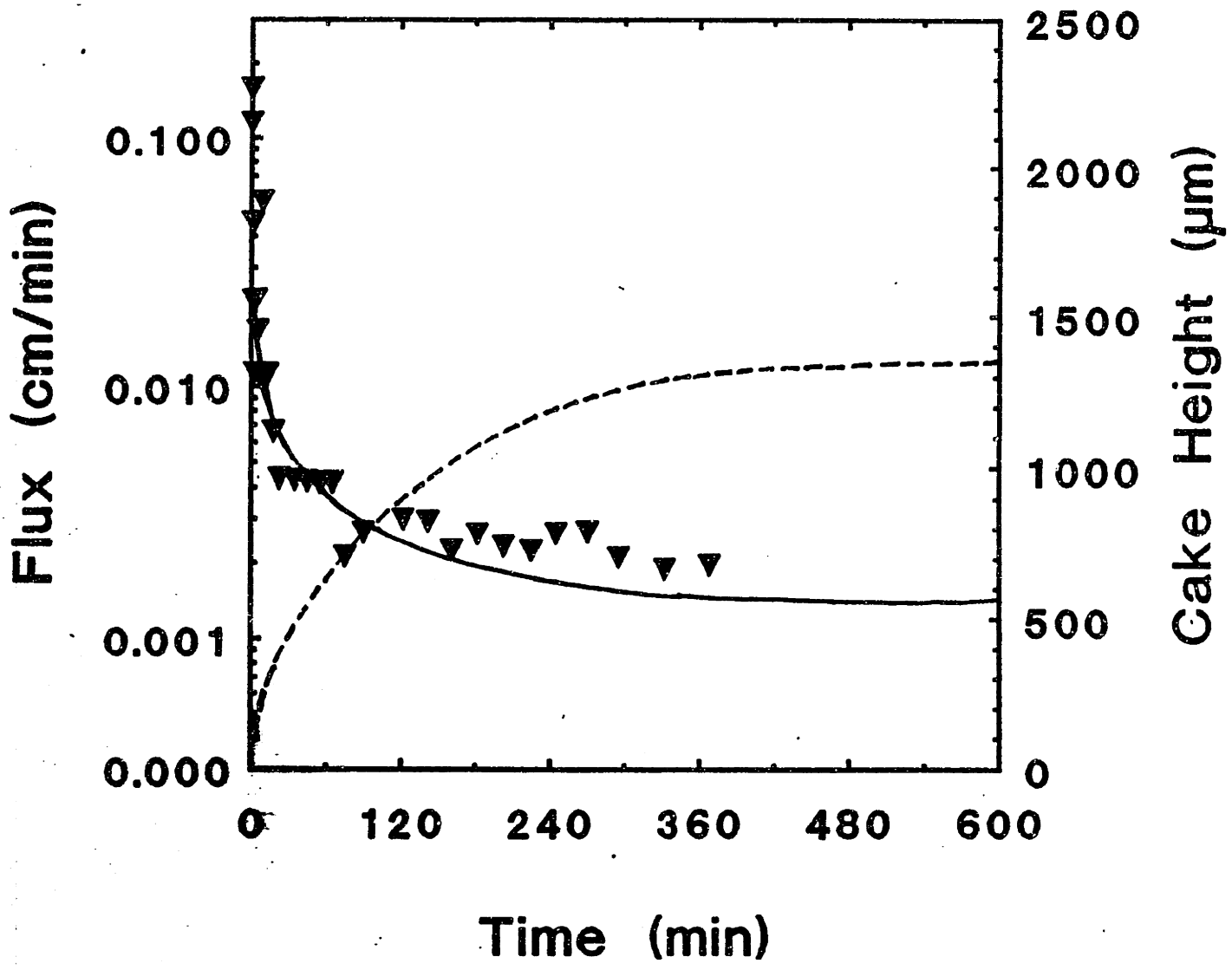

Figure 6-25. Experimental data and model predictions for filtration of a 7.7% suspension of 0.264 μm diameter latex particles at $P_{app,out}$ = 75 mmHg and $\overline{\gamma_{w,in}}$ = 55 s^{-1}.

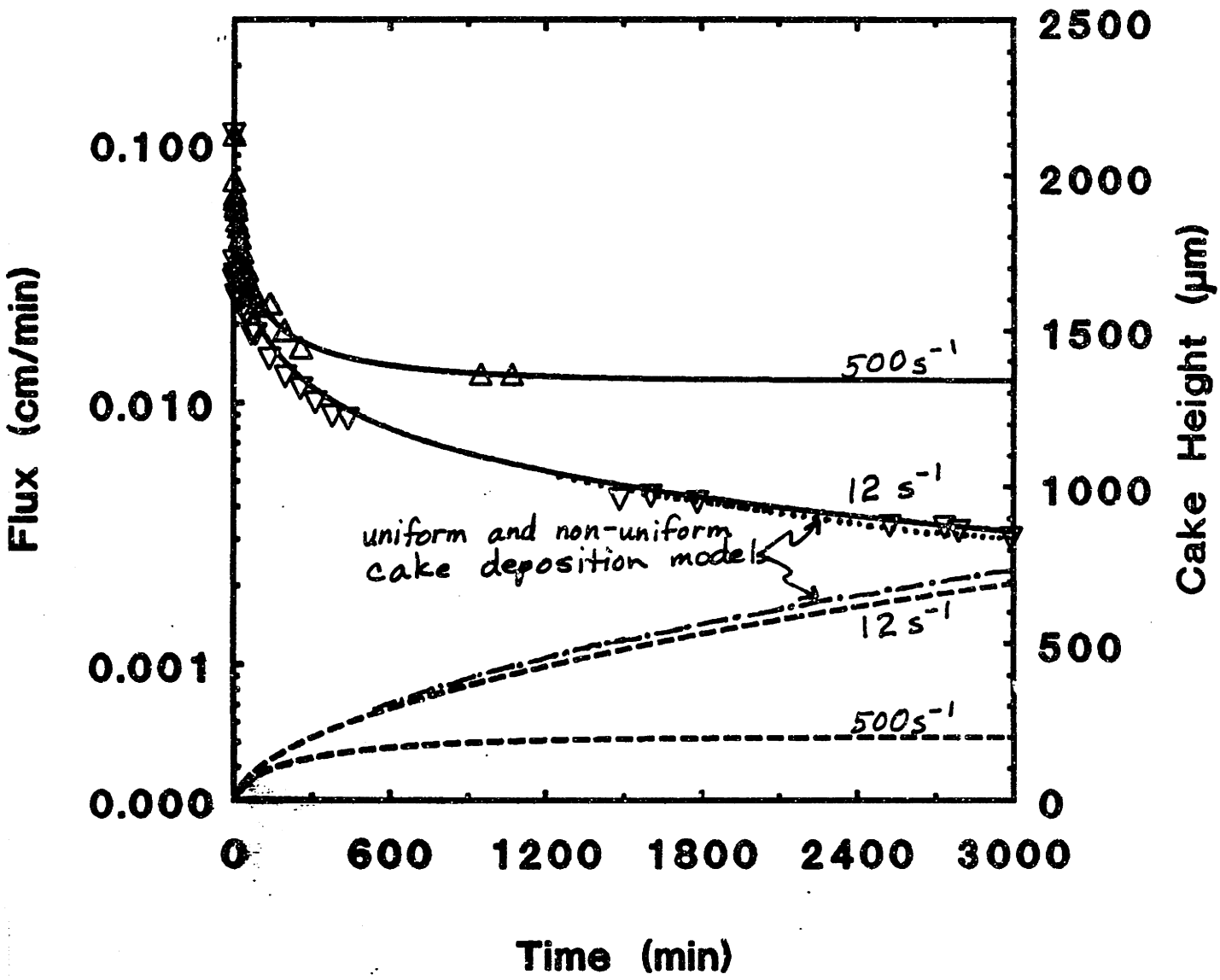

Figure 6-26. Experimental data and model predictions for filtration of a 0.2% suspension of 0.264 μm diameter latex particles at $P_{app,out}$ = 75 mmHg and two different inlet wall shear rates.

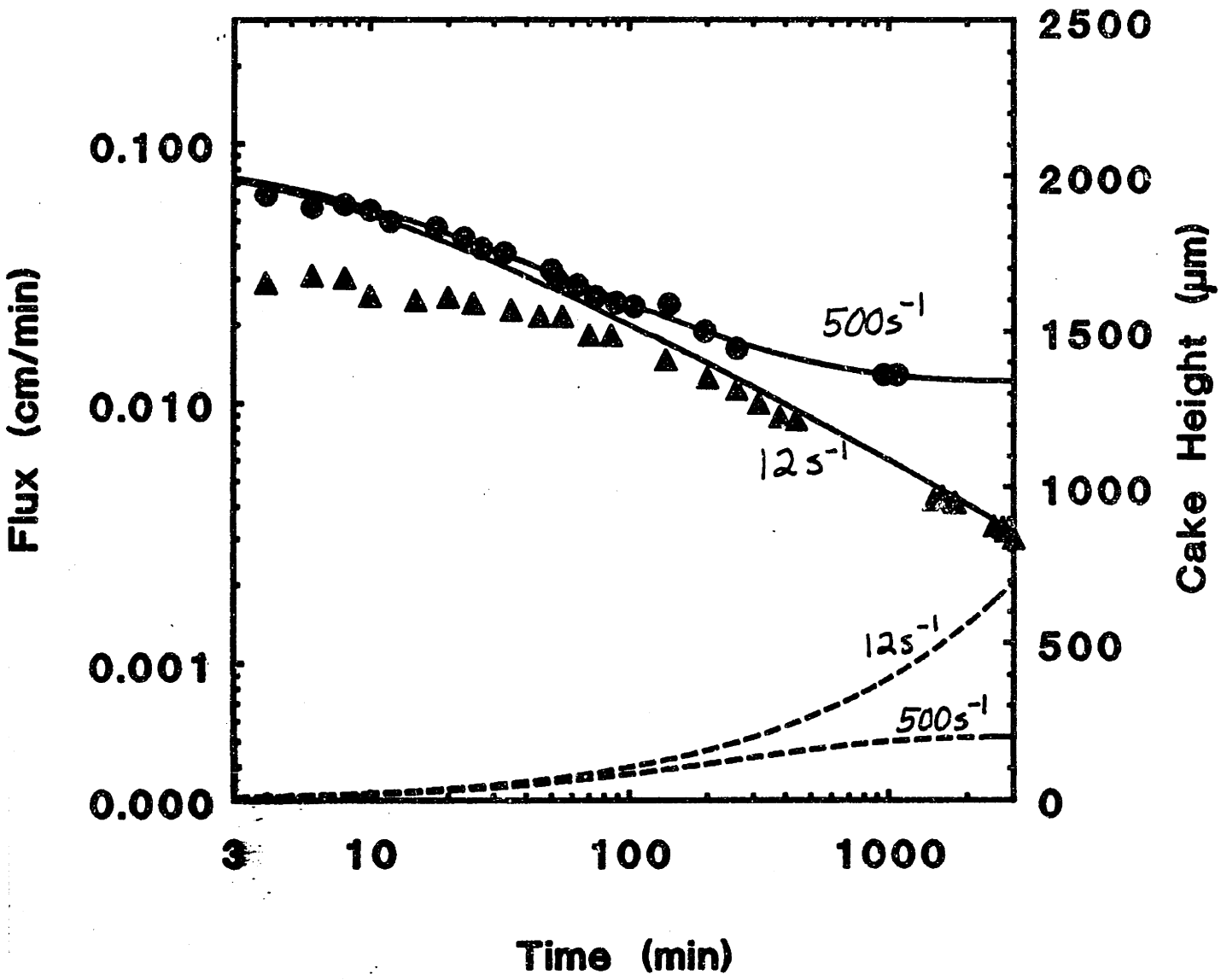

Figure 6-27. Experimental data and model predictions for filtration of a 0.2% suspension of 0.264 μm diameter latex particles at $P_{app,out}$ = 75 mmHg and two different inlet wall shear rates, re-plotted on log-log coordinates.

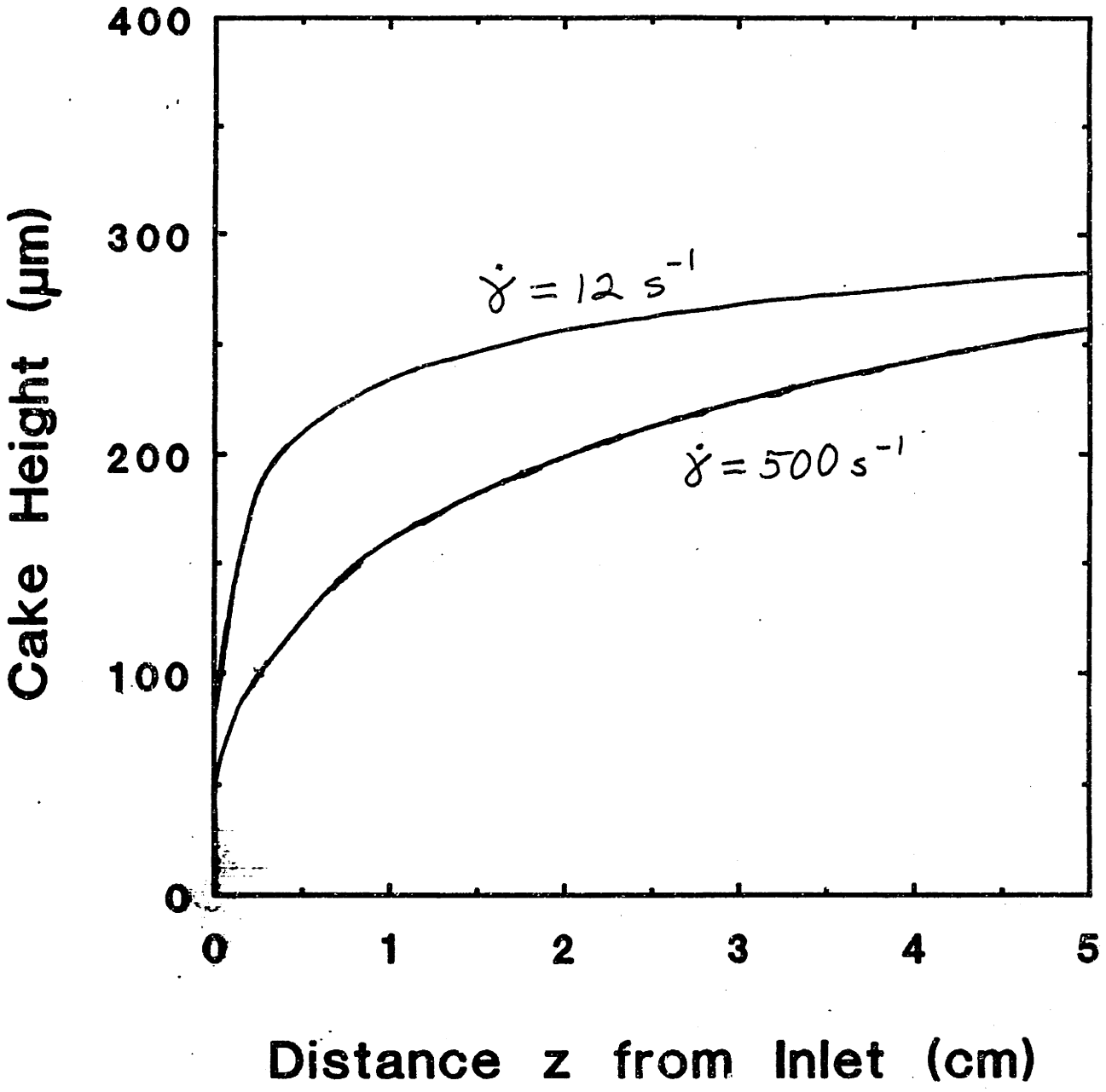

Figure 6-28. Predicted cake height vs. axial position at t=3000 min for filtration of a 0.2% suspension of 0.264 μm latex particles in single 4.66 mm ID hollow fibers at $P_{app,out}$ = 75 mmHg and two inlet wall shear rates.

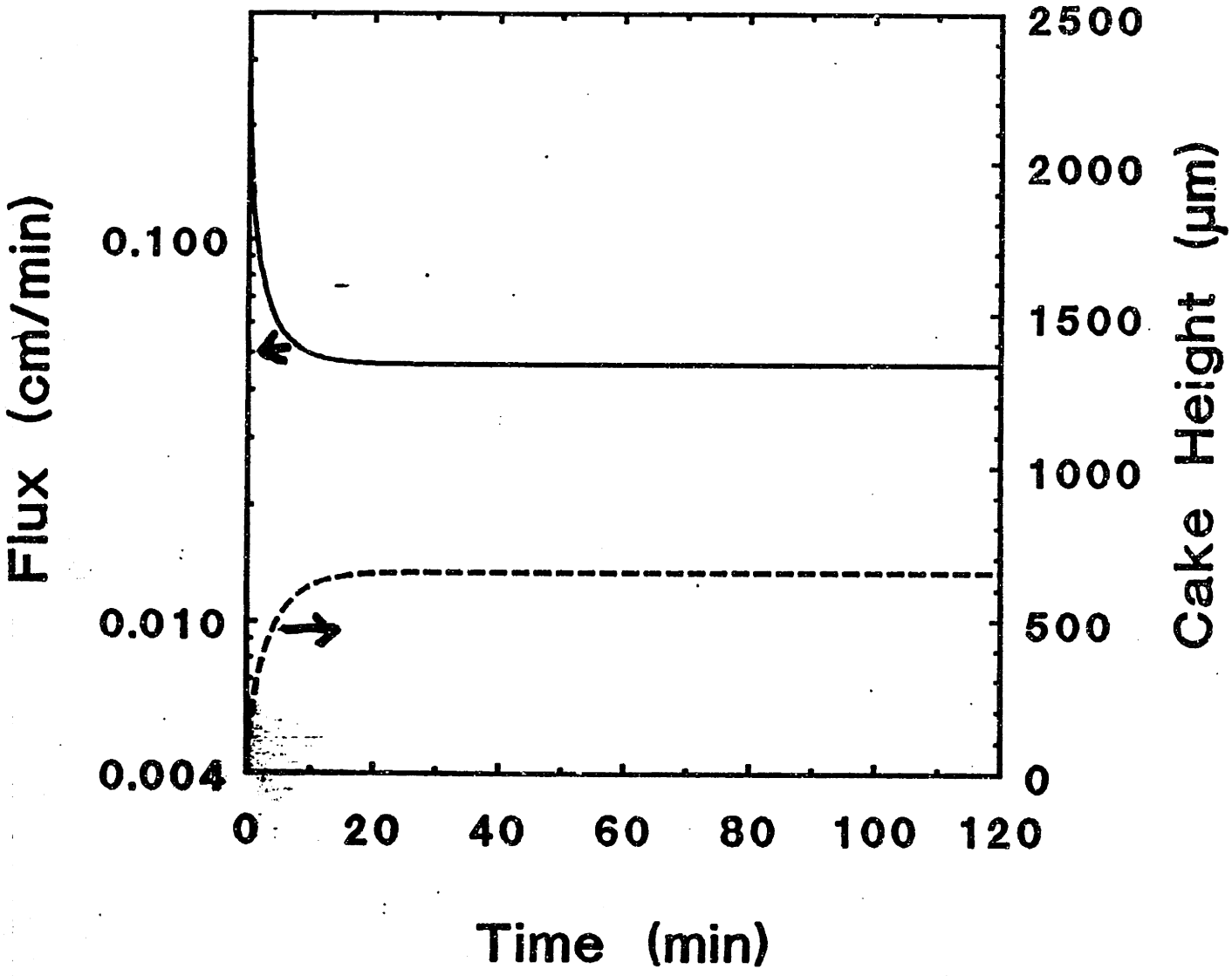

Figure 6-29. Predicted length-averaged flux and cake height as a function of time for the base case. (See Table II for parameter values.)

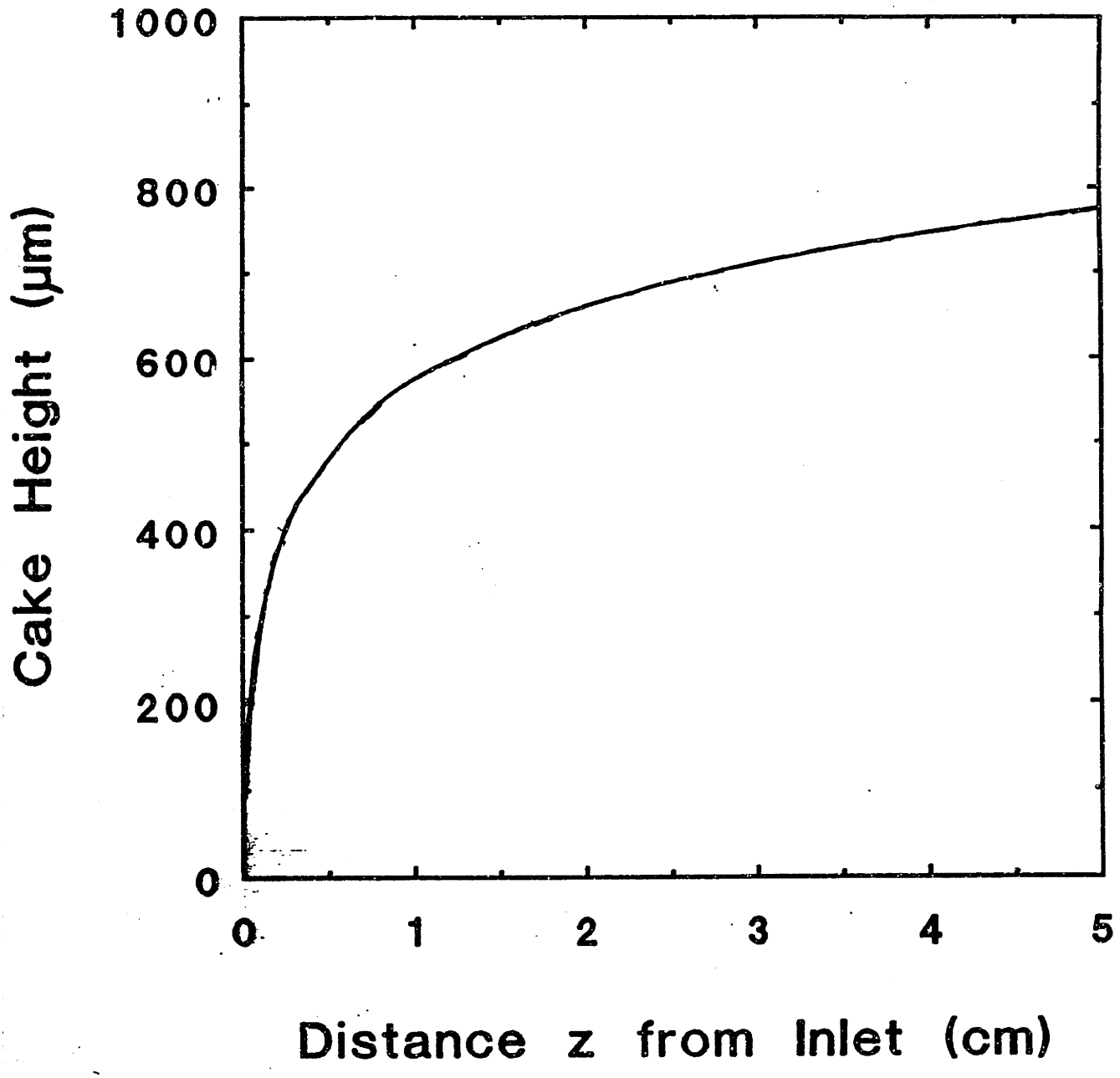

Figure 6-30. Predicted cake height as a function of axial distance for the base case. (See Table II for parameter values.)

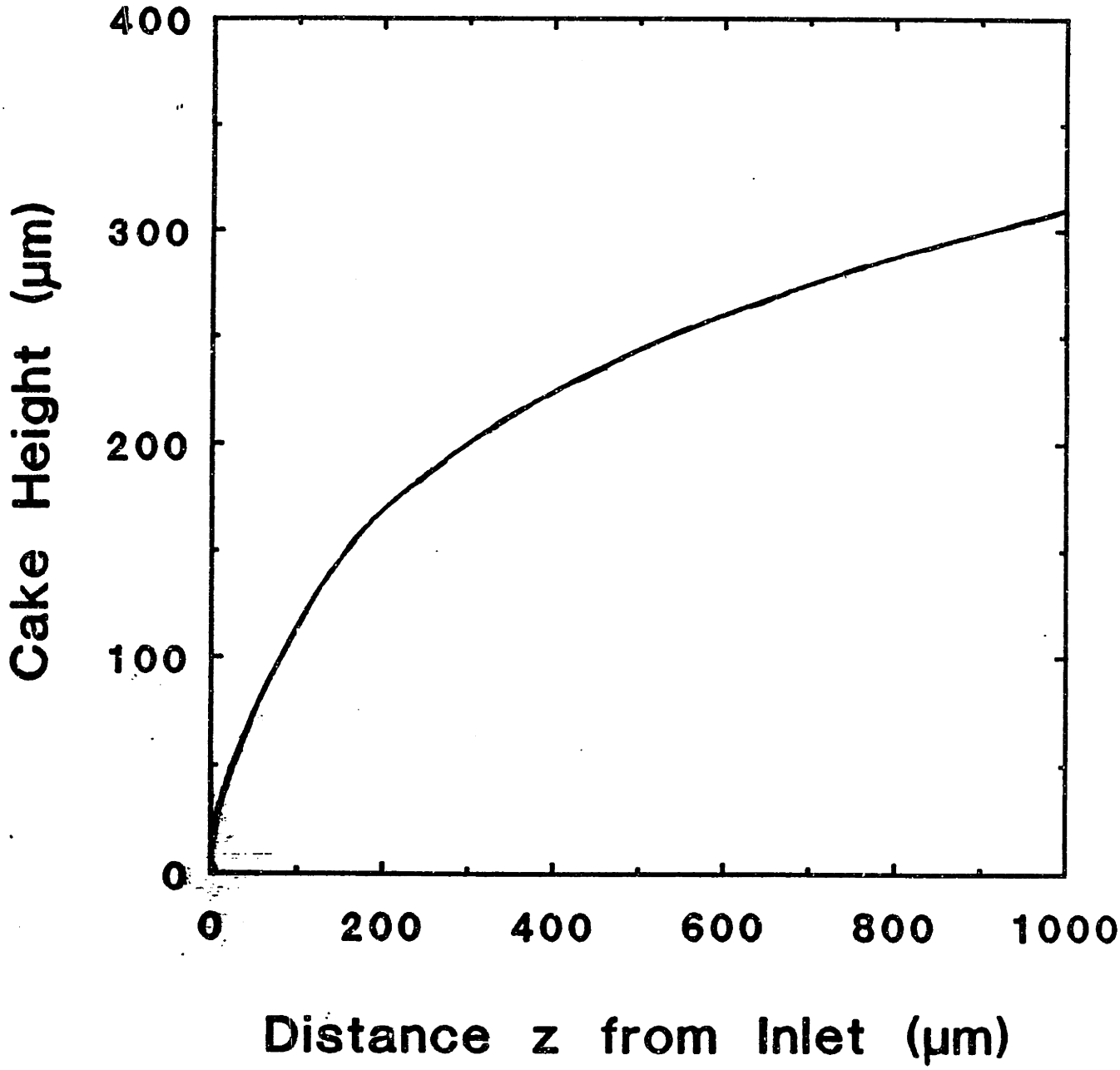

Figure 6-31. Predicted cake height as a function of axial distance for the base case, expanded to show inlet region. (See Table II for parameter values.)

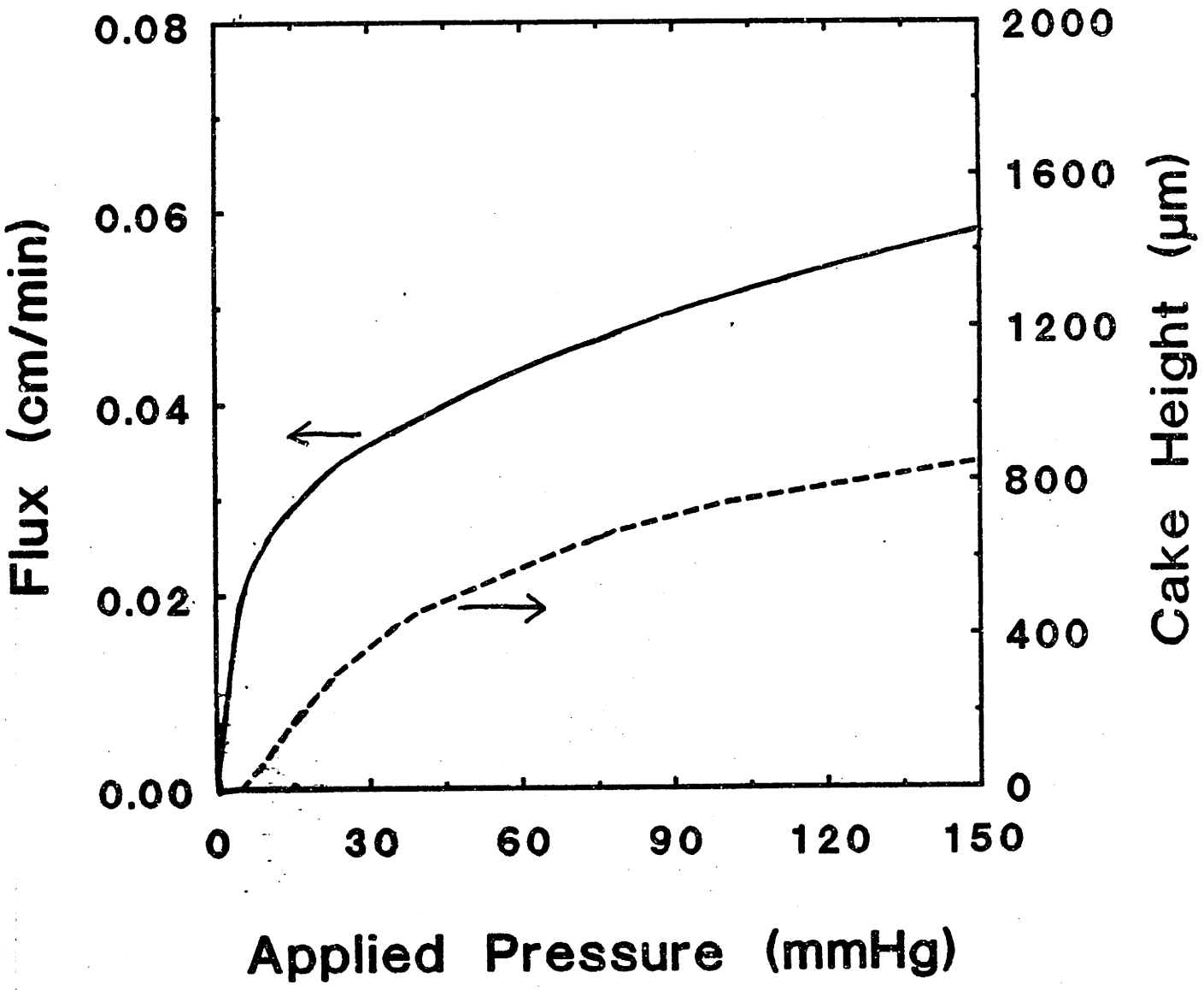

Figure 6-32. Predicted length-averaged steady-state flux and cake height as a function of applied pressure.

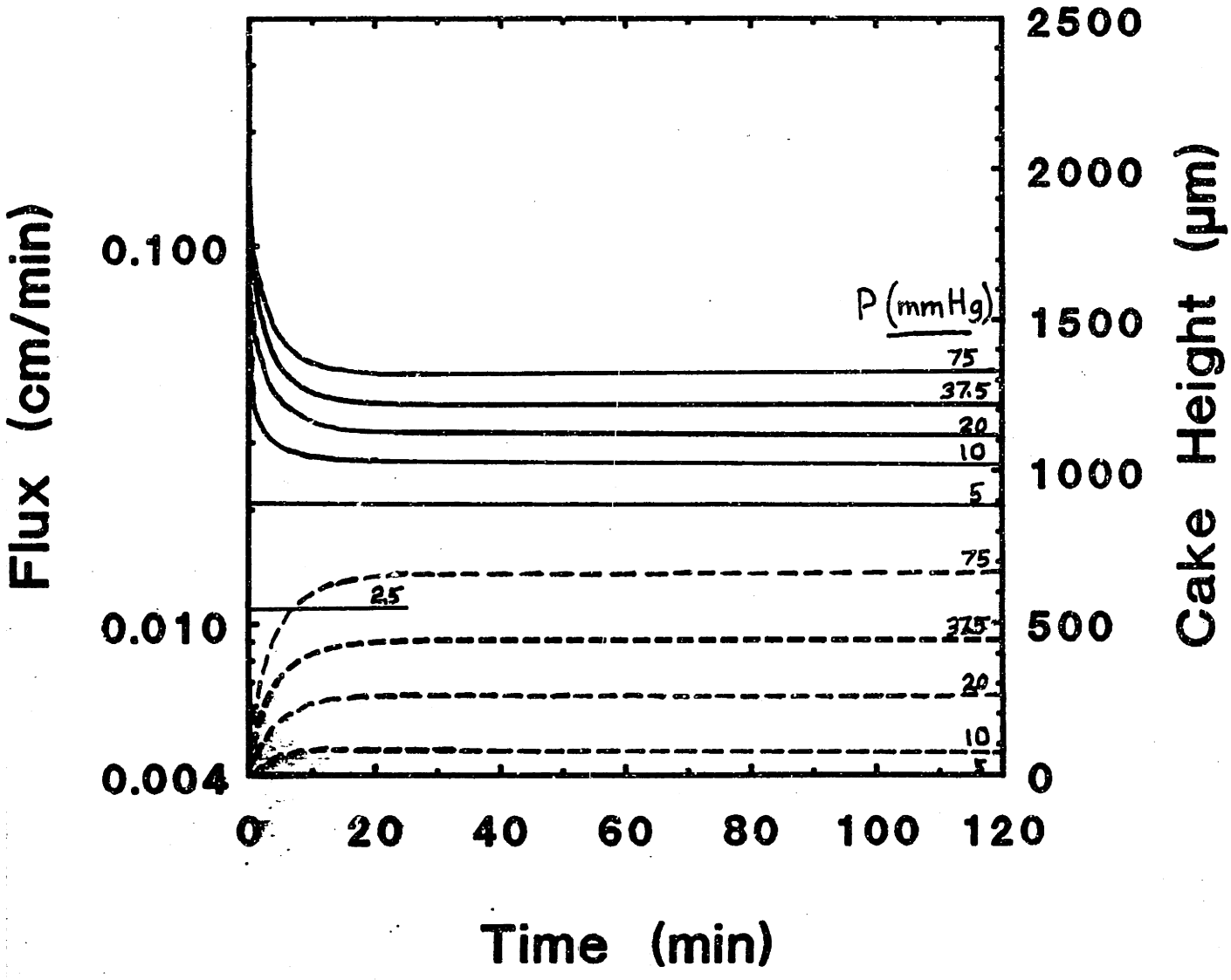

Figure 6-33. Predicted length-averaged steady-state flux and cake height as a function of time for several applied pressures.

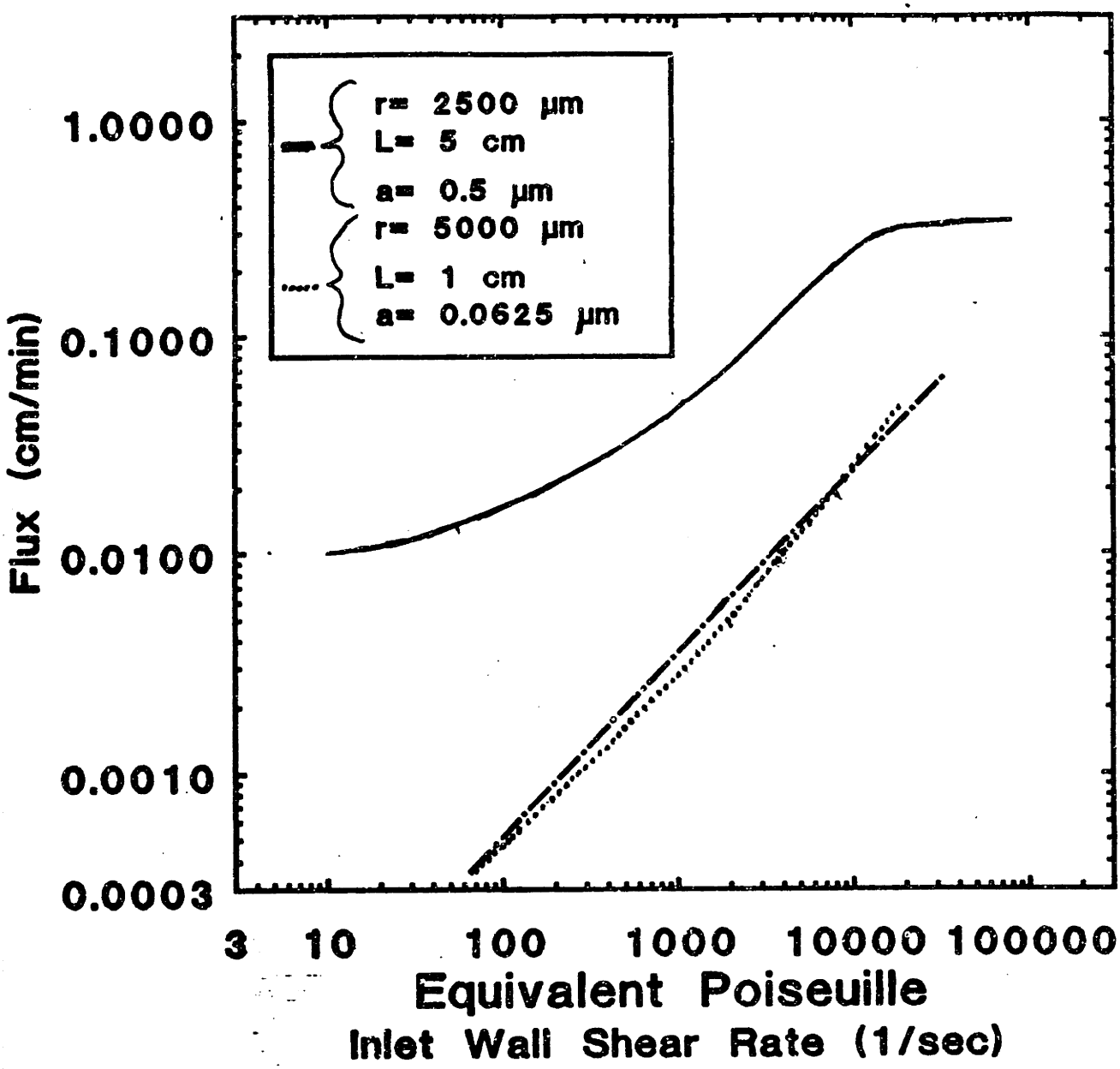

Figure 6-34. Predicted length-averaged steady-state flux as a function of equivalent Poiseuille inlet wall shear rate.

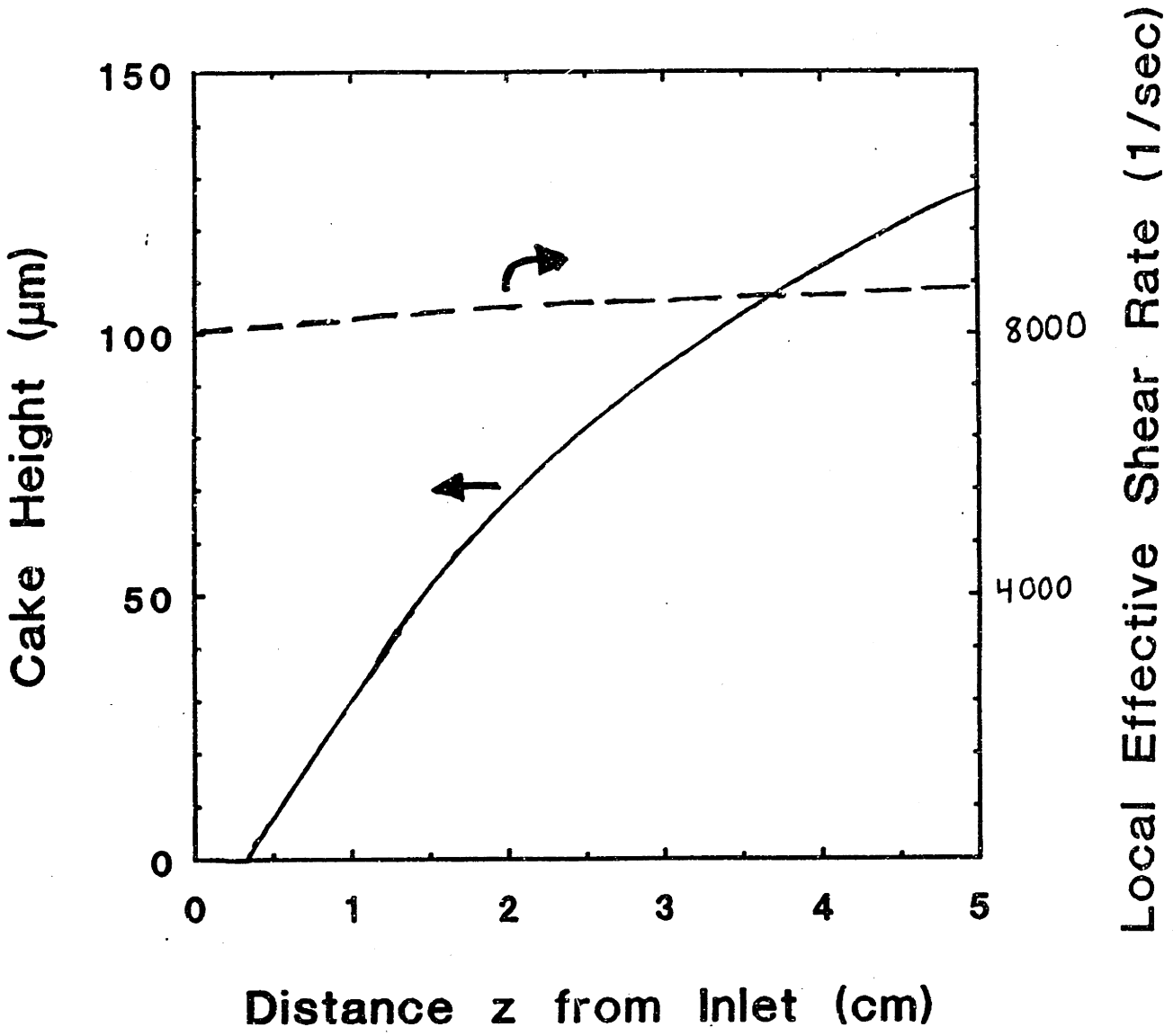

Figure 6-35. Cake height and local effective shear rate as a function of axial position for 0.125 μm diameter particles at an inlet wall shear rate of 8000 s^{-1}. (Other parameters same as base case values listed in Table II.)

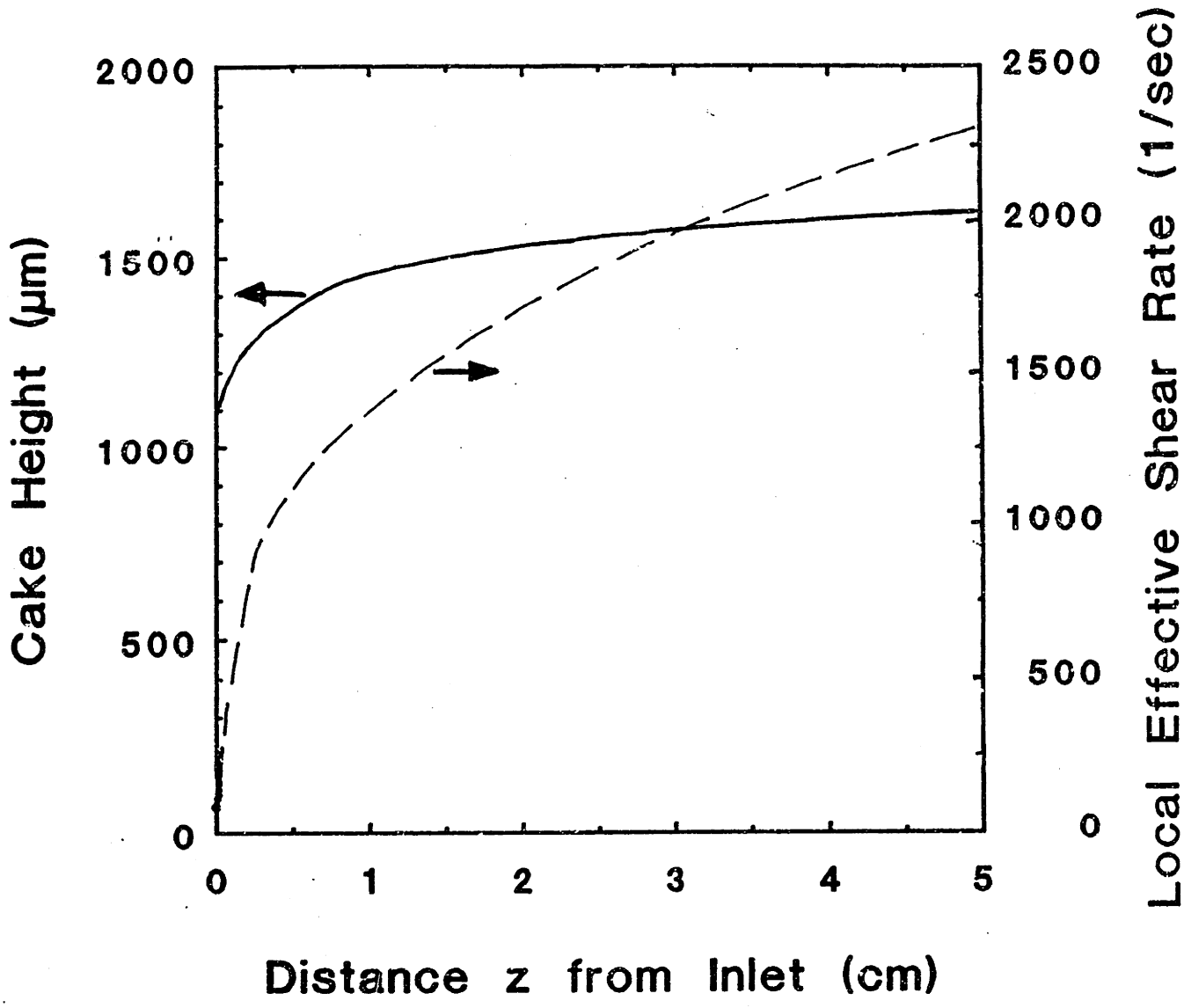

Figure 6-36. Cake height and local effective shear rate as a function of axial position for 1.0 μm diameter particles at an inlet wall shear rate of 100 s^{-1}. (Other parameters same as base case values listed in Table II.)

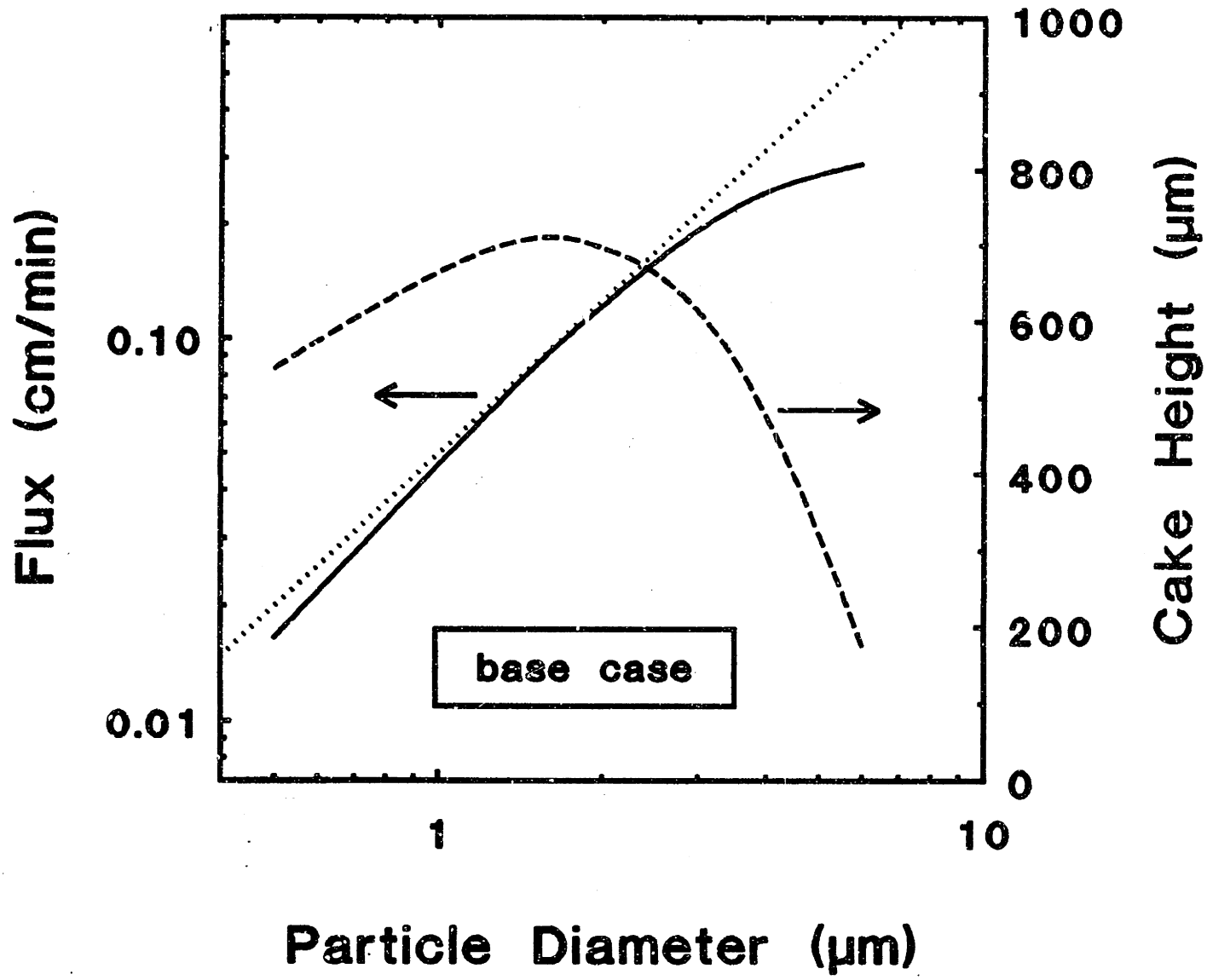

Figure 6-37. Predicted length-averaged steady-state flux and cake height as a function of particle diameter for the base case.

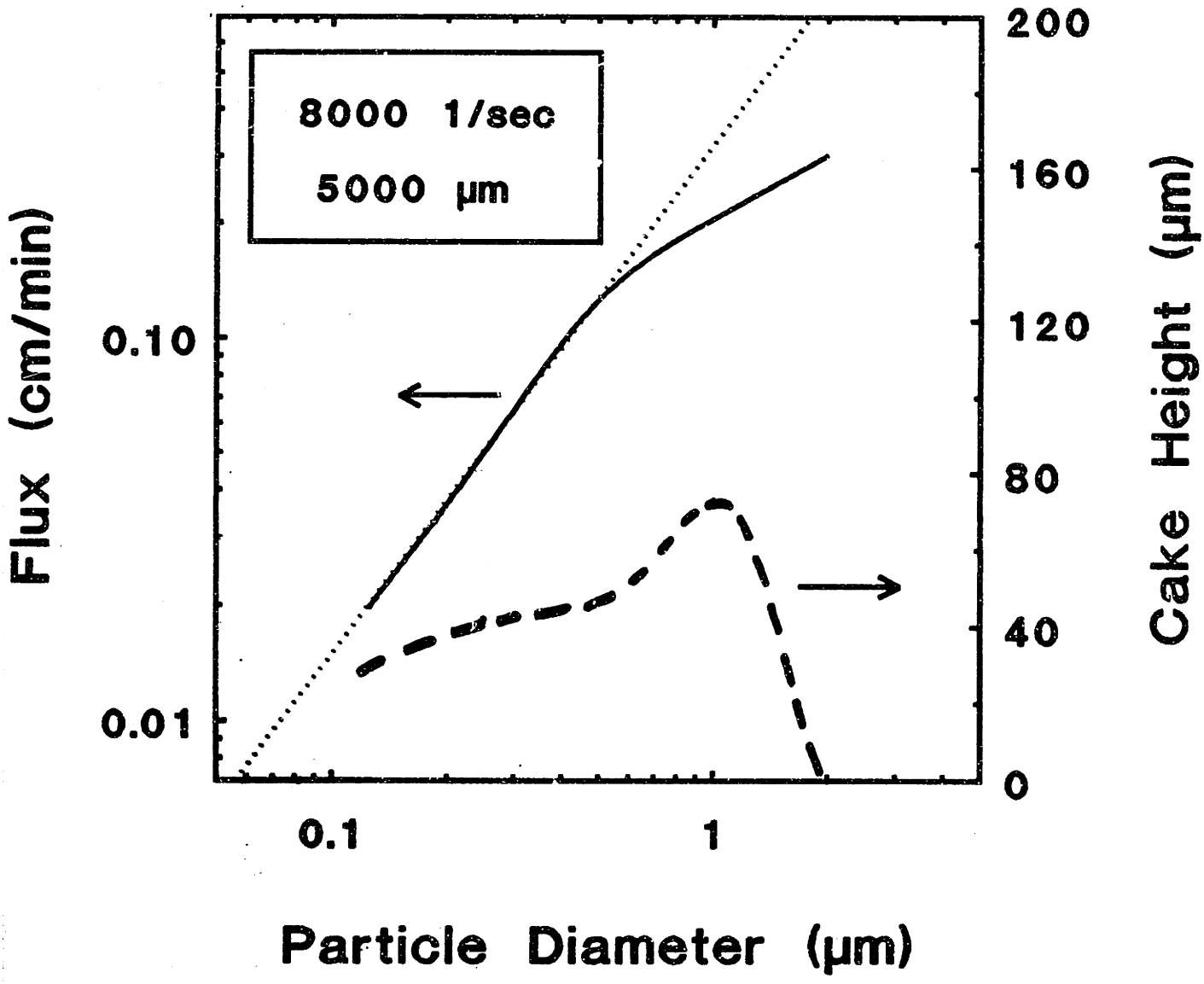

Figure 6-38. Predicted length-averaged steady-state flux and cake height as a function of particle diameter for a shear rate of 8000 s^{-1} and a fiber radius of 5000 μm (all other parameters same as the base case).

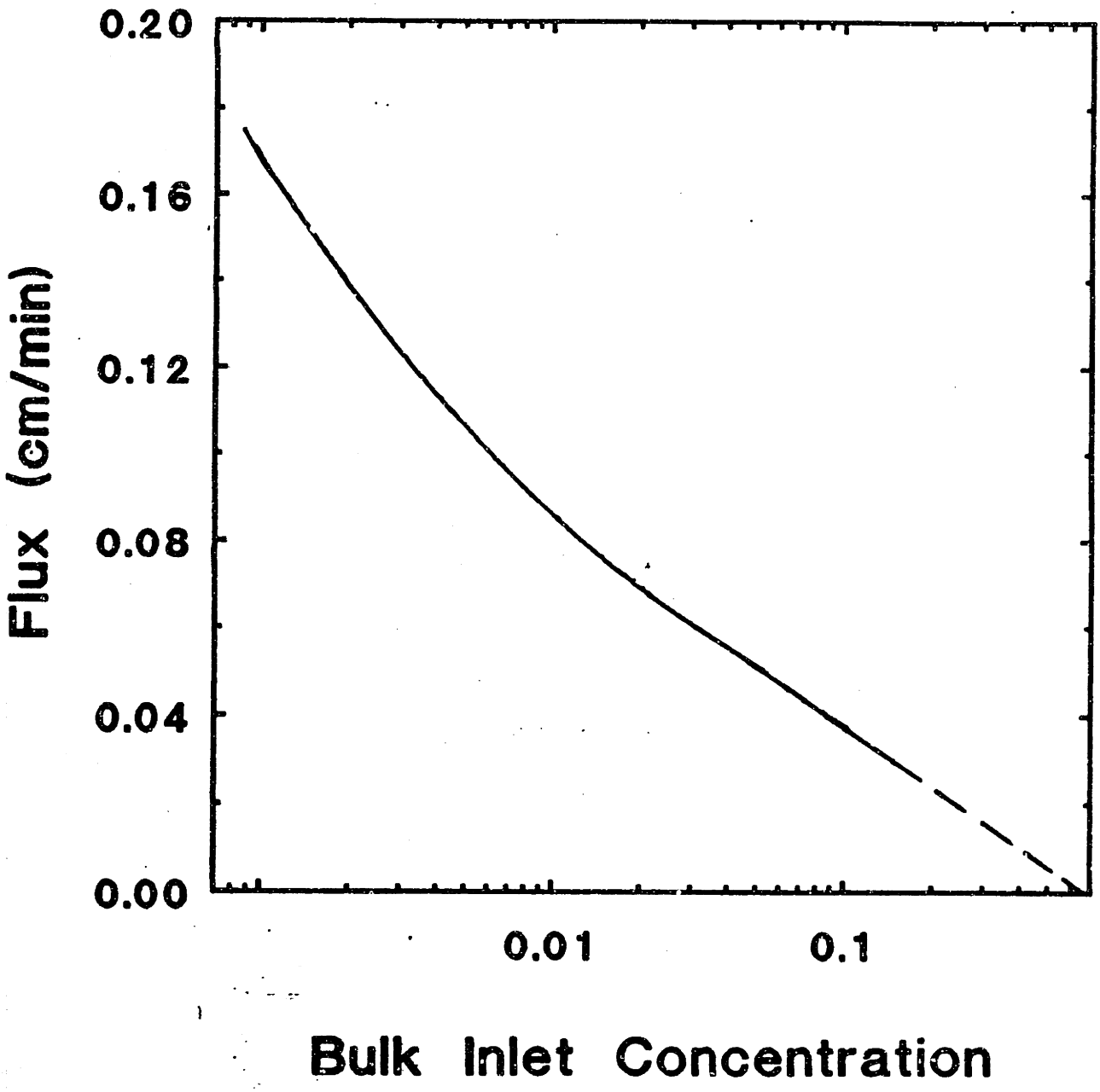

Figure 6-39. Predicted length-averaged steady-state flux as a function of bulk inlet concentration.

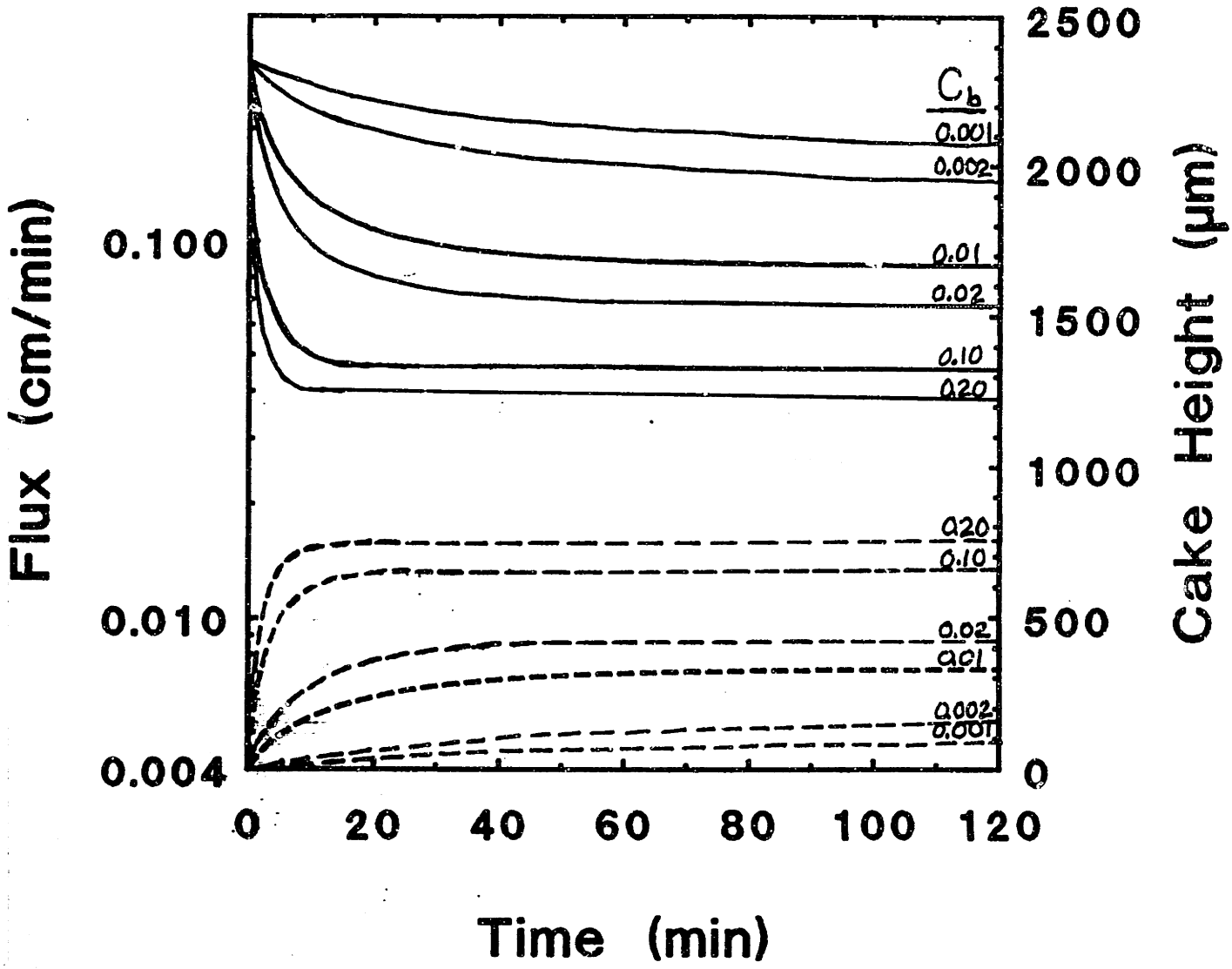

Figure 6-40. Predicted length-averaged steady-state flux and cake height as a function of time for several bulk inlet concentrations.

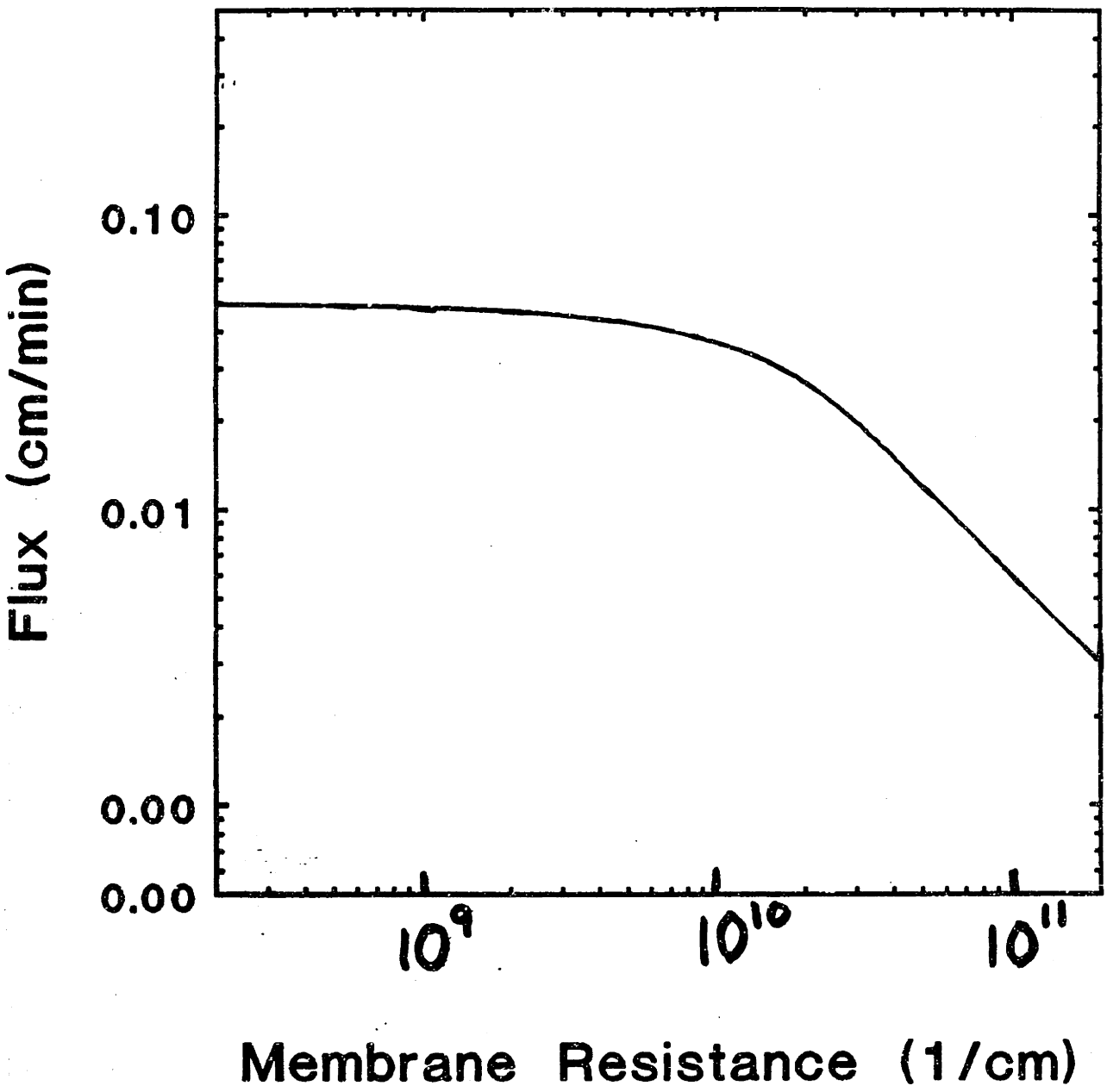

Figure 6-41. Predicted length-averaged steady-state flux as a function of membrane resistance.

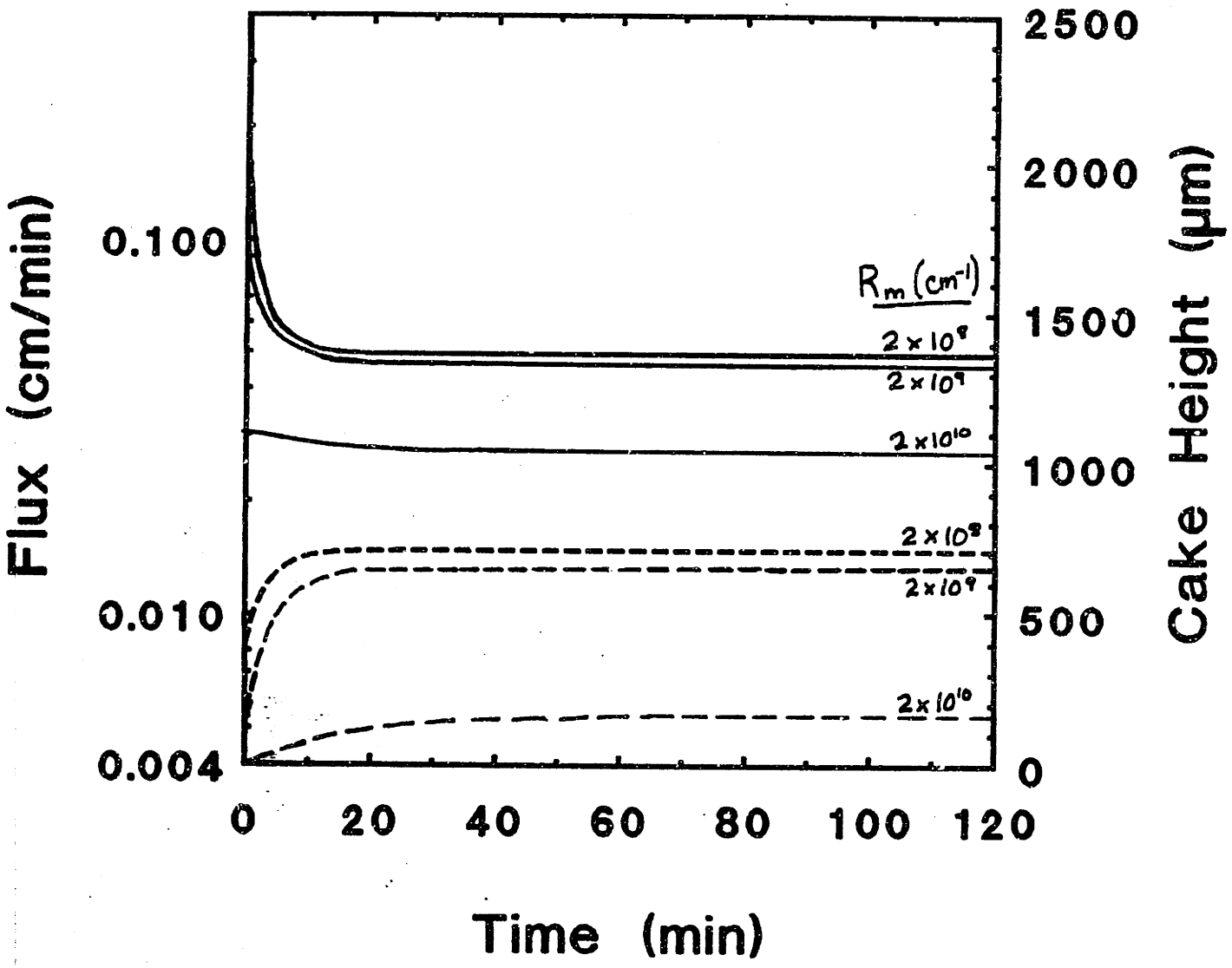

Figure 6-42. Predicted length-averaged steady-state flux and cake height as a function of time for several membrane resistances.

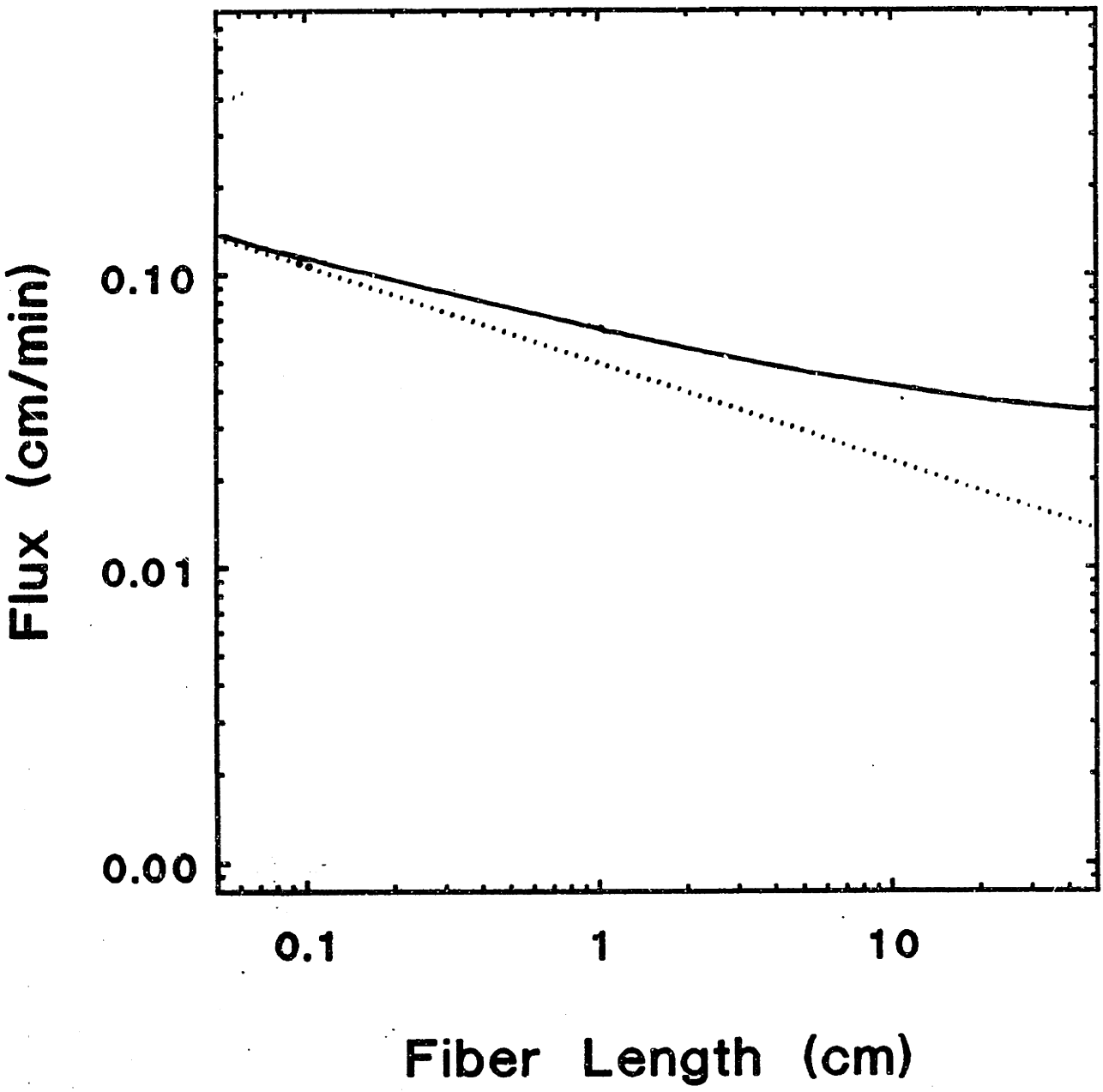

Figure 6-43. Predicted length-averaged steady-state flux as a function of fiber length.

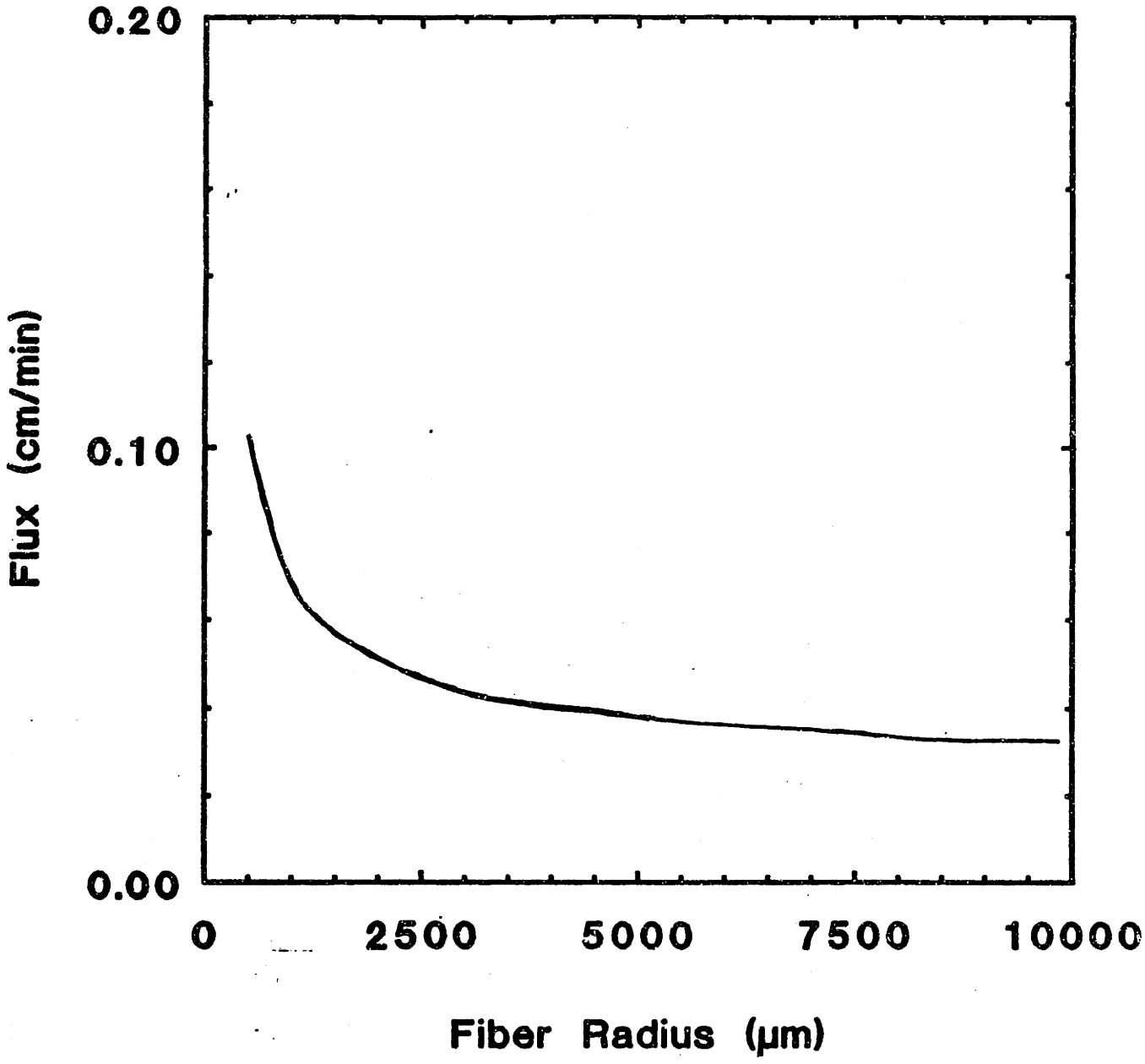

Figure 6-44. Predicted length-averaged steady-state flux as a function of fiber radius.

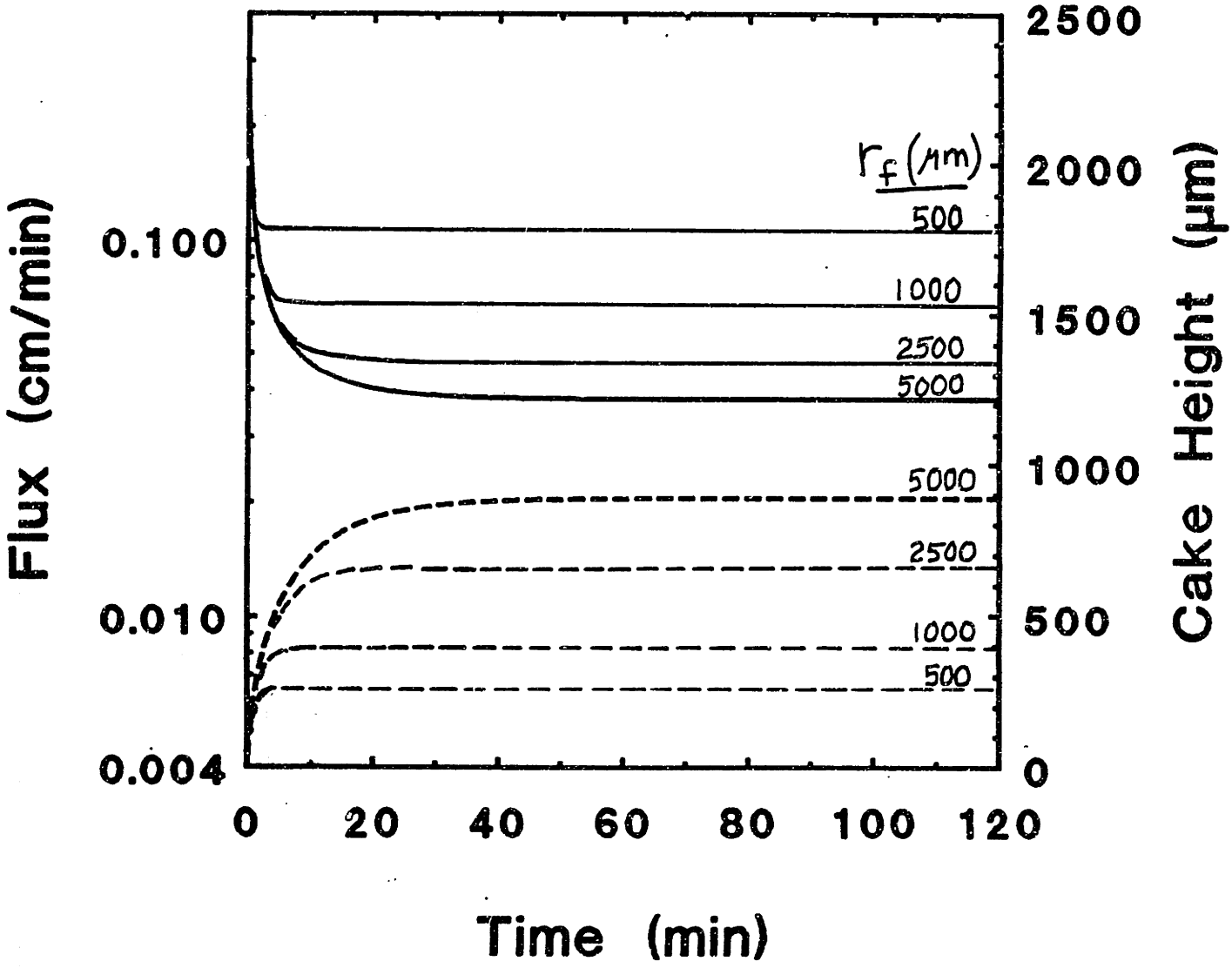

Figure 6-45. Predicted length-averaged steady-state flux and cake height as a function of time for several values of the fiber radius.

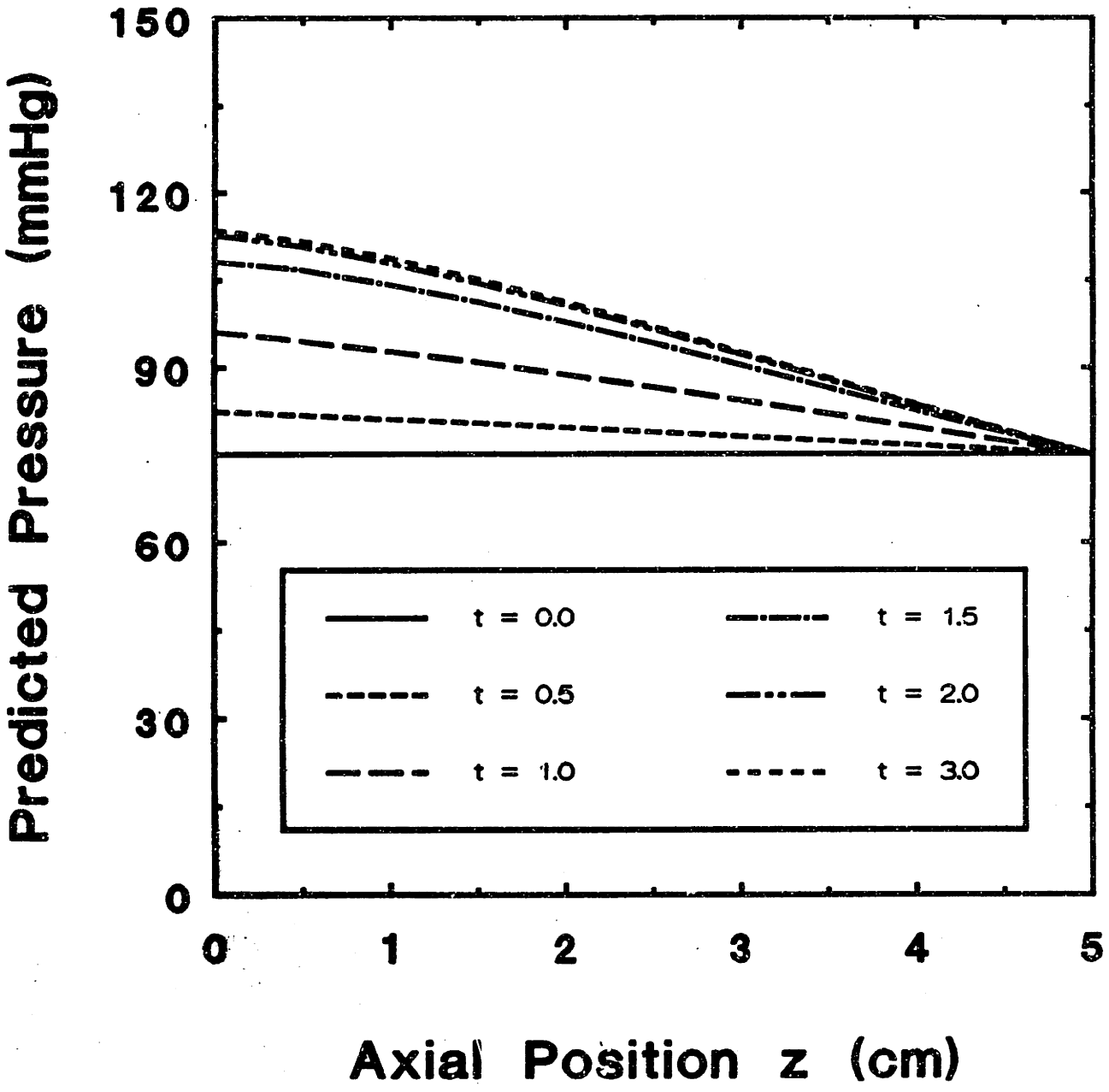

Figure 6-46. Predicted axial pressure profile at various times for the r_c = 500 μm case shown in Figure 6-45.

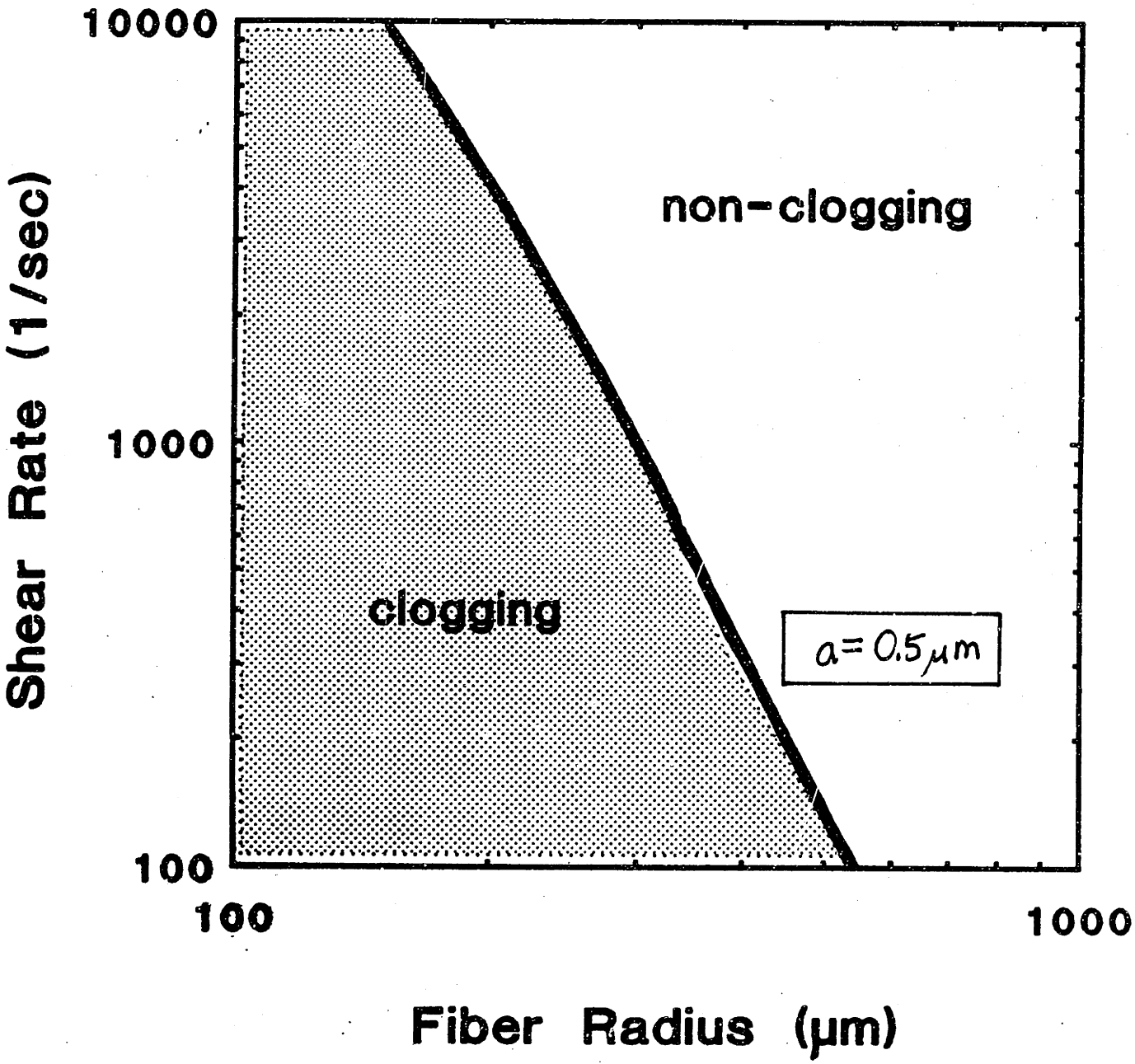

Figure 6-47. Predicted clogging and non-clogging regimes as a function of shear rate and fiber radius using base case values for all other parameters.

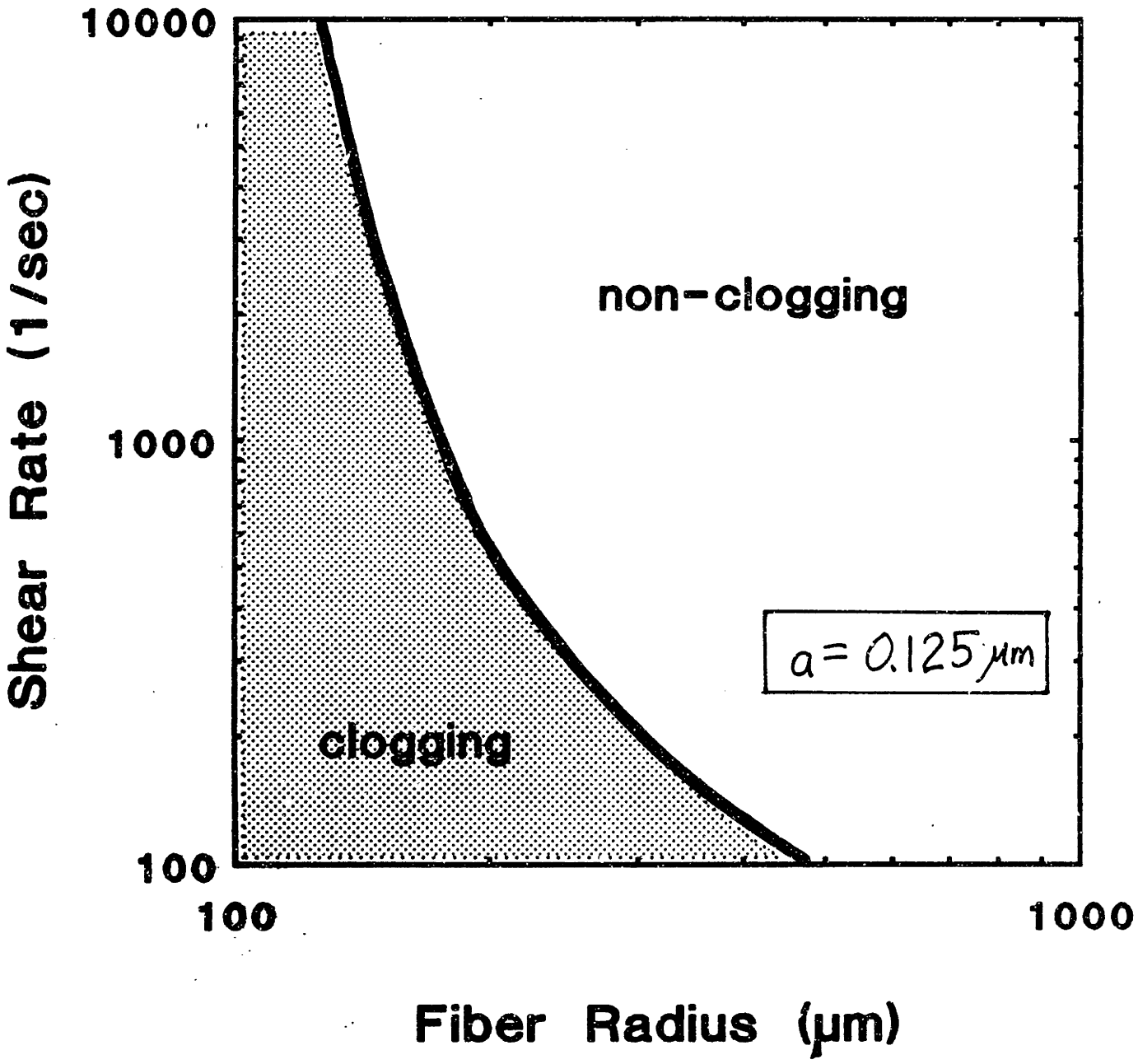

Figure 6-48. Predicted clogging and non-clogging regimes as a function of shear rate and fiber radius for a=0.125 μm, using base case values for all other parameters.

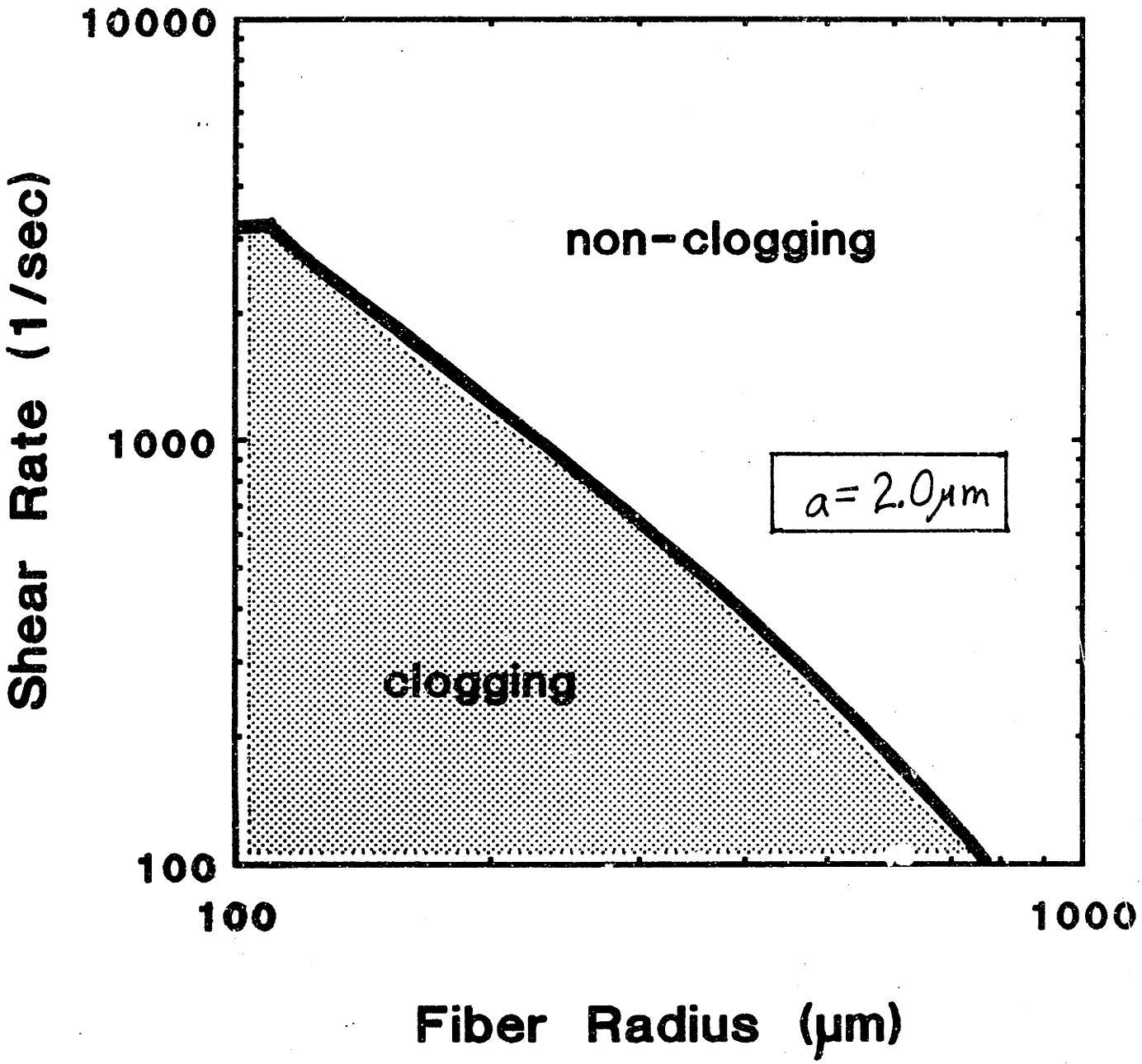

Figure 6-49. Predicted clogging and non-clogging regimes as a function of shear rate and fiber radius for a=2.0 μm, using base case values for all other parameters.

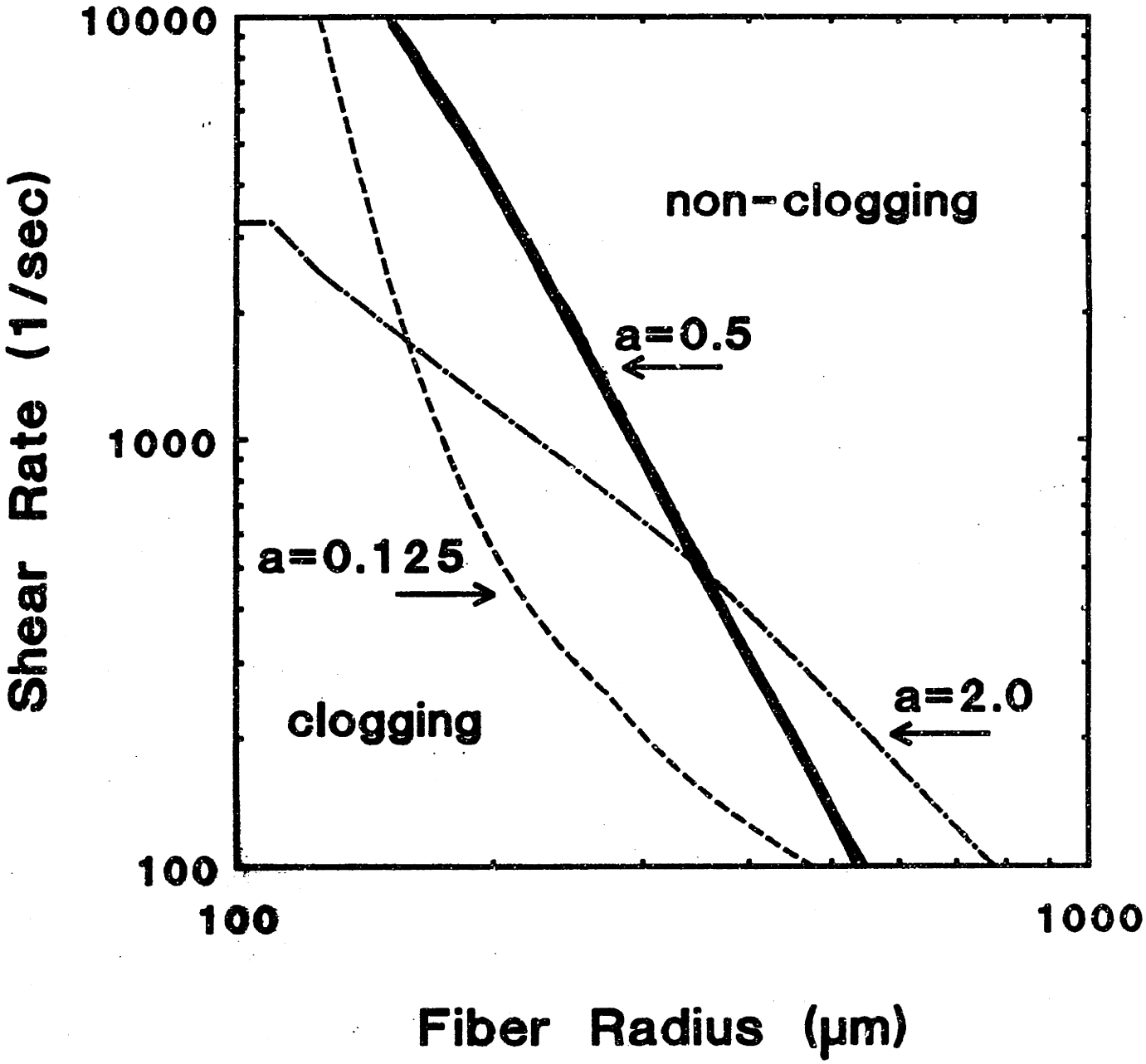

Figure 6-50. Predicted clogging and non-clogging regimes as a function of shear rate and fiber radius for various particle sizes, re-plotted from Figures 6-46 through 6-48.

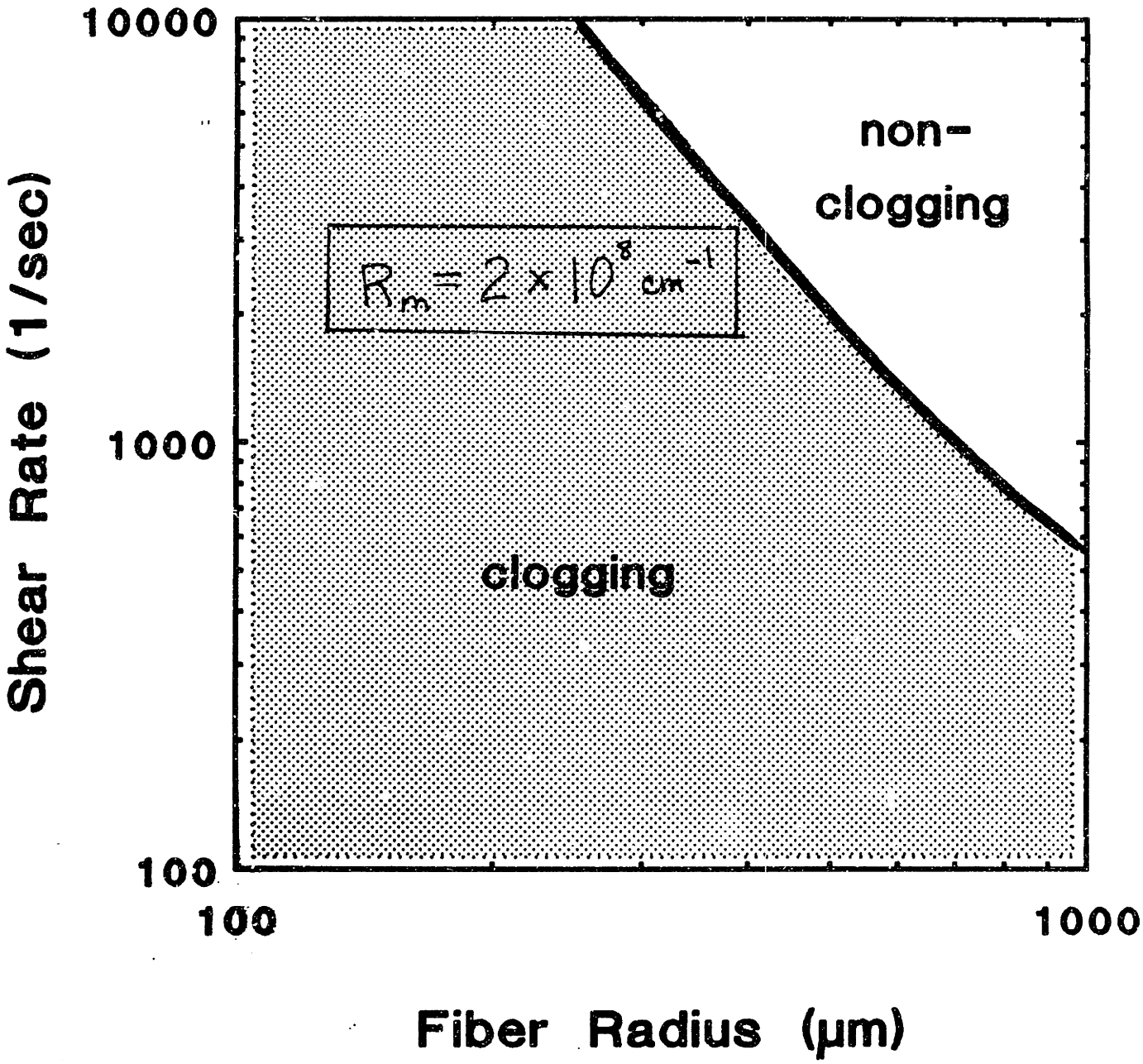

Figure 6-51. Predicted clogging and non-clogging regimes as a function of shear rate and fiber radius for $R_m = 2 \times 10^8$ cm^{-1}, using base case values for all other parameters.

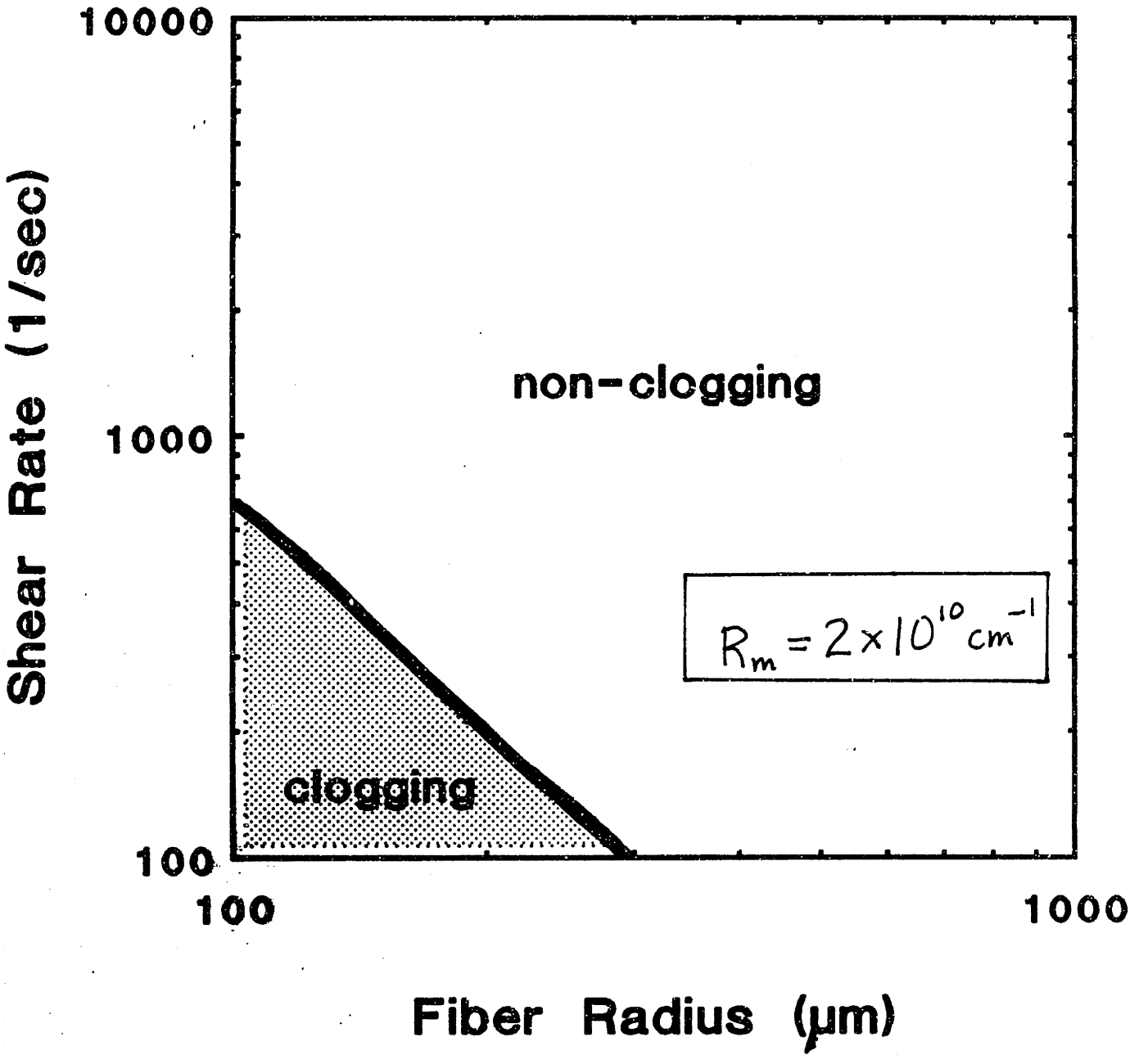

Figure 6-52. Predicted clogging and non-clogging regimes as a function of shear rate and fiber radius for $R_m = 2 \times 10^{10}\ cm^{-1}$, using base case values for all other parameters.

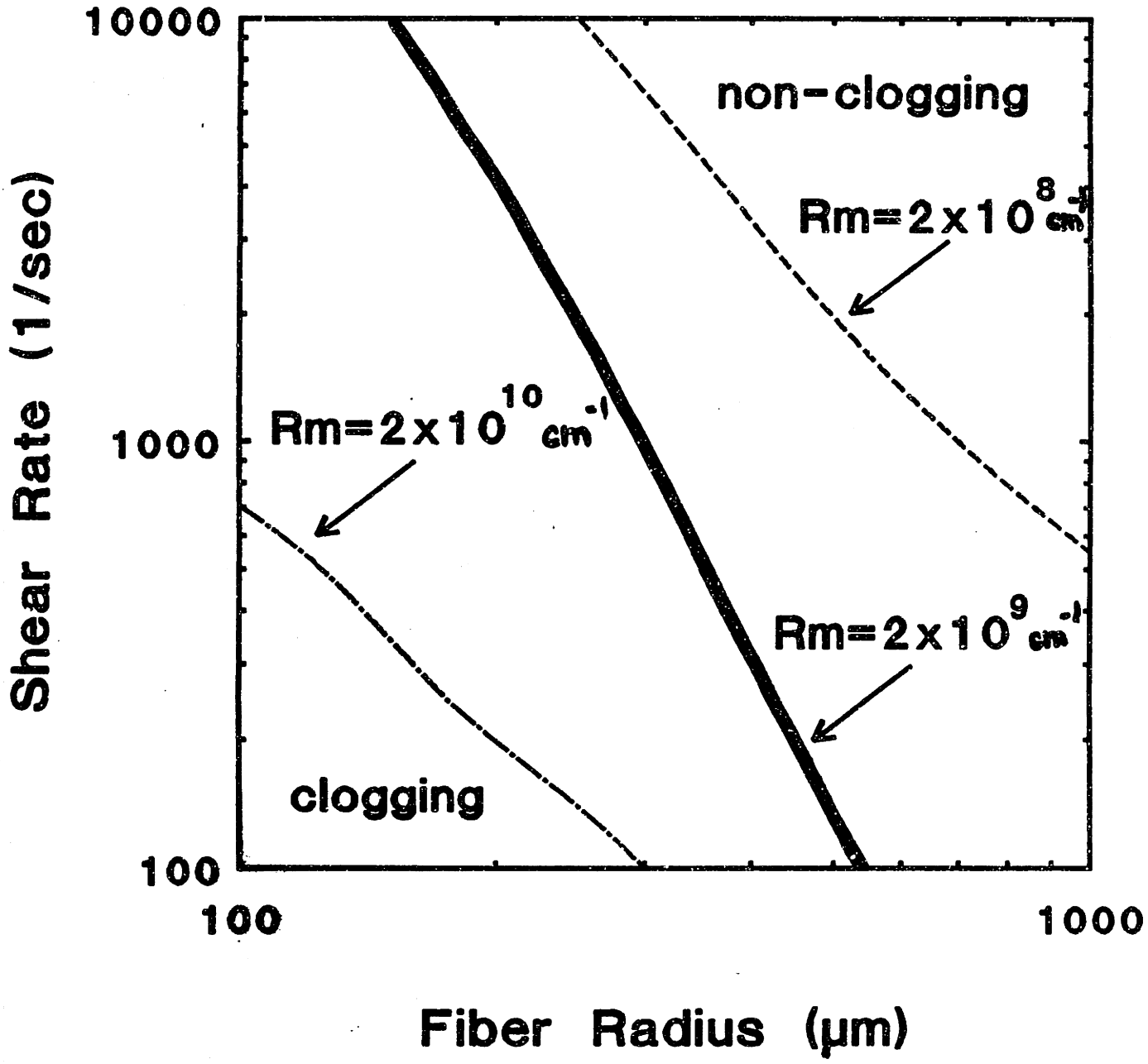

Figure 6-53. Predicted clogging and non-clogging regimes as a function of shear rate and fiber radius for various membrane resistances, re-plotted from Figures 6-46, 6-50, and 6-51.

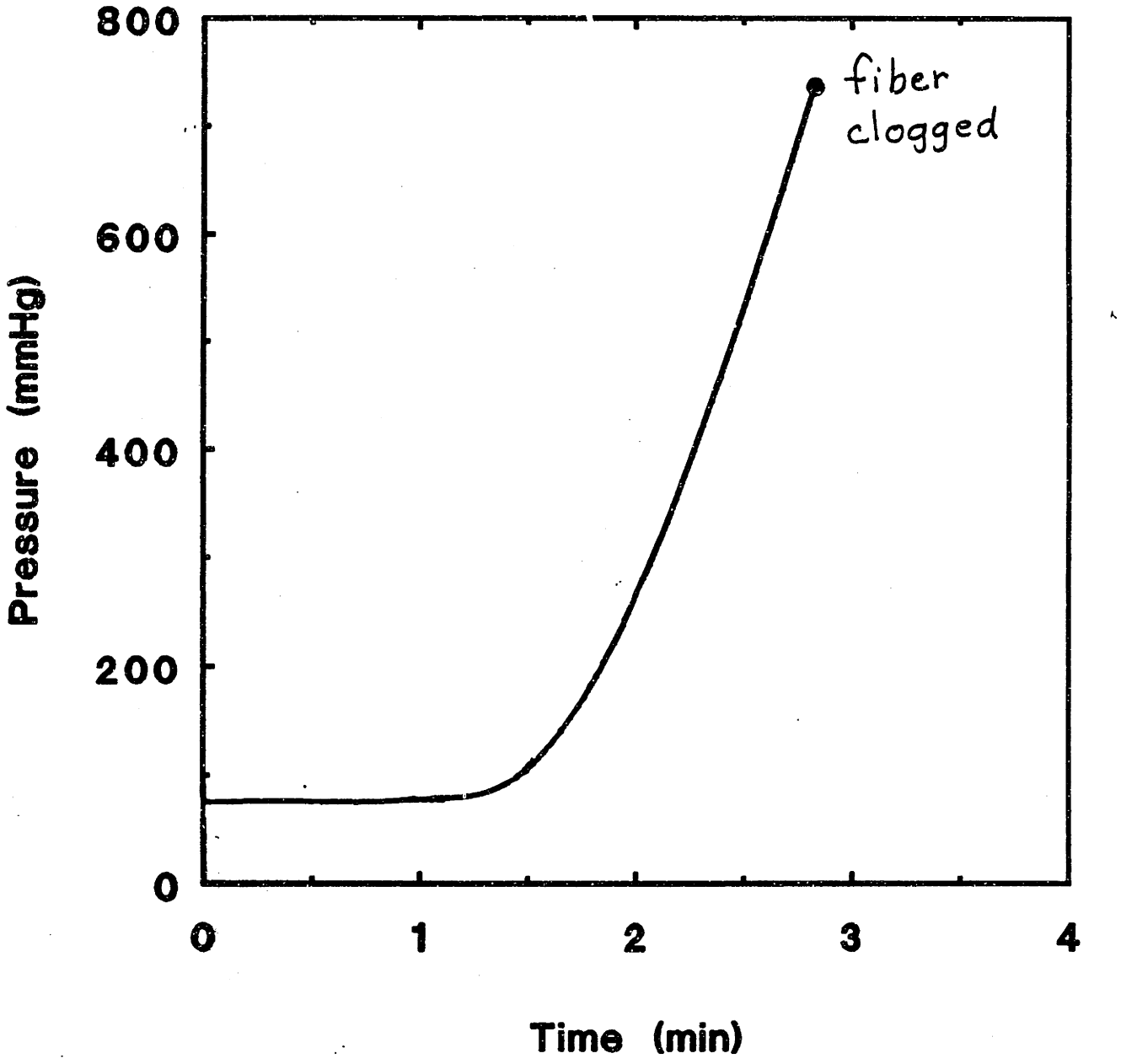

Figure 6-54. Inlet pressure as a function of time prior to clogging of a hollow fiber of r_f = 500 μm during filtration at an inlet wall shear rate of 150 s^{-1}.

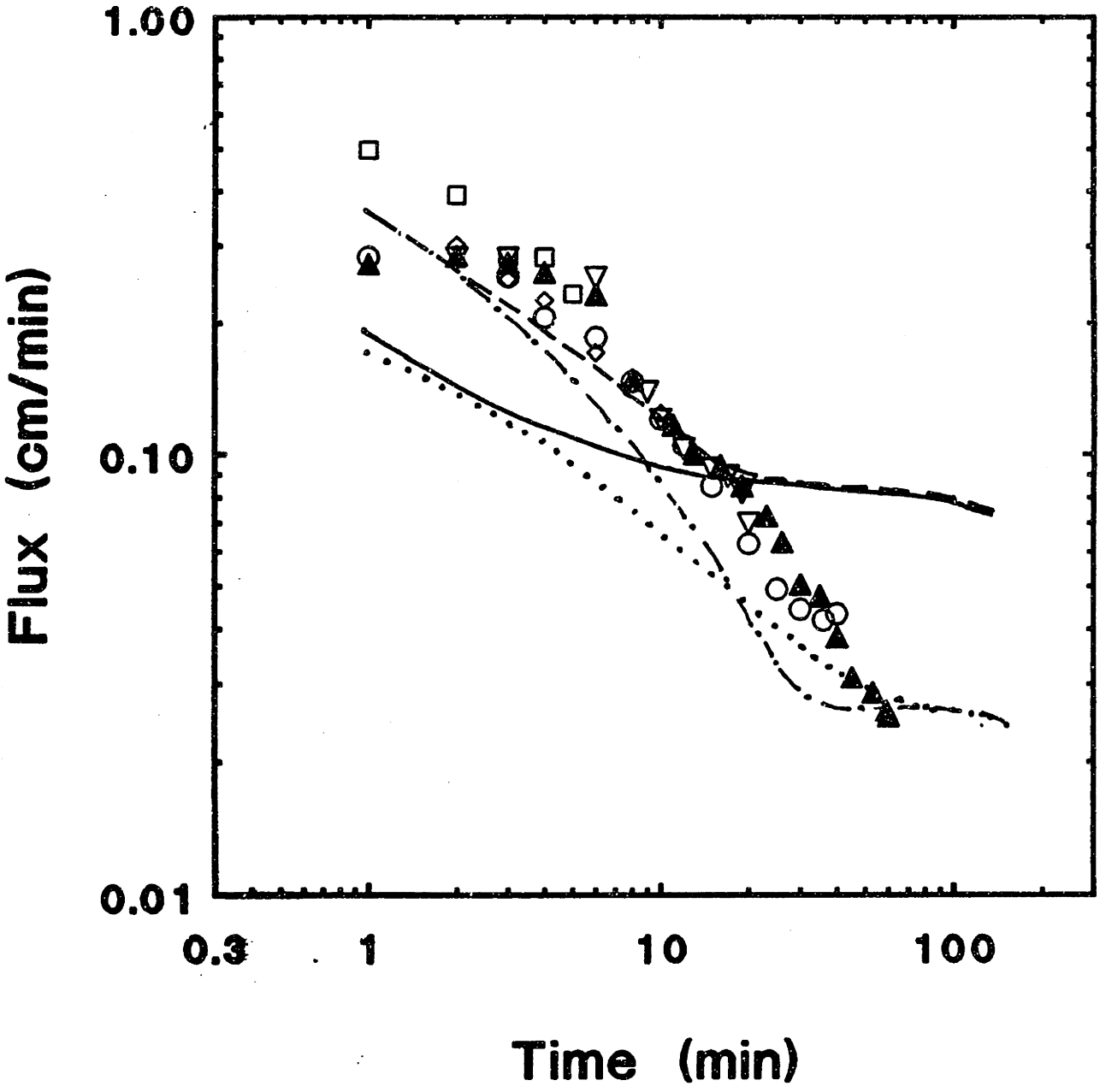

Figure 6-55. Predicted and measured flux during filtration of 0.65% yeast in 6% albumin in modified polysulfone (1 mm ID, 0.4 μm pore ID) hollow fibers, with an inlet wall shear rate of 80 s^{-1} and an outlet applied pressure of 70 mmHg.

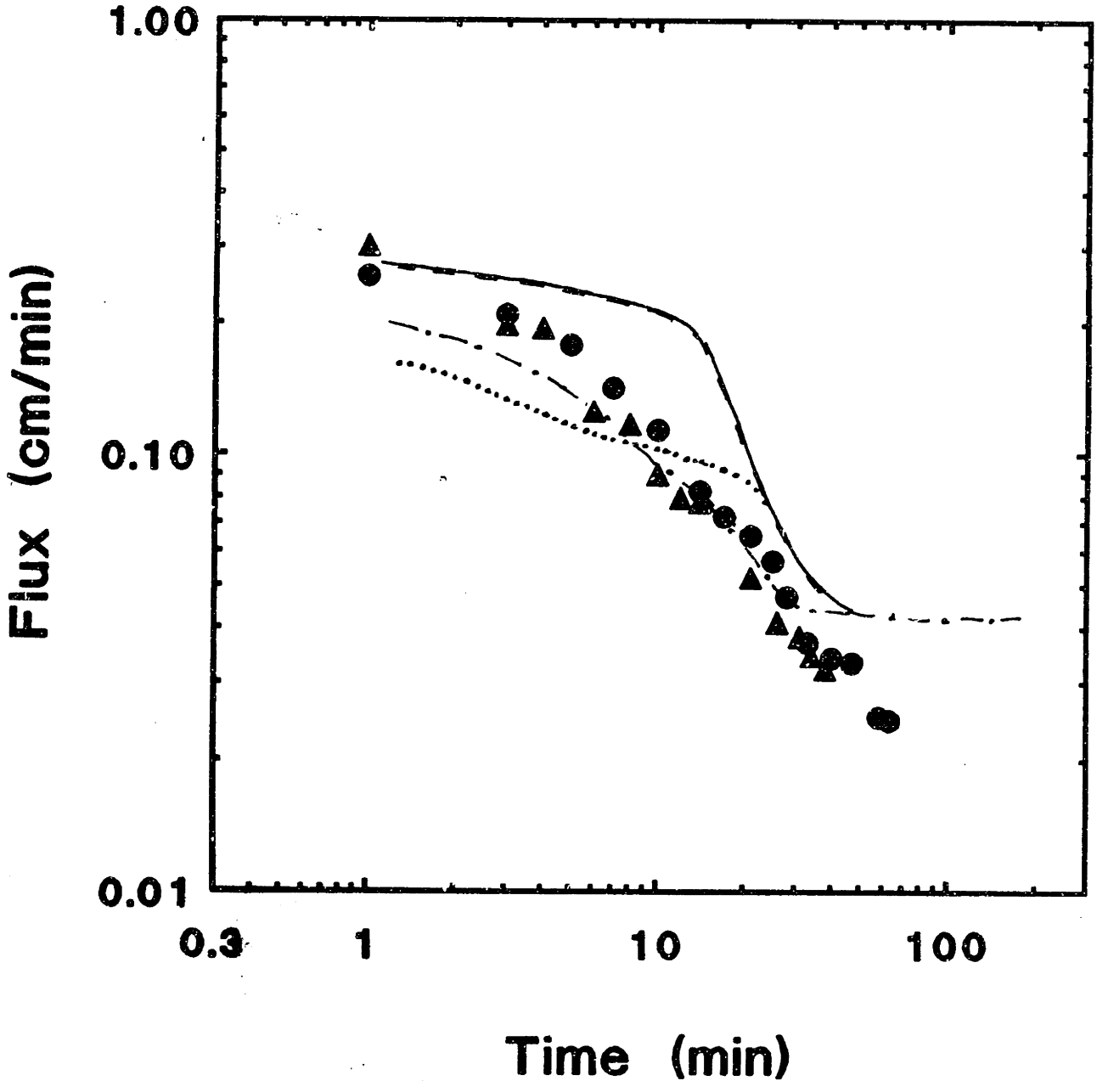

Figure 6-56. Predicted and measured flux during filtration of 0.65% yeast in 6% albumin in polypropylene (330 μm ID, 0.4 μm pore ID) hollow fibers, with an inlet wall shear rate of 800 s^{-1} and an outlet applied pressure of 70 mmHg.

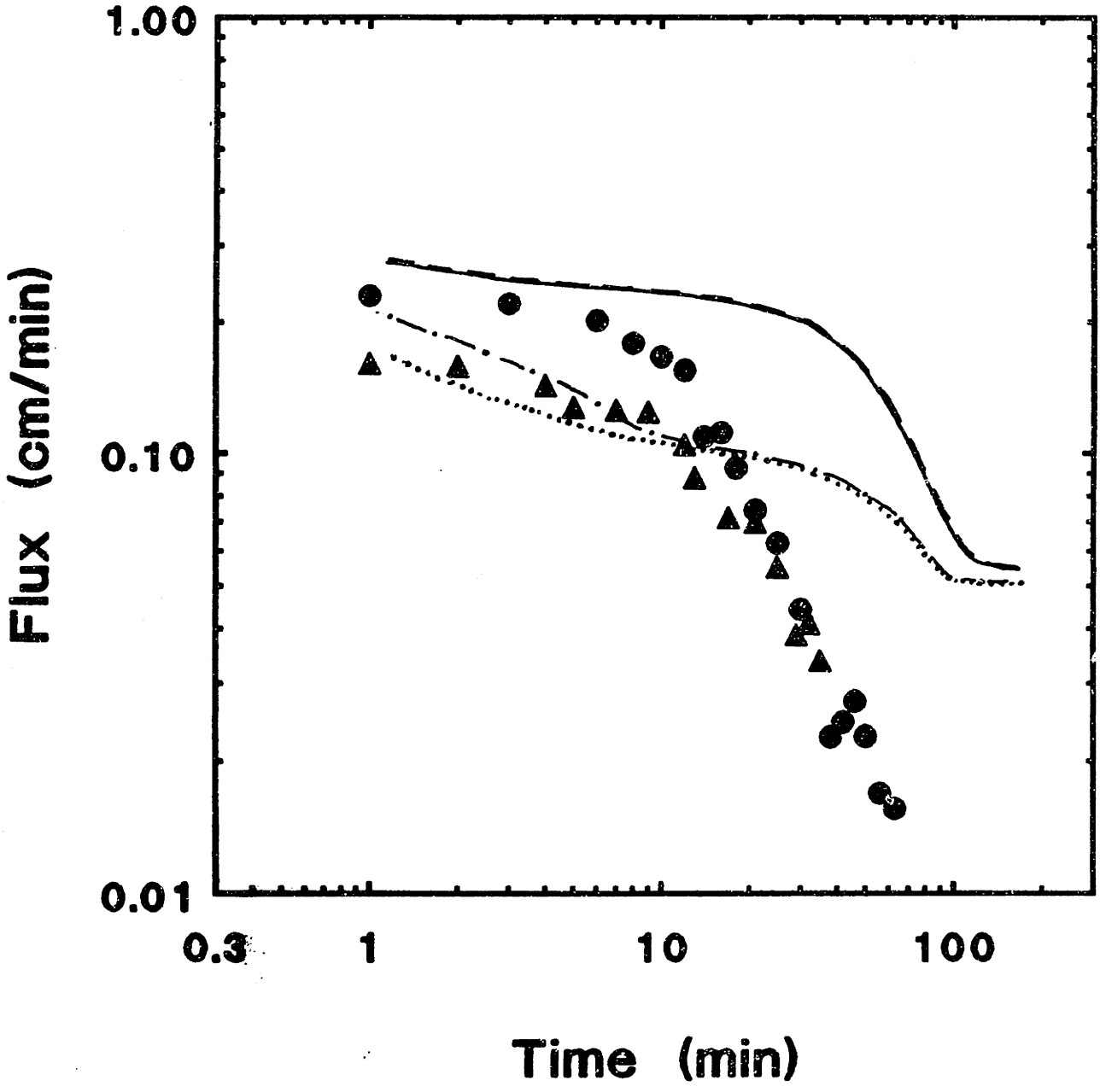

Figure 6-57. Predicted and measured flux during filtration of 0.65% yeast in 6% albumin in polyamide (320 μm ID, 0.35 μm pore ID) hollow fibers, with an inlet wall shear rate of 800 s^{-1} and an outlet applied pressure of 70 mmHg.

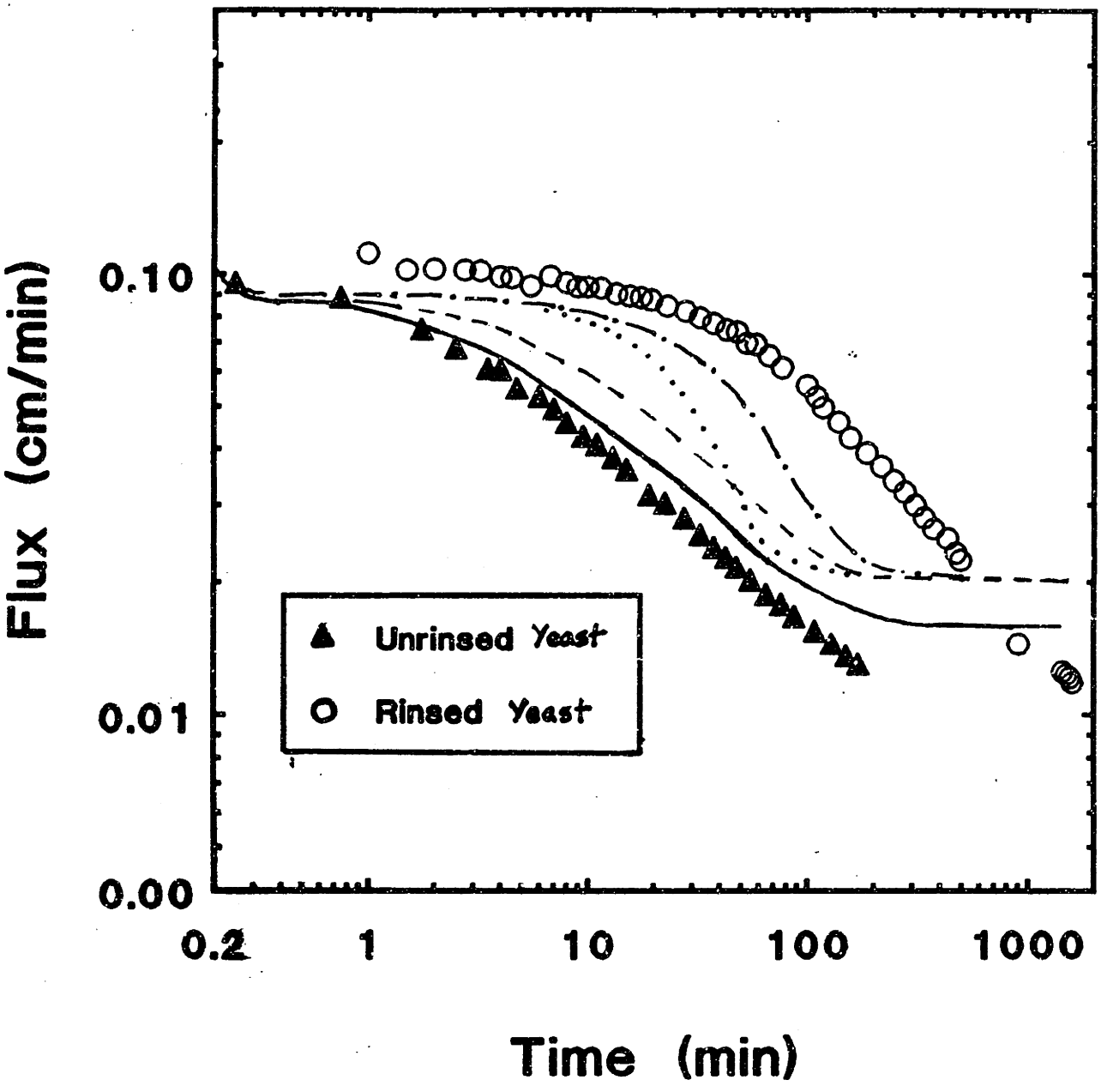

Figure 6-58. Predicted and measured flux during filtration of 2% suspensions of freshly-rehydrated yeast and 3x-rinsed yeast in media in polysulfone UF fibers (4.66 mm ID) hollow fibers, with $\gamma_{w,in} = 80\ s^{-1}$ and $P_{app,out} = 75$ mmHg.

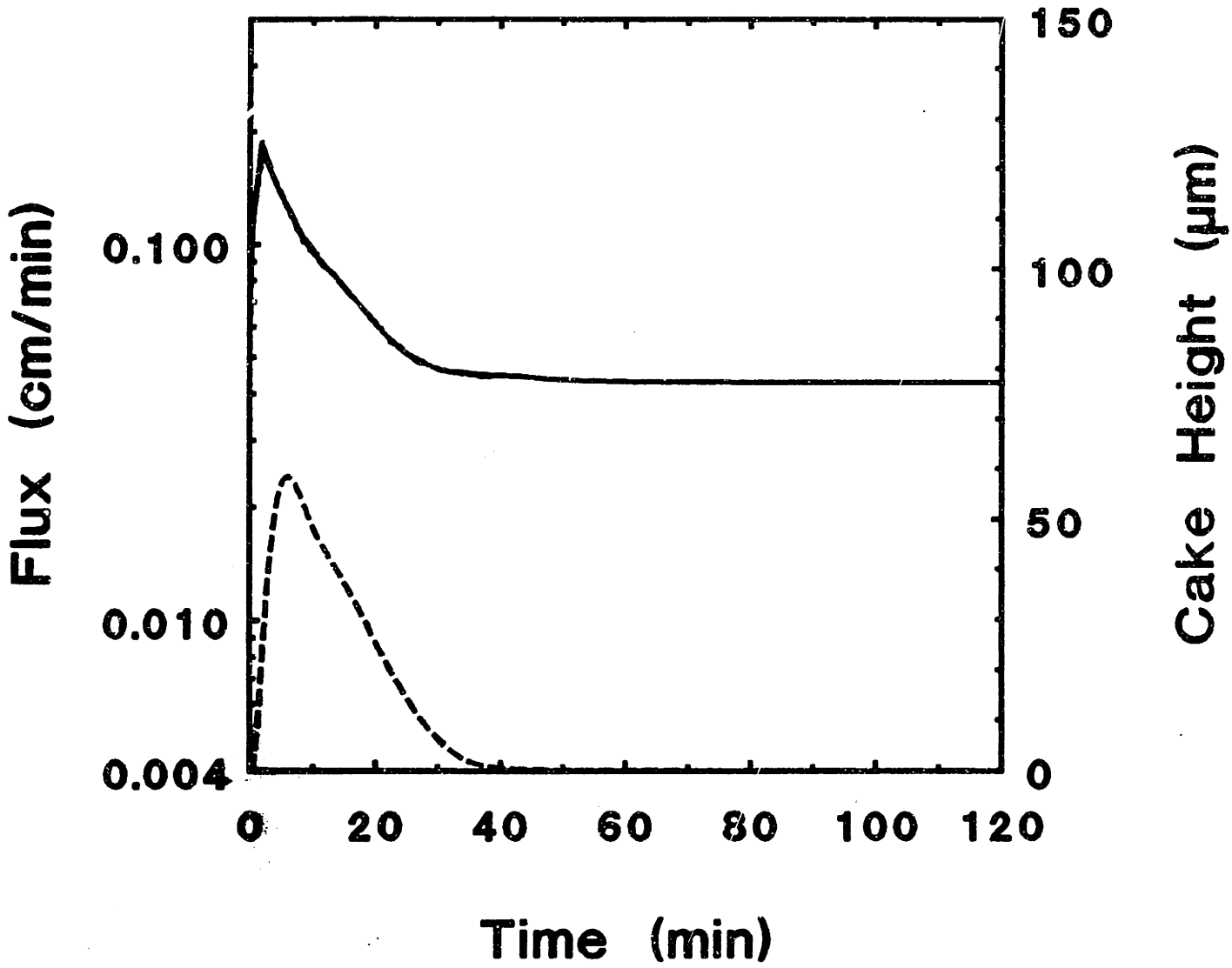

Figure 6-59. Predicted flux and cake thickness for filtration of 0.65% yeast in 6% albumin in polypropylene (330 μm ID, 0.4 μm pore ID) hollow fibers, with an inlet wall shear rate of 800 s^{-1} and an outlet applied pressure of 70 mmHg.

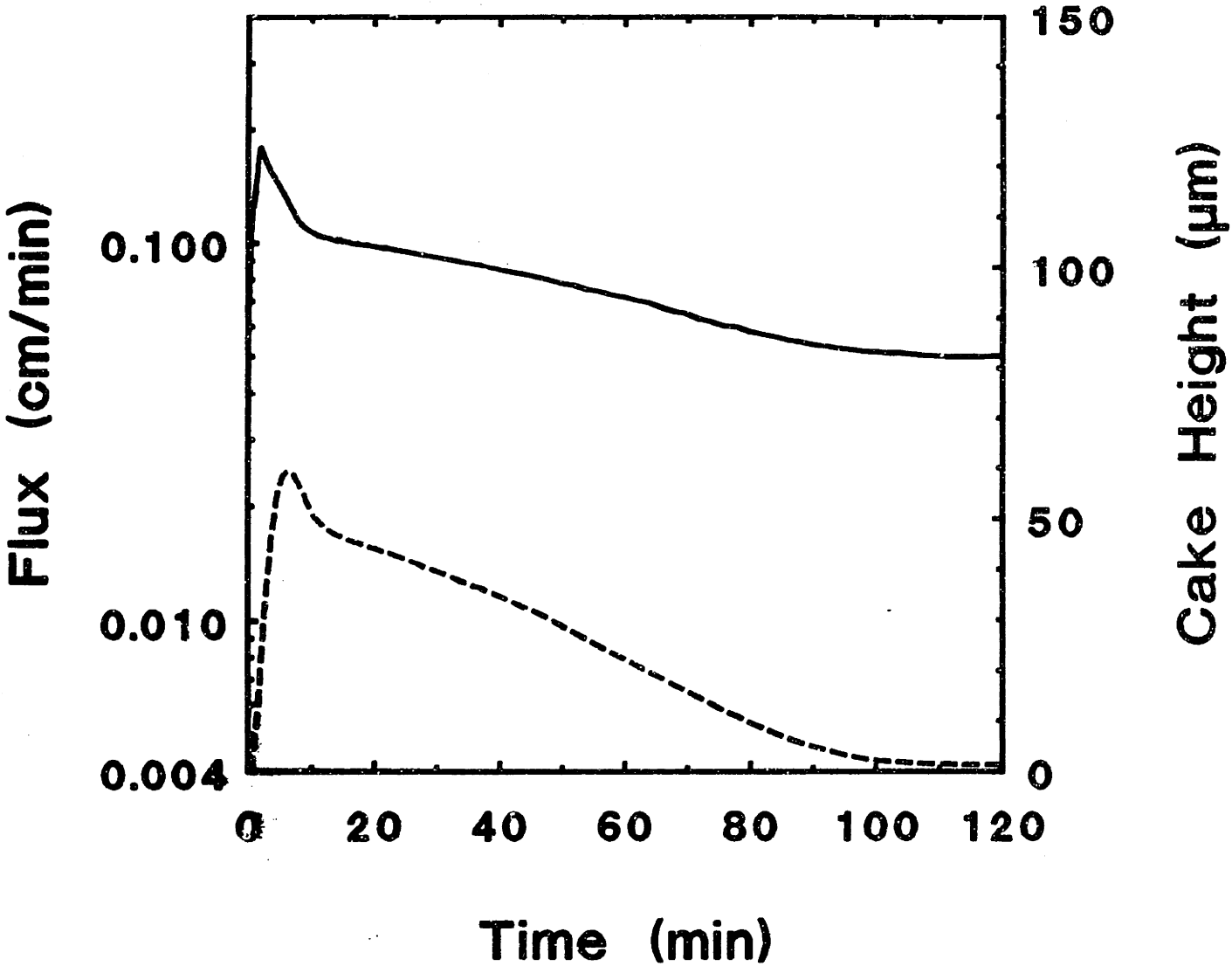

Figure 6-60. Predicted flux and cake thickness for filtration of 0.65% yeast in 6% albumin in polyamide (320 μm ID, 0.35 μm pore ID) hollow fibers, with an inlet wall shear rate of 800 s^{-1} and an outlet applied pressure of 70 mmHg.

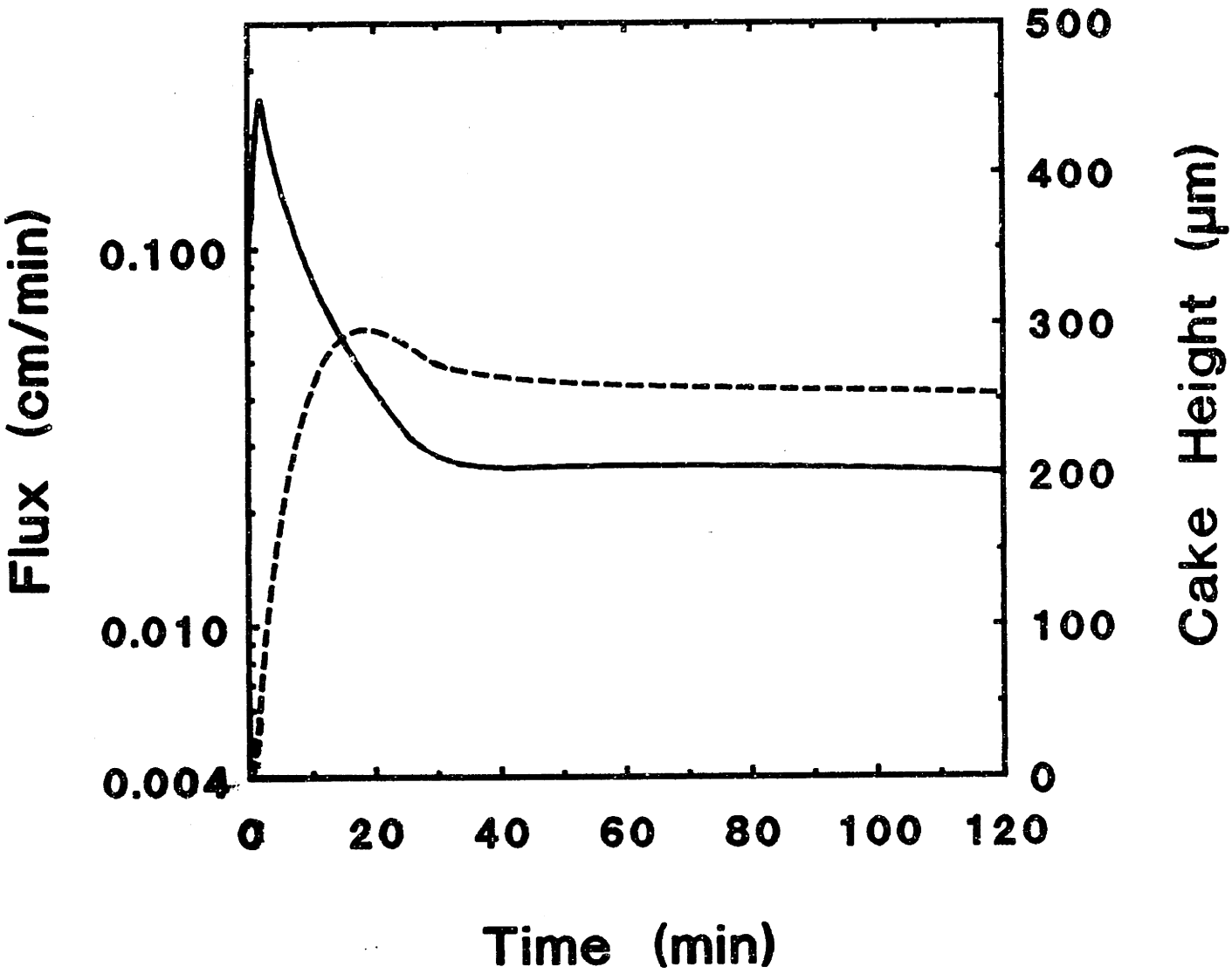

Figure 6-61. Predicted flux and cake thickness for filtration of 0.65% yeast in 5% albumin in modified polysulfone (1 mm ID, 0.4 μm pore ID) hollow fibers, with an inlet wall shear rate of 80 s^{-1} and an outlet applied pressure of 70 mmHg.

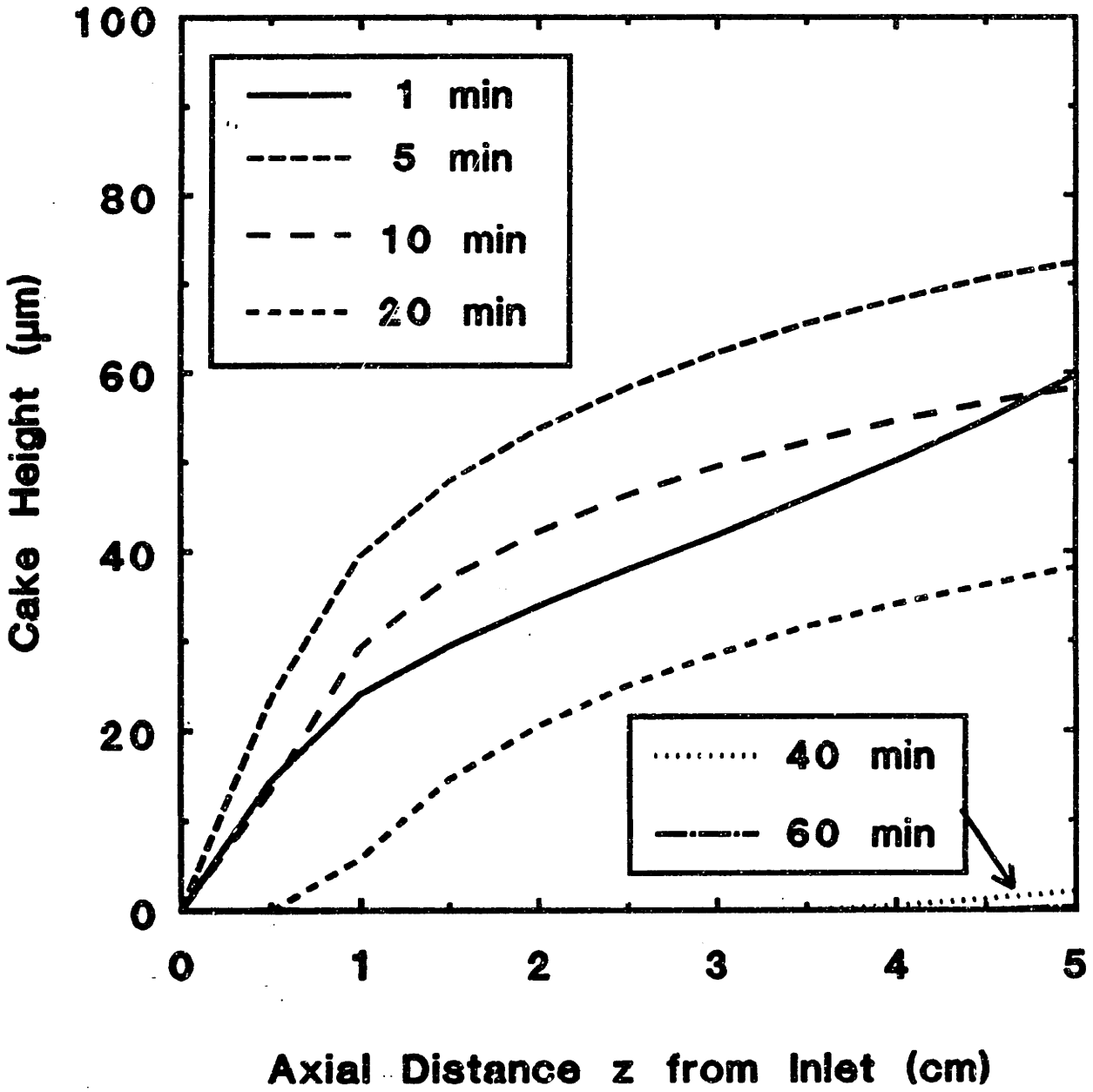

Figure 6-62. Predicted cake thickness as a function of axial position at several times for filtration of 0.65% yeast in 6% albumin in polypropylene hollow fibers, with $\gamma_{w,in}$=800 s^{-1} and $P_{app,out}$=70 mmHg.

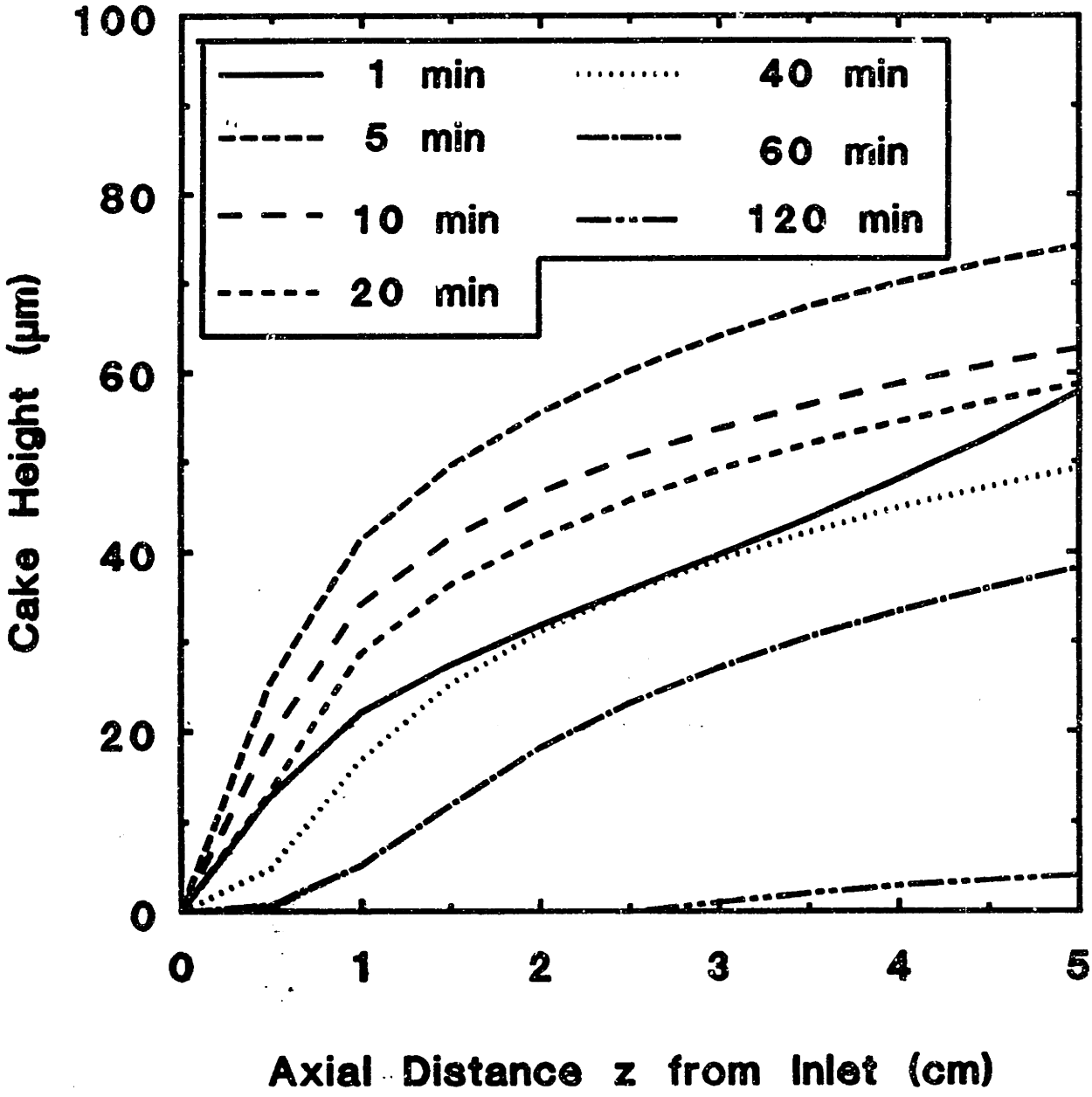

Figure 6-63. Predicted cake thickness as a function of axial position at several times for filtration of 0.65% yeast in 6% albumin in polyamide hollow fibers, with $\gamma_{w,in}$=800 s^{-1} and $P_{app,out}$=70 mmHg.

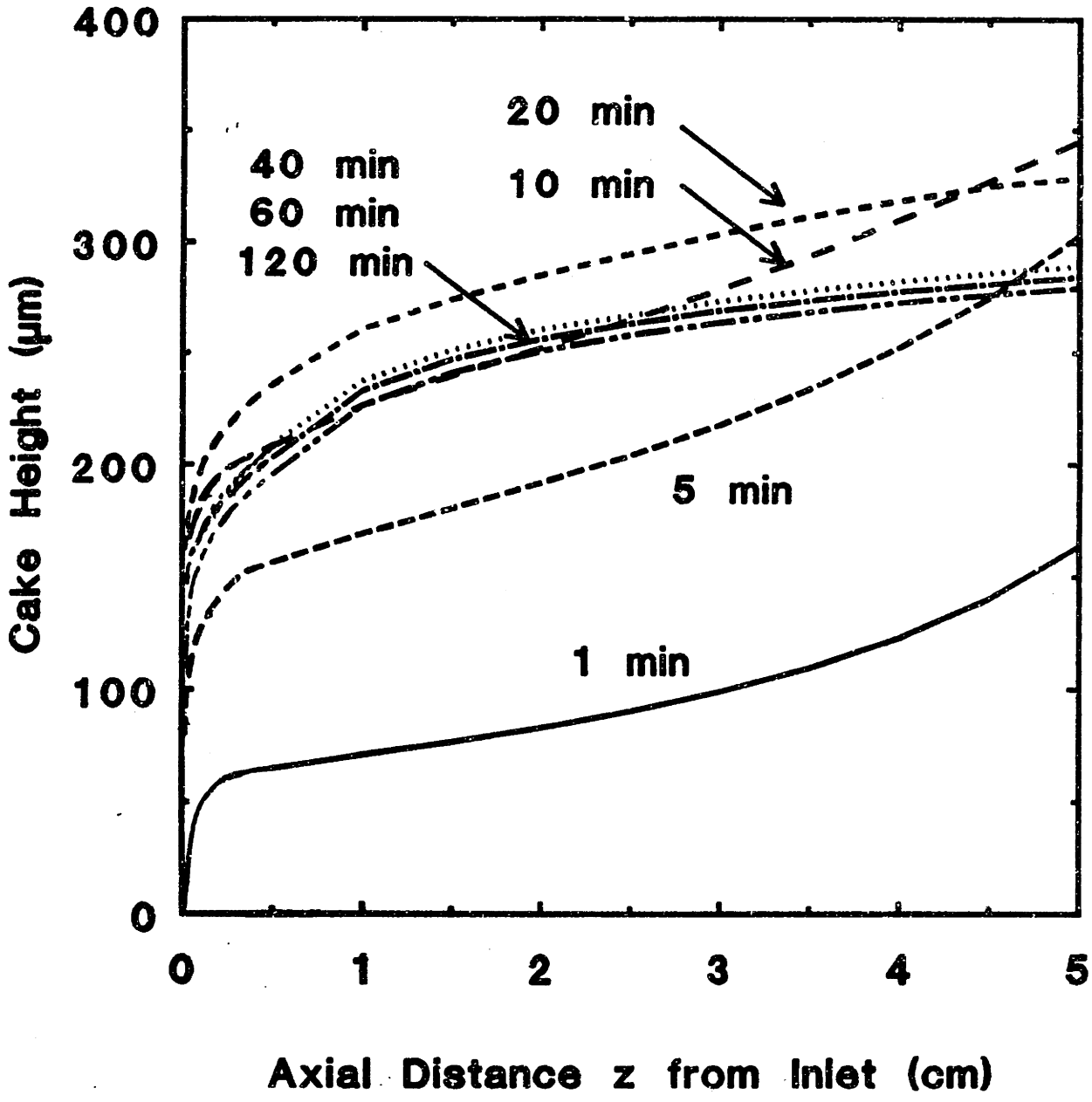

Figure 6-64. Predicted cake thickness as a function of axial position at several times for filtration of 0.65% yeast in 4% albumin in modified polysulfone hollow fibers, with $\gamma_{w,in}$=800 s^{-1} and $P_{app,out}$=70 mmHg.

```
THISFIL$ = "NUPART10.BAS": REVDATE$ = "11/29/88"

REM ***** TIME-DEPENDENT MODEL OF LATEX PARTICLE FILTRATION IN HOLLOW FIBERS,
REM         WITH AXIAL VARIATION IN BULK FLOW, CONC, P AND FLUXES *****

REM  This new version of the latex particle program was created from NEWPART5.
REM  Like the previous latex particle models, this version uses the Acrivos
REM  diffusivity and viscosity, and the Kozeny-Carman cake resistance.
REM  Unlike previous versions, the particle size is an input parameter so that
REM  a single version can be used for all latex particle calculations.  I have
REM  kept a number of features from ZYD4PP, including a time-dependent cake
REM  concentration (and cake resistance), a linear approach to the final
REM  outlet pressure (similar to Mitsuru Suzuki's experiments), integration
REM  along the axial direction at each timestep, iterating to determine the
REM  inlet pressure, and various corrections and improvements made along the
REM  way.  Unlike the yeast programs, this version does not include pore
REM  blockage.  (Second version contains option to continue calculations;
REM  third version adds Havg (t) to output and uses two output files;
REM  fourth version accounts for curvature in the Darcy's law term; and
REM  fifth version corrects Darcy equation and Havg calculation.  NUPART10
REM  adds the choice of using the numerically integrated Davg as choice 5.)

DEFDBL A-Z: DEFINT I-N: DIM SUM(1000): DIM DAVG(1000)

REM  Note: Variable values are output at each timestep, but only the
REM        current and immediately previous values are kept in memory.

REM Dimension arrays:

        ITMAX = 14: JTMAX = 12: NDIM = 5 * ITMAX * JTMAX
        DIM DT(ITMAX)
        DIM TIME(NDIM), SUMJCAKE(NDIM), FLOWSUM(NDIM), SUMH(NDIM)

REM Acrivos viscosity:

        DEF FNVISC (C) = (1 + 1.5 * C / (1 - C / .58)) ^ 2


REM Time-dependent cake concentration:

        DEF FNCCAKE (T)
                IF T < TAUCAKE THEN
                        FNCCAKE = CCAKEF - DELCCAKE * (TAUCAKE - T) / TAUCAKE
                ELSE
                        FNCCAKE = CCAKEF
                END IF
        END DEF

REM Kozeny-Carman cake resistance:

        DEF FNRC (CCAKE)
                 SO = 6 / (DIAM * .0001)
                CONSTKC = 5# * SO ^ 2
                EPS = 1 - CCAKE
                FNRC = CONSTKC * (1 - EPS) ^ 2 / EPS ^ 3
        END DEF

REM No pore blockage in this version:

        DEF FNBLOCK (H)
                FNBLOCK = 1
        END DEF

REM Acrivos diffusion coefficient:

        DEF FNDIFFA (Z) = Z ^ 2 * (1# + .5 * EXP(8.8 * Z))

REM The inlet pressure is gradually increased to its final value to avoid
REM clogging:

        DEF FNP (TLOCAL)
                IF TLOCAL < TAUP THEN
                        FNP = .1 * P0 + .9 * P0 * (TLOCAL / TAUP)
                ELSE FNP = P0
                END IF
        END DEF

REM No membrane resistance module input statement instead)

PRINT THISFIL$; " ", REVDATE$; " VERSION     Current Date and Time: "; DATE$; "
  => "; TIME$
PRINT ""

REM:  Input the required parameters (now includes time constant for Rc):

        REM $INCLUDE: 'C:\NORMA\QBASIC\INPUT18.BAS'

REM Store values of input parameters in the output file:

        OPEN OUTFILE1$ FOR OUTPUT AS #1
        PRINT #1, "This file is :  "; OUTFILE1$; " produced by :"
        PRINT #1, ""
        PRINT #1, THISFIL$; " - "; REVDATE$; " VERSION      at : "; TIME$; "
  => on : "; DATE$
        PRINT #1, ""
        PRINT #1, "Particle diameter (microns):  "; DIAM
        PRINT #1, "Fluid viscosity (cP):  "; VISCO
        PRINT #1, "Inlet bulk concentration:  "; CBO
        PRINT #1, "Final cake concentration:  "; CCAKEF
        PRINT #1, "Initial membrane resistance (cm-1):  ";
        PRINT #1, USING "+#.##^^^^"; RMO
        PRINT #1, "Final membrane resistance:  ";
        PRINT #1, USING "+#.##^^^^"; RMF
        PRINT #1, "Difference between initial and final cake concentrations:  ";
        PRINT #1, USING "+#.##^^^^"; DELCCAKE
        PRINT #1, "Time constant for cake compaction (min):  "; TAUCAKE
        PRINT #1, "Method for calculating Cavg:  "; MCAVG
        PRINT #1, "Final inlet pressure:  "; P0
        PRINT #1, "Time constant for pressure increase (min):  "; TAUP
        PRINT #1, "Inlet shear rate (sec-1):  "; GAMMA
        PRINT #1, "Fiber radius (microns):  "; RF
        PRINT #1, "Fiber length (cm):  "; XL
        IF M = 1 THEN PRINT #1, "Axial step size:  "; DELX
        PRINT #1, "Correction factor for diffusion term:  "; DIFFMULT
        PRINT #1, ""

REM Input the values of the numerical integration from a lookup table
REM    in which the integration step size was 0.001 (i.e. 0.1%):

        OPEN "C:\NORMA\QBASIC\LOOKUP.A58" FOR INPUT AS #2
        INPUT #2, NVALUES
        FOR I = 1 TO NVALUES
                INPUT #2, CONCEN, SUMM
                ICONC = INT(CONCEN * 1000)
                SUM(ICONC) = SUMM
        NEXT I
        CLOSE #2

REM If Davg is to be determined by the numerical integration method, then,
REM    input the values of the numerical integration from a lookup table
REM    in which the integration step size was 0.001 (i.e. 0.1%):
```


H. Computer Programs

```
        IF MCAVG = 5 THEN
                OPEN "C:\NORMA\QBASIC\DLOOKUP.CKC" FOR INPUT AS #2
                INPUT #2, NVALUES
                FOR I = 1 TO NVALUES
                        INPUT #2, CONCEN, DAVERAGE
                        ICONC = INT(CONCEN * 1000)
                        DAVG(ICONC) = DAVERAGE
                NEXT I
                CLOSE #2
        END IF

REM Set variable dimensions which are related to input parameters:

        DIM H(NL), OLDH(NL)

REM Set the cell-dependent parameters (in this case, for yeast):

        a = DIAM * .0001# / 2
        CBCRIT = .99# * CCAKEF

REM Calculate the constant part of the coefficients for the diffusion and
REM convection terms [note that 0.2569=0.538*(0.33)^(2/3) and that the
REM concentration part of the diffusivity is no longer constant because
REM it is evaluated at Cavg]:

       COEFF0 = DIFFMULT * .2569 * 60 * a ^ (4 / 3)
       COEFF2 = 1 / (.000000125# * VISC0)

REM Initialize loop parameters and calculate axial pressure drop per step:

        X = 0: SUMJCAKE = 0: FLOWMEM = 0: FLOWSUM = 0: SUMH = 0
        POUT = 0: DROP = 0: NSTEP = 0: PI = 3.14159
        BULKFLOO = 15 * PI * GAMMA * RF ^ 3 / 1000000000000#
        DPCRIT = .001 * P0
        STEPAREA = 2 * PI * RF * .0001# * DELX
        AREAMEMB = 2 * PI * RF * .0001# * XL

REM NOTE: These are timestep calculations and variable initializations
REM  which only need to be done once (24 timesteps of 5, 10, 15, 30 and
REM  60 s, then 36 steps of 2 min and 12 steps of 5 min)

        DT(1) = 1 / 12: DT(2) = 1 / 12: DT(3) = 1 / 6: DT(4) = 1 / 6
        DT(5) = .25: DT(6) = .25: DT(7) = .5: DT(8) = .5: DT(9) = 1#:
        DT(10) = 1#: DT(11) = 2#: DT(12) = 2#: DT(13) = 2#: DT(14) = 5#
REM        : DT(13) = 5#: DT(14) = 5#

        H = 0

REM ************************************************************
REM ***** Beginning of the iteration in time (outer loop): *****
REM ************************************************************

T = 0: NT = 0

CONTINUE: 'Entrance point for more calculations

FOR IT = 1 TO ITMAX
        DELT = DT(IT)
        FOR JT = 1 TO JTMAX

                NT = NT + 1
                T = T + DELT

                IF JT = JTMAX OR JT = JTMAX / 2 THEN
                        PRINT #1, " "
                        PRINT #1, " T = ";
```



```
                        PRINT #1, USING "####.##"; T
                        PRINT #1, ""
                END IF


REM Save the cake height as a function of axial position from the previous
REM    timestep in the OLDH array:

                FOR JJ = 1 TO NL

                        OLDH(JJ) = H(JJ)

                NEXT JJ


REM Set initial (X=0) values which are used only after successfully completing
REM     a timestep:

                OLDPOUT = POUT
                IF NT = 1 THEN AXIDPOLD = 0 ELSE AXIDPOLD = AXIALDP
                IF NT = 1 THEN AXIALDP = 0 ELSE AXIALDP = OLDPIN - OLDPOUT
REM Previous attempt to dampen oscillations:
REM      POUT = FNP(T) + (AXIALDP + AXIDPOLD) / 2#
                POUT = FNP(T) + AXIALDP
                OLDPIN = POUT
                NTLOOPS = 0
                PRINT ""
                PRINT "T=", T
                PRINT ""

REM Set the initial values which must be reset for each iteration of the
REM     timestep:

STARTX:         X = 0
                NTLOOPS = NTLOOPS + 1
                QBOUT = BULKFLOO
                CBOUT = CB0
                FLOWMEM = 0
                SUMJCAKE = 0
                FLOWSUM = 0
                SUMH = 0

                IF JT = JTMAX OR JT = JTMAX / 2 THEN
        PRINT #1, "    X     P     CB      H      SHEAR      DIFF FLUX      CONV
  => FLUX    MEM FLUX"
                END IF

REM ************************************************************************
REM ***** This is the beginning of the axial position (inner) loop *****
REM ************************************************************************

FOR NSTEP = 1 TO NL

        X = X + DELX

REM Set inlet values for this axial step equal to previous outlet values:

        QB = QBOUT
        CB = CBOUT
        PIN = POUT

REM Correct the previous timestep's value of H to account for compaction:

        H = OLDH(NSTEP) * FNCCAKE(T - DELT) / FNCCAKE(T)

REM Calculate the effective shear rate:
```

```
                GAMMAX = QB / (15 * PI * RF ^ 3 / 1000000000000#)
                IF H > DIAM THEN
                        EFFGAMMA = GAMMAX * (RF / (RF - H)) ^ 3
                ELSE
                        EFFGAMMA = GAMMAX
                END IF

REM Calculate the PDROP:

                CDROP = .0025# * VISCO * DELX * 60
                    IF H > DIAM THEN
                        PDROP = CDROP * FNVISC(CB) * EFFGAMMA / (RF - H)
                    ELSE
                        PDROP = CDROP * FNVISC(CB) * EFFGAMMA / RF
                    END IF


REM Calculate P from PIN and PDROP:

                P = PIN - PDROP / 2

REM Used only in version without inlet pressure correction:
REM                 IF P < 0 THEN
REM                         PRINT #1, "AXIAL PRESSURE DROP EXCEEDED APPLIED PRESSU
  => RE"
REM                         GOTO CLOG
REM                 END IF

                IF P < 0 THEN

        PRINT "Axial pressure drop too high, P = "; P; "at X = "; X
                        POUT = OLDPIN + 1# * ABS(P)
                        OLDPIN = POUT
        PRINT "repeating this timestep with PIN = "; POUT
        PRINT #1, "repeating this timestep with PIN = "; POUT
                        PRINT #1, USING "###.## ,"; X;
                        PRINT #1, USING "####.# ,"; P;
                        PRINT #1, USING "##.### ,"; CB;
                        PRINT #1, USING "####.# ,"; H;
                        PRINT #1, USING "###### ,"; EFFGAMMA;
                        PRINT #1, USING "+#.####^^^^ ,"; DIFF; CONVCAKE, CONVMEM
                        GOTO STARTX
                END IF



REM Calculate the fluxes for this axial step (note that coeff1 had to be
REM     recalculated because cb had changed).  Start by calling the numerical
REM     integration interpolating program with CB equal to the concentration
REM     at this axial position and time:

        REM $INCLUDE: 'C:\NORMA\QBASIC\INTERPO3.BAS'

REM The bulk viscosity (and therefore CB) appears in the coefficient for
REM the diffusion term:

        IF MCAVG = 1 THEN
                CAVG = FNCCAKE(T)
                DCAVG = FNDIFFA(CAVG)
        END IF

        IF MCAVG = 2 THEN
                CAVG = CB
                DCAVG = FNDIFFA(CAVG)
        END IF

        IF MCAVG = 3 THEN
                CAVG = (FNCCAKE(T) + CB) / 2
                DCAVG = FNDIFFA(CAVG)
        END IF

        IF MCAVG = 4 THEN
                CAVG = SQR(FNCCAKE(T) * CB)
                DCAVG = FNDIFFA(CAVG)
        END IF

        IF MCAVG = 5 THEN
                REM $INCLUDE: 'C:\NORMA\QBASIC\DINTERPO.BAS'
        END IF

REM* Diagnostic write:
REM*        PRINT "MCAVG = "; MCAVG
REM*        PRINT "CB = "; CB
REM*        PRINT "FNCCAKE(T) = "; FNCCAKE(T)
REM*        PRINT "CAVG = "; CAVG
REM*        PRINT "DCAVG = "; DCAVG

             COEFF1 = COEFF0 * FACTOR * FNVISC(CB) / DCAVG ^ (1 / 3)
               DIFF = COEFF1 * EFFGAMMA / (X - DELX / 2) ^ (1 / 3)
REM             CONVMEM = COEFF2 * P / (FNBLOCK(H) * FNRM(T) + FNRC(FNCCAKE(T))
  => * H * .0001#)

REM Note that the pore blockage term has been completely removed for clarity,
REM   and that this equation was corrected in version 5 of NEWPART:

  CONVMEM = COEFF2 * P / (FNRM(T) + FNRC(FNCCAKE(T)) * RF * .0001# * LOG(RF / (R
  => F - H)))

                IF H > DIAM THEN
                        CONVCAKE = CONVMEM * RF / (RF - H)
                ELSE
                        CONVCAKE = CONVMEM
                END IF
                FLUXNET = CONVCAKE - DIFF

REM This prevents numerically-induced oscillations:

                 IF ABS(FLUXNET / CONVMEM) < .00001 THEN FLUXNET = 0

REM These are running totals for calculating length-averaged fluxes (running
REM total for H is below):

                SUMJCAKE = SUMJCAKE + CONVCAKE
                FLOWMEM = CONVMEM * STEPAREA
                FLOWSUM = FLOWSUM + FLOWMEM

REM The increase or decrease in the cake height at this axial position
REM     (during this timestep) is calculated (with the constraint that the
REM     cake height >=0):

                DELH = 10000# * FLUXNET * DELT * CB / FNCCAKE(T)
                IF DELH < 0 AND ABS(DELH) > H THEN DELH = -ABS(H)

                H = H + DELH

REM Check that 0 < DELH < H:

                IF H < 0 THEN H = 0

                IF H >= RF - a * 10000# THEN
                        CLOG2$ = "FIBER CLOGGED BECAUSE CAKE FILLED CHANNEL"
```

```
                PRINT #1, CLOG2$
                GOTO CLOG
        END IF

REM Save the newly calculated height in its axial array:

        H(NSTEP) = H
        SUMH = SUMH + H


REM Use inlet values of Qb, Cb, and P to calculate outlet values:

        QBOUT = QB - FLOWMEM

        DCAKEVOL = .00000002# * PI * DELX * (RF - H - DELH / 2) * DELH
        CBOUT = (CB * QB - DCAKEVOL * FNCCAKE(T)) / QBOUT

        IF CB >= CBCRIT THEN
   CLOG1$ = "FIBER CLOGGED BECAUSE CRITICAL BULK CONCENTRATION EXCEEDED"
                PRINT #1, CLOG1$
                GOTO CLOG
        END IF

        POUT = P - PDROP / 2

REM Print out the variables for this axial step:

        IF JT = JTMAX OR JT = JTMAX / 2 THEN
                PRINT #1, USING "###.## ,"; X;
                PRINT #1, USING "####.# ,"; POUT;
                PRINT #1, USING "##.### ,"; CB;
                PRINT #1, USING "####.# ,"; H;
                PRINT #1, USING "###### ,"; EFFGAMMA;
               PRINT #1, USING "+#.###^^^^ ,"; DIFF; CONVCAKE, CONVMEM
                PRINT "T:"; T; "X:"; X; "H:"; H; "J:"; CONVMEM
        END IF

REM ************************************************
REM ***** End of axial position (inner) loop *****
REM ************************************************

NEXT NSTEP

REM Compare the calculated outlet pressure to the desired value and make a
REM      new guess of the inlet pressure if needed:

        OLDPERR = PERROR
        PERROR = FNP(T) - POUT
        IF ABS(PERROR) > DPCRIT THEN
                PRINT "POUT error too large, POUT = "; POUT

                IF NTLOOPS > 2 AND SGN(PERROR) <> SGN(OLDPERR) THEN
                        POUT = (OLDPIN + OLDERPIN) / 2
                ELSE
                        POUT = OLDPIN + PERROR
                END IF

                OLDERPIN = OLDPIN
                OLDPIN = POUT

                PRINT "...repeating this timestep with inlet pressure = "; POUT
                GOTO STARTX
        END IF


REM Save time and fluxes in (time) arrays for printing at end of output file:

        TIME(NT) = T
        SUMJCAKE(NT) = SUMJCAKE
        FLOWSUM(NT) = FLOWSUM
        SUMH(NT) = SUMH

        NEXT JT

REM ****************************************
REM ***** End of timestep (outer) loop *****
REM ****************************************

NEXT IT

REM Option to continue calculations:

BEEP:   FOR JJ = 1 TO 100: NEXT JJ: BEEP
        FOR KK = 1 TO 1000: NEXT KK
        BEEP: FOR JJ = 1 TO 100: NEXT JJ: BEEP
        FOR KK = 1 TO 1000: NEXT KK
        BEEP: FOR JJ = 1 TO 100: NEXT JJ: BEEP

NLOOPS = 0
PRINT ""
PRINT "For additional calculations with output every half hour,"
PRINT "choose a timestep size of 5 min, and NLOOPS = desired number of"
PRINT "hours (maximum=14).  (1 min=>output every 6 min, max 14/5 hours) "
PRINT ""

INPUT "Number of additional sets of 12 timesteps (NLOOPS):", NLOOPS
ITMAX = NLOOPS
IF NLOOPS > 0 THEN INPUT "Timestep size (min):", DTNLOOPS
FOR I = 1 TO JTMAX
        DT(I) = DTNLOOPS
NEXT I

IF NLOOPS > 0 THEN GOTO CONTINUE

GOTO FINISH

CLOG:   PRINT #1, "T = ";
        PRINT #1, USING "####.## ,"; T
        PRINT #1, USING "###.## ,"; X;
        PRINT #1, USING "####.# ,"; POUT;
        PRINT #1, USING "##.### ,"; CB;
        PRINT #1, USING "####.# ,"; H;
        PRINT #1, USING "###### ,"; EFFGAMMA;
        PRINT #1, USING "+#.###^^^^ ,"; DIFF; CONVCAKE, CONVMEM

FINISH: PRINT #1, ""
        PRINT #1, "For length-averaged flux and cake height data for this run,"
        PRINT #1, "see "; OUTFILE2$
        PRINT ""
        PRINT "Output files:  "; OUTFILE1$; " and "; OUTFILE2$
        CLOSE #1
        OPEN OUTFILE2$ FOR OUTPUT AS #1

        PRINT #1, "This file is :  "; OUTFILE2$: " produced by :"
        PRINT #1, ""
        PRINT #1, THISFIL$; " - "; REVDATE$; " VERSION      at : "; TIME$; "
  => on : "; DATE$
        PRINT #1, "For input parameters and stepwise data, see "; OUTFILE2$
        PRINT #1, ""

        PRINT #1, "  Time  JBarMem    AvgH     DelQ/Q        QbIN           QbOU
  => T      JBarCake"
```

```
PRINT "Finished at step number "; NSTEP - 1; " of total "; NL; " steps."


FOR IP = 1 TO NDIM

        IF TIME(IP) = 0 THEN GOTO DONE
        PRINT #1, USING "####.## ,"; TIME(IP);
        PRINT #1, USING "#.##### ,"; FLOWSUM(IP) / AREAMEMB;
        PRINT #1, USING "####.## ,"; SUMH(IP) / NL;
        PRINT #1, USING "#.##### ,"; FLOWSUM(IP) / BULKFLOO;
        PRINT #1, USING "+#.#####^^^^ ,"; BULKFLOO;
        PRINT #1, USING "+#.#####^^^^ ,"; BULKFLOO - FLOWSUM(IP);
        PRINT #1, USING "#.##### ,"; SUMJCAKE(IP) / NL

NEXT IP

BEEP:   FOR JJ = 1 TO 100: NEXT JJ: BEEP
        FOR KK = 1 TO 1000: NEXT KK
        BEEP: FOR JJ = 1 TO 100: NEXT JJ: BEEP

DONE: ' Breakout point to avoid printing 0 values

        CLOSE #1
```

375

```
REM                         INPUT18.BAS

REM ***** INPUT PROGRAM FOR NEWPART3, etc. *****
REM       (revised on 9/2 to include filename, on 9/4 to delete Rm, on 9/8 to
REM         replace DELH with DIFFMULT, on 9/15 to add CCAKE, and on 9/20 to
REM         replace final cake resistance with ratio of initial to final
REM         on 10/21 to change to CCAKEF and DELCCAKE, on 11/16 to add
REM         particle size, membrane resistance, fluid viscosity, and
REM         method of determining Cavg for particle version, on 11/17
REM         to make two output files, and on 11/29 to add choice 5)

INPUT "Name of Input Data File (C:SAME.IN=previous one; <CR>=none): ", INFILE$

REM Input from Keyboard:

IF INFILE$ = "" THEN
        INPUT "Particle Diameter (not radius!, in microns) : ", DIAM
        INPUT "Fluid Viscosity (cP) : ", VISCO
        INPUT "Inlet Bulk Concentration (vol. fract.) : ", CBO
        INPUT "Final Cake Concentration (vol. fract.) : ", CCAKEF
        INPUT "Difference between Initial and Final Cake Conc's: ", DELCCAKE
        INPUT "Time Constant for Cake Compaction (min) : ", TAUCAKE
        PRINT "Method of Calculating Cavg in Boundary Layer: 1 for Cw, 2 for Cb"
        INPUT "  3 for arith. avg, 4 for geom. mean, 5 for integral avg) : ", MC
  => AVG
        INPUT "Final Applied Pressure (mmHg) : ", PO
        INPUT "Time Constant for Pressure Increase (min) : ", TAUP
        INPUT "Wall Shear Rate (1/sec) : ", GAMMA
        INPUT "Membrane Resistance (_d_ format, cm-1) : ", RMCONST
        INPUT "Fiber Radius (microns) : ", RF
        INPUT "Fiber Length (cm) : ", XL
        INPUT "Specify axial step size (1) or number of steps (2)? ", M
        IF M = 1 THEN
                INPUT "Axial Step Size (cm) : ", DELX
                NL = CINT(XL / DELX)
        ELSE
                INPUT "Number of Steps : ", NL
                DELX = XL / NL
        END IF
        INPUT "Correction factor in diffusion term : ", DIFFMULT

        INPUT "Output pathname : ", PATHNAME$
        INPUT "Output filename (max 5 characters in name) : ", OUTNAME0$
        INPUT "Output file number : ", OUTNUM

ELSE
        OPEN INFILE$ FOR INPUT AS #1

        INPUT #1, DIAM
        PRINT "Particle Diameter (not radius!, in microns) : ", DIAM;
        INPUT " => ", DIAM2
        IF DIAM2 <> 0 THEN DIAM = DIAM2

        INPUT #1, VISCO
        PRINT "Fluid Viscosity (cP) : ", VISCO;
        INPUT " => ", VISCO2
        IF VISCO2 <> 0 THEN VISCO = VISCO2

        INPUT #1, CBO
        PRINT "Inlet Bulk Concentration (vol.fract.) : ", CBO; : INPUT " => ", C
  => BO2
        IF CBO2 <> 0 THEN CBO = CBO2

        INPUT #1, CCAKEF
        PRINT "Final Cake Concentration (vol.fract.) : ", CCAKEF; : INPUT " => "
  => , CCAKEF2
        IF CCAKEF2 <> 0 THEN CCAKEF = CCAKEF2

        INPUT #1, DELCCAKE
        PRINT "Difference between Initial and Final Cake Conc's: "; DELCCAKE;
        INPUT " => ", DELCCAK2
        IF DELCCAK2 <> 0 THEN DELCCAKE = DELCCAK2

        INPUT #1, TAUCAKE
        PRINT "Time Constant for Cake Compaction (min) : "; TAUCAKE;
        INPUT " => ", TAUCAKE2
        IF TAUCAKE2 <> 0 THEN TAUCAKE = TAUCAKE2

        INPUT #1, MCAVG
        PRINT "Method of Calculating Cavg in Boundary Layer: 1 for Cw, 2 for Cb"
        PRINT "  3 for arith. avg, 4 for geom. mean, 5 for integral avg) : ", MC
  => AVG;
        INPUT " => ", MCAVG2
        IF MCAVG2 <> 0 THEN MCAVG = MCAVG2


        INPUT #1, PO
        PRINT "Final Applied Pressure (mmHg) : ", PO; : INPUT " => ", PO2
        IF PO2 <> 0 THEN PO = PO2

        INPUT #1, TAUP
        PRINT "Time Constant for Pressure Increase (min) : "; TAUP;
        INPUT " => ", TAUP2
        IF TAUP2 <> 0 THEN TAUP = TAUP2

        INPUT #1, GAMMA
        PRINT "Wall Shear Rate (1/sec) : ", GAMMA; : INPUT " => ", GAMMA2
        IF GAMMA2 <> 0 THEN GAMMA = GAMMA2

        INPUT #1, RMCONST
        PRINT "Membrane Resistance (__D___ format, cm-1) : ";
        PRINT USING "   #.###^^^^^^^"; RMCONST;
        INPUT " => ", RMCONST2
        IF RMCONST2 <> 0 THEN RMCONST = RMCONST2

        INPUT #1, RF
        PRINT "Fiber Radius (microns) : ", RF; : INPUT " => ", RF2
        IF RF2 <> 0 THEN RF = RF2

        INPUT #1, XL
        PRINT "Fiber Length (cm) : ", XL; : INPUT " => ", XL2
        IF XL2 <> 0 THEN XL = XL2

        INPUT #1, M
        IF M = 1 THEN
                INPUT #1, DELX
                PRINT "Axial Step Size (cm):", DELX; : INPUT " => ", DELX2
                IF DELX2 <> 0 THEN DELX = DELX2
                NL = CINT(XL / DELX)
        ELSE
                INPUT #1, NL
                PRINT "Number of Axial Steps : ", NL; : INPUT " => ", NL2
                IF NL2 <> 0 THEN NL = NL2
                DELX = XL / NL
        END IF

        INPUT #1, DIFFMULT
        PRINT "Correction factor in diffusion term : ", DIFFMULT; : INPUT " => "
  => , DIFFMULT2
REM                 Note: in order to change from non-zero number to 0, have
REM                 to specify very small #, e.g. 1d-10, since 0 won't be read
REM                 in (the alternative is to have to type 1 every time)
```

```
                IF DIFFMULT2 <> 0 THEN DIFFMULT = DIFFMULT2

        INPUT #1, PATHNAME$
        INPUT #1, OUTNAME0$
        INPUT #1, OUTNUM
        OUTNUM = OUTNUM + 1
        EXT$ = ".OUT"
        PRINT "PATHNAME$ : "; PATHNAME$; : INPUT " => ", NEWPATH$
                IF NEWPATH$ <> "" THEN PATHNAME$ = NEWPATH$
        PRINT "OUTNAME0$ (5 characters or less) : "; OUTNAME0$; : INPUT " => ",
  => NEWNAME$
                IF NEWNAME$ <> "" THEN
                        OUTNAME0$ = NEWNAME$
                        OUTNUM = 1
                END IF
        PRINT "new OUTNUM (default=1 more than last): "; OUTNUM; : INPUT " => ",
  =>  NEWNUM
                IF NEWNUM <> 0 THEN OUTNUM = NEWNUM

END IF

REM Create output file names and print to confirm:

        IF OUTNUM < 10 THEN
                OUTNAME$ = OUTNAME0$ + LTRIM$(STR$(0))
        ELSE
                OUTNAME$ = OUTNAME0$
        END IF
        EXT1$ = "A.OUT"
        EXT2$ = "B.OUT"
        OUTFILE1$ = PATHNAME$ + OUTNAME$ + LTRIM$(STR$(OUTNUM)) + EXT1$
        OUTFILE2$ = PATHNAME$ + OUTNAME$ + LTRIM$(STR$(OUTNUM)) + EXT2$

        PRINT "Primary output file is "; OUTFILE1$
        PRINT "Secondary output file is "; OUTFILE2$

REM Save parameters for use in next run:

CLOSE #1
OPEN "C:SAME.IN" FOR OUTPUT AS #1
PRINT #1, DIAM
PRINT #1, VISCO
PRINT #1, CBO
PRINT #1, CCAKEF
PRINT #1, DELCCAKE
PRINT #1, TAUCAKE
PRINT #1, MCAVG
PRINT #1, PO
PRINT #1, TAUP
PRINT #1, GAMMA
PRINT #1, RMCONST
PRINT #1, RF
PRINT #1, XL
PRINT #1, M
IF M = 1 THEN PRINT #1, DELX ELSE PRINT #1, NL
PRINT #1, DIFFMULT
PRINT #1, PATHNAME$
PRINT #1, OUTNAME0$
PRINT #1, OUTNUM
CLOSE #1

REM The resistance is defined as a function for consistency with other modules:

DEF FNRM (T) = RMCONST
RMO = RMCONST
RMF = RMCONST
```

```
REM                    INTERP03.BAS

REM ***** PROGRAM FOR EVALUATING THE NUMERICAL INTEGRAL BY INTERPOLATING
REM     BETWEEN THE PREVIOUSLY CALCULATED VALUES STORED IN A LOOKUP TABLE *****

ICBLO = INT(CB * 1000)
ICBHI = ICBLO + 1
CBDIF = ICBHI - CB * 1000

REM Interpolate between the values of the integral at those concentrations:

LIMIT1 = 1000
LIMIT2 = 1

IF ICBLO > LIMIT1 OR ICBHI > LIMIT1 THEN
        PRINT "FIBER CLOGGED BECAUSE CRITICAL BULK CONCENTRATION EXCEEDED"
        PRINT #1, "FIBER CLOGGED BECAUSE CRITICAL BULK CONCENTRATION EXCEEDED"
        GOTO CLOG
END IF

IF ICBLO < 0 OR ICBHI < 0 THEN
        PRINT "DIVERGENCE--BULK CONCENTRATION < 0"
        PRINT #1, "DIVERGENCE--BULK CONCENTRATION < 0"
        GOTO CLOG
END IF

IF ICBLO < LIMIT2 THEN ICBLO = LIMIT2
IF ICBHI < LIMIT2 THEN ICBHI = LIMIT2

SUMDIF = SUM(ICBLO) - SUM(ICBHI)
FACTOR = SUM(ICBHI) + CBDIF * SUMDIF

REM DIAGNOSTIC WRITE:
REM PRINT "ICBLO = :",ICBLO,"ICBHI = :",ICBHI

REM "FACTOR" is the value of the integral for the bulk concentration CB (which
REM     will have units of volume fraction in the main program)
```

```
REM                         CONSTRM1

REM This is the constant membrane resistance module; it is used to predict
REM     fluxes with all membrane types in the absence of protein.

REM The suspending fluid is saline, so its viscosity is given by:

        VISCO = 1#

REM Input the membrane resistance:

        INPUT "Constant Membrane Resistance: "; RMCONST

REM To make this module consistent with the others the membrane resistance
REM     is define as a function:

        DEF FNRM (T) = RMCONST

        RM0 = FNRM(0)
        RMF = FNRM(180)

REM Test "function" for RM:

REM         T = 0
REM         FOR I = 1 TO 12
REM                 T = T + 10
REM                 PRINT T, FNRM(T)
REM         NEXT I
REM         PRINT "RM0 = "; RM0
REM         PRINT "RMF = "; RMF
```

```
REM                             PP3.BAS

REM This file is the third version of the module for the time-dependent
REM polypropylene membrane resistance, which increases more rapidly than
REM the PA resistance.  The program which calls this input file is called
REM SEPTPP.BAS.


REM Since this membrane resistance is used when 6% albumin is present, the
REM viscosity of the suspending fluid is not 1:

        VISCO = 1.5#

REM The following viscosity is used only in this subroutine:

        ALBVISC = VISCO * .000000125#
        ALBPRES = 71.3

REM These constants were determined by the 9/12/88 curve-fit for Mitsuru's
REM    6/18/88 data for the albumin permeability of the PP membranes:

        TERCEPT = .38#
        SLOPE = .36# / 26#
        A1PP = 1.113548#
        A2PP = 1.071265#
        A3PP = .139749#

REM Define function for main program:

        DEF FNRM (LOCALT)
                IF LOCALT < 16 THEN
                        ALBFLUX = TERCEPT - SLOPE * LOCALT
                ELSE
                        ALBFLUX = A1PP - A2PP * (1 - EXP(-A3PP * LOCALT))
                END IF
REM                PRINT "FLUX="; ALBFLUX;
                ALBLP = ALBFLUX / ALBPRES
                FNRM = 1 / (ALBLP * ALBVISC)
        END DEF

REM Calculate RMO and RMF:

        RMO = FNRM(0)
        RMF = FNRM(300)

REM Test the function:

REM         OPEN "SCRN:" FOR OUTPUT AS #2
REM         T = 0
REM         PRINT #2, " 5", FNRM(5)
REM         PRINT #2, " 10", FNRM(10)
REM         PRINT #2, " 15", FNRM(15)
REM         FOR I = 1 TO 15
REM                 T = T + 20
REM                 PRINT #2, T, FNRM(T)
REM         NEXT I
REM         CLOSE #2
```

```
REM                         PA3.BAS

REM This file is the third version of the module for the time-dependent
REM polyamide membrane resistance, which increases more slowly than
REM the PP resistance.  The program which calls this input file is called
REM SEPTPA.BAS.


REM This membrane resistance is used in the presence of 6% albumin so the
REM viscosity of the suspending fluid is no longer 1:

        VISCO = 1.5

REM This is the viscosity used in this subroutine:

        ALBVISC = VISCO * .000000125#

REM These constants were determined in the 9/12/88 curve-fit of Mitsuru's
REM albumin flux data taken on 6/22/88:

        AFLUX = .339779#
        BFLUX = -.004841408#
        CFLUX = .0000205173#
        ALBPRES = 71.3

REM Define function for main program:

        DEF FNRM (TLOCAL)
                IF TLOCAL > 120 THEN TLOCAL = 120
                ALBFLUX = AFLUX + BFLUX * TLOCAL + CFLUX * TLOCAL ^ 2
                ALBLP = ALBFLUX / ALBPRES
                FNRM = 1 / (ALBVISC * ALBLP)
        END DEF

REM Calculate RMO and RMF:

        RMO = FNRM(0)
        RMF = FNRM(300)

REM Test the function:

REM         OPEN "SCRN:" FOR OUTPUT AS #2
REM         T = 0
REM         FOR I = 1 TO 15
REM                 T = T + 20
REM                 PRINT #2, T, FNRM(T)
REM         NEXT I
REM         CLOSE #2
```

```
REM                    SEP2.BAS

REM This is the second version of the membrane resistance module for the
REM Sepracor polysulfone membranes, whose resistance stays fairly constant
REM longer than either the PA or PP membranes.  This module is called by the
REM SEPTSEP.BAS program.  On 9/20 I revised the final membrane resistance to
REM be the resistance at 180 min.

REM This membrane resistance is used when 6% albumin is present, so the
REM viscosity of the suspending fluid is not 1:

        VISC0 = 1.5

REM The following viscosity is used only in this subroutine:

        ALBVISC = VISC0 * .000000125#
        ALBPRES = 71.3

REM The parameters used here were determined on 9/8/88 from a curve-fit of
REM Mitsuru's 7/11/88 albumin permeability data:

        ASEP1 = .632798#
        ASEP2 = .003021255#
        ASEP3 = .078969#
        ASEP4 = .081668#

REM Here the membrane resistance function is defined for the main program:

DEF FNRM (TLOCAL)
        IF TLOCAL < 18 THEN TLOCAL = 18
        ALBFLUX = ASEP1 - ASEP2 * TLOCAL - ASEP3 * EXP(-ASEP4 * TLOCAL)
        ALBLP = ALBFLUX / ALBPRES
        FNRM = 1 / (ALBLP * ALBVISC)
END DEF

REM Calculate the initial and final membrane resistances:

        RM0 = FNRM(0)
        RMF = FNRM(180)

REM Test of the above function:

REM         T = 0
REM         OPEN "LPT1:" FOR OUTPUT AS #2
REM         PRINT #2, " 5", FNRMOLD(5), FNRM(5)
REM         PRINT #2, " 10", FNRMOLD(10), FNRM(10)
REM         PRINT #2, " 15", FNRMOLD(15), FNRM(15)

REM         FOR I = 1 TO 15
REM                 T = T + 20
REM                 PRINT #2, T, FNRMOLD(T), FNRM(T)
REM         NEXT I
REM         CLOSE #2
```

382

```
REM                          AA58LOOK.BAS

REM  ***** NUMERICAL INTEGRATION PROGRAM - ACRIVOS DIFF AND VISC  *****
REM (4/30 version creates lookup table"LOOKUP.A58" by integrating backward.
REM Notes: (1) "0.33" is not in the integral (2) 0.58 is max. concentration)

DEFDBL A-Z: DEFINT I-N

REM:  Define function to be integrated:

DEF FNF (Z) = Z * (1 + .5 * EXP(8.8 * Z)) / (1 + 1.5 * Z / (1 - Z / .58)) ^ 2

REM:  Input the integration limits and step size or number of steps:

INPUT "Initial lower integration limit:", XO
INPUT "Final lower integration limit:", XEND
INPUT "Upper integration limit:", XF
INPUT "Specify step size (1) or number of steps (2)"; J
IF J = 1 THEN INPUT "Step size:", DELX: GOTO 200
IF J = 2 THEN INPUT "Number of steps:", N: GOTO 210

REM:  Initialize variables before entering loop:

200 N = INT((XF - XO) / DELX): GOTO 220
210 DELX = (XF - XO) / N
220 X = XF: YLAST = FNF(XF): SUM = 0: NOUT = INT((XEND - XO) / DELX) + 1: DIM Y1
  => (N), Y2(N)

OPEN "A:LOOKUP.A58" FOR OUTPUT AS #1
PRINT #1, NOUT

REM:  Step down in x, calculate the trapezoid area and add it to the sum:

FOR I = 1 TO N
        X = X - DELX
        PRINT "X = ", X
        Y = FNF(X)
        AREA = DELX * (Y + YLAST) / 2!
        SUM = SUM + AREA
        YLAST = Y
        Y1(N + 1 - I) = X
        Y2(N + 1 - I) = SUM

REM If n=100 and nout=30, then m(100)....m(0) will be calculated
REM     but only the last 30 will be needed

NEXT I

REM Print out the results in ascending order:

FOR I = 1 TO NOUT
        PRINT #1, Y1(I), Y2(I)
NEXT I

PRINT #1, "XO              SUM"
PRINT #1, ""
PRINT #1, "XF = ", XF, "DELX = ", DELX
PRINT #1, ""
PRINT #1, "This is LOOKUP.A58 created by AA58LOOK.BAS at "; TIME$; " on "; DATE$

CLOSE #1
```

```
REM                          OTHERINT.BAS

REM Program created 1/5/88

DEFINT I-N
N = 580
DIM DAVG(N), CONC(N), SUMM(N)
OPEN "C:OTHERDAV.OUT" FOR OUTPUT AS #1
OPEN "C:OTHEROUT.DAT" FOR OUTPUT AS #2

REM Acrivos diffusivity:

DEF FNDIFFA (C) = C ^ 2 * (1# + .5 * EXP(8.8 * C))

REM Backwards numerical integration of D(C):

SUM = 0
DC = .001
CWALL = .57999
C = CWALL
Y = FNDIFFA(C)

FOR I = 1 TO N

        OLDY = Y
        C = C - DC
        Y = FNDIFFA(C)
        DELSUM = (Y + YOLD) * DC / 2
        SUM = SUM + DELSUM
        SUMM(I) = ABS(SUM)
        CONC(I) = ABS(C)

REM Calculation of average D from the integral:

        DAVG(I) = ABS(SUM / (CWALL - C))


NEXT I

REM Print out in ascending order:
        PRINT #2, N


FOR I = N TO 1 STEP -1

        PRINT USING "   #.#### "; CONC(I);
        PRINT ",";
        PRINT USING "   ##.##### "; SUMM(I);
        PRINT ",";
        PRINT USING "   ##.#####^^^^"; DAVG(I)

        PRINT #1, USING "   #.#### "; CONC(I);
        PRINT #1, ",";
        PRINT #1, USING "   ##.##### "; SUMM(I);
        PRINT #1, ",";
        PRINT #1, USING "   ##.#####^^^^"; DAVG(I)

        PRINT #2, USING "   #.#### "; CONC(I);
        PRINT #2, ",";
        PRINT #2, USING "   ##.#####^^^^"; DAVG(I)

NEXT I

CLOSE #1
CLOSE #2
```

```
THISFIL$ = "YEASTSEP.BAS": REVDATE$ = "12/29/88"

REM ***** TIME-DEPENDENT MODEL OF YEAST FILTRATION IN SEPRACOR HOLLOW FIBERS,
REM         WITH AXIAL VARIATION IN BULK FLOW, CONC, P AND FLUXES *****

REM This program was created from YEASTPP1.BAS.  It uses the Acrivos
REM diffusivity and viscosity from NUPART10, but the membrane and cake
REM resistances from ZYD4PP.  The cake compaction and CO2 buildup terms
REM are now separate.

DEFDBL A-Z: DEFINT I-N: DIM SUM(1000): DIM DAVG(1000)

REM  Note: Variable values are output at each timestep, but only the
REM        current and immediately previous values are kept in memory.

REM Dimension arrays:

        ITMAX = 14: JTMAX = 12: NDIM = 5 * ITMAX * JTMAX
        DIM DT(ITMAX)
        DIM TIME(NDIM), SUMJCAKE(NDIM), FLOWSUM(NDIM), SUMH(NDIM)

REM Acrivos viscosity:

        DEF FNVISC (C) = (1 + 1.5 * C / (1 - C / .58)) ^ 2

REM The final resistance of the cake is calculated from the local applied
REM pressure: (This equation was determined from the stagnant filtration
REM data for unrinsed, freshly-prepared yeast at room temperature.)

        RC1 = .001396
        RC2 = .3191
        RC3 = .047

        VISCSTAG = .000000125#
        RM100 = 40000000#

        DEF FNRC (P)

                HYDPERM = RC1 + RC2 * RC3 / (1 + RC3 * P) ^ 2
                FNRC = (1 / (VISCSTAG * HYDPERM) - RM100) / .01

        END DEF

REM This accounts for a linear buildup of CO2 in the cake during a time
REM period of length TAUCO2.  This increases the resistance of the cake
REM without affecting the yeast concentration in the cake.  The final
REM volume fraction occupied by the CO2 is FINALCO2.  (The way the cake
REM resistance lag term is set up this decreases the early-time resistance
REM and uses the experimentally-measured resistance as the final resistance.):

        DEF FNEPSCO2 (T)
                IF T < TAUCO2 THEN
                        FNEPSCO2 = FINALCC2 * T / TAUCO2
                ELSE
                        FNEPSCO2 = FINALCO2
                END IF
        END DEF

REM Time-dependent cake concentration due to compaction:

        DEF FNCCAKE (T)
                IF T < TAUCAKE THEN
                        FNCCAKE = CCAKEF - DELCCAKE * (TAUCAKE - T) / TAUCAKE
                ELSE
                        FNCCAKE = CCAKEF
                END IF
        END DEF

REM Lag in cake resistance due to time required for compaction and CO2 buildup:

        DEF FNRESLAG (T)
                EPS = 1 - FNCCAKE(T) - FNEPSCO2(T)
                EPSF = 1 - CCAKEF - FINALCO2
                IF T < TAUCAKE OR T < TAUCO2 THEN
                        FNRESLAG = (1 - EPS) ^ 2 * EPSF ^ 3 / ((1 - EPSF) ^ 2 *
  => EPS ^ 3)
                ELSE
                        FNRESLAG = 1
                END IF
        END DEF

REM The membrane resistance used below will be corrected to account for 40%
REM pore blockage if the cake height is > 1 cell layer, and will be a linear
REM function of cake height when there is less than a monolayer of coverage:

        PHIMAX = .4#
        DIAM = 6
        DEF FNBLOCK (H)
                IF H > DIAM THEN
                        PHI = PHIMAX
                ELSE
                        PHI = H * PHIMAX / DIAM
                END IF
                FNBLOCK = 1 / (1 - PHI)
        END DEF

REM Acrivos diffusion coefficient:

        DEF FNDIFFA (Z) = Z ^ 2 * (1# + .5 * EXP(8.8 * Z))

REM The inlet pressure is gradually increased to its final value to avoid
REM clogging:

        DEF FNP (TLOCAL)
                IF TLOCAL < TAUP THEN
                        FNP = .1 * P0 + .9 * P0 * (TLOCAL / TAUP)
                ELSE FNP = P0
                END IF
        END DEF

REM The membrane resistance program is called here (PP3=polypropylene with
REM albumin, PA3=polyamide with albumin, SEP2=Sepracor with albumin,
REM CONSTRM1=constant Rm, LINEAR=linearly increasing Rm to test negative DELH:

        REM $INCLUDE: 'C:\NORMA\QBASIC\SEP2.BAS'

PRINT THISFIL$; " ", REVDATE$; " VERSION     Current Date and Time: "; DATE$; "
  => "; TIME$
PRINT ""

REM:  Input the required parameters (now includes time constant for Rc):

        REM $INCLUDE: 'C:\NORMA\QBASIC\INPUT20.BAS'

REM Store values of input parameters in the output file:

        OPEN OUTFILE1$ FOR OUTPUT AS #1
        PRINT #1, "This file is :  "; OUTFILE1$; " produced by :"
        PRINT #1, ""
        PRINT #1, THISFIL$; " - "; REVDATE$; " VERSION      at : "; TIME$; "
  => on : "; DATE$
        PRINT #1, ""
```

```
        PRINT #1, "Fluid viscosity (cP):  "; VISCO
        PRINT #1, "Inlet bulk concentration:  "; CBO
        PRINT #1, "Final cake concentration:  "; CCAKEF
        PRINT #1, USING "+#.##^^^^"; RMO
        PRINT #1, "Final membrane resistance:  ";
        PRINT #1, USING "+#.##^^^^"; RMF
        PRINT #1, "Difference between initial and final cake concentrations:  ";
        PRINT #1, USING "+#.##^^^^"; DELCCAKE
        PRINT #1, "Time constant for cake compaction (min):  "; TAUCAKE
        PRINT #1, "Final volume fraction occupied by CO2:  ";
        PRINT #1, USING "+#.##^^^^"; FINALCO2
        PRINT #1, "Time constant for CO2 buildup (min):  "; TAUCO2
        PRINT #1, "Method for calculating Cavg:  "; MCAVG
        PRINT #1, "Final inlet pressure:  "; PO
        PRINT #1, "Time constant for pressure increase (min):  "; TAUP
        PRINT #1, "Inlet shear rate (sec-1):  "; GAMMA
        PRINT #1, "Fiber radius (microns):  "; RF
        PRINT #1, "Fiber length (cm):  "; XL
        IF M = 1 THEN PRINT #1, "Axial step size:  "; DELX
        PRINT #1, "Correction factor for diffusion term:  "; DIFFMULT
        PRINT #1, ""

REM Input the values of the numerical integration from a lookup table
REM     in which the integration step size was 0.001 (i.e. 0.1%):

        OPEN "C:\NORMA\QBASIC\LOOKUP.A58" FOR INPUT AS #2
        INPUT #2, NVALUES
        FOR I = 1 TO NVALUES
                INPUT #2, CONCEN, SUMM
                ICONC = INT(CONCEN * 1000)
                SUM(ICONC) = SUMM
        NEXT I
        CLOSE #2

REM If Davg is to be determined by the numerical integration method, then,
REM     input the values of the numerical integration from a lookup table
REM     in which the integration step size was 0.001 (i.e. 0.1%):

        IF MCAVG = 5 THEN
                OPEN "C:\NORMA\QBASIC\DLOOKUP.CKC" FOR INPUT AS #2
                INPUT #2, NVALUES
                FOR I = 1 TO NVALUES
                        INPUT #2, CONCEN, DAVERAGE
                        ICONC = INT(CONCEN * 1000)
                        DAVG(ICONC) = DAVERAGE
                NEXT I
                CLOSE #2
        END IF

REM Set variable dimensions which are related to input parameters:

        DIM H(NL), OLDH(NL)

REM Set the cell-dependent parameters (in this case, for yeast):

        A = .0003#
        CBCRIT = .99# * CCAKEF

REM Calculate the constant part of the coefficients for the diffusion and
REM convection terms [note that 0.2569=0.538*(0.33)^(2/3) and that the
REM concentration part of the diffusivity is no longer constant because
REM it is evaluated at Cavg]:

        COEFF0 = DIFFMULT * .2569 * 60 * A ^ (4 / 3)
        COEFF2 = 1 / (.000000125# * VISCO)
```



```
REM Initialize loop parameters and calculate axial pressure drop per step:

        X = 0: SUMJCAKE = 0: FLOWMEM = 0: FLOWSUM = 0: SUMH = 0
        POUT = 0: DROP = 0: NSTEP = 0: PI = 3.14159
        BULKFLOO = 15 * PI * GAMMA * RF ^ 3 / 1000000000000#
        DPCRIT = .001 * PO
        STEPAREA = 2 * PI * RF * .0001# * DELX
        AREAMEMB = 2 * PI * RF * .0001# * XL

REM NOTE: These are timestep calculations and variable initializations
REM  which only need to be done once (24 timesteps of 5, 10, 15, 30 and
REM  60 s, then 36 steps of 2 min and 12 steps of 5 min)

        DT(1) = 1 / 12: DT(2) = 1 / 12: DT(3) = 1 / 6: DT(4) = 1 / 6
        DT(5) = .25: DT(6) = .25: DT(7) = .5: DT(8) = .5: DT(9) = 1#:
        DT(10) = 1#: DT(11) = 2#: DT(12) = 2#: DT(13) = 2#: DT(14) = 5#
REM        : DT(13) = 5#: DT(14) = 5#

        H = 0

REM ************************************************************
REM ***** Beginning of the iteration in time (outer loop): *****
REM ************************************************************

T = 0: NT = 0

CONTINUE: 'Entrance point for more calculations

FOR IT = 1 TO ITMAX
        DELT = DT(IT)
        FOR JT = 1 TO JTMAX

                NT = NT + 1
                T = T + DELT

                IF JT = JTMAX OR JT = JTMAX / 2 THEN
                        PRINT #1, " "
                        PRINT #1, " T = ";
                        PRINT #1, USING "####.##"; T
                        PRINT #1, ""
                END IF


REM Save the cake height as a function of axial position from the previous
REM    timestep in the OLDH array:

                FOR JJ = 1 TO NL

                        OLDH(JJ) = H(JJ)

                NEXT JJ

REM Set initial (X=0) values which are used only after successfully completing
REM     a timestep:

                OLDPOUT = POUT
                IF NT = 1 THEN AXIDPOLD = 0 ELSE AXIDPOLD = AXIALDP
                IF NT = 1 THEN AXIALDP = 0 ELSE AXIALDP = OLDPIN - OLDPOUT
REM Previous attempt to dampen oscillations:
REM      POUT = FNP(T) + (AXIALDP + AXIDPOLD) / 2#
                POUT = FNP(T) + AXIALDP
                OLDPIN = POUT
                NTLOOPS = 0
                PRINT ""
                PRINT "T=", T
                PRINT ""
```

```
REM Set the initial values which must be reset for each iteration of the
REM     timestep:

STARTX:         X = 0
                NTLOOPS = NTLOOPS + 1
                QBOUT = BULKFLOO
                CBOUT = CB0
                FLOWMEM = 0
                SUMJCAKE = 0
                FLOWSUM = 0
                SUMH = 0

                IF JT = JTMAX OR JT = JTMAX / 2 THEN
        PRINT #1, "    X      P      CB       H       SHEAR       DIFF FLUX       CONV
  => FLUX     MEM FLUX"
                END IF

REM ************************************************************************
REM ***** This is the beginning of the axial position (inner) loop *****
REM ************************************************************************

FOR NSTEP = 1 TO NL

        X = X + DELX

REM Set inlet values for this axial step equal to previous outlet values:

        QB = QBOUT
        CB = CBOUT
        PIN = POUT

REM Correct the previous timestep's value of H to account for compaction:

        H = OLDH(NSTEP) * FNCCAKE(T - DELT) / FNCCAKE(T)

REM Calculate the effective shear rate:

                GAMMAX = QB / (15 * PI * RF ^ 3 / 1000000000000#)
                IF H > DIAM THEN
                        EFFGAMMA = GAMMAX * (RF / (RF - H)) ^ 3
                ELSE
                        EFFGAMMA = GAMMAX
                END IF

REM Calculate the PDROP:

                CDROP = .0025# * VISC0 * DELX * 60
                    IF H > DIAM THEN
                        PDROP = CDROP * FNVISC(CB) * EFFGAMMA / (RF - H)
                    ELSE
                        PDROP = CDROP * FNVISC(CB) * EFFGAMMA / RF
                    END IF


REM Calculate P from PIN and PDROP:

                P = PIN - PDROP / 2

REM Used only in version without inlet pressure correction:
REM                 IF P < 0 THEN
REM                         PRINT #1, "AXIAL PRESSURE DROP EXCEEDED APPLIED PRESSU
  => RE"
REM                         GOTO CLOG
REM                 END IF
                    IF P < 0 THEN

        PRINT "Axial pressure drop too high, P = "; P; "at X = "; X
                        POUT = OLDPIN + 1# * ABS(P)
                        OLDPIN = POUT
        PRINT "repeating this timestep with PIN = "; POUT
        PRINT #1, "repeating this timestep with PIN = "; POUT
                        PRINT #1, USING "###.## ,"; X;
                        PRINT #1, USING "####.# ,"; P;
                        PRINT #1, USING "##.### ,"; CB;
                        PRINT #1, USING "####.# ,"; H;
                        PRINT #1, USING "###### ,"; EFFGAMMA;
                        PRINT #1, USING "+#.###^^^^ ,"; DIFF; CONVCAKE, CONVMEM
                        GOTO STARTX
                END IF


REM Calculate the fluxes for this axial step (note that coeff1 had to be
REM     recalculated because cb had changed).  Start by calling the numerical
REM     integration interpolating program with CB equal to the concentration
REM     at this axial position and time:

        REM $INCLUDE: 'C:\NORMA\QBASIC\INTERPO3.BAS'

REM The bulk viscosity (and therefore CB) appears in the coefficient for
REM the diffusion term:

        IF MCAVG = 1 THEN
                CAVG = FNCCAKE(T)
                DCAVG = FNDIFFA(CAVG)
        END IF

        IF MCAVG = 2 THEN
                CAVG = CB
                DCAVG = FNDIFFA(CAVG)
        END IF

        IF MCAVG = 3 THEN
                CAVG = (FNCCAKE(T) + CB) / 2
                DCAVG = FNDIFFA(CAVG)
        END IF

        IF MCAVG = 4 THEN
                CAVG = SQR(FNCCAKE(T) * CB)
                DCAVG = FNDIFFA(CAVG)
        END IF

        IF MCAVG = 5 THEN
                REM $INCLUDE: 'C:\NORMA\QBASIC\DINTERPO.BAS'
        END IF

REM* Diagnostic write:
REM*            PRINT "MCAVG = "; MCAVG
REM*            PRINT "CB = "; CB
REM*            PRINT "FNCCAKE(T) = "; FNCCAKE(T)
REM*            PRINT "CAVG = "; CAVG
REM*            PRINT "DCAVG = "; DCAVG

             COEFF1 = COEFF0 * FACTOR * FNVISC(CB) / DCAVG ^ (1 / 3)
               DIFF = COEFF1 * EFFGAMMA / (X - DELX / 2) ^ (1 / 3)
REM             CONVMEM = COEFF2 * P / (FNBLOCK(H) * FNRM(T) + FNRC(FNCCAKE(T))
  => * H * .0001#)

REM Note that the pore blockage and resistance lag terms have been restored:
```

```
  CONVMEM = COEFF2 * P / (FNBLOCK(H) * FNRM(T) + FNRC(P) * FNRESLAG(T) * RF * .0
  => 001# * LOG(RF / (RF - H)))

              IF H > DIAM THEN
                      CONVCAKE = CONVMEM * RF / (RF - H)
              ELSE
                      CONVCAKE = CONVMEM
              END IF
              FLUXNET = CONVCAKE - DIFF

REM This prevents numerically-induced oscillations:

              IF ABS(FLUXNET / CONVMEM) < .00001 THEN FLUXNET = 0

REM These are running totals for calculating length-averaged fluxes (running
REM total for H is below):

              SUMJCAKE = SUMJCAKE + CONVCAKE
              FLOWMEM = CONVMEM * STEPAREA
              FLOWSUM = FLOWSUM + FLOWMEM

REM The increase or decrease in the cake height at this axial position
REM     (during this timestep) is calculated (with the constraint that the
REM     cake height >=0):

              DELH = 10000# * FLUXNET * DELT * CB / FNCCAKE(T)
              IF DELH < 0 AND ABS(DELH) > H THEN DELH = -ABS(H)

              H = H + DELH

REM Check that 0 < DELH < H:

              IF H < 0 THEN H = 0

              IF H >= RF - A * 10000# THEN
                      CLOG2$ = "FIBER CLOGGED BECAUSE CAKE FILLED CHANNEL"
                      PRINT #1, CLOG2$
                      GOTO CLOG
              END IF

REM Save the newly calculated height in its axial array:

              H(NSTEP) = H
              SUMH = SUMH + H


REM Use inlet values of Qb, Cb, and P to calculate outlet values:

              QBOUT = QB - FLOWMEM

              DCAKEVOL = .00000002# * PI * DELX * (RF - H - DELH / 2) * DELH
              CBOUT = (CB * QB - DCAKEVOL * FNCCAKE(T)) / QBOUT

              IF CB >= CBCRIT THEN
      CLOG1$ = "FIBER CLOGGED BECAUSE CRITICAL BULK CONCENTRATION EXCEEDED"
                      PRINT #1, CLOG1$
                      GOTO CLOG
              END IF

              POUT = P - PDROP / 2

REM Print out the variables for this axial step:

              IF JT = JTMAX OR JT = JTMAX / 2 THEN
                      PRINT #1, USING "###.## ,"; X;
                      PRINT #1, USING "####.# ,"; POUT;
```



```
                      PRINT #1, USING "##.### ,"; CB;
                      PRINT #1, USING "####.# ,"; H;
                      PRINT #1, USING "###### ,"; EFFGAMMA;
                     PRINT #1, USING "+#.###^^^^ ,"; DIFF; CONVCAKE, CONVMEM
                      PRINT "T:"; T; "X:"; X; "H:"; H; "J:"; CONVMEM
              END IF

REM ***********************************************
REM ***** End of axial position (inner) loop *****
REM ***********************************************

NEXT NSTEP

REM Compare the calculated outlet pressure to the desired value and make a
REM     new guess of the inlet pressure if needed:

        OLDPERR = PERROR
        PERROR = FNP(T) - POUT
        IF ABS(PERROR) > DPCRIT THEN
                PRINT "POUT error too large, POUT = "; POUT

                IF NTLOOPS > 2 AND SGN(PERROR) <> SGN(OLDPERR) THEN
                        POUT = (OLDPIN + OLDERPIN) / 2
                ELSE
                        POUT = OLDPIN + PERROR
                END IF

                OLDERPIN = OLDPIN
                OLDPIN = POUT

                PRINT "...repeating this timestep with inlet pressure = "; POUT
                GOTO STARTX
        END IF


REM Save time and fluxes in (time) arrays for printing at end of output file:

        TIME(NT) = T
        SUMJCAKE(NT) = SUMJCAKE
        FLOWSUM(NT) = FLOWSUM
        SUMH(NT) = SUMH

        NEXT JT

REM ***************************************
REM ***** End of timestep (outer) loop *****
REM ***************************************

NEXT IT

REM Option to continue calculations:

BEEP:   FOR JJ = 1 TO 100: NEXT JJ: BEEP
        FOR KK = 1 TO 1000: NEXT KK
        BEEP: FOR JJ = 1 TO 100: NEXT JJ: BEEP
        FOR KK = 1 TO 1000: NEXT KK
        BEEP: FOR JJ = 1 TO 100: NEXT JJ: BEEP

NLOOPS = 0
PRINT ""
PRINT "For additional calculations with output every half hour,"
PRINT "choose a timestep size of 5 min, and NLOOPS = desired number of"
PRINT "hours (maximum=14).  (1 min=>output every 6 min, max 14/5 hours) "
PRINT ""

INPUT "Number of additional sets of 12 timesteps (NLOOPS):", NLOOPS
```

```
ITMAX = NLOOPS
IF NLOOPS > 0 THEN INPUT "Timestep size (min):", DTNLOOPS
FOR I = 1 TO JTMAX
        DT(I) = DTNLOOPS
NEXT I

IF NLOOPS > 0 THEN GOTO CONTINUE

GOTO FINISH

CLOG:   PRINT #1, "T = ";
        PRINT #1, USING "####.## ,"; T
        PRINT #1, USING "###.## ,"; X;
        PRINT #1, USING "####.# ,"; POUT;
        PRINT #1, USING "##.### ,"; CB;
        PRINT #1, USING "####.# ,"; H;
        PRINT #1, USING "###### ,"; EFFGAMMA;
        PRINT #1, USING "+#.###^^^^ ,"; DIFF; CONVCAKE, CONVMEM

FINISH: PRINT #1, ""
        PRINT #1, "For length-averaged flux and cake height data for this run,"
        PRINT #1, "see "; OUTFILE2$
        PRINT ""
        PRINT "Output files:  "; OUTFILE1$; " and "; OUTFILE2$
        CLOSE #1
        OPEN OUTFILE2$ FOR OUTPUT AS #1

        PRINT #1, "This file is :  "; OUTFILE2$; " produced by :"
        PRINT #1, ""
        PRINT #1, THISFIL$; " - "; REVDATE$; " VERSION      at : "; TIME$; "
  => on : "; DATE$
        PRINT #1, "For input parameters and stepwise data, see "; OUTFILE2$
        PRINT #1, ""

        PRINT #1, "  Time  JBarMem    AvgH     DelQ/Q        QbIN           QbOU
  => T      JBarCake"

PRINT "Finished at step number "; NSTEP - 1; " of total "; NL; " steps."


FOR IP = 1 TO NDIM

        IF TIME(IP) = 0 THEN GOTO DONE
        PRINT #1, USING "####.## ,"; TIME(IP);
        PRINT #1, USING "#.##### ,"; FLOWSUM(IP) / AREAMEMB;
        PRINT #1, USING "####.## ,"; SUMH(IP) / NL;
        PRINT #1, USING "#.##### ,"; FLOWSUM(IP) / BULKFLOO;
        PRINT #1, USING "+#.#####^^^^ ,"; BULKFLOO;
        PRINT #1, USING "+#.#####^^^^ ,"; BULKFLOO - FLOWSUM(IP);
        PRINT #1, USING "#.##### ,"; SUMJCAKE(IP) / NL

NEXT IP

BEEP:   FOR JJ = 1 TO 100: NEXT JJ: BEEP
        FOR KK = 1 TO 1000: NEXT KK
        BEEP: FOR JJ = 1 TO 100: NEXT JJ: BEEP

DONE: ' Breakout point to avoid printing 0 values

        CLOSE #1
```

J. REFERENCES

Blatt, W. F., A. Dravid, A. S. Michaels, and L. Nelson (1970): Solute Polarization and Cake Formation in Membrane Ultrafiltration: Causes, Consequences, and Control Techniques, in Membrane Science and Technology J. E. Flinn, ed., Plenum Press, New York, pp. 47-97

Chudacek, M. W., and A. G. Fane (1984): The Dynamics of Polarisation in Unstirred and Stirred Ultrafiltration J. Memb. Sci. **21**: 145-160

Colton, C. K., L. W. Henderson, C. A. Ford, and M. J. Lysaght (1975): Kinetics of Hemodiafiltration. I. In Vitro Transport Characteristics of a Hollow-Fiber Blood Ultrafilter J. Lab. Clin. Med. **85**: 355

Darcy, H. P. G. (1856): Les Fontaines Publiques de la Ville de Dijon Dalmont, Paris

Davis, R. H., and D. T. Leighton (1987): Shear-induced Transport of a Particle Layer along a Porous Wall Chem. Eng. Sci. **42**(2): 275-281

Eckstein, E. C., D. G. Bailey, and A. H. Shapiro (1974): Self-Diffusion of Particles in Shear Flow of a Suspension J. Fluid Mech. **79**: 191

Kozeny, J. (1927): Hydralik, Springer-Verlag, Wein

Kozeny, J. (1927): Wasserkraft und Wasserwirtschaft **22**: 67,86

Leighton, D. T. (1985): The Shear-Induced Migration of Concentrated Suspensions, Ph. D. Thesis, Stanford University

Leighton, D. T., and A. A. Acrivos (1987): Measurement of the Shear-Induced Coefficient of Self-Diffusion in Concentrated Suspensions of Spheres J. Fluid Mech. **79**:109-131

Leveque, M. A. (1928): Les Lois de la Transmission de Chaleur par Convection Ann. Mines **13**:201

Reuss, M., Josic, D., Popovic, M., and W. K. Bronn (1979): Viscosity of Yeast Suspensions European J. Appl. Microbiol. **8**: 167-175

Romero, C. A., and R. H. Davis (1988): Global Model of Crossflow Microfiltration based on Hydrodynamic Particle Diffusion J. Memb. Sci. **39**: 157-185

Trettin, D. R., and M. R. Doshi (1980): Limiting Flux in Ultrafiltration of Macromolecular Solutions Chem. Eng. Comm. **4**: 507

Zydney, A. L. (1985): Cross-Flow Membrane Plasmapheresis: An Analysis of Flux and Hemolysis, Ph. D. Thesis, Massachusetts Institute of Technology

Zydney, A. L., and C. K. Colton (1982): Continuous Flow Membrane Plasmapheresis: Theoretical Models for Flux and Hemolysis Prediction Trans. Am. Soc. Artif. Intern. Organs **28**: 408

Zydney, A. L., and C. K. Colton (1986): A Concentration Polarization Model for the Filtrate Flux in Cross-Flow Microfiltration of Particulate Suspensions Chem. Eng. Commun. **47**: 1-21